CURRENT TRENDS IN MEDICINAL PLANT RESEARCH AND NEURODEGENERATIVE DISORDERS

EDITED BY: Muhammad Ayaz, Tahir Ali, Abdul Sadiq, Farhat Ullah and Muhammad Imran Naseer

PUBLISHED IN: Frontiers in Pharmacology and Frontiers in Neuroscience

frontiers Research Topics

ISSN 1664-8714
ISBN 978-2-88976-633-8
DOI 10.3389/978-2-88976-633-8

About Frontiers

Frontiers is more than just an open-access publisher of scholarly articles: it is a pioneering approach to the world of academia, radically improving the way scholarly research is managed. The grand vision of Frontiers is a world where all people have an equal opportunity to seek, share and generate knowledge. Frontiers provides immediate and permanent online open access to all its publications, but this alone is not enough to realize our grand goals.

Frontiers Journal Series

The Frontiers Journal Series is a multi-tier and interdisciplinary set of open-access, online journals, promising a paradigm shift from the current review, selection and dissemination processes in academic publishing. All Frontiers journals are driven by researchers for researchers; therefore, they constitute a service to the scholarly community. At the same time, the Frontiers Journal Series operates on a revolutionary invention, the tiered publishing system, initially addressing specific communities of scholars, and gradually climbing up to broader public understanding, thus serving the interests of the lay society, too.

Dedication to Quality

Each Frontiers article is a landmark of the highest quality, thanks to genuinely collaborative interactions between authors and review editors, who include some of the world's best academicians. Research must be certified by peers before entering a stream of knowledge that may eventually reach the public - and shape society; therefore, Frontiers only applies the most rigorous and unbiased reviews.
Frontiers revolutionizes research publishing by freely delivering the most outstanding research, evaluated with no bias from both the academic and social point of view. By applying the most advanced information technologies, Frontiers is catapulting scholarly publishing into a new generation.

What are Frontiers Research Topics?

Frontiers Research Topics are very popular trademarks of the Frontiers Journals Series: they are collections of at least ten articles, all centered on a particular subject. With their unique mix of varied contributions from Original Research to Review Articles, Frontiers Research Topics unify the most influential researchers, the latest key findings and historical advances in a hot research area! Find out more on how to host your own Frontiers Research Topic or contribute to one as an author by contacting the Frontiers Editorial Office: frontiersin.org/about/contact

CURRENT TRENDS IN MEDICINAL PLANT RESEARCH AND NEURODEGENERATIVE DISORDERS

Topic Editors:
Muhammad Ayaz, University of Malakand, Pakistan
Tahir Ali, University of Calgary, Canada
Abdul Sadiq, University of Malakand, Pakistan
Farhat Ullah, University of Malakand, Pakistan
Muhammad Imran Naseer, King Abdulaziz University, Saudi Arabia

Citation: Ayaz, M., Ali, T., Sadiq, A., Ullah, F., Naseer, M. I., eds. (2022). Current Trends in Medicinal Plant Research and Neurodegenerative Disorders. Lausanne: Frontiers Media SA. doi: 10.3389/978-2-88976-633-8

Table of Contents

frontiers | Frontiers in Pharmacology

EDITORIAL
published: 30 June 2022
doi: 10.3389/fphar.2022.922373

Editorial: Current Trends in Medicinal Plant Research and Neurodegenerative Disorders

Muhammad Ayaz[1]*, *Tahir Ali*[2,3], *Abdul Sadiq*[1], *Farhat Ullah*[1] and *Muhammad Imran Naseer*[4,5]

[1]Department of Pharmacy, Faculty of Biological Sciences, University of Malakand, Chakdara, Pakistan, [2]Calgary Prion Research Unit, Department of Comparative Biology and Experimental Medicine, Faculty of Veterinary Medicine, University of Calgary, Calgary, AB, Canada, [3]Hotchkiss Brain Institute, Cumming School of Medicine, University of Calgary, Calgary, AB, Canada, [4]Center of Excellence in Genomic Medicine Research, King Abdulaziz University, Jeddah, Saudi Arabia, [5]Department of Medical Laboratory Technology, Faculty of Applied Medical Sciences, King Abdulaziz University, Jeddah, Saudi Arabia

Keywords: Alzheime´s disease, natural products, neuroprotection, signaling pathways, oxidative stress

Editorial on the Research Topic

Current Trends in Medicinal Plant Research and Neurodegenerative Disorders

In natural product research, the ethnopharmacological approach is unique because it requires input from the cultural and social sciences. For the first time in 1967, the term "ethnopharmacology" was used as a book title "*Ethnopharmacological Search for Psychoactive Drugs*" (Efron et al., 1967). Ethnopharmacology is the scientific exploration of biologically active agents which are traditionally used or observed by man (Bruhn and Helmstedt, 1981). In many parts of the word, medicinal plants are considered as part of the traditional knowledge of a culture due to their significance in indigenous medical systems (Ayaz et al., 2019b). Thus, those studies which focus on the documentation of traditional uses of plants have ethnopharmacological relevance. The uses of medicinal plants have been described by many explorers, merchants, missionaries, and respective knowledgeable experts of healing and traditions which serve as a basis for ethnopharmacology-based drug development. Such knowledge has been widely used as a starting point for the development of drug (Heinrich, 2007).

The medicinal plants used by common people act as a significant part of all medical systems occurring in the world (Ayaz et al., 2017b; Ayaz et al., 2019c). It has been reported that in 17th century, an English housewife used Digitalis purpurea L. [Plantaginaceae] (foxglove) for the treatment of dropsy. After that, it was used by a physician WilliamWithering more systematically and he transformed this knowledge into medicine form that could be used by medical doctors (Griggs, 1981; Heinrich, 2010). Some of the ethno-pharmacologically driven natural products, identified during 19th century include morphine, emetine, strychnine, quinine, caffeine, coniine, atropine and capsaicin (Heinrich, 2010). Natural products are one of the most important sources of new drug leads. In past, crude materials isolated from various plants or their extracts were used as medicines for medical treatment and then after the second half of the 19th century due to rapid expansion of pharmaceutical industries the researchers started to develop and characterize various drugs from plant origin (Ovais et al., 2021; Heinrich, 2010). Chin et al., reported that among the marketed launched products, more than half of all new chemical entities are natural products or their derivatives (Sneader, 2005).

Since ancient times, natural products (NP) have been used as medicines to cure various illnesses (Ayaz et al., 2017a; Ayaz et al., 2020). As a source of therapeutic molecules, NP have historically proven their value and still act as an important pool for the recognition of novel drug leads (Atanasov et al., 2015). Galanthamine is a natural product obtained from several members of amaryllidaceae family and is commonly used for the treatment of Alzheimer's disease (AD). As per the ethnobotanical information, the development of galanthamine as anti-Alzheimer's drug consists

OPEN ACCESS

Edited by:
Javier Echeverria,
University of Santiago, Chile

Reviewed by:
Luca Rastrelli,
University of Salerno, Italy

***Correspondence:**
Muhammad Ayaz
ayazuop@gmail.com

Specialty section:
This article was submitted to Ethnopharmacology, a section of the journal Frontiers in Pharmacology

Received: *17 April 2022*
Accepted: *13 June 2022*
Published: *30 June 2022*

Citation:
Ayaz M, Ali T, Sadiq A, Ullah F and Naseer MI (2022) Editorial: Current Trends in Medicinal Plant Research and Neurodegenerative Disorders. Front. Pharmacol. 13:922373. doi: 10.3389/fphar.2022.922373

of three main periods, including early development (for the treatment of poliomyelitis), preclinical development (as anti-Alzheimer's drug in 1980s) and clinical development in 1990s (Heinrich and Teoh, 2004). In 1951, the acetylcholine esterase (AChE) inhibiting properties of galanthamine obtained from Galanthus woronowii Losinsk. [Amaryllidaceae] was proved by M. D. Mashkovsky and R. P. Kruglikojva-Lvov using *ex vivo* system of rat smooth muscle (Heinrich, 2010). Another example is the leaves extract of *Ginkgo biloba* L. [Ginkgoaceae], which is not considered to be a medicine in many countries but in other countries it is used to prevent dementia, memory deterioration and to enhances cognitive processes (Heinrich, 2010). Flavonoid glycosides were identified as active constituents in the leaf extracts of *G. biloba* L. in the mid of 1960 during initial research. The first patent on the complete extraction and standardization was filed in 1971 (in Germany) and 1972 (in France) (DeFeudis and Drieu, 2000). This example highlights the development of a standardized extract on the basis of traditional knowledge into an over-the-counter herbal medicine. In later years, many similar novel phytomedicines were development including *Hypericum perforatum* L. [Hypericaceae] (used for mild to moderate depression), Harpagophytumprocumbens (Burch.) DC. ex Meisn. [Pedaliaceae] (used for chronic pain), and Piper methysticum G. Forst. [Piperaceae] (used for relieving anxiety) (Collocott, 1927). Drug development for neurological disorders on the basis of ethnopharmacology persists to an exciting opportunity. According to the information available in the libraries of Swiss university, more than 150 plant species in different preparations have the potential for research and development (R&D) to develop new drugs against cognitive disorders (Adams et al., 2007).

Alzheimer's disease (AD) is a multifactorial and progressive neurodegenerative disease. AD is the major cause of dementia and clinically characterized by loss of cognition and memory functions. Currently, there are more than 50 million AD patients affected across the globe and this number is anticipated to double every 5 years and will increase to higher than 150 million by 2050. Besides the health problem for patients and their families, AD also represents a socioeconomic burden, with estimated global costs of US$1 trillion annually, which will be doubled by 2030 (Khalil et al., 2018; Saleem et al., 2021). Neuropathologically, AD is characterized by accumulation of plaques composed of aggregated amyloid-β (Aβ) and intraneuronal neurofibrillary tangles (NFTs) of hyperphosphorylated tau proteins. In early onset familial AD, Aβ generates from the proteolytic cleavage of amyloid precursor protein (APP), by the proteolytic and enzymatic action of β- and γ-secretases, a mechanism called amyloidogenic pathway. The Aβ aggregation and deficits in Aβ clearance led to the most neurotoxic AβO species. The hyperphosphorylation of tau proteins are also associated with amyloidogenic pathway. The hyperphosphorylated tau proteins aggregate intraneuronal and forming NFTs. According to amyloidogenic pathway the elevation of AβO induces hyperphosphorylation of tau proteins, resulting intraneuronal NFTs, resulting to synaptic and neuronal degeneration and subsequently cell death (Kunkle et al., 2019; Mahnashi et al., 2021). However, more than 95% of AD cases are sporadic with late onset and very heterogeneous neuropathology. Currently, there is no cure for AD. Hence, a better understanding of the contributing factors leading to neuropathology is essential to explore the underlying causes and mediating factors to cure AD.

The purpose of this editorial is to shed light on the recent development of compounds that could prevent or treat AD. The exact underlying cause of pathological changes in AD is still unknown. However, the therapeutic strategies were applied by targeting several pathological mechanisms including protein misfolding such as aggregation of Aβ and tau proteins, pro-inflammatory mediators (IL-1β, TNF-α, TLRs, NF-kβ) and neuroinflammation, oxidative damage and accumulated reactive oxygen species (ROS) as well as its associated pathways such as heme oxygenase-1 and nuclear factor-erythroid factor 2-related factor 2 (HO-1/Nrf2), aberrant cellular and energy homeostasis signaling (e.g., AMPK, SIRT1, mTOR etc) and signalling related with elevated phosphases and kinases, including MAPK/ERK, JNK, PI3K/Akt/GSK3β, as well as synaptic trafficking and its associated pathologies (Majd and Power, 2018; Yu et al., 2021).

Aging is a process that is the reason of many diseases such as cancer, heart diseases, diabetes, and many neurological disorders such as Huntington's disease (HD), Alzheimer's disease (AD), and Parkinson's disease (PD) (Tong et al., 2020). It has been reported in many studies that increased level of Reactive oxygen species (ROS) is reason of many neurodegenerative disease in different age-linked disorders such as diabetes, AD, and PD (Ovais et al., 2018; Saleem et al., 2021; Mahnashi et al., 2022). The increased ROS activate the destruction of the macromolecules such as lipids, proteins and DNA that is directly involved in the neurodegeneration through the disturbance of physiological activities of the brain (Ayaz et al., 2019a). The Research Topic, fifteen papers related to different aspects of neuroprotective drugs from natural sources were published. In the first study, Ahmad et al. reported that D-galactose (D-gal) effects neurological damage by inducing ROS signaling pathway while, Fisetin (natural flavonoid) play a protective potentials role against D-galactose-induced stress, neuroinflammation, and memory loss through adaptable anti-oxidant mechanisms, such as Sirt1/Nrf2 signaling, suppression of activated p-JNK/NF-kB signaling pathway and further downstream targets leading to inflammatory cytokines. Similarly, in another study showed neuroprotective effect of medicinal herb known as Bacopa monnieri (L.) Wettst. [Plantaginaceae], that is used as a brain tonic showed its neuroprotective effect PD when the compound extracted from Wettst extract (BME) in 1-methyl-4-phenyl-1,2,3,6-tetrahydropyridine (MPTP)-induced mice model. Further, more the BME exerts is effective and showed it neurorescue and neuroprotective and effects against MPTP-induced neurodegeneration of the nigrostriatal dopaminergic neurons. Further, it was also studied that BME help in slow down the disease progression and delay the process of neuronal damage in PD (Singh et al.). Bacopa monnieri(L.) Wettst. [Plantaginaceae] (BM) extract and the compounds isolated from it mainly used in many disease animal models. Previous studies revealed that Bacoside A may decrease the level of oxidative stress in the

CNS by increasing the activities of superoxide dismutase (SOD), glutathione peroxidase (GPx), glutathione reductase (GSR) and catalase level in brain (Comens, 1983). Furthermore, BM extract was also studies in a *Caenorhabditis elegans* model of 6-hydroxydopamine (6-OHDA)-induced Parkinson's disease (PD), and results showed that it may decrease the aggregation of α-synuclein by increasing the expression level of hsp-70 protein (Chowdhuri et al., 2002; Jadiya et al., 2011). Yet in another study, Pushparaj et al., evaluated an innovative tool (Next generation Knowledge discovery NGKD) to evaluate the AD-associated gene expression implicated in abnormal signaling pathways.

Rasool et al. have studied the role of antioxidants in Schizophrenic patients. The study was carried out on 288 Schizophrenic patients of both sexes and various ages. The study reveals that there is an alteration of liver function, increase of stress marker and decrease in the level of antioxidant in the patients. It was also concluded in the study that in patients with thyroid disorder, the deficiencies of certain vitamin (B6, B9 and B12) can lead to hyperhomocysteinemia which ultimately results in the decline of antioxidants and cause oxidative disorders. Panax ginsengC.A.Mey. [Araliaceae] is a perennial plant which has wide variety of useful applications. The major components of ginseng are ginsenosides and gintonin. Li et al. has compiled a literature review on the anti-Alzheimer effect of ginseng. Their literature conclusion reveals that ginseng has therapeutic effect in neurological disorders like Alzheimer. It was further summarized that it exerts the neuroprotective effect by targeting neuro-inflammation, amyloid plaques, mitochondria and function as an antioxidant. Though there is no clinically effective drug for the management of AD. However, the summary related to the clinical findings of ginseng in the management of AD have also been compiled.

Modern society is highly advanced and has many stressful stimuli in life and these event leads to depression (Post, 1992). Mood disorders due to the stressful life are become a serious problem for health that need serious attention (Gooren and Giltay, 2014). Recently, studies in male animals model with chronic stress showed nonorganic erectile dysfunction, testicular injury, less sexual motivation was reported (Chen et al., 2019). In china, for the control of emotion and to decrease sexual dysfunction a drug name as Bupleurum falcatum L. [Apiaceae] had been widely used. Its main active component is saikosaponin D (SSD) act as antidepressant. One of the study in this Research Topic investigated that SSD exposure help to restore sexual functions after chronically stressed mice and the brain mechanisms involved in these effects (Wang et al.). Salidroside (SLDS), a phenolic glycoside compound extracted from Rhodiola rosea L. [Crassulaceae] an old medicinal plant from China has been extensively used for the treatment of multiple inflammatory diseases. Yet in another study, SLDS was showed to exhibit protective against depressive behaviors via microglia activation (Fan et al.). The study revealed that SLDS exposure significantly declined microglial immuno-reactivity for both CD68 and Iba-1. Moreover, SLDS reserved microglial activation connecting the suppression of P38 MAPK, ERK1/2, and p65 NF-κB activation and thus decreased the expression level and release of neuroinflammatory cytokines in stress mice as well as in lipopolysaccharide (LPS)-induced primary microglia (Fan et al.). Further, it was also observed that SLDS changed morphology of microglial cells by reducing the phagocytic and the decreasing the ability of attachment in LPS-induced primary microglia. The results of the study showed that SLDS exposure may improve the depressive symptoms caused by chronic stress due to the unpredictable conditions and also having the potential therapeutic application of SLDS for the treatment of depression by controlling the microglia related neuroinflammation (Fan et al.). The Catha edulis (Vahl) Endl. [Celastraceae] (Khat) is most commonly known as a stimulant. The major constituents of Khat are cathinone and cathine. Abou-Elhamd et al. have evaluated the role of Khat extract in molecular signaling using SKOV3 cells. Their observations were that the extract have significant effect on molecular level using SKOV3 cells, and thus, can cause wide variety of neurological disorders. So, in countries where Khat leaves are chewed to induce excitement and euphorbia will have severe effects on the health. Lai et al. studied effect of carnosic acid on the levodopa (L-dopa)-induced dyskinesia (LID) in rats treated with 6-hydroxydopamine (6-OHDA). They proved that by regulating the D1R signaling, CA improves the development of LID in 6-OHDA-treated rats. This leads to prevention of L-dopa-induced apoptotic cell death through modulating the ERK1/2-c-Jun and inducing the parkin. This indicates beneficial role of CA in delaying development of LID in PD patients.

Wide variety of medicinal plants with its ethnomedicinal background are a big source of drug discovery. The *Centella asiatica* (L.) Urb. [Apiaceae] have been explored to have neuroprotective and anti-inflammatory properties. The plant exert its effect by protecting the mitochondria and have antioxidant properties (Wong et al.). Lee et al. tested herbal extract from *Glycyrrhiza* uralensis Fisch. ex DC. [Fabaceae], Atractylodes macrocephala Koidz. [Asteraceae], Panax ginseng C.A.Mey. [Araliaceae], *Astragalus* mongholicus Bunge [Fabaceae] to study the anti-inflammatory in the Muscle and Spinal Cord of an Amyotrophic Lateral Sclerosis Animal Model. They performed behavioral tests, including rotarod test and foot printing, immunohistochemistry, and Western blotting, in $hSOD1^{G93A}$ mice. Their experiments resulted in improved motor activity and reduced motor neuron loss in $hSOD1^{G93A}$ mice. They also found that the herbal extract reduced levels of oxidative stress-related proteins (HO1, NQO1, Bax, and ferritin) and inflammatory proteins ((GFAP, CD11b, and TNF-α)) in the skeletal muscles and spinal cord of $hSOD1^{G93A}$ mice.

Cerebral amyloid angiopathy (CAA) is considered by the accretion of β-amyloid (Aβ) in the walls of cerebral vessels, further causing the complications such as convexity subarachnoid hemorrhage, intracerebral hemorrhage as well as cerebral microinfarcts (Love et al., 2014). Dementia and strokes may develop in the patients with CAA-related intracerebral hemorrhage. Many experimental studies explained and demonstrated the pathology of more than 90% of AD patients have associated with CAA and leading to common pathogenic mechanisms. Possible causes of CAA include impaired Aβ removal from the brain through the system called as

intramural periarterial drainage (IPAD) (Saito et al., 2019). Moreover, CAA causes control of IPAD causing the limiting clearance. Early interference in CAA may help in the prevention of AD. In another paper published in this Research Topic, Saito et al., summarized that Taxifolin (dihydroquercetin) is a plant flavonoid is a safe and effective therapy for CAA. Taxifolin is a flavonoid extracted from plant is widely existing in the supplement product, which has been used to exhibit against anti-inflammatory effects, anti-oxidative effect and used as protective agents against the advanced glycation end products as well as mitochondrial damage. Further the flavonoid also showed that it help to facilitate disassembly and prevent oligomer formation and increase clearance of Aβ in CAA of mouse model. Taxifolin treatment also prevent the spatial reference memory impairment and cerebrovascular reactivity in CAA animal model. Further studied required to prove and explain the exact mechanism of Taxifolin that will help to use this drug with effectiveness and safe for the patients with CAA Saito et al. Corona virus disease (COVID-19) is a pandemic of the current era. The COVID-19 has the symptoms from simple common cold to more complex and even leading to the neuro-COVID complications. Pushparaj et al. has worked on the gene sequencing targeting the neuro-COVID. They were able to embark RNA sequencing and find out that some small organic molecules from natural or synthetic source can be useful in the treatment of neurological disorders related to COVID-19. Neuroprotective and anti-inflammatory effect of Pterostilbene was tested against Cerebral Ischemia/Reperfusion injury via suppression of COX-2 in middle cerebral artery occlusion (MCAO) rodent model by Yan et al. Treatment of Pterostilbene significantly reduced neurological score, infarct volume and brain edema. Hepatic parameters (ALT, AST and ALP), renal parameters (uric acid, creatinine, BUN and urea), lipid parameters (TG, HDL, LDL, TC and VLDL), antioxidant parameters (SOD, CAT, GSH, GPx, MDA), inflammatory cytokines (TNF-α, IL-1β, IL-6, and IL-10), inflammatory mediators (COX-2, PGE_2, iNOS) AND metalloproteinases (MMP) (MMP-2, and MMP-9) levels were improved. Results of these studies show that Pterostilbene is effective in the treatment of cerebral ischemic stroke and cerebral ischemia reperfusion.

Cerebral hypoperfusion (CH) causes neurological diseases like Alzheimer's-type dementia and vascular cognitive impairment and dementia. To find plant-based treatment for this problem, Liu et al. carried out experiments to unearth potential of Cucurbitacin E (steroidal tetracyclic terpene) in a rat model of CH. Treatment of the rats with Cucurbitacin E (CuE) for 28 days resulted in reduced CH-Induced neurological, sensorimotor and memory deficits, low lipid peroxidation (TBARS content) and protein carbonyls, increased GSH and catalase and diminished inflammatory cytokines (TNF-α, NF-κB, MPO, MMP-9, and iNOS). LDH, caspase-3, glutamate and acetylcholinesterase activities were decreased in Cu-E treated rats subjected to CH. Viable neuron density in the cortex was increased after treatment with CuE. These findings suggest that CuE is a potential compound against CH-associated disorders.

AUTHOR CONTRIBUTIONS

All authors listed have made a substantial, direct, and intellectual contribution to the work and approved it for publication.

REFERENCES

Adams, M., Gmünder, F., and Hamburger, M. (2007). Plants Traditionally Used in Age Related Brain Disorders-Aa Survey of Ethnobotanical Literature. *J. Ethnopharmacol.* 113 (3), 363–381. doi:10.1016/j.jep.2007.07.016

Atanasov, A. G., Waltenberger, B., Pferschy-Wenzig, E. M., Linder, T., Wawrosch, C., Uhrin, P., et al. (2015). Discovery and Resupply of Pharmacologically Active Plant-Derived Natural Products: A Review. *Biotechnol. Adv.* 33 (8), 1582–1614. doi:10.1016/j.biotechadv.2015.08.001

Ayaz, M., Ahmad, I., Sadiq, A., Ullah, F., Ovais, M., Khalil, A. T., et al. (2020). Persicaria Hydropiper (L.) Delarbre: A Review on Traditional Uses, Bioactive Chemical Constituents and Pharmacological and Toxicological Activities. *J. Ethnopharmacol.* 251, 112516. doi:10.1016/j.jep.2019.112516

Ayaz, M., Junaid, M., Ullah, F., Subhan, F., Sadiq, A., Ali, G., et al. (2017a). Anti-Alzheimer's Studies on β-Sitosterol Isolated from Polygonum Hydropiper L. *Front. Pharmacol.* 8, 697. doi:10.3389/fphar.2017.00697

Ayaz, M., Sadiq, A., Junaid, M., Ullah, F., Ovais, M., Ullah, I., et al. (2019a). Flavonoids as Prospective Neuroprotectants and Their Therapeutic Propensity in Aging Associated Neurological Disorders. *Front. Aging Neurosci.* 11, 155. doi:10.3389/fnagi.2019.00155

Ayaz, M., Sadiq, A., Junaid, M., Ullah, F., Subhan, F., and Ahmed, J. (2017b). Neuroprotective and Anti-aging Potentials of Essential Oils from Aromatic and Medicinal Plants. *Front. Aging Neurosci.* 9, 168. doi:10.3389/fnagi.2017.00168

Ayaz, M., Ullah, F., Sadiq, A., Kim, M. O., and Ali, T. (2019b). Editorial: Natural Products-Based Drugs: Potential Therapeutics against Alzheimer's Disease and Other Neurological Disorders. *Front. Pharmacol.* 10, 1417. doi:10.3389/fphar.2019.01417

Ayaz, M., Ullah, F., Sadiq, A., Ullah, F., Ovais, M., Ahmed, J., et al. (2019c). Synergistic Interactions of Phytochemicals with Antimicrobial Agents: Potential Strategy to Counteract Drug Resistance. *Chemico-biological Interact.* 308, 294–303. doi:10.1016/j.cbi.2019.05.050

Bruhn, J. G., and Helmstedt, B. (1981). Ethnopharmacology: Objectives, Principles and Perspectives. *Nat. Prod. as Med. agents*, 405–430.

Chen, G., Chen, J., Yang, B., Yu, W., Chen, Y., and Dai, Y. (2019). Dopamine D2 Receptors in the Basolateral Amygdala Modulate Erectile Function in a Rat Model of Nonorganic Erectile Dysfunction. *Andrologia* 51 (1), e13160. doi:10.1111/and.13160

Chowdhuri, D. K., Parmar, D., Kakkar, P., Shukla, R., Seth, P. K., and Srimal, R. C. (2002). Antistress Effects of Bacosides of Bacopa Monnieri: Modulation of Hsp70 Expression, Superoxide Dismutase and Cytochrome P450 Activity in Rat Brain. *Phytother. Res.* 16 (7), 639–645. doi:10.1002/ptr.1023

Collocott, E. E. V. (1927). Kava Ceremonial in Tonga. *J. Polyn. Soc.* 36 (141), 2

Comens, C. (1983). Fixed Drug Eruption. *Australas. J. Dermatol* 24 (1), 1–8. doi:10.1111/j.1440-0960.1983.tb00240.x

DeFeudis, F. V., and Drieu, K. (2000). Ginkgo Biloba Extract (EGb 761) and CNS Functions: Basic Studies and Clinical Applications. *Curr. Drug Targets* 1 (1), 25–58. doi:10.2174/1389450003349380

Efron, D. H., Holmstedt, B., and Kline, N. S. (1967). "Ethnopharmacologic Search for Psychoactive Drugs," in Proceedings of a symposium, San Francisco, CA, January, 1967. National Institute of Mental Health, Editor C. Chase, Md. (Washington, DC: American Association for the Advancement of Science), 468.

Gooren, L. J., and Giltay, E. J. (2014). Men and Women, So Different, So Similar: Observations from Cross-Sex Hormone Treatment of Transsexual Subjects. *Andrologia* 46 (5), 570–575. doi:10.1111/and.12111

Griggs, B. (1981). *Green Pharmacy: A History of Herbal Medicine*. London: Viking Press.

Heinrich, M., and Lee Teoh, H. (2004). Galanthamine from Snowdrop-Tthe Development of a Modern Drug against Alzheimer's Disease from Local Caucasian Knowledge. *J. Ethnopharmacol.* 92 (2-3), 147–162. doi:10.1016/j.jep.2004.02.012

Heinrich, M. (2010). Ethnopharmacology and Drug Discovery." in *Comprehensive Natural Products II*. Oxford: Elsevier, 351–381. doi:10.1016/b978-008045382-8.00666-3

Heinrich, M. (2007). W. Sneader, Drug Discovery: A History, John Wiley and Sons Ltd., Chichester (2005) 468 pp.; Numerous Figures (Mostly Chemical Line Drawings), Foreword by Arthur Hollman, ISBN 13: 978-0-471-89979-2 (HB), Â£ 85/978-0-471-89980-8 (PB), Â£ 34.95. *J. Ethnopharmacol.* 112, 596–597. doi:10.1016/j.jep.2007.04.017

Jadiya, P., Khan, A., Sammi, S. R., Kaur, S., Mir, S. S., and Nazir, A. (2011). Anti-Parkinsonian Effects of Bacopa Monnieri: Insights from Transgenic and Pharmacological *Caenorhabditis elegans* Models of Parkinson's Disease. *Biochem. Biophys. Res. Commun.* 413 (4), 605–610. doi:10.1016/j.bbrc.2011.09.010

Khalil, A. T., Ayaz, M., Ovais, M., Wadood, A., Ali, M., Shinwari, Z. K., et al. (2018). *In Vitro* cholinesterase Enzymes Inhibitory Potential and In Silico Molecular Docking Studies of Biogenic Metal Oxides Nanoparticles. *Inorg. Nano-Metal Chem.* 48 (9), 441–448. doi:10.1080/24701556.2019.1569686

Kunkle, B. W., Grenier-Boley, B., Sims, R., Bis, J. C., Damotte, V., Naj, A. C., et al. (2019). Genetic Meta-Analysis of Diagnosed Alzheimer's Disease Identifies New Risk Loci and Implicates Aβ, Tau, Immunity and Lipid Processing. *Nat. Genet.* 51 (3), 414–430. doi:10.1038/s41588-019-0358-2

Love, S., Chalmers, K., Ince, P., Esiri, M., Attems, J., Jellinger, K., et al. (2014). Development, Appraisal, Validation and Implementation of a Consensus Protocol for the Assessment of Cerebral Amyloid Angiopathy in Post-Mortem Brain Tissue. *Am. J. Neurodegener. Dis.* 3 (1), 19–32.

Mahnashi, M. H., Alqahtani, Y. S., Alyami, B. A., Alqarni, A. O., Alqahl, S. A., Ullah, F., et al. (2022). HPLC-DAD Phenolics Analysis, α-glucosidase, α-amylase Inhibitory, Molecular Docking and Nutritional Profiles of Persicaria Hydropiper L. *BMC Complement. Med. Ther.* 22 (1), 26–20. doi:10.1186/s12906-022-03510-7

Mahnashi, M. H., Alyami, B. A., Alqahtani, Y. S., Alqarni, A. O., Jan, M. S., Ayaz, M., et al. (2021). Neuroprotective Potentials of Selected Natural Edible Oils Using Enzyme Inhibitory, Kinetic and Simulation Approaches. *BMC complementary Med. Ther.* 21 (1), 1–14. doi:10.1186/s12906-021-03420-0

Majd, S., and Power, J. H. T. (2018). Oxidative Stress and Decreased Mitochondrial Superoxide Dismutase 2 and Peroxiredoxins 1 and 4 Based Mechanism of Concurrent Activation of AMPK and mTOR in Alzheimer's Disease. *Curr. Alzheimer Res.* 15 (8), 764–776. doi:10.2174/1567205015666180223093020

Ovais, M., Zia, N., Ahmad, I., Khalil, A. T., Raza, A., Ayaz, M., et al. (2018). Phyto-Therapeutic and Nanomedicinal Approaches to Cure Alzheimer's Disease: Present Status and Future Opportunities. *Front. Aging Neurosci.* 10, 284. doi:10.3389/fnagi.2018.00284

Ovais, M., Hoque, M. Z., Khalil, A. T., Ayaz, M., Ahmad, I., et al. (2021). "Mechanisms Underlying the Anticancer Applications of Biosynthesized Nanoparticles," in *Biogenic Nanoparticles for Cancer Theranostics* (Cambridge, MA: Elsevier), 229–248.

Post, R. M. (1992). Transduction of Psychosocial Stress into the Neurobiology of Recurrent Affective Disorder. *Am. J. psychiatry* 149 (8), 999–1010. doi:10.1176/ajp.149.8.999

Saito, S., Yamamoto, Y., and Ihara, M. (2019). Development of a Multicomponent Intervention to Prevent Alzheimer's Disease. *Front. Neurol.* 10, 490. doi:10.3389/fneur.2019.00490

Saleem, U., Akhtar, R., Anwar, F., Shah, M. A., Chaudary, Z., Ayaz, M., et al. (2021). Neuroprotective Potential of Malva Neglecta Is Mediated via Down-Regulation of Cholinesterase and Modulation of Oxidative Stress Markers. *Metab. Brain Dis.* 36 (5), 889–900. doi:10.1007/s11011-021-00683-x

Sneader, W. (2005). *Drug Discovery: A History*. New Jersey: John Wiley & Sons.

Tong, X., Li, X., Ayaz, M., Ullah, F., Sadiq, A., Ovais, M., et al. (2020). Neuroprotective Studies on Polygonum Hydropiper L. Essential Oils Using Transgenic Animal Models. *Front. Pharmacol.* 11, 580069. doi:10.3389/fphar.2020.580069

Yu, M., Zhang, H., Wang, B., Zhang, Y., Zheng, X., Shao, B., et al. (2021). Key Signaling Pathways in Aging and Potential Interventions for Healthy Aging. *Cells* 10 (3), 660. doi:10.3390/cells10030660

Conflict of Interest: The authors declare that the research was conducted in the absence of any commercial or financial relationships that could be construed as a potential conflict of interest.

Publisher's Note: All claims expressed in this article are solely those of the authors and do not necessarily represent those of their affiliated organizations, or those of the publisher, the editors and the reviewers. Any product that may be evaluated in this article, or claim that may be made by its manufacturer, is not guaranteed or endorsed by the publisher.

frontiers in Pharmacology

MINI REVIEW
published: 12 February 2021
doi: 10.3389/fphar.2021.643357

Taxifolin: A Potential Therapeutic Agent for Cerebral Amyloid Angiopathy

Satoshi Saito[1,2]*, *Masashi Tanaka*[3,4], *Noriko Satoh-Asahara*[4], *Roxana Octavia Carare*[1] and *Masafumi Ihara*[2]

[1]Faculty of Medicine, University of Southampton, Southampton, United Kingdom, [2]Department of Neurology, National Cerebral and Cardiovascular Center, Suita, Japan, [3]Department of Physical Therapy, Health Science University, Fujikawaguchiko, Japan, [4]Department of Endocrinology, Metabolism, and Hypertension Research, Clinical Research Institute, National Hospital Organization Kyoto Medical Center, Kyoto, Japan

Cerebral amyloid angiopathy (CAA) is characterized by the accumulation of β-amyloid (Aβ) in the walls of cerebral vessels, leading to complications such as intracerebral hemorrhage, convexity subarachnoid hemorrhage and cerebral microinfarcts. Patients with CAA-related intracerebral hemorrhage are more likely to develop dementia and strokes. Several pathological investigations have demonstrated that more than 90% of Alzheimer's disease patients have concomitant CAA, suggesting common pathogenic mechanisms. Potential causes of CAA include impaired Aβ clearance from the brain through the intramural periarterial drainage (IPAD) system. Conversely, CAA causes restriction of IPAD, limiting clearance. Early intervention in CAA could thus prevent Alzheimer's disease progression. Growing evidence has suggested Taxifolin (dihydroquercetin) could be used as an effective therapy for CAA. Taxifolin is a plant flavonoid, widely available as a health supplement product, which has been demonstrated to exhibit anti-oxidative and anti-inflammatory effects, and provide protection against advanced glycation end products and mitochondrial damage. It has also been shown to facilitate disassembly, prevent oligomer formation and increase clearance of Aβ in a mouse model of CAA. Disturbed cerebrovascular reactivity and spatial reference memory impairment in CAA are completely prevented by Taxifolin treatment. These results highlight the need for clinical trials on the efficacy and safety of Taxifolin in patients with CAA

Keywords: IPAD, clinical trial, treatment, Alzheimer's disease, cerebral amyloid angiopathy, Taxifolin

OPEN ACCESS

Edited by:
Tahir Ali,
University of Calgary, Canada

Reviewed by:
Gwangho Yoon,
Chonnam National University Medical School, South Korea
Amjad Khan,
Gyeongsang National University, South Korea
Haroon Badshah,
Abdul Wali Khan University Mardan, Pakistan

***Correspondence:**
Satoshi Saito
saitou.satoshi.43m@kyoto-u.jp

Specialty section:
This article was submitted to Neuropharmacology, a section of the journal Frontiers in Pharmacology

Received: *18 December 2020*
Accepted: *15 January 2021*
Published: *12 February 2021*

Citation:
Saito S, Tanaka M, Satoh-Asahara N, Carare RO and Ihara M (2021) Taxifolin: A Potential Therapeutic Agent for Cerebral Amyloid Angiopathy. Front. Pharmacol. 12:643357. doi: 10.3389/fphar.2021.643357

INTRODUCTION

Cerebral amyloid angiopathy (CAA) refers to the abnormal accumulation of amyloid proteins in the walls of cerebral vasculature (Love et al., 2014; Saito et al., 2020b). Seven amyloid proteins have so far been reported in CAA including β-amyloid (Aβ), cystatin C, transthyretin, gelsolin, prion protein, ABri/ADan and immunoglobulin light chain amyloid (Yamada, 2015). The most common form is Aβ-type CAA, which is present in over 90% cases of sporadic, non-familial age-related Alzheimer's disease (AD) (Saito and Ihara, 2016). The shared role of Aβ deposition in AD and CAA implies interaction between neurodegenerative and cerebrovascular processes (Saito et al., 2015). In this review, we discuss the pathophysiological basis of such interactions and how Taxifolin could act as a potential therapeutic agent for CAA.

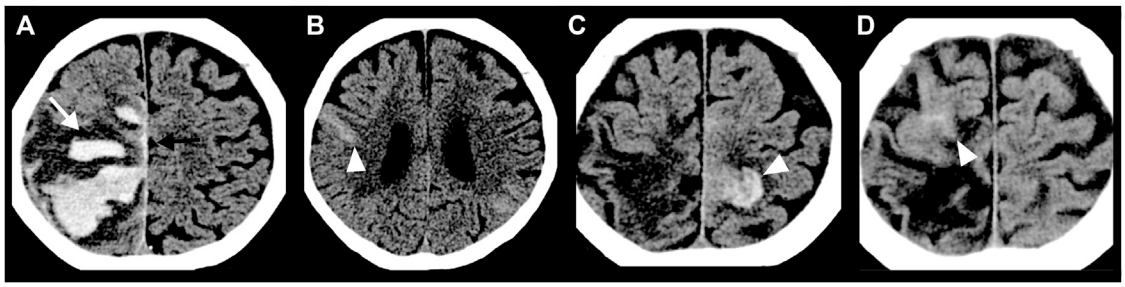

FIGURE 1 | Head CT images of an 84-year-old woman with CAA showing repeated non-traumatic intracranial hemorrhage over four months. **(A)** ICH presenting finger-like projections (white arrow) with SAH extension (black arrow). **(B)** Acute convexity SAH (arrowhead) at two months later than **A**. **(C)** Acute convexity SAH (arrowhead) at three months later than **A**. **(D)** Acute convexity SAH (arrowhead) at four months later than **A**.

CAA INDUCING CEREBROVASCULAR DISEASE

CAA induces smooth muscle cell degeneration, vessel wall thickening, luminal narrowing and concentric wall splitting, resulting in varying degrees of intracerebral hemorrhage (ICH) (Love et al., 2014). Lobar, but not deep, ICH is associated with CAA (Saito et al., 2020a). Finger-like projections and subarachnoid hemorrhage extension of lobar ICH, together with the ApoE4 genotype, are reliable diagnostic markers for CAA (Rodrigues et al., 2018; Renard et al., 2019) (**Figure 1A**). Cerebral microbleeds (CMBs) are commonly observed in patients with CAA. Strictly lobar CMBs are highly specific for CAA, while CMBs in deep brain may indicate hypertensive arteriopathy (Greenberg and Charidimou, 2018; Jung et al., 2020). The estimated annual incidence of CAA-related ICH is 5.3 per 100,000 people in the United Kingdom and 5.8 per 100,000 people in Japan; however, the incidence of ICH not resulting from CAA, and mainly associated with hypertensive arteriopathy, is 2.5-fold higher in Japan than the United Kingdom (Yakushiji et al., 2020). Early diagnosis of CAA is clinically important for guiding prognosis and treatment decisions. A recent prospective study, with a median follow-up time of 2.5 years, showed progression to dementia in more than 25% of patients with CAA-related ICH, even if no dementia had presented after the acute phase of ICH (Xiong et al., 2019). ICH recurrence was more frequent in patients with CAA than other potential causes (Pasi et al., 2018).

CAA is likely clinically underdiagnosed, due to the various clinical presentations outside of lobar ICH (Sakai et al., 2019; Fakan et al., 2020). Subarachnoid hemorrhage (SAH), resulting from bleeding into the subarachnoid space, known as "convexity SAH" in the acute phase (**Figures 1B–D**) and "superficial siderosis" in the chronic phase, can be induced by CAA (Saito et al., 2020a). Most CAA-induced bleeding into the subarachnoid space is limited without the involvement of the adjoining brain parenchyma (Kumar et al., 2010). Many convexity SAH are asymptomatic, though the risk of future intracranial hemorrhage and death of patients with CAA-convexity SAH is very high (Calviere et al., 2019; Saito et al., 2020a).

CAA also induces ischemic strokes consisting of both macro and microinfarcts (Saito et al., 2015; Saito and Ihara, 2016). Cerebral microinfarcts were originally defined as infarcts only visible by microscopy (Okamoto et al., 2012). However, technological advances in imaging modalities, such as ultra-high-field MRI, have enabled cerebral microinfarct observation (Ishikawa et al., 2020; Ter Telgte et al., 2020). AD and CAA patients frequently possess cortical cerebral microinfarcts near Aβ-laden vessels (Okamoto et al., 2009; Okamoto et al., 2012). Cerebral microinfarcts were replicated in CAA model mice following chronic cerebral hypoperfusion by bilateral common carotid artery stenosis (Okamoto et al., 2012). Impaired vasodilation due to vascular Aβ accumulation may contribute to cerebral microinfarct pathogenesis. AD and CAA patients have numerous, sometimes exceeding 1,000 (Westover et al., 2013), cerebral microinfarcts (van Rooden et al., 2014), which are likely to contribute to cognitive impairment (Saito et al., 2015).

CAA AS A CONTRIBUTOR TO NEURODEGENERATIVE DISORDER

CAA plays a pivotal role in the pathogenesis of dementia and is independently associated with cognitive decline (Boyle et al., 2015; Banerjee et al., 2018). Since there is little evidence for overproduction, the failure of clearance of Aβ peptides is a likely key factor in the pathological development of AD and CAA (Mawuenyega et al., 2010; Iturria-Medina et al., 2014). There is therefore increasing interest in developing agents that promote the safe elimination of Aβ from the brains of aged people (Saito and Ihara, 2014). The necessity of promoting Aβ clearance has been demonstrated in clinical trials using Aβ immunization. In AN-1792-vaccinated AD patients, the number and extent of parenchymal Aβ plaques diminished, while cerebrovascular Aβ accumulation and CAA increased (Nicoll et al., 2003; Patton et al., 2006). This finding was also observed in patients treated with solanezumab, a monoclonal anti-Aβ antibody (Roher et al., 2016). Antibody-solubilized Aβ appears to be removed from the cortex and re-deposited in the walls of the cerebral blood vessels via intramural periarterial clearance pathways (Carare et al., 2020).

Intramural periarterial drainage (IPAD), is a mechanism for the drainage of fluid and solutes from the brain along the walls of cerebral arteries (Tarasoff-Conway et al., 2015; Saito et al., 2019) (**Figure 2**). The central nervous system is devoid of lymph vessels.

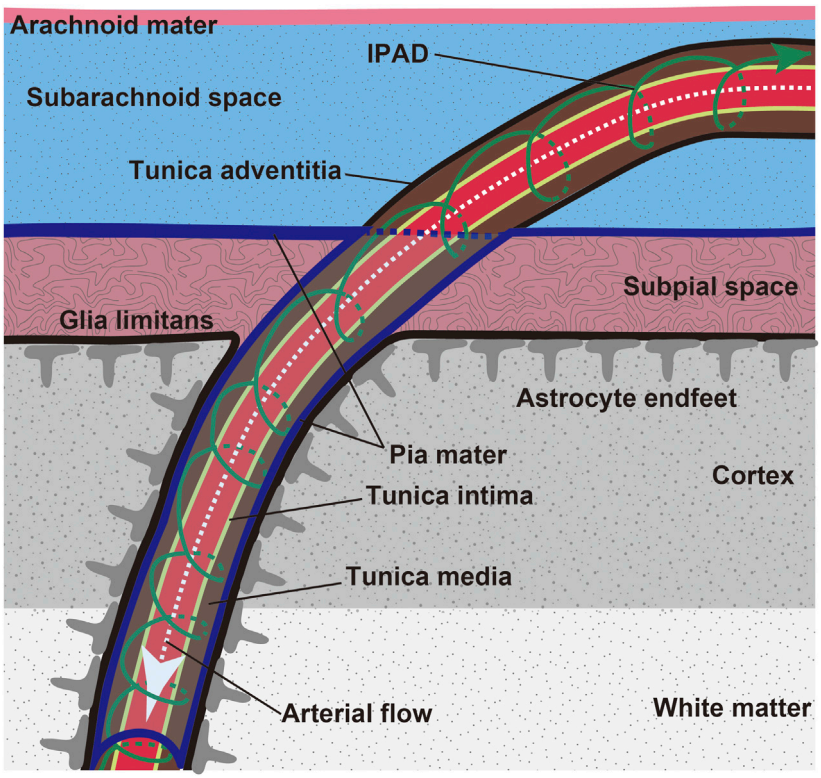

FIGURE 2 | Scheme of leptomeninges and penetration of leptomeningeal artery into the brain parenchyma. Brain waste is cleared through the IPAD route (green arrow). Aβ is preferentially deposited in the tunica media of the leptomeningeal and cortical arteries in CAA.

Instead, interstitial fluid and solutes within the extracellular matrix, including soluble Aβ, enter the IPAD pathways within the basement membranes of capillaries and continue to the basement membranes surrounding smooth muscle cells (SMCs) of the intracerebral and leptomeningeal arteries (Carare et al., 2020), which lead to the cervical lymph nodes (Piotrowska et al., 2020). This process has been examined in detail by several imaging methods including electron (Morris et al., 2016), confocal (Carare et al., 2008; MacGregor Sharp et al., 2020) and two-photon (Arbel-Ornath et al., 2013; Kim et al., 2020), microscopy. IPAD flow rapidly moves toward the leptomeningeal arteries where the deposition of Aβ is prominent in CAA (Keable et al., 2016). Aβ levels in the cerebrospinal fluid are decreased in CAA (Verbeek et al., 2009; van Etten et al., 2017), suggesting that Aβ transport is impeded in the IPAD pathways.

Transcytosis is another vascular-mediated Aβ clearance system closely associated with AD and CAA. The brain parenchyma is separated from capillary lumen by the blood brain barrier (BBB), which prevents passive exchange between the brain and blood, allowing controlled carrier-mediated bidirectional transport of nutrients and waste products (Sweeney et al., 2018; Sweeney et al., 2019). Several molecules, such as low-density lipoprotein receptor related protein-1 (LRP-1), are thought to be involved in Aβ efflux from brain to blood (Shibata et al., 2000; Deane et al., 2004). Aβ binds to LRP-1 at the abluminal side of the vascular endothelium, either as a free peptide or bound to ApoE2 and ApoE3. Aβ-ApoE2 and Aβ-ApoE3 complexes are rapidly cleared across the BBB into the blood, while Aβ bound to ApoE4 interacts poorly with LRP-1 and is less efficiently removed from brain (Deane et al., 2008). Aβ deposition is frequently found in the cerebral capillaries in subjects possessing the ApoE4 allele (Thal et al., 2008).

CAA is not merely a consequence of impaired IPAD or transcytosis but also an important contributor to these processes (Kim et al., 2020; Rosas-Hernandez et al., 2020). CAA damages arterial structure and function, leading to worsening of cerebrovascular function and cognition. Therefore, early intervention strategies against CAA could be key to preventing progression of AD.

Challenges in Developing Novel Therapies for CAA

Development of novel treatments for CAA has proved challenging, with no pharmaceutical agents currently available (Smith and Markus, 2020). While more than 100 trials are in progress for AD (Cummings et al., 2020), to our knowledge, there are no ongoing clinical trials for agents targeting CAA (The U.S. National Institutes of Health, 2020), though a clinical trial of minocycline, a tetracycline derivative with anti-inflammatory properties is being planned in the Netherlands. Previous clinical trials on agents targeting CAA have reported mixed

findings. Tramiprosate (3-amino-1-propanesulfonic acid), a low-molecular-weight ionic compound with preferential binding to soluble form of Aβ, has been shown to effectively block the deposition and facilitate the clearance of Aβ from the brains of transgenic mice expressing a double mutant (K670N/M671L and V717F) human *APP* gene (Gervais et al., 2007) but does not bind to insoluble fibrillar Aβ (Gervais et al., 2007). However, a phase-II trial of tramiprosate demonstrated no beneficial effects on CMBs despite causing no major safety issues (Greenberg et al., 2006; Gauthier et al., 2009; Aisen et al., 2011; Smith and Markus, 2020). In another trial, the anti-Aβ-monoclonal antibody, ponezumab was investigated in patients with CAA (Leurent et al., 2019). Ponezumab was well tolerated and plasma levels of $A\beta_{40}$ were increased in the ponezumab-treated group, suggesting effective removal from the brain. However, ponezumab did not improve visual task-related functional MRI activation, a marker for cerebrovascular reactivity (Leurent et al., 2019).

Taxifolin for CAA

Taxifolin is emerging as a viable safe therapeutic agent for the prevention and treatment of CAA. Taxifolin, also known as dihydroquercetin, is a bioactive flavanonol commonly found in grapes, citrus fruits, onions, green tea, olive oil, wine and several herbs such as milk thistle, French maritime bark, Douglas fir bark, and Smilacis Glabrae Rhizoma (Yang et al., 2016). Taxifolin is also widely used as a food additive and can be found in health supplement products including silymarin (Yang et al., 2016). Taxifolin has received increasing attention as a potential treatment for various diseases such as cancer, cardiovascular diseases, viral hepatitis, dyslipidemia and neurodegenerative disorders (Weidmann, 2012). It exhibits various pharmacological effects (Sunil and Xu, 2019), including anti-oxidant (Guo et al., 2015), advanced glycation end product suppressing (Harris et al., 2011), and mitochondrial protecting (Haraguchi et al., 1996) properties. Inhibition of Aβ fibril formation by Taxifolin has been demonstrated by using transmission electron microscopy imaging (Sato et al., 2013a; Sato et al., 2013b; Saito et al., 2017). Thioflavin T fluorescence assays have also shown that aggregated Aβ fibrils can be disaggregated by Taxifolin (Sato et al., 2013a), seemingly due to its chemical structure properties. Taxifolin is oxidized to form *o*-quinone on its B-ring. Since Lys16 and Lys28 are involved in the formation of β-sheets of Aβ, oxidized Taxifolin prevents the aggregation of Aβ as it covalently binds to Aβ at Lys16 and Lys28 residues (Sato et al., 2013b; Tanaka et al., 2019).

Aβ disassembly by Taxifolin treatment was confirmed *in vivo*. We administered Taxifolin or vehicle to a mouse model of CAA expressing the human *APP* gene with Swedish/Dutch/Iowa triple mutations (Saito et al., 2017). Filter trap assays showed a significant decrease in the concentration of Aβ oligomer in the soluble fraction of brain of Taxifolin-treated mice (Saito et al., 2017). However, the amount of total Aβ in the soluble fraction was similar between the Taxifolin-treated and vehicle-treated CAA mice, suggesting Taxifolin prevented the formation of Aβ oligomers from monomers (Saito et al., 2017). Furthermore, Taxifolin treatment prevented spatial memory deficits induced by injection of oligomeric Aβ into the hippocampus of wild-type mice (Wang et al., 2018). Decreased levels of Aβ oligomers by Taxifolin treatment were seen even in advanced stages of CAA (Saito et al., 2017). Higher blood Aβ levels were found in Taxifolin-treated CAA mice, suggesting facilitation of Aβ clearance from brain to blood. Taxifolin also fully restored both cerebrovascular reactivity and spatial reference memory in CAA mice (Saito et al., 2017). Higher expression of triggering receptor expressed on myeloid cell 2 (TREM2) is associated with the inflammation in the brain (Tanaka et al., 2020). We reported that Taxifolin suppressed inflammation, alleviating the accumulation of TREM2-expressing cells in the brains of CAA model mice (Inoue et al., 2019). Furthermore, Taxifolin suppressed glutamate levels and oxidative tissue damage, resulting in the amelioration of apoptotic cell death. In short, Taxifolin exhibits pleiotropic neuroprotective effects against CAA (Inoue et al., 2019).

FUTURE PERSPECTIVE

In light of the promising preclinical data outlined in this review, we are currently preparing a clinical trial of Taxifolin in CAA patients. Nevertheless, several caveats on the use of this exciting potential treatment option should be addressed. Firstly, preclinical studies have not demonstrated that Taxifolin mitigates or prevents ICH, suggesting this may represent an inappropriate efficacy outcome in a clinical trial. Considering that Taxifolin restores cerebrovascular reactivity in mice (Saito et al., 2017), improvement of the cerebrovascular reserve capacity may be a more suitable in evaluating efficacy in CAA patients; indeed, impaired vascular reactivity is an early manifestation of CAA (van Opstal et al., 2017). However, the use of a surrogate, instead of a clinical, endpoint as a primary outcome of the efficacy of a drug in a clinical trial of a common disease such as CAA remains controversial (Broich et al., 2011). Secondly, the optimal dose and usage of Taxifolin in humans should be assessed. We reported the inhibition of Aβ oligomer formation in mice using a high dose of Taxifolin (Saito et al., 2017). In our experiments, 3% Taxifolin was administered orally to mice weighing approximately 30 g and consuming 3–5 g chow a day. It is still unknown whether smaller doses of Taxifolin initiate Aβ disassembly *in vivo*. Daily doses of 100 mg per day of Taxifolin are frequently administered as a health supplement product. However, whether high doses of Taxifolin are safe and tolerated in humans has yet been established and the elimination half-life period of Taxifolin is short at less than 1 h (Saito et al., 2017). Thirdly, as many as 191 metabolites of Taxifolin were reported in rats (Yang et al., 2016). Given that some of the metabolites could exhibit anti-CAA effects as well as Taxifolin, individual differences in the metabolism of Taxifolin may affect the response on Aβ disassembly in each patient, meaning the safety of such derivatives should be also evaluated. Finally, the identification of predictive indicators of favorable response of Taxifolin on CAA should be prioritized. Heterogeneity and multimorbidity are common in the elderly (Barnett et al.,

2012), meaning the pharmacokinetic and pharmacodynamic effects of Taxifolin may vary in different individuals. However, the grouping of the patients based on the results of predictive indicators may facilitate more targeted, stratified or precision medicine treatments (Hampel et al., 2018).

CONCLUSION

Although numerous agents derived from natural plants now play pivotal roles in the prevention and treatment of various diseases, the importance of medicinal plant research may be underestimated in the field of AD and CAA. The beneficial effects demonstrated in preclinical studies suggest more promise for the clinical use of Taxifolin than other drug candidates for CAA. Future basic and clinical studies of this commonly used bioactive flavonoid could open new avenues for preemptive medicine for AD and CAA.

AUTHOR CONTRIBUTIONS

All the authors contributed to conceptualization and writing.

FUNDING

This work was supported by Grant-in-Aid for Japan Society for the Promotion of Science Fellows and Shimadzu Science Foundation (SS) as well as the Collaborative Research Project of Brain Research Institute, Niigata University (MI).

ACKNOWLEDGMENTS

We thank the late Yoko Okamoto for useful discussions, and Ahmad Khundakar at Newcastle University for editorial assistance.

REFERENCES

Aisen, P. S., Gauthier, S., Ferris, S. H., Saumier, D., Haine, D., Garceau, D., et al. (2011). Tramiprosate in mild-to-moderate Alzheimer's disease—a randomized, double-blind, placebo-controlled, multi-centre study (the Alphase Study). *Arch. Med. Sci.* 7 (1), 102–111. doi:10.5114/aoms.2011.20612

Arbel-Ornath, M., Hudry, E., Eikermann-Haerter, K., Hou, S., Gregory, J. L., Zhao, L., et al. (2013). Interstitial fluid drainage is impaired in ischemic stroke and Alzheimer's disease mouse models. *Acta Neuropathol.* 126 (3), 353–364. doi:10.1007/s00401-013-1145-2

Banerjee, G., Wilson, D., Ambler, G., Osei-Bonsu Appiah, K., Shakeshaft, C., Lunawat, S., et al. (2018). Cognitive impairment before intracerebral hemorrhage is associated with cerebral amyloid angiopathy. *Stroke* 49 (1), 40–45. doi:10.1161/STROKEAHA.117.019409

Barnett, K., Mercer, S. W., Norbury, M., Watt, G., Wyke, S., and Guthrie, B. (2012). Epidemiology of multimorbidity and implications for health care, research, and medical education: a cross-sectional study. *Lancet* 380 (9836), 37–43. doi:10.1016/S0140-6736(12)60240-2

Boyle, P. A., Yu, L., Nag, S., Leurgans, S., Wilson, R. S., Bennett, D. A., et al. (2015). Cerebral amyloid angiopathy and cognitive outcomes in community-based older persons. *Neurology* 85 (22), 1930–1936. doi:10.1212/WNL.0000000000002175

Broich, K., Weiergräber, M., and Hampel, H. (2011). Biomarkers in clinical trials for neurodegenerative diseases: regulatory perspectives and requirements. *Prog. Neurobiol.* 95 (4), 498–500. doi:10.1016/j.pneurobio.2011.09.004

Calviere, L., Viguier, A., Patsoura, S., Rousseau, V., Albucher, J. F., Planton, M., et al. (2019). Risk of intracerebral hemorrhage and mortality after convexity subarachnoid hemorrhage in cerebral amyloid angiopathy. *Stroke* 50 (9), 2562–2564. doi:10.1161/STROKEAHA.119.026244

Carare, R. O., Bernardes-Silva, M., Newman, T. A., Page, A. M., Nicoll, J. A., Perry, V. H., et al. (2008). Solutes, but not cells, drain from the brain parenchyma along basement membranes of capillaries and arteries: significance for cerebral amyloid angiopathy and neuroimmunology. *Neuropathol. Appl. Neurobiol.* 34 (2), 131–144. doi:10.1111/j.1365-2990.2007.00926.x

Carare, R. O., Aldea, R., Agarwal, N., Bacskai, B. J., Bechman, I., Boche, D., et al. (2020). Clearance of interstitial fluid (ISF) and CSF (CLIC) group—part of vascular professional interest area (PIA). *Alzheimers Dement (Amst)* 12 (1), e12053. doi:10.1002/dad2.12053

Cummings, J., Lee, G., Ritter, A., Sabbagh, M., and Zhong, K. (2020). Alzheimer's disease drug-development pipeline: few candidates, frequent failures. *Alzheimer's Res. Ther.* 6(1), e12050. doi:10.1002/trc2.12050

Deane, R., Sagare, A., Hamm, K., Parisi, M., Lane, S., Finn, M. B., et al. (2008). apoE isoform-specific disruption of amyloid beta peptide clearance from mouse brain. *J. Clin. Invest.* 118 (12), 4002–4013. doi:10.1172/JCI36663

Deane, R., Wu, Z., Sagare, A., Davis, J., Du Yan, S., Hamm, K., et al. (2004). LRP/amyloid beta-peptide interaction mediates differential brain efflux of Abeta isoforms. *Neuron* 43 (3), 333–344. doi:10.1016/j.neuron.2004.07.017

Fakan, B., Reisz, Z., Zadori, D., Vecsei, L., Klivenyi, P., and Szalardy, L. (2020). Predictors of localization, outcome, and etiology of spontaneous intracerebral hemorrhages: focus on cerebral amyloid angiopathy. *J. Neural. Transm.* 127 (6), 963–972. doi:10.1007/s00702-020-02174-2

Gauthier, S., Aisen, P. S., Ferris, S. H., Saumier, D., Duong, A., Haine, D., et al. (2009). Effect of tramiprosate in patients with mild-to-moderate Alzheimer's disease: exploratory analyses of the MRI sub-group of the Alphase study. *J. Nutr. Health Aging* 13 (6), 550–557. doi:10.1007/s12603-009-0106-x

Gervais, F., Paquette, J., Morissette, C., Krzywkowski, P., Yu, M., Azzi, M., et al. (2007). Targeting soluble Abeta peptide with Tramiprosate for the treatment of brain amyloidosis. *Neurobiol. Aging* 28 (4), 537–547. doi:10.1016/j.neurobiolaging.2006.02.015

Greenberg, S. M., and Charidimou, A. (2018). Diagnosis of cerebral amyloid angiopathy: evolution of the boston criteria. *Stroke* 49 (2), 491–497. doi:10.1161/STROKEAHA.117.016990

Greenberg, S. M., Rosand, J., Schneider, A. T., Creed Pettigrew, L., Gandy, S. E., Rovner, B., et al. (2006). A phase 2 study of tramiprosate for cerebral amyloid angiopathy. *Alzheimer Dis. Assoc. Disord.* 20 (4), 269–274. doi:10.1097/01.wad.0000213845.28624.f4

Guo, H., Zhang, X., Cui, Y., Zhou, H., Xu, D., Shan, T., et al. (2015). Taxifolin protects against cardiac hypertrophy and fibrosis during biomechanical stress of pressure overload. *Toxicol. Appl. Pharmacol.* 287 (2), 168–177. doi:10.1016/j.taap.2015.06.002

Hampel, H., Vergallo, A., Giorgi, F. S., Kim, S. H., Depypere, H., Graziani, M., et al. (2018). Precision medicine and drug development in Alzheimer's disease: the importance of sexual dimorphism and patient stratification. *Front. Neuroendocrinol.* 50, 31–51. doi:10.1016/j.yfrne.2018.06.001

Haraguchi, H., Mochida, Y., Sakai, S., Masuda, H., Tamura, Y., Mizutani, K., et al. (1996). Protection against oxidative damage by dihydroflavonols in Engelhardtia chrysolepis. *Biosci. Biotechnol. Biochem.* 60 (6), 945–948. doi:10.1271/bbb.60.945

Harris, C. S., Beaulieu, L. P., Fraser, M. H., McIntyre, K. L., Owen, P. L., Martineau, L. C., et al. (2011). Inhibition of advanced glycation end product formation by medicinal plant extracts correlates with phenolic metabolites and antioxidant activity. *Planta Med.* 77 (2), 196–204. doi:10.1055/s-0030-1250161

Inoue, T., Saito, S., Tanaka, M., Yamakage, H., Kusakabe, T., Shimatsu, A., et al. (2019). Pleiotropic neuroprotective effects of taxifolin in cerebral amyloid angiopathy. *Proc. Natl. Acad. Sci. U. S. A.* 116 (20), 10031–10038. doi:10.1073/pnas.1901659116

Ishikawa, H., Ii, Y., Shindo, A., Tabei, K. I., Umino, M., Ito, A. O., et al. (2020). Cortical microinfarcts detected by 3-tesla magnetic resonance imaging:

differentiation between cerebral amyloid angiopathy and embolism. *Stroke* 51 (3), 1010–1013. doi:10.1161/STROKEAHA.119.028202

Iturria-Medina, Y., Sotero, R. C., Toussaint, P. J., Evans, A. C., and Alzheimer's Disease Neuroimaging, I. (2014). Epidemic spreading model to characterize misfolded proteins propagation in aging and associated neurodegenerative disorders. *PLoS Comput. Biol.* 10 (11), e1003956. doi:10.1371/journal.pcbi.1003956

Jung, Y. H., Jang, H., Park, S. B., Choe, Y. S., Park, Y., Kang, S. H., et al. (2020). Strictly lobar microbleeds reflect amyloid angiopathy regardless of cerebral and cerebellar compartments. *Stroke* 51 (12), 3600–3607. doi:10.1161/STROKEAHA.119.028487

Keable, A., Fenna, K., Yuen, H. M., Johnston, D. A., Smyth, N. R., Smith, C., et al. (2016). Deposition of amyloid β in the walls of human leptomeningeal arteries in relation to perivascular drainage pathways in cerebral amyloid angiopathy. *Biochim. Biophys. Acta* 1862 (5), 1037–1046. doi:10.1016/j.bbadis.2015.08.024

Kim, S. H., Ahn, J. H., Yang, H., Lee, P., Koh, G. Y., and Jeong, Y. (2020). Cerebral amyloid angiopathy aggravates perivascular clearance impairment in an Alzheimer's disease mouse model. *Acta Neuropathol Commun* 8 (1), 181. doi:10.1186/s40478-020-01042-0

Kumar, S., Goddeau, R. P., Jr., Selim, M. H., Thomas, A., Schlaug, G., Alhazzani, A., et al. (2010). Atraumatic convexal subarachnoid hemorrhage: clinical presentation, imaging patterns, and etiologies. *Neurology* 74 (11), 893–899. doi:10.1212/WNL.0b013e3181d55efa

Leurent, C., Goodman, J. A., Zhang, Y., He, P., Polimeni, J. R., Gurol, M. E., et al. (2019). Immunotherapy with ponezumab for probable cerebral amyloid angiopathy. *Ann Clin Transl Neurol* 6 (4), 795–806. doi:10.1002/acn3.761

Love, S., Chalmers, K., Ince, P., Esiri, M., Attems, J., Jellinger, K., et al. (2014). Development, appraisal, validation and implementation of a consensus protocol for the assessment of cerebral amyloid angiopathy in post-mortem brain tissue. *Am J Neurodegener. Dis.* 3 (1), 19–32.

MacGregor Sharp, M., Saito, S., Keable, A., Gatherer, M., Aldea, R., Agarwal, N., et al. (2020). Demonstrating a reduced capacity for removal of fluid from cerebral white matter and hypoxia in areas of white matter hyperintensity associated with age and dementia. *Acta Neuropathol Commun* 8 (1), 131. doi:10.1186/s40478-020-01009-1

Mawuenyega, K. G., Sigurdson, W., Ovod, V., Munsell, L., Kasten, T., Morris, J. C., et al. (2010). Decreased clearance of CNS beta-amyloid in Alzheimer's disease. *Science* 330 (6012), 1774. doi:10.1126/science.1197623

Morris, A. W., Sharp, M. M., Albargothy, N. J., Fernandes, R., Hawkes, C. A., Verma, A., et al. (2016). Vascular basement membranes as pathways for the passage of fluid into and out of the brain. *Acta Neuropathol.* 131 (5), 725–736. doi:10.1007/s00401-016-1555-z

Nicoll, J. A., Wilkinson, D., Holmes, C., Steart, P., Markham, H., and Weller, R. O. (2003). Neuropathology of human Alzheimer disease after immunization with amyloid-beta peptide: a case report. *Nat. Med.* 9 (4), 448–452. doi:10.1038/nm840

Okamoto, Y., Ihara, M., Fujita, Y., Ito, H., Takahashi, R., and Tomimoto, H. (2009). Cortical microinfarcts in Alzheimer's disease and subcortical vascular dementia. *Neuroreport* 20 (11), 990–996. doi:10.1097/WNR.0b013e32832d2e6a

Okamoto, Y., Yamamoto, T., Kalaria, R. N., Senzaki, H., Maki, T., Hase, Y., et al. (2012). Cerebral hypoperfusion accelerates cerebral amyloid angiopathy and promotes cortical microinfarcts. *Acta Neuropathol.* 123(3), 381–394. doi:10.1007/s00401-011-0925-9

Pasi, M., Charidimou, A., Boulouis, G., Auriel, E., Ayres, A., Schwab, K. M., et al. (2018). Mixed-location cerebral hemorrhage/microbleeds: underlying microangiopathy and recurrence risk. *Neurology* 90(2), e119–e126. doi:10.1212/WNL.0000000000004797

Patton, R. L., Kalback, W. M., Esh, C. L., Kokjohn, T. A., Van Vickle, G. D., Luehrs, D. C., et al. (2006). Amyloid-beta peptide remnants in AN-1792-immunized Alzheimer's disease patients: a biochemical analysis. *Am. J. Pathol.* 169 (3), 1048–1063. doi:10.2353/ajpath.2006.060269

Piotrowska, A., Winter, K., Carare, R. O., and Bechmann, I. (2020). Vital functions contribute to the spread of extracellular fluids in the brain: comparison between life and death. *Front. Aging Neurosci.* 12, 15. doi:10.3389/fnagi.2020.00015

Renard, D., Parvu, T., and Thouvenot, E. (2019). Finger-like projections in lobar haemorrhage on early magnetic resonance imaging is associated with probable cerebral amyloid angiopathy. *Cerebrovasc. Dis.* 47(3–4), 121–126. doi:10.1159/000499032

Rodrigues, M. A., Samarasekera, N., Lerpiniere, C., Humphreys, C., McCarron, M. O., White, P. M., et al. (2018). The Edinburgh CT and genetic diagnostic criteria for lobar intracerebral haemorrhage associated with cerebral amyloid angiopathy: model development and diagnostic test accuracy study. *Lancet Neurol.* 17 (3), 232–240. doi:10.1016/S1474-4422(18)30006-1

Roher, A. E., Maarouf, C. L., Kokjohn, T. A., Belden, C., Serrano, G., Sabbagh, M. S., et al. (2016). Chemical and neuropathological analyses of an Alzheimer's disease patient treated with solanezumab. *Am J Neurodegener Dis.* 5 (4), 158–170.

Rosas-Hernandez, H., Cuevas, E., Raymick, J. B., Robinson, B. L., and Sarkar, S. (2020). Impaired amyloid beta clearance and brain microvascular dysfunction are present in the tg-SwDI mouse model of alzheimer's disease. *Neuroscience* 440, 48–55. doi:10.1016/j.neuroscience.2020.05.024

Saito, S., and Ihara, M. (2016). Interaction between cerebrovascular disease and Alzheimer pathology. *Curr. Opin. Psychiatr.* 29 (2), 168–173. doi:10.1097/YCO.0000000000000239

Saito, S., and Ihara, M. (2014). New therapeutic approaches for Alzheimer's disease and cerebral amyloid angiopathy. *Front. Aging Neurosci.* 6, 290. doi:10.3389/fnagi.2014.00290

Saito, S., Ikeda, Y., Ando, D., Carare, R. O., Ishibashi-Ueda, H., and Ihara, M. (2020a). Cerebral amyloid angiopathy presenting as massive subarachnoid haemorrhage: a case study and review of literature. *Front. Aging Neurosci.* 12, 538456. doi:10.3389/fnagi.2020.538456

Saito, S., McLaurin, J., and Carare, R. O. (2020b). Editorial: intramural vascular cells: key therapeutic targets for vascular cognitive impairment. *Front. Aging Neurosci.* 12, 615780. doi:10.3389/fnagi.2020.615780

Saito, S., Yamamoto, Y., and Ihara, M. (2019). Development of a multicomponent intervention to prevent alzheimer's disease. *Front. Neurol.* 10, 490. doi:10.3389/fneur.2019.00490

Saito, S., Yamamoto, Y., and Ihara, M. (2015). Mild cognitive impairment: at the crossroad of neurodegeneration and vascular dysfunction. *Curr. Alzheimer Res.* 12 (6), 507–512. doi:10.2174/1567205012666150530202508.

Saito, S., Yamamoto, Y., Maki, T., Hattori, Y., Ito, H., Mizuno, K., et al. (2017). Taxifolin inhibits amyloid-β oligomer formation and fully restores vascular integrity and memory in cerebral amyloid angiopathy. *Acta Neuropathol. Commun.* 5 (1), 26. doi:10.1186/s40478-017-0429-5

Sakai, K., Ueda, M., Fukushima, W., Tamaoka, A., Shoji, M., Ando, Y., et al. (2019). Nationwide survey on cerebral amyloid angiopathy in Japan. *Eur. J. Neurol.* 26 (12), 1487–1493. doi:10.1111/ene.14031

Sato, M., Murakami, K., Uno, M., Ikubo, H., Nakagawa, Y., Katayama, S., et al. (2013a). Structure-activity relationship for (+)-taxifolin isolated from silymarin as an inhibitor of amyloid β aggregation. *Biosci. Biotechnol. Biochem.* 77 (5), 1100–1103. doi:10.1271/bbb.120925

Sato, M., Murakami, K., Uno, M., Nakagawa, Y., Katayama, S., Akagi, K., et al. (2013b). Site-specific inhibitory mechanism for amyloid β42 aggregation by catechol-type flavonoids targeting the Lys residues. *J. Biol. Chem.* 288 (32), 23212–23224. doi:10.1074/jbc.M113.464222

Shibata, M., Yamada, S., Kumar, S. R., Calero, M., Bading, J., Frangione, B., et al. (2000). Clearance of Alzheimer's amyloid-ss(1-40) peptide from brain by LDL receptor-related protein-1 at the blood-brain barrier. *J. Clin. Invest.* 106 (12), 1489–1499. doi:10.1172/JCI10498

Smith, E. E., and Markus, H. S. (2020). New treatment approaches to modify the course of cerebral small vessel diseases. *Stroke* 51 (1), 38–46. doi:10.1161/STROKEAHA.119.024150

Sunil, C., and Xu, B. (2019). An insight into the health-promoting effects of taxifolin (dihydroquercetin). *Phytochemistry* 166, 112066. doi:10.1016/j.phytochem.2019.112066

Sweeney, M. D., Kisler, K., Montagne, A., Toga, A. W., and Zlokovic, B. V. (2018). The role of brain vasculature in neurodegenerative disorders. *Nat. Neurosci.* 21 (10), 1318–1331. doi:10.1038/s41593-018-0234-x

Sweeney, M. D., Zhao, Z., Montagne, A., Nelson, A. R., and Zlokovic, B. V. (2019). Blood-brain barrier: from physiology to disease and back. *Physiol. Rev.* 99 (1), 21–78. doi:10.1152/physrev.00050.2017

Tanaka, M., Saito, S., Inoue, T., Satoh-Asahara, N., and Ihara, M. (2019). Novel therapeutic potentials of taxifolin for amyloid-β-associated neurodegenerative diseases and other diseases: recent advances and future perspectives. *Int. J. Mol. Sci.* 20 (9). doi:10.3390/ijms20092139

Tanaka, M., Saito, S., Inoue, T., Satoh-Asahara, N., and Ihara, M. (2020). Potential therapeutic approaches for cerebral amyloid angiopathy and alzheimer's disease. *Int. J. Mol. Sci.* 21 (6). doi:10.3390/ijms21061992

Tarasoff-Conway, J. M., Carare, R. O., Osorio, R. S., Glodzik, L., Butler, T., Fieremans, E., et al. (2015). Clearance systems in the brain-implications for Alzheimer disease. *Nat. Rev. Neurol.* 11(8), 457–470. doi:10.1038/nrneurol.2015.119

Ter Telgte, A., Scherlek, A. A., Reijmer, Y. D., van der Kouwe, A. J., van Harten, T., Duering, M., et al. (2020). Histopathology of diffusion-weighted imaging-positive lesions in cerebral amyloid angiopathy. *Acta Neuropathol.* 139 (5), 799–812. doi:10.1007/s00401-020-02140-y

Thal, D. R., Griffin, W. S., de Vos, R. A., and Ghebremedhin, E. (2008). Cerebral amyloid angiopathy and its relationship to Alzheimer's disease. *Acta Neuropathol.* 115(6), 599–609. doi:10.1007/s00401-008-0366-2

The U.S. National Institutes of Health (2020). ClinicalTrials.gov. Available: https://clinicaltrials.gov/ (Accessed November 1, 2020).

van Etten, E. S., Verbeek, M. M., van der Grond, J., Zielman, R., van Rooden, S., van Zwet, E. W., et al. (2017). β-Amyloid in CSF: biomarker for preclinical cerebral amyloid angiopathy. *Neurology* 88 (2), 169–176. doi:10.1212/WNL.0000000000003486

van Opstal, A. M., van Rooden, S., van Harten, T., Ghariq, E., Labadie, G., Fotiadis, P., et al. (2017). Cerebrovascular function in presymptomatic and symptomatic individuals with hereditary cerebral amyloid angiopathy: a case-control study. *Lancet Neurol.* 16 (2), 115–122. doi:10.1016/S1474-4422(16)30346-5

van Rooden, S., Goos, J. D., van Opstal, A. M., Versluis, M. J., Webb, A. G., Blauw, G. J., et al. (2014). Increased number of microinfarcts in Alzheimer disease at 7-T MR imaging. *Radiology* 270 (1), 205–211. doi:10.1148/radiol.13130743

Verbeek, M. M., Kremer, B. P., Rikkert, M. O., Van Domburg, P. H., Skehan, M. E., and Greenberg, S. M. (2009). Cerebrospinal fluid amyloid beta(40) is decreased in cerebral amyloid angiopathy. *Ann. Neurol.* 66 (2), 245–249. doi:10.1002/ana.21694

Wang, Y., Wang, Q., Bao, X., Ding, Y., Shentu, J., Cui, W., et al. (2018). Taxifolin prevents β-amyloid-induced impairments of synaptic formation and deficits of memory via the inhibition of cytosolic phospholipase A2/prostaglandin E2 content. *Metab. Brain Dis.* 33 (4), 1069–1079. doi:10.1007/s11011-018-0207-5

Weidmann, A. E. (2012). Dihydroquercetin: more than just an impurity?. *Eur. J. Pharmacol.* 684(1-3), 19–26. doi:10.1016/j.ejphar.2012.03.035

Westover, M. B., Bianchi, M. T., Yang, C., Schneider, J. A., and Greenberg, S. M. (2013). Estimating cerebral microinfarct burden from autopsy samples. *Neurology* 80 (15), 1365–1369. doi:10.1212/WNL.0b013e31828c2f52

Xiong, L., Charidimou, A., Pasi, M., Boulouis, G., Pongpitakmetha, T., Schirmer, M. D., et al. (2019). Predictors for late post-intracerebral hemorrhage dementia in patients with probable cerebral amyloid angiopathy. *J. Alzheimers Dis.* 71 (2), 435–442. doi:10.3233/JAD-190346

Yakushiji, Y., Tanaka, J., Wilson, D., Charidimou, A., Noguchi, T., Kawashima, M., et al. (2020). Proportion of intracerebral haemorrhage due to cerebral amyloid angiopathy in the East and West: comparison between single hospital centres in Japan and the United Kingdom. *J. Neurol. Sci.* 416, 117037. doi:10.1016/j.jns.2020.117037

Yamada, M. (2015). Cerebral amyloid angiopathy: emerging concepts. *J Stroke* 17(1), 17–30. doi:10.5853/jos.2015.17.1.17

Yang, P., Xu, F., Li, H. F., Wang, Y., Li, F. C., Shang, M. Y., et al. (2016). Detection of 191 taxifolin metabolites and their distribution in rats using HPLC-ESI-IT-TOF-MS(n). *Molecules* 21 (9). doi:10.3390/molecules21091209

Conflict of Interest: The authors declare that the research was conducted in the absence of any commercial or financial relationships that could be construed as a potential conflict of interest.

frontiers in Pharmacology

ORIGINAL RESEARCH
published: 16 February 2021
doi: 10.3389/fphar.2021.625074

Saikosaponin D Rescues Deficits in Sexual Behavior and Ameliorates Neurological Dysfunction in Mice Exposed to Chronic Mild Stress

Zhuo Wang[1†], Jianwei Li[1†], Wei Wu[1†], Tao Qi[1], Zhansen Huang[1], Bo Wang[1], Shixiong Li[1], Chen Li[2], Jiuyang Ding[3], Yuanning Zeng[4], Peng Huang[5], Zhihua Zhou[6], Yanjun Huang[7], Jian Huang[2], Xiaohan Wang[2], Qiyuan Huang[8], Guanghuan Zhang[9], Pingming Qiu[2]* and Jun Chen[1]**

[1]Department of Infertility and Sexual Medicine, The Third Affiliated Hospital of Sun Yat-sen University, Guangzhou, China, [2]School of Forensic Medicine, Southern Medical University, Guangzhou, China, [3]School of Forensic Medicine, Guizhou Medical University, Guiyang, China, [4]Research Center for Good Practice in TCM Proessing Technology, Guangdong Pharmaceutical University, Guangzhou, China, [5]Foshan Maternal and Child Health Hospital, Affiliated Hospital of Southern Medical University, Foshan, China, [6]Department of Neurology, The First Affiliated Hospital, School of Clinical Medicine of Guangdong Pharmaceutical University, Guangzhou, China, [7]Department of Neurology, Zhujiang Hospital, Southern Medical University, Guangzhou, China, [8]School of Laboratory Medicine and Biotechnology, Southern Medical University, Guangzhou, China, [9]Department of Nutrition, Hospital of Integrated Traditional Chinese Medical and Western Medicine, Southern Medical University, Guangzhou, China

Often associated with sexual dysfunction (SD), chronic stress is the main contributing risk factor for the pathogenesis of depression. Radix bupleuri had been widely used in traditional Chinese medicine formulation for the regulation of emotion and sexual activity. As the main active component of Radix bupleuri, saikosaponin D (SSD) has a demonstrated antidepressant effect in preclinical studies. Herein, we sought to investigate the effect of SSD to restore sexual functions in chronically stressed mice and elucidate the potential brain mechanisms that might underly these effects. SSD was gavage administered for three weeks during the induction of chronic mild stress (CMS), and its effects on emotional and sexual behaviors in CMS mice were observed. The medial posterodorsal amygdala (MePD) was speculated to be involved in the manifestation of sexual dysfunctions in CMS mice. Our results revealed that SSD not only alleviated CMS-induced depressive-like behaviors but also rescued CMS-induced low sexual motivation and poor sexual performance. CMS destroyed astrocytes and activated microglia in the MePD. SSD treatment reversed the changes in glial pathology and inhibited neuroinflammatory and oxidative stress in the MePD of CMS mice. The neuronal morphological and functional deficits in the MePD were also alleviated by SSD administration. Our results provide insights into the central mechanisms involving the brain associated with sexual dysfunction. These findings deepen our understanding of SSD in light of the psychopharmacology of stress and sexual disorders, providing a theoretical basis for its potential clinical application.

Keywords: saikosaponin d, medial posterodorsal amygdala, sexual behaviour, emotion, stress

OPEN ACCESS

Edited by:
Muhammad Imran Naseer, King Abdulaziz University, Saudi Arabia

Reviewed by:
Syed Zaidi, King Abdulaziz University, Saudi Arabia
Shafiq Ur Rehman, Gyeongsang National University, South Korea

****Correspondence:***
Guanghuan Zhang
gzzhanggh@163.com
Pingming Qiu
qiupmfy@126.com
Jun Chen
jchen121121@hotmail.com

[†]These authors contributed equally to this work

Specialty section:
This article was submitted to Neuropharmacology, a section of the journal Frontiers in Pharmacology

Received: *02 November 2020*
Accepted: *06 January 2021*
Published: *16 February 2021*

Citation:
Wang Z, Li J, Wu W, Qi T, Huang Z, Wang B, Li S, Li C, Ding J, Zeng Y, Huang P, Zhou Z, Huang Y, Huang J, Wang X, Huang Q, Zhang G, Qiu P and Chen J (2021) Saikosaponin D Rescues Deficits in Sexual Behavior and Ameliorates Neurological Dysfunction in Mice Exposed to Chronic Mild Stress. Front. Pharmacol. 12:625074. doi: 10.3389/fphar.2021.625074

INTRODUCTION

Stressful stimuli are aplenty in modern society, and stressful life events are the main cause of depression (Hammen, 2018). Stress-related mood disorders have become a serious public health problem and drawn much attention (Becker and Kleinman, 2013; Ménard et al., 2016). Another great concern frequently overlooked is that depressed male patients who experience chronic stress often show reduced sexual interest, have difficulty with sexual arousal, and exhibit poor sexual function (Hosain et al., 2013; Breyer et al., 2014; Deumic et al., 2016). Indeed, the prevalence of these problems are much higher in depressed men than in the general population (El Yazidi et al., 2019). In experimental studies, chronic stress has also been reported to induce reduced sexual motivation, testicular injury, and nonorganic erectile dysfunction in male animals (Hou et al., 2014; Chen et al., 2019). Depression mainly occurs in young and middle-aged people (Bogren et al., 2018); sexual dysfunction in these men has a huge negative impact on the individuals' and couples' quality of life.

As an important component of the limbic system (Sokolowski and Corbin, 2012), the amygdala plays a key role in responding to emotional stimuli; its involvement in the pathophysiological response to stress had been well recognized (Drevets, 2003; Barry et al., 2017; Kedo et al., 2018). In addition, the amygdala also plays an important role in the arousal and execution of sexual behavior (Kühn and Gallinat, 2011; Seok et al., 2016). Direct bilateral electrical damage to the medial amygdala causes abnormal emotional behaviors in animals (Vinkers et al., 2010). The mating behaviors of male rats with a medial amygdala injury were severely impaired, while that of the rats with a basolateral amygdala injury remained unchanged (Kondo, 1992). The medial amygdala plays a dual role in both emotional processing and regulation of sexual behavior. The posterodorsal medial amygdala (MePD) is a subnucleus of the medial amygdala that expresses sex hormone receptors and is involved in regulating moods and sexual behavior (Rasia-Filho et al., 2012; Bergan et al., 2014). It can exert a regulatory effect on sexual motivation through its connection with downstream nuclear clusters (Holder and Mong, 2017). Sexual dysfunction in male patients with chronic stress-induced depression may be caused by a dysfunctional MePD in the central nervous system (CNS).

Common antidepressants have a long onset of action, accompanied by side effects of varying severity (Tollefson, 1991). Sexual dysfunction is one of the most commonly reported adverse effects of antidepressants (Montejo et al., 2019). Only few alternatives or supplemental drugs have been found to effectively alleviate the abovementioned symptoms. Therefore, there is an urgent need to identify and develop drugs that can clinically improve emotional dysfunctions, without disrupting sexual activity. Radix bupleuri is a widely used ingredient in traditional Chinese medicine (TCM) formulations for relieving depression. It plays a therapeutic role in the Xiaoyaosan (Liu et al., 2015), Sinisan (Wang et al., 2020), Chaihu-Shugan-San (Qiu et al., 2014), and other traditional antidepressant Chinese medicine formulae. Modern pharmacological studies have shown that saikosaponins are the main bioactive component of Radix bupleuri accounting for its antidepressant effects (Chao et al., 2020). Saikosaponin D (SSD) had a demonstrated antidepressant effect in multiple depression models (Li et al., 2017; Xu et al., 2019; Chao et al., 2020). However, it remains unknown whether SSD could ameliorate chronic stress-induced impairments of sexual activity. This study sought to explore the effect of SSD on chronic stress-induced depression and symptoms related to sexual dysfunction in male mice and elucidate its potential central mechanisms.

MATERIAL AND METHODS

Animals

C57 BL/6J adult male mice, aged 8–10 weeks, were provided by the Laboratory Animal Center of Southern Medical University (Guangzhou, Guangdong). All animals were raised in a single cage in a standard specific pathogen-free experimental environment (12 h light/dark cycle, with *ad libitum* access to dry food and clean water). The indoor temperature was maintained at 23 ± 1°C, and the humidity was maintained at 50–60%. Animal treatments, including anesthesia induction and euthanasia, were conducted in accordance with the Principle of Laboratory Animal Care (NIH Publication no. 85–23, revised 1985). All experimental procedures were conducted in accordance with the requirements of the China Animal Ethics Committee and were approved by the Animal Ethics Committee of The Third Affiliated Hospital of Sun Yat-sen University.

Chronic Mild Stress (CMS) Modeling and Drug Administration

In addition to those included in the control group, the remaining mice were subjected to chronic unpredictable stress. The procedures for CMS model development were adapted from a previous study (Qin et al., 2019). The stress paradigm included fasting, day/night reversal, forced swimming, noise, stroboscopy, restraint stress, water deprivation, and a wet cage; these stressors were randomly subjected 2–3 times every day. The unpredictable stimuli were administered in different ways for 7 weeks. After chronic stress stimulation for 3 weeks, the CMS mice were then randomly assigned to the SSD treatment group (CMS+SSD) or nontreated CMS group (CMS). The SSD dosage was adopted from previous validated research (Xu et al., 2019; Chao et al., 2020) (M3936, Abmole, Houston, TX, United States, >98%, 1 mg/kg; dissolved in saline and administered via gavage) and the treatment lasted three weeks; in contrast, the mice in the CMS group were treated with saline. In the preliminary experiment, we had used 1 mg/kg dosage in age-matched mice to verify the potential adverse effects of SSD. The SSD treatment had little effect on depressive and sexual behaviors of the mice, after which we performed the following experiments. All experiments were strictly implemented in accordance with the *3R* principles; each group had 20 mice. At the end of the CMS modeling and SSD treatment, the animals were used for behavioral, morphological, electrophysiological, and biochemical analyses. All animals were

assigned a numerical code and the investigators were always blinded to the treatment groups until the completion of data analysis.

Sucrose Preference Test

The sucrose preference test is the main method of testing the core symptom of CMS depression model-anhedonia (Cao et al., 2013). After 23 h of fasting and water abstinence, each mouse was provided with two bottles of water (weights measured in advance): one bottle contained 1% sucrose water and the other had pure water. Pure water consumption and sugar water consumption of the mice were calculated after 1 h. The percentage of sugar water consumption was calculated in terms of the total weights of liquid consumed.

Forced Swimming Test (FST)

The mice were placed in a swimming bucket filled with water at 24 ± 2°C, with a depth of 20 cm, for 6 min. The time the mice spent in immobility within the last 4 min was recorded. The duration of immobility was recorded when mice ceased struggling.

Y-Maze Preference Test

This experiment was conducted in a closed Y-shaped maze as previously described (Petrulis and Johnston, 1999). The maze was made of PVC plastic and consisted of three long arms and perforated plexiglass boxes were placed at the ends of two top arms. The animals were allowed to explore the animals behind the transparent perforated plexiglass boxes. The mice were allowed to move freely in the maze for 5 min, and the time spent exploring each end of the Y-maze was recorded.

Sexual Motivation Test

In reference to research on the sexual motivation of rats (Chu and Ågmo, 2016), we established a mouse model for the sexual motivation test. The experimental device used is similar to that used in rats. The equipment consisted of a rectangular open field having two chambers with openings on the diagonally opposite walls. The front of the chamber is made of a wire mesh, which allows the animals to see, smell and touch the animals in the chamber. Male and female animals are respectively placed in the two chambers. The virtual area in front of the cage is the motivation exploration area. A camera was suspended to track the movements of the animals, and the preference score was defined by female motivation area time/(female motivation area time + male motivation area time).

Sexual Behavior Test

The sexual interaction test was adapted from a previous study (Benelli et al., 2002). Briefly, the experiment was conducted in a quiet, dimly lit environment at nightphase. After three days of preadaptation to the experimental arena (20 min per day; arena area, 40 cm*40 cm*40 cm), the tested male mice were allowed to interact with aphrodisiac female mice (Grønli et al., 2005) for 30 min. The recorded masculine sexual behavior include the latency to first mount, mount frequency, intromission frequency, and the ratio of intromission and total mount.

Immunofluorescence Staining

Following paraformaldehyde perfusion and fixation, the mouse brains were dehydrated with 30% sucrose. After cryofixation and obtaining cryosections of the whole brain, the brain slices were incubated in 5% bovine serum albumin containing 0.5% Triton X-100 for 1 h, after which they were treated with the following primary antibodies: rabbit polyclonal anti-Iba1 (1:300; ab153696; Abcam) and rabbit polyclonal anti-glial fibrillary acid protein (GFAP) (1:300; ab7260; Abcam); the primary antibodies were incubated at overnight at 4°C. On the next day, following three washes with 0.1M phosphate-buffered saline (PBS), the slices were incubated with secondary antibody at room temperature for 1.5 h, mounted with DAPI-containing mounting medium, and sealed after washing again with PBS. Fluorescent images were acquired by confocal microscopy (Leica, Wetzlar, Germany) and analyzed using the Image J software.

Western Blotting

The brain protein samples were extracted using RIPA buffer containing a protease inhibitor cocktail (Roche, Basel, Switzerland), and the extracted proteins were electrophoresed in a 10–12% sodium dodecyl sulfate-polyacrylamide gel (Willget, China). Thereafter, the separated proteins were transferred onto polyvinylidene difluoride membranes; the membranes were then probed overnight with the following primary antibodies: mouse polyclonal anti-GFAP (1:800; cat# 3670; Cell Signaling Technology, MA, United States), rabbit polyclonal anti-MAP2 (1:800; cat# 4542; Cell Signaling Technology) and mouse polyclonal anti-GAPDH (1:2,000, sc-365062, Santa Cruz Biotechnology, TX, USA). On the next day, after washing, the membranes were incubated with horseradish peroxidase (HRP)-conjugated secondary antibody for 1 h at room temperature. The proteins were then visualized using an enhanced chemiluminescent substrate (ECL; Thermo Fisher Scientific, IL, United States).

ENZYME-LINKED IMMUNOSORBENT ASSAY (ELISA) DETERMINATION OF IL-1β AND IL-6

After behavior tests, the mice were sacrificed by cervical dislocation and MePD brains tissue were rapidly isolated on ice. The isolated brain tissue were homogenized in ice-cold phosphate buffer (pH 7.4) and centrifuged at 10, 000 g at 4°C for 15 min. The supernatants were collected and 100 μl supernatants were added in the plates to measure IL-1β and IL-6 with commercial ELISA kits (DY401 and DY406 respectively; R&D Systems, Minneapolis, United States) in accordance with the manufacturer's instructions. The optical density (OD) was measured with a microplate reader (PerkinElmer, Waltham, MA, United States) at a wavelength 450 nm and normalized to total soluble protein concentration with a BCA Protein Assay Kit (Cell Signaling Technology).

Reactive Oxygen Species (ROS) Measurement

Oxidative stress in the MePD was evaluated by determining the generation of ROS. Quantitative measurements of ROS were

performed using a double-sandwich ELISA method (ROS assay kit; QYE2656; Qualityard, Beijing, China) in accordance with the manufacturer's instructions. The OD value of each hole was measured sequentially with a microplate reader (PerkinElmer) with the wavelength of 450 nm and the values were expressed relative to the signal of controls.

Stereotaxic Surgery

Stereotaxic surgeries were conducted as previously described (Wang et al., 2019b). The mice were anesthetized with intraperitoneal injection of 4% pentobarbital sodium (40 ml/kg) and placed on a stereotaxic apparatus (RWD, Shenzhen, China). The scalp was shaved, and the skin was disinfected with 75% alcohol. The skin was cut along the median line of the exposed bone, and the subcutaneous tissue was separated to fully expose the skull. After drilling through the skull, above the MePD (AP -1.7; ML 2.0; DV -5.0) nucleus, adeno-associated viruses (AAV) expressing the green fluorescent protein (GFP; BrainVTA, Wuhan, China) was injected into the target site.

Confocal Image Analysis of Spine Density

The GFP-stained brain sections were observed under a confocal microscope (LSM510, Meta, Zeiss). For dendritic spine density analysis, z-series stacks were obtained with 10 consisted scans at a high zoom at 1 mm intervals in the Z-axis. The dendritic spines were sampled from 3–5 distal dendrites of all GFP-positive neurons. The density of dendritic spines in the MePD was measured using Image J software.

In vivo Electrophysiological Recordings

After the mice were placed on a stereotaxic apparatus and the skull was exposed, a glass electrode was slowly lowered toward the MePD to record neuronal activity. An electrical stimulation was delivered (STG4008 stimulator, Multichannel Systems, Germany) through the electrode—intensity, 0.1–0.9 mA; duration, 0.2 ms; frequency, 0.2–40 Hz. At the end of the experiments, only the data collected from the right stimulation sites were used for analyses.

Statistics

The GraphPad Prism 7.0 software was used to analyze the data and create the figures. Data are presented as mean ± standard error of mean (SEM) and analyzed using a Student's *t*-test or an analysis of variance, according to the different experiments. The significance level for all tests was set to $p/q < 0.05$.

RESULTS

SSD Alleviated CMS-Induced Depressive-like Behaviors in Mice

Adult male mice underwent a seven-week CMS paradigm andthe SSD administration started from the end of the third week of CMS induction. In the sucrose preference test to evaluate anhedonia, the percentage of sucrose consumption was significantly reduced in the CMS group than in the non-stressed control group; however, SSD treatment for three weeks significantly improved sucrose consumption (**Figure 1A**). The results of FST revealed that the CMS group showed significantly extended duration of immobility than the non-stressed control group. In contrast, SSD administration remarkably rescued this immobility in the FST (**Figure 1B**). Therefore, these findings indicate that SSD demonstrated antidepressant effects in a mouse model of CMS.

SSD Rescued CMS-Induced Low Sexual Motivation in Male Mice

In a previous study, the CMS-related rodent model had shown abnormally low sexual desire (Shen et al., 2020). In a mice Y-maze sexual preference test (**Figure 2A**), healthy male mice preferred to explore an estrous female mouse rather than a sexually active male mouse (**Figure 2B**); however, the CMS mice spent nearly the same amount of time around the male/female target arm. SSD treatment remarkably alleviated the adverse effects of CMS, with a statistically significant increase in the time spent exploring an estrous female mouse than a sexually active male mouse. In another sexual motivational test adapted from a rat study (**Figure 2C**), when the mice were allowed to freely explore the arena, similar to our abovementioned results, the CMS-induced male mice spent less time in the female zone than those in the control group. In addition, the SSD treatment restored female exploration behavior (**Figure 2D**). SSD administration improved the sexual motivation of the male CMS mice.

Effects of SSD on Sexual Performance in Male CMS Mice

After the sexual motivation test, we performed the sexual performance test assay to further assess the sexual performance of male CMS mice. In the sexual interaction test (**Figure 3A**), the latency to mount, number of mounts, number of intromissions, and the ratio between intromission and mount were recorded. SSD-treated CMS mice showed significantly reduced latency for first mouth with female mouse than vehicle-treated mice (**Figure 3B**). This further validated our previous results of the sexual motivation test. Moreover, SSD treatment significantly increased the number of mounts and intromission (**Figures 3C,D**), as well as increased the intromission ratio of male CMS mice to mount a female mouse (**Figure 3E**). SSD administration improved the overall sexual performance of male CMS mice.

Effects of SSD on Glial Pathology in the MePD

Similar to other amygdala subareas, the MePD mainly consists of two types of cells: neurons and glial cells. As a main glial cell type in the MePD, astrocytes are sensitive to environmental stress and may be affected in terms of their morphology and functions (Tynan et al., 2013), which can impact normal neural functions.

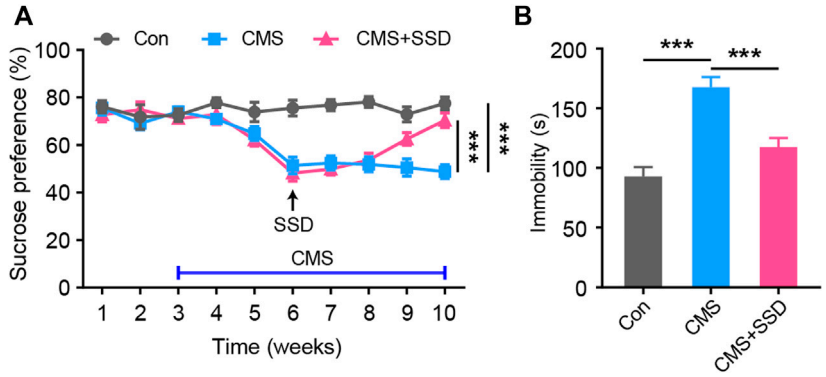

FIGURE 1 | The administration of saikosaponin D (SSD) induced antidepressant-like effects in chronic mild stress (CMS) mice. **(A)** Schematic of the experimental design; we used sucrose preference test to assess the depression-like behaviors of mice on a weekly basis. (n = 10, repeated-measures analysis of variance [ANOVA]). **(B)** Effects of SSD on depression-type behavior determined via forced swimming test (n = 9–11, one-way ANOVA). Data are presented as the mean ± standard error of mean. ***p < 0.001.

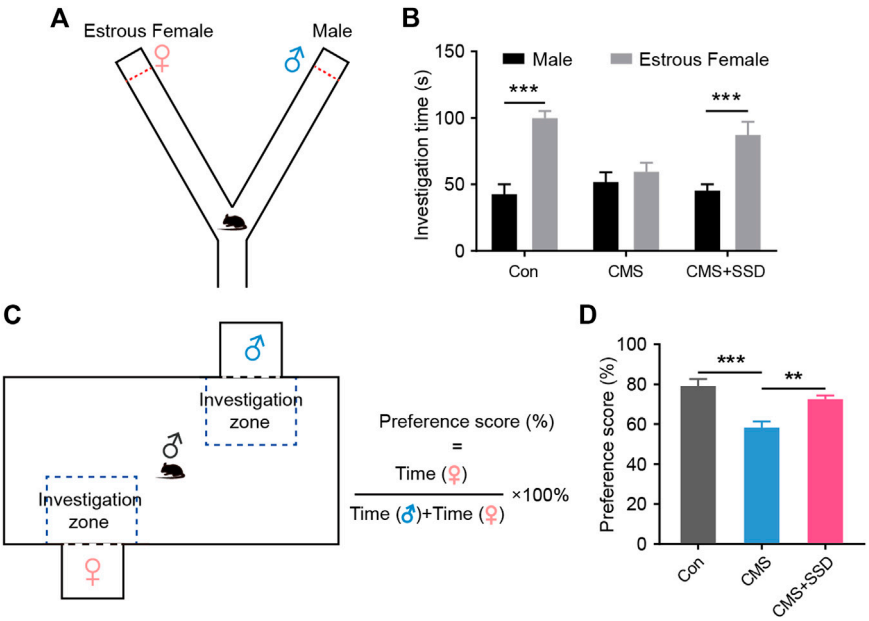

FIGURE 2 | The effect of saikosaponin D (SSD) on sexual preference and sexual motivation in chronic mild stress (CMS) mice. **(A)** Schematic of the Y-maze preference test. **(B)** The time spent exploring between male and estrous female. In the experimental design, we used sucrose preference test to assess depression-like behaviors of mice on a weekly basis. (n = 9, Bonferroni post hoc t-test, analysis of variance [ANOVA]). **(C)** Schematic of the mice sexual motivation test. **(D)** Preference scores for sexual motivation. (n = 9, Bonferroni post hoc t-test, ANOVA). Data are presented as the mean ± standard error of mean. **p < 0.01, ***p < 0.001.

In the MePD, we observed that the GFAP + astrocytic soma and primary processes responded sensitively to stress stimuli (**Figure 4A**). The animals in the CMS group had a lower GFAP + astrocyte density and shrunken astrocytic morphologies than those in the control group. The results of WB further confirmed the reduced GFAP expression in the MePD of CMS mice (**Figure 4B**); however, these deficits were reversed by SSD administration. Furthermore, chronic stress increased the number of Iba1-positive microglia and promote their activation in the MePD of CMS mice (**Figure 4A**).

Effects of SSD on Neuroinflammation and Oxidative Stress in the MePD

Nextly, we tested whether SSD could attenuated neuroinflammation and inhibiting the oxidative stress. We performed ELISA studies to measure the IL-1β and IL-6 in the MePD immediately after the behavioral tests. CMS increased the IL-1β and IL-6 levels as compared to control group, the treatment of SSD significantly decreased the IL-1β and IL-6 levels in MePD of the mice as compared to CMS group (**Figures 4C,D**). CMS induces significantly increased ROS production compared with

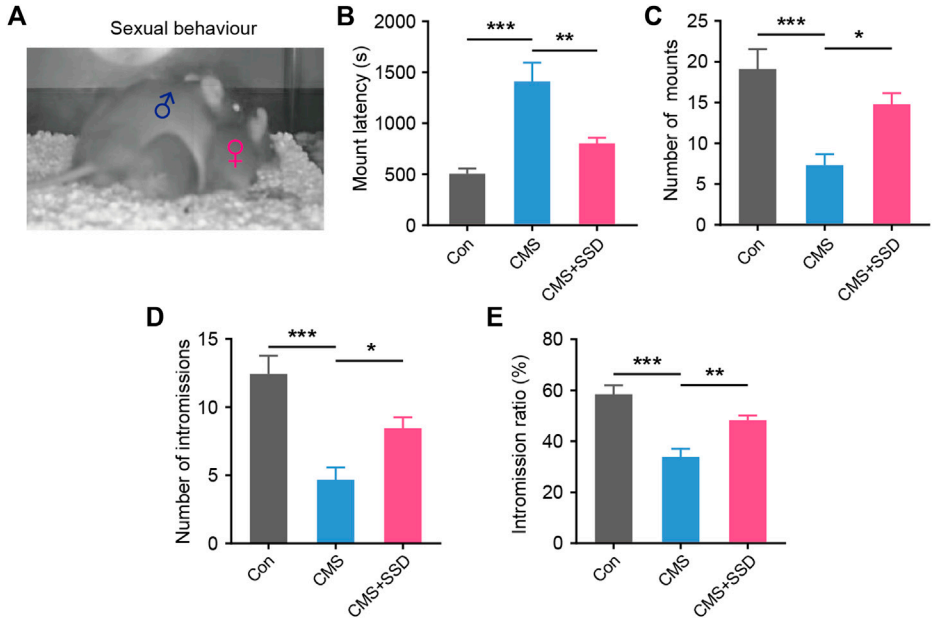

FIGURE 3 | The effect of saikosaponin D (SSD) on sexual activity parameters in CMS mice. **(A)** Schematic of the sexual activity experimental. Levels of sexual behavior after three weeks' SSD administration: **(B)** mounting latency; **(C)** total mount; **(D)** intromission frequency; **(E)** the time ratio of intromission and mount. (n = 9, one-way analysis of variance [ANOVA]). Data are presented as the mean ± standard error of mean. *$p < 0.05$, **$p < 0.01$, ***$p < 0.001$.

the control, however, SSD treatment effectively mitigate the elevation of the ROS levels in the MePD of the mice (**Figure 4E**).

Neural Plasticity in the MePD of CMS Mice After SSD Administration

Two weeks before the end of the CMS modeling, we infected MePD neurons with AAV-CMV-GFP. We measured the spine density in these local pyramidal neuronal cells that were tagged with GFP to reveal the morphological characteristics (**Figure 5A**). Spines protruding from second order dendrites were separately assessed for distal dendrites. The CMS mice showed significantly decreased spine density arising from the distal second order dendrites than that in the normal control mice (**Figure 5B**). The spines of dendrites in the SSD-treated group showed a significant reversion of the above-stated deficit. Consistent with the abovementioned observation, the expression of the neuronal marker MAP2 was decreased in CMS mice (**Figure 5C**), whereas MAP2 expression was significantly increased in the MePD of CMS+SSD mice.

Effects of SSD on Neural Firing Activity in the MePD

The firing rate of MePD neurons was measured by inserting an electrode into the brain (**Figures 6A,B**). CMS modeling significantly decreased the firing rate of MePD neurons (**Figure 6C**). This decreased neuronal firing was reversed in CMS+SSD group, which indicated that the restoration of the firing properties of the MePD may underpin the effects of SSD.

DISCUSSION

Mood disorders, such as depression, are mainly caused by chronic stress or stressful events, with a high lifetime prevalence of reaching 20% (Patten, 2003). Sexual dysfunction, characterized by decreased sexual motivation and impaired sexual performance, is a major comorbidity in men with depression (Clayton et al., 2013) and current therapies are only partially effective, with a slow onset of efficacy, and may even lead to more severe sexual dysfunction (Atmaca, 2020). In the present study, we found that treatment with SSD can not only generate a stable antidepressant effect but also significantly alleviate sexual dysfunctions in CMS mice. We explored the central brain mechanisms underlying chronic stress-induced sexual dysfunction in mice. Pathological changes and neuroinflammation were observed in the glial and neuronal cells of the MePD of CMS mice; they may be involved in the manifestation of stress-induced sexual dysfunction. We speculated that the restoration of sexual activity by SSD may be due to its participation in the neurotrophic protection of the MePD.

Antidepressants prescribed by psychiatrists, such as serotonin reuptake inhibitors, have the well-known adverse effect of affecting sexual activity (Ishak et al., 2013; Clayton et al., 2015); these drugs may further aggravate the negative consequences on depression-induced impairment in sexual activity and affect patients' quality of life, which could leading to patients' resistance to medication and treatment failure. These male patients with impaired sexual function often report these sexual symptoms and seek help from andrologists, who often lack in-depth understanding of the brain mechanisms implicated in

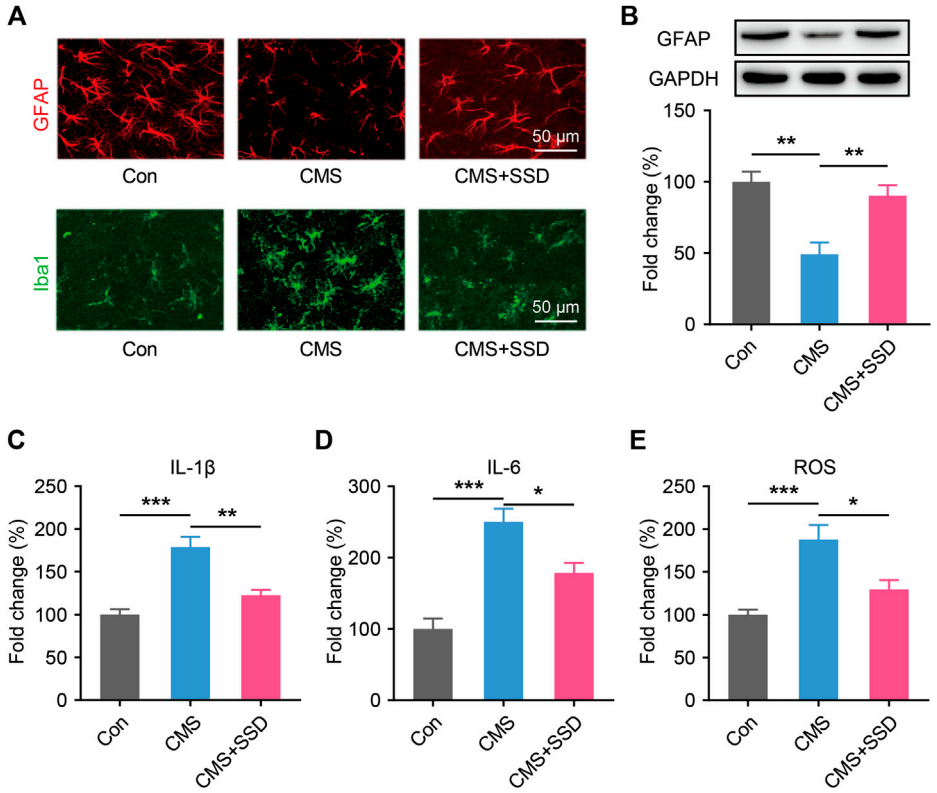

FIGURE 4 | The changes in glia markers, neuroinflammation and oxidative stress in the MePD. **(A)** Astrocytes and microglia were immunofluorescent staining with glial fibrillary acid protein (GFAP; red) and Iba1 (green) after CMS and saikosaponin D treatment. (Scale bar = 50 μm). **(B)** Expression patterns of GFAP by western blotting. (n = 5, one-way analysis of variance [ANOVA]). **(C–E)** IL-1β, IL-6 and reactive oxygen species in the MePD were detected by enzyme-linked immunosorbent assay and presented as fold change (%). (n = 5, one-way ANOVA). Data are presented as the mean ± standard error of mean. *$p < 0.05$, **$p < 0.01$, ***$p < 0.001$.

this syndrome; moreover, available treatments are mainly focused on providing symptomatic management, without a curative intent. Hence, there is an urgent need in this field for further interdisciplinary research.

The animal model of CMS has been widely used in studies on depression, which simulates various types of stress stimuli encountered by men in the current society (Brotto et al., 2001). The sexual dysfunction induced by this modeling strategy has been widely reported, such as reduced sexual motivation (Shen et al., 2020), nonorganic erectile dysfunction (Chen et al., 2019), impaired sexual behavior (Brotto et al., 2001), testicular damage (Hou et al., 2014), etc. In contrast, there is scarce information about the implications of central psychophysical mechanisms originating from the CNS. As a common clinical auxiliary therapy, TCM has been reported to have a therapeutic role in the regulation of emotions and sexual activity (Wang et al., 2019a; Ren et al., 2019). Bupleurum is the main ingredient in TCM prescriptions for the treatment of depression and sexual dysfunction (Lu et al., 2018). As the main active ingredient of Bupleurum, SSD has been reported to have antidepressant effects in rats (Li et al., 2017). However, it remains to be explored whether this effect involves modulation of sexual activity. Herein, we modeled CMS in mice and systematically analyzed the sexual motivation and performance of the CMS mice. SSD treatment improved depression-related behaviors in these mice, while also improving sexual motivation and performance. These findings are exciting and point toward the multi-modal effects of SSD.

Increasing evidence has revealed that the male reproduction system is extensively regulated by the CNS (Nadelhaft and Vera, 1996; Bancila et al., 2002), thus providing a new perspective to better understand related brain/reproductive system axis diseases. Sexual dysfunction caused by stress is not simply an symptom related to anhedonia associated with the reward system. As an instinctive behavior, sexual activity is linked to a conservative, intrinsic regulatory brain region (Kondo, 1992). Only few studies have analyzed stress-induced sexual dysfunction in terms of the pathophysiological and functional changes in the brain nuclei associated with sexual functions. As the subnucleus in the amygdala is closely related to sexual activity, MePD is evolutionarily conserved and plays an important role in arousal and the execution of human sexual behavior (Kühn and Gallinat, 2011; Seok et al., 2016). The MePD is considered to be a key integrator of systemic arousal and sexual sensory stimulation and is involved in both emotional regulation and sexual performance (Rasia-Filho et al., 2012; Bergan et al., 2014; Holder and Mong, 2017), thus we explore its potential

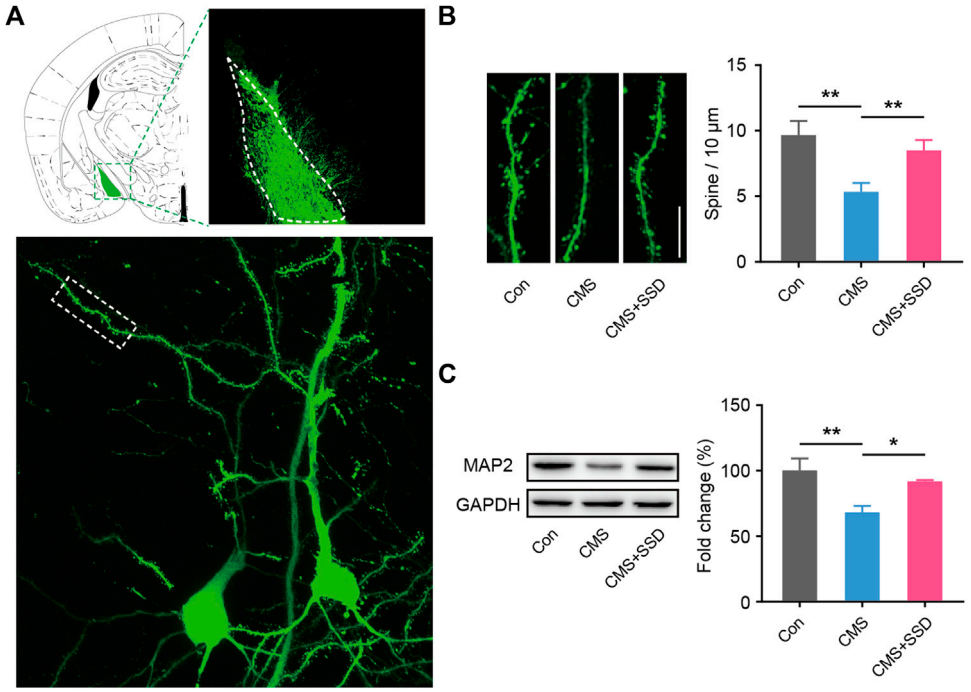

FIGURE 5 | Changes in neural spine density in the MePD. **(A)** Schematic of the viral injection, and the representative neuron imaged by Z-stacked confocal microscopy. **(B)** Spine density was expressed as the number of spines per 10 μm. (n = 12 slices from three mice, 5–6 neuron per slice, one-way analysis of variance [ANOVA]). (Scale bar = 10 μm). **(C)** MAP2 expression was determined by a western blotting analysis. (n = 5, one-way ANOVA). Data are presented as the mean ± standard error of mean. *p < 0.05, **p < 0.01.

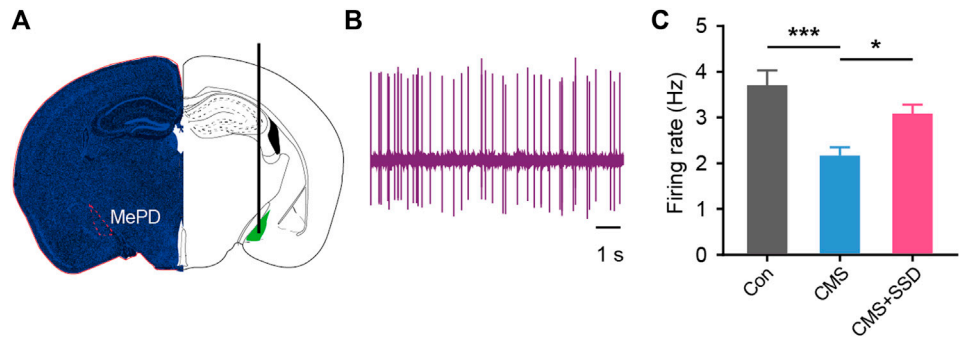

FIGURE 6 | Recording of the *in vivo* activity of MePD neurons. **(A,B)** Location of the recording site and spontaneous firing activity electrophysiological properties of recorded neurons. **(C)** Statistical results of firing rate of MePD neurons from each group. (n = 12, one-way analysis of variance). Data are presented as the mean ± standard error of mean. *p < 0.05, ***p < 0.001.

contribution in the psychological stresses-related sexual dysfunction.

Astrocytes are the most abundant cells in the CNS (Namihira and Nakashima, 2013) and have been found to play an important role in stress-induced behavioral abnormalities (Jun et al., 2018); however, their function in the MePD remains largely unknown. During CMS modeling, astrocytes, which are involved in the initiation of neuroinflammation, are activated in the hippocampus (Du Preez et al., 2021). However, regarding the astrocytes in the MePD, the depressive-like symptoms are associated with a decreased density and hypofunction of astrocytes, which is expected to contribute to synaptic dysfunction in the MePD. Our results showed that the number, volume, and protrusion length of MePD astrocytes were decreased in male mice experiencing chronic stress, thus reducing the plasticity of astrocytes in local brain regions. SSD had a protective effect on astrocytes, which could antagonize the CMS-induced damage to astrocytes and enhance their plasticity. Stress can cause a vicious cycle, increasing microglial activation and neuroinflammatory dysfunction (Calcia et al., 2016). In this

study, under condition of CMS, microglial activation and neuroinflammation were significantly increased in the MePD. CMS promoted proinflammatory microglial activation, microgliosis, and increased the concentration of inflammatory markers, such as interleukins, and increased ROS expression in the MePD. The effects of SSD in inhibiting microglia activation and neuroinflammation are consistent with those reported in previous reports (Su et al., 2020).

Chronic stress can significantly affect the synaptic plasticity and neuronal activity of the amygdala subnucleus (Marcuzzo et al., 2007), which suggests that CMS may produce changes in synaptic plasticity-related neural functions in the MePD. After observing the morphology of local neurons in the MePD, we found that the density of dendritic spines in the pyramidal neurons decreased significantly, suggesting weakened connections between the neurons. The electrophysiological results further showed impaired neuronal activity in the MePD, revealing that chronic stress caused synaptic plasticity-related impairment in neural functions in the MePD, and that SSD treatment can effectively reverse these changes. During the above processes, astrocytes are involved in the regulation of local neural activity (Chih and Roberts, 2003). Changes in astrocyte polarization were implicated in the abnormal neural information processing. Deepening understanding of the function of astrocytes and SSD's psychopharmacological target in the MePD are worthy of future research focus. In addition, the MePD receives projections from upstream brain regions and sends signals down to its related brain regions, the MePD-related circuit mechanisms implicated in this brain-related sexual dysfunction still warrant further investigation.

Taken together, our results have shown for the first time that SSD has a dual therapeutic effect on stress-induced depression and stress-induced sexual dysfunction. Our data provide significant evidence in support of the presence of glial and neural pathologies in an animal model of brain-related sexual dysfunction diseases (BRSDD). These findings broaden our psychopharmacological insights into the role of SSD and lay the foundation for the development of novel potential therapeutic strategies to treat BRSDD.

DATA AVAILABILITY STATEMENT

The raw data supporting the conclusions of this article will be made available by the authors, without undue reservation.

ETHICS STATEMENT

The animal study was reviewed and approved by Animal ethics committee of The Third Affiliated Hospital of Sun Yat-sen University.

AUTHOR CONTRIBUTIONS

Conceived and designed the research: JC, PQ, and GZ. Performed the experiments: ZW, JL,WW, TQ, ZH, BW, SL, CL, XW, JD., YZ, PH, ZZ, YH, JH, and QH Analyzed the data: ZW, JL, and WW Contributed reagents/materials/analysis tools: PH and QH Wrote the paper: JC and ZW. All authors edited and approved of the final manuscript.

FUNDING

This work was supported by grants from the National Natural Science Foundation of China (NSFC no. 81871158, 82001528), China Postdoctoral Science Foundation (no. 2020M672991), and Traditional Chinese Medicine Bureau of Guangdong Province Scientific Research Project (no. 20201340).

REFERENCES

Atmaca, M. (2020). Selective serotonin reuptake inhibitor-induced sexual dysfunction: current management perspectives. *Neuropsychiatr Dis. Treat.* 16, 1043–1050. doi:10.2147/ndt.s185757

Bancila, M., Giuliano, F., Rampin, O., Mailly, P., Brisorgueil, M. J., Calas, A., et al. (2002). Evidence for a direct projection from the paraventricular nucleus of the hypothalamus to putative serotoninergic neurons of the nucleus paragigantocellularis involved in the control of erection in rats. *Eur. J. Neurosci.* 16 (7), 1240–1248. doi:10.1046/j.1460-9568.2002.02184.x

Barry, T. J., Murray, L., Fearon, P., Moutsiana, C., Johnstone, T., and Halligan, S. L. (2017). Amygdala volume and hypothalamic-pituitary-adrenal axis reactivity to social stress. *Psychoneuroendocrinology*. 85, 96–99. doi:10.1016/j.psyneuen.2017.07.487

Becker, A. E., and Kleinman, A. (2013). Mental health and the global agenda. *N. Engl. J. Med.* 369 (1), 66–73. doi:10.1056/NEJMra1110827

Benelli, A., Bertolini, A., Zoli, M., Leo, G., Filaferro, M., Saltini, S., et al. (2002). Pharmacological manipulation of brain galaninergic system and sexual behavior in male mice. *Psychopharmacology (Berl).* 160 (3), 325–330. doi:10.1007/s00213-001-0992-z

Bergan, J. F., Ben-Shaul, Y., and Dulac, C. (2014). Sex-specific processing of social cues in the medial amygdala. *Elife.* 3, e02743. doi:10.7554/eLife.02743

Bogren, M., Brådvik, L., Holmstrand, C., Nöbbelin, L., and Mattisson, C. (2018). Gender differences in subtypes of depression by first incidence and age of onset: a follow-up of the Lundby population. *Eur Arch Psychiatry Clin. Neurosci*. 268 (2), 179–189. doi:10.1007/s00406-017-0778-x

Breyer, B. N., Cohen, B. E., Bertenthal, D., Rosen, R. C., Neylan, T. C., and Seal, K. H. (2014). Sexual dysfunction in male Iraq and Afghanistan war veterans: association with posttraumatic stress disorder and other combat-related mental health disorders: a population-based cohort study. *J. Sex. Med.* 11 (1), 75–83. doi:10.1111/jsm.12201

Brotto, L. A., Gorzalka, B. B., and LaMarre, A. K. (2001). Melatonin protects against the effects of chronic stress on sexual behaviour in male rats. *Neuroreport.* 12 (16), 3465–3469. doi:10.1097/00001756-200111160-00018

Calcia, M. A., Bonsall, D. R., Bloomfield, P. S., Selvaraj, S., Barichello, T., and Howes, O. D. (2016). Stress and neuroinflammation: a systematic review of the effects of stress on microglia and the implications for mental illness. *Psychopharmacology (Berl).* 233 (9), 1637–1650. doi:10.1007/s00213-016-4218-9

Cao, X., Li, L. P., Wang, Q., Wu, Q., Hu, H. H., Zhang, M., et al. (2013). Astrocyte-derived ATP modulates depressive-like behaviors. *Nat. Med.* 19 (6), 773–777. doi:10.1038/nm.3162

Chao, B., Huang, S., Pan, J., Zhang, Y., and Wang, Y. (2020). Saikosaponin d downregulates microRNA-155 and upregulates FGF2 to improve depression-like behaviors in rats induced by unpredictable chronic mild stress by negatively

regulating NF-κB. *Brain Res. Bull.* 157, 69–76. doi:10.1016/j.brainresbull.2020.01.008

Chen, G., Chen, J., Yang, B., Yu, W., Chen, Y., and Dai, Y. (2019). Dopamine D2 receptors in the basolateral amygdala modulate erectile function in a rat model of nonorganic erectile dysfunction *Andrologia.* 51 (1), e13160. doi:10.1111/and.13160

Chih, C. P., and Roberts, E. L., Jr. (2003). Energy substrates for neurons during neural activity: a critical review of the astrocyte-neuron lactate shuttle hypothesis. *J Cereb Blood Flow Metab.* 23 (11), 1263–1281. doi:10.1097/01.wcb.0000081369.51727.6f

Chu, X., and Ågmo, A. (2016). The adrenergic α2-receptor, sexual incentive motivation and copulatory behavior in the male rat. *Pharmacol. Biochem. Behav.* 144, 33–44. doi:10.1016/j.pbb.2016.02.008

Clayton, A. H., Gommoll, C., Chen, D., Nunez, R., and Mathews, M. (2015). Sexual dysfunction during treatment of major depressive disorder with vilazodone, citalopram, or placebo: results from a phase IV clinical trial. *Int. Clin. Psychopharmacol.* 30 (4), 216–223. doi:10.1097/yic.0000000000000075

Clayton, A. H., Kennedy, S. H., Edwards, J. B., Gallipoli, S., and Reed, C. R. (2013). The effect of vilazodone on sexual function during the treatment of major depressive disorder. *J. Sex. Med.* 10 (10), 2465–2476. doi:10.1111/jsm.12004

Deumic, E., Butcher, B. D., Clayton, A. D., Dindo, L. N., Burns, T. L., and Calarge, C. A. (2016). Sexual functioning in adolescents with major depressive disorder. *J Clin Psychiatry.* 77 (7), 957–962. doi:10.4088/JCP.15m09840

Drevets, W. C. (2003). Neuroimaging abnormalities in the amygdala in mood disorders. *Ann. N. Y. Acad. Sci.* 985, 420–444. doi:10.1111/j.1749-6632.2003.tb07098.x

Du Preez, A., Onorato, D., Eiben, I., Musaelyan, K., Egeland, M., Zunszain, P. A., et al. (2021). Chronic stress followed by social isolation promotes depressive-like behaviour, alters microglial and astrocyte biology and reduces hippocampal neurogenesis in male mice. *Brain Behav. Immun.* 91, 24–47. doi:10.1016/j.bbi.2020.07.015

El Yazidi, F. E., Boualame, A., Akammar, S., Zahrae Elfahiri, F., Aitbenlaassel, O., Adali, I., et al. (2019). [Prevalence and characteristics of sexual dysfunction among Moroccan patients consulting for a first depressive episode]. *Encephale.* 45 (6), 501–505. doi:10.1016/j.encep.2019.06.003

Grønli, J., Murison, R., Fiske, E., Bjorvatn, B., Sørensen, E., Portas, C. M., et al. (2005). Effects of chronic mild stress on sexual behavior, locomotor activity and consumption of sucrose and saccharine solutions. *Physiol. Behav.* 84 (4), 571–577. doi:10.1016/j.physbeh.2005.02.007

Hammen, C. (2018). Risk factors for depression: an autobiographical review. *Annu. Rev. Clin. Psychol.* 14, 1–28. doi:10.1146/annurev-clinpsy-050817-084811

Holder, M. K., and Mong, J. A. (2017). The role of ovarian hormones and the medial amygdala in sexual motivation. *Curr. Sex Health Rep.* 9 (4), 262–270. doi:10.1007/s11930-017-0131-4

Hosain, G. M., Latini, D. M., Kauth, M., Goltz, H. H., and Helmer, D. A. (2013). Sexual dysfunction among male veterans returning from Iraq and Afghanistan: prevalence and correlates. *J. Sex. Med.* 10 (2), 516–523. doi:10.1111/j.1743-6109.2012.02978.x

Hou, G., Xiong, W., Wang, M., Chen, X., and Yuan, T. F. (2014). Chronic stress influences sexual motivation and causes damage to testicular cells in male rats. *J. Sex. Med.* 11 (3), 653–663. doi:10.1111/jsm.12416

Ishak, W. W., Christensen, S., Sayer, G., Ha, K., Li, N., Miller, J., et al. (2013). Sexual satisfaction and quality of life in major depressive disorder before and after treatment with citalopram in the STAR*D study. *J Clin Psychiatry.* 74 (3), 256–261. doi:10.4088/JCP.12m07933

Jun, M., Xiaolong, Q., Chaojuan, Y., Ruiyuan, P., Shukun, W., Junbing, W., et al. (2018). Calhm2 governs astrocytic ATP releasing in the development of depression-like behaviors. *Mol Psychiatry.* 23 (4), 1091. doi:10.1038/mp.2017.254

Kühn, S., and Gallinat, J. (2011). A quantitative meta-analysis on cue-induced male sexual arousal. *J. Sex. Med.* 8 (8), 2269–2275. doi:10.1111/j.1743-6109.2011.02322.x

Kedo, O., Zilles, K., Palomero-Gallagher, N., Schleicher, A., Mohlberg, H., Bludau, S., et al. (2018). Receptor-driven, multimodal mapping of the human amygdala. *Brain Struct. Funct.* 223 (4), 1637–1666. doi:10.1007/s00429-017-1577-x

Kondo, Y. (1992). Lesions of the medial amygdala produce severe impairment of copulatory behavior in sexually inexperienced male rats. *Physiol. Behav.* 51 (5), 939–943. doi:10.1016/0031-9384(92)90074-c

Li, H. Y., Zhao, Y. H., Zeng, M. J., Fang, F., Li, M., Qin, T. T., et al. (2017). Saikosaponin D relieves unpredictable chronic mild stress induced depressive-like behavior in rats: involvement of *HPA axis and hippocampal neurogenesis.* 234 (22), 3385–3394. doi:10.1007/s00213-017-4720-8

Liu, C. C., Wu, Y. F., Feng, G. M., Gao, X. X., Zhou, Y. Z., Hou, W. J., et al. (2015). Plasma-metabolite-biomarkers for the therapeutic response in depressed patients by the traditional Chinese medicine formula Xiaoyaosan: a (1)H NMR-based metabolomics approach. *J. Affect. Disord.* 185, 156–163. doi:10.1016/j.jad.2015.05.005

Lu, J., Fu, L., Qin, G., Shi, P., and Fu, W. (2018). The regulatory effect of Xiaoyao San on glucocorticoid receptors under the condition of chronic stress. *Cell Mol Biol (Noisy-le-grand).* 64 (6), 103–109. doi:10.14715/cmb/2018.64.6.17

Ménard, C., Hodes, G. E., and Russo, S. J. (2016). Pathogenesis of depression: insights from human and rodent studies. *Neuroscience.* 321, 138–162. doi:10.1016/j.neuroscience.2015.05.053

Marcuzzo, S., Dall'oglio, A., Ribeiro, M. F., Achaval, M., and Rasia-Filho, A. A. (2007). Dendritic spines in the posterodorsal medial amygdala after restraint stress and ageing in rats. *Neurosci. Lett.* 424 (1), 16–21. doi:10.1016/j.neulet.2007.07.019

Montejo, A. L., Calama, J., Rico-Villademoros, F., Montejo, L., González-García, N., and Pérez, J. (2019). A real-world study on antidepressant-associated sexual dysfunction in 2144 outpatients: the SALSEX I study. *Arch. Sex. Behav.* 48 (3), 923–933. doi:10.1007/s10508-018-1365-6

Nadelhaft, I., and Vera, P. L. (1996). Neurons in the rat brain and spinal cord labeled after pseudorabies virus injected into the external urethral sphincter. *J. Comp. Neurol.* 375 (3), 502–517. doi:10.1002/(sici)1096-9861(19961118)375:3<502::aid-cne11>3.0.co;2-n

Namihira, M., and Nakashima, K. (2013). Mechanisms of astrocytogenesis in the mammalian brain. *Curr. Opin. Neurobiol.* 23 (6), 921–927. doi:10.1016/j.conb.2013.06.002

Patten, S. B. (2003). Recall bias and major depression lifetime prevalence. *Soc Psychiatry Psychiatr Epidemiol.* 38 (6), 290–296. doi:10.1007/s00127-003-0649-9

Petrulis, A., and Johnston, R. E. (1999). Lesions centered on the medial amygdala impair scent-marking and sex-odor recognition but spare discrimination of individual odors in female golden hamsters. *Behav. Neurosci.* 113 (2), 345–357. doi:10.1037//0735-7044.113.2.345

Qin, X. H., Wu, Z., Dong, J. H., Zeng, Y. N., Xiong, W. C., Liu, C., et al. (2019). Liver soluble epoxide hydrolase regulates behavioral and cellular effects of chronic stress. *Cell Rep.* 29 (10), 3223–3234.e6. doi:10.1016/j.celrep.2019.11.006

Qiu, J., Hu, S. Y., Shi, G. Q., and Wang, S. E. (2014). Changes in regional cerebral blood flow with Chaihu-Shugan-San in the treatment of major depression. *Pharmacogn Mag.* 10 (40), 503–508. doi:10.4103/0973-1296.141775

Rasia-Filho, A. A., Haas, D., de Oliveira, A. P., de Castilhos, J., Frey, R., Stein, D., et al. (2012). Morphological and functional features of the sex steroid-responsive posterodorsal medial amygdala of adult rats. *Mini Rev. Med. Chem.* 12 (11), 1090–1106. doi:10.2174/138955712802762211

Ren, F., Ma, Z., Shen, Y., Li, G., You, Y., Yu, X., et al. (2019). Effects of Chaihu-Shugan-San capsule for psychogenic erectile dysfunction: study protocol of a randomized placebo-controlled trial. *Medicine (Baltim.).* 98 (46), e17925. doi:10.1097/md.0000000000017925

Seok, J. W., Sohn, J. H., and Cheong, C. (2016). Neural substrates of sexual arousal in heterosexual males: event-related fMRI investigation. *J. Physiol. Anthropol.* 35, 8. doi:10.1186/s40101-016-0089-3

Shen, Y., He, D., He, L., Bai, Y., Wang, B., Xue, Y., et al. (2020). Chronic psychological stress, but not chronic pain stress, influences sexual motivation and induces testicular autophagy in male rats. *Front. Psychol.* 11, 826. doi:10.3389/fpsyg.2020.00826

Sokolowski, K., and Corbin, J. G. (2012). Wired for behaviors: from development to function of innate limbic system circuitry. *Front. Mol. Neurosci.* 5, 55. doi:10.3389/fnmol.2012.00055

Su, J., Pan, Y. W., Wang, S. Q., Li, X. Z., Huang, F., and Ma, S. P. (2020). Saikosaponin-d attenuated lipopolysaccharide-induced depressive-like behaviors via inhibiting microglia activation and neuroinflammation. *Int Immunopharmacol.* 80, 106181. doi:10.1016/j.intimp.2019.106181

Tollefson, G. D. (1991). Antidepressant treatment and side effect considerations. *J Clin Psychiatry.* 52 (Suppl), 4–13.

Tynan, R. J., Beynon, S. B., Hinwood, M., Johnson, S. J., Nilsson, M., Woods, J. J., et al. (2013). Chronic stress-induced disruption of the astrocyte network is

driven by structural atrophy and not loss of astrocytes. *Acta Neuropathol.* 126 (1), 75–91. doi:10.1007/s00401-013-1102-0

Vinkers, C. H., Bijlsma, E. Y., Houtepen, L. C., Westphal, K. G., Veening, J. G., Groenink, L., et al. (2010). Medial amygdala lesions differentially influence stress responsivity and sensorimotor gating in rats. *Physiol. Behav.* 99 (3), 395–401. doi:10.1016/j.physbeh.2009.12.006

Wang, B., Lu, S., Zhang, C., Zhu, L., Li, Y., Bai, M., et al. (2020). Quantitative proteomic analysis of the liver reveals antidepressant potential protein targets of Sinisan in a mouse CUMS model of depression. *Biomed. Pharmacother.* 130, 110565. doi:10.1016/j.biopha.2020.110565

Wang, L., Zhang, Y., Du, X., Ding, T., Gong, W., and Liu, F. (2019a). Review of antidepressants in clinic and active ingredients of traditional Chinese medicine targeting 5-HT1A receptors. *Biomed. Pharmacother.* 120, 109408. doi:10.1016/j.biopha.2019.109408

Wang, Z., Zeng, Y. N., and Yang, P. (2019b). Axonal iron transport in the brain modulates anxiety-related behaviors. *Nat Chem Biol.* 15 (12), 1214–1222. doi:10.1038/s41589-019-0371-x

Xu, L., Su, J., Guo, L., Wang, S., Deng, X., and Ma, S. (2019). Modulation of LPA1 receptor-mediated neuronal apoptosis by Saikosaponin-d: a target involved in depression. *Neuropharmacology.* 155, 150–161. doi:10.1016/j.neuropharm.2019.05.027

Conflict of Interest: The authors declare that the research was conducted in the absence of any commercial or financial relationships that could be construed as a potential conflict of interest.

frontiers in Pharmacology

ORIGINAL RESEARCH
published: 25 February 2021
doi: 10.3389/fphar.2021.612078

Fisetin Rescues the Mice Brains Against D-Galactose-Induced Oxidative Stress, Neuroinflammation and Memory Impairment

*Sareer Ahmad, Amjad Khan, Waqar Ali, Myeung Hoon Jo, Junsung Park, Muhammad Ikram and Myeong Ok Kim**

Division of Life Science and Applied Life Science (BK 21 Plus), College of Natural Sciences, Gyeongsang National University, Jinju, South Korea

Herein, we have evaluated the protective potentials of Fisetin against D-galactose-induced oxidative stress, neuroinflammation, and memory impairment in mice. D-galactose (D-gal) causes neurological impairment by inducing reactive oxygen species (ROS), neuroinflammation, and synaptic dysfunction, whereas fisetin (Fis) is a natural flavonoid having potential antioxidant effects, and has been used against different models of neurodegenerative diseases. Here, the normal mice were injected with D-gal (100 mg/kg/day for 60 days) and fisetin (20 mg/kg/day for 30 days). To elucidate the protective effects of fisetin against D-galactose induced oxidative stress-mediated neuroinflammation, we conducted western blotting, biochemical, behavioral, and immunofluorescence analyses. According to our findings, D-gal induced oxidative stress, neuroinflammation, synaptic dysfunctions, and cognitive impairment. Conversely, Fisetin prevented the D-gal-mediated ROS accumulation, by regulating the endogenous anti-oxidant mechanisms, such as Sirt1/Nrf2 signaling, suppressed the activated *p*-JNK/NF-kB pathway, and its downstream targets, such as inflammatory cytokines. Hence, our results together with the previous reports suggest that Fisetin may be beneficial in age-related neurological disorders.

Keywords: d-galactose, fisetin, neurodegeneration, aging model, phytonutrient

OPEN ACCESS

Edited by:
Muhammad Ayaz,
University of Malakand, Pakistan

Reviewed by:
Sagheer Ahmed,
Shifa Tameer-e-Millat University, Pakistan
Waqas Tahir,
University of Calgary, Canada
Faheem Ullah,
Florida International University, United States

****Correspondence:***
Myeong Ok Kim
mokim@gnu.ac.kr

Specialty section:
This article was submitted to Ethnopharmacology, a section of the journal Frontiers in Pharmacology

Received: *30 September 2020*
Accepted: *08 January 2021*
Published: *25 February 2021*

Citation:
Ahmad S, Khan A, Ali W, Jo MH, Park J, Ikram M and Kim MO (2021) Fisetin Rescues the Mice Brains Against D-Galactose-Induced Oxidative Stress, Neuroinflammation and Memory Impairment. Front. Pharmacol. 12:612078. doi: 10.3389/fphar.2021.612078

INTRODUCTION

Aging is a cause of several chronic diseases, including diabetes mellitus, cardiovascular diseases, cancer, and neurological disorders such as Alzheimer's disease (AD), Parkinson's disease (PD), and Huntington's disease (HD) (Khan et al., 2018). Several studies have indicated that elevated ROS level is responsible for different neurodegenerative conditions in various age-associated disorders such as AD, PD, and diabetes (Olanow, 1993; Khan et al., 2019a). The elevated oxidative stress triggers cellular damage to the macromolecules (proteins, lipids, and DNA), which disturbs the physiological functions of the central nervous system (CNS), leading to neurodegeneration (Paradies et al., 2011). Thus, the neurodegeneration caused by elevated oxidative stress could be a therapeutic target to tackle age-related diseases neurodegenerative diseases. To develop neuroprotective strategies against age-related neurological disease, different animal models have been developed. One of the known models is the D-gal injected animal model.

Chronic administration of D-gal induces brain aging and accelerates artificial senescence which is used for different anti-aging pharmacological research (Cui et al., 2006). D-gal is a monosaccharide, which exists throughout the body. At higher concentrations, in the presence of galactose oxidase, it converts to hydrogen peroxide and aldose, causing disposition of a superoxide anion, oxygen-derived free radicals, and cellular damage (Lu et al., 2007). Chronic administration of D-galactose for 2 months induces cognitive and memory impairment through the accumulated ROS, mitochondrial deficits, neuroinflammation, and neurodegeneration (Zhang et al., 2007).

Recently, the use of phytonutrients and medicinal herbs have gained a special interest to treat neurological disorders such as AD (Huang and Mucke, 2012; Shah et al., 2017b). Among the phytonutrients, Fisetin (3,7,3′,4′-tetrahydroxyflavone), a natural flavonoid is found in different fruits, such as legumes, mangoes, kiwis, strawberries, grapes, cucumbers, nuts, beans, and onions. Fisetin has shown strong anticarcinogenic, anti-inflammatory, antioxidant, neurotrophic, and neuroprotective effects against different neurodegenerative diseases (Khan et al., 2013; Currais et al., 2014; Echeverry et al., 2015; Maher, 2015).

Here, we explore the underlying neuroprotective mechanism of Fis against D-gal-induced aging in mice. We have targeted the main cell survival mechanisms of the brain, such as silent information regulator transcript-1 (SIRT1), Nuclear factor erythroid 2-related factor 2 (Nrf-2), and Heme oxygenase (HO-1). The Sirt1 is a nicotinamide adenine dinucleotide (NAD)-dependent nuclear histone deacetylase, which is involved in the modulation of several cell survival mechanisms, e.g., regulation of calorie restriction and improving the lifespan, cellular metabolic processes, cells senescence, apoptotic cell death, oxidative stress, neuroinflammation, histones deacetylating and non-histone proteins in the body. The deacetylation by SIRT1 may inhibit the transcriptional activation of NF-kB, and neuroinflammation (Shah et al., 2017a).

The transcription factor Nrf2 encodes antioxidant enzymes, regulates the repair of damaged proteins and organelles, neuroinflammation, and mitochondrial homeostasis. The function of Nrf2 is affected in several neurodegenerative conditions, such as Alzheimer's disease, Parkinson's (Khan et al., 2020), and multiple sclerosis. Pharmacological modulators of Nrf2 have shown promising effects in neurodegenerative conditions.

Prion disease is a group of neurodegenerative diseases affecting humans and animal species. The conversion of a non-pathogenic normal cellular protein (PrP^{c}) into an abnormal pathogenic form prion protein scrapie (PrP^{Sc}), is considered the cause of the disease. The PrP^{Sc} aggregates in the individual's brain, causing an elevation of oxidative stress, by reducing the expression of Nrf2. And, boosting the level of Nrf2 may reduce the severity of the disease (Shah et al., 2018). Studies have suggested that regulation of Nrf2 may provide an opportunity to delay the progression of this disease (Dinkova-Kostova et al., 2018; Ikram et al., 2019a).

Among the neuroinflammatory factors, Mitogen-Activated Protein Kinases (MAPK), such as *p*-JNK play a critical role in the execution of neuroinflammation. Another factor is the NF-kB, which regulates multiple adaptive and innate immune functions and serves as a pivotal mediator of inflammatory reaction (Liu et al., 2017). The activation of NF-κB has been widely implicated in the normal aging processes, which aggravates the release of inflammatory cytokines and activation of astrocytes and microglial cells, such as ionized calcium-binding adaptor molecule 1 (Iba-1), and GFAP respectively (Ullah et al., 2020b; Kim et al., 2020).

The present study was undertaken to analyze the effects of Fisetin against D-gal-induced elevated ROS, neuroinflammation, and cognitive dysfunction in mice. Herein, we hypothesize that Fisetin may reduce oxidative stress and neuroinflammation by regulating cell survival (SIRT1/Nrf2) and inflammatory (*p*-JNK) mechanisms. Collectively, here we hypothesize that Fisetin may regulate the oxidative stress-mediated neuroinflammation, apoptotic cell death and cognitive dysfunctions in D-gal treated mice.

MATERIALS AND METHODS

Animals Handling, Grouping, and Ethical Approval

The study included wild-type mice (C57BL/6N) having 26–29 g of body weight and 9 weeks of age. The mice were obtained from Samtako Bio (Osan, South Korea). The study was conducted under the approved guidelines of the Institutional Animal Care and Use Committee (IACUC) of the Division of Applied Life Science, Gyeongsang National University, South Korea (approval ID: 125). To acclimatize, all animals (total number of mice = 60, the number of mice per group = 20, and 10 mice for Western blot and 10 for immunofluorescence analysis) were kept for 7 days in the animal house under a 12/12 h light/dark cycle at control temperature (23°C) with 60 ± 10% humidity. The animals were freely provided with food and water.

Chemicals and Antibodies

Fisetin (Lot#SLBF3913V) and D-galactose (sc-202564) were procured from Sigma-Aldrich Chemical Co. (St. Louis, MO, United States). The drugs were dissolved in 0.1% dimethyl sulfoxide (DMSO) and the final volume was adjusted with normal saline (0.9% saline). The control mice were injected with normal saline.

The antibodies used in the current studies are: SIRT1 (sc-74465), anti-Nrf2 (sc-722), anti-HO-1 (sc-136,961), P-JNK (sc-625), anti-p-NF-κβ (sc-136,548), anti-Iba-1 (sc-32,725),anti-GFAP (sc-33673) anti-interleukin (IL-1β) (sc-32,294), anti-tumor necrosis factor-α (TNF-α) (sc-52,746), NOS-2 (sc-651), anti-Bax (sc-7480) anti-Bcl2 (sc-7382), cleaved Caspase-3 (sc-7272), anti-PARP-1 (sc-8007), anti-PSD-95 (sc-71,933), anti-synaptosomal-associated protein 23 (SNAP-25), and anti-β-actin (sc-47,778) (Santa Cruz Biotechnology, Dallas, TX, United States). The primary antibodies were diluted in 1× TBST (1:1,000), and secondary anti-mouse HRP (horseradish peroxidase) conjugated (Promega Ref# W402) and anti-rabbit HRP conjugated (Promega Ref# W401) were diluted 1:10,000 in

1 M TBST (Promega, Fitchburg, WI, United States); the secondary antibodies (anti-mouse Ref# A11029 and anti-rabbit Ref# 32,732) used in the immunofluorescence studies were diluted in 1:100 in 1 M PBS.

Mice Grouping and Drugs Administration

The mice were randomly divided into the following three groups 1) Mice injected with saline as a control group. 2) Mice administered with D-gal (100 mg/kg/day i. p for 2 months, one month before, and one month co-treated with Fisetin). 3) Mice administered with D-gal and Fis (20 mg/kg/day i. p for 1 month). The alone group was not considered for the analysis, as no side effects of Fis have been reported previously. The dose of Fis was selected based on previously conducted studies (Rehman et al., 2017). After the completion of the treatment, the behavioral study of the male mice was conducted by using the Y-maze test followed by the Morris water maze (MWM) **Figure 1**.

Y-Maze Test

To conduct the behavioral studies, the mice were randomly divided into three groups, and the cages were labeled with numbers (so that the experimenters were unaware of the mice grouping). Y-maze test was conducted to analyze the spatial working memory, as performed previously (Khan et al., 2018; Muhammad et al., 2019). The Y-maze had three arms, having 50 cm in length, 10 cm in width, and 20 cm in height. The mouse was put at the center of the maze and allowed to explore the maze for 8 min (three times), and the arm entries were observed visually. The Spontaneous alternation was defined as the consecutive entry of the mice into the three arms in coinciding triplet sets. The alternation behavior (% age) was calculated as successive triplet sets/(total number of arm entries–2) × 100.

Morris Water Maze Test

The apparatus used for the MWM is made up of a circular water tank 40 cm in height and 100 cm in diameter. The tank was filled with water (23 ± 1°C) to a depth of 15.5 cm and was made opaque by adding non-toxic white ink. A platform (20 cm in height, 10 cm in diameter) was placed 1 cm below the water surface in one quadrant. The mice were trained for four consecutive days (four trials per day). The latency to reach the hidden platform was calculated for each trial. After completion of the training the probe test was conducted, where the mice were subjected to swim freely in the tank for 1 min (in the absence of platform). Here, the time spent in the target quadrant, and three non-quadrants (right, left, and opposite), and the number of crossings were recorded through a video detective system (SMART, Panlab Harvard Apparatus, United States).

Protein Extraction From Mice Brains for the Western Blot

After the behavioral studies, the mice were sacrificed and the brains were extracted and the sections (cortex and hippocampus) were carefully dissected, and homogenized in PRO-PREP extraction solution (iNtRON, Seoul South Korea). After homogenization, the brain tissues were centrifuged at 13,000 rpm at 4°C for 24 min, and the supernatants were collected and preserved at (−80°C) for further experimentations.

Western Blotting

The amount of protein loaded in each well was calculated using the Bio-Rad solution (Bio-Rad protein assay kit, Bio-Rad Laboratories, CA, United States) (Muhammad et al., 2018; Khan et al., 2019a). Equal amounts of proteins 18–20 µg were loaded in the gel under similar experimental conditions. A broad-range prestained protein marker (GangNam STAIN™, iNtRON) was loaded for the determination of the exact molecular weight. To avoid the non-specific binding the membranes were blocked in 5% (w/v) skim milk and incubated with the primary antibodies (overnight at 4°C). The membranes were washed and treated with horseradish peroxidase-conjugate (HRP)-a secondary antibody, and the expressions were detected using an ECL detection reagent, according to the instructions (Amersham, Uppsala, Sweden). The optical densities of the bands were analyzed through ImageJ software.

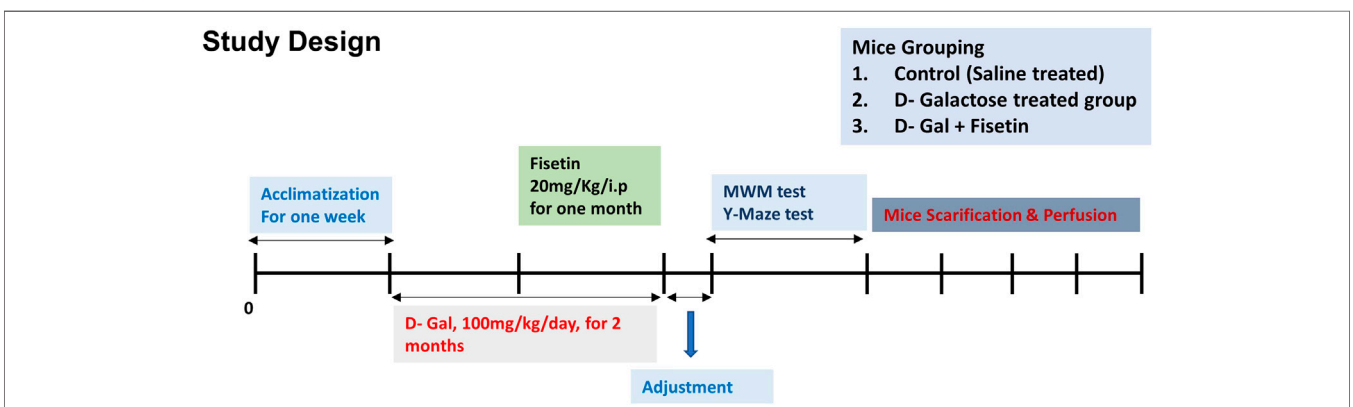

FIGURE 1 | Study design and animal treatments. Figure showing the mice grouping, handling, drug treatment, and experimental design.

Preparation of the Samples for the Immunofluorescence Studies

The mice were perfused transcardially with saline followed by transfusion with ice-cold 4% neutral buffer paraformaldehyde. The brains were fixed in 4% paraformaldehyde for 72 h, followed by incubation in 20% sucrose for 48 h. After that, the brains were fixed in the frozen O.C.T. compound (Tissue-Tek O.C.T. compound medium, Sakura Finetek United States, Inc., Torrance, CA, United States). The 14 μm coronal plane sections were cut using a CM 3050 S Cryostat (Leica, Berlin Germany). The sections were taken on the gelatin-coated slide and used for further experiments.

Immunofluorescence Staining

The immunofluorescence staining was conducted as described previously (Ikram et al., 2019b; Muhammad et al., 2019). The slides were washed with 0.01 M PBS, followed by incubation for 1 h in 2% normal goat serum and 0.3% Triton X-100 in PBS. After that, the slides were treated with primary antibodies diluted in PBS. After the primary antibody treatment, the slides were treated with appropriate secondary antibodies (TRITC or FITC-labeled) (Santa Cruz Biotechnology, Dallas Texas United States). For the nuclear staining, the slides were incubated with 4′,6-diamidino-2-phenylindole (DAPI). The immunoreaction was visualized using a confocal laser-scanning microscope (Fluoview FV 1000 MPE, Olympus, Tokyo, Japan). Through ImageJ, the relative integrated densities were evaluated among the experimental groups, which sums all of the pixels within a region and gives a total value. And the obtained values were compared among the experimental groups.

ROS and LPO Assays

The ROS assay was conducted according to the established protocols (Ikram et al., 2019b). The assay is based on the oxidation of 7-dichlorodihydrofluorescein diacetate (DCFH-DA) to 2, 7-dichlorodihydrofluorescein (DCF). In short, the brain tissue homogenates (Cortical and Hippocampal) were used for this assay. The tissue homogenate was diluted in 1 ml of Locke's buffer (1:20 ratio), 10 ml of DCFH-DA (5 mM), and 0.2 ml of tissue to a final concentration of 5 mg tissue/mL, followed by incubation for 15 min to get a fluorescent DCF. The converted fluorescent DCF was measured using a spectrofluorometer (excitation at 484 nm and emission at 530 nm). A parallel blank was used for background fluorescence (conversion of DCFH-DA in the absence of homogenate). The data has been presented as picomole DCF formed per minute per milligram of the protein. For the evaluation of LPO, the free malondialdehyde (MDA) was analyzed in the brain samples, for which MDA colorimetric/fluorometric kit (Cat #K739–100) was used, a detailed description has been given previously (Badshah et al., 2019).

Fluoro-Jade B Staining

The Fluoro-Jade B (Burlington, MA, United States, Cat #AG310, Lot #2159662) staining was performed as conducted previously (Ikram et al., 2019b). The slides were dipped in 1% sodium hydroxide and 80% ethanol for 5 min, followed by treatment with 70% ethanol for 2 min. After that, the slides were rinsed with D-water and transferred into a potassium permanganate solution (0.06%) for 10 min, washed with D-water, and kept in 0.1% acetic acid solution and 0.01% Fluoro-Jade B solution for 20 min. After the treatment, the slides were washed with D-water and dried. The sections were covered, and the images were taken using a confocal laser microscope (FV 1000, Olympus, Tokyo, Japan). And, the integrated density was used for the immunofluorescence intensity, for which the ImageJ software (wsr@nih.gov, https://imagej.nih.gov/ij/) was used.

Evaluations and Statistical Analysis

ImageJ software was used to measure the values for western blot and immunofluorescence analysis. The data has been presented as mean ± SEM (three independent experiments for 20 mice per group: 10 for immunofluorescence and 10 for Western blot). For statistical analysis, we used GraphPad Prism v6 (GraphPad Software), where one-way ANOVA followed by student's t-test was used to differentiate among the experimental groups. p values less than 0.05 was considered to be statistically significant $^{*}p < 0.05$, $^{**}p < 0.01$ represent control vs. D-gal treated mice, $\#p < 0.05$, $\#\#p < 0.01$ represent D-gal vs. D-gal + Fis.

RESULTS

Effects of Fisetin Against D-Galactose-Induced Oxidative Stress in Mice Brains

To analyze the antioxidant effects of Fisetin, we performed the ROS and LPO assays, which showed that D-gal increased the levels of LPO and ROS, which were partially reduced with the administration of Fisetin (**Figures 2A**,**B**). Also, we analyzed the expression of SIRT1/Nrf-2 and HO-1 in the experimental mice brains through western blot. According to our findings, there was a significant downregulation in the expression of SIRT1, Nrf-2, and HO-1 in the D-gal-injected mice brains, compared to the control group. Notably, these markers were upregulated in the D-gal + Fisetin co-treated mice, compared to the D-Gal injected mice (**Figure 2C**). These results were further confirmed with the immunofluorescence analysis, which showed that Fisetin significantly enhanced the expression of SIRT1 and Nrf-2 in the Fisetin-treated mice brains (**Figures 2D**,**E**).

Protective Effects of Fisetin Against D-Gal-Induced Neuroinflammation in Mice Brains

The elevated ROS level may induce the expression of JNK and NF-kB, which contributes to neuroinflammation in animal models (Rehman et al., 2017). So, we evaluated the expression of *p*-JNK, Iba-1, and GFAP in the experimental groups through the immunofluorescence analysis. According to our findings, there was a significant increase in the expression of *p*-JNK,

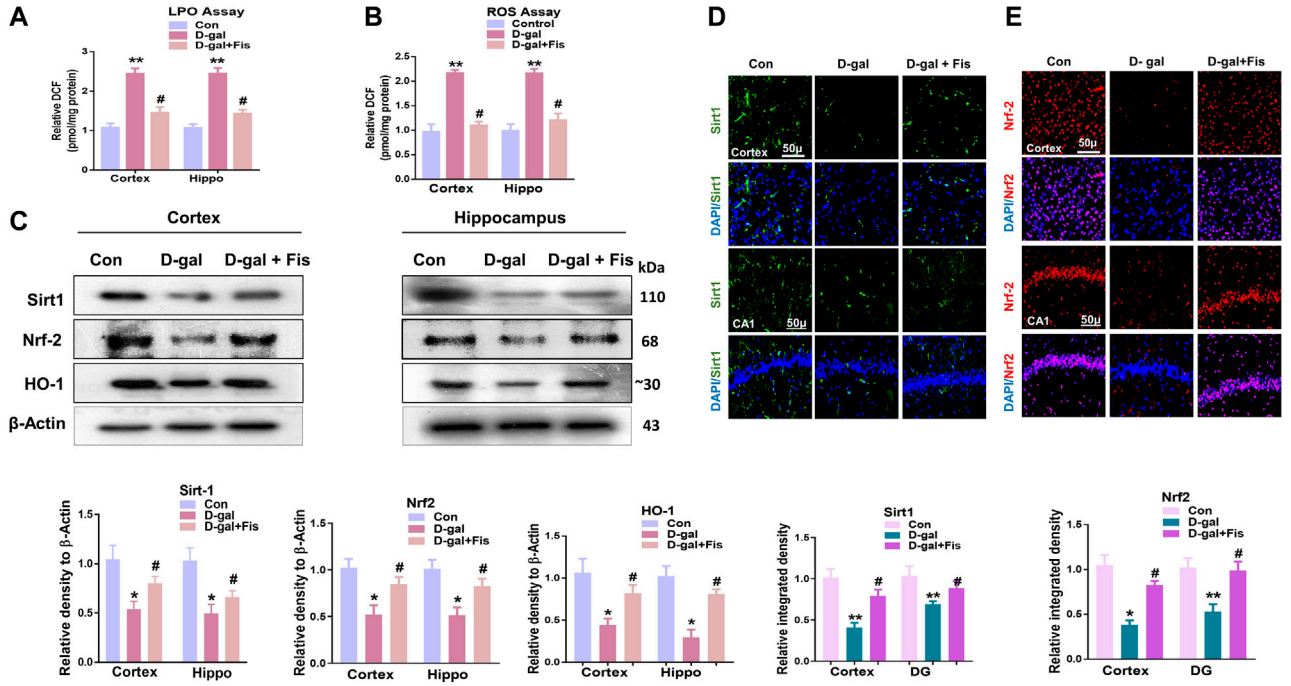

FIGURE 2 | Fisetin regulates Sirt-1/Nrf2/HO-1 signaling pathway in mice brains (A and B). LPO and ROS assays *in vivo*. **(C)**. Western blots results of SIRT1/Nrf2/HO-1 in the experimental groups, with respective bar graphs. β- Actin was used as a loading control **(D and E)**. Immunofluorescence images of SIRT1 and Nrf2 with respective bar graphs Magnifications ×10. Scale bar 50 μm $n = 10$ mice per group for western blot and immunofluorescence analysis, number of experiments = 3. $^{*}p < 0.05$, $^{**}p < 0.01$ represent control vs. D-gal treated mice, $\#p < 0.05$, $\#\#p < 0.01$ represent D-gal vs. D-gal + fisetin. LPO: Lipid peroxidation, ROS: Reactive Oxygen Species, Con: Control, D-gal: D-galactose, Fis: Fisetin, Hippo: *Hippocampus*.

Iba-1, and GFAP in the D-gal treated mice brains, which was reduced in the D-gal + Fis co-treated groups (**Figures 3A–C**). Moreover, the western blot results also showed that D-gal-treated mice showed increased expression of p- JNK, JNK p-NF-Kβ, NF-Kβ, Iba-1, GFAP, IL-1β, TNF-α, and NOS-2 in the D-gal-treated mice brains, whereas Fisetin significantly reduced the expression of these markers compared to the D-gal-treated mice (**Figure 3D**).

Effects of Fisetin on the Expressions of Apoptotic Markers in the Mice Brains

The elevated oxidative stress causes the activation of *p*-JNK which may mediate the apoptotic signalings (Tournier et al., 2000; Liu and Lin, 2005). To show the effects of Fisetin against apoptotic cell death, we analyzed the expressions of cleaved Caspase-3, cleaved PARP-1, and Bax, and Bcl-2 in the D-gal-treated mice brains. Our findings suggested that Fisetin significantly reduced the expression of pro-apoptotic markers (cleaved-Caspase-3. Cleaved-PARP-1 and Bax), and enhanced the expression of anti-apoptotic markers (Bcl-2) in the Fisetin-injected mice brains (**Figure 4A**). Further, the immunofluorescence results of Caspase-3 showed enhanced activation of Caspase-3 in D-gal-treated mice brains which were reduced in the Fisetin-treated mice brains (**Figure 3B**). Similarly, the Fluorojad B staining also showed reduced Fluorojad B positive cells in fisetin-treated mice brains, compared to the D-gal injected mice (**Figure 3C**).

Effects of Fisetin Against the Synaptic Dysfunctions in the D-Gal Treated Mice

Next, we evaluated the expressions of synaptic proteins in the experimental groups. According to our findings, there was a significant downregulation in the expression of synaptic proteins such as SNAP-25 and PSD-95 in the D-gal treated mice compared to the control group, which were upregulated in the Fisetin-treated group (**Figure 5A**). Moreover, the immunofluorescence analyses also showed reduced expression of PSD-95 in the D-gal-treated mice brains compared to the control group, which were upregulated in the Fisetin-treated mice brains (**Figure 5B**). Collectively, our findings suggested that Fisetin reversed the D-gal-induced synaptic dysfunction in D-galactose-treated mice brains (**Figure 5**).

Effects of Fisetin Against Cognitive Dysfunctions in D-Gal Treated Mice

To assess the effects of fisetin on the cognitive dysfunctions, we performed Y-maze followed by MWM tests. For the evaluation of the spatial working memory, the Y-maze test was conducted. Our results indicated that D-gal-injected mice exhibited less number of spontaneous alternations compared to the saline-treated control mice. Fisetin enhanced the spontaneous alternation behavior (%), showing that Fis restored the spatial working memory of the D-gal-injected mice (**Figure 6A**). Moreover, the arm entries were also considered, to analyze the effects of

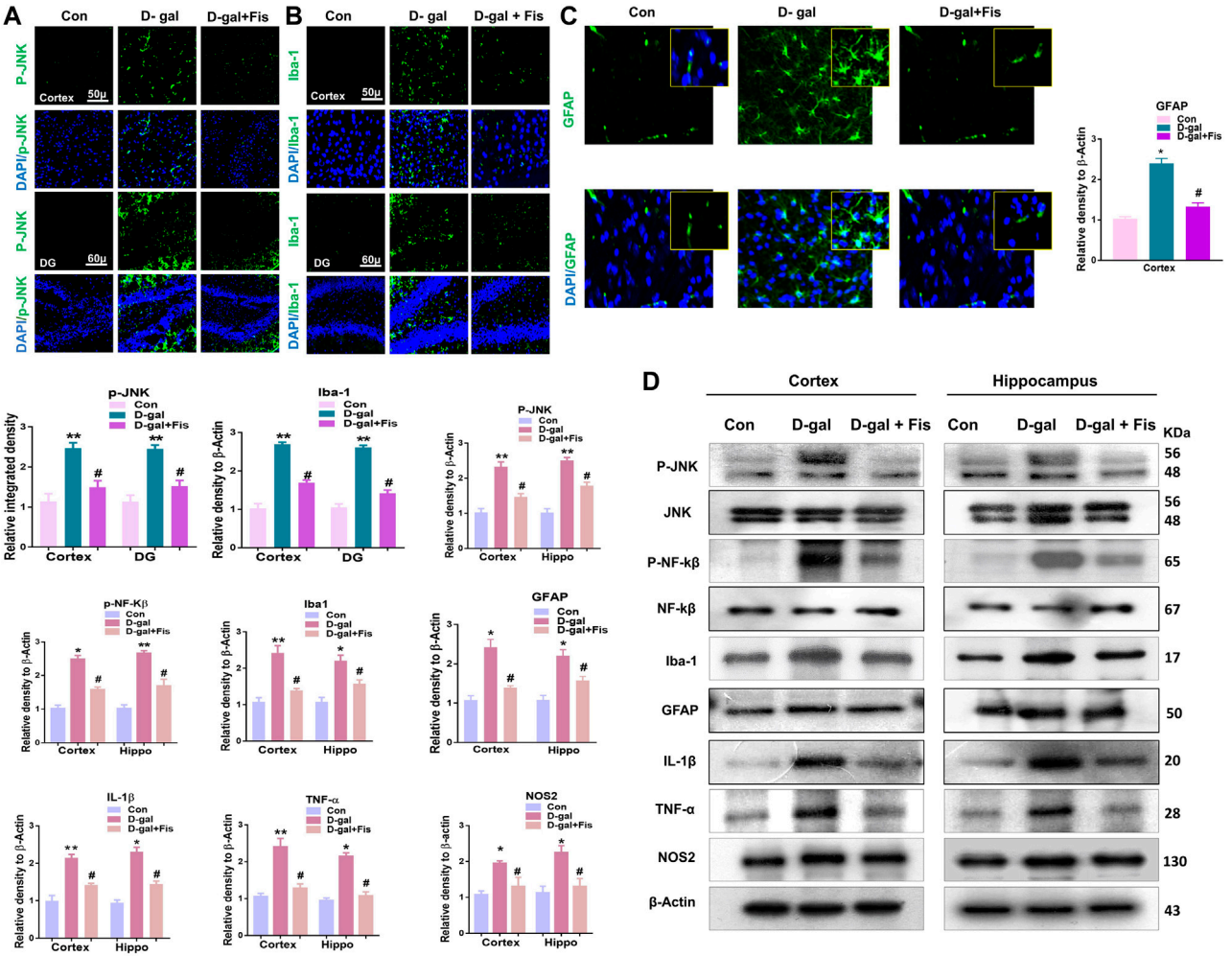

FIGURE 3 | Fisetin ameliorates the expression of JNK and its associated inflammatory mediators in D-galactose injected mice (A,B and C). Immunofluorescence results of *p*-JNK, Iba-1, and GFAP in the experimental mice's brains. **(D)**. Western blot results of *p*-JNK, JNK p-NF-Kβ, NF-Kβ, IL-1β, Iba-1, GFAP, TNF-α, and NOS-2 in the experimental mice's brains. β- Actin was used as a loading control. $n = 10$ mice per group for western blot and immunofluorescence analysis, number of experiments = 3. $^{*}p < 0.05$, $^{**}p < 0.01$ represent control vs. D-gal treated mice, $\#p < 0.05$, $\#\#p < 0.01$ represent D-gal vs. D-gal + fisetin. LPO: Lipid peroxidation, ROS: Reactive Oxygen Species, Con: Control, D-gal: D-galactose, Fis: Fisetin, Hippo: *Hippocampus*, DG: Dentate Gyrus.

Fisetin on the motor performance of mice, which suggested that the number of arm entries was markedly upregulated with the administration of Fisetin, compared to the D-gal treated mice as shown in (**Figure 6B**).

For the analysis of the memory formation, we performed the MWM test. In the MWM test, the mice were trained to find a submerged hidden platform, if failed to find the platform, the mice were guided to the platform. After the training session, we analyzed the time required to arrive at the hidden platform position. The D-gal-injected mice took more time (increased latency time) to reach the hidden platform compared to the control mice. Interestingly, Fisetin reversed the D-galactose effects and enhanced the memory function, as indicated by the mice taking less time to arrive at the hidden platform compared to the D-gal-treated mice (**Figures 6C,D**). Furthermore, a probe test was conducted, which demonstrated that Fisetin reversed the D-galactose effects, and increased the number of platform crossings, time spent in the target quadrant (**Figures 6E,F**). Also, we checked the swimming speed, to show the effects of Fisetin on motor performance. According to our findings, fisetin significantly improved the swimming speed of the mice in the MWM test, compared to the D-galactose injected mice (**Figure 6G**).

DISCUSSION

The current study was investigated the antioxidant and neuroprotective effects of Fisetin against D-galactose-induced oxidative stress, neuroinflammation, and memory dysfunctions in mice. Our findings suggested that D-gal induces oxidative stress, neuroinflammation, apoptotic cells, and memory impairment in mice. Interestingly, these effects were markedly reduced with the administration of Fisetin, as confirmed by western blotting, immunofluorescence analysis, and behavioral studies.

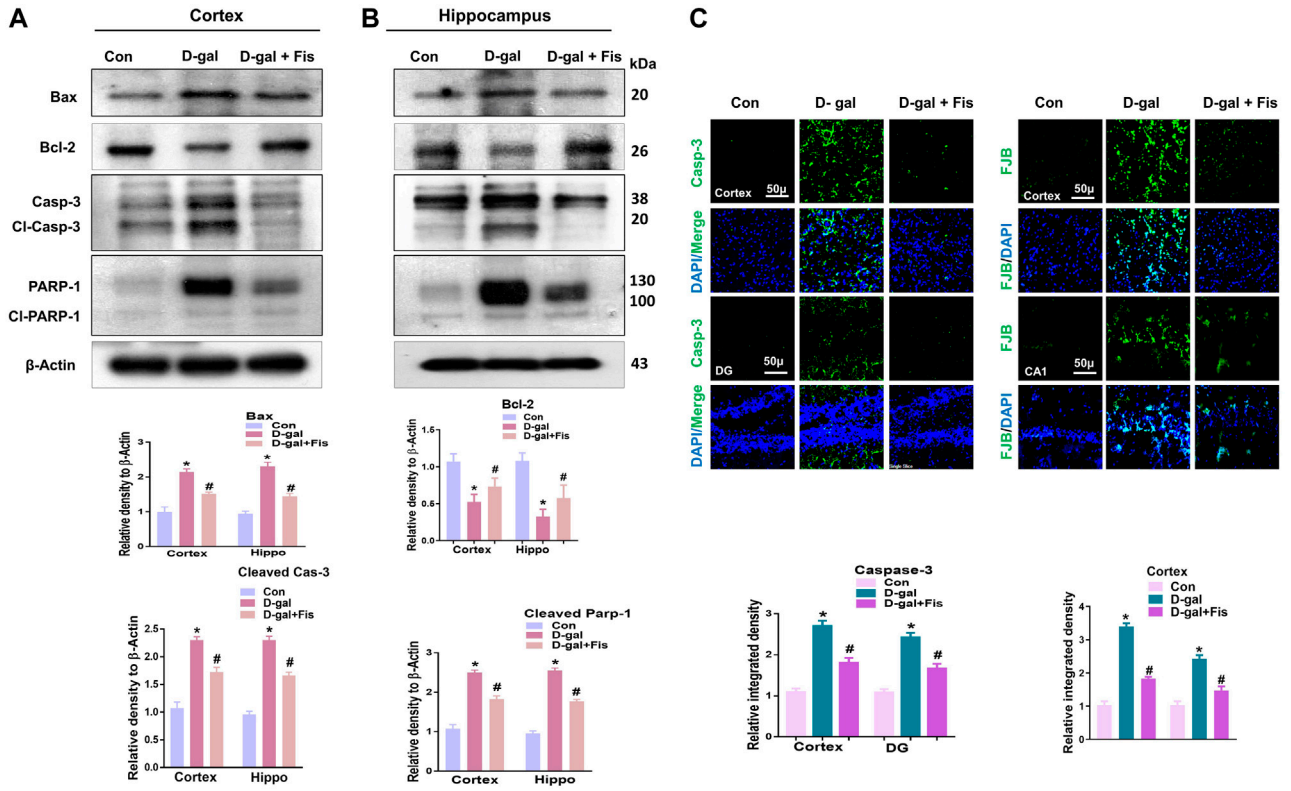

FIGURE 4 | Effects of Fisetin against the apoptotic cell death in the D-gal-treated mice Brains. **(A)**. Western blots results of Bax, Bcl2, cleaved caspase-3, and cleaved PARP-1 in the mice brains **(B and C)** Immunofluorescence results of caspase-3 and flourojade-B in the experimental mice brains. β- Actin was used as a loading control. Values are the means ± SEM from three independent experiments. Magnifications ×10, Scale bar 50 μm *n* = 10 mice per group for western blot and immunofluorescence analysis, number of experiments = 3. *Significantly different from normal mice # significantly different from D-gal-treated mice, respectively; **p* < 0.05, ***p* < 0.01 represent control vs. D-gal treated mice, #*p* < 0.05, ##*p* < 0.01 represent D-gal vs. D-gal + fisetin. Con: Control, D-gal: D-galactose, Fis: Fisetin, Hippo: *Hippocampus*, DG: Dentate Gyrus.

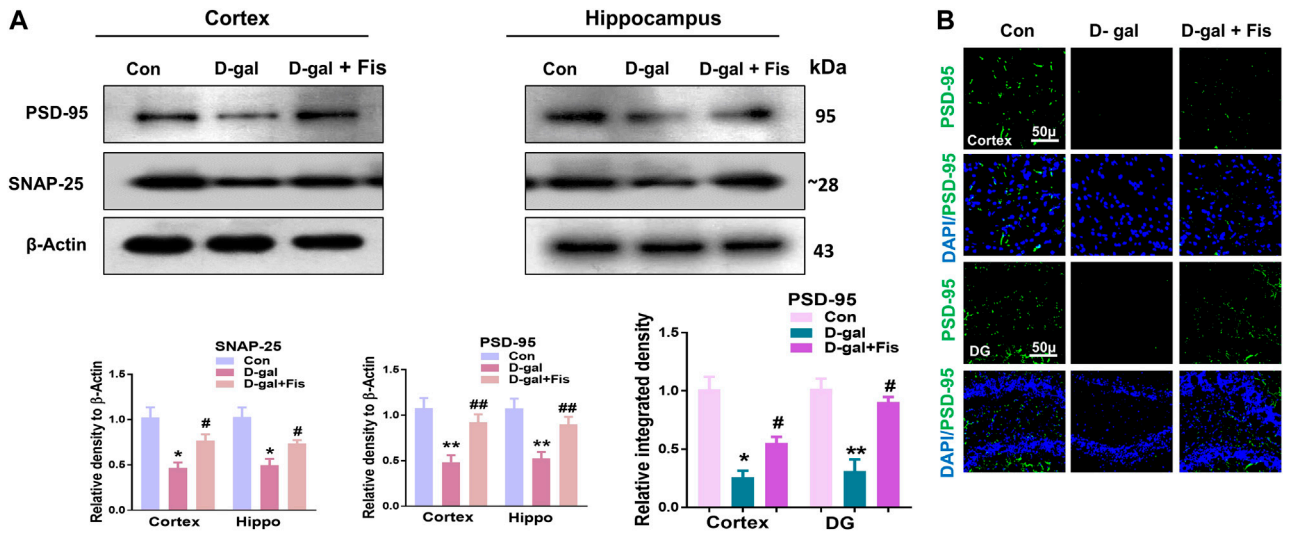

FIGURE 5 | Effects of Fisetin against the synaptic dysfunction in D-gal-treated mice. **(A)**. Western blot resulted in SNAP-25 and PSD-95 in the experimental mice, β-Actin was used as a loading control. **(B)**. Immunofluorescence images of PSD-95 in the cortex and hippocampus of the treated groups. Magnification ×10. Scale bar 50 μm *n* = 10 mice per group for western blot and immunofluorescence analysis, number of experiments = 3. **p* < 0.05, ***p* < 0.01 represent control vs. D-gal treated mice, #*p* < 0.05, ##*p* < 0.01 represent D-gal vs. D-gal + Fis. Con: Control, D-gal: D-galactose, Fis: Fisetin, Hippo: *Hippocampus*, DG: Dentate Gyrus.

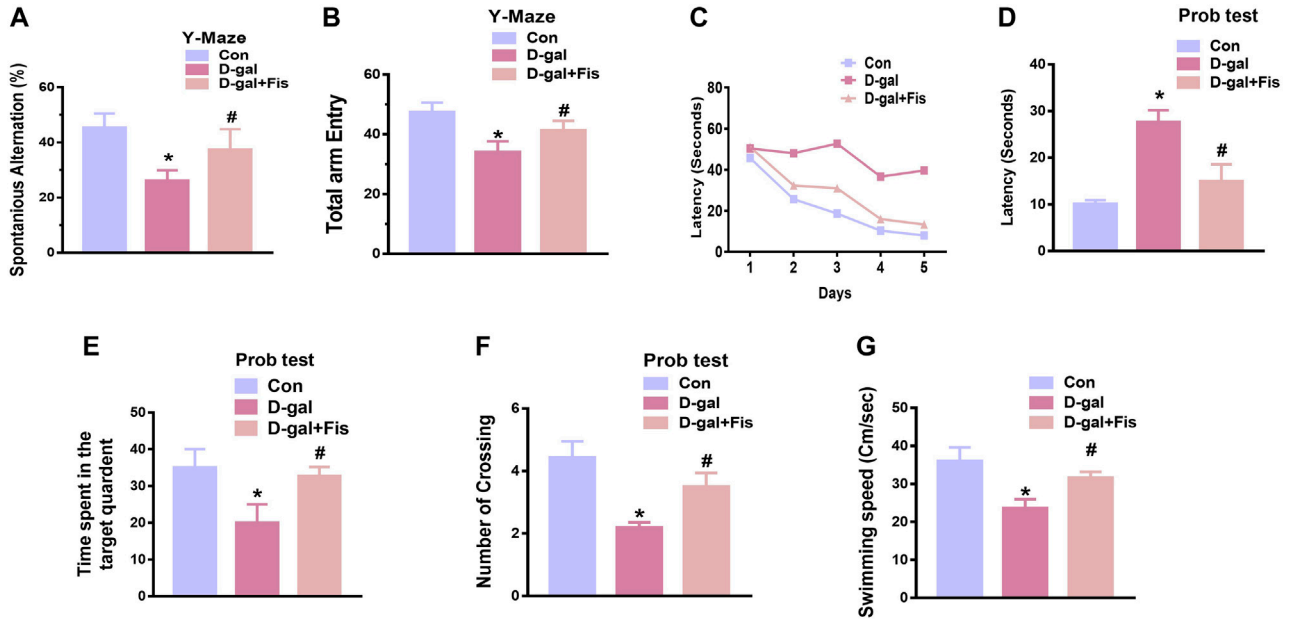

FIGURE 6 | Fisetin improved cognitive functions in the D-gal-injected mice (A and B). Histograms showing the spontaneous alternation behavior (%) and the number of arm entries in the Y-maze test. **(C)**. Latency to reach the hidden platform during the training days. **(D)**. Latency on day fifth. **(E)**. The time spent in the target quadrant during the probe test on day 5. **(F)**. The number of crossings over the hidden platform location during the probe test on day 5. **(G)**. The swimming speed of the mice in the MWM test. n = 10 mice per group for behavioral analysis, number of experiments = 3. *$p < 0.05$ represents control vs. D-gal treated mice, #$p < 0.05$, represents D-gal vs. D-gal + Fis. Con: Control, D-gal: D-galactose, Fis: Fisetin, Hippo: *Hippocampus*.

Here, we have targeted the four cardinal features of D-galactose-induced aging, i.e., oxidative stress, neuroinflammation, synaptic dysfunction, and memory impairment. Oxidative stress is the result of an imbalance in the pro-oxidant/antioxidant homeostasis leading to the generation of toxic reactive oxygen species (ROS) (Niedzielska et al., 2016). The elevated oxidative stress induces neuroinflammation and neurodegeneration in age-related diseases such as AD (Ikram et al., 2019a) and PD, and other toxin-based animal models of neurodegeneration (Khan et al., 2019a; Badshah et al., 2019).

Several studies have suggested that D-galactose induces aging in animal models, by inducing oxidative stress and neuroinflammation, which aggravate the aging process (Chang et al., 2014). The oxidative stress may be induced by several mechanisms, such as suppression of the endogenous ROS regulators, and inducing lipid peroxidation. As, during aging, there is a significant reduction in the expression of SIRT1, which is vital for different neuronal survival by reducing oxidative stress (Salminen et al., 2013). Also, the cells are endowed with an antioxidant defense mechanism mediated by Nrf2, which activates the transcription of proteins involved in oxidative stress and cytotoxicity (Xue et al., 2012). As activation of Nrf-2 targets several genes such as HO-1, which provide a defense against oxidative stress, neuroinflammation, and neuronal apoptosis, offering a substantial resistance against oxidative stress-induced neurodegeneration (Johnson et al., 2008).

To show the effects of Fisetin against the elevated oxidative stress, we analyzed the expression of SIRT1, Nrf2, and HO-1 in the experimental groups, which suggested that Fisetin significantly regulated the elevated oxidative stress in D-galactose-injected mice brains. As, the downregulation of Sirt1, Nrf-2, and HO-1 in the D-gal treated mice brain, is per the previously conducted studies (Chen et al., 2019). The findings suggest that the D-galactose-induced oxidative stress may be partly due to suppression of the endogenous antioxidant mechanisms, as suggested previously (Ahmad et al., 2019). Interestingly, Fisetin attenuated the oxidative stress, as shown by the ROS and LPO assays.

Another main contributor to the progression of neurodegeneration is inflammation (Ikram et al., 2020), as several studies have shown that D-gal-induces oxidative stress, which activates the inflammatory and apoptotic cell death pathways (Rehman et al., 2019). Several factors are responsible for the induction of neuroinflammation, such as activation of *p*-JNK, p-NF-kβ (Muhammad et al., 2019; Ali et al., 2020), and activation of astrocytes and microglial cells, as components of the innate immune system (Muhammad et al., 2019), which are activated with oxidative stress. Previous studies have suggested that chronic administration of D-gal causes activation of Caspases via *p*-JNK/NF-kβ, which are involved in the neurodegeneration (Lu et al., 2010; Khan et al., 2019a). Nuclear factor-kB, a family of homo- and heterodimeric transcription factors, playing a role in the homeostasis of the various transcription genes in response to different stimuli such as infection, inflammation, and DNA damage-induced oxidative stress (Hayden and Ghosh, 2004), and may result in activation of inflammatory mediators such as

IL-1β, TNF-α, and NOS2. Activation of NF-kB has been reported in old-aged mice (Barco and Marie, 2011). In 2013, Rehman et al. suggested that D-gal activates the *p*-JNK/NF-kB pathway (Rehman et al., 2017). Consistent with previous studies, our findings suggested increased expression of *p*-JNK/NF-κB in the D-galactose-injected mice, which were reduced in the Fisetin treated mice. The activation of *p*-JNK/NF-κB elicits other neuroinflammatory mediators and apoptosis. So, we analyzed the expression of IL-1β, TNFα, and NOS2, and other apoptotic markers such as cleaved caspases-3, cleavage PARP-1, Bcl-2, and Bax in the experimental groups, which suggested that fisetin possess strong anti-inflammatory and anti-apoptotic effects. For further confirmation, we used Fluoro-Jade B staining, which showed that, with the administration of Fisetin, there was a significant reversal in the loss of neuronal markers in the D-gal treated mice. The effects of Fisetin against neurodegeneration is in accordance with the previous studies conducted on aluminum (Prakash and Sudhandiran, 2015).

Our findings together with the previously conducted studies on the role of fisetin suggest that Fisetin has pronounced anti-inflammatory effects on neuroinflammation and apoptotic cell death (Ahmad et al., 2019). There is convincing evidence that Fisetin may inhibit the neuroinflammatory mediators, such as suppression of microglia and astrocytes (Chuang et al., 2014), as the activated astrocytes and microglia are the cardinal features of several neurodegenerative diseases (Ullah et al., 2020a) or it may reduce the inflammation by reducing the oxidative stress (Althunibat et al., 2019). The exact role of fisetin against the neuroinflallamtion needed further eluciadation.

Synaptic dysfunction has been extensively reported in age-related diseases such as AD (Ali et al., 2018). However, the exact mechanism by which D-gal causes synaptic dysfunction and neurological disorders remain unclear. Like neuroinflammation, the synaptic dysfunction may be directly triggered with the elevated oxidative stress or due to the activation of the inflammatory mediators, as both of these may affect cognition and synaptic functioning.

CONCLUSION

Collectively our results suggested that Fisetin may attenuate oxidative stress, neuroinflammation, neurodegeneration, and memory impairment in D-gal-treated mice via regulation of SIRT1, Nrf2/HO-1, and *p*-JNK/NF-kB-mediated neuroinflammation. Our study is strongly supporting the previously conducted studies on the role of Fisetin, showing that Fisetin is neuroprotective, by modulating the ionic homeostasis, thereby regulating the vital processes in the neurodegenerative conditions (Singh et al., 2019). Another study also conducted on fisetin, showing that Fisetin abrogated the D-gal induced oxidative stress and neuroinflammation by regulating the inflammatory mediators (IL-1β and TNF-α) and autophagy-related markers (Atg-3 and Beclin-1) (Singh et al., 2018). Previously conducted studies were solely based on the biochemical parameters, no behavioral studies were conducted to support the overall hypotheses. Here, we have conducted detailed synaptic and behavioral studies, which strongly supports the notion that Fisetin may regulate the age-related synaptic and memory impairment in mice. Furthermore, the SIRT1, Nrf2/HO-1 signaling regulated by fisetin is not limited to oxidative stress, and other proteins that affect neuronal apoptosis, inflammatory cytokines, cell survival, and memory performance should also be investigated. As depicted in **Figure 7**.

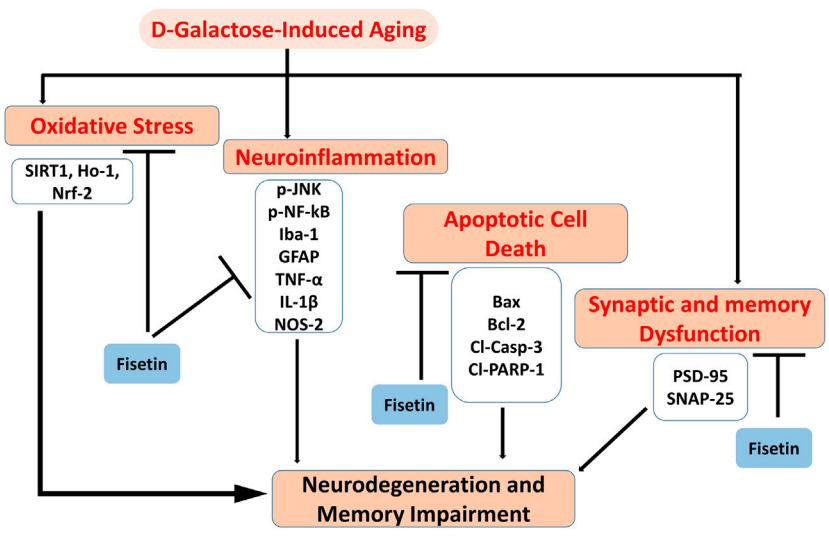

FIGURE 7 | Graphical Abstract. The diagram showing that D-galactose causes activation of oxidative stress, neuroinflammation, apoptotic cell death, and synaptic dysfunctions, and cognitive dysfunctions. Interestingly, Fisetin may exert multi-targeted neuroprotective effects by reducing oxidative stress, neuroinflammation, apoptotic cell death, and synaptic dysfunctions.

DATA AVAILABILITY STATEMENT

The original contributions presented in the study are included in the article/**Supplementary Material**, further inquiries can be directed to the corresponding author.

ETHICS STATEMENT

The animal study was reviewed and approved by Institutional Animal Care and Use Committee (IACUC) of the Division of Applied Life Science, Gyeongsang National University, South Korea (approval ID: 125).

AUTHOR CONTRIBUTIONS

SA designed and wrote the main manuscript, and performed and analyzed the *in vivo* experiments. AK helped in mice treatment. WA helped in western blot. MJ, JP, and MI prepared the final draft, and carefully reviewed the manuscript. MK comprehended the study, provided critical suggestions, and overall managed the current study. All the authors listed in the manuscript have agreed upon and reviewed the manuscript and provided feedback.

FUNDING

This research was supported by the Neurological Disorder Research Program of the National Research Foundation (NRF) funded by the Korean Government (MSIT) (2020M3E5D9080660).

SUPPLEMENTARY MATERIAL

The Supplementary Material for this article can be found online at: https://www.frontiersin.org/articles/10.3389/fphar.2021.612078/full#supplementary-material.

REFERENCES

Ahmad, A., Ali, T., Rehman, S. U., and Kim, M. O. (2019). Phytomedicine-based potent antioxidant, fisetin protects CNS-insult LPS-induced oxidative stress-mediated neurodegeneration and memory impairment. *J. Clin. Med.* 8(6), 850. doi:10.3390/jcm8060850

Ali, T., Kim, T., Rehman, S. U., Khan, M. S., Amin, F. U., Khan, M., et al. (2018). Natural dietary supplementation of anthocyanins via PI3K/Akt/Nrf2/HO-1 pathways mitigate oxidative stress, neurodegeneration, and memory impairment in a mouse model of Alzheimer's disease. *Mol. Neurobiol.* 55, 6076–6093. doi:10.1007/s12035-017-0798-6

Ali, W., Ikram, M., Park, H. Y., Jo, M. G., Ullah, R., Ahmad, S., et al. (2020). Oral administration of alpha linoleic acid rescues aβ-induced glia-mediated neuroinflammation and cognitive dysfunction in C57bl/6N mice. *Cells* 9(3), 667. doi:10.3390/cells9030667

Althunibat, O. Y., Al Hroob, A. M., Abukhalil, M. H., Germoush, M. O., Bin-Jumah, M., and Mahmoud, A. M. (2019). Fisetin ameliorates oxidative stress, inflammation and apoptosis in diabetic cardiomyopathy. *Life Sci.* 221, 83–92. doi:10.1016/j.lfs.2019.02.017

Badshah, H., Ikram, M., Ali, W., Ahmad, S., Hahm, J. R., and Kim, M. O. (2019). Caffeine may abrogate LPS-induced oxidative stress and neuroinflammation by regulating nrf2/TLR4 in adult mouse brains. *Biomolecules* 9(11), 719. doi:10.3390/biom9110719

Barco, A., and Marie, H. (2011). Genetic approaches to investigate the role of CREB in neuronal plasticity and memory. *Mol. Neurobiol.* 44, 330–349. doi:10.1007/s12035-011-8209-x

Chang, L., Liu, X., Liu, J., Li, H., Yang, Y., Liu, J., et al. (2014). D-galactose induces a mitochondrial complex I deficiency in mouse skeletal muscle: potential benefits of nutrient combination in ameliorating muscle impairment. *J. Med. Food* 17, 357–364. doi:10.1089/jmf.2013.2830

Chen, P., Chen, F., and Zhou, B. H. (2019). Leonurine ameliorates D-galactose-induced aging in mice through activation of the Nrf2 signalling pathway. *Aging* 11, 7339–7356. doi:10.18632/aging.101733

Chuang, J. Y., Chang, P. C., Shen, Y. C., Lin, C., Tsai, C. F., Chen, J. H., et al. (2014). Regulatory effects of fisetin on microglial activation. *Molecules* 19, 8820–8839. doi:10.3390/molecules19078820

Cui, X., Zuo, P., Zhang, Q., Li, X., Hu, Y., Long, J., et al. (2006). Chronic systemic D-galactose exposure induces memory loss, neurodegeneration, and oxidative damage in mice: protective effects of R-alpha-lipoic acid. *J. Neurosci. Res.* 84, 647–654. doi:10.1002/jnr.20899

Currais, A., Prior, M., Dargusch, R., Armando, A., Ehren, J., Schubert, D., et al. (2014). Modulation of p25 and inflammatory pathways by fisetin maintains cognitive function in Alzheimer's disease transgenic mice. *Aging Cell* 13, 379–390. doi:10.1111/acel.12185

Dinkova-Kostova, A. T., Kostov, R. V., and Kazantsev, A. G. (2018). The role of Nrf2 signaling in counteracting neurodegenerative diseases. *FEBS J.* 285, 3576–3590. doi:10.1111/febs.14379

Echeverry, C., Arredondo, F., Martínez, M., Abin-Carriquiry, J. A., Midiwo, J., and Dajas, F. (2015). Antioxidant activity, cellular bioavailability, and iron and calcium management of neuroprotective and nonneuroprotective flavones. *Neurotox. Res.* 27, 31–42. doi:10.1007/s12640-014-9483-y

Hayden, M. S., and Ghosh, S. (2004). Signaling to NF-kappaB. *Genes Dev.* 18, 2195–2224. doi:10.1101/gad.1228704

Huang, Y., and Mucke, L. (2012). Alzheimer mechanisms and therapeutic strategies. *Cell* 148, 1204–1222. doi:10.1016/j.cell.2012.02.040

Ikram, M., Muhammad, T., Rehman, S. U., Khan, A., Jo, M. G., Ali, T., et al. (2019a). Hesperetin confers neuroprotection by regulating nrf2/TLR4/NF-kappaB signaling in an abeta mouse model. *Mol. Neurobiol.* 56(9), 6293–6309. doi:10.1007/s12035-019-1512-7

Ikram, M., Saeed, K., Khan, A., Muhammad, T., Khan, M. S., Jo, M. G., et al. (2019b). Natural dietary supplementation of curcumin protects mice brains against ethanol-induced oxidative stress-mediated neurodegeneration and memory impairment via nrf2/TLR4/RAGE signaling. *Nutrients* 11(5), 1082. doi:10.3390/nu11051082

Ikram, M., Ullah, R., Khan, A., and Kim, M. O. J. C. (2020). Ongoing research on the role of gintonin in the management of neurodegenerative disorders. *Cells*, 9, 1464. doi:10.3390/cells9061464

Johnson, J. A., Johnson, D. A., Kraft, A. D., Calkins, M. J., Jakel, R. J., Vargas, M. R., et al. (2008). The Nrf2-ARE pathway: an indicator and modulator of oxidative stress in neurodegeneration. *Ann. N. Y. Acad. Sci.* 1147, 61–69. doi:10.1196/annals.1427.036

Khan, A., Ali, T., Rehman, S. U., Khan, M. S., Alam, S. I., Ikram, M., et al. (2018). Neuroprotective effect of quercetin against the detrimental effects of LPS in the adult mouse brain. *Front. Pharmacol.* 9, 1383. doi:10.3389/fphar.2018.01383

Khan, A., Ikram, M., Hahm, J. R., and Kim, M. O. J. A. (2020). Antioxidant and anti-inflammatory effects of citrus flavonoid hesperetin: special focus on neurological disorders. *Antioxidants*, 9, 609. doi:10.3390/antiox9070609

Khan, A., Ikram, M., Muhammad, T., Park, J., and Kim, M. O. (2019a). Caffeine modulates cadmium-induced oxidative stress, neuroinflammation, and cognitive impairments by regulating nrf-2/HO-1 in vivo and in vitro. *J. Clin. Med.* 8(5), 680. doi:10.3390/jcm8050680

Khan, N., Syed, D. N., Ahmad, N., and Mukhtar, H. (2013). Fisetin: a dietary antioxidant for health promotion. *Antioxidants Redox Signal* 19, 151–162. doi:10.1089/ars.2012.4901

Kim, S., Nam, Y., Kim, C., Lee, H., Hong, S., Kim, H. S., et al. (2020). Neuroprotective and anti-inflammatory effects of low-moderate dose

ionizing radiation in models of Alzheimer's disease. *Int. J. Mol. Sci.* 21(10), 3678. doi:10.3390/ijms21103678

Liu, J., and Lin, A. (2005). Role of JNK activation in apoptosis: a double-edged sword. *Cell Res.* 15, 36–42. doi:10.1038/sj.cr.7290262

Liu, T., Zhang, L., Joo, D., and Sun, S. C. (2017). NF-κB signaling in inflammation. *Signal Transduct Target Ther* 2, 17023. doi:10.1038/sigtrans.2017.23

Lu, J., Wu, D. M., Zheng, Y. L., Hu, B., and Zhang, Z. F. (2010). Purple sweet potato color alleviates D-galactose-induced brain aging in old mice by promoting survival of neurons via PI3K pathway and inhibiting cytochrome C-mediated apoptosis. *Brain Pathol.* 20, 598–612. doi:10.1111/j.1750-3639.2009.00339.x

Lu, J., Zheng, Y. L., Wu, D. M., Luo, L., Sun, D. X., and Shan, Q. (2007). Ursolic acid ameliorates cognition deficits and attenuates oxidative damage in the brain of senescent mice induced by D-galactose. *Biochem. Pharmacol.* 74, 1078–1090. doi:10.1016/j.bcp.2007.07.007

Maher, P. (2015). How fisetin reduces the impact of age and disease on CNS function. *Front. Biosci.* 7, 58–82. doi:10.2741/425

Muhammad, T., Ali, T., Ikram, M., Khan, A., Alam, S. I., and Kim, M. O. (2018). Melatonin rescue oxidative stress-mediated neuroinflammation/neurodegeneration and memory impairment in scopolamine-induced amnesia mice model. *J. Neuroimmune Pharmacol.* 14(2), 278–294. doi:10.1007/s11481-018-9824-3

Muhammad, T., Ikram, M., Ullah, R., Rehman, S. U., and Kim, M. O. (2019). Hesperetin, a citrus flavonoid, attenuates LPS-induced neuroinflammation, apoptosis and memory impairments by modulating TLR4/NF-kappaB signaling. *Nutrients* 11(3), 648. doi:10.3390/nu11030648

Niedzielska, E., Smaga, I., Gawlik, M., Moniczewski, A., Stankowicz, P., Pera, J., et al. (2016). Oxidative stress in neurodegenerative diseases. *Mol. Neurobiol.* 53, 4094–4125. doi:10.1007/s12035-015-9337-5

Olanow, C. W. (1993). A radical hypothesis for neurodegeneration. *Trends Neurosci.* 16, 439–444. doi:10.1016/0166-2236(93)90070-3

Paradies, G., Petrosillo, G., Paradies, V., and Ruggiero, F. M. (2011). Mitochondrial dysfunction in brain aging: role of oxidative stress and cardiolipin. *Neurochem. Int.* 58, 447–457. doi:10.1016/j.neuint.2010.12.016

Prakash, D., and Sudhandiran, G. (2015). Dietary flavonoid fisetin regulates aluminium chloride-induced neuronal apoptosis in cortex and hippocampus of mice brain. *J. Nutr. Biochem.* 26, 1527–1539. doi:10.1016/j.jnutbio.2015.07.017

Rehman, S. U., Shah, S. A., Ali, T., Chung, J. I., and Kim, M. O. (2017). Anthocyanins reversed D-galactose-induced oxidative stress and neuroinflammation mediated cognitive impairment in adult rats. *Mol. Neurobiol.* 54, 255–271. doi:10.1007/s12035-015-9604-5

Rehman, S. U., Ikram, M., Ullah, N., Alam, S. I., Park, H. Y., Badshah, H., et al. (2019). Neurological enhancement effects of melatonin against brain injury-induced oxidative stress, neuroinflammation, and neurodegeneration via AMPK/CREB signaling. *Cells* 8(7), 760. doi:10.3390/cells8070760

Salminen, A., Kaarniranta, K., and Kauppinen, A. (2013). Crosstalk between oxidative stress and SIRT1: impact on the aging process. *Int. J. Mol. Sci.* 14, 3834–3859. doi:10.3390/ijms14023834

Shah, S. A., Khan, M., Jo, M. H., Jo, M. G., Amin, F. U., and Kim, M. O. (2017a). Melatonin stimulates the SIRT1/nrf2 signaling pathway counteracting lipopolysaccharide (LPS)-Induced oxidative stress to rescue postnatal rat brain. *CNS Neurosci. Ther.* 23, 33–44. doi:10.1111/cns.12588

Shah, S. A., Yoon, G. H., Chung, S. S., Abid, M. N., Kim, T. H., Lee, H. Y., et al. (2017b). Novel osmotin inhibits SREBP2 via the AdipoR1/AMPK/SIRT1 pathway to improve Alzheimer's disease neuropathological deficits. *Mol. Psychiatr.* 22, 407–416. doi:10.1038/mp.2016.23

Shah, S. Z. A., Zhao, D., Hussain, T., Sabir, N., Mangi, M. H., and Yang, L. (2018). p62-Keap1-NRF2-ARE pathway: a contentious player for selective targeting of autophagy, oxidative stress and mitochondrial dysfunction in prion diseases. *Front. Mol. Neurosci.* 11, 310. doi:10.3389/fnmol.2018.00310

Singh, S., Garg, G., Singh, A. K., Tripathi, S. S., and Rizvi, S. I. (2019). Fisetin, a potential caloric restriction mimetic, modulates ionic homeostasis in senescence induced and naturally aged rats. *Arch. Physiol. Biochem.*, 15(193), 171–179. doi:10.1080/13813455.2019.1662452

Singh, S., Singh, A. K., Garg, G., and Rizvi, S. I. (2018). Fisetin as a caloric restriction mimetic protects rat brain against aging induced oxidative stress, apoptosis and neurodegeneration. *Life Sci.* 193, 171–179. doi:10.1016/j.lfs.2017.11.004

Tournier, C., Hess, P., Yang, D. D., Xu, J., Turner, T. K., Nimnual, A., et al. (2000). Requirement of JNK for stress-induced activation of the cytochrome c-mediated death pathway. *Science* 288, 870–874. doi:10.1126/science.288.5467.870

Ullah, F., Asgarov, R., Venigalla, M., Liang, H., Niedermayer, G., Münch, G., et al. (2020a). Effects of a solid lipid curcumin particle formulation on chronic activation of microglia and astroglia in the GFAP-IL6 mouse model. *Sci. Rep.* 10, 2365. doi:10.1038/s41598-020-58838-2

Ullah, F., Liang, H., Niedermayer, G., Münch, G., and Gyengesi, E. (2020b). Evaluation of phytosomal curcumin as an anti-inflammatory agent for chronic glial activation in the GFAP-IL6 mouse model. *Front. Neurosci.* 14, 170. doi:10.3389/fnins.2020.00170

Xue, M., Rabbani, N., Momiji, H., Imbasi, P., Anwar, M. M., Kitteringham, N., et al. (2012). Transcriptional control of glyoxalase 1 by Nrf2 provides a stress-responsive defence against dicarbonyl glycation. *Biochem. J.* 443, 213–222. doi:10.1042/BJ20111648

Zhang, X. L., Jiang, B., Li, Z. B., Hao, S., and An, L. J. (2007). Catalpol ameliorates cognition deficits and attenuates oxidative damage in the brain of senescent mice induced by D-galactose. *Pharmacol. Biochem. Behav.* 88, 64–72. doi:10.1016/j.pbb.2007.07.004

Conflict of Interest: The authors declare that the research was conducted in the absence of any commercial or financial relationships that could be construed as a potential conflict of interest.

frontiers in Pharmacology

ORIGINAL RESEARCH
published: 16 March 2021
doi: 10.3389/fphar.2021.616413

Neuroprotective and Neurorescue Mode of Action of *Bacopa monnieri* (L.) Wettst in 1-Methyl-4-phenyl-1,2,3,6-tetrahydropyridine-Induced Parkinson's Disease: An *In Silico* and *In Vivo* Study

Babita Singh[1], *Shivani Pandey*[1]*, *Mohammad Rumman*[1], *Shashank Kumar*[2], *Prem Prakash Kushwaha*[2], *Rajesh Verma*[3] *and Abbas Ali Mahdi*[1]

[1]Department of Biochemistry, KGMU, Lucknow, India, [2]Molecular Signaling and Drug Discovery Laboratory, Department of Biochemistry, Central University of Punjab, Punjab, India, [3]Department of Neurology, KGMU, Lucknow, India

OPEN ACCESS

Edited by:
Muhammad Imran Naseer, King Abdulaziz University, Saudi Arabia

Reviewed by:
Peter Natesan Pushparaj, King Abdulaziz University, Saudi Arabia
Noman Bin Abid, Gyeongsang National University, South Korea

***Correspondence:**
Shivani Pandey
shivanipandey@kgmcindia.edu
drshivaninbc@gmail.com

Received: *12 October 2020*
Accepted: *19 January 2021*
Published: *16 March 2021*

Citation:
Singh B, Pandey S, Rumman M, Kumar S, Kushwaha PP, Verma R and Mahdi AA (2021) Neuroprotective and Neurorescue Mode of Action of Bacopa monnieri *(L.) Wettst in 1-Methyl-4-phenyl-1,2,3,6-tetrahydropyridine-Induced Parkinson's Disease: An* In Silico *and* In Vivo *Study. Front. Pharmacol. 12:616413. doi: 10.3389/fphar.2021.616413*

Ethnopharmacological Relevance: Parkinson's disease (PD) is characterized by progressive death of dopaminergic neurons. The presently used medicines only tackle the symptoms of PD, but none makes a dent on the processes that underpin the disease's development. Herbal medicines have attracted considerable attention in recent years. *Bacopa monnieri* (L.) *Wettst* (Brahmi) has been used in Indian Ayurvedic medicine to enhance memory and intelligence. Herein, we assessed the neuroprotective role of *Bacopa monnieri* (L.) *Wettst* on Parkinson's disease.

Aim of the Study: *Bacopa monnieri* (L.) *Wettst*, a medicinal herb, is widely used as a brain tonic. We investigated the neuroprotective and neurorescue properties of *Bacopa monnieri* (L.) *Wettst* extract (BME) in 1-methyl-4-phenyl-1,2,3,6-tetrahydropyridine (MPTP)-induced mice model of PD.

Materials and Methods: The mice model of MPTP-induced PD is used in the study. In the neuroprotective (BME + MPTP) and neurorescue (MPTP + BME) experiments, the animals were administered 40 mg/kg body weight BME orally before and after MPTP administration, respectively. Effect of BME treatment was evaluated by accessing neurobehavioral parameters and levels of dopamine, glutathione, lipid peroxide, and nitrites. An *in silico* study was performed using AutoDock Tools 1.5.6 (ADT).

Results: A significant recovery in behavioral parameters, dopamine level, glutathione level, lipid peroxides, and nitrite level was observed in BME-treated mice. Treatment with BME before or after MPTP administration has a protective effect on dopaminergic neurons, as evidenced by a significant decrease in GFAP immunostaining and expression of inducible nitric oxide synthase (iNOS) in the substantia nigra region; however, the degree of improvement was more prominent in mice receiving BME treatment before MPTP administration. Moreover, the *in silico* study revealed that the constituents of BM,

including bacosides, bacopasides, and bacosaponins, can inactivate the enzyme monoamine oxidase B, thus preventing the breakdown of MPTP to MPP+.

Conclusion: Our results showed that BME exerts both neuroprotective and neurorescue effects against MPTP-induced degeneration of the nigrostriatal dopaminergic neurons. Moreover, BME may slow down the disease progression and delay the onset of neurodegeneration in PD.

Keywords: neurodegeneration, antioxidants, *Bacopa monnieri*, substantia nigra, iNOS

INTRODUCTION

Bacopa monnieri (L.) *Wettst* (Brahmi, BM) is a reputed drug of Ayurveda (Bammidi et al., 2011). It belongs to *Scrophulariaceae* family, which represents 220 genera with more than 4,500 species, and typically grows in the wetlands of southern India and Australia. Of all the Indian herbs, BM was, and still considered as, the premier herb for treating brain disorders and age-related mental decline as well as for improving cognitive functions. BM has been utilized as a brain tonic, diuretic, antidepressant, revitalizer of sensory organs, cardiotonic, antianxiety, and anticonvulsant agent (Chopra et al., 1956, 2004). Animals treated chronically with BM extract showed improved acquisition skills and improved retention in learning tasks (Prisila Dulcy et al., 2012; Yadav et al., 2014a; Yadav et al., 2014b; Balaji et al., 2015).

The main constituents of BM are dammarane type of triterpenoid saponins called bacosides, with jujubogenin or pseudojujubogenin moieties as a glycone unit. The main alkaloids include brahmine, nicotine, and herpestine, along with D-mannitol, apigenin, hersaponin, monnierasides I–III, cucurbitacins, and plantainoside B. Bacosides are a family of 12 acknowledged analogs. Novel saponins called bacopasides I–XII have been identified recently. Bacoside A, which is a blend of bacoside A3, bacopaside II, bacopasaponin C, and a jujubogenin isomer of bacosaponin C, is the most studied compound of BM (Aguiar and Borowski, 2013).

BM extract as well as its isolated compounds has been studied extensively in animal models of various diseases. A previous study showed that Bacoside A could reduce oxidative stress in the brain by enhancing the activities of superoxide dismutase (SOD), catalase, glutathione peroxidase (GPx), and glutathione reductase (GSR) (Commens, 1983). Moreover, in a *Caenorhabditis elegans* model of 6-hydroxydopamine (6-OHDA)-induced Parkinson's disease (PD), BM extract could reduce α-synuclein aggregation by inducing the expression of stress-buffer protein hsp-70 (Chowdhuri et al., 2002; Jadiya et al., 2011). Our previous study showed that chronic 1-methyl-4-phenyl-1,2,3,6-tetrahydropyridine (MPTP) administration induces PD-like symptoms in mice and cotreatment with BM extract could ameliorate the motor defects and increase the number of dopaminergic neurons in the substantia nigra of PD animals (Singh et al., 2017). We also reported that the neuroprotective effect of BM extract was mediated via upregulation of antiapoptotic protein Bcl2 (Singh et al., 2017). In a rat model of rotenone-induced PD, BM extract could ameliorate motor defects by reducing oxidative stress in the substantia nigra, hippocampus, striatum, cortex, and brain stem regions.

BM extract has low toxicity and exerts apparent beneficial effects as a nootropic (Pravina et al., 2007; Aguiar and Borowski, 2013). BM extract is used as a dietary supplement (KeenMind or CDRI08, Soho Flordis International) and is approved by the Food and Drug Administration (FDA). Although BM is widely available and BM extract is used as herbal medicine, the mechanisms of action of BM have yet to be delineated.

Parkinson's disease (PD) is the second most common neurodegenerative disorder, and about 1% of the population over 60 years of age is affected by this disease (de Rij et al., 2000). In PD, the loss of dopamine-producing neurons is mainly responsible for PD-associated symptoms. Since the neurotransmitter dopamine is associated with the motor activity, therefore, loss of dopaminergic neurons leads to tremors, muscle rigidity, and bradykinesia. Moreover, PD also affects cognition, mental state, sleep, personality, and behavior leading to depression and anxiety (Cheng et al., 2010). The etiology of PD is still not clearly understood. At present, the available treatments for PD improve few symptoms of the disease. However, these treatment modalities have suboptimal efficacy and low efficiency. Thus, there is an urgent need to develop novel neuroprotective or disease-modifying treatments for PD. Natural products or herbal compounds are of particular interest as they can be used to develop novel drugs that could help in preventing or delaying the PD-associated neurodegeneration.

The present study aimed to evaluate the effects of pre- and posttreatment with BM extract on PD-associated motor defects and neuroinflammation employing an MPTP-induced mice model of PD. Further, the study also aimed to explore the neuroprotective mode of action of BM extract through an *in silico* study. Our results suggest that both pretreatment (neuroprotective) and posttreatment (neurorescue) with BM extract ameliorate the motor defects in PD mice. Moreover, both pre- and posttreatment with BM extract reduce oxidative stress, increase the dopamine levels, decrease the inflammation, and suppress microglial activation in the substantia nigra region of the MPTP-treated mice brain. Employing an *in silico* approach, we identified the probable active BM phytoconstituents that might be involved in its neuroprotective and neurorescue properties.

MATERIALS AND METHODS

Animals and Treatment

In this study, Swiss albino mice were used. Animals were obtained from the breeding colony of Indian Institute of Toxicology Research (IITR), Lucknow, India. All animal experiments were performed after obtaining approval from the Institutional Animal Ethics Committee (IAEC, letter no. 39/IAH/PHARMA/14).

Animals were maintained under 12–12 h light-dark cycles with an ambient temperature (25°C) and controlled humidity, along with free access to drinking water and pellet diet (Hindustan Lever Ltd., Mumbai, India).

Experimental Schedule

Bacopa monnieri (L.) *Wettst* extract (BME) was purchased from Natural Remedies Pvt. Ltd., Bangalore, India (BM/10015).

For experimental design, mice were randomly divided into the following four groups (n = 8 in each group): Group I: animals received 0.5 ml of normal saline (intraperitoneal (i.p.) for 3 weeks) served as control or vehicle group; Group II: animals received MPTP (30 mg/kg body weight, i.p.) on the 8th day of the experiment, twice with a gap of 16 h to induce PD-like symptoms (MPTP group) (Yadav et al., 2014a; Yadav et al., 2014b); Group III: animals received BME treatment (40 mg/kg body weight/day, p. o.) for 1 week (Singh et al., 2016; Rai et al., 2003; Singh et al., 2017; Singh et al., 2020) followed by MPTP treatment on the 8th day of the experiment, twice with a gap of 16 h, and BME treatment continued for another 2 weeks (neuroprotective experiment, BME + MPTP group); and Group IV: animals received MPTP on the first day of the experiment followed by BME treatment (40 mg/kg body weight/day, p.o.) for 3 weeks (neurorescue experiment, MPTP + BME group).

At the end of the entire treatment, neurobehavioral tests were performed to evaluate the motor functions. After that, the animals were sacrificed and the brain was dissected out for further biochemical analysis.

Neurobehavioral Studies

Footprinting Test

Footprint analysis was performed to assess limb coordination in all mice groups as described previously (Yadav et al., 2014a; Yadav et al., 2014b). Briefly, animals were trained to walk across a white sheet of paper without stopping. At end of the drug treatment, the forepaw of mice was dipped in blank ink and the animals were allowed to walk freely on a white sheet of paper. The stride length was measured as the distance between the centers of the ipsilateral adjacent footprints (Yadav et al., 2014a; Yadav et al., 2014b).

Rotarod Test

The rotarod test was carried out using the Rotomex (Columbus Instruments, USA) instrument to evaluate the motor coordination in animals. The apparatus consisted of an iron rod with nonslip surface (3 cm diameter, 30 cm length). Prior to the drug treatment, animals were trained by placing them on the rotating rod (10 rpm) for 300 s. After the treatment, the fall time of animals from the rotating rod was recorded (Rai et al., 2016).

Grip Strength Test

To measure the forelimb strength in mice, the grip strength test was used as described previously (Terry et al., 2003).

Neurochemical Studies

After the behavioral tests, mice were anesthetized using ketamine/xylene (60 mg/kg) and sacrificed via cervical dislocation followed by decapitation to ensure minimum pain. The whole brain was dissected out and frozen directly until further analyses. The substantia nigra was carefully dissected out from both the hemispheres of each mice brain and stored at −80°C until further use.

Oxidative stress was evaluated by measuring the levels of malondialdehyde (MDA), nitrite, and glutathione (GSH) in the substantia nigra region.

Malondialdehyde (MDA) Estimation

Malondialdehyde levels can be the indicator of lipid peroxidation. MDA is a reactive three-carbon di-aldehyde formed as a byproduct of polyunsaturated fatty acid (PUFA) peroxidation. In the brain tissue, the lipid peroxidation level (LPO) was estimated according to the method described previously (Ohkawa et al., 1979) with few modifications. Briefly, the assay mixture was incubated at room temperature for 5 min followed by the addition of 20% acetic acid (0.6 ml) and further incubation for another 5 min. After this, 0.8% thiobarbituric acid (TBA) (0.6 ml) was added to the mixture and incubated in a boiling water bath for 1 h. The reaction mixture was cooled and centrifuged, and the absorbance was recorded at 532 nm. LPO was measured as nanomoles MDA/mg protein.

Nitrite Estimation

Nitrite levels were determined in the supernatant of the tissue homogenate as described previously (Granger et al., 1996). Briefly, tissue homogenate was incubated with sodium nitrite (10 mM), ammonium chloride (0.7 mM), and Griess reagent (0.1% N-naphthylethylenediamine and 1% sulfanilamide in 2.5% phosphoric acid). The reaction mixture was incubated at room temperature for 30 min, and the absorbance was measured at 540 nm. The nitrite content was calculated using a standard curve of sodium nitrite (10–100 μM). Nitrite levels were expressed as μmoles/ml.

Glutathione (GSH) Estimation

GSH was estimated in the tissue homogenate by 5,5′dithiobis-(2-nitrobenzoic acid) (DTNB)-glutathione reductase coupled assay as described previously (Anderson 1985). Briefly, 1.0 ml of the brain tissue homogenate was deprotonated by adding 1.0 ml of 10% TCA and centrifuged at 6000 g for 5 min. 0.5 ml aliquot from the clear supernatant was mixed with 0.5 ml double distilled water. Thereafter, 2 ml of 0.4 M Tris buffer and 0.1 ml DTNB were added to it with continuous mixing. GSH reacts with DTNB to produce a yellow-colored chromogen. The absorbance was measured at 412 nm. GSH content in the sample was calculated using a standard curve (GSH 200–1,600 nmole), and the results were expressed as nmole/g tissue.

Dopamine Estimation by HPLC

The dopamine (DA) level was estimated in the isolated substantia nigra homogenate using HPLC (Yadav et al., 2014a; Yadav et al., 2014b). Briefly, the samples were homogenized in 0.17 M perchloric acid using a Polytron homogenizer. The homogenates were centrifuged at 33000 g (Biofuge Stratos, Heaureas, Germany) at 4°C.Then, 20 μL of the supernatant

was injected into an HPLC pump (Model 1,525, binary gradient pump) fitted with a C18 column (Spherisorb, RP C18, 5 mm particle size, 4.6 mm i.d. × 250 mm at 30°C) connected to an ECD (Model 2,465, Waters, Milford, MA, USA) at a potential of +0.8 V with a glassy carbon working electrode vs. Ag/AgCl reference electrode. The mobile phase consisted of 32 mM citric acid, 12.5 mM disodium hydrogen orthophosphate, 1.4 mM sodium octyl sulfonate, 0.05 mM EDTA, and 16% (v/v) methanol (pH 4.2) at a flow rate of 1.2 ml/min. The chromatogram was recorded and analyzed using Empower software (Version 2.0).

Enzyme-Linked Immunosorbent Assay (ELISA)

TNF-α protein levels were measured in the substantia nigra homogenates using a commercially available kit for ELISA (Diaclone).

GFAP Immunostaining

Sections of the substantia nigra region were blocked in blocking buffer (PBS containing 2% normal goat serum) for 2 h. Sections were then incubated with monoclonal mouse anti-GFAP antibody (1:1,000) overnight at room temperature. Then, sections were washed with PBS thrice and incubated with biotinylated anti-mouse IgG (1:500) for 2 h at room temperature and subsequently in avidin peroxidase (1:500 dilution) for 2 h. DAB (Sigma) was used to visualize the immunoreactivity. The stained sections were dehydrated and mounted using a coverslip. For quantification, images were acquired on the Nikon Eclipse TiBR imaging system using a ×10 objective. ImageJ software was used to determine the fraction of GFAP positive area.

Gene Expression Analysis by Quantitative Real-Time PCR

Total RNA was isolated from the substantia nigra region using TRIzol reagent. Genomic DNA was removed using RNase-free DNase (Ambion). RNA pellets were resuspended in DEPC-treated water (Ambion). Equal amounts of RNA were reverse transcribed using the Superscript first-strand cDNA synthesis kit with Oligo-dT (Invitrogen, USA) and diluted in nuclease-free water (Ambion) to a final concentration of 10 ng/μL. Real-time q-PCR was performed to detect changes in mRNA expression using the SYBR green and ABI Prism 7900 HT Sequence Detection System (Applied Biosystems; Foster City, CA). Beta-actin was used as internal control. Relative expression was calculated using the delta Ct method (Tiwari et al., 2014).

The primers used for qPCR were iNOS forward 5′-CCCTTCCGAAGTTTCTGGCAGCAGC-3′and iNOS reverse 5′-GGCTGTCAGAGCCTCGTGGCTTTGG-3'.

In Silico Study

Ligand Screening and Preparation

NCBI PubChem compounds database and literature on BM phytochemicals were used to take an idea for the selection of active phytoconstituents from BM for the present study (http://www.ncbi.nlm.nih.gov/pccompound). As per the literature, bacosides, bacopasides, and bacopasaponins form the major proportion of active phytochemicals in BM. The PubChem compound search tool was used to find the natural and/or synthetic analogs of the active phytoconstituents. Thirty-one analogs of bacosides (N = 2), bacopasides (N = 20), and bacopasaponins (N = 9) were used for further *in silico* study. The standard known inhibitors for different targeted proteins were retrieved from the literature. The 3D/2D structure of phytochemicals and various inhibitors of their respective protein were retrieved from NCBI PubChem in SDF format. Open Babel molecule format converter was used to perform conversion of 2D structure into 3D conformation (O'Boyle et al., 2011)

Screening and Preparation of Ligand Receptor

The 3D structures of various ligand-receptor proteins were downloaded from RCSB-protein data bank in PDB file (Berman et al., 2000). The bulkier structure of MAO-A protein (enzyme) was divided into two (Chain A and Chain B) separate PDB files. Chain C (Nrf2) of PDB 3ZGC and Chain A (neuronal calcium sensor 1) of PDB 5AER were deleted to obtain KEAP1 and D2 dopamine receptor proteins, respectively. Protein models were cleaned and optimized by removing ligands as well as other heteroatoms (acetate ion and $H_2O$for KEAP1; Mg, S-adenosylmethionine, 3,5-Dinitrocatechol, K and H_2O for COMT; N-[3-(2,4-Dichlorophenoxy)Propyl]-N-Methyl-N-Prop-2-Ynylamine and FAD for MAO-A; FAD, H_2O and (5R)-5-{4-[2-(5-ethylpyridin-2-yl)ethoxy]benzyl}-1,3-thiazolidine-2,4-dione for MAO-B; 5′-S-(3-{[(3R)-1,2,3,4-tetrahydroisoquinolin-3-ylcarbonyl]amino}propyl)-5′-thioadenosine, 2-Amino-2-Hydroxymethyl-Propane-1,3-Diol and H_2O for PNMT; L-Dopamine, Adenosine-3′-5′-diphosphate and H_2O for PST; β-D-Galactose, SO_4, Uridine-5′-Diphosphate, Mn and H_2O for UGT; 1-benzyl-1H-indole-2,3-dione, Na, 1,2-Ethanediol, Guanidine and H_2O for ALDH1A1; 3-chloro-5-ethyl-N-{[(2S)-1-ethylpyrrolidin-2-yl]methyl}-6-hydroxy-2-methoxybenzamide and Maltose for D3 dopamine receptor and Ca, K and H_2O for D2 dopamine receptor). Energy minimization was done by using the Swiss-PDB Viewer (v4.1) software.

Molecular Docking Stimulation

For docking experiments, the ligand-receptor proteins and the ligands were loaded into AutoDock Tools 1.5.6 (ADT) (Sanner 1999). Gasteiger partial charges assigned after merging nonpolar hydrogen and torsions were applied to the ligands by rotating all rotatable bonds. Docking calculations were carried out on the protein models. Polar hydrogen atoms, Kollman charges, and solvation parameters were added with the aid of AutoDock tools. AutoDock 4.2 offers the option of three search algorithms to explore the space of active binding with different efficacy. We used the Lamarckian genetic algorithm (LGA) in this study.

Visualization of the Results

LigPlot$^+$ was used to visualize the hydrogen bonds as well as the exact distance between residues of KEAP1 (Kelch-like-ECH-associated

protein 1) receptor protein and different atoms of bacopaside-XII. PyMOL (v1.1) software was used for visualization of the interaction pattern in different receptor protein and ligand. Molecular surface structure was obtained by PyMOL software.

Statistical Analysis

Data are represented as mean ± standard deviation (SD). Comparison between the treated and the untreated groups was performed using one-way analysis of variance (ANOVA), followed by the Student–Newman–Keuls test (InStat3 package program). $p < 0.05$ was considered statistically significant.

RESULTS

Neurobehavioral Studies

To evaluate the efficacy of BME in ameliorating MPTP-induced behavioral deficits, we studied neurobehavioral changes using rotarod test, grip strength test, and foot printing test. MPTP-induced mice exhibited a significant decrease ($p < 0.05$) in the time spent on the rotarod as compared with control mice (**Figure 1A**), which is in agreement with previous studies (Singh et al., 2020). Both, pre- and posttreatment with BME significantly increased the time spent on the rotarod in MPTP-treated mice. Interestingly, mice receiving BME treatment before MPTP lesioning (BME + MPTP group) exhibited a more significant ($p < 0.001$) increase compared with mice receiving BME treatment after MPTP lesioning (MPTP + BME) ($p < 0.05$). Further, grip strength was significantly decreased in mice treated with MPTP compared with the control group (**Figure 1B**). An improvement in the grip strength was observed in both pretreatment (BME + MPTP) and posttreatment (MPTP + BME) groups compared with the MPTP-induced group. Similar to the rotarod test, the increase in the pretreatment group (BME + MPTP) was significantly more compared with the posttreatment group (MPTP + BME) in the grip strength test. In the footprinting test, we observed that MPTP treatment induced walking errors in mice ($p < 0.05$). Pre- and posttreatment with BME ameliorated the walking errors in MPTP-induced mice (**Figure 1C**). Taken together, these results suggest that both pre- and posttreatment with BME could ameliorate the motor deficits in MPTP-treated PD mice.

Biochemical Analysis

In the MPTP-induced group, a significant increase ($p < 0.001$) in the levels of lipid peroxides and nitrite in the substantia nigra region was observed compared with control mice. Both, pre- and posttreatment with BME decreased the levels of lipid peroxides and nitrite; however, the decrease was more significant in the BME + MPTP group ($p < 0.001$) than in the MPTP + BME group ($p < 0.05$) (**Figure 1D**). Moreover, a significant decrease ($p < 0.001$) in the GSH level (**Figure 1E**) was observed in the MPTP-induced group compared with the control group. Pre- or posttreatment with BME increased the GSH levels in MPTP-treated mice. The increase in the BME + MPTP group was more significant ($p < 0.001$) than the MPTP + BMP group ($p < 0.05$). As shown in **Figure 1F,** a significant decrease in the DA level was observed in MPTP-induced mice ($p < 0.001$) when compared with the control group, indicating death of dopaminergic neurons in the MPTP-induced animals. Pre- and posttreatment with BME restored the levels of DA. The effect was more pronounced in the BME + MPTP group ($p < 0.01$) than in the MPTP + BME group ($p < 0.05$). A significant increase ($p < 0.001$) in the TNF-α level was observed in the substantia nigra of the MPTP-induced group as compared with the control group, which was restored significantly in both pre- and posttreated groups ($p < 0.01$ and $p < 0.05$, respectively) (**Figure 1G**).

Immunohistochemistry

The neuroprotective/neurorescue effect of BME was assessed by staining the activated astrocytes. In MPTP-induced mice, the number of GFAP positive astrocytes was significantly higher compared with the control animals (**Figures 2A,B**). In both MPTP + BME and BME + MPTP groups, a significant decrease in GFAP immunoreactivity was observed as compared with the MPTP group (**Figures 2A,B**). The decrease in GFAP positive astrocytes in SNpc of BME + MPTP and MPTP + BME group confirms the neuroprotective/neurorescue action of BME on astrocytes.

Expression Studies

MPTP administration significantly increased the mRNA level of iNOS ($p < 0.001$) (**Figure 2C**), which was significantly restored in the BME + MPTP ($p < 0.01$) and MPTP + BME ($p < 0.05$) groups.

Molecular Docking with Different Targeted Ligand-Receptor Proteins

Molecular docking tools were employed to explore the oxidative stress activity of BM phytochemicals. Docking results of dopamine receptor and ligand MPP^+ showed very high affinity. MPP^+ binds with D2 and D3 dopamine receptor with a binding energy of −4.9 and 7.9 kcal/mol, respectively, as shown in molecular surface structure (**Figures 3A,B**). The docking scores for known standard inhibitors of D2 (eticlopride, raclopride) and D3 (raclopride) dopamine receptor were −4.7, −4.5, and −6.7 kcal/mol, respectively (**Table 1**).

Major phytoconstituent of BM phytochemicals, bacosides, bacopasides, and bacopasaponins showed interesting binding affinity with KEAP1 receptor protein (**Table 1**). The docking studies revealed that bacopaside-XII has the highest affinity for KEAP1 and binds with the lowest energy (−14.7 kcal/mol) among thirty docked compounds as shown in molecular surface structure (**Figure 3C**). Out of 30, 27 compounds showed better binding affinity than the standard KEAP1 inhibitor CDDO-Me (−9.9 kcal/mol). Bacopaside A (PubChCID-11079173), bacopaside B (PubChem CID-11113741), and bacopasaponin F (PubChem CID -16216038) showed comparatively lesser binding affinity than the standard. The docking values for the entire test BM phytoconstituents and standard inhibitor with KEAP1 protein are given in **Table 1**. Residues Pro384, Tyr572, Asn382, Pro384, Ser383, Arg380, Asn 387, and Asp389 of KEAP1 receptor protein were involved in the formation of hydrogen bonds (nine) with bacopaside-XII (**Figure 3D**).

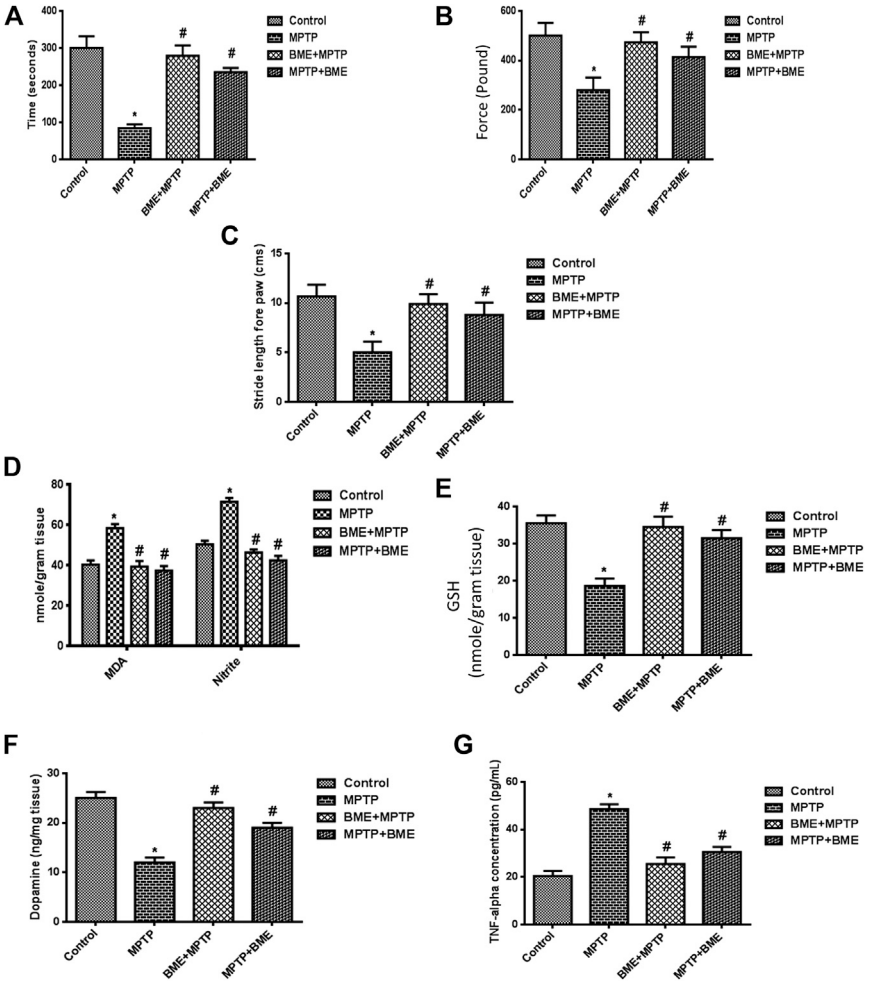

FIGURE 1 | Assessment of neurobehavioral and biochemical parameters in treated and untreated groups. **(A)** The rotarod test was performed in all the groups of animals, and a significant perfection in the time of stay on the rotarod was found in BME pretreated mice compared with the MPTP group. **(B)** The grip strength test was significantly reduced in the MPTP mouse as compared with control. The protective effect was found on forelimb grip strength in pre- and posttreatment of the BME group (BME + MPTP and MPTP + BME). **(C)** Effect of *Bacopa monnieri* (L.) *Wettst* extract (BME) on stride forepaw length. MPTP mice showed decreased stride forepaw length as compared with control. **(D)** Levels of lipid peroxides and nitrite. **(E)** Effect of BME treatment (before and after) in mice on the GSH level. **(F)** Levels of dopamine. **(G)** Effect of pre- and posttreatment of BME extract on the TNF-α level. Values are expressed in mean ± SD. *: compared with the control group, #: compared with the MPTP-treated group. $p < 0.05$ was considered as significant.

BM phytochemicals were also docked with the enzymes (MAO-A, MAO-B, COMT, ALDH, PNMT, PST, and UGT) involved in dopamine degradation pathway, and results were compared with the standard known inhibitors (**Table 1** and **Figures 4A–H**).

Out of the entire test BM phytoconstituents, bacopaside-XII showed the highest binding energy of −13.3 kcal/mol with MAO-B enzyme (**Table 1**). By using the PyMOL visualization tool, the different residues of MAO-B, namely, Ile477, Glu466, Lys190, His431, and Arg67, were identified to be involved in the formation of hydrogen bonds with bacopaside-XII (**Figure 4E**). Bacopaside-XII binds to COMT, MAO-A Chain A, MAO-A Chain B, MAO-B, PNMT, PST, UGT, and ALDH1A1 with highest binding affinity than other docked test compounds, ranging from −11.1 to −15.5 kcal/mol (**Table 1**). The PyMOL visualization tool revealed that different residues of UGT (Gln318, Arg247, Gly278, His779, Arg277, Leu280, Arg156), PST (Arg78, Gln63, Lys16, Arg213), MOA-A (Arg356, Gln327, Glu492, Trp116, Thr204), MAO-B (Ile477, Glu466, Lys190, His431, Arg67), ALDH1A1 (Ser234, Ser235, Ala231), PNMT (Trp123, Glu144, Trp113, Arg145, Arg148, Phe121), and COMT (Gln195) were involved in the formation of hydrogen bonding with bacopaside-XII (**Figures 4A–H**).

DISCUSSION

An understanding of the detailed mechanism of PD progression is required for the development of an effective neuroprotective therapeutic approach to halt or to slow the disease progression.

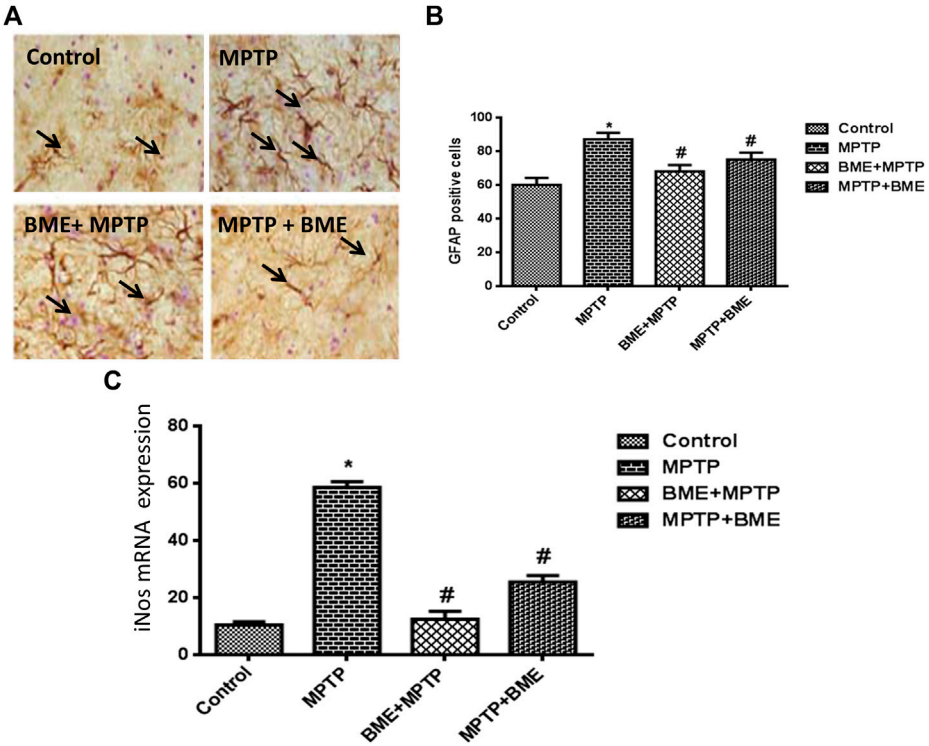

FIGURE 2 | Immunohistochemical studies of astrocytes and quantitative estimation of iNOS mRNA. **(A)** Immunostained representative in brain tissue sections of the substantia nigra (SN), showing astrocyte marker GFAP immunoreactivity in control and all treated animals. **(B)** Bar diagram showing the number of GFAP fibers in the SN region of different groups. Each bar represents mean ± SD. Data are shown as percentages relative to untreated controls. **(C)** q-PCR estimation of iNOS mRNA, beta-actin was used as internal normalizer. $p < 0.05$ was considered as significant. *: comparison of the control group and # comparison of the MPTP-treated group. $p < 0.05$ was considered as significant.

The mouse model of MPTP-induced PD is widely used to test new treatment interventions for the disease. Intraperitoneal administration of MPTP in mice causes motor-function-related problems, activation of proinflammatory cytokines, oxidative stress, and alterations in the neurotransmitters level (Singh et al., 2016). 1-Methyl-4-phenylpyridinium (MPP+) is a toxic metabolite of MPTP, which specially inhibits complex I (NADH dehydrogenase) of the mitochondrial electron transport chain leading to a decrease in ATP generation, thereby causing death of dopaminergic neurons in the SNpc region of the brain (Hutter-Saunders et al., 2012). Loss of dopaminergic neurons is not only due to decreased mitochondrial function but also due to the increased levels of proinflammatory cytokines and reactive oxygen species (ROS). Degeneration of the membrane lipids produces high levels of intracellular ROS, which ultimately leads to the loss of membrane integrity and dopaminergic neurodegeneration. Oxidative stress is one of the major causes of neurodegeneration. Dopaminergic neurons of the nigrostriatal area are more susceptible to oxidative damage as this area is allied with high-energy consumption and has low levels of the antioxidant GSH (Yamaguchi and Shen, 2007). Therefore, ROS scavenging antioxidants might play a crucial role in preventing PD progression by inhibiting ROS-induced neurodegeneration.

Bacopa monnieri (L.) *Wettst* is a well-known dietary antioxidant. Several *in vitro* and animal studies have established that BME inhibits oxidative stress by reducing the formation of free radicals in the brain (Kumar et al., 2012; Shinomol and Bharath, 2012). Studies also showed the neuroprotective role of BME, but there is a lacuna in the studies of neuroprotective and neurorescue effects of BME. To the best of our knowledge, this study is the first to demonstrate neuroprotective and neuroreparative (neurorescue) effect of BME in the MPTP-induced model of PD.

Animals were treated with BME (40 mg/kg bw) orally before and after MPTP administration. The BME dose was chosen based on our earlier studies, where BME has been found to protect against MPTP-induced neurodegeneration (Singh et al., 2016). Although several groups have characterized the chemical components of BME, active components or chemical entities responsible for neuroprotective and neurorescue action of BME are not evidently defined yet.

In the present study, mice treated with MPTP showed a huge decline in motor activity as evaluated by different neurobehavioral tests (grip strength, footprinting, and rotarod test), which is in accordance with previous studies (Singh et al., 2016). The decreased time spent by the MPTP-treated mice on the rotarod is attributed to loss of the dopaminergic neurons

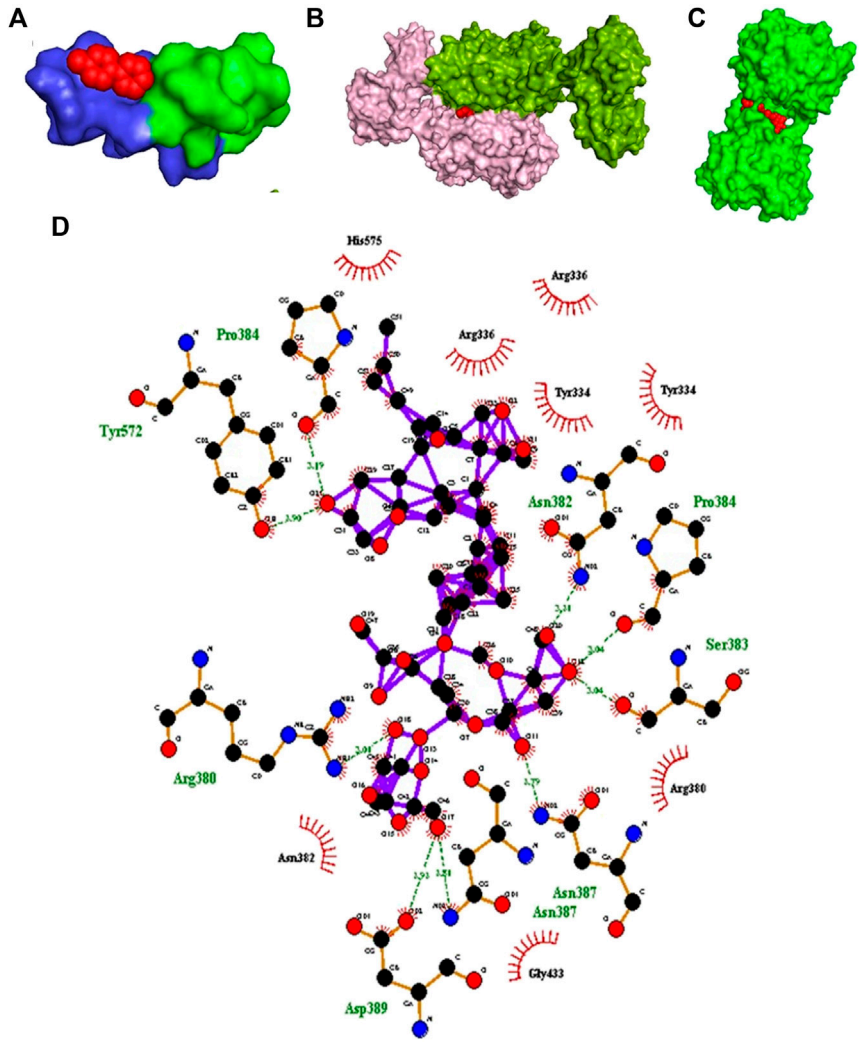

FIGURE 3 | *In silico* study. **(A)** Molecular surface structure of D2 dopamine receptor (PDB: 5AER) (Chain B-light green and Chain C-blue) in complex with MPP+ (red in color). **(B)** Molecular surface structure of D3 dopamine receptor (PDB: 3PBL) (Chain A-light pink and Chain B-green color) in complex with MPP + toxin (red color). **(C)** Molecular surface structure of KEAP1 protein (PDB: 3ZGC) (green color) in complex with bacopaside-XII (red sphere). **(D)** LigPlot depicting schematic representation of hydrogen bonds and hydrophobic interactions between bacopaside-XII and KEAP1 protein.

within the basal ganglia, especially in the mid brain region of substantia nigra (Schwarting et al., 1991). Previous studies showed that decrease in the stride length is significantly associated with the magnitude of neuronal loss in the SN region of the brain (Fernagut et al., 2002). Oral BME administration before or after MPTP lesioning significantly improved the motor functions, suggesting neuroprotective/neurorescue effect of BME on dopaminergic neurons against MPTP-induced toxicity. Our behavioral studies indicate that BME might play an essential role in enhancing the grip power in the PD mice model, supporting its neuroprotective/neurorescue potential. Our findings correlate well with those of the earlier studies from our group as well as from others (Schwarting et al., 1991; Fernagut et al., 2002; Singh et al., 2016).

Results of our study demonstrated that injection of MPTP toxin upregulated the levels of lipid peroxides and nitrite and reduced the GSH level in the substantia nigra region. Administration of BME (pre- and posttreatment) reduced the oxidative stress. Our results can be explained by the fact that BME possesses strong radical scavenging activity (Simpson et al., 2015; Singh et al., 2016).

Dopamine is the most important neurotransmitter involved in the control of motor activities and movement. Previous studies showed that, in human PD patients, the level of catecholamines is lower compared with healthy controls (Hinterberger, 1971; Piggott et al., 1999). We postulate that an increase in the levels of dopamine in both treatment groups (pre- and posttreatment) might be due to the capability of BME to prevent degradation of DA or inhibit reuptake of DA. It might also be possible that the increased levels of DA in the BME-treated mice might be due to the neuroprotective effect of BME on dopaminergic neurons. Nevertheless, our findings that BME

TABLE 1 | Binding energy of *B. monnieri* phytoconstituents and standard inhibitors with different proteins involved in antioxidant defense system, locomotion physiology, and dopamine degradation pathway.

S. No	PubChem ID	Ligand name	Proteins*										
			P1	P2	P3	P4	P5	P6	P7	P8	P9	P10	P11
1	5213	Silybin	—	—	—	—	—	—	−10.3	—	—	—	—
2	6407	Chloral	—	—	—	—	—	—	—	—	−3.6	—	—
3	26757	Selegiline	—	−7	−7	−5.1	—	—	—	—	—	—	—
4	57267	Eticlopride	—	—	—	—	—	—	—	—	—	—	−4.7
5	121938	LY134046	—	—	—	—	−7.1	—	—	—	—	—	—
6	400769	CDDO-Me	—	—	—	—	—	—	—	−9.9	—	—	—
7	3033769	Raclopride	—	—	—	—	—	—	—	—	—	−6.7	−4.5
8	5280863	Kaempferol	—	—	—	—	—	−10.4	—	—	—	—	—
9	5464105	Nitecapone	−6.3	—	—	—	—	—	—	—	—	—	—
10	9876264	Bacopaside II	−6.8	−8.2	−9.8	−9	−7.6	−10.4	−9.1	−11	−8.9	—	—
11	10605023	Bacopasaponin G	−7.9	−9.9	−8.8	−9.2	−8.5	−9.4	−8.6	−11	−9	—	—
12	10629555	Bacopaside X	−8	−9.5	−9.8	−9.3	−8.3	−9.9	−9.8	−10.8	−10.2	—	—
13	10865594	Bacopaside IV	−7.4	−9	−10.3	−10	−8.2	−9.2	−9.5	−11.5	−8.9	—	—
14	11079173	Bacopaside A	−5	−6.4	−6.4	−6.3	−5.4	−6.5	−7.7	−7.3	−7	—	—
15	11113741	Bacopaside B	−8.4	−8.6	−8.3	−9.2	−7.7	−6.8	−8.1	−8.5	−9.3	—	—
16	11145924	Bacopaside C	−7.2	−10.1	−9.1	−7.9	−7.3	−7.8	−10.3	−10.1	−9.8	—	—
17	11949626	Bacopaside N1	−7.3	−8.8	−8.8	−8.6	−7.9	−8.7	−9.2	−10.9	−8.6	—	—
18	15922618	Bacopaside III	−7	−10	−10.1	−10.1	−8.9	−9.8	−10.1	−12.6	−9.7	—	—
19	16216038	Bacosaponin F	−7.1	−8.1	−8.7	−8.3	−7.8	−8.8	−7.5	−9.2	−9.6	—	—
20	21574494	Bacopaside N2	−7.4	−10.8	−8.4	−9.3	−7.8	−9.5	−10.1	−10	−9.3	—	—
21	21599442	Bacopaside I	−7.7	−10.6	−9.3	−8.9	−8	−9.6	−9.5	−11.1	−9.2	—	—
22	44421667	Bacopaside VII	−6.9	−10.4	−10.3	−9.6	−8.2	−9.7	−10.2	−10.4	−9.4	—	—
23	44421668	Bacopaside I	−7.2	−10.3	−9.4	−8.9	−7.9	−9.2	−10.2	−10.8	−9.1	—	—
24	53398644	Bacoside A	−6.8	−7.5	−7.4	−7.8	−7.6	−7.7	−8.7	−11.3	−7.5	—	—
25	71312546	Bacopaside I	−7.9	−10.1	−10.1	−9.3	−8	−8.9	−9.7	−10.4	−9.7	—	—
26	90472275	Bacopaside II	−7	−10.3	−9.3	−8.9	−9.1	−8.6	−10.8	−9.9	−9.1	—	—
27	91827005	Bacoside A3	−7	−8.8	−8.7	−8.8	−7.9	−8.7	−9.8	−9.9	−8.8	—	—
28	101062564	Bacopasaponin E	−7	−8.7	−10.7	−9	−8.2	−8.9	−8.8	−11	−9.5	—	—
29	1,01219808	Bacopaside V	−8	−11.1	−11.2	−9.6	−8.2	−9.8	−10	−12	−10.1	—	—
30	101995276	Bacopasaponin A	−8.1	−9.1	−9.7	−9.2	−8.2	−9.2	−9.8	−12.3	−8.9	—	—
31	101996847	Bacopasaponin B	−7.5	−10	−9.4	−10.3	−8.4	−8.8	−10	−10.4	−8.9	—	—
32	101996848	Bacopasaponin C	−8.2	−9.8	−9.5	−9.1	−8.7	−9.9	−9.5	−10.2	−9.1	—	—
33	102000288	Bacopasaponin D	−7.4	−11.8	−11.9	−9.3	−7.7	−8.5	−10	−9.9	−8.7	—	—
34	102080690	Bacopaside VI	−7.7	−9.8	−9.4	−9.1	−9.2	−9.4	−10.4	−11.4	−9.8	—	—
35	102080691	Bacopaside VII	−7.3	−9.7	−9.3	−9.5	−8.6	−10	−10.2	−10.1	−8.6	—	—
36	102080692	Bacopaside VIII	−7.2	−8.4	−9.5	−8.9	−8.4	−9.1	−8.9	−10.3	−8.3	—	—
37	102418532	Bacopaside XI	−8	−9.5	−11.2	−8.9	−8.8	−9.2	−10.2	−10.3	−8.2	—	—
38	102418533	Bacopaside XII	−11.1	−14	−14.8	−13.3	−13.8	−12.9	−13.1	−14.7	−15.5	—	—
39	118856250	Bacopasaponin C	−8.2	−9.8	−10.4	−9.4	−8.5	−9.3	−10	−10.3	−9.6	—	—
40	39484	MPP^+	—	—	—	—	—	—	—	—	—	−7.9	−4.9

*Proteins. *P1: COMT; P2: MAO-A Chain A; P3: MAO-A Chain B; P4: MAO-B; P5: PNMT; P6: PST; P7: UGT; P8: KEAP1; P9: ALDH1A1; P10: D3 dopamine receptor; P11: D2 dopamine receptor (S. no. 1 to 9 represent standard ligand for their respective protein).*

treatment increases the levels of DA corroborate with previous studies (Ghosh et al., 2009).

MPTP intoxication can stimulate the production of various proinflammatory molecules within the substantia nigra region (Ghosh et al., 2009). Our previous study showed that treatment with BME could attenuate the increased expression of these proinflammatory molecules in MPTP-induced mice (Singh et al., 2017). We found that MPTP intoxication led to a marked increase in gliosis as evidenced by increased number of GFAP positive neurons in the SNpc region. Thus, MPTP administration causes microglial activation and increases the expression of iNOS in the substantia nigra region of the brain (Liberatore et al., 1999), leading to the production of nitric oxide, eventually causing neuronal death. Our results showed that MPTP treatment increased the production of nitric oxide possibly by increasing the levels of iNOS. Increased iNOS activity enhances nitric oxide production, which promotes dopaminergic neuronal death by nitrosative/oxidizing damage and other respiratory deficiency (Tsang and Chung, 2009). Our results showed that MPTP intoxication increases the number of GFAP expressing cells and the transcript levels of iNOS in mice, and BME (pre- and posttreatment) ameliorates these changes. Thus, the neuroprotective and neurorescue effects of BME may involve the regulation of antioxidant enzymes and transcription factors by compounds present in BME.

In agreement with previous studies, our study showed that the toxin MPTP induces phenotypes associated with Parkinson's disease in mice such as decreased levels of dopamine and GSH; increased levels of MDA, iNOS, and TNF-α; and increased numbers of GFAP positive astrocytes. Moreover, our

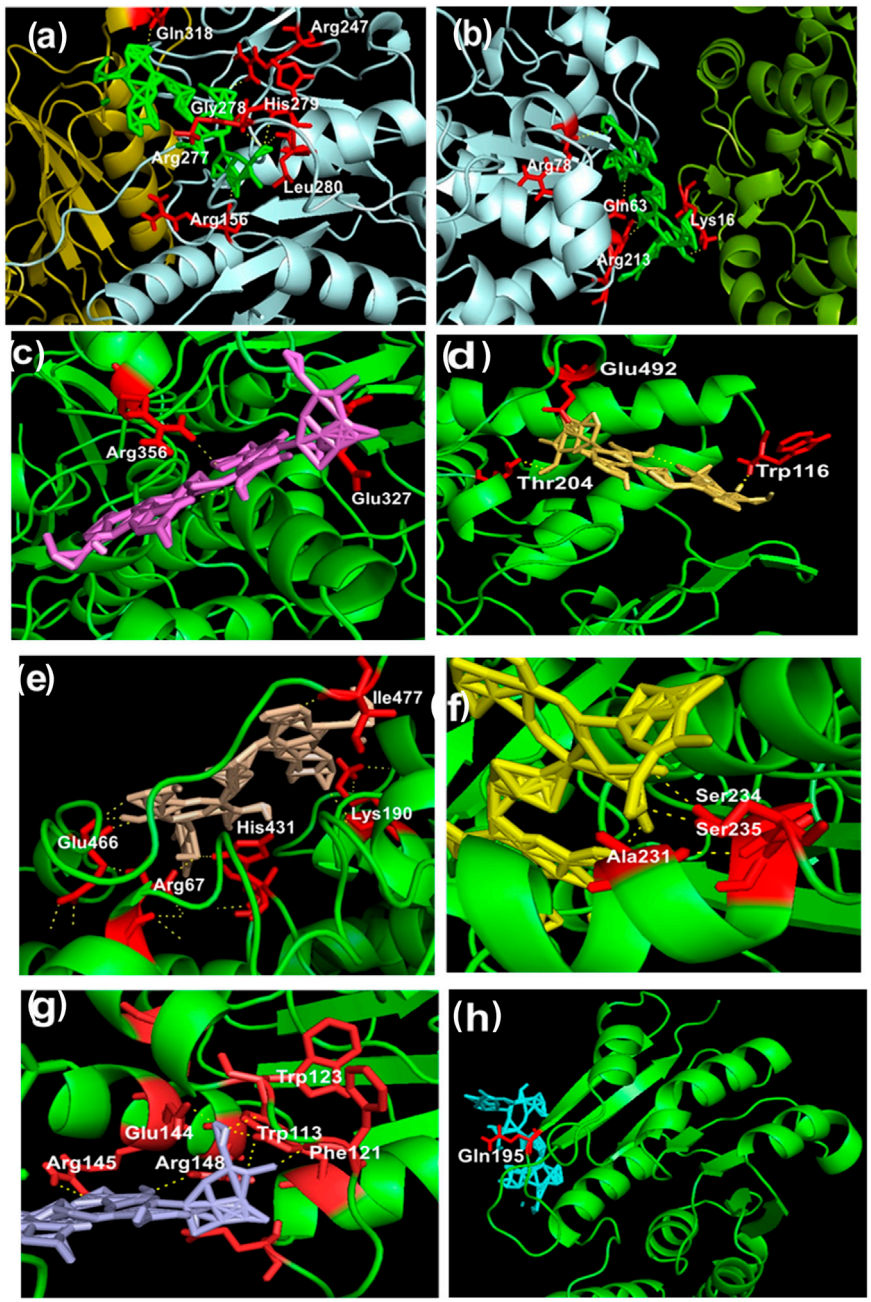

FIGURE 4 | (A–H) Representation of intermolecular hydrogen bonds between bacopaside-XII and various dopamine degradation enzymes. **(A)** UGT (PDB: 3PBL): Chain A pale cyan; Chain B deep olive; red color residues and green color bacopaside-XII. **(B)** PST (PDB: 2A3R): Chain A split pea; Chain B pale cyan; red color residues and green color bacopaside-XII. **(C)** MAO-A Chain A (PDB: 2BXS): Chain A green color; red color residues and violet color bacopaside-XII. **(D)** MAO-A Chain B (PDB: 2BXS): Chain B green color; red color residues and yellow orange color bacopaside-XII. **(E)** MAO-B (PDB: 4A79): Chain A and Chain B in green color; red color residues and wheat color bacopaside-XII. **(F)** ALDH1A1 (PDB: 4WP7): Chain A green color; red color residues and yellow color bacopaside-XII. **(G)** PNMT (PDB: 4MQ4): Chain A and Chain B in green color; red color residues and light blue color bacopaside-XII. **(H)** COMT (PDB: 3BWM): Chain A green color; red color residue and cyan color bacopaside-XII.

results suggest that pretreatment with BME is more effective in ameliorating the neurotoxicity in the MPTP-induced mice model of PD as compared with posttreatment of BME. This indicates that prior intake of BME might be more helpful in preventing neurodegeneration as well as in slowing down the disease progression (neuroprotective effect) as compared with post intake of BME (neurorescue effects). However, further studies are required to understand the mode of action of BME and to identify the active component(s) of BME responsible for neuroprotective and neurorescue effects.

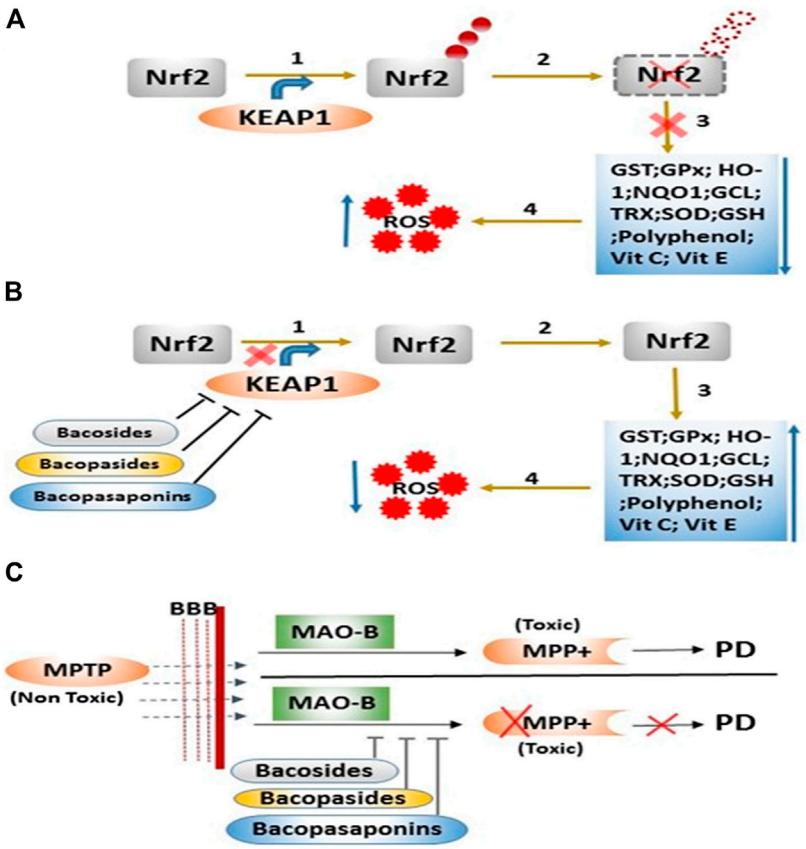

FIGURE 5 | Mode of action of *B. monnieri* phytoconstituents on the regulation of the antioxidant system and metabolic degradation of MPTP. **(A)** Step 1: ubiquitination of Nrf2 protein via KEAP1 protein, Step 2: degradation of Nrf2 protein, Step 3: downregulation of various enzymatic and nonenzymatic antioxidants, and Step 4: enhancement of reactive oxygen species (ROS). **(B)** Step 1: inhibition of KEAP1 protein via *B. monnieri* phytochemicals, Step 2: inhibition of Nrf2 degradation, Step 3: expression of enzymatic and nonenzymatic antioxidants, and Step 4: decrease in the ROS level. **(C)** *B. monnieri* phytochemicals inhibit the degradation of MPTP (nontoxic) into MPP+ (toxic) product through the binding with catalyzing enzyme MAO-B.

Our *in silico* study suggests that BM phytoconstituents (mainly bacopaside-XII) have the ability to block KEAP1 protein. Thus, it may be inferred that inhibition of KEAP1 protein further inhibits the Cullin 3-mediated ubiquitination of Nrf2 protein and thereby upregulates the expression (through Nrf2) of antioxidant enzymes (**Figures 3E,F**). We, therefore, postulate that these phytochemicals act as natural drug to counter KEAP1-mediated oxidative stress.

The enhanced levels of DA in the MPTP + BME group could be due to the protective effect of BME on dopaminergic neurons. Another possibility is that BM phytoconstituents may inhibit the enzymes involved in the DA degradation pathway. There are several distinct dopamine degradation pathways that act via the set of enzymes such as monoamine oxidase A and B (MAO-A and -B), catechol-O-methyl transferase (COMT), aldehyde dehydrogenase (ALDH), UDP-glucuronosyltransferases (UGT), phenol sulfur-transferase (PST), and phenylethanolamine N-methyltransferase (PNMT) acting in sequence (Meiser et al., 2013). We performed the molecular docking study to dock various enzymes involved in DA degradation, with BM phytoconstituents. Result showed that BM phytochemicals (bacosides, bacopaside, and bacosaponins) have the ability to inhibit all the abovementioned enzymes involved in DA degradation (**Figure 5**; **Table 1**).

CONCLUSION

Both, *in vivo* and *in silico* data indicate that BM phytochemicals have the ability to maintain DA concentrations in the mice brain by either increasing dopamine synthesis or inhibiting DA degradation. An understanding of the pathophysiology and etiology of PD at cellular and molecular levels is the clinical need of the hour. For neuroprotective disease-modifying therapy, identifying the molecular targets is essential in the field of PD basic research. Thus, our study may offer a therapeutic approach for treating this neurodegenerative disease.

DATA AVAILABILITY STATEMENT

The original contributions presented in the study are included in the article/Supplementary Material; further inquiries can be directed to the corresponding author.

ETHICS STATEMENT

The animal study was reviewed and approved by the Institutional Animal Ethical Committee (ethical clearance letter no. 39/IAH/PHARMA/14).

AUTHOR CONTRIBUTIONS

BS and SP conceived the presented idea and planned the experiments. SP verified the analytical methods and supervised the findings of this work. BS designed the model, carried out the experiments, and analyzed the data. BS wrote the manuscript with input from all authors. MR contributed to sample preparation and the interpretation of the results. BS and MR contributed to implementation of the research, to the analysis of the results, and to the writing of the manuscript. SK and PK contributed to *in silico* work design and developed the theoretical framework and the interpretation of these results. BS, SP, MR, and SK drafted the manuscript and designed the figures. RV and AM were involved in planning and supervised the work. SP, RV, and AM were in charge of overall direction and planning. All authors provided critical feedback and helped shape the research, analysis, and manuscript preparation. All authors approved the manuscript for submission.

FUNDING

This study was funded by the Council of Science and Technology, Uttar Pradesh (UPCST) (CST/SERPD/D-2794).

ACKNOWLEDGMENTS

The authors are thankful to the Council of Science and Technology, Uttar Pradesh (UPCST), Lucknow, for financial support and to the Developmental Toxicology Division, Indian Institute of Toxicology Research (IITR), Lucknow, for providing support and experimental facility.

REFERENCES

Anon (2004). Bacopa monniera. Monograph *Altern. Med. Rev.* 9(1): 79–85.

Aguiar, S., and Borowski, T. (2013). Neuropharmacological review of the nootropic herb Bacopa monnieri. *Rejuvenation Res.* 16 (4), 313–326. doi:10.1089/rej.2013.1431

Anderson, M. E. (1985). Determination of glutathione and glutathione disulfide in biological samples. *Meth Enzymol.* 113, 548–555. doi:10.1016/s0076-6879(85)13073-9

Balaji, B., Kumar, E. P., and Kumar, A. (2015). Evaluation of standardized Bacopa monniera extract in sodium fluoride-induced behavioural, biochemical, and histopathological alterations in mice. *Toxicol. Ind. Health* 31 (1), 18–30. doi:10.1177/0748233712468018

Bammidi, S. R., Volluri, S. S., Chippada, S. C., Avanigadda, S., and Vangalapati, M. (2011). A review on pharmacological studies of Bacopa monniera. *J. Chem. Biol. Phys. Sci. (Jcbps)* 1 (2), 250.

Berman, H. M., Westbrook, J., Feng, Z., Gilliland, G., Bhat, T. N., Weissig, H., et al. (2000). The protein data bank. *Nucleic Acids Res.* 28 (1), 235–242. doi:10.1093/nar/28.1.235

Cheng, H. C., Ulane, C. M., and Burke, R. E. (2010). Clinical progression in Parkinson's disease and the neurobiology of axons. *Ann. Neurol.* 67 (6), 715–725. doi:10.1002/ana.21995

Chopra, R., Nayar, L., and Chopra, I. (1956). *Glossary of Indian medicinal plants*, New Delhi: Council of Scientific and Industrial Research,.

Chowdhuri, D. K., Parmar, D., Kakkar, P., Shukla, R., Seth, P. K., and Srimal, R. C. (2002). Antistress effects of bacosides of Bacopa monnieri: modulation of Hsp70 expression, superoxide dismutase and cytochrome P450 activity in rat brain. *Phytother Res.* 16 (7), 639–645. doi:10.1002/ptr.1023

Commens, C. (1983). Fixed drug eruption. *Australas. J. Dermatol.* 24 (1), 1–8. doi:10.1111/j.1440-0960.1983.tb00240.x

de Rij, M., Launer, L., Berger, K., Breteler, M., Dartigues, J., Baldereschi, M., et al. (2000). Prevalence of Parkinson's disease in europe: a collaborative study of population-based cohorts. Neurologic diseases in the elderly research group. *Neurology* 54 (11 Suppl. 5), S21–S23.

Fernagut, P. O., Diguet, E., Labattu, B., and Tison, F. (2002). A simple method to measure stride length as an index of nigrostriatal dysfunction in mice. *J. Neurosci. Methods* 113, 123–130.

Ghosh, A., Roy, A., Matras, J., Brahmachari, S., Gendelman, H. E., and Pahan, K. (2009). Simvastatin inhibits the activation of p21ras and prevents the loss of dopaminergic neurons in a mouse model of Parkinson's disease. *J. Neurosci.* 29, 13543–13556.

Granger, D. L., Taintor, R. R., Boockvar, K. S., and Hibbs, J. B., Jr (1996). Measurement of nitrate and nitrite in biological samples using nitrate reductase and Griess reaction. *Meth Enzymol.*, 142–151. doi:10.1016/s0076-6879(96)68016-1

Hinterberger, H. (1971). The biochemistry of catecholamines in relation to Parkinson's disease. *Aust. New Zealand J. Med.* 1, 14–18.

Hutter-Saunders, J. A., Gendelman, H. E., and Mosley, R. L. (2012). Murine motor and behavior functional evaluations for acute 1-methyl-4-phenyl-1,2,3,6-tetrahydropyridine (MPTP) intoxication. *J. Neuro. Pharmacol.* 7 (1), 279–288. doi:10.1007/s11481-011-9269-4

Jadiya, P., Khan, A., Sammi, S. R., Kaur, S., Mir, S. S., and Nazir, A. (2011). Anti-Parkinsonian effects of Bacopa monnieri: insights from transgenic and pharmacological *Caenorhabditis elegans* models of Parkinson's disease. *Biochem. Biophys. Res. Commun.* 413 (4), 605–610. doi:10.1016/j.bbrc.2011.09.010

Kumar, R. R., Kathiravan, K., and Muthusamy, R. (2012). Bacopa monniera a potent neuroprotector against transient global cerebral ischemia induced hippocampal damage and memory function. *Int. J. Anatom. Sci.* 3, 26–32.

Liberatore, G. T., Jackson-Lewis, V., Vukosavic, S., Mandir, A. S., Vila, M., McAuliffe, W. G., et al. (1999). Inducible nitric oxide synthase stimulates dopaminergic neurodegeneration in the MPTP model of Parkinson disease. *Nat. Med.* 5, 1403.

Meiser, J., Weindl, D., and Hiller, K. (2013). Complexity of dopamine metabolism. *Cell Commun. Signal.* 11 (1), 34. doi:10.1186/1478-811X-11-34

O'Boyle, N. M., Banck, M., James, C. A., Morley, C., Vandermeersch, T., and Hutchison, G. R. (2011). Open Babel: an open chemical toolbox. *J. Cheminform* 3, 33. doi:10.1186/1758-2946-3-33

Ohkawa, H., Ohishi, N., and Yagi, K. (1979). Assay for lipid peroxides in animal tissues by thiobarbituric acid reaction. *Anal. Biochem.* 95 (2), 351–358. doi:10.1016/0003-2697(79)90738-3

Piggott, M., Marshall, E., Thomas, N., Lloyd, S., Court, J., Jaros, E., et al. (1999). Dopaminergic activities in the human striatum: rostrocaudal gradients of uptake sites and of D1 and D2 but not of D3 receptor binding or dopamine. *Neuroscience* 90, 433–445.

Pravina, K., Ravindra, K., Goudar, K., Vinod, D., Joshua, A., Wasim, P., et al. (2007). Safety evaluation of BacoMind in healthy volunteers: a phase I study. *Phytomedicine* 14 (5), 301–308. doi:10.1016/j.phymed.2007.03.010

Prisila Dulcy, C., Singh, H. K., Preethi, J., and Rajan, K. (2012). Standardized extract of Bacopa monniera (BESEB CDRI-08) attenuates contextual associative

learning deficits in the aging rat's brain induced by D-galactose. *J. Neurosci. Res.* 90 (10), 2053–2064. doi:10.1002/jnr.23080

Rai, D., Bhatia, G., Palit, G., Pal, R., Singh, S., and Singh, H. K. (2003). Adaptogenic effect of Bacopa monniera (brahmi). *Pharmacol. Biochem. Behav.* 75 (4), 823–830. doi:10.1016/s0091-3057(03)00156-4

Rai, S. N., Yadav, S. K., Singh, D., and Singh, S. P. (2016). Ursolic acid attenuates oxidative stress in nigrostriatal tissue and improves neurobehavioral activity in MPTP-induced Parkinsonian mouse model. *J. Chem. Neuroanat.* 71, 41–49. doi:10.1016/j.jchemneu.2015.12.002

Sanner, M. F. (1999). *Python*: a programming language for software integration and development. *J. Mol. Graph Model.* 17 (1), 57–61.

Schwarting, R., Bonatz, A., Carey, R., and Huston, J. (1991). Relationships between indices of behavioral asymmetries and neurochemical changes following mesencephalic 6-hydroxydopamine injections. *Brain Res.* 554, 46–55.

Shinomol, G. K., and Bharath, M. S. (2012). Neuromodulatory propensity of Bacopa monnieri leaf extract against 3-nitropropionic acid-induced oxidative stress: in vitro and in vivo evidences. *Neurotox. Res.* 22, 102–114.

Simpson, T., Pase, M., and Stough, C. (2015). Bacopa monnieri as an antioxidant therapy to reduce oxidative stress in the aging brain. *Evid. Based Complemen. Alternat. Med.* 2015.

Singh, B., Pandey, S., Rumman, M., and Mahdi, A. A. (2020). Neuroprotective effects of Bacopa monnieri in Parkinson's disease model. *Metab. Brain Dis.* 35 (3), 517–525. doi:10.07/s11011-019-00526-w10.1007/s11011-019-00526-w

Singh, B., Pandey, S., Verma, R., Ansari, J. A., and Mahdi, A. A. (2016). Comparative evaluation of extract of Bacopa monnieri and Mucuna pruriens as neuroprotectant in MPTP model of Parkinson's disease. *Int. J. Experimen. Biol.* 54, 758–766.

Singh, B., Pandey, S., Yadav, S. K., Verma, R., Singh, S. P., and Mahdi, A. A. (2017). Role of ethanolic extract of Bacopa monnieri against 1-methyl-4-phenyl-1,2,3,6-tetrahydropyridine (MPTP) induced mice model via inhibition of apoptotic pathways of dopaminergic neurons. *Brain Res. Bull.* 135, 120–128. doi:10.1016/j.brainresbull.2017.10.007

Terry, A. V., Stone, J., Buccafusco, J., Sickles, D., Sood, A., and Prendergast, M. (2003). Repeated exposures to subthreshold doses of chlorpyrifos in rats: hippocampal damage, impaired axonal transport, and deficits in spatial learning. *J. Pharmacol. Exp. Ther.* 305 (1), 375–384. doi:10.1124/jpet.102.041897

Tiwari, S. K., Agarwal, S., Seth, B., Yadav, A., Nair, S., Bhatnagar, P., et al. (2014). Curcumin-loaded nanoparticles potently induce adult neurogenesis and reverse cognitive deficits in Alzheimer's disease model via canonical Wnt/β-catenin pathway. *ACS Nano* 8 (1), 76–103. doi:10.1021/nn405077y

Tsang, A. H., and Chung, K. K. (2009). Oxidative and nitrosative stress in Parkinson's disease. *Biochim. Biophys. Acta* 1792, 643–650.

Yadav, K. D., Reddy, K., and Kumar, V. (2014a). Beneficial effect of Brahmi Ghrita on learning and memory in normal rat. *Ayu* 35 (3), 325. doi:10.4103/0974-8520.153755

Yadav, S. K., Prakash, J., Chouhan, S., Westfall, S., Verma, M., Singh, T. D., et al. (2014b). Comparison of the neuroprotective potential of Mucuna pruriens seed extract with estrogen in 1-methyl-4-phenyl-1,2,3,6-tetrahydropyridine (MPTP)-induced PD mice model. *Neurochem. Int.* 65, 1–13. doi:10.1016/j.neuint.2013.12.001

Yamaguchi, H., and Shen, J. (2007). Absence of dopaminergic neuronal degeneration and oxidative damage in aged DJ-1-deficient mice. *Mol. Neurodegen.* 2, 10.

Conflict of Interest: The authors declare that the research was conducted in the absence of any commercial or financial relationships that could be construed as a potential conflict of interest.

frontiers in Pharmacology

ORIGINAL RESEARCH
published: 29 April 2021
doi: 10.3389/fphar.2021.646287

Role of Oxidative Stress and the Identification of Biomarkers Associated With Thyroid Dysfunction in Schizophrenics

Mahmood Rasool[1,2], Arif Malik[3], Shamaila Saleem[4], Muhammad Abdul Basit Ashraf[4], Altaf Qadir Khan[5], Sulayman Waquar[3], Ayesha Zahid[3], Sumaira Shaheen[6], Muhammad Abu-Elmagd[1,2], Kalamegam Gauthaman[1,2] and Peter Natesan Pushparaj[1,2]*

[1]Department of Medical Laboratory Technology, Faculty of Applied Medical Sciences, King Abdulaziz University, Jeddah, Saudi Arabia, [2]Center of Excellence in Genomic Medicine Research, King Abdulaziz University, Jeddah, Saudi Arabia, [3]Institute of Molecular Biology and Biotechnology (IMBB), The University of Lahore, Lahore, Pakistan, [4]University College of Medicine and Dentistry, The University of Lahore, Lahore, Pakistan, [5]Department of Psychiatry, Ameer-Ud-Din Medical College, Lahore, Lahore, Pakistan, [6]Center for Research in Molecular Medicine, The University of Lahore, Lahore, Pakistan

OPEN ACCESS

Edited by:
Muhammad Ayaz,
University of Malakand, Pakistan

Reviewed by:
Ali Saber Abdelhameed,
King Saud University, Saudi Arabia
Muhammad Asif,
Balochistan University of Information Technology, Pakistan
Ihsan Ullah,
University of Swabi, Pakistan

***Correspondence:**
Mahmood Rasool
mahmoodrasool@yahoo.com

Specialty section:
This article was submitted to Neuropharmacology, a section of the journal Frontiers in Pharmacology

Received: 25 December 2020
Accepted: 23 March 2021
Published: 29 April 2021

Citation:
Rasool M, Malik A, Saleem S, Ashraf MAB, Khan AQ, Waquar S, Zahid A, Shaheen S, Abu-Elmagd M, Gauthaman K and Pushparaj PN (2021) Role of Oxidative Stress and the Identification of Biomarkers Associated With Thyroid Dysfunction in Schizophrenics. Front. Pharmacol. 12:646287. doi: 10.3389/fphar.2021.646287

Background: Schizophrenia is associated with a deficiency of dietary antioxidants like vitamin B6, B9, and B12 resulting in defective methylation leading to hyperhomocysteinemia. Hyperhomocysteinemia causes mitochondrial DNA damage, oxidative stress, vascular damage, and lipid peroxidation. Oxidative stress and increase in reactive oxygen species result in 8-oxodG production which induces apoptosis of both astrocytes and thyrocytes thus predisposing them to thyroid dysfunction and neurodegeneration. Furthermore, the presence of excessive free radicals increases thyroid thermogenesis causing hyperthyroidism or its excess may cause hypothyroidism by inhibiting iodide uptake. In the present study, we evaluated the various biomarkers associated with thyroid dysfunction in schizophrenics.

Materials and Methods: 288 patients suffering from schizophrenia and 100 control subjects were screened for liver function tests (LFTs) such as alanine aminotransferase (ALT), aspartate aminotransferase (AST), alkaline phosphatase (ALP), and total bilirubin (TB). Also, the stress markers, namely malondialdehyde (MDA), homocysteine, cysteine, methionine, the thyroid profile including triiodothyronine (T3), thyroxine (T4), thyroid-stimulating hormone (TSH), thyroxine peroxide antibody (TPO-Ab); TSH receptor-Ab (TSHr-Ab), dietary antioxidants, lipids, cytokines, aminoacids and hormones, vitamins and trace elements, and other biochemical parameters.

Results: The LFTs showed elevated levels of ALT (45.57 ± 4.87 Vs. 26.41 ± 3.76 U/L), AST (40.55 ± 1.34 Vs. 21.92 ± 3.65 U/L), ALP (121.54 ± 4.87 Vs. 83.76 ± 5.87 U/L), and total bilirubin (2.63 ± 0.987 Vs. 1.10 ± 0.056 mg/dl), in schizophrenics than controls. Increased levels of MDA (3.71 ± 0.967 Vs. 1.68 ± 0.099) and homocysteine (17.56 ± 2.612 Vs. 6.96 ± 1.987 μmol/L were observed in schizophrenics compared to the controls, indicating increased stress. Levels of cysteine and methionine were decreased in schizophrenics than the controls (1.08 ± 0.089 Vs. 4.87 ± .924 μmol/L and 17.87 ± 1.23 Vs. 99.20 ± 5.36 μmol/L). The levels of TPO-Ab (IU/ml), Tg-Ab (pmol/L), and

TSHr-Ab (IU/L) were observed to be higher in the patients' group as compared to control subjects (9.84 ± 2.56 Vs. 5.81 ± 1.98, 55.50 ± 2.98 Vs. 32.95 ± 2.87 and 2.95 ± 0.0045 Vs. 1.44 ± 0.0023 respectively). Levels of Vitamin B6, B9, and B12 were also significantly decreased in the patients compared to the healthy controls.

Conclusion: The schizophrenics, demonstrated altered liver function, increased stress markers, and decreased dietary antioxidants. Reduced primary and secondary antioxidant levels, may result in hyperhomocysteinemia and cause further DNA and mitochondrial damage. Therefore, homocysteine and/or prolactin levels may serve as candidate prognostic markers for schizophrenia. Also, both neurological symptoms and the susceptibility to thyroid disorders may be prevented in the initial stages of this debilitating disorder by appropriate dietary supplementation of antioxidants which can rectify a reduction in primary and secondary antioxidants, and disturbed prolactin-serotonin-dopamine interactions in schizophrenics.

Keywords: schizophrenia, hyperhomocysteinemia, oxidative stress, autoimmune thyroid diseases, biomarkers, antioxidants, reactive oxygen species, prolactin

INTRODUCTION

Schizophrenia is a neuropsychiatric disorder manifested by disruptive thinking, quantifiable language disturbances, perception, and self-sense (Barnham et al., 2004; Ciobica et al., 2011). It is characterized by disturbances in behavior, thinking ability, and gross distortion from reality (Ciobica et al., 2011). Among the psychiatric disorders, schizophrenia accounts for 1.1% of adults with nearly 21 million individuals being affected in the United States alone (Santos et al., 2012). It is among the seven most disabling diseases in patients between 20–45 years of age being more common than cardiovascular diseases, HIV, and diabetes. The identified causative agents for schizophrenia are stress, malnutrition, genetics, drugs, and alcohol abuse (Svrakic et al., 2013). The symptoms of schizophrenia are categorized into three groups: general (depression and hostility), positive (delusions and hallucinations), and negative (anhedonia and violation) (Barnham et al., 2004; Tamminga and Holcomb, 2005).

Schizophrenics have susceptibility toward thyroid disorders, and the reduction in catalase (CAT) levels results in elevated hydrogen peroxide (H_2O_2) thereby playing a potential role in thyroid hormogenesis (Adam-Vizi and Chinopoulos, 2006). Oxidative stress occurs in both astrocytes and thyrocytes as there is an increase in pro-oxidants and a decrease in antioxidants due to an increase in the production or decrease in the processing of reactive oxygen species (ROS) (Li et al., 2006). In schizophrenia, there is either reduction in primary antioxidants levels including superoxide dismutase (SOD), CAT and glutathione peroxidase (GPx), or a decrease in the secondary antioxidants such as glutathione, vitamins B6 (pyridoxine), B9 (folate), B12 (cobalamin), C, D, and E (Schweizer et al., 2008; Mitchell et al., 2014). The deficiency in vitamins B6, B9, and B12 leads to enhanced homocysteine levels resulting in decreased glutathione and vitamins C and E levels mediating oxidative insult leading to neurotoxic effects (Lindqvist et al., 2017; Mikkelsen et al., 2017). Reduced vitamin C levels induce serotonin reduction and dopamine induction but on the other hand, levels of trace elements including copper and zinc have opposite effects resulting in hyperprolactinemia mediated depression (Pohl et al., 2011). Vitamin E has thyroid hormone suppressive action thus its deficient levels induce hyperthyroidism (Subudhi and Chainy, 2010).

The disturbed serotonin-dopamine-prolactin interactions are one side of the picture while the other aspect is deranged thyroid functions including higher thyroid-stimulating hormone (TSH) levels indicating hypothyroidism (Petrulea et al., 2012). It has been shown that dietary lack of L-arginine and an increase in asymmetrical dimethylarginine (ADMA) due to hyperhomocysteinemia reduces nitric oxide synthase (NOS) dependent nitric oxide (NO) production leading to schizophrenic symptoms. Glutamate is an important amino acid in the production of both glutathione and NO, and its deficiency mediates schizophrenic symptoms (Koga et al., 2011). Phenylalanine and tyrosine ultimately produce dopamine, but their reduced levels also induce an imbalanced serotonin-dopamine-prolactin relationship (Liao and Ya-Mei, 2014). In schizophrenics, there may be dietary insufficiency or poor exposure to sunlight resulting in vitamin D deficiency, which makes them susceptible to autoimmune thyroid disorders and is reflected by higher thyroid antibody levels (Kivity et al., 2011). The present study aimed to 1) determine the levels of primary and secondary antioxidants in the serum of schizophrenics, 2) assess homocysteine levels and their relation to thyroid dysfunction, 3) examine serotonin-dopamine-prolactin interactions and hyperprolactinemia mediated depression (HMD), 4) observe the schizophrenics susceptibility to thyroid disorders by measuring their thyroid profile and 5) elucidate vitamin D levels and their effects in rendering the schizophrenics to autoimmune thyroid disorders (AITDs).

MATERIALS AND METHODS

Subjects

Two hundred and eighty-eight newly diagnosed patients (males and females) suffering from schizophrenia in the age group of

13–73 years were considered and included in the prospective study at the Department of Psychiatry, Social Security Hospital Lahore, Fountain House Lahore, and Mental Hospital Lahore, Lahore, Pakistan. One hundred sex and age-matched healthy individuals free from schizophrenia with an age range between 15 and 70 years were considered as controls. The study was conducted according to the ethical committee approval of the Institute of Molecular Biology and Biotechnology (IMBB), The University of Lahore (UOL) (IRB/IMBB/UOL/ph-984). Before the start of the study, written informed consent was obtained from all participants of the study according to Helsinki's declaration.

Inclusion and Exclusion Criteria

Newly diagnosed schizophrenia patients were included and any subject with a history of smoking, alcohol intake, or on antiparkinsonian/antipsychotic medications was excluded from the study (Duval et al., 2010; Bredin et al., 2013). All control subjects were healthy with no history of chronic diseases such as diabetes mellitus, liver diseases, and cancer (Duval et al., 2010; Duval et al., 2020).

Blood Samples

Blood samples were collected from the cubital vein of each subject in appropriate tubes (with or without anticoagulant) for separation of plasma and serum separately. Plasma was separated immediately and for the serum separation, the blood samples were allowed to clot by leaving the sample at room temperature for 30 min. The clotted blood sample was then centrifuged at 3,000 rpm for 10 min and the clear supernatant was collected. Both the plasma and serum were aliquoted and stored at -80°C until analysis.

Biochemical Analysis

All patients were assessed for their demographic profile and screened for their fasting blood glucose (FBG), gamma-glutamyl transferase (GGT), albumin (ALB), blood urea nitrogen (BUN), bicarbonate (HCO_3), uric acid, and bilirubin using a semi-automated clinical chemistry analyzer as described before (Kumari et al., 2020).

Estimation of Lipid Profile

The lipid profiles including total cholesterol (TCh), triglycerides (TGL), high-density lipoproteins (HDL), low-density lipoproteins (LDL) were estimated using commercially available kits (Sigma-Aldrich, United States).

Liver Function Tests

Assays for liver function tests (LFTs) were performed including aspartate aminotransferase (AST), alanine aminotransferase (ALT), alkaline phosphatase (ALP), and total bilirubin (TB) using commercially available kits (Sigma-Aldrich, United States).

Estimation of Antioxidant Profile

Glutathione was estimated based on the method described Moron et al., 1979. The 100 µl of plasma was taken and added 0.02 M (2.4 µl) EDTA and ice-cooled (10 min), Followed by the addition of 2 ml distilled water. To this 50.0 µl of TCA (50%) was added and incubated on ice for 15 min. Samples were then centrifuged (3,500 rpm). The supernatant was removed and added with 2 ml of 0.15 M Tris. HCl and 0.05 ml (DTNB). Absorbance was measured at 412 nm. Catalase (CAT) was determined by the method of Aebi, 1974. 100 µl of the sample was added to the tube followed by 1.9 ml of phosphate buffer and 1 ml of H_2O_2. The absorbance was measured after every minute at 240 nm. Superoxide dismutase (SOD) was estimated as per Kakkar et al., 1984. The 100 µl of the sample was taken in the tube, added with 1.2 ml of PBS, 100 µl of phenazine methosulfate, 300 µl of NBT, and 200 µl of NADH. Thereafter, 100 µl of Glacial acetic acid and 4 ml of 2-propanol were added further in the tube and centrifuged at 3,000 rpm for 10 min. The absorbance was taken at 560 nm. Glutathione peroxidase (GPX) was analyzed by Goldberg and Spooner, 1983, and Glutathione Reductase (GR) using commercially available kits (Sigma-Aldrich, United States). Malondialdehyde (MDA) was estimated using the method described by Ohkawa et al., 1979. 200 µl of the sample was taken in the tube, to which 200 µl of 8.1% SDS and 1.5 ml of 20% acetic acid were added. Later 1.5 ml of 0.8% TBA and 600 µl of distilled water along with 4 ml of 2-propanol was supplemented. It was centrifuged (4,000 rpm, 10 min) and the supernatant was removed for measuring absorbance at 532 nm using a UV-1100 spectrophotometer. Advanced Oxidative Protein Products (AOPPS) was estimated by the method of Witko-Sarsat et al., 1998. 200 µl of the sample was first diluted with PBS, then 10 µl of KI (1.16 M), and 20 µl of acetic acid was added. The sample was centrifuged at 5,000 rpm for 5 min and absorbance was measured at 340 nm on UV-spectrophotometer. Advanced glycation end products (AGEs) were estimated based on the method provided by Kalousova et al., 2002.

Nitric Oxide (NO) was estimated based on the method described before (Rasool et al., 2016). 100 µl of Griess Reagent was added with 300 µl of sample and supplemented with 2.6 ml of distilled water followed by incubation (30 min). The absorbance was measured at 548 nm. On the other hand, the myeloperoxidase (MPO), nitric oxide synthase (NOS), C - reactive protein (CRP), and ferritin levels were estimated using a commercial kit from Sigma-Aldrich, United States.

Thyroid Profile

The thyroid profile [triiodothyronine (T3), thyroxine (T4), thyroid-stimulating hormone (TSH), thyroid-stimulating hormone receptor antibodies (TSHr-Ab), thyroid peroxidase (TPO), thyroglobulin (TG), levels of reverse triiodothyronine (rT3), levels were also measured using commercially available kits (Sigma Diagnostics, United States).

Estimation of Vitamins and Trace Elements

Vitamin C was estimated based on the method described by Chinoy et al.,1986. 100 µl of the sample was added with 400 µl of TCA 5% and centrifuged at 3,000 rpm for 10 min. 320 µl of supernatant was separated and added with 130 µl of DTC and allowed to heat at 90° for 1 h. It was later ice-cooled and added with 600 µl of sulphuric acid then subjected to absorbance at 520 nm (Rasool et al., 2017). Vitamin E was estimated by the method of Rosenberg, 1992. 200 µl of the sample was supplemented with 200 µl of ethanol, 200 µl of n-hexane, and

TABLE 1 | Demographic/physical characteristics.

Characteristics	Schizophrenics (n = 288)	Control (n = 100)
Age (Yrs)	13–73	15–70
Male (n)	162	47
Females (n)	126	53
Weight (kg)	21-77	20-80
SBP (mmHg)	133.48	130.21
DBP (mmHg)	84.59	81.24
BMI (kg/m^2)	21.87	20.76

distilled water. It was then centrifuged at 3,000 rpm for 10 min and added with 25 µl of Bathophenanlhroline, 75 µl of ferric chloride, and 50 µl of Orthophosphoric Acid. Its absorbance was taken at 536 nm (Rasool et al., 2017). Both Vitamin A and Vitamin D were measured based on the methods described by Rutkowski and Grzegorczyk, 2007 and Arneson and Arneson, 2013 respectively. The vitamins (B6, B9, and B12) were estimated using the methods described before (Shaik and Gan, 2013). Sodium (Na) and potassium (K) were estimated by taking their absorbance with the help of a flame photometer (Kumar and Gill, 2018) and other trace elements in plasma were estimated based on the methods described previously (Bolann et al., 2007).

Estimation of IL-2, IL-6, and TNF-alpha

Cytokines such as interleukins (IL-2, IL-6), and tumor necrosis factor-alpha (TNF-α) were analyzed using respective commercial enzyme-linked immunosorbent assay (ELISA) kits (BioVendor, Czech Republic).

Aminoacids and Hormonal Profiles

The plasma aminoacids were estimated using the methods described by Shimbo et al., 2010. The levels of dopamine, serotonin, and prolactin were estimated using commercially available kits (Enzo Life Sciences Inc., United States).

Statistical Analysis

All the statistical analysis was performed using SPSS version 21(IBM SPSS, United States). Variables were assessed with One-way ANOVA ($p < 0.05$) and Pearson Correlation was plotted.

RESULTS

The results from age and sex-matched controls and schizophrenics, in general, represent the physiological and biochemical parameters indicating the susceptibility and development of thyroid disorders in schizophrenics. The controls were selected to match the demographic profile of age, weight, body mass index (BMI), gender distribution, systolic, and diastolic blood pressure (**Table 1**).

Lipid Profile

The lipid profile of the schizophrenic patients was compared with the same number of controls (**Table 2**). The value of total cholesterol (Tch) was higher in schizophrenics (5.10 ± 1.76 mg/dl) than the control (4.49 ± 0.978 mg/dl). The LDL levels was also higher in schizophrenics (2.91 ± 0.564 mg/dl) than the control (2.31 ± 0.876 mg/dl). However, both the increases in Tch and LDL were statistically not significant. The levels of HDL was decreased in schizophrenics (1.31 ± 0.654 mg/dl) compared to the control (1.67 ± 0.265 mg/dl). Triglyceride levels was increased in schizophrenics (2.49 ± 0.056 mg/dl) compared to healthy control (1.40 ± 0.097 mg/dl). Both the decrease in HDL (p = 0.044) and the increase in triglycerides (p = 0.037) were statistically significant.

Liver Profile

Higher levels of ALT (45.57 ± 4.87 Vs. 26.41 ± 3.76 U/L), AST (40.55 ± 1.34 Vs. 21.92 ± 3.65 U/L), ALP (121.54 ± 4.87 Vs. 83.76 ± 5.87 U/L) and total bilirubin (2.63 ± 0.987 Vs. 1.10 ± 0.056 mg/dl) were found in schizophrenics in comparison to the corresponding controls (**Table 3**) and these increases in values were highly significant (p = 0.010, 0.014, 0.018 and 0.034 respectively). The levels of total protein (6.57 ± 1.56 mg/dl vs. 6.46 ± 1.65 mg/dl) in schizophrenics and controls respectively did not show much difference. However, serum albumin was significantly (p = 0.045) reduced in schizophrenics (2.71 ± 0.765 mg/dl) compared with healthy controls (2.79 ± 0.456 mg/dl).

Antioxidant Profile

The various antioxidant parameters evaluated demonstrated a correlation between schizophrenics and the development or progression of thyroid disorders. The MDA levels (nmol/ml) varied significantly (p = 0.0213) and demonstrated elevated levels (3.71 ± 0.967) in schizophrenics than the healthy group (1.68 ± 0.099) (**Table 4**). The critical role of ROS and reactive nitrogen species (RNS) in the development of schizophrenia and its progression towards thyroid disorders is evident by the enzymatic and non-enzymatic antioxidants profile including SOD (µg/dl), GSH (µg/dl), CAT (µmol/mol of protein), GPx (mmol/dl) and GR (µmol/ml) respectively. All the above biomarkers showed very significant variations (**Table 4**). The levels of SOD (0.11 ± 0.0034 Vs. 0.45 ± 0.0056), GSH (4.48 ± 0.965 Vs. 9.06 ± 1.75), CAT (2.30 ± 0.0564 Vs. 3.67 ± 0.0376) and GPx (6.67 ± 0.987 Vs. 8.06 ± 1.87) were reduced in schizophrenics compared to the control. On the other hand, GR levels were higher in the patients relative to control (4.29 ± 0.365 Vs. 1.69 ± 0.002). Pro-oxidant levels including NO, NOS, and oxidative damage products like AOPsP, AGEs, and 8-OHdG showed a significant difference among themselves (p = 0.423, 0.017, 0.0110, 0.0287, and 0.0011 respectively). The levels of NO (23.27 ± 3.87 Vs. 56.33 ± 7.45 ng/ml) and NOS (7.87 ± 1.87 Vs. 56.76 ± 2.67 U/L) were decreased, while the levels of AOPPs (1.43 ± 0.0043 Vs. 0.90 ± 0.0067 ng/ml), AGEs (2.77 ± 0.0046 Vs. 2.57 ± 0.0045 ng/ml) and 8-OHdG (2.76 ± 0.0067 Vs. 1.18 ± .0045 ng/ml) were increased in the subjects versus controls.

Cytokine Profile

Cytokines have pleiotropic functions and serve as potential prognostic and diagnostic variables to establish the severity, stage, and treatment of a given disease. The data shown in (**Table 4**) depicted that cytokines including IL-2, IL-6, and

TABLE 2 | Lipid profiles of schizophrenics versus controls.

Variables	Schizophrenics vs. control (mean ± SD)				*p*-values (< 0.05)
	Control	Schizophrenics	Schizophrenics (male)	Schizophrenics (female)	
TCh (mg/dl)	4.49 ± 0.978	5.10 ± 1.76	5.27 ± 1.76	4.97 ± 1.74	0.066
LDL (mg/dl)	2.31 ± 0.876	2.91 ± 0.564	2.89 ± 0.331	2.92 ± 0.86	0.097
HDL (mg/dl)	1.67 ± 0.265	1.31 ± 0.654	1.33 ± 0.422	1.30 ± 0.564	0.044
Tg (mg/dl)	1.40 ± 0.097	2.49 ± 0.056	2.50 ± 0.076	2.48 ± 0.069	0.037

TABLE 3 | Hepatic profiles of schizophrenics versus controls.

Variables	Schizophrenics vs. control (mean ± SD)				*p*-values (< 0.05)
	Control	Schizophrenics	Schizophrenics (male)	Schizophrenics (female)	
ALT (U/L)	26.41 ± 3.76	45.57 ± 4.87	41.97 ± 6.98	48.38 ± 4.98	.010
AST (U/L)	21.92 ± 3.65	40.55 ± 1.34	42.11 ± 4.76	39.45 ± 2.87	.014
ALP (U/L)	83.76 ± 5.87	121.54 ± 4.87	127.53 ± 8.65	131.55 ± 10.65	.018
ALB (mg/dl)	3.61 ± .978	2.71 ± .765	2.79 ± .456	2.64 ± .762	.045
T.Bili (mg/dl)	1.10 ± .056	2.63 ± .987	2.85 ± .564	2.47 ± .675	.034
TP (mg/dl)	6.46 ± 1.65	6.57 ± 1.56	6.58 ± 1.78	6.55 ± 1.33	.087

TABLE 4 | Antioxidant profiles of schizophrenics versus controls.

Variables	Schizophrenics vs. control (mean ± SD)				*p*-values (< 0.05)
	Control	Schizophrenics	Schizophrenics (male)	Schizophrenics (female)	
MDA (nmol/L)	1.68 ± .099	3.71 ± .967	3.77 ± .365	3.66 ± .331	.0213
SOD (μg/dl)	0.45 ± .0056	0.11 ± .0034	0.11 ± .0076	0.11 ± .0056	.0423
GSH (μmol/L)	9.06 ± 1.75	4.48 ± .965	4.13 ± 1.089	4.76 ± 1.78	.0376
CAT (μmol/mol of protein)	3.67 ± .0376	2.30 ± .0564	2.16 ± .076	2.40 ± .067	.0187
GGT (U/L)	44.154.87	57.99 ± 5.87	56.95 ± 6.76	58.79 ± 3.98	.0245
CRP (mg/dl)	1.08 ± .0037	1.45 ± .0022	1.47 ± .0067	1.44 ± .0045	.0354
IL-6 (pg/ml)	3.73 ± 2.76	6.69 ± 3.87	6.61 ± 1.87	6.76 ± .96	.0010
IL-2 (pg/ml)	2.65 ± 1.56	5.34 ± 1.77	6.65 ± 1.87	4.03 ± 1.02	.0310
TNF-α (pg/ml)	30.42 ± 3.87	31.60 ± 5.76	31.78±3.87	31.47 ± 3.08	.0332
AOPPs (ng/ml)	0.90 ± .0067	1.43 ± .0043	1.35 ± .0065	1.49 ± .090	.0110
AGEs (ng/ml)	2.57 ± .0045	2.77 ± .0046	2.77 ± .0031	2.77 ± .0027	.0287
NO (ng/ml)	23.27 ± 3.87	56.33 ± 7.45	56.58 ± 6.64	56.13 ± 7.87	.0423
GPx (μmol/L)	8.06 ± 1.87	6.67 ± .987	6.61 ± 1.78	6.71 ± 1.33	.0187
GRx (μmol/L)	1.69 ± .0023	4.29 ± .365	3.91 ± .0076	4.58 ± .192	.0214

TNF-α play a considerable role in the development of schizophrenia. The levels of IL-2 (pg/ml) (5.34 ± 1.77 Vs. 2.65 ± 1.56), IL-6 (pg/ml) (6.69 ± 3.87 Vs. 3.73 ± 2.76) and TNF-α (pg/ml) (31.60 ± 5.76 Vs. 30.42 ± 3.87) were increased in schizophrenics than the control subjects and varied significantly ($p < 0.05$) among each other.

Thyroid Hormone Profile

The thyroid function tests and related antibodies exhibited a diverse representation among schizophrenics and control and displayed a statistical significance ($p < 0.05$). Higher levels of freeT4 (21.30 ± 2.87 Vs. 10.66 ± 1.87 pmol/L) and TSH (5.09 ± 1.98 Vs. 2.00 ± 0.0045 mIU/L) and lower levels of freeT3 (3.85 ± 0.99 Vs. 4.58 ± 1.09 pg/ml) were observed in schizophrenics compared to controls (**Table 5**). Elevated levels of thyroid antibodies also revealed the development of autoimmune thyroid disorders (AITDs) in schizophrenia subjects. The levels of TPO-Ab (IU/ml), TG-Ab (pmol/L), and TSHr-Ab (IU/L) were observed to be higher in the patients' group as compared to control subjects (9.84 ± 2.56 Vs. 5.81 ± 1.98, 55.50 ± 2.98 Vs. 32.95 ± 2.87 and 2.95 ± 0.0045 Vs. 1.44 ± 0.0023 respectively). The increases in FT4, TSH, and thyroid antibodies in schizophrenics indicate the association of schizophrenia with thyroid disorders.

Vitamins and Trace Elements Profile

The levels of water-soluble vitamins tested in schizophrenia showed significant decrease in their levels compared to the control (**Table 6**). The decreased levels of Vit B6 (23.98 ± 3.65 nmol/L), Vit B9 (1.97 ± 0.034 nmol/L), Vit B12 (89.98 ± 10.25 pmol/L) and Vit C (0.36 ± 0.0035 nmol/L) were recorded in schizophrenics susceptible to AITDs in comparison to healthy controls (Vit B6 87.67 ± 7.24, Vit B9 2.78 ± 0.092, Vit B12 234.65 ± 11.87 and Vit C 0.54 ± 0.0034

TABLE 5 | Thyroid hormone profiles of schizophrenics versus controls.

Variables	Schizophrenics vs. control (mean ± SD)				*p* values (< 0.05)
	Control	Schizophrenics	Schizophrenics (male)	Schizophrenics (female)	
FT4 (pmol/L)	10.66 ± 1.87	21.30 ± 2.87	21.36 ± 3.98	21.25 ± 4.65	.0457
FT3 (μg/dl)	4.58 ± 1.09	3.85 ± .99	3.88±.86	3.82 ± .778	.0344
TSH (IU/L)	2.00 ± .0045	5.09 ± 1.98	4.89 ± .997	5.24 ± 1.08	.0214
TgAb (IU/L)	32.95 ± 2.87	55.50 ± 2.98	55.48 ± 5.76	55.51 ± 5.64	.0409
TPOAb (IU/L)	5.81 ± 1.98	9.84 ± 2.56	10.20 ± 3.87	9.55 ± 1.56	.0345
TSHRAb (IU/L)	1.44 ± .0023	2.95 ± .0045	2.94 ± .0034	2.97 ± .0033	.0351

TABLE 6 | Vitamin profiles of schizophrenics versus controls.

Variables	Schizophrenics vs. control (mean ± SD)				*p*-values (< 0.05)
	Control	Schizophrenics	Schizophrenics (male)	Schizophrenics (female)	
Vitamin A(nmol/L)	6.01 ± 1.76	4.33 ± 1.62	4.42 ± 1.56	4.25 ± .921	.0417
Vitamin C(nmol/L)	0.54 ± .0034	0.36 ± .0035	0.37 ± .0016	0.36 ± .0035	.0315
Vitamin E(nmol/L)	0.28 ± .0045	0.25 ± .0035	0.23 ± .0061	0.26 ± .0026	.0431
Vitamin D(pmol/L)	15.82 ± 1.98	9.57 ± 1.89	9.55 ± 2.87	9.59 ± 1.92	.0271
Vitamin-B6 (nmol/L)	87.67 ± 7.24	23.98 ± 3.65	21.98 ± 2.76	25.98 ± 1.92	.0190
Vitamin-B9 (nmol/L)	2.78 ± .092	1.97 ± .034	1.78 ± .065	2.16± ± .0924	.0267
Vitamin-B12 (pmol/L)	234.65 ± 11.87	89.98 ± 10.25	79.87 ± 11.87	100.09 ± 6.63	.0023

TABLE 7 | Trace elements profile of schizophrenics versus controls.

Variables	Schizophrenics vs. control (mean ± SD)				P-values (< 0.05)
	Control	Schizophrenics	Schizophrenics (male)	Schizophrenics (female)	
Zn (mg/kg)	0.16 ± 0.0023	0.27 ± 0.0027	0.27 ± 0.0014	0.27 ± 0.0025	0.006
Cu (mg/kg)	1.51 ± 0.0026	0.95 ± 0.0067	0.91 ± 0.0053	0.98 ± 0.0063	0.0067
Fe (μmol/L)	1.23 ± 0.0093	1.36 ± 0.0034	1.34 ± 0.0039	1.37 ± 0.0036	0.0454
Ferritin (μg/L)	1.12 ± 0.0033	1.83 ± 0.0092	1.82 ± 0.0023	1.84 ± 0.0024	0.0645
Selenium (ppm)	0.0293 ± 0.000956	0.0075 ± 0.00043	0.0056 ± 0.00073	0.0094 ± 0.00051	0.0319

respectively). All the above decreases were statistically significant compared to the control [Vit B6 ($p = 0.0190$), Vit B9 ($p = 0.0267$), Vit B12 ($p = 0.0023$) and Vit C ($p = 0.0315$)]. The levels of fat-soluble vitamins were also reduced during disease severity. The levels of Vit A (4.33 ± 1.62 Vs. 6.01 ± 1.76 nmol/L), Vit E (0.25 ± 0.0035 Vs. 0.28 ± 0.0045 nmol/L) and Vit D (9.57 ± 1.89 Vs. 15.82 ± 1.98 pmol/L) were significantly lower in schizophrenics relative to control ($p < 0.05$) **(Table 6)**. Significantly, reduced levels of trace elements (Se 5.5 ± 0.78 Vs. 4.21 ± 0.02), Zn 0.27 ± 0.0027 Vs. 0.16 ± 0.0023 mg/kg, Cu 0.95 ± 0.0067 Vs. 1.51 ± 0.0026 mg/kg, Fe 1.36 ± 0.0034 Vs. 1.23 ± 0.0093 μmol/L and ferritin 1.83 ± 0.0092 Vs. 1.12 ± 0.0033 μg/L) were recorded in schizophrenics **(Table 7)**. As these trace elements play an important role in the proper functioning of anti-oxidative enzymes but their lower levels suggested improper activity of these enzymes which was most likely resulting in oxidative stress-mediated damage.

Aminoacids and Hormonal Profiles

The facts regarding different amino acids displayed a clear picture of their eminent involvement in the initiation of schizophrenia and its progression to thyroid disorders represented in (**Table 8**). The levels of sulfur-containing amino acids (homocysteine, cysteine, and methionine) were found to be significantly regulated (**Table 8**). The homocysteine levels were significantly elevated ($p = 0.000$) in schizophrenics (17.56 ± 2.612 Vs. 6.96 ± 1.987 μmol/L), while cysteine and methionine were significantly decreased ($p = 0.034$ and $p = 0.014$) than the control (1.08 ± 0.089 Vs. 4.87 ± 0.924 μmol/L and 17.87 ± 1.23 Vs. 99.20 ± 5.36 μmol/L). The reason behind this variation may be due to reduced Vit B6, B9 and B12 so that homocysteine can neither be trans-sulfurated nor methylated properly resulting in oxidative stress. The levels of non-essential amino acids (glutamate, arginine, and tyrosine) were markedly reduced in schizophrenics in contrast to the corresponding control (12.70 ± 4.62 Vs. 19.77 ± 3.76 μmol/L, 91.65 ± 3.98 Vs. 95.35 ± 4.76 μmol/L, and 65.90 ± 7.54 Vs. 67.56 ± 3.76 μmol/L) while glycine was increased (267.87 ± 6.63 Vs. 256.73 ± 7.87 μmol/L). The reduction in glutamate levels resulted in oxidative injury while decreased arginine levels depict a fall in NO resulting in neurocognitive decline. The essential amino acids including phenylalanine, leucine, and threonine were higher in

TABLE 8 | Amino acids and hormonal profile of schizophrenics versus controls.

Variables	Schizophrenics vs. Control (Mean ± SD)				*p*-values (< 0.05)
	Control	Schizophrenics	Schizophrenics (Male)	Schizophrenics (Female)	
Homocysteine (μmol/L)	6.96 ± 1.987	17.56 ± 2.612	19.56 ± 3.712	15.56 ± 2.87	.000
Glutamate (mmol/L)	19.77 ± 3.76	12.70 ± 4.62	13.02 ± 3.76	12.46 ± 2.78	.0145
Methionine (μmol/L)	99.20 ± 5.36	17.87 ± 1.23	15.54 ± 2.87	20.20 ± 1.97	.0012
Cysteine (μmol/L)	4.87 ± .924	1.08 ± .089	0.99 ± .025	1.17 ± .092	.034
NOS (U/L)	7.87 ± 1.87	56.76 ± 2.67	45.76 ± 3.561	67.76 ± 2.76	.0176
Serotonin (ng/ml)	196.98 ± 6.35	77.98 ± 7.01	69.76 ± 6.26	86.20 ± 7.27	.0017
Dopamine (pg/ml)	7.98 ± 1.82	3.78 ± .92	2.87 ± .729	4.69 ± .623	.0014
Prolactin (ng/ml)	15.76 ± 2.65	32.43 ± 1.67	29.76 ± 2.87	35.10 ± 3.78	.000
8-OHdG (ng/ml)	1.18 ± .0045	2.76 ± .0067	1.98 ± .0032	3.54 ± .0056	.0011
Glycine (μmol/L)	256.73 ± 7.87	267.87 ± 6.63	270.34 ± 9.53	265.40 ± 6.43	.0498
Leucine (μmol/L)	145.35 ± 3.87	155.35 ± 6.64	159.36 ± 3.98	151.34 ± 8.54	.156
Phenylalanine (μmol/L)	63.87 ± 4.87	64.76 ± 4.98	65.36 ± 3.98	63.40 ± 7.54	.287
Tyrosine (μmol/L)	67.56±3.76	65.90 ± 7.54	63.36 ± 2.89	62.54 ± 6.34	.0942
Threonine (μmol/L)	129.76 ± 4.67	134.35 ± 6.98	132.76 ± 4.43	135.94 ± 3.98	.0425
Arginine (μmol/L)	95.35 ± 4.76	91.65 ± 3.98	92.79 ± 6.45	90.51 ± 6.43	.0052

schizophrenia patients (64.76 ± 4.98 μmol/L, 155.35 ± 6.64 μmol/L, and 134.35 ± 6.98 μmol/L) relative to the control (63.87 ± 4.87 μmol/L, 145.35 ± 3.87 μmol/L, and 129.76 ± 4.67 μmol/L). The hormonal levels (dopamine, serotonin, and prolactin) were also assessed. Dopamine levels were decreased (3.78 ± 0.92 Vs. 7.98 ± 1.82 pg/ml) while an increasing trend was observed in serotonin and prolactin (PRL) among schizophrenics in comparison to the control (196.98 ± 6.35 Vs. 77.98 ± 7.01 ng/ml and 32.43 ± 1.67 Vs. 15.76 ± 2.65 ng/ml). An increase in serotonin together with a decrease in dopamine is associated with hyperprolactinemia mediated depression (HMD).

DISCUSSION

The present study showed that in schizophrenics susceptible to thyroid disorders, deficiency in vitamins B6, B9, and B12 mediates hyperhomocysteinemia resulting in the reduction of antioxidative enzymes leading to oxidative injury. Hyperhomocysteinemia in turn increases asymmetric dimethylarginine (ADMA) levels thereby inhibiting the NOS activity causing the reduction in NO levels, an important mediator in synaptic plasticity and memory. The levels of glutamate and cysteine were lower in schizophrenics, mediating oxidative insult while the decline in arginine levels result in decreased NO levels leading to schizophrenic symptoms. Reduction in Cu and an increase in Zn levels result in lower dopamine and higher serotonin levels leading to hyperprolactinemia mediated depression (HMD). The lower vitamin D levels in schizophrenics may be due to poor nutrition or inadequate sunlight exposure, which in turn increases susceptibility to autoimmune thyroid disorders, as they additionally have raised thyroid antibodies. The increase in thyroid-stimulating hormone (TSH) indicated hypothyroidism while the higher level of H_2O_2 resulted in not only hypothyroidism as well as hyperthyroidism (Kivity et al., 2011).

The dietary antioxidants including the vitamins pyridoxine (B6), folic acid (B9), and cobalamin (B12) have gained marked attention as they have a significant role in the prevention of oxidative damage and donation of a methyl group in the production of proteins, lipids, nucleic acids, neurotransmitters, and hormones (Mitchell et al., 2014). It has been proposed that increased levels of vitamins B6, B9, and B12 cause a reduction in homocysteine levels which helps consolidation of working memory. In contrast, their deficiency can result in hyperhomocysteinemia which may induce problems in neurocognitive abilities and behavior (Moustafa et al., 2014). The present study also demonstrated an inverse correlation between homocysteine and vitamins B6 (r = -0.298), B9 (r = -0.523) and B12 (r = -0.498). Thyroid hormones have a positive effect on homocysteine levels by two different mechanisms. Firstly, thyroid hormones can cause a reduction in methionine synthase (MS) and methylenetetrahydrofolate reductase (MTHFR) levels in the liver, involved in the remethylation of homocysteine (Ayav et al., 2005). Secondly, the glomerular filtration rate was most likely reduced by low thyroid hormone levels (Diekman et al., 2001). The effect of these two mechanisms leads to high homocysteine levels (T3 Vs. Homocysteine, r = 0.387, and T4 Vs. homocysteine, r = 0.399).

Hyperhomocysteinemia has a positive effect on ADMA, an inhibitor of NOS, and thus reduces NO levels, a potent vasodilator resulting in microvascular damage in the brain (Keil et al., 2004). The current study also demonstrated an inverse correlation with NOS (Homocysteine Vs. NOS, r = -0.576). This is associated with decreased vascular supply to the brain and thyroid tissue which leads to their atrophy in schizophrenics. Another effect of oxidative stress is lipid peroxidation, in which peroxides (MDA) are produced and combines with NO to produce peroxynitrite in the presence of total plasma peroxidases which further increases lipid peroxidation and causes a reduction in NO levels (Akiibinu et al., 2012), which was similar to the results of the present study (MDA Vs. NO, r = -0.387). NO has an important role in neurotransmission, memory maintenance, cognitive abilities, and synaptic plasticity. Therefore, it usually becomes utilized with a limited amount being available for these vital functions. NO controls the spine growth by mainly involving the

postsynaptic regulation of actin cytoskeleton protein through cGMP-PKG cascade which in turn is responsible for actin polymerization in a phosphorylation-dependent manner and is implicated in the synapse formation (Nikonenko et al., 2013). In the case of malnutrition, there is an inadequate intake of L-arginine which results in the deficiency of NO in schizophrenics, as both have a positive correlation (L-arginine Vs. NO, r = 0.299). Malondialdehyde (MDA) reduces membrane stability and also plays a role in DNA damage by forming adducts (Frey et al., 2007). This study reveals a positive correlation between MDA and 8 oxodG, the end product of DNA damage (MDA Vs. 8 oxodG, r = 0.756).

Homocysteine-mediated oxidative stress is considered as one of the significant mechanisms for the toxicity of homocysteine in neuronal cells. In vascular and neuronal cells, auto-oxidation of homocysteine can occur which causes disturbances in redox homeostasis resulting in defective redox signaling mechanisms (Zou and Banerjee, 2005). This effect can be elaborated by increasing ROS production and NO deactivation. In the mitochondria of both astrocytes and thyrocytes, N-acetyl cysteine is converted into cysteine by deacetylation which then reacts with glutamate to form gamma-glutamate-cysteine in the presence of glutamate-cysteine ligase catalytic unit. Gamma-glutamate-cysteine combines with glycine to form glutathione in the presence of glutathione synthetase (Wood et al., 2009). In schizophrenia, amino acids including cysteine and glutamate, and antioxidant enzymes are decreased in astrocytes and thyrocytes simultaneously thus ROS is increased (Erdamar et al., 2008). Glutamate is also a progenitor of NO and a positive correlation was observed between NO and glutamate (NO Vs. glutamate, r = 0.442). Due to an increase in superoxide free radicals, DNA damage causes telomere shortening/erosion which allows the formation of adducts i.e., 8-oxodG and 8-oxoGuo thus result in apoptosis of thyrocytes and astrocytes (Nishioka and Arnold, 2004). This cell death causes ventricular enlargement and hippocampal volume reduction which leads to schizophrenic symptoms and atrophy of the thyroid gland (Nishioka and Arnold, 2004). Hydrogen peroxide is an important factor in thyroid hormogenesis. The increase in H_2O_2 enhances the conversion of iodide into iodine, the coupling of monoiodotyrosine (MIT) and diiodotyrosine (DIT), and synthesis of RT3 leads to hyperthyroidism (Chen et al., 2011). On the other hand, it is also suggested that the increase in H_2O_2 causes inhibition of iodide uptake and organification which results in hypothyroidism (Moreno et al., 2002). High H_2O_2 also induces cell death by activating apoptosis signal-regulating kinase and also favors inflammation (Poljak et al., 2006).

Hyperhomocysteinemia causes cytotoxic effects by reducing antioxidants such as Vit C or E and N-acetylcysteine (Weiss et al., 2003), and the current study demonstrated an inverse correlation of homocysteine with both Vit C (r = -0.498) and E (r = -0.354). Vit C, another antioxidant acts as a cofactor for 5-hydroxytryptophan and dopamine beta-hydroxylase which mediates the conversion of tryptophan to serotonin and dopamine to norepinephrine respectively (Cooper, 1961). Dietary lack of Vit C causes a reduction in serotonin levels and also an increase in dopamine levels (Yamamoto and Novotney, 1998) and the current study also showed a positive correlation of Vit C with serotonin (r = 0.343) and an inverse with dopamine (r = -0.459). Vit E acts as an antioxidant to prevent peroxides (MDA) formation involved in lipid peroxidation and thus functions as a membrane stabilizer (Niki et al., 1995). Its levels are markedly reduced in schizophrenic patients, cause lipid peroxidation leading to DNA and cell membrane damage in both thyroid and brain tissues (Petrulea et al., 2012). In the present study, Vit E showed an inverse correlation with both MDA (r = -0.339) and 8-oxodG (r = -0.576). Vit E has a suppressing effect on thyroid activity and also on oxidants thus its supplementation in hyperthyroidism may have a positive role in the reduction of thyroid hormone levels and oxidative damage (Prabakaran et al., 2004). In line with the above, an inverse correlation between Vit E and thyroid hormones (T3, r = -0.221 and T4, r = -0.287) was observed in the present study (**Table 9**).

Schizophrenia and elevated heavy metals have a strong association (Wolf et al., 2006; Vural et al., 2010; Liu et al., 2015).

TABLE 9 | Pearsons' correlation coefficients of prominent variables in the development of thyroid dysfunction in schizophrenics.

Variables	Correlation coefficients	$p < (0.05)$
Homocysteine Vs. L-Arginine	–(.676)	0.034
Homocysteine Vs. NOS	–(.576)	0.041
Homocysteine Vs. Vit-E	–(.354)	0.023
Homocysteine Vs. Vit-C	–(.4.98)	0.044
Homocysteine Vs. Vit-B6	–(.298)	0.001
Homocysteine Vs. Vit-B9	–(.523)	0.026
Homocysteine Vs. Vit-B12	–(.498)	0.033
Homocysteine Vs. T3	+(.387)	0.043
Homocysteine Vs. T4	+(.399)	0.020
Homocysteine Vs. MDA	+(.801)	0.019
MDA Vs. 8OHdG	+(.756)	0.017
MDA Vs. Vit-E	–(.339)	0.030
MDA Vs. NO	–(.387)	0.013
Vit-E Vs. T3	–(.221)	0.021
Vit-E Vs. T4	–(.287)	0.034
Vit-E Vs. 8OHdG	–(.576)	0.021
Vit-C Vs. Serotonin	+(.434)	0.041
Vit-C Vs. Dopamine	–(.459)	0.028
L-Arginine Vs. NO	+(.229)	0.042
Cu Vs. Zn	–(.398)	0.011
Cu Vs. Dopamine	+(.427)	0.018
Se Vs. GPx	+(.598)	0.025
Iron Vs. Catalase	+(.644)	0.025
Prolactin Vs. Dopamine	–(.867)	0.002
Prolactin Vs. Serotonin	+(.745)	0.010
Prolactin Vs. IL-6	–(.246)	0.023
Prolactin Vs. IL-2	+(.301)	0.017
Prolactin Vs. TNF-α	+(.465)	0.039
Glutamate Vs. NO	+(.442)	0.045
Zn Vs. NOS	+(.421)	0.018
Zn Vs. SOD	+(.334)	0.041
Vit-D Vs. TPO-Ab	–(.791)	0.006
Vit-D Vs. TSH	–(.673)	0.000
Vit-D Vs. TSHr-Ab	–(.591)	0.028
Vit-D Vs. Tg-Ab	–(.437)	0.019
Vit-D Vs. ALP	–(.391)	0.022
Vit-D Vs. ALT	–(.891)	0.010
Vit-D Vs. AST	–(.403)	0.019
Vit-D Vs. IL-6	–(.721)	0.003
Vit-D Vs. IL-2	–(.614)	0.011
Vit-D Vs. TNF-α	–(.811)	.0190

The metallothionein, a metal removing protein is required for heavy metals removal, but malfunctioning transcription processes of this protein are reported in schizophrenics (Wolf et al., 2006). The other common factor in schizophrenia is copper (Cu) toxicity which mediates elevated catecholamine oxidation; the resultant end products are harmful hallucinogens (Liu et al., 2015). In contrast, a recent finding revealed that Cu is decreased in schizophrenics (Vural et al., 2010). It is essential for the proper functioning of superoxide dismutase (SOD), dopamine beta-hydroxylase, and tyrosine hydroxylase, and therefore diminished levels of Cu cause oxidative stress and abnormal dopamine nor-epinephrine interaction (Pataracchia, 2008) and we observed a positive correlation for Cu with dopamine (r = 0.427). It has been also proposed that low thyroid function permits heavy metal retention as there is reduced hepatic synthesis of metallothionein (Gupta and Kar, 1983). Heavy metals hamper T4 to T3 conversion by restraining peripheral enzymes (van Vliet et al., 2007). Zinc (Zn) deficiency is an antagonist to Cu (Yanik et al., 2004), the present study also revealed an inverse correlation between these two metals (Cu Vs. Zn, r = -0.398). Zinc is essential for other important functions such as serotonin synthesis, proper functioning of metallothionein, the formation of Cu, Zn, SOD, and activation of NOS. It is important in the prevention of oxidative damage, reduction of lipid peroxidation in neurons, and thus plays a major role in maintaining the blood-brain barrier (Malik, A et al., 2016). The present study suggested that the decreased Cu levels mediate the lowering of dopamine levels while increased Zn levels cause elevated serotonin levels, resulting in hyperprolactinemia leading to hyperprolactinemia mediated depression (HMD), as reported in a recent study (Wysokiński and Kłoszewska, 2014). An inverse correlation between PRL and dopamine (r = -0.867) while a positive correlation between PRL and serotonin (r = 0.745) was observed in the current study. The levels of phenylalanine were increased but that of tyrosine was lowered in schizophrenics. Phenylalanine is converted into tyrosine in the presence of phenylalanine hydroxylase and it ultimately produces dopamine. But in schizophrenia, the activity of this enzyme is affected by cytokines (interferon-γ) and ROS which decreases cofactor 6 R-L-erythroid-5,6,7,8-tetrahydrobiopterin (BH4) required for its proper functioning (Liao and Ya-Mei, 2014). The increase in TSH response to TRH has been recognized, having a direct effect on the thyroid gland resulting in hyperthyroidism (Duval et al., 2010). Contrary to this effect, it is reported that there is a reduction in TSH response to TRH in depression which leads to hypothyroidism (Asare et al., 2014). Selenium (Se) and iron (Fe) deficit are also common in schizophrenics as they act as cofactors for glutathione peroxidase (GPx) and catalase (CAT) respectively thus their deficiency results in oxidative damage (Pataracchia, 2008). The current study demonstrated a positive correlation between Se and GPx (r = 0.598) and also between Fe and CAT (r = 0.664) **(Table 9)**.

It has been revealed that individuals with Vit D deficiency are two times more prone to develop schizophrenia, and its deficiency leads to a seasonal affective disorder (SAD), a state of depression that may arise from decreased sunlight exposure and poor nutrition (Bischoff-Ferrari et al., 2006). The levels of antibody titer represent that thyroid peroxidase-antibody (TPOAb), thyroid-stimulating hormone receptor-antibody (TSHrAb), and thyroglobulin-antibody (TgAb) were raised in the patients suffering from schizophrenia along with thyroid dysfunction. A strong inverse relationship between Vit D and the presence of anti-thyroid antibodies in patients deficient in Vit D was revealed (Virupaksha et al., 2014). The present study also represents inverse correlation between Vit D and thyroid antibodies namely TPO-Ab (r = -0.791), TSHr-Ab (r = -0.591) and TG-Ab (r = -0.338*). In the current study, Vit D showed inverse correlation with inflammatory cytokines namely, IL-2 (r = -0.614), IL-6 (r = -0.721) TNF-α (r = -0.811). The enhanced inflammatory response mediates up-regulation of autoimmune response resulting in autoimmune thyroid disorders (AITDs) including Hashimoto's thyroiditis and Graves' disease. This decrease in Vit D may be due to deranged liver functions as observed in this study by raised hepatic enzymes including ALT, ALP, and AST, contrary to the findings of Virupaksha et al., 2014 when a high inverse correlation was observed between Vit D and the following hepatic enzymes namely, ALT (r = -0.891), AST (r = -0.403) and ALP (r = -0.391). The deficient 1, $25(OH)_2D_3$ levels in schizophrenics results in an increase in homocysteine levels by blocking the activity of cystathionine β-synthase (CBS) and also inhibit NOS dependent NO production leading to cognitive decline (Malik, A. A et al., 2016), similar correlations of Vit D with homocysteine (r = 0.502) and NOS (r = 0.411).

Figure 1 describes that in the mitochondria of astrocytes and thyrocytes, methionine is converted into S-adenosylmethionine (SAM) in the presence of MATI/II which is then converted into S-adenosylhomocysteine (SAH) by glycine N-methyltransferase (GNMT) so that methylation of neurotransmitters occurs. SAH is transformed into homocysteine, mediated by S-adenosylhomocysteine hydrolase (SAHH). Homocysteine has two routes, one is to remethylate into methionine in the presence of methionine synthase (MS), vitamin B9 and vitamin B12 act as a cofactor for it. The methyl group is provided by methyltetrahydrofolate (CH3-THF), formed from tetrahydrofolate (THF) in the presence of serine hydroxymethyltransferase (SHMT), methyltetrahydrofolate reductase (MTHFR), and vitamin B6. The other route is that homocysteine is converted into cystathionine-by-cystathionine synthase beta (CSβ) and then into N-acetylcysteine (NAC) which requires vitamin B6 as a cofactor. NAC is then converted into cysteine by deacetylation which then combines with glutamate and glycine to form glutathione (GSH). In schizophrenia, glutathione is reduced due to polymorphism of its gene, and deficiency of vitamin B6, B9, and B12 may be due to reduced dietary intake, malabsorption, and genetic dysfunction. Thus, it leads to hyperhomocysteinemia which causes oxidative stress, vascular damage, DNA damage, mitochondrial dysfunction, and apoptosis of both astrocytes and thyrocytes. Furthermore, in schizophrenics, antioxidant enzymes such as SOD, GPx, and CAT are also reduced. Thus, there is a dual cause of an increase in oxidative stress. This causes DNA damage and apoptosis leading to hippocampal volume reduction and ventricular enlargement in the brain and thyroid atrophy as well. Lipid peroxidation produces peroxide (MDA) which forms peroxynitrite when combined with nitric oxide (NO) in the brain coming from blood vessels, produced by L-arginine and oxygen in the presence of nitric oxide synthase (NOS). NO has an important role in vasodilation, memory maintenance, neurotransmission, and cognition. NO synthesis is

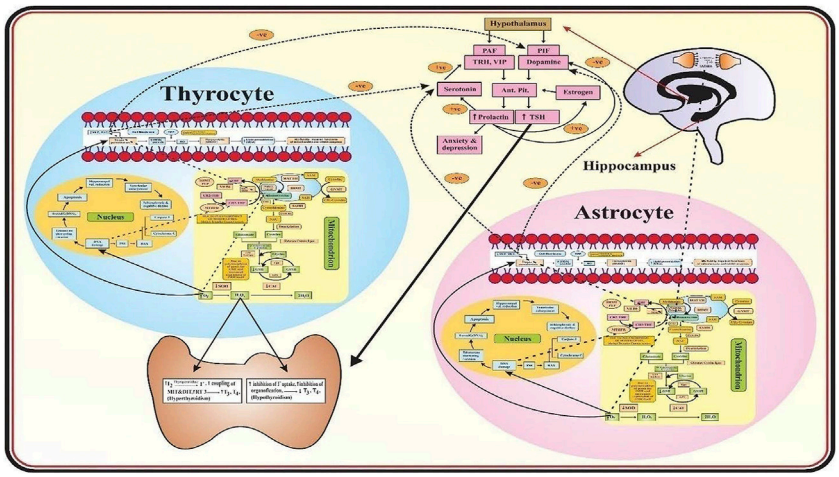

FIGURE 1 | Mechanism of Thyroid Dysfunction in Schizophrenics. The role of oxidative stress and the biomarkers associated with thyroid dysfunction in schizophrenics.

affected in schizophrenia by hyperhomocysteinemia by increasing asymmetrical dimethyl aspartate (ADMA), an inhibitor of NOS, and also due to L-arginine dietary lack. Thus, microvasculature is destroyed resulting in decreased blood supply to the brain and thyroid tissues proceeding to apoptosis. The peroxides (MDA) cause DNA damage which ultimately leads to astrocytes and thyrocytes apoptosis. In thyrocytes, hydrogen peroxide (H_2O_2) is used in the synthesis of thyroid hormone as it acts on thyroperoxidase (TPO) mediated reactions. Thus, the increase in H_2O_2- causes hyperthyroidism (Song et al., 2007). The rise in H_2O_2 causes inhibition of iodide uptake and organification resulting in hypothyroidism (Song et al., 2007; Szanto et al., 2019). In the hypothalamus, prolactin (PRL) activating factors (TRH and VIP) and PRL inhibiting factor (dopamine) are released which act on the anterior pituitary to produce PRL and TSH. In schizophrenics, hyperprolactinemia occurs as PRL increases estrogen which induces more production of PRL. PRL also enhances serotonin synthesis which increases PRL activating factors and reduces dopamine, thus more hyperprolactinemia occurs leading to anxiety and depression. TSH is also increased and acts on the thyroid resulting in hyperthyroidism. Hyperhomocysteinemia also reduces the levels of vitamin C and E, the dietary antioxidants in schizophrenia. The reduction in vitamin C causes a decrease in serotonin and dopamine as it acts on enzymes that mediate their synthesis and processing. Vitamin E reduces lipid peroxidation thus has a significant role in membrane stabilization. Hence, the reduction in vitamin E may substantially elevate the lipid peroxidation levels resulting in mitochondrial and cell membrane damage and apoptosis of astrocytes and thyrocytes in schizophrenics.

CONCLUSION

In the present study, schizophrenics demonstrated altered liver function, increased stress markers, and decreased dietary antioxidants. The reduced levels of primary and secondary antioxidants may subsequently result in hyperhomocysteinemia and increased ROS leading to DNA and mitochondrial damage. Moreover, we found that in schizophrenics susceptible to thyroid disorders, deficiency in vitamins B6, B9, and B12 mediates hyperhomocysteinemia resulting in the reduction of antioxidative enzymes leading to oxidative injury. Hyperhomocysteinemia in turn increases ADMA levels thereby inhibiting the NOS activity causing a decrease in NO levels, an important mediator in synaptic plasticity and memory. The levels of glutamate and cysteine were lower in schizophrenics, mediating oxidative insult while the decline in arginine levels result in decreased NO levels leading to schizophrenic symptoms. Besides, the reduction in Cu and an increase in Zn levels result in lower dopamine and higher serotonin levels leading to HMD. Also, the lower vitamin D levels in schizophrenics increase their susceptibility to autoimmune thyroid disorders. In conclusion, homocysteine and/or PRL levels may serve as candidate prognostic markers for schizophrenia. Besides, both neurological symptoms and the susceptibility to thyroid disorders may be prevented in the initial stages of this debilitating disorder by appropriate dietary supplementation of antioxidants which can rectify a reduction in primary and secondary antioxidants, and disturbed prolactin-serotonin-dopamine interactions in schizophrenics.

DATA AVAILABILITY STATEMENT

The raw data supporting the conclusions of this article will be made available by the authors, without undue reservation.

ETHICS STATEMENT

The study was conducted according to the Ethical Committee approval of the Institute of Molecular Biology and Biotechnology

(IMBB), the University of Lahore (IRB/IMBB/UOL/ph-984). Before the start of the study, written informed consent was obtained from all participants of the study according to Helsinki's Declaration. The patients/participants provided their written informed consent to participate in this study.

AUTHOR CONTRIBUTIONS

MR, AM, SS, AZ, MA, AK, SW, AZ, and SSH were involved in the conceptualization of the manuscript, generation and analysis of data. ME, KG, and PP were involved in the review and editing of the manuscript.

FUNDING

We acknowledge this project funded by King Abdulaziz City for Science and Technology (KACST), Riyadh, Kingdom of Saudi Arabia, under grant number 13-MED2437-03. We acknowledge with thanks the KACST and the Science and Technology Unit, King Abdulaziz University for the technical and financial support.

REFERENCES

Adam-Vizi, V., and Chinopoulos, C. (2006). Bioenergetics and the formation of mitochondrial reactive oxygen species. *Trends Pharmacol. Sci.* 27, 639–645. doi:10.1016/j.tips.2006.10.005

Aebi, H. (1974). "Catalase," in *Methods of enzymatic analysis*. Editor H. U. Bergmeyer (New York and London: Academic Press), 673–677.

Akiibinu, M. O., Ogundahunsi, O. A., and Ogunyemi, E. O. (2012). Inter-relationship of plasma markers of oxidative stress and thyroid hormones in schizophrenics. *BMC Res. Notes* 5, 169. doi:10.1186/1756-0500-5-169

Arneson, W. L., and Arneson, D. L. (2013). Current methods for routine clinical laboratory testing of vitamin D levels. *Lab. Med.* 44, e38–e42. doi:10.1309/LMONQZQ27TIN7XFS

Asare, G. A., Tetteh, R., Amedonu, E., Asiedu, B., and Doku, D. (2014). Toxicity, deficiency and dysmetabolism of trace elements in Ghanaian clinically stable schizophrenics. *Open Access Maced J. Med. Sci.* 2, 293–298. doi:10.3889/oamjms.2014.049

Ayav, A., Alberto, J. M., Barbe, F., Brunaud, L., Gerard, P., Merten, M., et al. (2005). Defective remethylation of homocysteine is related to decreased synthesis of coenzymes B2 in thyroidectomized rats. *Amino Acids* 28, 37–43. doi:10.1007/s00726-004-0151-z

Barnham, K. J., Masters, C. L., and Bush, A. I. (2004). Neurodegenerative diseases and oxidative stress. *Nat. Rev. Drug Discov.* 3, 205–214. doi:10.1038/nrd1330

Bischoff-Ferrari, H. A., Giovannucci, E., Willett, W. C., Dietrich, T., and Dawson-Hughes, B. (2006). Estimation of optimal serum concentrations of 25-hydroxyvitamin D for multiple health outcomes. *Am. J. Clin. Nutr.* 84, 18–28. doi:10.1093/ajcn/84.1.18

Bolann, B. J., Rahil-Khazen, R., Henriksen, H., Isrenn, R., and Ulvik, R. J. (2007). Evaluation of methods for trace-element determination with emphasis on their usability in the clinical routine laboratory. *Scand. J. Clin. Lab. Invest.* 67 (4), 353–366. doi:10.1080/00365510601095281

Bredin, S., Warburton, D., and Lang, D. (2013). The health benefits and challenges of exercise training in persons living with schizophrenia: a pilot study. *Brain Sci.* 3, 821–848. doi:10.3390/brainsci3020821

Chen, C.-S., Kuo, Y.-T., Tsai, H.-Y., Li, C.-W., Lee, C.-C., Yen, C.-F., et al. (2011). Brain biochemical correlates of the plasma homocysteine level: a proton magnetic resonance spectroscopy study in the elderly subjects. *Am. J. Geriatr. Psychiatry* 19, 618–626. doi:10.1097/JGP.0b013e318209ddf1

Chinoy, N. J., Mehta, R. R., Seethalakshmi, L., Sharma, J. D., Chinoy, M. R., Ciobica, A., et al. (1986). Effects of vitamin C deficiency on physiology of male reproductive organs of Guinea pigs. *Int J FertilPsychiatr. Danub.* 31, 232–239.

Ciobica, A., Padurariu, M., Dobrin, I., Stefanescu, C., and Dobrin, R. (2011). Oxidative stress in schizophrenia - focusing on the main markers. *Psychiatria Danubina* 23 (3), 237–245.

Cooper, J. R. (1961). The role of ascorbic acid in the oxidation of tryptophan to 5-hydroxytryptophan. *Ann. N. Y Acad. Sci.* 92, 208–211. doi:10.1111/j.1749-6632.1961.tb46120.x

Diekman, M. J. M., van der Put, N. M., Blom, H. J., Tijssen, J. G. P., and Wiersinga, W. M. (2001). Determinants of changes in plasma homocysteine in hyperthyroidism and hypothyroidism. *Clin. Endocrinol. (Oxf).* 54, 197–204. doi:10.1046/j.1365-2265.2001.01170.x

Duval, F., Mokrani, M.-C., Erb, A., Danila, V., Gonzalez Lopera, F., and Jeanjean, L. (2020). Dopaminergic, noradrenergic, adrenal, and thyroid abnormalities in psychotic and affective disorders. *Front. Psychiatry* 11, 533872. doi:10.3389/fpsyt.2020.533872

Duval, F., Mokrani, M.-C., Lopera, F. G., Diep, T. S., Rabia, H., and Fattah, S. (2010). Thyroid axis activity and suicidal behavior in depressed patients. *Psychoneuroendocrinology* 35, 1045–1054. doi:10.1016/j.psyneuen.2010.01.005

Erdamar, H., Demirci, H., Yaman, H., Erbil, M. K., Yakar, T., Sancak, B., et al. (2008). The effect of hypothyroidism, hyperthyroidism, and their treatment on parameters of oxidative stress and antioxidant status. *Clin. Chem. Lab. Med.* 46, 1004–1010. doi:10.1515/CCLM.2008.183

Frey, B. N., Andreazza, A. C., Kunz, M., Gomes, F. A., Quevedo, J., Salvador, M., et al. (2007). Increased oxidative stress and DNA damage in bipolar disorder: a twin-case report. *Prog. Neuro-Psychopharmacology Biol. Psychiatry* 31, 283–285. doi:10.1016/j.pnpbp.2006.06.011

Gupta, P., and Kar, A. (1983). Cadmium induced thyroid dysfunction in chicken: hepatic type I iodothyronine 5'-monodeiodinase activity and role of lipid peroxidation. *Comp. Biochem. Physiol. C, Pharmacol. Toxicol. Endocrinol.* 123, 39–44. doi:10.1016/s0742-8413(99)00007-9

Kakkar, P., Das, B., and Viswanathan, P. N. (1984). A modified spectrophotometric assay of superoxide dismutase. *Indian J. Biochem. Biophys.* 21, 130–132.

Kalousová, M., Skrha, J., and Zima, T. (2002). Advanced glycation end-products and advanced oxidation protein products in patients with diabetes mellitus. *Physiol. Res.* 51 (6), 597–604.

Keil, U., Bonert, A., Marques, C. A., Strosznajder, J. B., Müller-Spahn, F., Müller, W. E., et al. (2004). Elevated nitric oxide production mediates beta-amyloid-induced mitochondria failure. *Pol. J. Pharmacol.* 56, 631–634.

Kivity, S., Agmon-Levin, N., Zisappl, M., Shapira, Y., Nagy, E. V., Dankó, K., et al. (2011). Vitamin D and autoimmune thyroid diseases. *Cell. Mol. Immunol.* 8, 243–247. doi:10.1038/cmi.2010.73

Koga, M., Serritella, A. V., Messmer, M. M., Hayashi-Takagi, A., Hester, L. D., Snyder, S. H., et al. (2011). Glutathione is a physiologic reservoir of neuronal glutamate. *Biochem. Biophysical Res. Commun.* 409, 596–602. doi:10.1016/j.bbrc.2011.04.087

Kumar, V., and Gill, K. D. (2018). To estimate sodium and potassium in serum by using flame photometer. *Basic concepts in clinical biochemistry: a practical guide*. Singapore: Springer. doi:10.1007/978-981-10-8186-6_36

Kumari, S., Bahinipati, J., Pradhan, T., and Sahoo, D. P. (2020). Comparison of test performance of biochemical parameters in semiautomatic method and fully automatic analyzer method. *J. family Med. Prim. Care* 9 (8), 3994–4000. doi:10.4103/jfmpc.jfmpc_845_19

Li, H.-c., Chen, Q.-z., Ma, Y., and Zhou, J.-f. (2006). Imbalanced free radicals and antioxidant defense systems in schizophrenia: a comparative study. *J. Zhejiang Univ. - Sci. B* 7, 981–986. doi:10.1631/jzus.2006.B0981

Liao, W. T., and Ya-Mei, B. (2014). Major depressive disorder induced by prolactinoma-a case report. *Gen. Hosp. Psychiatry* 36, 1251–1252. doi:10.1016/j.genhosppsych.2013.01.010

Lindqvist, D., Dhabhar, F. S., James, S. J., Hough, C. M., Jain, F. A., Bersani, F. S., et al. (2017). Oxidative stress, inflammation and treatment response in major depression. *Psychoneuroendocrinology* 76, 197–205. doi:10.1016/j.psyneuen.2016.11.031

Liu, T., Lu, Q.-B., Yan, L., Guo, J., Feng, F., Qiu, J., et al. (2015). Comparative study on serum levels of 10 trace elements in schizophrenia. *Plos. One.* 10, e0133622. doi:10.1371/journal.pone.0133622

Malik, A. A., Saleem, S., Ashraf, M. A. B., and Qazi, M. H. (2016). 1, 25-dihydroxyvitamin D3, a potential role player in the development of thyroid disorders in schizophrenics. *Pak. J. Med. Sci.* 32, 1370–1374. doi:10.12669/pjms.326.11157

Malik, A., Saleem, S., Ashraf, M. A. B., Asif, M., Waquar, S., Qazi, M. H., et al. (2016). Role of extrapolative factors in the development of Hyperprolactinemia Mediated Depression (HMD) in schizophrenics susceptible to thyroid disorders. *Int.J.Biosci.* 9, 183–189.

Mikkelsen, K., Stojanovska, L., Prakash, M., and Apostolopoulos, V. (2017). The effects of vitamin B on the immune/cytokine network and their involvement in depression. *Maturitas* 96, 58–71. doi:10.1016/j.maturitas.2016.11.012

Mitchell, E. S., Conus, N., and Kaput, J. (2014). B vitamin polymorphisms and behavior: evidence of associations with neurodevelopment, depression, schizophrenia, bipolar disorder and cognitive decline. *Neurosci. Biobehavioral Rev.* 47, 307–320. doi:10.1016/j.neubiorev.2014.08.006

Moreno, J. C., Bikker, H., Kempers, M. J. E., van Trotsenburg, A. S. P., Baas, F., de Vijlder, J. J. M., et al. (2002). Inactivating mutations in the gene for thyroid oxidase 2 (THOX2) and congenital hypothyroidism. *N. Engl. J. Med.* 347, 95–102. doi:10.1056/NEJMoa012752

Moron, M., Depierre, J., and Mannervik, B. (1979). Levels of glutathione, glutathione reductase and glutathione S-transferase activities in rat lung and liver. *Biochim. Biophys. Acta (Bba) - Gen. Subjects* 582 (1), 67–78. doi:10.1016/0304-4165(79)90289-7

Moustafa, A. A., Hewedi, D. H., Eissa, A. M., Frydecka, D., and Misiak, B. a. (2014). Homocysteine levels in schizophrenia and affective disorders-focus on cognition. *Front. Behav. Neurosci.* 8, 343. doi:10.3389/fnbeh.2014.00343

Niki, E., Noguchi, N., Tsuchihashi, H., and Gotoh, N. (1995). Interaction among vitamin C, vitamin E, and beta-carotene. *Am. J. Clin. Nutr.* 62, 1322S–1326S. doi:10.1093/ajcn/62.6.1322S

Nikonenko, I., Nikonenko, A., Mendez, P., Michurina, T. V., Enikolopov, G., and Muller, D. (2013). Nitric oxide mediates local activity-dependent excitatory synapse development. *Proc. Natl. Acad. Sci.* 110, E4142–E4151. doi:10.1073/pnas.1311927110

Nishioka, N., and Arnold, S. E. (2004). Evidence for oxidative DNA damage in the hippocampus of elderly patients with chronic schizophrenia. *Am. J. Geriatr. Psychiatry* 12, 167–175. doi:10.1097/00019442-200403000-00008

Ohkawa, H., Ohishi, N., and Yagi, K. (1979). Assay for lipid peroxides in animal tissues by thiobarbituric acid reaction. *Anal. Biochem.* 95, 351–358. doi:10.1016/0003-2697(79)90738-3

Pataracchia, R. J. (2008). Orthomolecular treatment for schizophrenia. *J. Orthomol. Med.* 23, 95–105.

Petrulea, M., Adriana, M., and Ileana, D. (2012). Oxidative stress and antioxidant status in hypo and hyperthyroidism. *INTECH* 10, 197–236.

Pohl, H. R., Roney, N., and Abadin, H. G. (2011). Metal ions affecting the neurological system. *Met. Ions Life Sci.* 8, 247–262.

Poljak, A., Grant, R., Austin, C. J. D., Jamie, J. F., Willows, R. D., Takikawa, O., et al. (2006). Inhibition of indoleamine 2,3 dioxygenase activity by H2O2. *Arch. Biochem. Biophys.* 450, 9–19. doi:10.1016/j.abb.2006.03.003

Prabakaran, S., Swatton, J. E., Ryan, M. M., Huffaker, S. J., Huang, J.-J., Griffin, J. L., et al. (2004). Mitochondrial dysfunction in schizophrenia: evidence for compromised brain metabolism and oxidative stress. *Mol. Psychiatry* 9, 684–697. doi:10.1038/sj.mp.4001511

Rasool, M., Ashraf, M. A. B., Malik, A., Waquar, S., Khan, S. A., Qazi, M. H., et al. (2017). Comparative study of extrapolative factors linked with oxidative injury and anti-inflammatory status in chronic kidney disease patients experiencing cardiovascular distress. *PLoS One* 12 (2), e0171561. doi:10.1371/journal.pone.0171561

Rasool, M., Malik, A., Basit Ashraf, M. A., Parveen, G., Iqbal, S., Ali, I., et al. (2016). Evaluation of matrix metalloproteinases, cytokines and their potential role in the development of ovarian cancer, *PLoS One*, 11, e0167149. doi:10.1371/journal.pone.0167149

Rutkowski, M., and Grzegorczyk, K. (2007). Modifications of spectrophotometric methods for antioxidative vitamins determination convenient in analytic practice. *Acta Scientiarum Polonorum Technologia Alimentaria* 6 (3), 17–28.

Santos, N. C., Costa, P., Ruano, D., Macedo, A., Soares, M. J., Valente, J., et al. (2012). Revisiting thyroid hormones in schizophrenia. *J. Thyroid Res.* 2012, 1. doi:10.1155/2012/569147

Schweizer, U., Chiu, J., and Köhrle, J. (2008). Peroxides and peroxide-degrading enzymes in the thyroid. *Antioxid. Redox Signaling* 10, 1577–1592. doi:10.1089/ars.2008.2054

Shaik, M. M., and Gan, S. H. (2013). Rapid resolution liquid chromatography method development and validation for simultaneous determination of homocysteine, vitamins B(6), B(9), and B(12) in human serum. *Indian J. Pharmacol.* 45 (2), 159–167. doi:10.4103/0253-7613.108303

Shimbo, K., Kubo, S., Harada, Y., Oonuki, T., Yokokura, T., Yoshida, H., et al. (2010). Automated precolumn derivatization system for analyzing physiological amino acids by liquid chromatography/mass spectrometry. *Biomed. Chromatogr.* 24 (7), 683–691. doi:10.1002/bmc.1346

Song, Y., Driessens, N., Costa, M., De Deken, X., Detours, V., Corvilain, B., et al. (2007). Roles of hydrogen peroxide in thyroid physiology and disease. *J. Clin. Endocrinol. Metab.* 92, 3764–3773. doi:10.1210/jc.2007-0660

Subudhi, U., and Chainy, G. B. N. (2010). Expression of hepatic antioxidant genes in l-thyroxine-induced hyperthyroid rats: regulation by vitamin E and curcumin. *Chemico-Biological Interactions* 183, 304–316. doi:10.1016/j.cbi.2009.11.004

Svrakic, D. M., Zorumski, C. F., Svrakic, N. M., Zwir, I., and Cloninger, C. R. (2013). Risk architecture of schizophrenia. *Curr.Opin.Psychiatry.* 26, 188–195. doi:10.1097/YCO.0b013e32835d8329

Szanto, I., Pusztaszeri, M., and Mavromati, M. (2019). H2O2 metabolism in normal thyroid cells and in thyroid tumorigenesis: focus on NADPH oxidases. *Antioxidants (Basel, Switzerland)*, 8, 126. doi:10.3390/antiox8050126

Tamminga, C. A., and Holcomb, H. H. (2005). Phenotype of schizophrenia: a review and formulation. *Mol. Psychiatry* 10, 27–39. doi:10.1038/sj.mp.4001563

van Vliet, J., Oates, N. A., and Whitelaw, E. (2007). Epigenetic mechanisms in the context of complex diseases. *Cell. Mol. Life Sci.* 64, 1531–1538. doi:10.1007/s00018-007-6526-z

Virupaksha, H. G., Kumar, A., and Nirmala, B. P. (2014). Migration and mental health: an interface. *J. Nat. Sci. Biol. Med.* 5, 233–239. doi:10.4103/0976-9668.136141

Vural, H., Demirin, H., Kara, Y., Eren, I., and Delibas, N. (2010). Alterations of plasma magnesium, copper, zinc, iron and selenium concentrations and some related erythrocyte antioxidant enzyme activities in patients with Alzheimer's disease. *J. Trace Elem. Med. Biol.* 24, 169–173. doi:10.1016/j.jtemb.2010.02.002

Weiss, N., Heydrick, S. J., Postea, O., Keller, C., Keaney, J. F., Jr, and Loscalzo, J. (2003). Influence of hyperhomocysteinemia on the cellular redox state - impact on homocysteine-induced endothelial dysfunction. *Clin. Chem. Lab. Med.* 41, 1455–1461. doi:10.1515/CCLM.2003.223

Witko-Sarsat, V., Friedlander, M., Nguyen Khoa, T., Capeillère-Blandin, C., Nguyen, A. T., Canteloup, S., et al. (1998). Advanced oxidation protein products as novel mediators of inflammation and monocyte activation in chronic renal failure, *J. Immunol.*, 161. 2524–2532.

Wolf, T. L., Kotun, J., and Meador-Woodruff, J. H. (2006). Plasma copper, iron, ceruloplasmin and ferroxidase activity in schizophrenia. *Schizophrenia Res.* 86, 167–171. doi:10.1016/j.schres.2006.05.027

Wood, S. J., Yücel, M., Pantelis, C., and Berk, M. (2009). Neurobiology of schizophrenia spectrum disorders: the role of oxidative stress. *Ann. Acad. Med. Singap.* 38, 396–6.

Wysokiński, A., and Kłoszewska, I. (2014). Level of thyroid-stimulating hormone (TSH) in patients with acute schizophrenia, unipolar depression or bipolar disorder. *Neurochem. Res.* 39, 1245–1253. doi:10.1007/s11064-014-1305-3

Yamamoto, B. K., and Novotney, S. (1998). Regulation of extracellular dopamine by the norepinephrine transporter. *J. Neurochem.* 71, 274–280. doi:10.1046/j.1471-4159.1998.71010274.x

Yanik, M., Kocyigit, A., Tutkun, H., Vural, H., and Herken, H. (2004). Plasma manganese, selenium, zinc, copper, and iron concentrations in patients with schizophrenia. *Bter* 98, 109–118. doi:10.1385/BTER:98:2:109

Zou, C.-G., and Banerjee, R. (2005). Homocysteine and redox signaling. *Antioxid. Redox Signaling* 7, 547–559. doi:10.1089/ars.2005.7.547

Conflict of Interest: The authors declare that the research was conducted in the absence of any commercial or financial relationships that could be construed as a potential conflict of interest.

frontiers in Pharmacology

ORIGINAL RESEARCH
published: 10 May 2021
doi: 10.3389/fphar.2021.666885

Unraveling the *Catha edulis* Extract Effects on the Cellular and Molecular Signaling in SKOV3 Cells

Alaa Sayed Abou-Elhamd[1,2†], *Gauthaman Kalamegam*[3†,4], *Farid Ahmed*[3,4], *Mourad Assidi*[3,4], *Abdulmajeed Fahad Alrefaei*[5], *Peter Natesan Pushparaj*[3,4†] and *Muhammad Abu-Elmagd*[3,4*†]

[1]Department of Anatomy and Histology, Faculty of Veterinary Medicine, Assiut University, Assiut, Egypt, [2]Department of Respiratory Therapy, College of Applied Medical Sciences, Jazan University, Jazan, Saudi Arabia, [3]Department of Medical Laboratory Technology, Faculty of Applied Medical Sciences, King Abdulaziz University, Jeddah, Saudi Arabia, [4]Center of Excellence in Genomic Medicine Research, King Abdulaziz University, Jeddah, Saudi Arabia, [5]Department of Biology, Jamoum University College, Umm Al-Qura University, Mecca, Saudi Arabia

Khat (*Catha edulis* (Vahl) Endl.) is an evergreen flowering shrub used as a stimulant in many regions worldwide including East Africa, the Arabian Peninsula, Europe, and the United States. Chewing leaves of khat induces excitement and euphoria, which are primarily attributed to two major constituents, cathinone and cathine. Khat also contains other important constituents such as cathedulins. A considerable number of studies reported side effects induced by the khat extracts to both embryos and adults. These include teratogenicity and developmental retardation, oral cancer and ulcers, high blood pressure, and myocardial infarction. So far, little attention has been paid to the effects of khat extracts on the molecular signaling interactions. We aimed in this study to investigate this through evaluating the effects of khat extracts on SKOV3, a human ovarian adenocarcinoma cell line. We show, by *in vitro* assays, that khat induces several cellular defects including reduced cell size, cell membrane damage, and apoptosis. At high khat extract concentrations, the cell metabolic activity, cell cycle, and cellular proliferation were affected. RT-qPCR analysis showed an increase in the gene expression of the apoptotic marker BAX, the tumor suppressor p53, and the inflammatory cytokine IL-6. Protein expression analysis by immunostaining showed downregulation of β-catenin, E-cadherin, and Ki-67 and upregulation of FZD8 and SPRY2, suggesting that Wnt and FGF signaling were implicated. SwissTargetPrediction *in silico* analysis showed that khat constituents cathine, cathinone, catheduline K2, and catheduline E5 bind to family A G-protein-coupled receptor, cause many neurological diseases and disorders such as Alzheimer's, schizophrenia, depression, and anxiety, and induce many ovarian cancer-related diseases. The analysis also showed that important signaling pathways such as CREB, Wnt, FGF, IL-6, and ERK/MAPK, and that of the endometrial cancer, and cell cycle were implicated. Upstream regulators of cathine and cathinone were found to potentially target several molecules including interleukin-8, MMP2, PLAU, and micro-RNAs. In conclusion, khat induces significant cellular and molecular changes that could potentially cause a wide range of serious diseases and syndromes. Such an impact could have a heavy burden on the health care system in the countries where khat is consumed.

Keywords: molecular signaling, gene expression, FGF, microRNAs, khat, SKOV3

OPEN ACCESS

Edited by:
Tahir Ali,
University of Calgary, Canada

Reviewed by:
Tarek Mohamed Abd El-Aziz,
The University of Texas Health Science Center at San Antonio, United States
Amr El-Demerdash,
John Innes Centre, United Kingdom

****Correspondence:***
Muhammad Abu-Elmagd
mabuelmagd@kau.edu.sa

†These authors have contributed equally to this work

Specialty section:
This article was submitted to Ethnopharmacology, a section of the journal Frontiers in Pharmacology

Received: *11 February 2021*
Accepted: *30 March 2021*
Published: *10 May 2021*

Citation:
Abou-Elhamd AS, Kalamegam G, Ahmed F, Assidi M, Alrefaei AF, Pushparaj PN and Abu-Elmagd M (2021) Unraveling the Catha edulis *Extract Effects on the Cellular and Molecular Signaling in SKOV3 Cells. Front. Pharmacol. 12:666885. doi: 10.3389/fphar.2021.666885*

INTRODUCTION

Khat (*Catha edulis* (Vahl) Endl.) is an evergreen shrub grown in the Horn of Africa and the Arab Peninsula (Al-Qirim et al., 2002; Wabe, 2011). Chewing khat leaves is a common practice among people in these countries due to its stimulant and sympathomimetic effects (Al-Qirim et al., 2002; Dimba et al., 2004; Al-Zubairi et al., 2008). At least 200 constituents in the khat leaves have been recently identified (Kiros, 2020). Khat leaves contain a considerable number of alkaloids, among which major active constituents are cathinone (S-(-)-2-amino-1-phenyl-1-propanone), cathine (1S, 2S-norpseudoephedrine), 62 highly complex cathedulins (polyhydroxylated sesquiterpenes), flavonoids, glycosides, ascorbic acid, tannins, sterols, triterpenes, and smaller amounts of 1*R*, 2*S*-norephedrine (Halbach, 1972; Kalix and Braenden, 1985; Kite et al., 2003; Wabe, 2011; Alsanosy et al., 2020; Kiros, 2020). Young and mature khat leaves constituent analysis has been recently well-documented. This hierarchical cluster analysis showed that cathine and cathinone were the major components and associated with significant cytotoxicity (Alsanosy et al., 2020). The use of khat for medicinal treatment is not yet fully understood, but it has been used to treat serious diseases such as gonorrhea, asthma, chest complications, depression, gastric ulcers, obesity, and tiredness (reviewed by Kiros, 2020).

Problems associated with repeated khat consumption such as psychiatric morbidity (Al-Habori et al., 2002; Pennings et al., 2008), myocardial infarction (Al-Motarreb et al., 2002a), muscle toxicity, and rhabdomyolysis (Mohan et al., 2019), as well as hypertension and tachycardia (Kuczkowski, 2005) have been evident. Khat also causes adverse effects on the gastrointestinal tract such as esophagitis and gastritis (Gunaid et al., 1995). Khat intake has been shown to have a direct relationship with oral cancers with signs of cytotoxic effects at the site of mastication (Soufi et al., 1991; Ali et al., 2004). Interestingly, the evidence for the direct link between khat consumption and oral cancer induction has recently shown a great deal of controversies (Al-Maweri et al., 2020; Chong et al., 2020). Some khat extracts cytotoxic effects were reported in ovarian cancer (Elhag et al., 1999). The toxicity symptoms caused by heavy khat consumption were attributed to the harmful effects of its polyphenolic contents (Abdelwahab et al., 2018).

In rats, khat extracts induced apoptosis, degeneration of hepatocytes (Al-Habori et al., 2002; Al-Mamary et al., 2002; Ageely et al., 2014), embryotoxicity, and severe teratogenicity (Islam et al., 1994; Abou-Elhamd et al., 2018). In male rats, it impaired the process of spermiogenesis (Abou-Elhamd et al., 2020), while in females, it increased the oxidative stress markers (Arafa et al., 2019).

At the cellular level, khat causes genetic damage in human T-lymphoblastoid cell lines (Barkwan et al., 2004) and rapid cell death in HL-60, Jurkat, and NB4 leukemia cell lines (Dimba et al., 2003).

Literature evidence from both *in vitro* and *in vivo* studies indicated that khat extracts have significant cytotoxic and apoptotic effects against some human cancer cell lines (Dimba et al., 2003; Bredholt et al., 2009; Alsanosy et al., 2020). Ovarian cancer ranks fifth most common among cancers in women and is associated with high morbidity and mortality. SKOV3 is an epithelial-like human ovarian adenocarcinoma cell line derived from the ascites of an ovarian serous cystadenocarcinoma. To understand whether khat extract has any inhibitory or cytotoxic effects on ovarian cancer cells, we, in the present study, evaluated the effects of khat extracts on SKOV3 using both *in vitro* and *in silico* platforms. We showed significant changes in the gene and protein expression of several known molecular markers. We also identified many signaling pathways implicated by the khat extracts such as FGF signaling, Wnt signaling, and micro-RNAs.

MATERIALS AND METHODS

Ethical Approval

The ethical approval for the use of SKOV3 was obtained from the Bioethics Committee of the King Abdulaziz University *vide* approval number (33-15/KAU). Khat extracts were processed and obtained from the Biology Department, Jazan University, and its use was approved by the Research Ethics Committee of the Medical Research Center, Jazan University (approval number REC/ MRC/ JU, 30/01/2017).

Khat Extraction

Two bundles weighing 393 g of fresh khat (genus: *Catha edulis* (Vahl) Endl., family: Celastraceae, order: Celastrales, class: Magnoliopsida) was provided by the Substances Abuse and Research Center, Jazan University, Jazan, Saudi Arabia, on the 12th of January 2019. Khat extraction was carried out as soon as the khat bundles were received to avoid the loss of the active ingredients. The average length of the selected khat green leaves for the extract preparation was 4–6 cm. Khat leaves (126 g) were washed in distilled water, chopped on a metal plate, and crushed by a blender. Methanolic khat extraction was carried out as previously described (Abou-Elhamd et al., 2020). In brief, crushed leaves were immersed in 100 ml methanol (Sigma-Aldrich, Taufkirchen, Germany) and kept on a rotary shaker for 2 h. The mixture was filtrated through an 11 mm filter paper (Grade 1, Whatman, Kent, United Kingdom). The filtrate was kept overnight on a stirrer at 45°C to allow the methanol to evaporate (Kimani et al., 2008). Dried khat methanolic crude extract weighed 65.5 g from which we obtained approximately 34 g of usable khat extracts. Cathine and cathinone concentrations in the khat extracts were measured in the Poison Control Medicinal Chemistry Legitimacy Jazan Center, Jazan, Ministry of Health, Saudi Arabia, and were 305 μg/ml and 114 μg/ml, respectively. Khat extracts were stored at −20°C until used as required. Khat extracts were solubilized before being used in the experiments by a tissue culture grade phosphate-buffered saline without calcium and magnesium (PBS^-) and sonicated for 3 min (50 Hz, 37°C).

Culture of the Human Ovarian Cancer Cell Line (SKOV3)

SKOV3 was purchased from the European Collection of Authenticated Cell Cultures (ECACC, Wiltshire, England).

The SKOV3 cells were cultured in the basal Rosewell Park Memorial Institute (RPMI) 1640 medium supplemented with 10% fetal bovine serum (FBS), 2 mM GlutaMAX, and 1% antibiotics (penicillin-streptomycin). The frozen vials containing SKOV3 cells were rapidly thawed in 37°C water bath using the standard thawing procedure. The cells were cultured in a humidified 5% CO_2 incubator at 37°C.

Cell Morphology

SKOV3 cells were seeded at a density of 2×10^4 cells/well in a 24-well plate and allowed to attach overnight. SKOV3 cells serving as negative controls were treated with PBS^- with volumes equal to the added khat extracts. The cells were then treated with various concentrations of the khat extracts (10 µg/ml, 30 µg/ml, 100 µg/ml, 300 µg/ml, 1 mg/ml, 3 mg/ml, and 10 mg/ml) for 24–72 h and cultured in a 5% CO_2 incubator at 37°C. Cell morphology was investigated every 24 h by phase-contrast microscopy (Nikon Instruments, Tokyo, Japan).

Cell Metabolic Activity (MTT) Assay

SKOV3 cells were plated and cultured as stated above, and MTT assay was carried out at 24, 48, and 72 h following treatment with khat extracts at different concentrations (10 µg/ml, 30 µg/ml, 100 µg/ml, 300 µg/ml, 1 mg/ml, 3 mg/ml, and 10 mg/ml). The cell metabolic activity and hence their proliferation/inhibition was determined using MTT assay according to the manufacturer's instructions (Sigma-Aldrich, Germany). The spun media was removed, and 200 ml of fresh culture medium containing 20 µl MTT reagent (3-(4, 5-dimethyl thiazolyl-2)-2, 5-diphenyltetrazolium bromide; Sigma, MO, United States) was added to each well. The cells were incubated under standard culture conditions for 4 h. The medium was removed, and the insoluble formazan crystals were solubilized using DMSO (200 ml/well). The absorbance was obtained at 570 nm with a background reference of 630 nm, using a SpectraMax i3 Multimode Reader (Molecular Devices, Sunnyvale, CA, United States).

Cell Cycle Assay

SKOV3 cells were seeded at a density of 1×10^5 cells/T-25cm^2 tissue culture flask and treated with khat extracts at the following concentrations: 10 µg/ml, 30 µg/ml, and 300 µg/ml for 48 h. The control and treated cells were fixed in 70% ice-cold ethanol by dropwise addition, to avoid clumping of cells, and left overnight at 4°C. The fixed cells were then washed with PBS^- and stained with propidium iodide (PI, 50 µg/ml) in PBS^- containing 50 µg/ml RNase-A and 0.1% Triton X-100. The cells were analyzed using a FACS III Aria flow cytometer (BD Biosciences, CA, United States), and the results were computed with FACSDiva™ software (BD Biosciences, CA, United States).

Apoptosis (Annexin V-PI) Assay

SKOV3 cells were plated and treated with khat extracts as in the above experiment. Cells were treated with khat extracts at the following concentrations: 10 µg/ml, 30 µg/ml, and 300 µg/ml for 48 h. Both the control and treated cells were then trypsinized, centrifuged (1000 rpm × 5 min), and pelleted. The cell pellet was washed once in cold PBS^- and twice in 1X binding buffer with centrifugation (1000 rpm × 5 min) in between washing steps. The final cell pellet was resuspended in freshly prepared PI (Sigma, St Louis, MO, United States) and Annexin V-APC (BD Biosciences, CA, United States) solution and incubated for 15 min in the dark at room temperature. The stained samples were then analyzed for the various stages of the apoptotic cells using a FACS III Aria flow cytometer (BD Biosciences, CA, United States), and the results were computed with FACSDiva™ software (BD Biosciences, CA, United States).

TABLE 1 | Genes and primers' sequence details.

Gene	Primer sequence
BAX	F: 5′-TGGAGCTGCAGAGGATGATTG-3′
	R: 5′-GCTGCCACTCGGAAAAAGAC-3′
IL6	F: 5′-CCACTCACCTCTTCAGAA-3′
	R: 5′-GCGCAAAATGAGATGAGT-3′
p53	F: 5′-GCGCACAGAGGAAGAGAATC-3′
	R: 5′-CTCTCGGAACATCTCGAAGC-3′
GAPDH	F: 5′-ACCACAGTCCATGCCATCAC-3′
	R: 5′-TCCACCACCCTGTTGCTGTA-3′

Gene Expression Analysis (Quantitative Real-Time PCR)

SKOV3 cells were treated with khat extracts as mentioned above and were analyzed for the apoptosis, cell cycle, and inflammation-related gene expression using quantitative real-time PCR (RT-qPCR). The total RNA was extracted using a Pure Link RNA Mini Kit (Ambion, Thermo Fisher Scientific, United Kingdom). Quantity and quality were analyzed using Nanodrop™ (Nanodrop Technologies, Wilmington, DW, United States). First-strand cDNA synthesis was done using random hexamers (High-Capacity cDNA Reverse Transcription Kit, Applied Biosystems) with the inclusion of on-column deoxyribonuclease (DNase-I) treatment. Gene expression of BAX (apoptosis regulator, also known as BCL-2-like protein 4), p53 (tumor suppressor), and IL-6 (interleukin, acts as a proinflammatory cytokine and an anti-inflammatory myokine) were analyzed. The primer sequences used are provided in **Table 1** (Abu-Elmagd et al., 2017). Gene expression analysis was performed using a StepOnePlus™ real-time PCR System (Applied Biosystems, United States) with SYBR Green Master Mix. Relative quantitation was done using the comparative $2^{-\Delta\Delta Ct}$ method.

Immunohistochemistry

SKOV3 control cells and 700 µg/ml of khat extract-treated cells on coverslips were fixed in 4% formaldehyde/PBS for 10 min at room temperature and then rinsed twice in ice-cold PBS/Tween-20 (PBST). Cells were then treated with 2% H_2O_2 for 10 min to block the endogenous peroxidase expression, washed with PBST, and then permeabilized with Triton X-100 for 10 min. Cells were washed with PBST and blocked with 10% goat serum, after which each coverslip was treated at 4°C with an anti-human primary antibody of β-catenin (Leica Biosystems, IL, United States) (mouse

monoclonal, 6003258, 1:100 dil.), E-cadherin (Dako, CA, United States) (mouse monoclonal, M7240, 1:100 dil.), Frizzled-8 (FZD8, Rabbit, ab155093, 1:100 dil.), Sprouty-2 (SPRY2, mouse monoclonal, SC-100862, 1:250 dil.), and Ki-67 (mouse monoclonal, M-7240). After overnight incubation in the primary antibody, cells were washed with PBST and blocked with 10% goat serum. The secondary antibody was applied, and the color was detected according to Dako REAL detection system manufacturer's instructions (Dako, CA, United States, cat. no. K5001). Cells were then treated with biotinylated secondary antibody for 20 min, washed with PBST, and then treated with streptavidin peroxidase for 20 min. The color was developed using Dako DAB color substrate and counter-stained with hematoxylin. The slides were dehydrated with ascending grades of ethanol and mounted with xylene-based mounting media. Images were captured using an Olympus BX53 microscope (Tokyo, Japan).

In Silico Analysis

SwissTargetPrediction

The machine-readable formats of the cathine ($C_9H_{13}NO$), cathinone ($C_9H_{11}NO$), catheduline K2 ($C_{40}H_{51}NO_{19}$), and catheduline E5 ($C_{59}H_{64}N_2O_{23}$) structures were obtained, based on both canonical and from the PubChem Database (Kim, 2016; Kim et al., 2016). In the present study, the putative molecular targets of the cathine, cathinone, and both cathedulins were obtained using SwissTargetPrediction (http://www.swisstargetprediction.ch/) (Gfeller et al., 2014) (**Supplementary Figure S1**). Canonical and isomeric SMILES of cathine, cathinone, catheduline K2, and catheduline E5 were used as input sequences in the SwissTargetPrediction webserver to virtually screen the molecular targets (Daina and Zoete, 2019). The SwissTargetPrediction virtual screening tool uses the "similarity principle" to predict the most probable targets of bioactive molecules such as cathine, cathinone, catheduline K2, and catheduline E5 (Gfeller et al., 2013; Gfeller et al., 2014). In this virtual reverse screening tool, the putative binding predictions are accomplished from 376,342 experimentally active analogous compounds in 2D and 3D that strongly interact with 3,068 well-recognized protein targets (Huang et al., 2018; Daina and Zoete, 2019). In the latest version of the SwissTargetPrediction, the dataset is based on ChEMBL23, and putative protein targets are ranked based on a score that merges both 2D and 3D similarity values of an active molecule to the query molecules such as cathine, cathinone, catheduline K2, and catheduline E5 (Daina et al., 2019). Importantly, the ranking of the targets rather than the absolute values of scores or probabilities is the most meaningful parameter. A maximum of 100 probable protein targets was obtained as an output from the SwissTargetPrediction tool (Gfeller et al., 2014; Daina et al., 2019).

WebGestalt Analysis of Cathine and Cathinone Targets

WebGestalt (wGSEA) is an open-source platform (http://webgestalt.org/) that facilitates a more flexible, comprehensive, and interactive functional enrichment analysis of differentially expressed proteins (DEPs) or differentially expressed genes (DEGs) (Liao et al., 2019). The newest version of the wGSEA identifies 155,175 functional groups, 342 gene identifiers, and 12 major organisms with an additional option for including user-defined functional databases (Liao et al., 2019; Bahlas et al., 2020). The DEPs or DEGs derived from medium- to large-scale omics experiments can be classified based on biological, molecular, and cellular functions using the wGSEA web tool. To functionally classify the cathine- and cathinone-induced putative protein targets, the Over Representation Analysis (ORA) module of the wGSEA was chosen (**Supplementary Figure S1)**, the preferred organism was *Homo sapiens*, and gene ontology (biological, cellular, and molecular functions) and disease databases such as OMIM, GLAD4U, and DisGeNET were selected for further downstream analyses (Liao et al., 2019; Bahlas et al., 2020). The default parameters for the enrichment analysis such as the minimum number of IDs (5), the maximum number of IDs (2000), the Benjamini Hochberg (BH) method for computing the False Discovery (FDR) Rate ($p < 0.05$), and the significance level (Top 10) were applied for each wGSEA analysis (Bahlas et al., 2020).

Open Targets Platforms

The Open Targets Platform (https://www.targetvalidation.org/) was utilized to uncover the cathine and cathinone molecular targets associated with cell proliferation disorders, ovarian diseases, and psychiatric disorders (Koscielny et al., 2017; Carvalho-Silva et al., 2018; Ochoa et al., 2021). The evidence from various omics studies, text mining of scientific publications, *in vivo* models, and disease relevant drugs were utilized in the Open Targets Platform to score and rank target-disease associations and assist target prioritization (Khaladkar et al., 2017; Carvalho-Silva et al., 2018; Ochoa et al., 2021). Here, the query lists, along with the putative molecular targets of cathine and cathinone, were used to decipher the cell proliferation, ovarian, psychiatric, and nervous system disorders, and diseases significantly ($p < 0.05$) regulated by these molecules and their associated molecular networks.

Ingenuity Pathway Analysis

Ingenuity Pathway Analysis (IPA) software (Qiagen Inc., MD, United States) has a cutting edge, up to date next generation knowledge base that consists of clarified scientific information from publications, databases, and other relevant resources (Jafri et al., 2019; Bahlas et al., 2020). Here, we applied the IPA to functionally annotate the protein clusters and identified biologically significant disease-specific pathways regulated by cathine and cathinone molecular targets. The putative molecular targets of cathine and cathinone was subjected to Core Analysis in the IPA to delineate biologically relevant canonical pathways, diseases, biological and pathological functions, upstream regulators, causal networks, and nondirectional unique networks, using the right-tailed Fisher Exact Test and Benjamini Hochberg Correction (BHC) for multiple testing ($p < 0.05$).

RESULTS

Khat Extract and SKOV3 Cells Morphology

The untreated control of SKOV3 cells demonstrated normal attachment, morphology, growth, and proliferation. Treatment

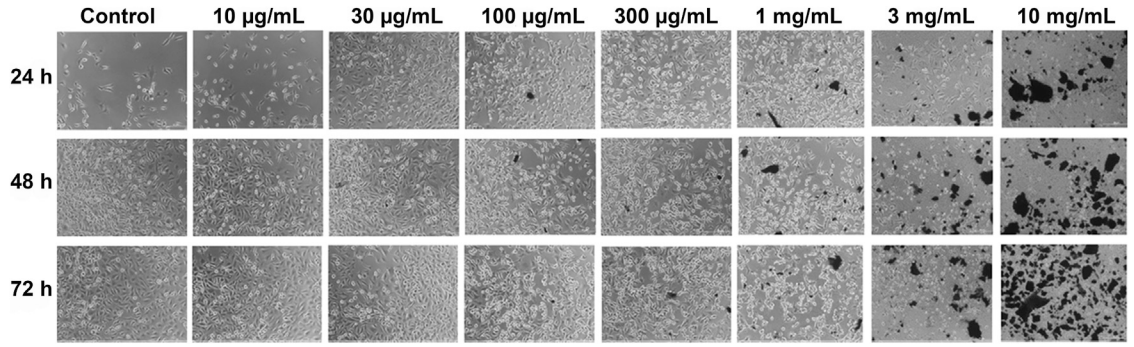

FIGURE 1 | Representative phase-contrast images of the ovarian cancer cell line (SKOV3) following treatment with khat extracts at different concentrations (10, 30, 100, 300 µg/ml, 1, 3, 10 mg/ml) and different time points (24, 48, and 72 h). Compared to control, the SKOV3 cells exposed to khat extracts demonstrated cell growth inhibition and death with increasing concentration of the extract. Magnification 10x.

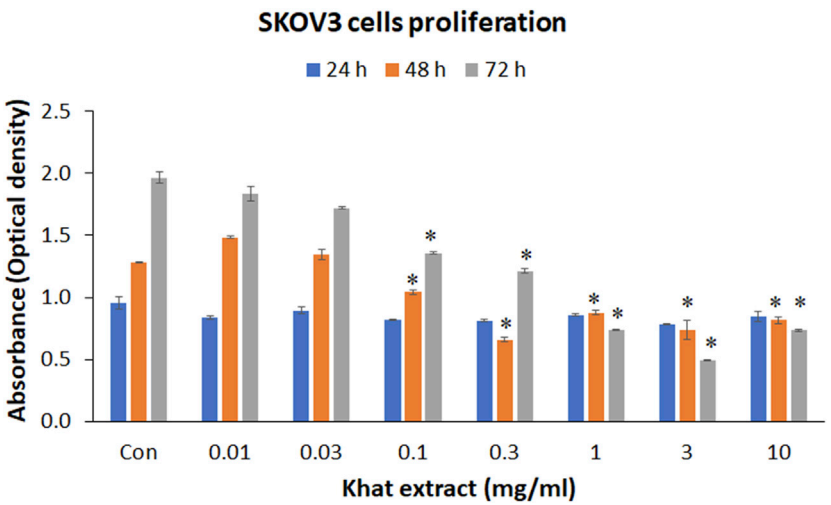

FIGURE 2 | Cell metabolic activity (MTT assay) of SKOV3 following treatment with khat extracts at different concentrations (10, 30, 100, 300 µg/ml; 1, 3, 10 mg/ml) and different time points (24, 48, and 72 h). There was a decrease in cell metabolic activity reflecting cell proliferation with increasing concentration of the extract especially at 48 and 72 h compared to the control. Values are expressed as mean ± SEM of three different experiments.*Statistical significance ($p < 0.05$).

with different concentrations (10, 30, 100, and 300 µg/ml; 1, 3, and 10 mg/ml) of khat extracts for 24–72 h showed variable inhibition of SKOV3 cell growth and proliferation compared to the control (**Figure 1**). There were no changes in cell morphology or proliferation at lower concentrations compared to the control. However, higher concentrations of khat extracts, especially 1 mg/ml, 3 mg/ml, and 10 mg/ml and extended culture period (48 and 72 h), showed different morphological changes such as shrinkage in cell size, damage to cell membranes, and loss of cell adherence, culminating in cell death compared to control (**Figure 1**).

Khat Extract and SKOV3 Cells Metabolic Activity

MTT assay demonstrated an indirect increase, reflecting the increase in cell numbers with extended duration of culture. However, following treatment with different concentrations (10, 30, 100, and 300 µg/ml; 1, 3, and 10 mg/ml) of khat extracts for 24–72 h, a mild to moderate decline in the metabolic activity of the SKOV3 cells was observed with most concentrations compared to the control (**Figure 2**). The observed reduction in metabolic activity after treatment for 24 h at various concentrations of khat extracts as stated above was 12.32, 6.34, 14.22, 14.92 10.13, 18.21, and 11.36%. These mean decreases compared to the control were statistically not significant (**Figure 2**).

At 48 h, the 10 and 30 µg/ml concentrations of khat extracts demonstrated an increase by 15.84 and 5.28%, respectively, compared to the control, these increases were not statistically significant. The rest of the concentrations (100 and 300 µg/ml; 1, 3, and 10 mg/ml) of khat extracts demonstrated a decrease by 18.68, 48.65, 31.55, 42.30, and 36.19% compared to the control.

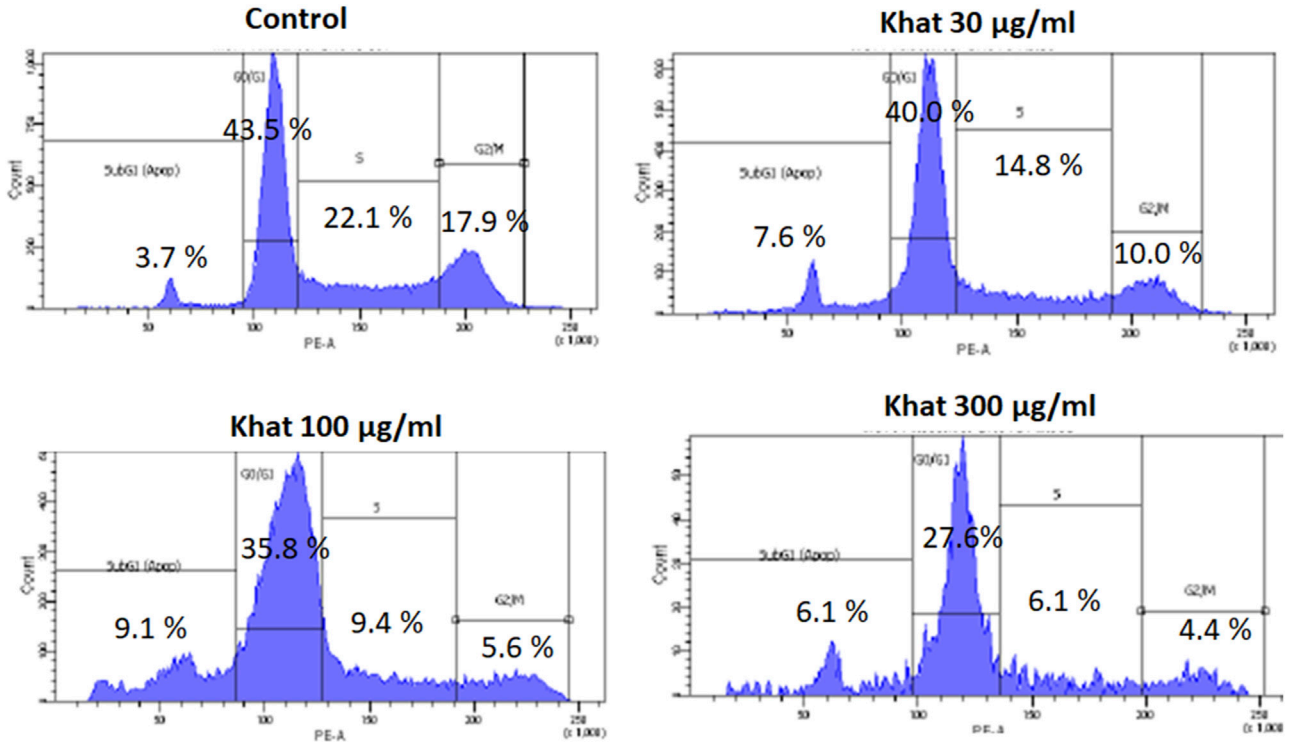

FIGURE 3 | Cell cycle (Propidium iodide assay) of SKOV3 following treatment with khat extracts at different concentrations (30 µg/ml, 100 µg/ml, and 300 µg/ml) for 48 h. There was a mild increase in the sub-G1 phase of the cell cycle indicative of apoptosis.

All these mean decreases in values were statistically significant (**Figure 2**).

Treatment of SKOV3 cells with khat extracts for 72 h demonstrated a decrease in the metabolic activity by 6.57, 12.52, 31.05, 38.40, 62.39, 74.85, and 62.72% compared to the control. All these mean decreases in values except for the 10 and 30 µg/ml concentrations were statistically significant (**Figure 2**).

Khat Extract and Cell Cycle Assay

The cell cycle (propidium iodide) assay evaluated after treatment of SKOV3 cells with 30, 100, and 300 µg/ml of khat extracts for 48 h demonstrated an increase in the sub-G1 SKOV3 cells' population by 3.9, 5.4, and 2.4%, respectively, compared to the control in the representative histogram (**Figure 3**). The "S" phase of the cell cycle demonstrated a decrease by 7.8, 12.7, and 16.0%, respectively, compared to the control (**Figure 3**). The "G2M" phase of the cell cycle demonstrated a decrease by 7.9, 12.3, and 13.3%, respectively, compared to the control (**Figure 3**).

Khat Extract and Cell Apoptosis Assay

The apoptosis (Annexin V-APC) assay evaluated with 30, 100, and 300 µg/ml of khat extracts for 48 h demonstrated a decrease in the apoptotic cells' population compared to the control (**Figure 4**). The mean percentage values of the apoptotic cells were 2.2, 2.0, and 3.1% for the concentrations of 30, 100, and 300 µg/ml, respectively, compared to the control (**Figure 4**). The percentage of cells representing the cell debris population was increased by 24.4, 25.5, and 18.1% compared to the control (**Figure 4**).

Khat Extract and Gene Expression Assay

The quantitative RT-PCR analysis was carried out following treatment of SKOV3 cells with 30, 100 and 300 µg/ml of khat extracts for 48 h demonstrated a mild increase in the expression of both apoptosis-related BAX and p53 genes and inflammation-related IL-6 gene (**Figure 5**). The fold increases were as follows: BAX (0.81, 1.18, and 0.28); p53 (0.88, 2.48, and 1.69); and IL-6 (0.81, 0.40, and 0.10) with 30 µg/ml, 100 µg/ml, and 300 µg/ml of khat extracts, respectively, compared to the control (**Figure 5**). The proapoptotic BAX gene and the tumor suppressor p53 gene showed an overall increase compared to the control, although the higher concentration demonstrated a relative decrease. However, the inflammatory gene IL-6 was increased compared to the control; it demonstrated a decline with an increase in concentrations of khat extracts.

Analysis of the Effects of Khat Extract by Immunostaining

The endogenous protein expression of several molecular markers was tested on khat SKOV3–treated cells at 700 µg/ml for 48 h alongside the untreated control cells by immunostaining. These markers were applied to specifically test the khat extract effects on important molecular and cellular signaling such as Wnt and FGF signaling, cellular adhesion, and cellular proliferation. The markers

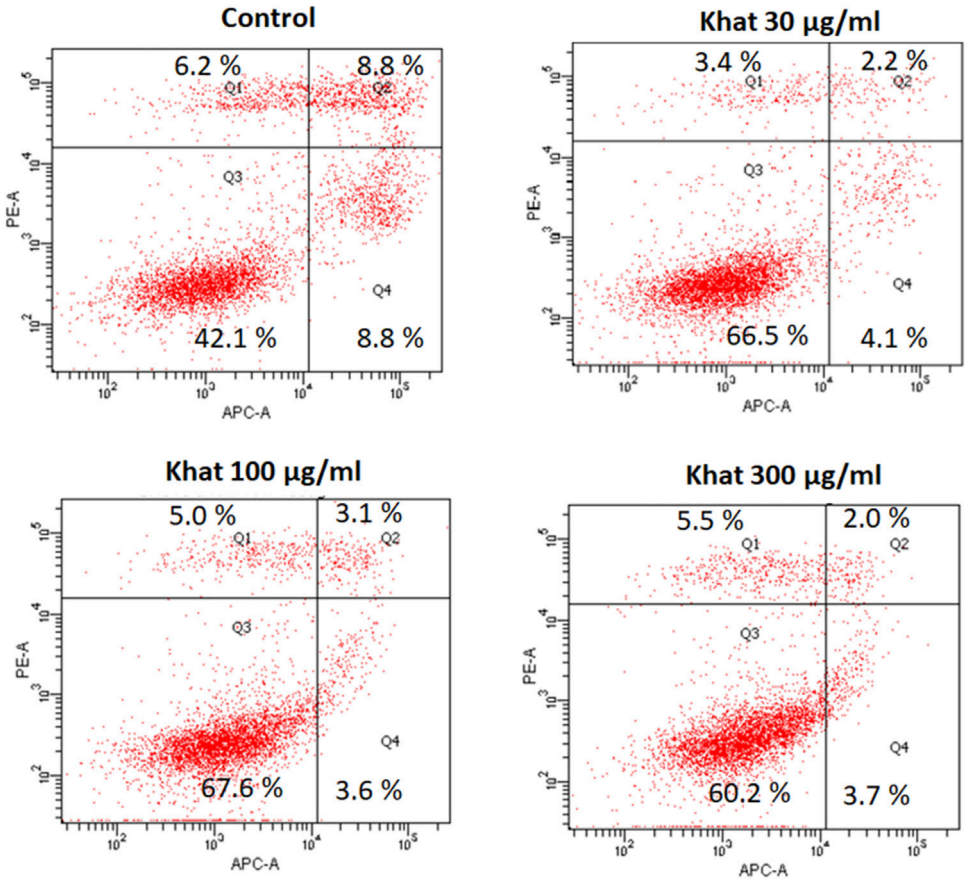

FIGURE 4 | Apoptosis (annexin V-APC assay) of SKOV3 following treatment with khat extracts at different concentrations (30 µg/ml, 100 µg/ml, and 300 µg/ml) for 48 h. The control cells demonstrated more positive staining with annexin V-APC which showed a decreasing trend with increasing concentration of the khat extract.

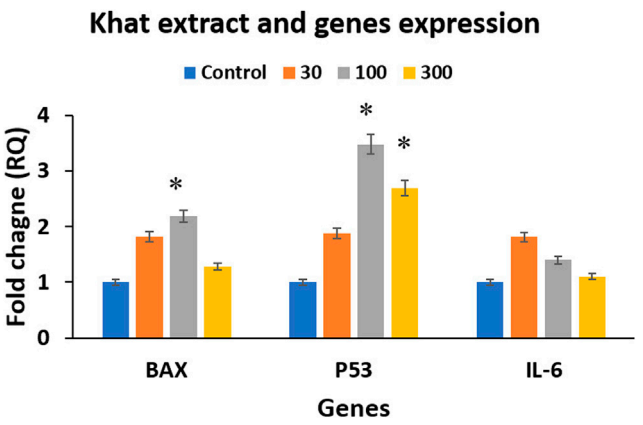

FIGURE 5 | Gene expression analysis using RT-qPCR analysis of the treated and untreated SKOV3 cells showing BAX, p53, and IL-6 expression following treatment with 30, 100, and 300 µg/ml of khat extracts for 48 h. GAPDH was used as the internal control, and the data were quantified using the comparative $2^{-\Delta\Delta Ct}$ method. The values are expressed as mean ± SEM from triplicate samples of two independent experiments.

used were β-catenin and Frizzled-8 (Wnt signaling pathway molecules), E-cadherin (CAM or cell adhesion molecule), Sprouty-2 (FGF/MAP kinase signaling inhibitor), and Ki-67 (nonhistone nuclear protein marker for cell proliferation) (**Figure 6**). In SKOV3 khat extract treated cells, we observed downregulation of the protein expression of β-catenin, E-cadherin, and Ki-67 (**Figures 6B,D,F**) in comparison with their corresponding untreated controls (**Figures 6A,C,E**). A reduction in the nucleoli number was also observed which was demarcated by the Ki-67 expression (**Figure 6F**) in comparison with the untreated control cells (**Figure 6E**). A considerable upregulation of Frizzled-8 and Sprouty-2 expression (**Figures 6H,J**) in comparison with the untreated SKOV3 control (**Figures 6G,I**) was also observed.

In Silico Analysis

Prediction of the Molecular Targets of Cathine, Cathinone, Catheduline K2, and Catheduline E5 Using SwissTargetPrediction

SwissTargetPrediction was performed for cathine (**Figure 7A**), cathinone (**Figure 7B**), catheduline K2 (**Figures 8A,C**), and

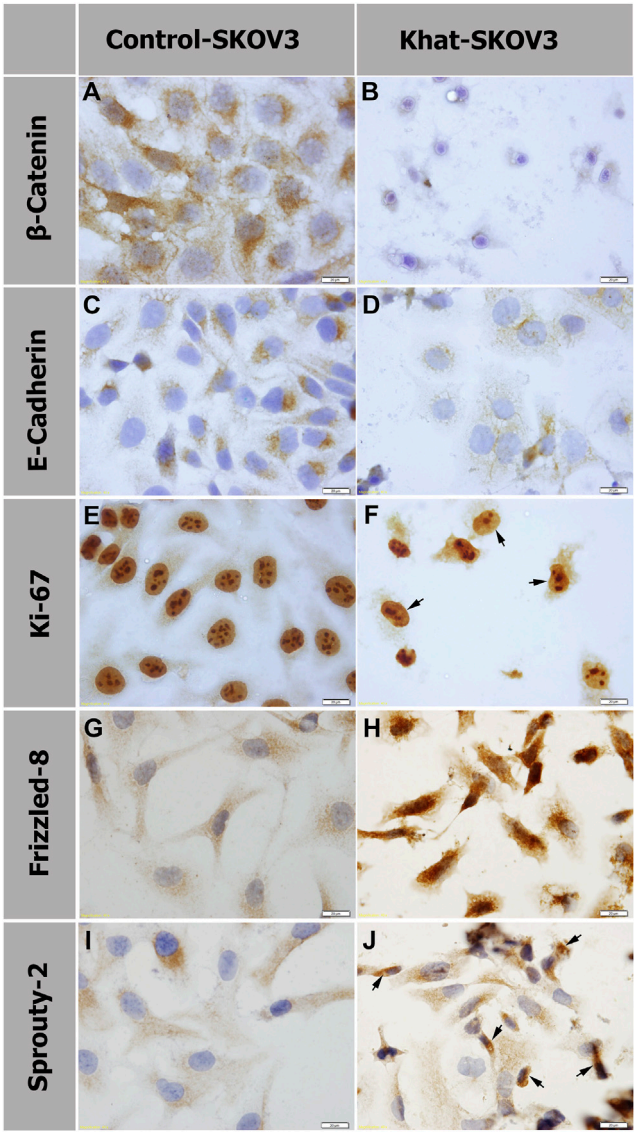

FIGURE 6 | Protein expression analysis by immunostaining of β-catenin **(A, B)**, E-cadherin **(C , D)**, Ki-67 **(E, F)**, Frizzled-8 **(G, H)**, and Sprouty 2 **(I, J)** of SKOV3 cells treated with 700 μg/ml of khat extract alongside the untreated SKOV3 control cells. Panels **(B, D, F)** show downregulation of β-catenin, E-cadherin, and Ki-67, respectively, in comparison with the corresponding untreated control **(A, C, E)**. Panels **(H, J)** show increased expression of FZD8 and SPRY2, respectively, in comparison with the untreated control **(G, I)**. Arrows in **(F)** indicate SKOV3 khat-treated cells with a reduction in the nucleoli number. Arrows in **(J)** indicate SKOV3 khat-treated cells with an elevated SPRY2 expression.

catheduline E5 (**Figures 8B,D**) using both canonical and isomeric Simplified Molecular Input Line Entry System (SMILES) codes (**Supplementary Table S1**) computed by OEChem (Version 2.1.5). The cathine and cathinone have the highest percentage of binding (32 and 15%, respectively) with family A G-protein coupled receptors (**Figures 7A,B**). For the cathedulins K2 and E5, one hundred top targets analysis showed that these compounds show high affinity to bind to the proteases, kinases, and Family A G protein-coupled receptor (**Figures 8C,D**). This is in addition to other targets such as cytochrome p450, nuclear receptor, and voltage-gated ion channel.

Over Representation Analysis (ORA) of the Molecular Targets of Cathine and Cathinone Using WebGestalt

All the putative molecular targets of cathine and cathinone were obtained using isomeric SMILES (**Supplementary Table S1**) as input molecules in wGSEA to perform the ORA. GO Slim Summary for cathine and cathinone molecular targets in humans displaying biological process, cellular component, and molecular function are shown in (**Figure 9**).

The putative target list contains 100 user IDs for either cathine or cathinone. 88 user IDs for cathine were unambiguously mapped to 88 unique Entrez gene IDs and 13 user IDs, while 97 user IDs for cathinone were unambiguously mapped to 97 unique Entrez gene IDs and three user IDs cannot be mapped to any Entrez gene ID. The GO Slim summary for cathine was based upon the 88 unique Entrez gene IDs. Among 88 unique Entrez gene IDs, 6 IDs were annotated to the selected functional categories as well as the reference list, which was used for the enrichment analysis (**Figure 9A**). Similarly, the GO Slim summary for cathinone was based upon the 97 unique Entrez gene IDs. Among 97 unique Entrez gene IDs, 9 IDs were also annotated in the same way (**Figure 9B**).

The reference lists consist of all mapped Entrez gene IDs from the selected platform genome. The ORA using OMIM, GLAD4U, and DisGeNET disease databases showed that the putative protein targets of both cathine and cathinone significantly (**Supplementary Figure S2**, indicated by the false discovery rate (FDR ≤ 0.05) in dark blue) regulate many diseases and disorders such as schizophrenia, Alzheimer's disease, mental depression, and other major depressive disorders, anxiety disorders, and migraine disorders.

Identification of Cathine and Cathinone-Induced Molecular Targets in Cell Proliferation Disorders, Ovarian Diseases, and Psychiatric Disorders

The Open Targets Platform was used to determine the association between diseases with the putative molecular targets of both cathine and cathinone (**Supplementary Figure S1**). Our findings showed that 879 types of cell proliferation disorders (**Supplementary Table S2**), 13 different types of ovarian diseases (**Supplementary Table S3**), and 322 types of psychiatric disorders (**Supplementary Table S4**) were significantly ($p < 0.05$) affected by the molecular targets of cathine. The 13 types of ovarian diseases significantly ($p < 0.05$) regulated by cathine were noticeably cancer-related diseases.

Additionally, our findings showed that 1,156 types of cell proliferation disorders (**Supplementary Table S5**), 43 different types of ovarian diseases (**Supplementary Table S6**), and 408 types of psychiatric diseases (**Supplementary Table S7**) were significantly ($p < 0.05$) affected by the molecular targets of cathinone. The 43 types of ovarian diseases significantly ($p < 0.05$) regulated by cathinone were predominantly related to ovarian cancer disease, ovarian insufficiency, ovarian

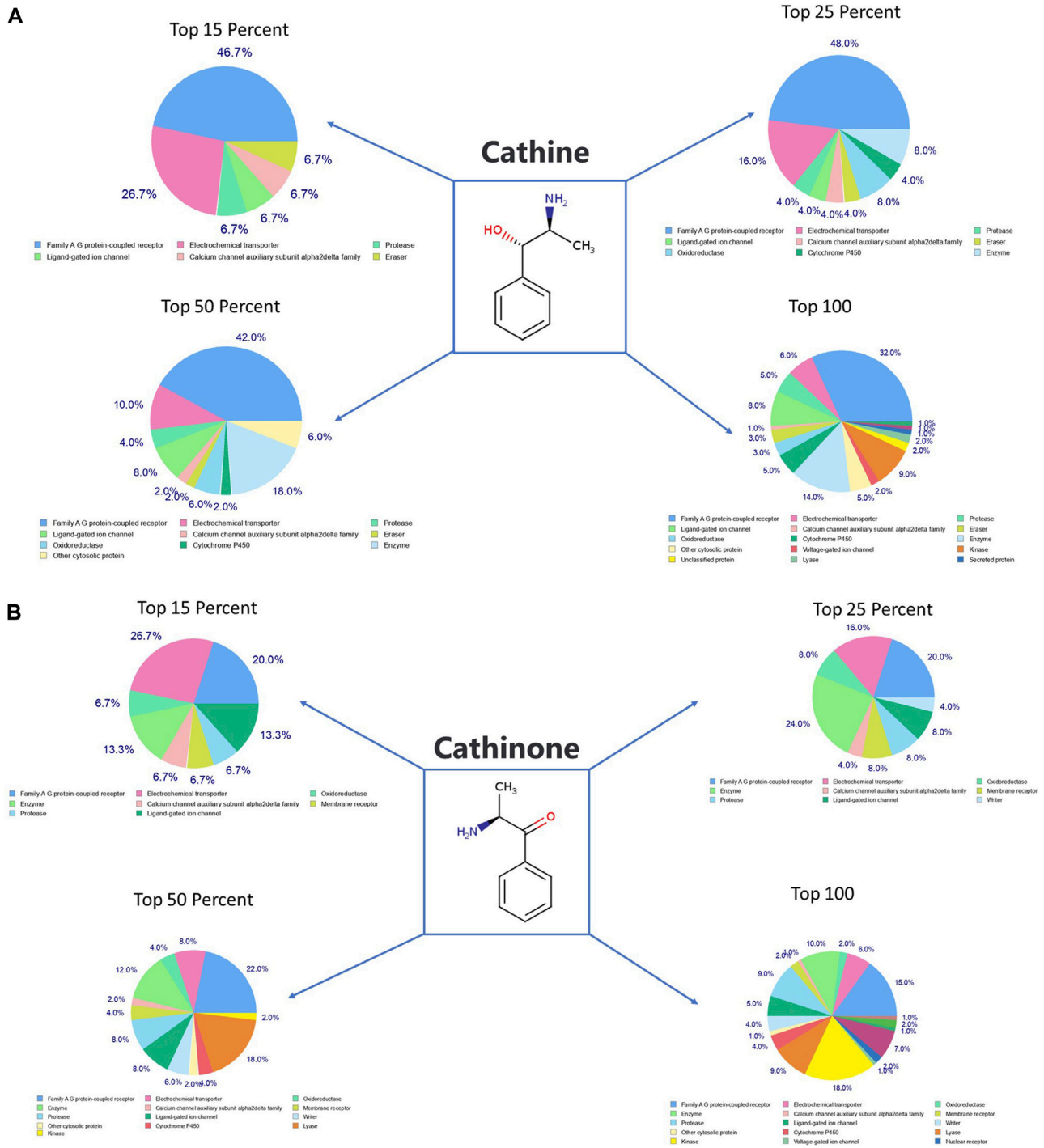

FIGURE 7 | SwissTargetPrediction analysis for cathine **(A)** (PubChem CID 441457) and cathinone **(B)** (PubChem CID 62258) showing top targets for both components. Cathine and cathinone have the highest percentage of binding (32 and 15%, respectively) with family A G-protein-coupled receptors.

dysfunction leading to infertility, rare female infertility due to an anomaly of the ovarian function of genetic origin, osteosclerosis-ichthyosis-premature ovarian failure, and ovarian endometriosis. (**Supplementary Table S6**).

Ingenuity Pathway Analysis of the Putative Protein Targets of Cathine and Cathinone

We used the IPA to decode the canonical pathways, upstream regulators, causal functions, diseases and biofunctions,

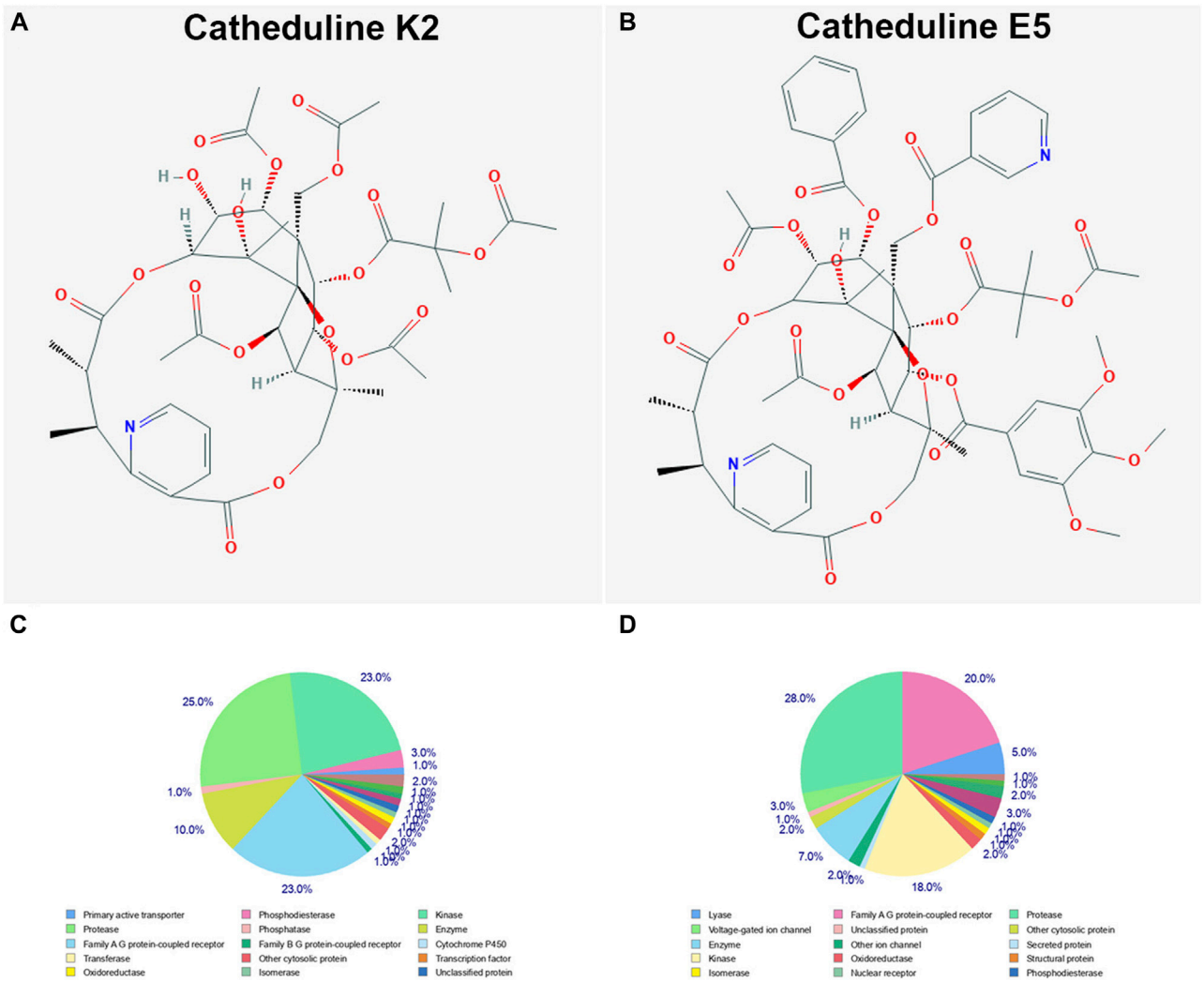

FIGURE 8 | SwissTargetPrediction analysis of two members of the cathedulins khat constituents, catheduline K2 **(A)** (PubChem CID 101290208), and catheduline E5 **(B)** (PubChem CID 124201484) showing top 100 targets for both components **(C, D),** respectively. Both cathedulins have the potential to highly bind with the protease, kinase, and Family A G protein-coupled receptor in addition to other potential targets.

pathological functions, and nondirectional unique networks that are significantly impacted by both cathine and cathinone. The IPA core analysis of the putative molecular targets of cathine (**Supplementary Table S8**) and cathinone (**Supplementary Table S9**) revealed that canonical pathways such as G-protein coupled receptor signaling, dopamine receptor signaling, serotonin receptor signaling, CREB-signaling in neurons, Wnt signaling, FGF signaling, IL-6 signaling, ERK/MAPK signaling, endometrial cancer signaling, and cell cycle were significantly affected ($p < 0.05$). Furthermore, the diseases and biofunctions such as psychological disorders and many neurological diseases were potentially regulated ($p < 0.05$) by cathine (**Supplementary Table S10**) and cathinone (**Supplementary Table S11**).

Interestingly, the IPA core analysis identified 250 upstream regulators of cathine to target CXCL8 (Interleukin-8), and 43 regulators to target PLAU and its receptor PLAUR (**Supplementary Table S12**). On the other hand, the analysis identified 33 upstream regulators of cathinone (not the cathine) to target MMP2 and 62 regulators to target PLAU and its receptor PLAUR (**Supplementary Table S13**).

The IPA analysis identified several upstream micro-RNA regulators. For the cathine, these were miR-16-1-3p, miR-30, miR-30c-5p, miR-31-5p, miR-146a-5p, mir-204, miR-373, miR-424-3p, miR-511-5p, and miR-542-3p (**Supplementary Table S12**). For the cathinone, these were: miR-9, miR-9-5p, miR-30c-5p, miR-31, miR-34a-5p, miR-103, miR-222-5p, miR-296, miR-451a, miR-491-5p, miR-1180, miR-1275, and miR-1285-3p (**Supplementary Table S13**).

DISCUSSION

Khat plant is a widespread stimulant which is recreationally munched by many people in Africa, Asia, Europe, and the

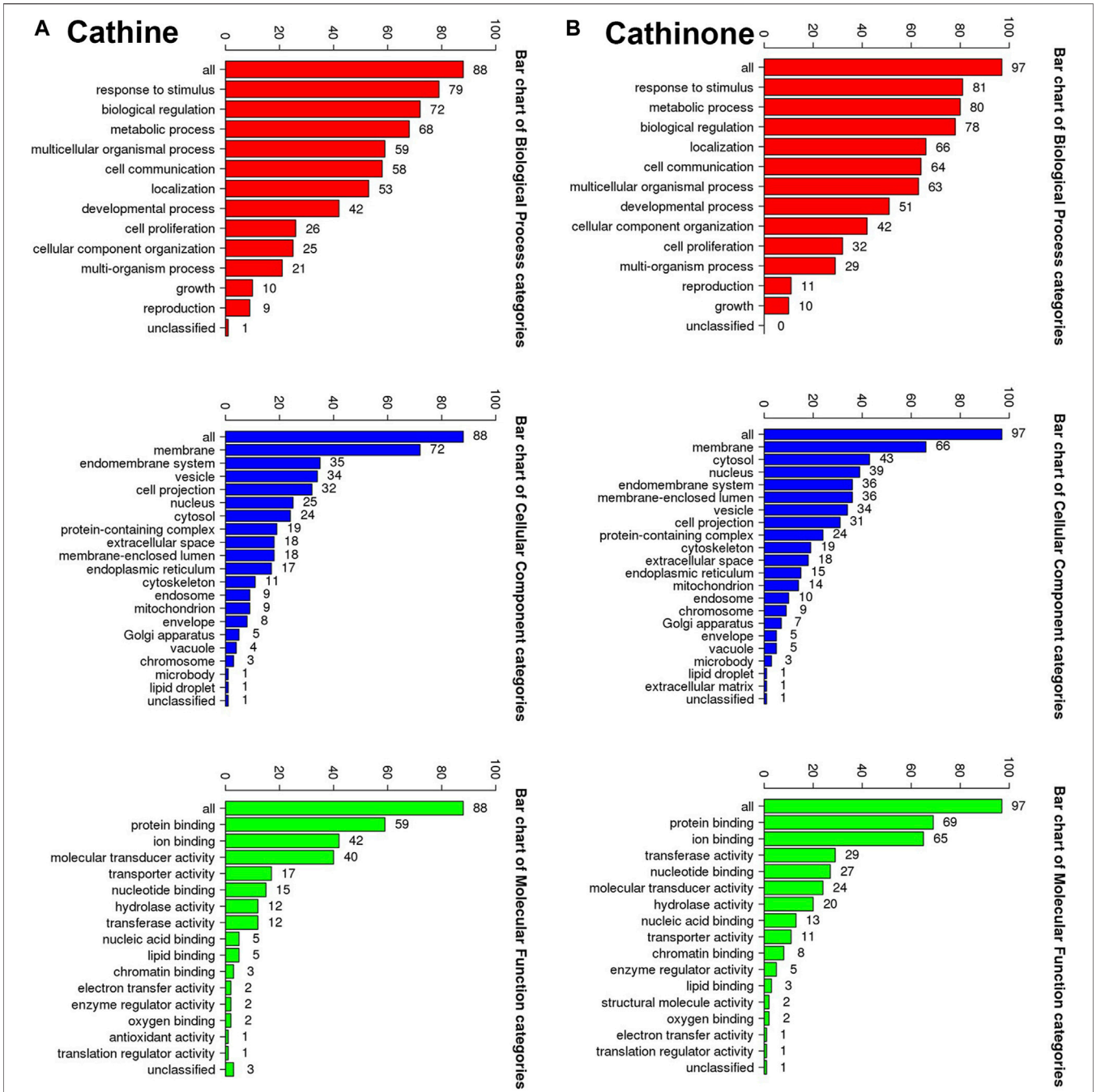

FIGURE 9 | The GO Slim analysis. The summaries are based upon the 88 and 97 unique Entrez gene IDs for the putative protein targets of cathine **(A)** and cathinone **(B)**, respectively. Potential effects on the biological process (bars in red), cellular component (bars in blue) and molecular function (bars in green). The height of each bar characterizes the number of IDs in the user list and in the category.

United States with an estimate of more than 20 million users (El-Menyar et al., 2015). Many studies have shown that khat induces a series of adverse effects during embryonic development and illnesses in adulthood. These include teratogenicity, cancer, and adverse effects on the nervous, cardiovascular, digestive, genitourinary, reproductive, metabolic, and endocrine systems (reviewed by Wabe, 2011). In this study, we evaluated the effects of khat on the human ovarian adenocarcinoma SKOV3 cell line. We detected several cellular and molecular adverse effects, including shrinkage in the cell size, damage to the cell membrane, loss of cell adherence, cell death, metabolic decline, decrease in the "S" and "G2" cell cycle phases, and decrease in the apoptotic cells' population. Similar effects of inhibition of cell proliferation and cell growth, shrinkage of

cells and increased apoptosis were shown after khat extracts treatment in human hepatocytes HepG2 (Taha et al., 2014), rat cardiomyoblasts H9c2 (Mohan et al., 2016), and Madin–Darby bovine kidney cell line (Ageely et al., 2016). It was also previously shown that khat induced a reduction in cell viability and apoptosis in other different cell lines such as L02 human hepatic cell line (Abid et al., 2013) and human breast cancer cell line MDA-MB-231 (Lu et al., 2017). It has been shown that khat induced apoptosis through a mechanism involving activation of caspase-1, -3, and -8 (Dimba et al., 2004).

We tested the khat effects on apoptosis, tumorigenesis, and inflammation using BAX, p53, and IL-6, respectively, and showed an overall increase in the expression of these important genes. Our results agree with several studies that tested the effects of khat on the expression of these markers but using different cell lines. Abid et al. (2013) showed an increase in BAX expression after khat extracts treatment to the human liver cell line L02. An increase of p53 expression and a G1-phase arrest was previously reported after the khat extracts treatment of human oral keratinocytes and oral fibroblasts (Lukandu et al., 2008). An increase in the IL-6 expression in the brain tissue was previously reported after khat extracts treatment *in vivo* in mice (Ali et al., 2015).

Khat extracts treatment in rats showed stress-related effects on the ovaries due to an imbalance between ROS and the production of antioxidants (Arafa et al., 2019). Similar ROS inhibition induced by khat extracts treatment was reported using murine monocytic macrophages RAW 264.7 cell line (Abdelwahab et al., 2018). It has also been reported that khat induces intracellular ROS in the human fetal hepatocyte L02 cell line resulting in consecutive activation of JNK and ERK signaling pathways (Abid et al., 2013). This, in turn, decreased cell viability and increased apoptosis. In the current study, the effects of khat extracts treatment on ROS were not tested; however, ROS may have been similarly affected in SKOV3 cells.

We aimed to analyze possible molecular signaling pathways after khat extracts treatment to decipher the involved mechanisms of action. Among several signaling pathways, Wnt signaling (represented by β-catenin and FZD8 expression), FGF signaling (represented by SPRY2 expression, FGF negative regulator), and cellular adhesion (represented by E-Cadherin) were tested using respective antibodies against these markers. Despite their crucial roles during many cellular events, these signaling pathways have not been previously analyzed following khat extracts treatment. We showed in the current study that β-catenin expression was severely reduced after khat extracts treatment. This suggests that canonical Wnt signaling through β-catenin was modulated. Interestingly, we also showed that FZD8 (Wnt receptor) expression was strongly elevated in comparison with the untreated SKOV3 control cells. It was previously shown that elevated FZD8 expression was linked with the airway proinflammation induction and associated with chronic bronchitis (Spanjer et al., 2016). As mentioned above, we showed by RT-qPCR an increase in the proinflammation IL-6 expression which could be the trigger for FZD8 expression upregulation. This explanation is supported by some reported evidence linking Wnt/β-catenin signaling with both anti-inflammation and proinflammation functions (Ma and Hottiger, 2016). We also showed that SPRY2 expression was upregulated following treatment with khat extracts. SPRY2 is a negative regulator of FGF signaling, so upregulation of its expression would lead to blocking of the FGF signaling through a negative feedback loop. Compromising FGF signaling might explain some of the cellular damage obtained in our results. We also observed a reduction in E-cadherin expression. It has been previously reported that SPRY2 overexpression inhibited the induction of the transcriptional repressor E-cadherin in the SKOV3 ovarian adenocarcinoma cell line (Cheng et al., 2016).

Our *in silico* results from various analyses showed that cathine, cathinone, catheduline K2, and catheduline E5 potentially induce several neurological and psychological diseases and symptoms. Our findings agree with earlier results reported by other studies (Odenwald et al., 2005; Hoffman and Al'absi, 2010; El-Setouhy et al., 2016). However, potential induction of several neural disorders we report here by the khat constituents such as developmental disorder of mental health, neurodevelopmental disorder with epilepsy, motor developmental delay, macrocephaly, developmental delay with seizures, and developmental delay associated with premature aging appearance ($p < 0.05$) (**Supplementary Tables S4, S7**) have not been previously reported. Further experimental validation of these results would complement the *in silico* analysis and is highly recommended.

Additionally, the IPA analysis results (**Supplementary Tables S2, S5, S8, S9**) supported our immunostaining findings which showed that the khat extract affected cell proliferation, Wnt signaling, FGF signaling, and cell adhesion in SKOV3 cells. Besides, the IPA analysis showed that upstream targets of the cathine and cathinone abundantly target MMP2, PLAU, and its receptor PLAUR, and IL-8. It has been previously shown that MMP2 functions as an early marker for ovarian cancer metastasis (Kenny and Lengyel, 2009). The urokinase plasminogen activator (PALU) was shown to play an important role during ovulation in animal models (Ogiwara et al., 2015). Interestingly, IL-8 was shown to increase cell proliferation and correlate with increased MMP2 expression in ovarian cancer (Wang et al., 2012).

The IPA analysis identified several members of the micro-RNAs as potential upstream regulators of the cathine and cathinone. These micro-RNAs have previously been reported to have different important roles in ovarian cancer regulation, prognosis, and/or diagnosis (Alshamrani, 2020; Aziz et al., 2020; Ferreira et al., 2020). Hence, our present analysis could provide potential directions for future studies on the further elucidation of these micro-RNAs' regulations of the cellular and molecular events induced by khat. In summary, our study identifies several crucial molecular signaling pathways mediated by khat extracts treatment and not been previously identified.

CONCLUSIONS

We examined the cellular and molecular side effects of khat extracts on the human ovarian adenocarcinoma SKOV3 cell line,

aiming mainly at deciphering the implicated signaling pathways. We showed by several *in vitro* assays that khat extracts affects the cellular integrity of SKOV3, including size, membrane, metabolic activity, proliferation, and survival. At the gene and protein levels, expression of BAX, p53, IL-6, FZD8, and SPRY2 was increased while β-catenin, E-cadherin, and Ki-67 was decreased. Our *in silico* analysis revealed that khat extracts' major constituents namely cathine, cathinone, and cathedulins are potentially associated with Alzheimer's, schizophrenia, depression, anxiety, and ovarian cancer. Signaling pathways of CREB, Wnt, FGF, IL-6, and ERK/MAPK were among other pathways significantly affected. Besides, the upstream regulators including IL-8, MMP2, PLAU, and an array of micro-RNAs were potentially involved in the khat signaling.

DATA AVAILABILITY STATEMENT

The original contributions presented in the study are included in the article/**Supplementary Material**, and further inquiries can be directed to the corresponding author.

AUTHOR CONTRIBUTIONS

MA-E, GK, ASA-E, FA, PP: Project design, supervision, experimental execution, and data analysis. FA, GK: Flow cytometry experiments and data analysis. MA-E, KG: RT-qPCR experiments and analysis. MA-E: Immunostaining experimental work and analysis. PP and MA-E: in silico analysis. MA-E, GK, ASA-E, FA, PP, MA, AR: All data analysis and interpretation, writing up, editing, and revision of the manuscript. All authors approved the final version of the manuscript.

FUNDING

The authors extend their appreciation to the Deputyship for Research and Innovation, Ministry of Education in Saudi Arabia, for funding this research work through the project number (1033).

ACKNOWLEDGMENTS

The authors would like to sincerely thank Andrea Münsterberg, Professor of the Developmental Biology at the School of Biological Sciences, University of East Anglia, Norwich, United Kingdom, for her proofreading of the manuscript and valuable and critical comments. They would also like to thank the technical staff at the Center of Excellence in Genomic Medicine Research, King Abdulaziz University, for their valuable help and support during the work.

SUPPLEMENTARY MATERIAL

The Supplementary Material for this article can be found online at: https://www.frontiersin.org/articles/10.3389/fphar.2021.666885/full#supplementary-material

REFERENCES

Abdelwahab, S. I., Alsanosy, R., Mohamed Elhassan Taha, M., and Mohan, S. (2018). Khat induced toxicity: role on its modulating effects on inflammation and oxidative stability. *Biomed. Res. Int.* 2018, 5896041. doi:10.1155/2018/5896041

Abid, M. D. N., Chen, J., Xiang, M., Zhou, J., Chen, X., and Gong, F. (2013). Khat (catha edulis) generates reactive oxygen species and promotes hepatic cell apoptosis *via* MAPK activation. *Int. J. Mol. Med.* 32, 389–395. doi:10.3892/ijmm.2013.1394

Abou-Elhamd, A. S., Ageely, H., Abu-Elmagd, M., and Zayed, A. E. (2018). Catha edulis forsk mediates embryotoxic effects in rats: an experimental study. *Int. J. Morphol.* 36, 1087–1094. doi:10.4067/s0717-95022018000301087

Abou-Elhamd, A. S., Sumayli, S., Steger, K., Ali, A. K. M., and Zayed, A. E. (2020). Effect of khat (catha edulis forsk) extract on testicular maturation in pre-pubertal and pubertal rats: a morphological and biochemical study. *Anatomia, Histologia, Embryologia.* 50, 271–283. doi:10.1111/ahe.12626

Abu-Elmagd, M., Alghamdi, M. A., Shamy, M., Khoder, M. I., Costa, M., Assidi, M., et al. (2017). Evaluation of the effects of airborne particulate matter on bone marrow-mesenchymal stem cells (BM-MSCs): cellular, molecular and systems biological approaches. *Int. J. Environ. Res. Public Health.* 14. 440. doi:10.3390/ijerph14040440

Ageely, H. M., El-Nagar, M. M., Abouelmagd, A., Abou-Elhamd, A. S., Kelany, M. E., and Pati, B. R. (2014). Khat extract mediated morphological and histochemical alterations in rat liver. *Int. J. Adv. Res.* 2, 971–980.

Ageely, H. M., Agag, A. E., Mohan, S., and Shehata, A. (2016). (khat) Induces apoptosis in Madin-Darby bovine kidney cell line. *Pharmacogn Mag.* 12, S454–S459. doi:10.4103/0973-1296.191456

Al-Habori, M., Al-Aghbari, A., Al-Mamary, M., and Baker, M. (2002). Toxicological evaluation of Catha edulis leaves: a long term feeding experiment in animals. *J. ethnopharmacology* 83, 209–217. doi:10.1016/s0378-8741(02)00223-4

Ali, A. A., Al-Sharabi, A. K., Aguirre, J. M., and Nahas, R. (2004). A study of 342 oral keratotic white lesions induced by qat chewing among 2500 Yemeni. *J. Oral Pathol. Med.* 33, 368–372. doi:10.1111/j.1600-0714.2004.00145.x

Ali, E., Hegazy, H. G., and Mosaad, R. (2015). Interaction between pro-inflammatory cytokines and brain oxidative stress biomarkers of khat, cathinone and pseudoephedrine hydrochloride intoxication in male mice. *Afr. J. Pharm. Pharmacol.* 9, 585–594. doi:10.5897/AJPP2015.4291

Al-Mamary, M., Al-Habori, M., Al-Aghbari, A., and Baker, M. (2002). Investigation into the toxicological effects of Catha edulis leaves: a short term study in animals. *Phytotherapy Research: Int. J. Devoted Pharmacol. Toxicol. Eval. Nat. Product. Derivatives* 16, 127–132. doi:10.1002/ptr.835

Al-Maweri, S. A., Al-Soneidar, W. A., and Alqahtani, K. W. (2020). Evaluation of khat (Catha edulis) use as a risk factor of cancer: a systematic review (Chong et al., 2020). *Asian Pac. J. Cancer Prev.* 21, 2181–2182. doi:10.31557/apjcp.2020.21.8.2181

Al-Motarreb, A., Al-Kebsi, M., Al-Adhi, B., and Broadley, K. (2002a). Khat chewing and acute myocardial infarction. *Heart* 87, 279–280. doi:10.1136/heart.87.3.279

Al-Qirim, T. M., Shahwan, M., Zaidi, K. R., Uddin, Q., and Banu, N. (2002). Effect of khat, its constituents and restraint stress on free radical metabolism of rats. *J. Ethnopharmacology* 83, 245–250. doi:10.1016/s0378-8741(02)00251-9

Alsanosy, R., Alhazmi, H. A., Sultana, S., Abdalla, A. N., Ibrahim, Y., Al Bratty, M., et al. (2020). Phytochemical screening and cytotoxic properties of ethanolic extract of young and mature khat leaves. *J. Chem.* 2020, 7897435. doi:10.1155/2020/7897435

Alshamrani, A. A. (2020). Roles of microRNAs in ovarian cancer tumorigenesis: two decades later, what have we learned? *Front. Oncol.* 10, 1084. doi:10.3389/fonc.2020.01084

Al-Zubairi, A. S., Ismail, P., Pei, C. P., Abdul, A. B., and Ali, R. S. (2008). Short-term repeated dose biochemical effects of catha edulis (khat). *Int. J. Trop. Med.* 3, 19–25.

Arafa, N., Al Sabi, Z., and Faqihi, K. (2019). Effect of khat on ovarian oxidative stress in female rats. *Afr. J. Biol. Sci.* 15, 53–62. doi:10.21608/ajbs.2019.63987

Aziz, N. B., Mahmudunnabi, R. G., Umer, M., Sharma, S., Rashid, M. A., Alhamhoom, Y., et al. (2020). MicroRNAs in ovarian cancer and recent advances in the development of microRNA-based biosensors. *Analyst* 145, 2038–2057. doi:10.1039/c9an02263e

Bahlas, S., Damiati, L. A., Al-Hazmi, A. S., and Pushparaj, P. N. (2020). Decoding the role of sphingosine-1-phosphate in asthma and other respiratory system diseases using next generation knowledge discovery platforms coupled with luminex multiple analyte profiling technology. *Front. Cel. Dev. Biol.* 8, 444. doi:10.3389/fcell.2020.00444

Barkwan, S. S., Barnett, C. R., Barnett, Y. A., Tomkins, P. T., and Fokunang, C. N. (2004). Evaluation of the cytotoxic and genotoxic potential of khat (catha edulis forsk) extracts on human T lymphoblastoid cell line. *J. Med. Sci.* 4, 110–114. doi:10.3923/jms.2004.110.114

Bredholt, T., Dimba, E. A., Hagland, H. R., Wergeland, L., Skavland, J., Fossan, K. O., et al. (2009). Camptothecin and khat (Catha edulis Forsk.) induced distinct cell death phenotypes involving modulation of c-FLIPL, Mcl-1, procaspase-8 and mitochondrial function in acute myeloid leukemia cell lines. *Mol. Cancer* 8, 101. doi:10.1186/1476-4598-8-101

Carvalho-Silva, D., Pierleoni, A., Pignatelli, M., Ong, C., Fumis, L., Karamanis, N., et al. (2018). Open targets platform: new developments and updates two years on. *Nucleic Acids Res.* 47, D1056–D1065. doi:10.1093/nar/gky1133

Cheng, J-C., Chang, H-M., Xiong, S., So, W-K., and Leung, P. C. K. (2016). Sprouty2 inhibits amphiregulin-induced down-regulation of E-cadherin and cell invasion in human ovarian cancer cells. *Oncotarget* 7, 81645–81660. doi:10.18632/oncotarget.13162

Chong, Z. X., Ho, W. Y., Yan, P., and Alshagga, M. A. (2020). Evaluation of khat (Catha edulis) use as a risk factor of cancer: a systematic review. *Asian Pac. J. Cancer Prev.* 21, 881–895. doi:10.31557/apjcp.2020.21.4.881

Daina, A., and Zoete, V. (2019). Application of the SwissDrugDesign online resources in virtual screening. *Int. J. Mol. Sci.* 20. doi:10.3390/ijms20184612

Daina, A., Michielin, O., and Zoete, V. (2019). SwissTargetPrediction: updated data and new features for efficient prediction of protein targets of small molecules. *Nucleic Acids Res.* 47, W357–W364. doi:10.1093/nar/gkz382

Dimba, E., Gjertsen, B. T., Francis, G. W., Johannessen, A. C., and Vintermyr, O. K. (2003). Catha edulis(Khat) induces cell death by apoptosis in leukemia cell lines. *Ann. N. Y Acad. Sci.* 1010, 384–388. doi:10.1196/annals.1299.070

Dimba, E. A. O., Gjertsen, B. T., Bredholt, T., Fossan, K. O., Costea, D. E., Francis, G. W., et al. (2004). Khat (Catha edulis)-induced apoptosis is inhibited by antagonists of caspase-1 and -8 in human leukaemia cells. *Br. J. Cancer* 91, 1726–1734. doi:10.1038/sj.bjc.6602197

Elhag, H., Mossa, J. S., and El-Olemy, M. M. (1999). *Antimicrobial and cytotoxic activity of the extracts of khat callus cultures*. West Lafayette, USA: Center for New Crops & Plant ProductsInd.

El-Menyar, A., Mekkodathil, A., Al-Thani, H., and Al-Motarreb, A. (2015). Khat use: history and heart failure. *Oman Med. J.* 30, 77–82. doi:10.5001/omj.2015.18

El-Setouhy, M., Alsanosy, R. M., Alsharqi, A., and Ismail, A. A. (2016). Khat dependency and psychophysical symptoms among chewers in jazan region, Kingdom of Saudi Arabia. *Biomed. Res. Int.* 2016, 2642506. doi:10.1155/2016/2642506

Ferreira, P., Roela, R. A., Lopez, R. V. M., and Del Pilar Estevez-Diz, M. (2020). The prognostic role of microRNA in epithelial ovarian cancer: a systematic review of literature with an overall survival meta-analysis. *Oncotarget* 11, 1085–1095. doi:10.18632/oncotarget.27246

Gfeller, D., Michielin, O., and Zoete, V. (2013). Shaping the interaction landscape of bioactive molecules. *Bioinformatics* 29, 3073–3079. doi:10.1093/bioinformatics/btt540

Gfeller, D., Grosdidier, A., Wirth, M., Daina, A., Michielin, O., and Zoete, V. (2014). SwissTargetPrediction: a web server for target prediction of bioactive small molecules. *Nucleic Acids Res.* 42, W32–W38. doi:10.1093/nar/gku293

Gunaid, A. A., Sumairi, A. A., Shidrawi, R. G., Al-Hanaki, A., Al-Haimi, M., Al-Absi, S., et al. (1995). Oesophageal and gastric carcinoma in the Republic of Yemen. *Br. J Cancer* 71, 409–410.

Halbach, H. (1972). Medical aspects of the chewing of khat leaves. *Bull. World Health Organ.* 47, 21–29.

Hoffman, R., and Al'Absi, M. (2010). Khat use and neurobehavioral functions: suggestions for future studies. *J. ethnopharmacology* 132, 554–563. doi:10.1016/j.jep.2010.05.033

Huang, H., Zhang, G., Zhou, Y., Lin, C., Chen, S., Lin, Y., et al. (2018). Reverse screening methods to search for the protein targets of chemopreventive compounds. *Front. Chem.* 6, 138. doi:10.3389/fchem.2018.00138

Islam, M. W., Al-Shabanah, O. A., Al-Harbi, M. M., and Al-Gharably, N. M. A. (1994). Evaluation of teratogenic potential of khat (Catha edulis Forsk.) in rats. *Drug Chem. Toxicol.* 17, 51–68. doi:10.3109/01480549409064046

Jafri, M. A., Kalamegam, G., Abbas, M., Al-Kaff, M., Ahmed, F., Bakhashab, S., et al. (2019). Deciphering the association of cytokines, chemokines, and growth factors in chondrogenic differentiation of human bone marrow mesenchymal stem cells using an ex vivo osteochondral culture system. *Front. Cel. Dev. Biol.* 7, 380. doi:10.3389/fcell.2019.00380

Kalix, P., and Braenden, O. (1985). Pharmacological aspects of the chewing of khat leaves. *Pharmacol. Rev.* 37, 149–164.

Kenny, H. A., and Lengyel, E. (2009). MMP-2 functions as an early response protein in ovarian cancer metastasis. *Cell Cycle* 8, 683–688. doi:10.4161/cc.8.5.7703

Khaladkar, M., Koscielny, G., Hasan, S., Agarwal, P., Dunham, I., Rajpal, D., et al. (2017). Uncovering novel repositioning opportunities using the open targets platform. *Drug Discov. Today* 22, 1800–1807. doi:10.1016/j.drudis.2017.09.007

Kim, S., Thiessen, P. A., Bolton, E. E., Chen, J., Fu, G., Gindulyte, A., et al. (2016). PubChem Substance and Compound databases. *Nucleic Acids Res.* 44, D1202–D1213. doi:10.1093/nar/gkv951

Kim, S. (2016). Getting the most out of PubChem for virtual screening. *Expert Opin. Drug Discov.* 11, 843–855. doi:10.1080/17460441.2016.1216967

Kimani, S. T., Patel, N. B., and Kioy, P. G. (2008). Effect of single and daily khat (Catha edulis) extract on locomotor behaviour in CBA mice. *Scientific Res. Essay* 3, 187–196. doi:10.1016/j.bbr.2008.05.022

Kiros, T. (2020). Non-alkaloidal compounds from khat (Catha edulis) leaves. *Biology, Medicine, Nat. Product. Chem.* 9, 81–89. doi:10.14421/biomedich.2020.92.81-89

Kite, G. C., Ismail, M., Simmonds, M. S. J., and Houghton, P. J. (2003). Use of doubly protonated molecules in the analysis of cathedulins in crude extracts of khat (Catha edulis) by liquid chromatography/serial mass spectrometry. *Rapid Commun. Mass. Spectrom.* 17, 1553–1564. doi:10.1002/rcm.1085

Koscielny, G., An, P., Carvalho-Silva, D., Cham, J. A., Fumis, L., Gasparyan, R., et al. (2017). Open Targets: a platform for therapeutic target identification and validation. *Nucleic Acids Res.* 45, D985–D994. doi:10.1093/nar/gkw1055

Kuczkowski, K. (2005). Herbal ecstasy: cardiovascular complications of khat chewing in pregnancy. *Acta Anaesthesiol Belg.* 56, 19–21.

Liao, Y., Wang, J., Jaehnig, E. J., Shi, Z., and Zhang, B. (2019). WebGestalt 2019: gene set analysis toolkit with revamped UIs and APIs. *Nucleic Acids Res.* 47, W199–w205. doi:10.1093/nar/gkz401

Lu, Y., Li, Y., Xiang, M., Zhou, J., and Chen, J. (2017). Khat promotes human breast cancer MDA-MB-231 cell apoptosis *via* mitochondria and MAPK-associated pathways. *Oncol. Lett.* 14, 3947–3952. doi:10.3892/ol.2017.6708

Lukandu, O. M., Costea, D. E., Dimba, E. A., Neppelberg, E., Bredholt, T., Gjertsen, B. T., et al. (2008). Khat induces G1-phase arrest and increased expression of stress-sensitive p53 and p16 proteins in normal human oral keratinocytes and fibroblasts. *Eur. J. Oral Sci.* 116, 23–30. doi:10.1111/j.1600-0722.2007.00508.x

Ma, B., and Hottiger, M. O. (2016). Crosstalk between Wnt/β-Catenin and NF-κB signaling pathway during inflammation. *Front. Immunol.* 7, 378. doi:10.3389/fimmu.2016.00378

Mohan, S., Abdelwahab, S., Hobani, Y., Syam, S., Al-Zubairi, A., Al-Sanousi, R., et al. (2016). *Catha edulis* extract induces H9c2 cell apoptosis by increasing reactive oxygen species generation and activation of mitochondrial proteins. *Phcog Mag.* 12, 321–326. doi:10.4103/0973-1296.185732

Mohan, S., Shaheen, E., El-Amir, Y., Khadashi, H., Ncibi, S., Farasani, A., et al. (2019). Catha edulis-induced skeletal muscle toxicity in experimental rats *via* regulation of rhabdomyolysis biomarkers. *Phcog Mag.* 15, 359. doi:10.4103/pm.pm_142_19

Ochoa, D., Hercules, A., Carmona, M., Suveges, D., Gonzalez-Uriarte, A., Malangone, C., et al. (2021). Open targets platform: supporting systematic drug-target identification and prioritisation. *Nucleic Acids Res.* 49, D1302–D1310. doi:10.1093/nar/gkaa1027

Odenwald, M., Neuner, F., Schauer, M., Elbert, T., Catani, C., Lingenfelder, B., et al. (2005). Khat use as risk factor for psychotic disorders: a cross-sectional and case-control study in Somalia. *BMC Med.* 3, 5. doi:10.1186/1741-7015-3-5

Ogiwara, K., Hagiwara, A., Rajapakse, S., and Takahashi, T. (2015). The role of urokinase plasminogen activator and plasminogen activator inhibitor-1 in follicle rupture during ovulation in the teleost medaka. *Biol. Reprod.* 92, 10. doi:10.1095/biolreprod.114.121442

Pennings, E. J. M., Opperhuizen, A., and Van Amsterdam, J. G. C. (2008). Risk assessment of khat use in the Netherlands: a review based on adverse health effects, prevalence, criminal involvement and public order. *Regul. Toxicol. Pharmacol.* 52, 199–207. doi:10.1016/j.yrtph.2008.08.005

Soufi, H. E., Kameswaran, M., and Malatani, T. (1991). Khat and oral cancer. *J. Laryngol. Otol.* 105, 643–645. doi:10.1017/s0022215100116913

Spanjer, A. I. R., Menzen, M. H., Dijkstra, A. E., Van Den Berge, M., Boezen, H. M., Nickle, D. C., et al. (2016). A pro-inflammatory role for the Frizzled-8 receptor in chronic bronchitis. *Thorax* 71, 312–322. doi:10.1136/thoraxjnl-2015-206958

Taha, M., Abdelwahab, S. I., and Al-Sanousi, R. (2014). *In vitro* hepatotoxcity of Catha edulis Forsk. (khat) phenolic-rich extract on human hepatocytes. *J. Appl. Pharm. Sci.* 4, 42–46. doi:10.7324/JAPS.2014.4118

Wabe, N. T. (2011). Chemistry, pharmacology, and toxicology of khat (catha edulis forsk): a review. *Addict. Health* 3, 137–149.

Wang, Y., Xu, R. C., Zhang, X. L., Niu, X. L., Qu, Y., Li, L. Z., et al. (2012). Interleukin-8 secretion by ovarian cancer cells increases anchorage-independent growth, proliferation, angiogenic potential, adhesion and invasion. *Cytokine* 59, 145–155. doi:10.1016/j.cyto.2012.04.013

Conflict of Interest: The authors declare that the research was conducted in the absence of any commercial or financial relationships that could be construed as a potential conflict of interest.

frontiers in Pharmacology

REVIEW
published: 02 June 2021
doi: 10.3389/fphar.2021.688490

Neuroprotective Potentials of Panax Ginseng Against Alzheimer's Disease: A Review of Preclinical and Clinical Evidences

Jing Li[1†], Qingxia Huang[1,2†], Jinjin Chen[1], Hongyu Qi[1], Jiaqi Liu[1], Zhaoqiang Chen[1], Daqing Zhao[1], Zeyu Wang[3] and Xiangyan Li[1]**

[1]Jilin Ginseng Academy, Key Laboratory of Active Substances and Biological Mechanisms of Ginseng Efficacy, Ministry of Education, Jilin Provincial Key Laboratory of Bio-Macromolecules of Chinese Medicine, Changchun University of Chinese Medicine, Changchun, China, [2]Research Center of Traditional Chinese Medicine, College of Traditional Chinese Medicine, Changchun University of Chinese Medicine, Changchun, China, [3]Department of Scientific Research, Changchun University of Chinese Medicine, Changchun, China

OPEN ACCESS

Edited by:
Muhammad Ayaz,
University of Malakand, Pakistan

Reviewed by:
Amjad Khan,
Gyeongsang National University, South Korea
Cláudia Pereira,
University of Coimbra, Portugal

***Correspondence:**
Zeyu Wang
zeyu781022@163.com
Xiangyan Li
xiangyanli1981@163.com

†These authors have contributed equally to this work

Specialty section:
This article was submitted to Ethnopharmacology, a section of the journal Frontiers in Pharmacology

Received: 30 March 2021
Accepted: 10 May 2021
Published: 02 June 2021

Citation:
Li J, Huang Q, Chen J, Qi H, Liu J, Chen Z, Zhao D, Wang Z and Li X (2021) Neuroprotective Potentials of Panax Ginseng Against Alzheimer's Disease: A Review of Preclinical and Clinical Evidences. Front. Pharmacol. 12:688490. doi: 10.3389/fphar.2021.688490

Alzheimer's disease (AD), a neurodegenerative disorder, is a major health concern in the increasingly aged population worldwide. Currently, no clinically effective drug can halt the progression of AD. *Panax ginseng* C.A. Mey. is a well-known medicinal plant that contains ginsenosides, gintonin, and other components and has neuroprotective effects against a series of pathological cascades in AD, including beta-amyloid formation, neuroinflammation, oxidative stress, and mitochondrial dysfunction. In this review, we summarize the effects and mechanisms of these major components and formulas containing *P. ginseng* in neuronal cells and animal models. Moreover, clinical findings regarding the prevention and treatment of AD with *P. ginseng* or its formulas are discussed. This review can provide new insights into the possible use of ginseng in the prevention and treatment of AD.

Keywords: Alzeheimer's disease, ginseng (*Panax ginseng* C.A. Meyer), ginsenosidase, gintonin, neuroprotection

INTRODUCTION

Alzheimer's disease (AD) is a neurodegenerative disorder and is one of the most common causes of dementia in the elderly population (Jia et al., 2020). The global costs in 2030 due to dementia could be much higher than the predictions made by the World Alzheimer Report 2015, reaching $2.54 trillion (Jia et al., 2018). According to the Alzheimer's Association, the incidence and prevalence, mortality and morbidity, use and costs of care, and the overall impact on the caregivers and society of AD are increasingly major concerns (Alzheimer's Association, 2020). The prevention and treatment of AD has become a global problem due to the increasingly aged population worldwide (Alzheimer's Association, 2020; Ikram et al., 2020). AD clinically manifests as apathy, anxiety, cognitive and functional decline, and the emergence of neuropsychiatric symptoms (Johansson et al., 2020; Cummings, 2021).

AD pathogenesis is defined by the extracellular deposition of beta-amyloid (Aβ) and tau hyperphosphorylation (Vaz and Silvestre, 2020). Aβ plaque formation is thought to be the main cause of AD symptoms, including memory deficit, due to its neurotoxic effect (Yankner et al., 1989; Sonawane et al., 2021). Aβ is derived from Aβ protein precursors (AβPPs) through the amyloidogenic pathway (Hwang et al., 2012; Kwon et al., 2019). Aβ accumulation accelerates tau

phosphorylation (p-tau) during AD development (Gomes et al., 2019), whereas normal tau phosphorylation is essential for neuronal plasticity and axonal outgrowth (Arendt and Bullmann, 2013). Hyperphosphorylated tau protein is released from microtubules and self-assembles into neurotoxic insoluble aggregates such as intracellular neurofibrillary tangles (NFTs) (JeffKuret, 2008). The toxic effects of senile plaques composed of Aβ peptides and NFTs on the brain cholinergic system, mitochondria, and axonal transport result in oxidative stress, intracellular Ca^{2+} overload, apoptosis, and glutamate dysregulation (Bader Lange et al., 2008; Aalinkeel et al., 2018). In addition, the senile plaques produce more Aβ peptides through microglial activation and release of pro-inflammatory cytokines. The treatments for AD approved by the Food and Drug Administration are mainly based on reducing acetylcholine (ACh) levels and glutamate excitotoxicity and inhibiting Aβ protein deposition in the brain; approved drugs include donepezil, rivastigmine hydrogen tartrate, galanthamine, and huperzine-A (Li et al., 2019; Kareti and P, 2020; Pardridge, 2020). Although these drugs can result in symptomatic improvement, they cannot reverse AD progression and cause various adverse effects after long-term use.

Panax ginseng C.A. Mey. (ginseng) is a well-known and valuable medicinal herb that has been widely used in China and other East Asian countries as traditional Chinese medicine and health food (Shi et al., 2019). Recent studies demonstrated that ginseng extracts, active components (ginsenosides and gintonin), and ginseng formulas can improve the symptoms of AD patients and inhibit the progression of AD by reducing the deposition of Aβ and tau protein hyperphosphorylation. These effects may be mediated by mitochondrial function, neuron conduction, apoptosis, calcium ions, and reactive oxygen species (ROS) (Rajabian et al., 2019; Guo et al., 2021). Ginsenosides, which are mainly classified into protopanaxadiol (PPD) and protopanaxatriol (PPT), according to their sapogenin, can result in significant improvement in AD symptoms (Im and Nah, 2013; Kim et al., 2018; Piao et al., 2020). Previous studies have confirmed that β-site APP cleaving enzyme 1 (BACE1, β-secretase) inhibitors can inhibit the formation of Aβ (Karpagam et al., 2013), and acetylcholinesterase (AChE) inhibition can improve cognitive and memory function (Park et al., 2017). Molecular dynamics analysis combined with enzyme activity experiments showed that ginsenosides CK, F1, Rh1, and Rh2 are potential BACE1 inhibitors, inhibiting the formation of Aβ (Karpagam et al., 2013). In addition, ginsenosides F1, Rd, Rk3, 20(S)-Rg3, F2, and Rb2 possess strong AChE inhibitory activities, which can improve cognitive and memory function (Nah, 2012; Yang et al., 2019a). Gintonin, a component of ginseng, is a bioactive glycolipoprotein that forms nonsaponin multimers (Pyo et al., 2011; Nah, 2012; Jakaria et al., 2020; Choi et al., 2021). Recent studies have shown that gintonin can affect the activation of the phosphatidic acid receptor, which is involved in hemolysis, reducing the formation of Aβ and improving learning and memory abilities (Lee et al., 2018a; Kim et al., 2018). In addition, gintonin can also reduce the symptoms and progress of AD through neurogenesis, autophagy stimulation, anti-apoptosis effects, anti-oxidative stress, and anti-inflammatory activities (Choi et al., 2021).

We first introduce the effects and mechanisms of ginsenosides, gintonin, and ginseng formulas in the prevention and treatment of AD based on the extensive *in vitro* and *in vivo* studies. Then, we summarize the clinical findings regarding the prevention and treatment of AD with ginseng or its formulas. This review can provide new insights into the possible use of ginseng in AD treatment.

EFFECTS AND MECHANISMS OF GINSENG IN PREVENTING AND TREATING AD

Ginsenosides

It has been reported that many ginsenosides can target the following pathological processes of AD: (1) inhibiting Aβ aggregation and tau hyperphosphorylation, (2) protecting against neuroinflammation and apoptosis, (3) increasing the secretion of neurotrophic factors, and (4) improving mitochondrial dysfunction.

Aβ Aggregation and Tau Hyperphosphorylation

In $Aβ_{1–40}$-induced AD rats, ginsenoside Rb1 can improve learning and memory by altering the amyloidogenic process of APP into a nonamyloidogenic process (Lin et al., 2019). Ginsenoside Rb1, an agonist of peroxisome proliferator–activated receptor-γ (PPARγ), could lower cholesterol levels and reduce the cytotoxicity induced by $Aβ_{25–35}$ by decreasing lipid peroxidation and protecting the rigidity of the cytoskeleton and the membrane surface in PC12 cells (Changhong et al., 2021). Ginsenoside Rd increases soluble APP-α (sAPPα) levels and reduces extracellular Aβ levels, enhancing cognitive and memory functions of ovariectomized rats (Yan et al., 2017). Ginsenoside Re inhibits the activity of BACE1 by increasing PPARγ expression at the mRNA and protein levels in N2a/APP695 cells and thereby reduces the generation of $Aβ_{1–40}$ and $Aβ_{1–42}$ (Cao et al., 2016). Another research showed that ginsenoside Rg1 can downregulate cyclin-dependent kinase 5 (CDK5) expression to inhibit the phosphorylation of PPARγ and the activity of its targets, BACE and insulin-degrading enzyme (IDE), reducing Aβ levels, and exerting neuroprotective effects against AD (Quan et al., 2020). In SweAPP-SK cells with mutant APP, Rg3 treatment significantly enhances neprilysin (NEP) gene expression, reducing the levels of $Aβ_{40}$ and $Aβ_{42}$ (Yang et al., 2009).

With respect to tau hyperphosphorylation, Rd pretreatment can maintain the functional balance between glycogen synthase kinase 3β (GSK-3β) and protein phosphatase 2A (PP-2A), inhibiting tau phosphorylation (Li et al., 2013). Moreover, Rd inhibits the hyperphosphorylation of tau protein at Ser199/202, Ser396, or Ser404, induced by okadaic acid microinfusion in rats and cortical neurons, increasing the PP-2A activity and protecting against AD (Li et al., 2011). Collectively, these results suggest that ginsenosides Rb1, Rd, Re, and Rg1 can inhibit Aβ aggregation to regulate the phosphorylation of tau protein in the prevention and treatment of AD.

TABLE 1 | Summary of effects and mechanisms of ginsenosides in neuronal cells and animal models.

Ref	Ginsenosides	Model	Inducer	Experimental model	Mechanism	Effects
Zhao et al. (2014)	Rg1	AD	$A\beta_{25-35}$	NG108-15 neuroglial cells	TLR3, TLR4, NF-κB, TRAF-6, TNF-α, IFN-β, iNOS↓	Neuroinflammation
Li et al. (2019)	Rg1	AD		3 × Tg-AD mice	Arachidonic acid, 11b-PGF2a, cytc p450, enzyme prostaglandin-F synthase, tryptophan, lysine↓	Oxidative stress, inflammation reaction
Yang et al. (2020)	Rg1	AD		SAMP8 mice	Activated microglia cells, activated astrocytes, iNOS, Aβ↓	Oxidative stress, neuroinflammation
Xu et al. (2019)	Rg1	Neuronal damage	H_2O_2	Hippocampal neurons cells	β-Galactosidase, ROS, caspase-3, NOX2, p22phox, NLRP1, ASC, caspase-1, IL-1β, IL-18↓	Oxidative stress, apoptosis, neuroinflammation
Quan et al. (2020)	Rg1	AD	$A\beta_{1-42}$	Rat hippocampal neurons cells	p-PPARγ, CDK5, BACE1, APP, Aβ1-42↓ IDE↑	Apoptosis, Aβ degradation and reduction
Nie et al. (2017)	Rg1	AD		3 × Tg-AD mice	SYN2, CPLX2, SNP25, PSD-95↑	Modulating the expression of the proteins of memory and depression
Cui et al. (2020)	Rg2	AD	$A\beta_{25-35}$	Male SD rats	Caspase-3, Bax↓ Bcl-2, p-Akt↑	Apoptosis
Cui et al. (2017)	Rg2		$A\beta_{25-35}$	PC12 cells	LDH, $[Ca^{2+}]i$, ROS, caspase-3, Bax↓ p-Akt, Bcl-2↑	Mitochondrial dysfunction, apoptosis
Li et al. (2007)	Rg2		Glutamate	PC12 cells	$[Ca^{2+}]i$, MDA, NO, calpain II, caspase-3↓	Anti-oxidation, anti-apoptosis
Joo et al. (2008)	Rg3	AD	$A\beta_{42}$	BV-2 microglial cells	TNFα, IL-1β, iNOS↓	Neurotoxicity, microglial activation, inflammation
Lee et al. (2013)	Rg3	AD/learning and memory impairments	D-Galactose/ LPS	Adult male SD rats	Caspase-3, caspase-9, Bax, AIF, cyto C, Bcl-2, TNF-α, IL-1β, COX-2↓	Mitochondrial dysfunction, energy metabolism, ETC, amino acid metabolism, purine metabolism, anti-apoptosis, neuroinflammation
Aalinkeel et al. (2018)	PLGA-Rg3 NPs	AD	$A\beta_{1-42}$	C6/THP-1 cells	Cyto C, ROS, TNF-α, IL-1β↓	Aβ plaques, AβPP-A4, oxidative stress, mitochondrial dysfunction, neuroinflammation
Lin et al. (2019)	Rb1	AD	$A\beta_{1-40}$	Male Wistar rats	IL-1β, Aβ, GFAP↓	Aβ plaques, neuroinflammation
Wang et al. (2018)	Rb1	AD	$A\beta_{1-40}$	Male SD rats	Bax, caspase-3↓ Bcl-2↑	Apoptosis
Changhong et al. (2021)	Rb1	AD	$A\beta_{25-35}$	PC12 cells	Cholesterol, ROS, lipid peroxidation↓ PPARγ↑	Apoptosis, PPARγ activation, cholesterol reduction
Zhao et al. (2018)	Rb1	AD	$A\beta_{1-40}$	Male SD rats	Nestin, GFAP, NSE, NSCs, NPCs↑	Promote the proliferation and differentiation of endogenous NSCs
Yang et al. (2020)	Rg3 + Rb1	AD		SAMP8 mice	TNF-α, activated microglia cells, activated astrocytes, ASC, caspase-1, iNOS, Aβ↓	Oxidative stress, neuroinflammation
Han et al. (2019)	F1	AD		Old APP/PS1 mice	Aβ plaque↓ pCREB, BDNF↑	Amyloid protein (Aβ) accumulation
Du et al. (2018)	Rf	AD	$A\beta_{42}$	N2A cells	ROS, Ca^{2+}, IFN-γ↓ Mmp, IL-13↑	Apoptosis, neuroinflammation, oxidative stress
Yang et al. (2019b)	CK	Memory impaired	Scopolamine hydrobromide	ICR mice	SOD, GSH-PX, Bcl-2, IDE, Nrf2, HO-1↑ MDA, Bax, caspase-3, APP, BACE1, PS1, Aβ, Keap1↓	Aβ plaques, neurotoxicity, oxidative stress, apoptosis
Chen et al. (2019)	CK	AD	$A\beta_{1-42}$	HT22 cells	IRS2, IDE, GLUT1, GLUT3↑ GSK3β, tau↓	Aβ intake and accumulation, energy metabolism disorder
Park et al. (2012)	CK	Inflammation	LPS	Male C57BL/6 mice/ BV2 microglial cells/ primary cultured microglia	Number of activated microglia, NO, TNF-α, IL-1β, iNOS, IL-6, MCP-1, MMP-3, MMP-9, ROS, NADPH, MAPKS↓ CREB↑	Microglial activation, NF-κB/ap-1 activities suppresses inflammatory molecules

(Continued on following page)

TABLE 1 | (*Continued*) Summary of effects and mechanisms of ginsenosides in neuronal cells and animal models.

Ref	Ginsenosides	Model	Inducer	Experimental model	Mechanism	Effects
Liu et al. (2019)	Re	AD	$A\beta_{25-35}$	SH-SY5Y cells	Caspase-3/7, caspase-9, cyt C, ASK-1, JNK, Bax, ROS↓ Caspase-8, caspase-12→ MMP, ATP, Bcl-2/Bax, GSH, SOD, Gpx↑	Mitochondrial apoptosis, oxidative damage, oxidative stress
Cao et al. (2016)	Re	AD		N2A/APP695 cells	sAPPβ, C99, BACE1↓ PPARγ protein and mRNA↑	Aβ production
Li et al. (2018)	Re	AD	$A\beta_{25-35}$	Male kunming mice	Tryptophan↓ LPC, hexadecasphinganine, phytosphingosine, phenylalanine↑	Metabolomics
Liu et al. (2012)	Rd	AD	$A\beta_{1-40}$	Male SD rats	IL-1β, IL-6, TNF-α, S100β mRNA, PC, HNE, caspase-3↓ IL-10, HSP70 mRNA↑	Inflammation, oxidative stress, apoptosis
Liu et al. (2015a)	Rd	AD		APP transgenic mice	IL-1β, IL-6, TNF-α, S100β mRNA, NF-κB p65↓ IL-10↑	Inflammation, NF-κB
Li et al. (2013)	Rd	AD		APP transgenic mice	GSK-3β, Tyr216↓ Ser9, PP-2A↑	p-tau
Liu et al. (2015b)	Rd	AD	$A\beta_{25-35}$	Primary cultured hippocampal neurons cells	ROS, Bax mRNA, caspase-3, cyto C mRNA↓ SOD, GSH-Px, Bcl-2 mRNA↑	Oxidative stress, neuronal apoptosis
Li et al. (2011)	Rd	AD	Okadaic acid	Adult male SD rats/ Cortical neurons cells	Tau↓ P-2A↑	Tau
Yan et al. (2017)	Rd	AD	Ovariectomy/ Inhibitor	Adult female rats/ HT22 hippocampal neuronal cells	BACE1, Aβ↓ sAPPα, ADAM↑	Activating estrogen-like activity
Kim et al. (2014)	Re + rd			Neuro2a cells	ChAT, VAChT, ach, MAP-2, p75, p21, TrkA↑	Cholinergic markers

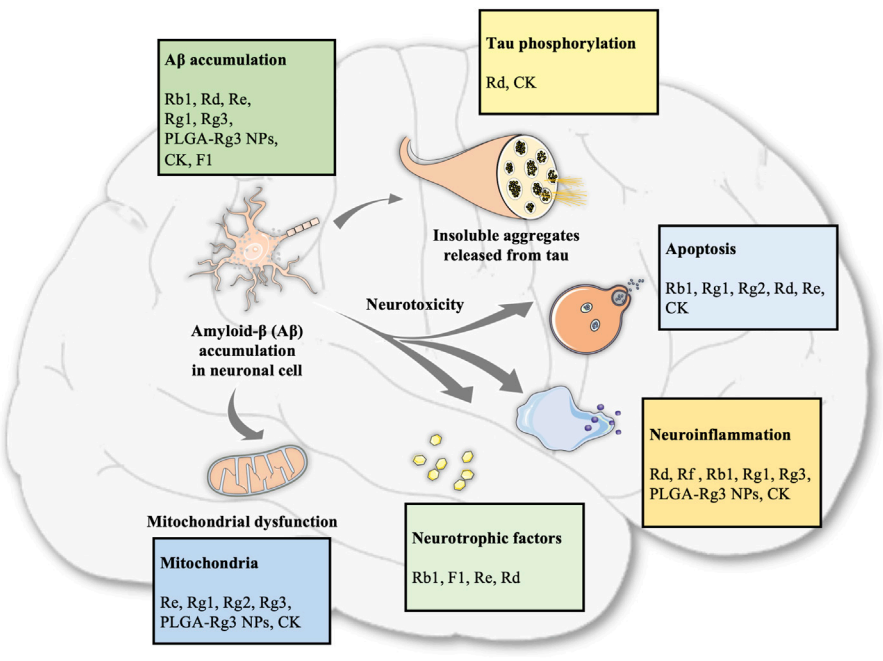

FIGURE 1 | Summary of different ginsenoside monomers involved in various pathological processes of AD.

Neuroinflammation

Neuroinflammation is a continuous process that is implicated in the preclinical, moderate, and late stages of AD (Sung et al., 2020). In APP transgenic mice, Rd pretreatment at 10 mg/kg significantly suppresses the NF-κB pathway activity, reducing the generation of pro-inflammatory cytokines, such as interleukin-1 beta (IL-1β), IL-6, tumor necrosis factor-α (TNF-α), and S100 calcium-binding protein B (S100β), which can improve learning and memory abilities (Liu et al., 2015a). Meanwhile, Rd exerts obvious anti-inflammatory, anti-oxidative, and anti-apoptotic effects by reducing caspase-3 expression and apoptosis of normal cells in $A\beta_{1-40}$-induced AD model rats (Liu et al., 2012). Ginsenoside Rf significantly alleviates Aβ-induced neuronal death in N2A cells and memory deficits in Aβ-treated mice by alleviating inflammation and enhancing Aβ degradation, which suggests that Rf decreases Aβ-induced neurotoxicity during AD development (Du et al., 2018). Ginsenoside Rg1 can reduce the NADPH oxidase 2 (NOX2)–mediated ROS production and neuronal apoptosis, which in turn inhibits the nucleotide-binding domain and leucine-rich repeat pyrin domain–containing protein 1 (NLRP1) inflammasome in H_2O_2-induced hippocampal neurons (Xu et al., 2019). Moreover, the combination of Rb1 with Rg1 can reduce brain Aβ production by regulating multiple processes, including NLRP3 inflammasome, TNF-α levels, oxidative stress, and astrocyte and microglia activation (Yang et al., 2020). Rb1 has a stronger effect on reducing the levels of apoptosis-related proteins in the hippocampus, and Rg1 has a stronger effect in decreasing iNOS levels and activating glial cells (Yang et al., 2020). In addition, ginsenoside Rg1 suppresses the TLR3/4 signaling pathway to decrease inflammatory factors in $A\beta_{25-35}$-induced NG108-15 cells (Zhao et al., 2014). In lipopolysaccharide (LPS)-induced rats, Rg3 administration significantly alleviates cognitive impairment by inhibiting the expression of pro-inflammatory mediators (TNF-α, IL-1β, and cyclooxygenase 2 [COX-2]) in the brain (Lee et al., 2013). In $A\beta_{42}$-treated BV-2 cells, the binding of NF-κB p65 to its DNA consensus sequences and TNF-α expression in activated microglia are effectively reduced by Rg3 treatment (Joo et al., 2008). Compound K (CK), a metabolite biotransformed from ginsenosides Rb1, Rb2, and Rc (Oh and Kim, 2016), can suppress various inflammatory molecules in LPS-stimulated BV2 cells and primary microglia by regulating the mitogen-activated protein kinase (MAPKs), NF-κB/AP-1, and HO-1/ARE signaling pathways (Park et al., 2012). These *in vitro* and *in vivo* findings indicate that major ginsenosides can alleviate inflammation in hippocampal neurons and microglia by mainly regulating the NF-κB pathway and NLRP3 inflammasome.

Neurotrophic Factors

Neurotrophic factors are endogenous proteins that maintain survival and differentiated functions of neurons, including the brain-derived neurotrophic factor (BDNF) and tropomyosin-related kinases (Trks) A, B, and C (Schindowski et al., 2008). A study showed that Rb1 can promote endogenous neural stem cell proliferation and differentiation by increasing the protein levels of Nestin, glial fibrillary acidic protein (GFAP), and nucleotide sugar epimerase (NSE), thereby improving cognitive function of AD rats (Zhao et al., 2018). Ginsenoside F1 can decrease phosphorylated cAMP-response element binding protein (CREB) and increase cortical BDNF levels in the hippocampus, reducing Aβ plaques and improving memory function of APP/PS1 double-transgenic AD mice (Han et al., 2019). With respect to other neurotrophic factors, the gene and protein expression levels of the nerve growth factor receptor p75 and TrkA in Neuro2a cells are increased by ginsenoside Re and Rd, which suggest that the NGF-TrkA signaling pathway mediates the ginsenoside-induced neuroprotective effects against AD progression (Kim et al., 2014).

Apoptosis

The balance between of pro-apoptotic and anti-apoptotic factors in brain tissue plays important roles in improving cognitive and memory functions in AD. Rb1 administration significantly reduces the levels of Bax and cleaved caspase-3 and enhances Bcl-2 levels in the hippocampus to prevent cognitive deficit of $A\beta_{1-40}$-induced rats (Wang et al., 2018; Lin et al., 2019). In $A\beta_{25-35}$-induced PC12 cells and hippocampal CA1 neurons, Rg2 improves cell survival and inhibits apoptosis by promoting the Bcl-2/Bax ratio and attenuating the cleavage of caspase-3, which is mediated by the enhancement of PI3K/Akt signaling (Cui et al., 2017; Cui et al., 2020). Meanwhile, $A\beta_{25-35}$-induced oxidative stress and neuronal apoptosis are, obviously, ameliorated by Rd by keeping the oxidation–anti-oxidation balance and regulating apoptotic proteins, such as Bax, Bcl-2, and cytochrome c (Cyto C) (Liu et al., 2015b). In Aβ-induced SH-SY5Y cells, Re can elevate the ratio of Bcl-2/Bax and reduce the release of Cyto C to maintain mitochondrial function by regulating the apoptosis signal–regulating kinase 1 (ASK1)/JNK/Bax and Nrf2/HO-1 pathways (Liu et al., 2019). Ginsenoside Rg2 significantly attenuates glutamate-induced neurotoxic effects through mechanisms related to anti-oxidative (malondialdehyde [MDA] and nitrogen oxide [NO]) and anti-apoptotic (caspase-3) mechanisms (Li et al., 2007). In a scopolamine-exposed AD mouse model, CK was found to enhance Nrf2/Keap1 signaling, increasing the anti-oxidative activity and reducing neuronal apoptosis, which can regulate the balance between Aβ production and clearance and improve memory function (Yang et al., 2019b). Taken together, ginsenosides Rb1, Rg2, Re, and Rd can regulate apoptosis-related proteins, including Bcl-2, Bax, and Cyto C, reducing Aβ-induced or tau protein–induced neurotoxicity during AD development.

Mitochondrial Dysfunction

Mitochondrial dysfunction, including mtDNA lesions and reduced electron transport chain (ETC) enzyme function, is found in the brains of AD subjects, highlighting potential treatment strategies for AD (Perez Ortiz and Swerdlow, 2019). Metabolomic analysis showed that Re treatment can restore metabolic profiling including lecithin, amino acids, and sphingolipids, to exert protective effects in AD mice (Li et al., 2018). Rg1 can improve memory impairment and depression-like behavior in 3 × Tg-AD mice by upregulating the expression of the depression and memory-related proteins complexin-2 (CPLX2),

TABLE 2 | Summary of effects and mechanisms of extracts or fractions from ginseng in neuronal cells and animal models.

Ref	Extract/fraction	Model	Inducer	Experimental model	Mechanisms	Effects
Lee et al. (2017)	Red ginseng oil	AD	$A\beta_{25-35}$	PC12 cells	Ca^{2+}, Bax, caspase-3, caspase-9, PARP-1, JNK, p38 NF-κB, iNOS, COX-2, PGE2, NO, TNF-α↓ MMP, Bcl-2↑	Mitochondrial dysfunction, apoptosis, neuroinflammation
Lee et al. (2018b)	Red ginseng oil	AD	$A\beta_{25-35}$	PC12 cells	iNOS, p-NF-κB, COX-2, p-IκB, p38, p-ERK, p-JNK, Ca^{2+}, Bax, caspase-8, caspase-9, caspase-3, RARP-1, TNF-α, IL-1β, NO, PGE2, iNOS, COX-2, p-p65↓ MMP, Bcl-2↑	Oxidative stress, apoptotic responses, pro-inflammatory mediators
Shin et al. (2021)	Nonsaponin fraction with rich polysaccharide (NFP) from red ginseng	AD	$A\beta_{1-42}$	14 months old SD rats/5 × FAD mice/HT22 cells	Iba-1(+) area↓ NeuN-positive cells, mitochondrial numbers, mitochondrial dynamics, OCR, ATP, mitochondrial respiration↑ Defective brain mitochondrial dynamics, number of DCX (+) neurons, dendritic morphology	Aβ deposition, neuroinflammation, neurodegeneration, mitochondrial dysfunction, impaired adult neurogenesis, cognitive dysfunction
Shin et al. (2019)	KRG extracts	AD	$A\beta_{1-42}$	5 × FAD mice/HT22 cells	4G8 (+) arealba-1 (+), GFAP (+), Ki-67 (+),DCX (+)↓ Nonmitochondrial respiration↓ OCR, basal respiration, ATP-linked respiration Maximal respiration capacity↑	Aβ accumulation, neuroinflammation, impaired adult neurogenesis, neuronal death, cognitive dysfunction, mitochondrial dysfunction

synapsin-2 (SYN2), and synaptosomal-associated protein 25 (SNP25) (Nie et al., 2017). In AD rats, Rg3 can prevent cognitive impairment by directly or indirectly improving mitochondrial dysfunction, ETC function, and amino acid/purine metabolism (Zhang et al., 2019). In Aβ-induced HT22 cells, CK treatment can regulate abnormal expression of proteins related to energy metabolism, promoting Aβ degradation and inhibiting tau expression (Chen et al., 2019).

Overall, the neuroprotective effects of ginsenosides against AD are mediated by the regulation of Aβ accumulation, inflammation, apoptosis, neurotrophic factors, and mitochondrial function, as shown in **Table 1** and **Figure 1**.

Gintonin

The role of gintonin in the prevention and treatment of AD has been evaluated for many years. Gintonin exerts anti-AD effects by affecting Aβ plaque deposition, sAβPPα release, the cholinergic system, neurotrophic factors, autophagy and apoptosis, and G protein–coupled lysophosphatidic acid (LPA) receptors. Gintonin administration attenuates Aβ plaque deposition and stimulates sAβPPα release, improving memory impairment in mice with AD, suggesting that gintonin results in the formation of the beneficial sAβPPα rather than neurotoxic Aβ (Hwang et al., 2012). With respect to the cholinergic system, gintonin can increase choline acetyltransferase expression, causing the release of ACh and attenuating Aβ-induced cholinergic impairments in a transgenic AD mouse model (Kim et al., 2015a). The release and expression of the vascular endothelial growth factor (VEGF) in cortical astrocytes are stimulated by gintonin, which may be mediated by the LPA1/3 receptor or other receptors, exerting neuroprotective effects against hypoxia insults (Kim et al., 2016; Choi et al., 2019). Moreover, gintonin can induce autophagic flux in astrocytes *via* activation of the AMPK-mTOR signaling pathway and efficiently suppress the production of NO by regulating MAPK and NF-κB pathways (Saba et al., 2015; Rahman et al., 2020). Importantly, gintonin, an LPA receptor ligand, can interact with LPA receptors, which are abundantly expressed in astrocytes to induce transient increases in intracellular Ca^{2+} concentrations ($[Ca^{2+}]i$), affecting neurotransmitter release and synaptic transmission and subsequently enhancing cognition. However, ginsenosides or other active components in ginseng have no effect on $[Ca^{2+}]i$, which may be related to the chemical characteristics of gintonin and its action on G protein-coupled receptors (Im and Nah, 2013; Kim et al., 2015b; Choi et al., 2015).

Other Extracts or Fractions of Ginseng

Apart from ginsenosides and gintonin, extracts or fractions from ginseng have also been widely investigated to explore their molecular mechanisms against AD in a series of cell and animal models. Ginseng extracts result in a reduction of Aβ amount, which may be related to multiple targets, including the balance between mitochondrial fusion and fission, basal respiration, and neuroinflammation attenuation in the AD brain (Chen et al., 2006; Shin et al., 2019). The Korean red ginseng extract, which may regulate alternative pathways such as mitochondrial dysfunction and Aβ degradation/clearance, inhibits tau aggregation but has no direct effect on $A\beta_{1-42}$ accumulation (Shin et al., 2020). The oil from red ginseng, containing linoleic acid, β-sitosterol, and stigmasterol, exhibits protective effects against $A\beta_{25-35}$-induced damage through inhibition of the NF-κB and MAPK pathway–mediated inflammation and apoptosis (Lee et al., 2018b). Red ginseng oil can also downregulate the p38/-JNK/-NF-κB pathway to

TABLE 3 | Summary of effects and mechanisms of formulas containing ginseng in neuronal cells and animal models.

Ref	Formulas	Medicines	Model	Inducer	Experimental model	Mechanism	Effects
Yang et al. (2017)	Fuzheng Quxie Decoction	Renshen, huan glian, and chuanxiong (9:6:5)	AD		SAMP8 mice	p-tau↓ p-PP2A, NR2A, nissl bodies↑	p-tau
An et al. (2018)	SQYZ granules	Ginsenoside Rg1, astragaloside a, and baicalin	AD		APP/PS1 double transgenic mice	Aβ42, dynamin-1↓ MAPK3, TCA (dalt, Fabp5, ldhb, Glo1, Eno1), HSP↑ Atp5b, Dmxl1	Aβ deposition, neuroinflammation, stress responses, energy metabolism
Ren et al. (2020)	Shenqi yizhi granules	*Panax ginseng*, *Astragalus membranaceus*, and *Scutellaria baicalensis* Georgi (2:4:3)	AD		APP/PS1 double transgenic mice	Mdhc, PKM, ATP, HSP↑ acetyl-CoA	Energy metabolism, stress response, cytoskeleton, synaptic transmission, signal transduction, amino acid metabolism
Guo et al. (2019)	Kai-xin-san	*Panax ginseng*, *Polygala tenuifolia* Willd, *Poria cocos* (Schw.) Wolf, and *Acorus tatarinowii* Schott (3:2:3:2)	AD	$A\beta_{25-35}$	SD rats/PC12 cells	AChE, Bcl-2, ROS, TNF-α, IL-1β↓ Ach, Bax, cleaved-caspase-3, p-PI3K, *p*-Akt, and *p*-GSK-3β↑ PI3K/Akt, tau	Oxidative stress, neuroinflammation, apoptosis, Aβ deposition, cytoskeleton
Cao et al. (2018)	Kai-xin-san	*Ginseng Radix et Rhizoma*, *Polygalae Radix*, *Acori Tatarinowii*, and *Poria* (3:2:2:3)			Primary mouse astrocytes cells	MMP-9, TIMP-1→ NGF, BDNF, CREB, tPA↑	cAMP-dependent pathway, synthesis of neurotrophic factors *via* regulation of the tPA system
Liu et al. (2020)	GAPT, GEPT, or jinsiwei	Ginseng, epimedium, polygala, and tuber curcumae	Learning and memory-disordered model	Scopolamine	6 months old male ICR mice	MDA, AChE, ROS↓ ChAT, SOD, GPX, Ach↑	Protecting cholinergic neurons, reducing oxidative stress injury, neuroprotective
Seo et al. (2018)	P. *montana* and red ginseng extracts	Hongshen and gegen	Neurodegeneration	TMT	5 weeks old male ICR mice	AChE↓ Catalase, MDA↑	Ach, oxidative stresses
Shi et al. (2018)	Rg1 and *Acori graminei Rhizoma*	Ginsenoside Rg1 and shichangpu	AD	$A\beta_{1-42}$	SAMP8 mice/ Primary hippocampal neurons cells/PC12 cells	HMOX1↓ mir-873-5p↑	Apoptosis

suppress pro-inflammatory mediators, and caspase-3/PARP-1 signaling, inhibiting mitochondria-mediated apoptosis and protecting against Aβ-induced injury (Lee et al., 2017). In addition, the nonsaponin polysaccharide fraction, from ginseng, mitigates Aβ-induced neuronal dysfunction and improves mitochondrial respiration in the subiculum of the 5 × FAD mice model (Shin et al., 2021). Collectively, these results indicate that ginseng extracts and fractions have neuroprotective roles, improving mitochondrial dysfunction and inhibiting inflammation and apoptosis (**Table 2**). Importantly, the active components of these ginseng extracts should be further identified.

Formulas Containing Ginseng or Combination Treatment

Formulas containing ginseng and drug combinations can be used to achieve treatment efficacy and reduced toxicity. Currently, several decoctions containing ginseng are investigated to confirm the neuroprotective effects and identify the active components. Fuzheng Quxie decoction includes ginsenosides Rg1, Re, Rb1, and coptisine, which can cross the blood–brain barrier to inhibit tau hyperphosphorylation in the hippocampus, inhibiting learning and memory impairments in SAMP8 mice (Yang et al., 2017). The anti-neuroinflammatory effects of the Shenqi Yizhi formula in the 5 × FAD mice model may be mediated by active components including ginsenoside Rg1, astragaloside A, and baicalin by influencing energy metabolism, cytoskeleton, and stress reaction (An et al., 2018; Ren et al., 2020). Shengmai San can inhibit $A\beta_{1-42}$ production to improve spatial learning and memory of APP/PS1 mice (Zhang et al., 2018). Kaixin San (KXS), a well-known formula that has been used in clinical settings for a long time, has various pharmacological effects; for instance, protecting nerve cells and preventing AD (Lv et al., 2014; Wang et al., 2019). The active components of KXS have been identified as ginsenoside Rf, ginsenoside F1, and

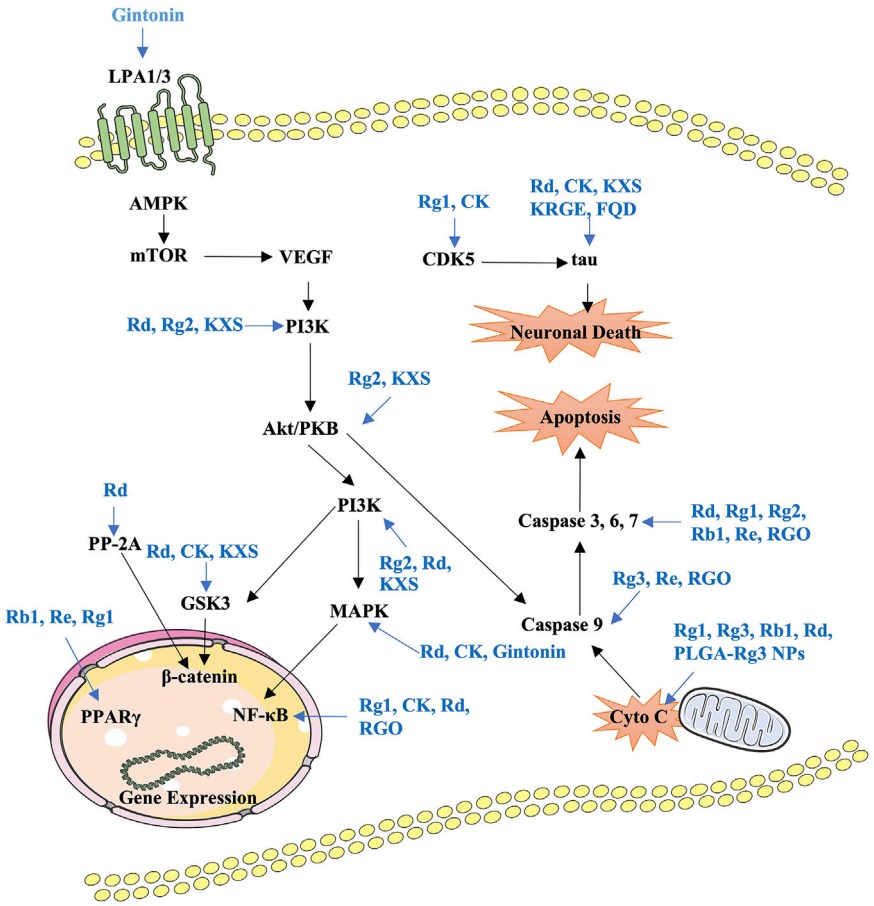

FIGURE 2 | Summary of the functional effects of ginseng on AD *via* multiple links across regulatory mechanisms and multitarget effects. LPA, lysophosphatidic acid; KXS, Kaixin-San; PP-2A, protein phosphatase 2A; RGO, red Ginseng oil; Cyto C, cytochrome C.

dehydropachymic acid, which can activate cAMP-dependent signaling and promote neurotrophic factor synthesis in primary astrocytes and AD mice (Cao et al., 2018; Wang et al., 2019). Importantly, system biology analysis has validated that KXS has multitarget synergistic effects on the amelioration of AD features (Guo et al., 2019). Ninjin-yoei-to (NYT), a formula containing 14 herbs, can promote the production of nerve growth factor in rat embryo astrocytes after incubation for 24 h (Yabe et al., 2003). Additionally, GAPT (Jinsiwei), a combination of several active components, can reduce the AChE activity and expression and increase ACh synthesis to improve cholinergic nerve function, reducing the learning and memory impairments in scopolamine-induced mice (Liu et al., 2020). Pretreatment with *P. montana* and red ginseng extracts significantly reduces catalase and AChE activities, inhibiting trimethyltin-induced neuronal cell death, oxidative stress, and learning and memory impairments (Seo et al., 2018). Ginsenoside Rg1 combined with the Acori graminei rhizoma extract can reverse the effect of $A\beta_{1-42}$ accumulation by regulating the expression of miR-873-5p in PC12 cells and SAMP8 mice (Shi et al., 2018). The current findings of formulas or combination treatment in AD have been summarized in **Table 3**. *In vitro* and *in vivo* preclinical studies have demonstrated that ginsenosides, gintonin, and other active components from ginseng or formulas containing ginseng mainly regulate PI3K/Akt, AMPK-mTOR, MAPK, GSK-3β/CDK5, NF-κB, and mitochondrial apoptotic signaling pathways to improve key pathological processes of AD development (**Figure 2**).

CLINICAL TRIALS OF GINSENG, FORMULAS, OR DIETARY SUPPLEMENTS CONTAINING GINSENG

At present, very few clinical trials investigating the effects of ginseng intervention on AD are ongoing or completed. Most clinical trials focus on ginseng or red ginseng extract and employ the Alzheimer's Disease Assessment Scale (ADAS) and the Mini-Mental State Examination (MMSE) scores to monitor cognitive performances. After ginseng treatment for 12 weeks, the cognitive subscale of ADAS and the MMSE score are significantly improved, indicating that ginseng has positive effect on the cognitive performance of AD patients (Lee et al., 2008). After administration with heat-processed ginseng (4.5 g/day) for 24 weeks, cognitive function and behavioral symptoms in patients

TABLE 4 | Summary of clinical trials of ginseng interventions in AD patients.

Ref	Medicine	Model	Sample size	Inclusion criteria	Evaluative criteria	Results
Lee et al. (2008)	Ginseng	AD	Control group (n = 39), ginseng group (n = 58)	1. NINDS-ADRDA 2. Patients without other neurodegenerative disorders or cognitive impairments 3. The use of drugs for concomitant conditions was permitted	MMSE, ADAS	Ginseng as a cognitive enhancer for AD patients
Kudoh et al. (2016)	Ninjin-yoei-to (renshen yangrong tang)	Mild to moderate probable AD	Donepezil (n = 11), donepezil + NYT (n = 12)	1. Patients diagnosed with AD between 65 and 85 years of age 2. Patients who scored 15–23 points on the MMSE after treatment with donepezil (5 mg/day) for more than 8 months, but who did not exhibit any significant change in cognitive function 3. Patients without an otherwise healthy condition	MMSE, ADAS-J cog, NPI	No significant differences between the two groups
Heo et al. (2012)	Heat-processed ginseng	AD	1.5 g/day (n = 10), 3 g/day (n = 10), 4.5 g/day (n = 10), control (n = 10)	1. Age older than 50 years 2. MMSE score of ≤20 3. CDR score of ≥1 4. Without psychiatric disorder, seizure disorder, or a medical condition 5. Without cognitive impairment due to stroke, neoplasia, infection, hypoxic brain injury, or medications	ADAS, MMSE	Significant improvement on the MMSE and ADAS. Higher dose group (4.5 g/day) showed improvements in ADAS and MMSE score as early as at 12 weeks, which sustained for 24-week follow-up
Heo et al. (2008)	Korean red ginseng	AD	Low-dose (4.5 g/day, n = 15), high-dose (9 g/day, n = 15), control (n = 31)	1. Aged older than 50 years and baseline MMSE score of≥10 and ≤26 2. Patients were without psychiatric disorder, seizure disorder, or a medical condition that would limit the completeness of the study 3. Patients without cognitive disorder caused by stroke, hypoxic brain, cerebral neoplasia, infection, and medications	ADAS, K-MMSE, CDR	High-dose KRG group was significant improvement on the ADAS and CDR but normally improved on the MMSE after 12 weeks of KRG therapy when compared with those in the control group
Yakoot et al. (2013)	Memo® (combining of lyophilized royal jelly, extracts of *G. biloba* and *P. ginseng*)	AD	Experimental group (n = 30) control group (n = 30)	1. Aged 50–80 years, complaining of memory impairment or forgetfulness 2. Satisfying the clinical criteria of memory complaint, normal activities of daily living, abnormal memory for age, and no documented dementia	MMSE	Beneficial in treating the cognitive decline that occurs during the aging process as well as in the early stages of pathologic cognitive impairment of insidious-onset vascular dementia and in AD

with moderately severe AD are improved at 12 weeks, which is sustained for the next 12-week follow-up (Heo et al., 2012). AD patients in the high-dose (9 g/day) Korean red ginseng group show significant improvements on the ADAS and Clinical Dementia Rating scales after 12-week therapy compared with the control group (Heo et al., 2008). In a larger-sized study, oral administration of Memo®, a triple formula (750 mg lyophilized royal jelly, 120 mg *Ginkgo biloba* extract, and 150 mg ginseng extract) for 4 weeks was shown to exert beneficial effects on cognition during aging and pathologic cognitive impairment in the early stages of AD (Yakoot et al., 2013). Furthermore, a combination of NYT and donepezil is more effective for AD patients with mild depression compared with donepezil-only (Kudoh et al., 2016). In addition, no adverse reactions occurred in all clinical studies, which suggests that ginseng can be used safely and has better tolerance for the patients with AD. The findings from clinical trials have been summarized in **Table 4**, which preliminarily indicates that ginseng treatment is safe and has a positive effect on cognition in patients with AD. However, it is essential to conduct more and high-quality clinical trials to evaluate the protective and therapeutic effects of ginseng, formulas containing ginseng, and combinations with other drugs in patients with different stages of AD and explore the underlying molecular mechanisms.

CONCLUSION

In this review, we summarize our recent findings regarding the effects of ginseng on AD and cognitive and memory dysfunction.

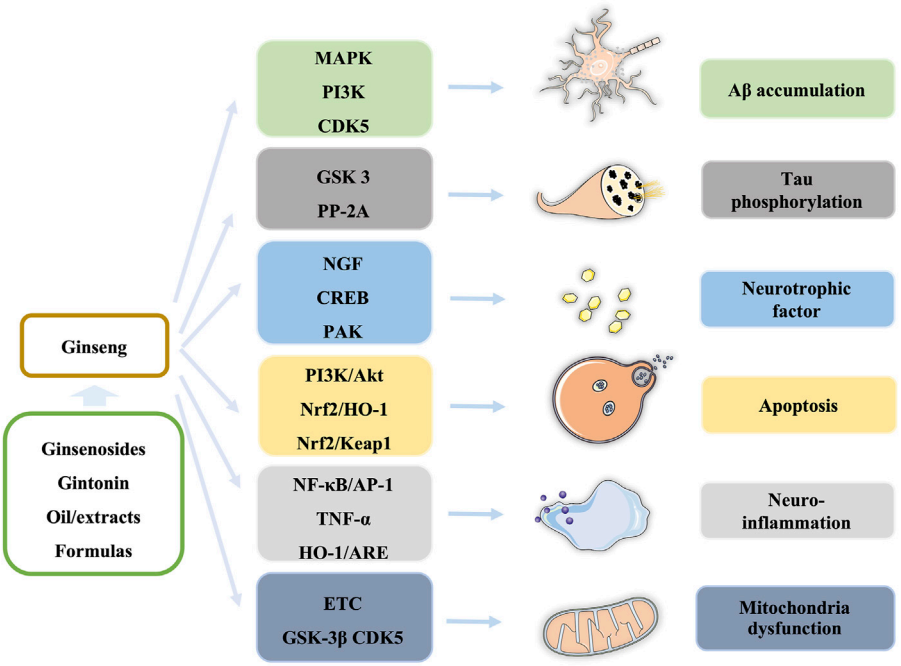

FIGURE 3 | Summary of ginseng components and the affected pathways in the pathological process of AD.

Ginsenosides, gintonin, extracts/fractions from ginseng, and formulas containing ginseng are widely studied in cells and animal models, which demonstrate that ginseng exerts neuroprotective effects in the prevention and treatment of AD through regulating multiple signaling pathways, such as PI3K/Akt, AMPK-mTOR, and NF-κB pathways, to block or improve pathological processes, including Aβ accumulation, tau phosphorylation, neuroinflammation, neurotrophic factors, apoptosis, and mitochondrial dysfunction in different stages of AD (**Figure 3**).

However, in preclinical and clinical studies of the effects of ginseng on AD, three important aspects should be considered: 1) Most studies focus on ginsenosides and gintonin with different chemical characteristics. The molecular mechanisms underlying the effects of ginsenosides and gintonin in the regulation of Aβ accumulation, neuroinflammation, and neurotrophic factors are similar, but only gintonin can interact with LPA receptors to mediate transient increases in $[Ca^{2+}]i$ regulating neurotransmitter release and improving cognition. 2) A series of cell models, such as PC12, SH-SY5Y, SweAPP-SK, and hippocampal neurons and several animal models, such as SAMP8, 5 × FAD, and 3 × Tg-AD mice are used to evaluate the neuroprotective effects of ginseng. Based on the current preclinical findings, we think that long-term interventions with ginseng or its formulas are critical to improve cognitive features for AD patients in early stages, which should be validated in larger and multicenter clinical trials. 3) Key pathological procedures of AD, including Aβ synthesis and degradation, neurotoxicity, and mitochondrial function, are potential targets for ginseng treatments. However, the molecular targets and binding sites of ginsenosides, gintonin, and other components in the prevention and treatment of AD remain unclear. Therefore, the network of targets of ginseng needs to be explored in the future. Collectively, this review can provide new insights into the possible use of ginseng in the prevention and treatment of AD.

AUTHOR CONTRIBUTIONS

JinL and QH collected, analyzed, and reviewed the literature and wrote the main manuscript; JinL, JC, HQ, JiaL, and ZC added/checked references and assembled figures/tables; DZ and ZW revised the manuscript; XL and ZW designed and supervised the final version of the manuscript. All authors have read and agreed to the published version of the manuscript.

FUNDING

This study was supported by the National Key Research and Development Program of China (2017YFC1702103), National Natural Science Foundation of China (U19A2013), and Science and Technology Development Plan Project of Jilin Province (20190101010JH, 202002053JC).

REFERENCES

Aalinkeel, R., Kutscher, H. L., Singh, A., Cwiklinski, K., Khechen, N., Schwartz, S. A., et al. (2018). Neuroprotective Effects of a Biodegradable Poly(lactic-Co-Glycolic Acid)-Ginsenoside Rg3 Nanoformulation: a Potential Nanotherapy for Alzheimer's Disease?. *J. Drug Target.* 26, 182–193. doi:10.1080/1061186x.2017.1354002

Alzheimer's Association (2020). *Alzheimer's Disease Facts and Figures. Alzheimer's & Dementia : The Journal of the Alzheimer's Association*.

An, H., Wei, D., Qian, Y., Li, N., and Wang, X. (2018). SQYZ Granules, a Traditional Chinese Herbal, Attenuate Cognitive Deficits in AD Transgenic Mice by Modulating on Multiple Pathogenesis Processes. *Am. J. Transl Res.* 10, 3857–3875.

Arendt, T., and Bullmann, T. (2013). Neuronal Plasticity in Hibernation and the Proposed Role of the Microtubule-Associated Protein Tau as a "master Switch" Regulating Synaptic Gain in Neuronal Networks. *Am. J. Physiol. Regulatory, Integr. Comp. Physiol.* 305, R478–R489. doi:10.1152/ajpregu.00117.2013

Bader Lange, M. L., Cenini, G., Piroddi, M., Mohmmad Abdul, H., Sultana, R., Galli, F., et al. (2008). Loss of Phospholipid Asymmetry and Elevated Brain Apoptotic Protein Levels in Subjects with Amnestic Mild Cognitive Impairment and Alzheimer Disease. *Neurobiol. Dis.* 29, 456–464. doi:10.1016/j.nbd.2007.11.004

Cao, C., Xiao, J., Liu, M., Ge, Z., Huang, R., Qi, M., et al. (2018). Active Components, Derived from Kai-Xin-San, a Herbal Formula, Increase the Expressions of Neurotrophic Factor NGF and BDNF on Mouse Astrocyte Primary Cultures via cAMP-dependent Signaling Pathway. *J. Ethnopharmacol.* 224, 554–562. doi:10.1016/j.jep.2018.06.007

Cao, G., Su, P., Zhang, S., Guo, L., Zhang, H., Liang, Y., et al. (2016). Ginsenoside Re Reduces Aβ Production by Activating PPARγ to Inhibit BACE1 in N2a/APP695 Cells. *Eur. J. Pharmacol.* 793, 101–108. doi:10.1016/j.ejphar.2016.11.006

Changhong, K., Peng, Y., Yuan, Z., and Cai, J. (2021). Ginsenoside Rb1 Protected PC12 Cells from Aβ25-35-Induced Cytotoxicity via PPARγ Activation and Cholesterol Reduction. *Eur. J. Pharmacol.* 893, 173835. doi:10.1016/j.ejphar.2020.173835

Chen, F., Eckman, E. A., Eckman, C. B., Chen, F., Eckman, E. A., and Eckman, C. B. (2006). Reductions in Levels of the Alzheimer's Amyloid β Peptide after Oral Administration of Ginsenosides. *FASEB j.* 20, 1269–1271. doi:10.1096/fj.05-5530fje

Chen, X., Li, H., Yang, Q., Lan, X., Wang, J., Cao, Z., et al. (2019). Ginsenoside Compound K Ameliorates Alzheimer's Disease in HT22 Cells by Adjusting Energy Metabolism. *Mol. Biol. Rep.* 46, 5323–5332. doi:10.1007/s11033-019-04988-0

Choi, S.-H., Kim, H.-J., Cho, H.-J., Park, S.-D., Lee, N.-E., Hwang, S.-H., et al. (2019). Gintonin-mediated Release of Astrocytic Vascular Endothelial Growth Factor Protects Cortical Astrocytes from Hypoxia-Induced Cell Damages. *J. ginseng Res.* 43, 305–311. doi:10.1016/j.jgr.2018.05.006

Choi, S.-H., Lee, R., Nam, S. M., Kim, D.-G., Cho, I.-H., Kim, H.-C., et al. (2021). Ginseng Gintonin, Aging Societies, and Geriatric Brain Diseases. *Integr. Med. Res.* 10, 100450. doi:10.1016/j.imr.2020.100450

Choi, S., Jung, S., Lee, B., Kim, H., Hwang, S., Kim, H., et al. (2015). Ginseng Pharmacology: a New Paradigm Based on Gintonin-Lysophosphatidic Acid Receptor Interactions. *Front. Pharmacol.* 6, 245. doi:10.3389/fphar.2015.00245

Cui, J., Shan, R., Cao, Y., Zhou, Y., Liu, C., and Fan, Y. (2020). Protective Effects of Ginsenoside Rg2 against Memory Impairment and Neuronal Death Induced by Aβ25-35 in Rats. *J. Ethnopharmacol* 266, 113466. doi:10.1016/j.jep.2020.113466

Cui, J., Wang, J., Zheng, M., Gou, D., Liu, C., and Zhou, Y. (2017). Ginsenoside Rg2 Protects PC12 Cells against β-amyloid25-35-induced Apoptosis via the Phosphoinositide 3-kinase/Akt Pathway. *Chemico-Biological Interactions* 275, 152–161. doi:10.1016/j.cbi.2017.07.021

Cummings, J. (2021). New Approaches to Symptomatic Treatments for Alzheimer's Disease. *Mol. Neurodegener* 16, 2. doi:10.1186/s13024-021-00424-9

Du, Y., Fu, M., Wang, Y. T., and Dong, Z. (2018). Neuroprotective Effects of Ginsenoside Rf on Amyloid-β-Induced Neurotoxicity *In Vitro* and *In Vivo*. *Jad* 64, 309–322. doi:10.3233/jad-180251

Gomes, L. A., Hipp, S. A., Rijal Upadhaya, A., Balakrishnan, K., Ospitalieri, S., Koper, M. J., et al. (2019). Aβ-induced Acceleration of Alzheimer-Related τ-pathology Spreading and its Association with Prion Protein. *Acta Neuropathol.* 138, 913–941. doi:10.1007/s00401-019-02053-5

Guo, M., Shao, S., Wang, D., Zhao, D., and Wang, M. (2021). Recent Progress in Polysaccharides from Panax Ginseng C. A. Meyer. *Food Funct.* 12, 494–518. doi:10.1039/d0fo01896a

Guo, S., Wang, J., Wang, Y., Zhang, Y., Bi, K., Zhang, Z., et al. (2019). Study on the Multitarget Synergistic Effects of Kai-Xin-San against Alzheimer's Disease Based on Systems Biology. *Oxid Med. Cel Longev* 2019, 1707218. doi:10.1155/2019/1707218

Han, J., Oh, J. P., Yoo, M., Cui, C. H., Jeon, B. M., Kim, S. C., et al. (2019). Minor Ginsenoside F1 Improves Memory in APP/PS1 Mice. *Mol. Brain* 12, 77. doi:10.1186/s13041-019-0495-7

Heo, J.-H., Lee, S.-T., Chu, K., Oh, M. J., Park, H.-J., Shim, J.-Y., et al. (2008). An Open-Label Trial of Korean Red Ginseng as an Adjuvant Treatment for Cognitive Impairment in Patients with Alzheimers Disease. *Eur. J. Neurol.* 15, 865–868. doi:10.1111/j.1468-1331.2008.02157.x

Heo, J.-H., Lee, S.-T., Chu, K., Oh, M. J., Park, H.-J., Shim, J.-Y., et al. (2012). Heat-processed Ginseng Enhances the Cognitive Function in Patients with Moderately Severe Alzheimer's Disease. *Nutr. Neurosci.* 15, 278–282. doi:10.1179/1476830512y.0000000027

Hwang, S. H., Shin, E.-J., Shin, T.-J., Lee, B.-H., Choi, S.-H., Kang, J., et al. (2012). Gintonin, a Ginseng-Derived Lysophosphatidic Acid Receptor Ligand, Attenuates Alzheimer's Disease-Related Neuropathies: Involvement of Non-amyloidogenic Processing. *Jad* 31, 207–223. doi:10.3233/jad-2012-120439

Ikram, M., Ullah, R., Khan, A., and Kim, M. O. (2020). Ongoing Research on the Role of Gintonin in the Management of Neurodegenerative Disorders. *Cells* 9. doi:10.3390/cells9061464

Im, D.-s., and Nah, S.-y. (2013). Yin and Yang of Ginseng Pharmacology: Ginsenosides vs Gintonin. *Acta Pharmacol. Sin* 34, 1367–1373. doi:10.1038/aps.2013.100

Jakaria, M., Azam, S., Go, E. A., Uddin, M. S., Jo, S. H., and Choi, D. K. (2020). Biological Evidence of Gintonin Efficacy in Memory Disorders. *Pharmacol. Res.* 163, 105221. doi:10.1016/j.phrs.2020.105221

JeffKuret, N. S. H. a. (2008). Tau Aggregation and Toxicity in Tauopathic Neurodegenerative Diseases. *J. Alzheimer's Dis.* 14, 417–422. doi:10.3233/jad-2008-14409

Jia, J., Wei, C., Chen, S., Li, F., Tang, Y., Qin, W., et al. (2018). The Cost of Alzheimer's Disease in China and Re-estimation of Costs Worldwide. *Alzheimer's Demen.* 14, 483–491. doi:10.1016/j.jalz.2017.12.006

Jia, L., Quan, M., Fu, Y., Zhao, T., Li, Y., Wei, C., et al. (2020). Dementia in China: Epidemiology, Clinical Management, and Research Advances. *Lancet Neurol.* 19, 81–92. doi:10.1016/s1474-4422(19)30290-x

Johansson, M., Stomrud, E., Lindberg, O., Westman, E., Johansson, P. M., van Westen, D., et al. (2020). Apathy and Anxiety Are Early Markers of Alzheimer's Disease. *Neurobiol. Aging* 85, 74–82. doi:10.1016/j.neurobiolaging.2019.10.008

Joo, S. S., Yoo, Y. M., Ahn, B. W., Nam, S. Y., Kim, Y.-B., Hwang, K. W., et al. (2008). Prevention of Inflammation-Mediated Neurotoxicity by Rg3 and its Role in Microglial Activation. *Biol. Pharm. Bull.* 31, 1392–1396. doi:10.1248/bpb.31.1392

Kareti, S. R., and P, S. (2020). In Silico Molecular Docking Analysis of Potential Anti-alzheimer's Compounds Present in Chloroform Extract of Carissa Carandas Leaf Using Gas Chromatography MS/MS. *Curr. Ther. Res.* 93, 100615. doi:10.1016/j.curtheres.2020.100615

Karpagam, V., Sathishkumar, N., Sathiyamoorthy, S., Rasappan, P., Shila, S., Kim, Y.-J., et al. (2013). Identification of BACE1 Inhibitors from Panax Ginseng Saponins-An Insilco Approach. *Comput. Biol. Med.* 43, 1037–1044. doi:10.1016/j.compbiomed.2013.05.009

Kim, H.-J., Jung, S.-W., Kim, S.-Y., Cho, I.-H., Kim, H.-C., Rhim, H., et al. (2018). Panax Ginseng as an Adjuvant Treatment for Alzheimer's Disease. *J. Ginseng Res.* 42, 401–411. doi:10.1016/j.jgr.2017.12.008

Kim, H.-J., Kim, D.-J., Shin, E.-J., Lee, B.-H., Choi, S.-H., Hwang, S.-H., et al. (2016). Effects of Gintonin-Enriched Fraction on Hippocampal Cell Proliferation in Wild-type Mice and an APPswe/PSEN-1 Double Tg Mouse Model of Alzheimer's Disease. *Neurochem. Int.* 101, 56–65. doi:10.1016/j.neuint.2016.10.006

Kim, H.-J., Shin, E.-J., Lee, B.-H., Choi, S.-H., Jung, S.-W., Cho, I.-H., et al. (2015a). Oral Administration of Gintonin Attenuates Cholinergic Impairments by Scopolamine, Amyloid-β Protein, and Mouse Model of Alzheimer's Disease. *Mol. Cell* 38, 796–805. doi:10.14348/molcells.2015.0116

Kim, H., Lee, B.-H., Choi, S.-H., Kim, H.-J., Jung, S.-W., Hwang, S.-H., et al. (2015b). Gintonin Stimulates Gliotransmitter Release in Cortical Primary Astrocytes. *Neurosci. Lett.* 603, 19–24. doi:10.1016/j.neulet.2015.07.012

Kim, M. S., Yu, J. M., Kim, H. J., Kim, H. B., Kim, S. T., Jang, S. K., et al. (2014). Ginsenoside Re and Rd Enhance the Expression of Cholinergic Markers and Neuronal Differentiation in Neuro-2a Cells. *Biol. Pharm. Bull.* 37, 826–833. doi:10.1248/bpb.b14-00011

Kudoh, C., Arita, R., Honda, M., Kishi, T., Komatsu, Y., Asou, H., et al. (2016). Effect of Ninjin'yoeito, a Kampo (Traditional Japanese) Medicine, on Cognitive Impairment and Depression in Patients with Alzheimer's Disease: 2 Years of Observation. *Psychogeriatrics* 16, 85–92. doi:10.1111/psyg.12125

Kwon, O. H., Cho, Y. Y., Kim, T.-W., and Chung, S. (2019). O-GlcNAcylation of Amyloid-β Protein Precursor by Insulin Signaling Reduces Amyloid-β Production. *Jad* 69, 1195–1211. doi:10.3233/jad-190060

Lee, B.-H., Choi, S.-H., Kim, H.-J., Park, S.-D., Rhim, H., Kim, H.-C., et al. (2018a). Gintonin Absorption in Intestinal Model Systems. *J. Ginseng Res.* 42, 35–41. doi:10.1016/j.jgr.2016.12.007

Lee, B., Sur, B., Park, J., Kim, S.-H., Kwon, S., Yeom, M., et al. (2013). Ginsenoside Rg3 Alleviates Lipopolysaccharide-Induced Learning and Memory Impairments by Anti-inflammatory Activity in Rats. *Biomolecules Ther.* 21, 381–390. doi:10.4062/biomolther.2013.053

Lee, S.-T., Chu, K., Sim, J.-Y., Heo, J.-H., and Kim, M. (2008). Panax Ginseng Enhances Cognitive Performance in Alzheimer Disease. *Alzheimer Dis. Assoc. Disord.* 22, 222–226. doi:10.1097/wad.0b013e31816c92e6

Lee, S., Youn, K., Jeong, W., Ho, C., and Jun, M. (2017). Protective Effects of Red Ginseng Oil against Aβ-Induced Neuronal Apoptosis and Inflammation in PC12 Cells. *Int. J. Mol. Sci.* 18. doi:10.3390/ijms18102218

Lee, S., Youn, K., and Jun, M. (2018b). Major Compounds of Red Ginseng Oil Attenuate Aβ25-35-Induced Neuronal Apoptosis and Inflammation by Modulating MAPK/NF-κB Pathway. *Food Funct.* 9, 4122–4134. doi:10.1039/c8fo00795k

Li, G., Zhang, N., Geng, F., Liu, G., Liu, B., Lei, X., et al. (2019). High-throughput Metabolomics and Ingenuity Pathway Approach Reveals the Pharmacological Effect and Targets of Ginsenoside Rg1 in Alzheimer's Disease Mice. *Sci. Rep.* 9, 7040. doi:10.1038/s41598-019-43537-4

Li, J., Liu, Y., Li, W., Wang, Z., Guo, P., Li, L., et al. (2018). Metabolic Profiling of the Effects of Ginsenoside Re in an Alzheimer's Disease Mouse Model. *Behav. Brain Res.* 337, 160–172. doi:10.1016/j.bbr.2017.09.027

Li, L., Liu, J., Yan, X., Qin, K., Shi, M., Lin, T., et al. (2011). Protective Effects of Ginsenoside Rd against Okadaic Acid-Induced Neurotoxicity *In Vivo* and *In Vitro*. *J. Ethnopharmacol.* 138, 135–141. doi:10.1016/j.jep.2011.08.068

Li, L., Liu, Z., Liu, J., Tai, X., Hu, X., Liu, X., et al. (2013). Ginsenoside Rd Attenuates Beta-Amyloid-Induced Tau Phosphorylation by Altering the Functional Balance of Glycogen Synthase Kinase 3beta and Protein Phosphatase 2A. *Neurobiol. Dis.* 54, 320–328. doi:10.1016/j.nbd.2013.01.002

Li, N., Liu, B., Dluzen, D. E., and Jin, Y. (2007). Protective Effects of Ginsenoside Rg2 against Glutamate-Induced Neurotoxicity in PC12 Cells. *J. Ethnopharmacol.* 111, 458–463. doi:10.1016/j.jep.2006.12.015

Lin, J., Gao, S., Wang, T., Shen, Y., Yang, W., Li, Y., et al. (2019). Ginsenoside Rb1 Improves Learning and Memory Ability through its Anti-inflammatory Effect in Aβ1-40 Induced Alzheimer's Disease of Rats. *Am. J. Transl Res.* 11, 2955–2968.

Liu, J.-f., Yan, X.-d., Qi, L.-s., Li, L., Hu, G.-y., Li, P., et al. (2015b). Ginsenoside Rd Attenuates Aβ25-35-Induced Oxidative Stress and Apoptosis in Primary Cultured Hippocampal Neurons. *Chemico-Biological Interactions* 239, 12–18. doi:10.1016/j.cbi.2015.06.030

Liu, J., Yan, X., Li, L., Li, Y., Zhou, L., Zhang, X., et al. (2015a). Ginsenoside Rd Improves Learning and Memory Ability in APP Transgenic Mice. *J. Mol. Neurosci.* 57, 522–528. doi:10.1007/s12031-015-0632-4

Liu, J., Yan, X., Li, L., Zhu, Y., Qin, K., Zhou, L., et al. (2012). Ginsennoside Rd Attenuates Cognitive Dysfunction in a Rat Model of Alzheimer's Disease. *Neurochem. Res.* 37, 2738–2747. doi:10.1007/s11064-012-0866-2

Liu, M., Bai, X., Yu, S., Zhao, W., Qiao, J., Liu, Y., et al. (2019). Ginsenoside Re Inhibits ROS/ASK-1 Dependent Mitochondrial Apoptosis Pathway and Activation of Nrf2-Antioxidant Response in Beta-Amyloid-Challenged SH-Sy5y Cells. *Molecules* 24. doi:10.3390/molecules24152687

Liu, Z., Qin, G., Mana, L., Dong, Y., Huang, S., Wang, Y., et al. (2020). GAPT Regulates Cholinergic Dysfunction and Oxidative Stress in the Brains of Learning and Memory Impairment Mice Induced by Scopolamine. *Brain Behav.* 10, e01602. doi:10.1002/brb3.1602

Lv, C., Li, Q., Zhang, X., He, B., Xu, H., Yin, Y., et al. (2014). Simultaneous Quantitation of Polygalaxanthone III and Four Ginsenosides by Ultra-fast Liquid Chromatography with Tandem Mass Spectrometry in Rat and Beagle Dog Plasma after Oral Administration of Kai-Xin-San: Application to a Comparative Pharmacokinetic S. *J. Sep. Sci.* 37, 1103–1110. doi:10.1002/jssc.201400058

Nah, S.-Y. (2012). Gintonin: a Novel Ginseng-Derived Ligand that Targets G Protein- Coupled Lysophosphatidic Acid Receptors. *Cdt* 13, 1659–1664. doi:10.2174/138945012803529947

Nie, L., Xia, J., Li, H., Zhang, Z., Yang, Y., Huang, X., et al. (2017). Ginsenoside Rg1 Ameliorates Behavioral Abnormalities and Modulates the Hippocampal Proteomic Change in Triple Transgenic Mice of Alzheimer's Disease. *Oxid Med. Cel Longev* 2017, 6473506. doi:10.1155/2017/6473506

Oh, J., and Kim, J.-S. (2016). Compound K Derived from Ginseng: Neuroprotection and Cognitive Improvement. *Food Funct.* 7, 4506–4515. doi:10.1039/c6fo01077f

Pardridge, W. M. (2020). Treatment of Alzheimer's Disease and Blood-Brain Barrier Drug Delivery. *Pharmaceuticals (Basel)* 13. doi:10.3390/ph13110394

Park, J.-S., Shin, J. A., Jung, J.-S., Hyun, J.-W., Van Le, T. K., Kim, D.-H., et al. (2012). Anti-inflammatory Mechanism of Compound K in Activated Microglia and its Neuroprotective Effect on Experimental Stroke in Mice. *J. Pharmacol. Exp. Ther.* 341, 59–67. doi:10.1124/jpet.111.189035

Park, K., Kim, E., Han, H., Shim, Y., Kwon, J., Ku, B., et al. (2017). Efficacy and Tolerability of Rivastigmine Patch Therapy in Patients with Mild-To-Moderate Alzheimer's Dementia Associated with Minimal and Moderate Ischemic white Matter Hyperintensities: A Multicenter Prospective Open-Label Clinical Trial. *PloS one* 12, e0182123. doi:10.1371/journal.pone.0182123

Perez Ortiz, J. M., and Swerdlow, R. H. (2019). Mitochondrial Dysfunction in Alzheimer's Disease: Role in Pathogenesis and Novel Therapeutic Opportunities. *Br. J. Pharmacol.* 176, 3489–3507. doi:10.1111/bph.14585

Piao, X., Zhang, H., Kang, J. P., Yang, D. U., Li, Y., Pang, S., et al. (2020). Advances in Saponin Diversity of Panax Ginseng. *Molecules* 25. doi:10.3390/molecules25153452

Pyo, M.-K., Choi, S.-H., Shin, T.-J., Hwang, S.-H., Lee, B.-H., Kang, J.-Y., et al. (2011). A Simple Method for the Preparation of Crude Gintonin from Ginseng Root, Stem, and Leaf. *J. Ginseng Res.* 35, 209–218. doi:10.5142/jgr.2011.35.2.209

Quan, Q., Li, X., Feng, J., Hou, J., Li, M., and Zhang, B. (2020). Ginsenoside Rg1 Reduces βamyloid Levels by Inhibiting CDK5induced PPARγ Phosphorylation in a Neuron Model of Alzheimer's Disease. *Mol. Med. Rep.* 22, 3277–3288. doi:10.3892/mmr.2020.11424

Rahman, M. A., Hwang, H., Nah, S.-Y., and Rhim, H. (2020). Gintonin Stimulates Autophagic Flux in Primary Cortical Astrocytes. *J. ginseng Res.* 44, 67–78. doi:10.1016/j.jgr.2018.08.004

Rajabian, A., Rameshrad, M., and Hosseinzadeh, H. (2019). Therapeutic Potential of Panax Ginseng and its Constituents, Ginsenosides and Gintonin, in Neurological and Neurodegenerative Disorders: a Patent Review. *Expert Opin. Ther. Patents* 29, 55–72. doi:10.1080/13543776.2019.1556258

Ren, J., Wei, D., An, H., Zhang, J., and Zhang, Z. (2020). Shenqi Yizhi Granules Protect hippocampus of AD Transgenic Mice by Modulating on Multiple Pathological Processes. *J. Ethnopharmacol.* 263, 112869. doi:10.1016/j.jep.2020.112869

Saba, E., Jeon, B. R., Jeong, D. H., Lee, K., Goo, Y. K., Kwak, D., et al. (2015). A Novel Korean Red Ginseng Compound Gintonin Inhibited Inflammation by MAPK and NF-Kb Pathways and Recovered the Levels of Mir-34a and Mir-93 in RAW 264.7 Cells. *Evid. Based Complement. Alternat Med.* 2015, 624132. doi:10.1155/2015/624132

Schindowski, K., Belarbi, K., and Buée, L. (2008). Neurotrophic Factors in Alzheimer's Disease: Role of Axonal Transport. *Genes Brain Behav.* 7 (Suppl. 1), 43–56. doi:10.1111/j.1601-183x.2007.00378.x

Seo, Y.-M., Choi, S. J., Park, C. K., Gim, M. C., and Shin, D.-H. (2018). Synergistic Effect of Korean Red Ginseng and Pueraria montana Var. Lobata against

Trimethyltin-Induced Cognitive Impairment. *Food Sci. Biotechnol.* 27, 1193–1200. doi:10.1007/s10068-018-0362-9

Shi, R., Zhang, S., Cheng, G., Yang, X., Zhao, N., and Chen, C. (2018). Ginsenoside Rg1 and Acori Graminei Rhizoma Attenuates Neuron Cell Apoptosis by Promoting the Expression of miR-873-5p in Alzheimer's Disease. *Neurochem. Res.* 43, 1529–1538. doi:10.1007/s11064-018-2567-y

Shi, Z. Y., Zeng, J. Z., and Wong, A. S. T. (2019). Chemical Structures and Pharmacological Profiles of Ginseng Saponins. *Molecules* 24. doi:10.3390/molecules24132443

Shin, S. J., Jeon, S. G., Kim, J. I., Jeong, Y. O., Kim, S., Park, Y. H., et al. (2019). Red Ginseng Attenuates Aβ-Induced Mitochondrial Dysfunction and Aβ-Mediated Pathology in an Animal Model of Alzheimer's Disease. *Int. J. Mol. Sci.* 20. doi:10.3390/ijms20123030

Shin, S. J., Nam, Y., Park, Y. H., Kim, M.-J., Lee, E., Jeon, S. G., et al. (2021). Therapeutic Effects of Non-saponin Fraction with Rich Polysaccharide from Korean Red Ginseng on Aging and Alzheimer's Disease. *Free Radic. Biol. Med.* 164, 233–248. doi:10.1016/j.freeradbiomed.2020.12.454

Shin, S. J., Park, Y. H., Jeon, S. G., Kim, S., Nam, Y., Oh, S. M., et al. (2020). Red Ginseng Inhibits Tau Aggregation and Promotes Tau Dissociation *In Vitro*. *Oxid Med. Cel Longev* 2020, 7829842. doi:10.1155/2020/7829842

Sonawane, S., Uversky, V., and Chinnathambi, S. (2021). Baicalein Inhibits Heparin-Induced Tau Aggregation by Initializing Non-toxic Tau Oligomer Formation. *Cell Commun. signaling : CCS* 19, 16. doi:10.1186/s12964-021-00704-3

Sung, P. S., Lin, P. Y., Liu, C. H., Su, H. C., and Tsai, K. J. (2020). Neuroinflammation and Neurogenesis in Alzheimer's Disease and Potential Therapeutic Approaches. *Int. J. Mol. Sci.* 21. doi:10.3390/ijms21030701

Vaz, M., and Silvestre, S. (2020). Alzheimer's Disease: Recent Treatment Strategies. *Eur. J. Pharmacol.* 887, 173554. doi:10.1016/j.ejphar.2020.173554

Wang, X.-j., Zhang, A.-h., Kong, L., Yu, J.-b., Gao, H.-l., Liu, Z.-d., et al. (2019). Rapid Discovery of Quality-Markers from Kaixin San Using Chinmedomics Analysis Approach. *Phytomedicine* 54, 371–381. doi:10.1016/j.phymed.2017.12.014

Wang, Y., Li, Y., Yang, W., Gao, S., Lin, J., Wang, T., et al. (2018). Ginsenoside Rb1 Inhibit Apoptosis in Rat Model of Alzheimer's Disease Induced by Aβ1-40. *Am. J. Transl Res.* 10, 796–805.

Xu, T. Z., Shen, X. Y., Sun, L. L., Chen, Y. L., Zhang, B. Q., Huang, D. K., et al. (2019). Ginsenoside Rg1 Protects against H2O2-induced N-euronal D-amage D-ue to I-nhibition of the NLRP1 I-nflammasome S-ignalling P-athway in H-ippocampal N-eurons I-n vitro. *Int. J. Mol. Med.* 43, 717–726. doi:10.3892/ijmm.2018.4005

Yabe, T., Tuchida, H., Kiyohara, H., Takeda, T., and Yamada, H. (2003). Induction of NGF Synthesis in Astrocytes by Onjisaponins of Polygala Tenuifolia, Constituents of Kampo (Japanese Herbal) Medicine, Ninjin-Yoei-To. *Phytomedicine* 10, 106–114. doi:10.1078/094471103321659799

Yakoot, M., Salem, A., and Helmy, S. (2013). Effect of Memo®, a Natural Formula Combination, on Mini-Mental State Examination Scores in Patients with Mild Cognitive Impairment. *Cia* 8, 975–981. doi:10.2147/cia.s44777

Yan, X., Hu, G., Yan, W., Chen, T., Yang, F., Zhang, X., et al. (2017). Ginsenoside Rd Promotes Non-amyloidogenic Pathway of Amyloid Precursor Protein Processing by Regulating Phosphorylation of Estrogen Receptor Alpha. *Life Sci.* 168, 16–23. doi:10.1016/j.lfs.2016.11.002

Yang, L., Hao, J., Zhang, J., Xia, W., Dong, X., Hu, X., et al. (2009). Ginsenoside Rg3 Promotes Beta-Amyloid Peptide Degradation by Enhancing Gene Expression of Neprilysin. *J. Pharm. Pharmacol.* 61, 375–380. doi:10.1211/jpp/61.03.0013

Yang, Q., Lin, J., Zhang, H., Liu, Y., Kan, M., Xiu, Z., et al. (2019b). Ginsenoside Compound K Regulates Amyloid β via the Nrf2/Keap1 Signaling Pathway in Mice with Scopolamine Hydrobromide-Induced Memory Impairments. *J. Mol. Neurosci.* 67, 62–71. doi:10.1007/s12031-018-1210-3

Yang, Y., Jia, X., Feng, J., Wang, Z., Cao, Y., Liu, J., et al. (2017). Fuzheng Quxie Decoction Ameliorates Learning and Memory Impairment in SAMP8 Mice by Decreasing Tau Hyperphosphorylation. *Evid. Based Complement. Alternat Med.* 2017, 5934254. doi:10.1155/2017/5934254

Yang, Y., Li, S., Huang, H., Lv, J., Chen, S., Pires Dias, A. C., et al. (2020). Comparison of the Protective Effects of Ginsenosides Rb1 and Rg1 on Improving Cognitive Deficits in SAMP8 Mice Based on Anti-neuroinflammation Mechanism. *Front. Pharmacol.* 11, 834. doi:10.3389/fphar.2020.00834

Yang, Y., Liang, X., Jin, P., Li, N., Zhang, Q., Yan, W., et al. (2019a). Screening and Determination for Potential Acetylcholinesterase Inhibitory Constituents from Ginseng Stem-Leaf Saponins Using Ultrafiltration (UF)-LC-ESI-MS 2. *Phytochem. Anal.* 30, 26–33. doi:10.1002/pca.2787

Yankner, B., Dawes, L., Fisher, S., Villa-Komaroff, L., Oster-Granite, M., and Neve, R. (1989). Neurotoxicity of a Fragment of the Amyloid Precursor Associated with Alzheimer's Disease. *Science* 245, 417–420. doi:10.1126/science.2474201

Zhang, A. H., Yu, J.-B., Sun, H., Kong, L., Wang, X. Q., Zhang, Q.-Y., et al. (2018). Identifying Quality-Markers from Shengmai San Protects against Transgenic Mouse Model of Alzheimer's Disease Using Chinmedomics Approach. *Phytomedicine* 45, 84–92. doi:10.1016/j.phymed.2018.04.004

Zhang, Y., Yang, X., Wang, S., and Song, S. (2019). Ginsenoside Rg3 Prevents Cognitive Impairment by Improving Mitochondrial Dysfunction in the Rat Model of Alzheimer's Disease. *J. Agric. Food Chem.* 67, 10048–10058. doi:10.1021/acs.jafc.9b03793

Zhao, B.-S., Liu, Y., Gao, X.-Y., Zhai, H.-Q., Guo, J.-Y., and Wang, X.-Y. (2014). Effects of Ginsenoside Rg1 on the Expression of Toll-like Receptor 3, 4 and Their Signalling Transduction Factors in the NG108-15 Murine Neuroglial Cell Line. *Molecules* 19, 16925–16936. doi:10.3390/molecules191016925

Zhao, J., Lu, S., Yu, H., Duan, S., and Zhao, J. (2018). Baicalin and Ginsenoside Rb1 Promote the Proliferation and Differentiation of Neural Stem Cells in Alzheimer's Disease Model Rats. *Brain Res.* 1678, 187–194. doi:10.1016/j.brainres.2017.10.003

Conflict of Interest: The authors declare that the research was conducted in the absence of any commercial or financial relationships that could be construed as a potential conflict of interest.

frontiers in Pharmacology

ORIGINAL RESEARCH
published: 08 June 2021
doi: 10.3389/fphar.2021.635762

Salidroside Improves Chronic Stress Induced Depressive Symptoms Through Microglial Activation Suppression

*Yang Fan, Yajuan Bi and Haixia Chen**

School of Pharmaceutical Science and Technology, Tianjin University, Tianjin, China

Depression is a severe neurological disorder highly associated with chronic mental stress stimulation, which involves chronic inflammation and microglial activation in the central nervous system (CNS). Salidroside (SLDS) has been reported to exhibit anti-neuroinflammatory and protective properties on neurological diseases. However, the mechanism underlying the effect of SLDS on depressive symptoms has not been well elaborated. In the present study, the effects of SLDS on depressive behaviors and microglia activation in mice CNS were investigated. Behavioral tests, including Forced swimming test (FST), Open field test (OFT) and Morris water maze (MWM) revealed that SLDS treatment attenuated the depressive behaviors in stress mice. SLDS treatment significantly reduced the microglial immunoreactivity for both Iba-1 and CD68, characteristic of deleterious M1 phenotype in hippocampus of stress mice. Additionally, SLDS inhibited microglial activation involving the suppression of ERK1/2, P38 MAPK and p65 NF-κB activation and thus reduced the expression and release of neuroinflammatory cytokines in stress mice as well as in lipopolysaccharide (LPS)-induced primary microglia. Also, SLDS changed microglial morphology, attachment and reduced the phagocytic ability in LPS-induced primary microglia. The results demonstrated that SLDS treatment could improve the depressive symptoms caused by unpredictable chronic stress, indicating a potential therapeutic application of SLDS in depression treatment by interfering microglia-mediated neuroinflammation.

Keywords: salidroside, neuroinflammation, microglia, depressive behavior, LPS

OPEN ACCESS

Edited by:
Tahir Ali,
University of Calgary, Canada

Reviewed by:
Paul Willner,
Swansea University, United Kingdom
Tahir Ali,
Peking University, China

****Correspondence:***
Haixia Chen
chenhx@tju.edu.cn

Specialty section:
This article was submitted to Neuropharmacology, a section of the journal Frontiers in Pharmacology

Received: *30 November 2020*
Accepted: *25 May 2021*
Published: *08 June 2021*

Citation:
Fan Y, Bi Y and Chen H (2021) Salidroside Improves Chronic Stress Induced Depressive Symptoms Through Microglial Activation Suppression. Front. Pharmacol. 12:635762. doi: 10.3389/fphar.2021.635762

INTRODUCTION

Based on the statistical analysis from the World Health Organization, over 450 million people suffer from depression and it will rise to the top financial burden among all the diseases in 2030 (Ustun et al., 2004; Smith 2014; Kato and Kanba, 2015). Typical clinical symptoms of depression include significant and long-term depressive mood, insensitivity, anhedonia and vital exhaustion (Ellis et al., 2004; Szatmari et al., 2018). Further progression may even lead to suicidal tendencies (Mitchell and Malhi 2004). The pathogenesis of depression is still unclear, however multiple studies suggested that chronic mental stress might be one of the critical pathogenic factors during depression formation and progression (Patriquin and Mathew 2017; da Estrela et al., 2020). Recent studies have shown that long-term stress impacts multiple aspects of biological systems, such as neuroendocrine, autonomic regulation, and behaviors (Sterlemann et al., 2008). This long-term stimulation eventually leads to a

failure in normal stress responses and brain inflammation, and finally causes mental disorders (Goshen et al., 2008; Patriquin and Mathew 2017).

Many studies have revealed that microglia cells are involved in the formation and development of depression (Singhal and Baune 2017; Deng et al., 2020). Neuroinflammation is a key driver of the pathological process in depression, and is primarily regulated by resident macrophages, which are microglia in the central nervous system (CNS). Microglia normally maintains ramified morphology in the resting state. Upon brain injury, microglia can be activated and transit into the amoeboid morphology, followed by release of multiple pro-inflammatory cytokines which further damage to nearby neurons (Fan et al., 2017). Microglia activation involves two functionally different states, deleterious state (M1 phenotype) and beneficial state (M2 phenotype) depending on the activation conditions and methods. In the presence of lipopolysaccharide (LPS), microglia cells are activated to M1 phenotype and lead to produce and secrete pro-inflammatory cytokines such as TNF-α and IL-6, IL-18, NO, and ROS (He et al., 2019; Laffer et al., 2019; Ahmed et al., 2021; Zong et al., 2020). In contrast, IL-4 or IL-10 induce microglia cells into M2 phenotype which tunes down the M1 phenotype and secretes brain-derived neurotrophic factor (BDNF), transforming growth factor-β (TGF-β) and nerve growth factor (NGF) to repair tissue and extracellular matrix components in CNS(Wei and Jonakait 1999; Szczepanik et al., 2001; Laffer et al., 2019; Yi et al., 2020). LPS is a classic inflammatory trigger that activates M1 phenotype, induces inflammatory response, further leading to inflammatory cytokines expression alterations and cerebral injuries (Nakagawa and Chiba 2014). Iba1 is the protein which widely and specifically expressed in the microglia all over the CNS and used as a microglia marker, while CD68 is a transmembrane protein widely expressed in activated microglia (M1 phenotype) upon LPS induction (Leaw et al., 2017). The morphological changes of microglia cells are closely related to their activation state and are the first sign to be observed in the multi-step microglia activation. These changes include thickening and retraction of processes and the increase in cell body size (Tynan et al., 2010; Fan et al., 2018). Vimentin filaments are parts of the intermediate filament system whose dynamic properties are important for cellular flexibility and vimentin has been revealed as a key component involved in microglia activation (Jiang et al., 2013). Focal adhesions refer to the physical connection between the extracellular matrix and the cell actin cytoskeleton, which are mediated by integrins. They are of fundamental importance in regulating cellular adhesion, mechanical sensing, and signals controlling for cell growth and differentiation (Ilic et al., 1995; Ruggiero et al., 2018). Paxillin has been reported to be phosphorylated by p38 MAPK and ERK1/2 at the residue Ser83 and its phosphorylation is involved in microglial activation and phagocytosis (Huang et al., 2004; Fan et al., 2018). Hippocampus is one of the important functional area of the brain which is responsible for the storage transformation of long-term memory and orientation (Colombo et al., 2001; Shi et al., 2018). Recent research has also highlighted its strong functional linkage to anxiety and depressive behaviors (Lee et al., 2002; Feng et al., 2020). The activation of microglia is pathological characteristics of patients with depression, which results in the release of extensive levels of proinflammatory cytokines in brain and causes neuronal apoptosis (Jiang et al., 2020; Wang T., et al., 2020). Therefore, inhibition of the deleterious microglial activation and migration might be a promising therapeutic strategy to ameliorate depressive symptoms. However, it is still in shortage of clinical drug alternatives.

Salidroside (SLDS), a phenolic glycoside compound, is extracted from a traditional Chinese medicinal plant, *Rhodiola rosea*. For centuries, this herb has been widely used by Chinese to treat multiple inflammatory diseases. Modern investigations have shown that SLDS has potent protective effects against hepatitis, colitis, skeletal muscle atrophy, and myocardial injury by alleviating excessive inflammation (Hu B et al., 2014; Huang et al., 2019; Liu et al., 2019; Wang N. et al., 2020). Especially, SLDS plays a neuroprotective role in both preclinical models of Alzheimer disease and cerebral ischemia by regulating microglia activation and distribution (Zhang et al., 2016; Liu et al., 2018; Wang et al., 2018; Zuo et al., 2018; Wang H. et al., 2020). Studies showed that SLDS could reduce the blood-brain barrier injury by activating the PI3K/Akt signaling pathway, decrease microvascular endothelial cells apoptosis, increase neuron cells viability and promote M2 macrophage/microglial polarization, thus improving functional recovery after cerebral ischemia (Liuet al., 2018; Wang et al., 2018; Zuo et al., 2018). In addition, SLDS could improve learning and memory impairment by suppressing SIRT1/NF-κB pathway and inhibiting the release of TNF-α, IL-1β and IL-6 (Gao et al., 2016). All these studies indicated that SLDS might become a promising new implement in attenuating depression by modulating microglial activation. Therefore, the goal of this study was to open up new horizons for the medicinal value of SLDS against depression by examining behavioral effects of SLDS and its effects in microglial cell cultures.

MATERIALS AND METHODS

Chemicals

SLDS (98% purity; Solarbio) was dissolved in phosphate buffered saline (PBS) at 50 μm. LPS (≥99% purity; Solarbio) was suspended in PBS at 1 mg/ml.

Animals

Male C57BL/6 mice (20 ± 2 g, 6 weeks old) were purchased from HuaFuKang (Beijing, China) and raised at Institute of Radiation Medicine (Tianjin, China). All the mice were raised individually at 22 ± 1°C, at humidity of 40–50%, with 12 h light/dark cycle. Free access to water and food. Body weight was measured every week. The animal experiments were all proved by the Institutional Animal Care and Use Committee of Institute of Radiation Medicine, Chinese Academy of Medical Sciences.

Chronic Stress Procedure and Drug Treatment

The mice were divided into three groups (10 mice each). Both stress groups were exposed to unpredictable stressors for 28 days using a strategy shown in **Table 1** (Nollet et al., 2013; Willner

TABLE 1 | Chronic stress strategies.

Days	Chronic stress strategies	Injection
1	Change to new cage and Food fasting	no
2	Shaking home cage and Water fasting	no
3	50 ml centrifuge constraint and Wet mattress	no
4	Switch to dirty cage and Hot temperature	no
5	Shaking home cage and Food fasting	no
6	50 ml centrifuge constraint and Water fasting	no
7	Rest and Change to new cage	no
8	Hot temperature and Food fasting	no
9	Switch to dirty cage and Water fasting	no
10	50 ml centrifuge constraint and Hot temperature	no
11	Switch to dirty cage and Food fasting	no
12	Shaking home cage and Water fasting	no
13	50 ml centrifuge constraint and Food fasting	no
14	Rest and Change to new cage	no
15	Shaking home cage and Food fasting	yes
16	Switch to dirty cage and Water fasting	yes
17	Hot temperature and Food fasting	yes
18	50 ml centrifuge constraint and Water fasting	yes
19	Shaking home cage and Hot temperature	yes
20	Hot temperature and Water fasting	yes
21	Rest and Change to new cage	yes
22	50 ml centrifuge constraint and Hot temperature	yes
23	Switch to dirty cage and Food fasting	yes
24	Shaking home cage and Water fasting	yes
25	50 ml centrifuge constraint and Food fasting	yes
26	Hot temperature and Water fasting	yes
27	Shaking home cage and Switch to dirty cage	yes
28	Rest and Change to new cage	yes

2017). Random stress strategies include: 24 h Food fasting; 24 h Water fasting; 12 h 50 ml centrifuge tube confinement; 24 h wet mattress; 24 h dirt cage; 30 min hot temperature; 15 min/2 times home cage shake. After 14 days, stressed groups began the intraperitoneal injection with PBS (100 μL/mice) or SLDS (10 mg/kg) every day.

Sucrose Preference Test

Socrose preference test (SPT) was conducted according to the method described previously (Feng et al., 2020). They were tested on the initial days (the 1st day and the day before it) and final days (the 28th day and the day after it). Mice were adjusted to habituate to the presence of two identical drinking bottles before it started. On the day of the tests, mice were exposed to the identical bottles randomly and individually, with one-containing 1% sucrose and another tap water for 2 days. After chronic stress procedure, test was repeat again. The position of the two bottles (right/left) was varied randomly from trial to trial to prevent place-preference by the animals. The percentage of sucrose intake over total intake was calculated as the relative sucrose intake preference.

Forced Swimming Test

FST was conducted as described by Feng et al. (Feng et al., 2020). It has been recognized as one of the most common animal models for the evaluation of antidepressant-like activity in rodents, due to its sensitivity to a broad range of antidepressant drugs (Cryan et al., 2002; Taliaz et al., 2010). The most important advantage of FST is that it is easy to operate and the data is collected and analyzed quickly. The mice were tested on the initial day (the 1st day) and final day (the 28th day). Briefly, mice were put into the transparent plastic buckets gently and separately. The transparent plastic buckets (30 cm in height × 20 cm in diameter) were filled with water of 12 cm high and maintained at 25 ± 2°C. Mice were kept in the water for 6 min and their behaviors were recorded in the last 4 min. When a mouse floated upright and hold its head above the water with a small amount of movements, it can be considered to be immobile.

Open Field Test

OFT was conducted the day after FST as described (Sevastre-Berghian et al., 2020). OFT has been reported as a scientifically valid method to evaluate the general locomotivity and anxiety levels in animal experiments (Sevastre-Berghian et al., 2020; Zhang et al., 2020). Briefly, the open field (Techman software, China) 36 cm × 36 cm was surrounded by walls. The open field area was divided into 25 same small squares with lines. Each mouse was placed in the middle of the area and started to record. Mice were allowed to freely explore the new environment for 5 min. Data were obtained and analyzed using the Techman software Behavior analyzing system.

Morris Water Maze Test

MWM was conducted the day after OFT as described (Bassett et al., 2021). Briefly, in a round water tank (30 cm in height × 100 cm in diameter) filled with water (25 ± 1°C) that was dyed white with milk, a platform was hidden in the water at a specific position. The tank was divided into four quadrants and marked 1, 2, 3 and 4. Mice were given free swimming until they reach the platform. Mice were guided manually to the platform where they were allowed to stay 60 s if the mice couldn't reach the platform in 90 s. After 6 days of training, the mice were tested on the 7th day with the platform being removed. The mice were allowed to swim freely for 60 s to test their spatial memory for the location of removed platform. Data were obtained and analyzed using the Top Scan Lite-Top View Behavior analyzing system (Noldus Information Technology, United States).

Spontaneous Locomotor Activity Test

Spontaneous locomotor activity test (SLAT) was conducted at the days before and after treatment (Nicolas et al., 2006). Mice were treated with either vehicle (Con group) or 50 μm SLDS (SLDS group) for 7 consecutive days. Data were obtained and analyzed using a Techman software Behavior analyzing system for 10 min in an empty box (36 cm × 36 cm with walls surrounded).

Brain Tissue Collection

After behavioral experiments, mice were anesthetized and killed. The brain was dissected and split along the longitudinal fissure into the left and right hemispheres. The hippocampus from the right hemispheres was evenly segmented and homogenized for ELISA, western blotting or qRT-PCR, while the left hemispheres were fixed in 4% paraformaldehyde at 4°C to further process for immunofluorescence staining.

TABLE 2 | Primers used in the real-time PCR assay.

Gene		Oligonucleotide Sequence	Length (bp)
TNF-α	Forward	5′ CTCAAGCCCTGGTATGAGCC 3′	20
	Reverse	5′ GGCTGGGTAGAGAACGGATG 3′	20
IL-1β	Forward	5′ CCTGCAGCTGGAGAGTGTGGAT 3′	22
	Reverse	5′ TGTGCTCTGCTTGTGAGGTGCT 3′	22
IL-6	Forward	5′ GGAGCCCACCAAGAACGATA 3′	20
	Reverse	5′ CAGGTCTGTTGGGAGTGGTA 3′	20
IL-18	Forward	5′ ACGTGTTCCAGGACACAACA 3′	20
	Reverse	5′ GGCGCATGTGTGCTAATCAT 3′	20
GAPDH	Forward	5′ AGCCTCGTCCCGTAGACAAAA 3′	21
	Reverse	5′ TGGCAACAATCTCCACTTTGC 3′	21

Cell Culture

Brain tissues of newborn mice C57BL/6 were cut in pieces with scissors and further dissociated by pipetting. Cells pelleted by centrifuge were suspended in DMEM with 10% fetal bovine serum premium (AusGeneX PTY LTD, Australia) and plated in culture flask. After incubation at 37°C with 5% CO_2 for 12 days, primary microglia cells were taken off by shaking at 280–310 rpm for 1 h and seeded on the new plates. When cells reached 80% confluence, 1 μg/ml LPS alone or with 50 μM SLDS was given for 24 h.

PC12 cells (generous gift from Gao Wenyuan at Tianjin University, China) were cultured in DMEM containing 10% fetal bovine serum premium and 10% Horse Serum (Gibco, China) at 37°C with 5% CO_2.

Cell Viability Assay

CCK-8 kit (Biosharp, China) was utilized to estimate the cell viability according to the manufacturer's instructions. Briefly, primary microglia or PC12 cells were seeded at the density of 5×10^3 cells per well. After 24 h incubation, cells were treated SLDS in different concentration (0, 50, 100, or 200 μM) with or without 1 μg/ml LPS (Wang et al., 2018) for 24 h. For apoptosis assay, primary microglia were pretreated with 50 μM SLDS with or without 1 μg/ml LPS for 12 h. Then the supernatant, defined as conditioned medium (CM) were collected to cultivate PC12 cells for 48 h (CM group) or with supplement of LPS (CM-LPS) or LPS and SLDS (CM-LPS+SLDS). After cultivation, PC12 cells were incubated with CCK-8 solution for 2 h at 37°C. The absorbance was measured at 450 nm with a microplate reader (TECAN, Switzerland).

Western Blotting

The lysates of primary microglia or brain tissue obtained from animal experiment mentioned above (25 μg/lane) were separated by 10% SDS-PAGE and then transferred at 12V to PVDF membrane (Millipore, United States) for 70 min using a semi-dry transfer apparatus (Bio-Rad). The membranes were blocked at room temperature (RT) for 1 h with blocking buffer (Solarbio) and then incubated with different primary antibodies overnight at 4°C. Rabbit polyclonal antibodies against phospho-p42/44 MAPK, p42/44 MAPK, phospho-p38 MAPK, p38 MAPK, phospho-NF-κB p65, NF-κB p65, iNOS (1:5000, CST), phospho-paxillin Ser83 and mouse polyclonal antibodies against paxillin (1:2500, ECM biosciences), α-Tubulin (1:10000, CST) were used. After incubation with a HRP-conjugated secondary antibody, the immunoreactive signals were visualized using Amersham Imager 600 (GE Life Sciences).

ELISA

Inflammation cytokines were measured using ELISA assay (Lanpai Bio, China). Briefly, protein concentration from brain samples or cell cultures were determined by using a BCA kit and equal amount of proteins from different samples were quantitatively analyzed with IL-1β, IL-6, IL-18 and TNF-α according to the manufacturer's instruction.

Real-Time PCR

Total RNA from brain samples or cell cultures was isolated by Eastep Super RNA isolation kit (Promega, China). Total RNA concentration was determined by a Nanodrop Spectrophotometer (Thermo Fisher Scientific, United States). cDNA synthesis was performed in PCR system (Eppendorf, Germany) using HiScript Q RT SuperMix kit (Vazyme, China) with 800 ng RNA in a total 10 μl reaction system. Subsequently, cDNA was diluted for 15 times and 5 μl of the dilute was mixed with Ultra SYBR mixture low ROX (CW biotech, China) for real-time PCR in a Quant Studio 6 Flex real-time PCR instrument (Thermo Fisher Scientific, China). The primers used for qRT-PCR are listed in **Table 2**.

Immunofluorescence Microscopy

Brain samples from left hemispheres were fixed in the 4% paraformaldehyde and embedded in OCT-freeze medium after sucrose cryoprotection. Brain tissues were sectioned in 25 μm thick using a cryostat (CM 1950; Germany). For the immunofluorescence assay, sections were blocked using 5% goat serum in TBS at RT for 30 min followed by the incubation with rabbit Iba-1 (Proteitech, United States) and mouse CD68 (BioLegend, United States) antibodies at 4°C overnight. After 3 washes with TBST, the sections were further incubated with corresponding secondary antibodies (Immunoway Biotech, China). After 3 times rinsing, sections were mounted with Dapi+ Fluorsave mounting medium (Calbiochem, United States).

Primary microglia cells were with 4% paraformaldehyde and permeabilized with 0.2% Triton X-100 in PBS. After washing, cells were blocked followed by incubation with rabbit anti-vimentin or mouse anti-paxillin at 4°C overnight. After incubation with corresponding secondary antibody, cells were washed and mounted.

For phagocytosis assay, 1 μl Alexa594-labeled latex beads (Thermo Fisher) were added to the new cell culture medium to replace the previous medium. The primary microglia cells were fixed and F-actin was visualized with Alexa 488 labeled phalloidin. The images were documented using a Nikon A1$^+$ microscope system.

Statistical Analysis

All the data were analyzed using Prism 8 Software. SPT, FST, SLAT and training day's data in MWM were analyzed using two-way ANOVA. The rest experiments were analyzed using one-way ANOVA and Tukey correction for multiple testing between categories. $P < 0.05$ was considered as statistically significant.

RESULTS

SLDS Attenuated the Depressive Symptoms in Chronic Stress Exposed Mice.

To determine whether SLDS treatment has the effects on the depressive symptoms of chronic stress induced mice, randomly grouped mice were left untreated (control group), subjected to unpredictable stress (stress + vehicle group) or injected with SLDS during stress challenge (stress + SLDS group). After 28 days, there was no significant difference in mice body weight among three groups (**Figure 1B**). And then three behavioral tests, FST, MWM and OFT were performed to evaluate the therapeutic effects (**Figure 1A**).

In FST, the results showed that there was no statistically significant difference in immobility time among three groups before the chronic stress procedure. However, the immobility time was significantly increased in mice of the stress group after four weeks of chronic stress procedure. In contrast, the duration of immobility in stress+ SLDS group was half less than that of the stress group (**Figure 1C**). These results suggested that SLDS might exhibit antidepressant-like activity.

Subsequent OFT results showed that the total distance of motion was reduced in mice exposed to chronic stress for four weeks, and tendency of motionlessness was increased compared to that of the control group (p <0.05). While in SLDS treatment group, the movement distance and location preference of mice were comparable to that of the control group (**Figures 1D–G**). These results suggested that chronic stress could induce locomotor activity decrease and SLDS might ameliorate the symptoms significantly.

After OFT, the spatial learning and memory abilities of mice had been monitored with MWM. Results showed that the stress group had a significantly longer path length and increased escape latency compared to the control group during the consecutive 6 training days. However, in SLDS treated group, the path length and escape latency were significantly decreased (**Figures 1H,I**). On the 7th day, when probe trials were conducted to evaluate the spatial memory abilities, the stress group had a lower frequency of swimming around the original platform position. On the contrary, the stress + SLDS group showed a significantly increased swimming time in the target quadrant and increased frequency in swimming across the original platform position (**Figures. 1K,L**). These results indicated that SLDS treatment significantly improved the impaired spatial learning and memory caused by chronic stress.

However, for SPT there were no significant difference among all three groups (data were not shown). It might be due to the long-term water deprivation and high temperature environment which resulted in the drinking behavioral alteration. Meanwhile, to examine whether the increased activity of SLDS treated group in FST and MWM was due to a locomotor activity stimulating effect from SLDS, we conducted spontaneous locomotor activity test. The results showed no statistically difference between control group and SLDS alone group, excluding the possibility that the improved behavior in SLDS treated mice was caused by an increase in locomotor activity (**Figure 1M**).

SLDS Suppressed Microglial Activation and Pro-Inflammatory Cytokines Release in Hippocampus of Chronic Stress Exposed Mice.

In order to visualize and quantify the activated microglia in hippocampus, cryosections of hippocampus from different groups were labeled with Iba1 and CD68. There were no significant differences in the amount of Iba-1 positive microglia cells among all three groups (**Figures 2A,B**). However, after SLDS treatment, the amount of CD68 positive activated microglia cells was significantly reduced compared with the stress group, indicating that the SLDS suppressed microglial activation (**Figures 2A,C**).

Next, we investigated whether SLDS attenuated pro-inflammatory cytokines release in the hippocampus of chronic stress induced mice. Quantitative RT-PCR results revealed that the mRNA levels of IL-1β, IL-6, IL-18 and TNF-α were significantly enhanced in stress group compared with those of control (**Figure 2D**, p <0.05). On the contrary, the expression levels of these pro-inflammatory cytokines were significantly reduced after SLDS treatment. Then the expression of IL-1β, IL-6, IL-18 and TNF-α in a protein level was evaluated by using ELISA assay. Consistent with the results of qRT-PCR, the protein levels of IL-1β, IL-6, IL-18 and TNF-α were significantly enhanced in stress group compared to those of control, while SLDS treatment significantly attenuated their expression (**Figure 2E**, p <0.05).

SLDS Inhibited Inflammatory Pathway Signaling in Hippocampus of Chronic Stress Exposed Mice.

To further determine whether SLDS attenuates inflammatory response in the chronic stress induced mice and reveal the underlying mechanism, we examined the activation of p42/p44

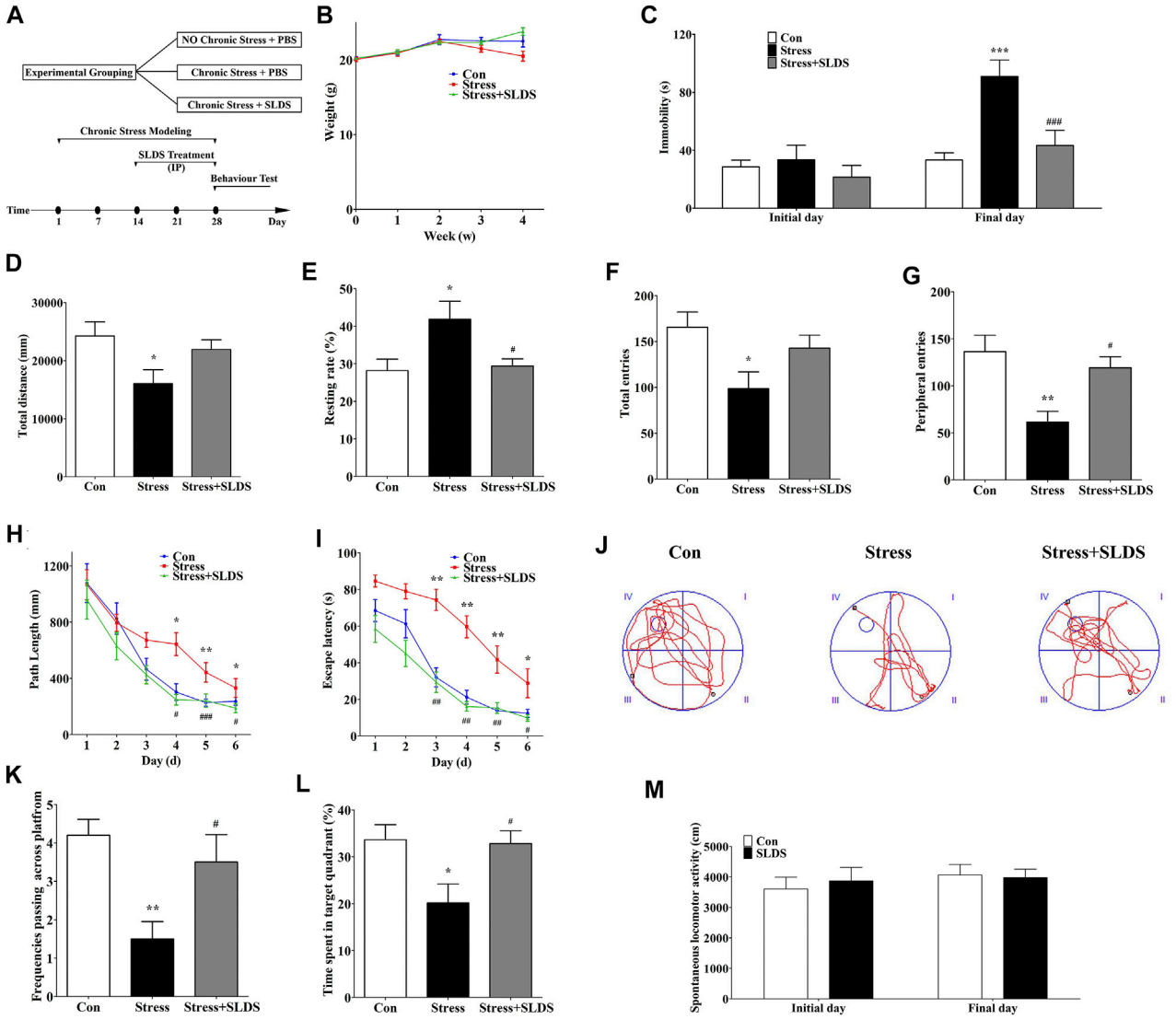

FIGURE 1 | SLDS attenuated the depressive symptoms in chronic stress exposed mice. **(A)** The timeline for chronic stress induction, SLDS treatment, and behavior evaluation (FST, MWM and OFT); **(B)** The body weight measurements during four weeks chronic stress exposure; **(C)** The duration of immobility in FST (Source of variation: interaction $F(2, 54) = 4.861$, $P = 0.0114$, treatment factor $F(2, 54) = 8.296$, $P = 0.0007$, initial/final days comparison $F(1, 54) = 15.67$, $P = 0.0002$; **(D)** The total path length distance in OFT [$F(2,27) = 3.752$, $P = 0.0365$]; **(E)** The rate of mice motionless in OFT [$F(2,27) = 4.825$, $P = 0.0158$]; **(F)** The total number of entries in OFT [$F(2,27) = 4.332$, $P = 0.0233$]; **(G)** The number of peripheral entries in OFT [$F(2,27) = 8.076$, $P = 0.0018$]; **(H)** The path length of mice during the navigation test of MWM (Source of variation: interaction $F(10, 208) = 1.407$, $P = 0.179$, Treatment factor $F(2, 208) = 13.68$, $P < 0.0001$, Days factor $F(5, 208) = 21.15$, $P < 0.0001$); **(I)** The escape latency of mice during the navigation test of MWM (Source of variation: interaction $F(10, 208) = 1.554$, $P = 0.1226$, Treatment factor $F(2, 208) = 56.55$, $P < 0.0001$, Days factor $F(5, 208) = 39.05$, $P < 0.0001$); **(J)** Representative diagram in the probe trial in MWM; **(K)** The frequency of passing across the virtual platform in MWM [$F(2,27) = 6.577$, $P = 0.0047$]; **(L)** The time spent in target quadrant at 7th day trial in MWM [$F(2,27) = 5.062$, $P = 0.0136$]; **(M)** The locomotor activity in SLAT (Source of variation: interaction $F(1, 36) = 0.2360$, $P = 0.6301$, treatment factor $F(1, 36) = 0.0526$, $P = 0.8198$, initial/final day comparison $F(1, 36) = 0.5920$, $P = 0.4467$. All data are presented as mean ± SD (n = 10/group). * $P < 0.05$, ** $P < 0.01$, compare to control group; # $P < 0.05$ ## $P < 0.01$ ###$P < 0.005$, compare to stress group.

MAPK (ERK1/2), p38 MAPK, NF-κB and iNOS. Activation of ERK1/2, p38 MAPK and NF-κB have been highly cited in activated microglia. It is also an important pathway to activate neuroinflammation. The activation state of ERK1/2, p38 MAPK, NF-κB and the expression level of iNOS were analyzed by Western blotting. Our results showed that chronic stress increased the phosphorylation of ERK1/2, p38 MAPK, NF-κB p65 in the mice hippocampus area, which was prohibited in the SLDS treated group (**Figures 2F–H**). iNOS is an inducible nitric oxide synthase that is induced after brain injury and neuroinflammation. It also has been reported as the downstream product of the p38 MAPK signaling pathway (Yoshida et al., 2020). In this study, the upregulated iNOS expression induced by stress

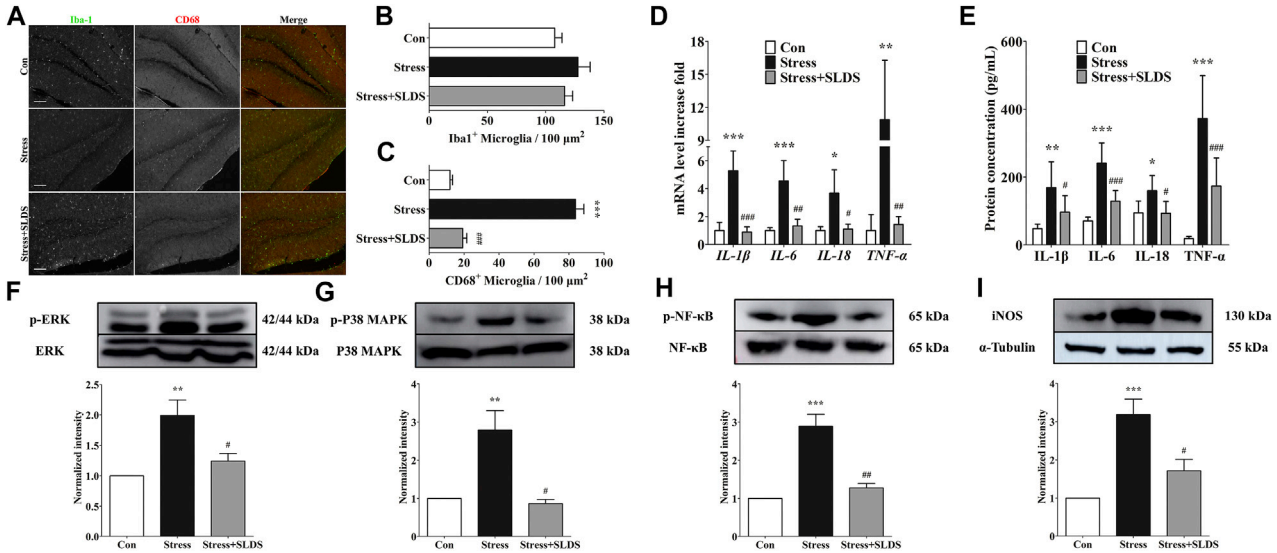

FIGURE 2 | SLDS suppressed microglia activation and pro-inflammatory cytokines release in hippocampus of chronic stress exposed mice. **(A)** Representative images illustrating microglia stained with Iba-1 and CD68 antibodies in hippocampal sections. Scale bar, 100 μm; **(B)** Number of Iba-1 positive microglia in hippocampal sections [$F(2,27) = 1.515$, $P = 0.2568$]; **(C)** Number of CD68 positive microglia in hippocampal sections [$F(2,27) = 151.9$, $P < 0.0001$]; **(D)** mRNA level of IL-1β [$F(2,9) = 35.23$, $P < 0.0001$], IL-6 [$F(2,9) = 19.28$, $P = 0.0006$], IL-18 [$F(2,9) = 9.481$, $P = 0.0061$] and TNF-α [$F(2,9) = 12.61$, $P = 0.0025$] in hippocampus determined by qRT-PCR ($n = 4$); **(E)** The secretion level of IL-1β [$F(2,15) = 8.063$, $P = 0.0042$], IL-6 [$F(2,15) = 29.19$, $P < 0.0001$], IL-18 [$F(2,15) = 5.890$, $P = 0.0129$] and TNF-α [$F(2,15) = 24.66$, $P < 0.0001$] in hippocampus determined using ELISA ($n = 4$); **(F)** P-ERK1/2 [$F(2,9) = 10.15$, $P = 0.0049$] in hippocampal area tissue; **(G)** P-p38 MAPK [$F(2,12) = 13.05$, $P = 0.0010$] in hippocampal area tissue; **(H)** P-p65 NF-κB [$F(2,15) = 28.59$, $P < 0.0001$] in hippocampal area tissue; **(I)** iNOS expression [$F(2,15) = 14.42$, $P = 0.0003$] in hippocampal area tissue. All data are presented as mean ± SD. * $P < 0.05$, ** $P < 0.01$, *** $P < 0.005$, compare to control group; # $P < 0.05$, ## $P < 0.01$, ### $P < 0.005$, compare to stress group.

challenge was also attenuated by SLDS (**Figure 2I**). These data indicated that inflammation-related signaling pathways were most likely inhibited by SLDS treatment after exposure to chronic stress.

SLDS Reduced the Levels of Proinflammatory Cytokines in LPS Induced Primary Microglia.

In order to further examine whether SLDS has the same beneficial effects towards LPS insulting *in vitro*, primary microglia was cultured and stimulated by LPS. The cytotoxicity of SLDS on primary microglia were firstly evaluated. Different concentrations (0, 50, 100 and 200 μM) of SLDS with or without LPS 1 μg/ml were used to treat primary microglia and the survival rate of cells was determined. It showed that SLDS had no cytotoxicity in primary microglia at settled concentrations (**Figures 3A,B**). Then the effects of a relatively low concentration of SLDS on the expression and release of proinflammatory cytokines in LPS induced inflammatory response were investigated. qRT-PCR results showed that SLDS significantly reduced mRNA expression of IL-1β, IL-6, IL-18 and TNF-α (**Figure 3C**, $p < 0.05$). ELISA results also revealed a reduction in secreted IL-1β, IL-6, IL-18 and TNF-α upon SLDS treatment (**Figure 3D**). It could be concluded that SLDS exhibited anti-proinflammatory effects on LPS induces inflammatory responses in primary microglia.

SLDS Decreased LPS Induced Inflammation Through Prohibiting the Same Pathway in Primary Microglia.

Previous studies revealed p38 MAPK, ERK1/2 and NF-κB signaling is an important pathway in the transcriptional regulation of proinflammatory cytokines (Xiao et al., 2002; Dong et al., 2014), and iNOS involves in nitric oxide secretion. Given the beneficial effects of SLDS on LPS induced inflammatory response of primary microglia, it was wondered whether SLDS could prohibit the inflammatory signaling pathway in primary microglia as same as the brain tissue sample. In this study, Western blotting assay for phosphorylation of ERK1/2, p38 MAPK, NF-κB and expression level of iNOS had been performed. The results revealed that SLDS significantly attenuated activation of ERK1/2, p38 MAPK, NF-κB and expression level of iNOS in LPS-stimulated primary microglia (**Figures 3E–G**), which were consistent with the results that were found in chronic stress exposed mice.

SLDS Inhibits Microglial Morphological Alterations and Phagocytic Ability in LPS Induced Primary Microglia.

In order to determine morphological alterations in microglial cells upon LPS challenging, the length of vimentin filaments was

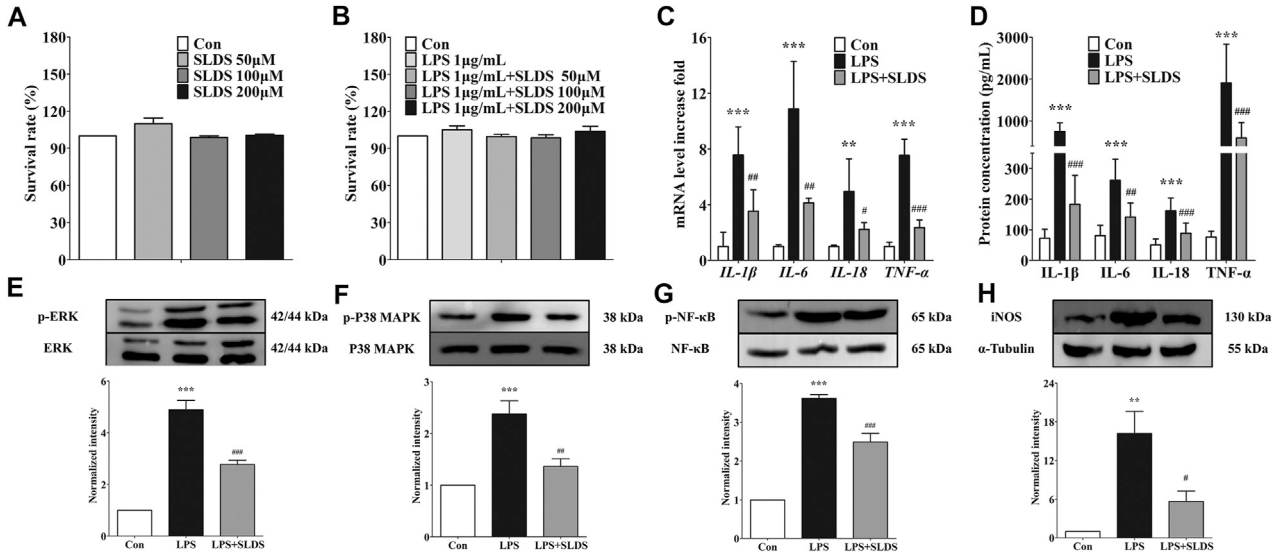

FIGURE 3 | SLDS reduced the levels of proinflammatory cytokines and suppressed microglial activation in LPS induced primary microglia. **(A)** The cell viability with SLDS (0, 50, 100 and 200 μM) alone [$F(3,12) = 1.524$, $P = 0.2588$] in primary microglia; **(B)** The cell viability with SLDS (0, 50, 100 and 200 μM) and LPS 1 μg/ml [$F(4,31) = 0.6963$, $P = 0.6003$] in primary microglia; **(C)** mRNA levels of IL-1β [$F(2,9) = 17.54$, $P = 0.0008$], /L-6 [$F(2,9) = 25.80$, $P = 0.0002$], IL-18 [$F(2,9) = 8.516$, $P = 0.0084$] and TNF-α [$F(2,9) = 81.80$, $P < 0.0001$] in primary microglia ($n = 4$); **(D)** The secretion levels of IL-1β [$F(2,21) = 57.51$, $P = < 0.0001$], IL-6 [$F(2,21) = 19.17$, $P < 0.0001$], IL-18 [$F(2,21) = 21.64$, $P < 0.0001$] and TNF-α [$F(2,21) = 23.71$, $P < 0.0001$] in primary microglia ($n = 4$); *(E)* P-ERK1/2 [$F(2,15) = 72.91$, $P < 0.0001$] in primary microglia; **(F)** P-p38 MAPK [$F(2,12) = 17.38$, $P = 0.0003$] in primary microglia; **(G)** P-p65 NF-κB [$F(2,9) = 86.64$, $P < 0.0001$] in primary microglia; **(H)** iNOS expression [$F(2,11) = 12.46$, $P = 0.0015$] in primary microglia. All data are presented as mean ± SD. ** P <0.01, ***P <0.005, compare to control group; # $P < 0.05$ ## P <0.01 ###$P < 0.005$, compare to LPS treated group.

determined, which were in parallel to the longitudinal axis of primary microglia cells. The results showed that the length of vimentin filaments was significantly shortened in LPS induced primary microglia, which resulted in the changes in cell shape and size (**Figures 4A,B**). However, SLDS significantly reduced the loss of vimentin filaments (**Figures 4A,B**, $p<0.05$).

We further wondered whether alterations in cell shape and size of microglia affected assembly of focal adhesions. The focal adhesion was examined using the paxillin, which was a component of focal adhesions in primary microglia. The amount of focal adhesions was significantly enhanced in LPS induced primary microglia, and in contrast, SLDS restored focal adhesion numbers comparable to a condition of the resting primary microglia, which was consistent with its inhibition of cell spreading (**Figures 4A,C**). Western blotting analysis showed SLDS suppressed the enhanced phosphorylation at Ser83 in paxillin induced by LPS in primary microglia (**Figure 4D**).

The morphological changes and cell adhesion of microglia cells might eventually affect their phagocytic activity. Therefore, we further examined whether the phagocytic ability of primary microglia was affected by SLDS after exposed to LPS by using fluorescent beads. Phagocytosis assay showed primary microglia exhibited stronger phagocytic ability after LPS stimulation, while SLDS could significantly diminish LPS induced phagocytic activity, which was consistent with morphology and adhesion analysis results (**Figures 4E,F**).

SLDS Prevented Neuronal Apoptosis in Chronic Stress Exposed Mice and Decreased Microglial Neurotoxicity in PC12 Cells.

Microglial activation induced by chronic stress causes neuronal apoptosis. In apoptotic cells, compaction, condensation and segregation of the nuclear chromatin appear. We used Dapi staining to determine whether SLDS could reduce neuronal apoptosis. The immunofluorescence microscopy assay revealed that SLDS could distinctly reduce the amount of apoptotic nucleus in hippocampus of chronic stress exposed mice (**Figures 5A,B**). To further conform this effect of SLDS, we cultured PC12 cells with CM derived from primary microglia cultures to detect the microglial neurotoxicity. A CCK-8 kit was used to detect whether SLDS exhibited cytotoxicity to PC12 cells. The results showed that SLDS exhibited no cytotoxicity in PC12 cells at the detected concentrations (**Figures 5C,D**). It showed that the viability of PC12 cells was significantly increased in CM from primary microglia cultures with SLDS pretreatment (**Figure 5E**). Furthermore, flow cytometry assay with Annexin V/PI staining was used to evaluate neuroprotective properties of SLDS. Results showed that CM from primary microglia cultures pretreated with SLDS significantly reduced apoptosis in PC12 cells (**Figures 5F,G**). In conclusion, SLDS might achieve neuroprotective functions by inhibiting microglial activation.

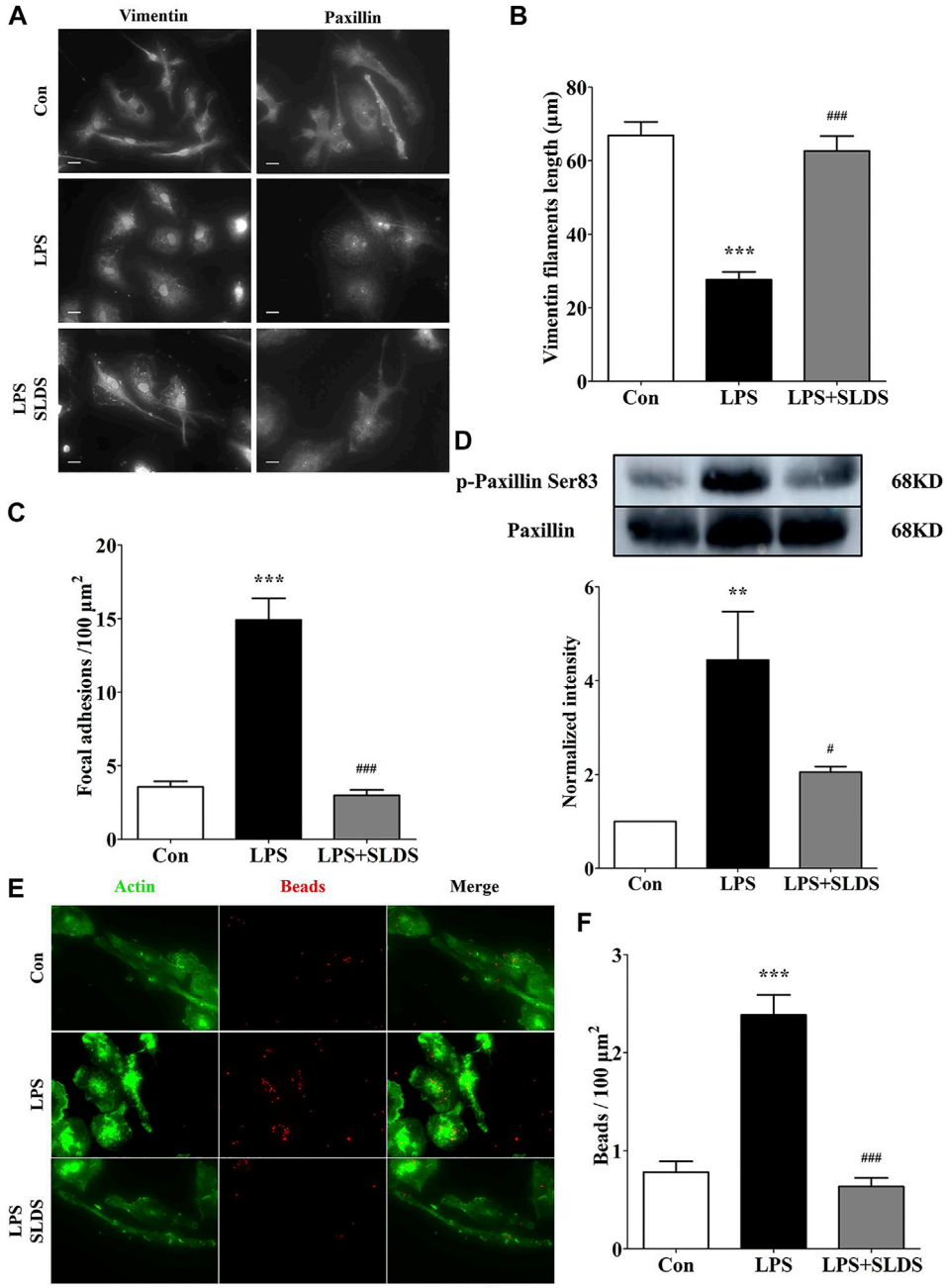

FIGURE 4 | SLDS inhibited microglial morphological alterations and phagocytic ability in LPS induced primary microglia. **(A)** Representative images illustrating primary microglia stained with vimentin and paxillin antibodies, scale bar: 10 μm; **(B)** The length of vimentin filaments in primary microglia [$F(2,60) = 39.11$, $P < 0.0001$]; **(C)** The number of focal adhesions in primary microglia [$F(2,36) = 55.93$, $P < 0.0001$]; **(D)** P-paxillin at Ser83 [$F(2,9) = 8.705$, $P = 0.0079$] in primary microglia; **(E)** Representative images illustrating microglial phagocytosis; **(F)** The number of beads engulfed by primary microglia [$F(2,59) = 35.24$, $P < 0.0001$]. All data are presented as mean ± SD. ** P <0.01, ***P <0.005, compare to control group; # $P < 0.05$, ###$P < 0.005$, compare to LPS treated group.

DISCUSSION

In this study, we illustrated that SLDS treatment relieved the depressive symptoms induced via unpredictable chronic stress in mice and reduced the amount of deleterious activated microglia (CD68 positive) in hippocampus. It was found that SLDS treatment inactivated ERK1/2, p38 MAPK, NF-κB signaling, suppressed iNOS expression, and caused impaired phagocytosis and reduced the expression and release of pro-inflammatory cytokines (**Figure 6**). These findings underpinned a possible molecular mechanism that underlies the beneficial effects of SLDS in relieving the behavioral and cognitional disorders in a depressive mouse

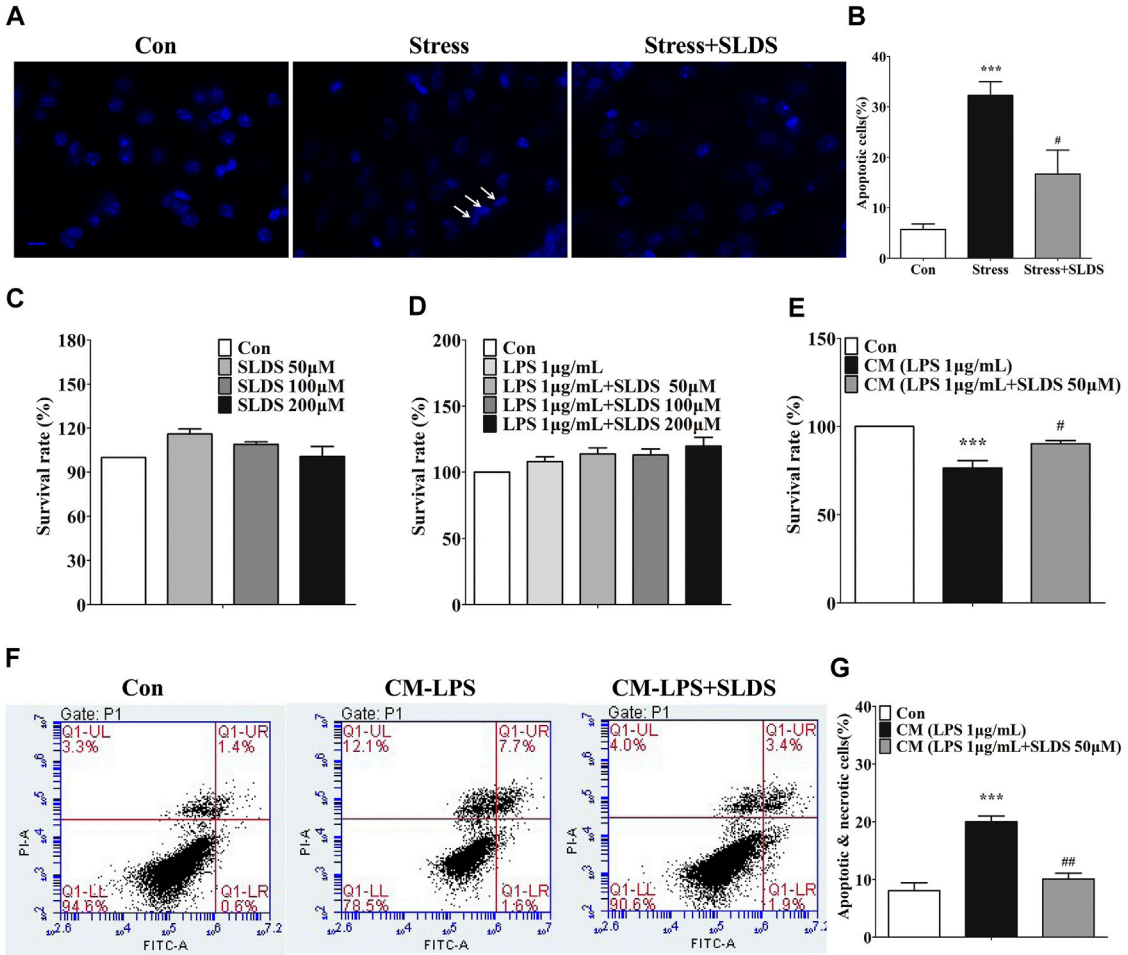

FIGURE 5 | SLDS prevented neuronal apoptosis in chronic stress exposed mice and decreased microglial neurotoxicity in PC12 cells. **(A)** Representative images illustrating apoptotic cells in hippocampal sections, scale bar: 10 μm; **(B)** Quantification of apoptotic cells in the hippocampus of mice [$F(2,13) = 18.20$, $P = 0.0002$]. All data are presented as mean ± SD. ***P <0.005, compare to control group; #P <0.05, compare to stress group. **(C)** The cell viability for PC12 cells treated with SLDS (0, 50, 100 and 200 μM) alone [$F(3,8) = 3.611$, $P = 0.0650$]; **(D)** The cell viability for PC12 cells treated with SLDS (0, 50, 100 and 200 μM) and LPS 1 μg/ml [$F(4,10) = 2.766$, $P = 0.0874$]; **(E)** The cell viability for PC12 cells treated with CM [$F(2,13) = 18.20$, $P = 0.0002$]; **(F)** Representative images illustrating the flow cytometry analysis for PC12 cells; **(G)** The percentage of apoptotic and necrotic PC12 cells assessed using flow cytometry analysis [$F(2,9) = 19.79$, $P = 0.0005$]. All data are presented as mean ± SD. ***P <0.005, compare to control group; ##P <0.01, ###P < 0.005, compare to CM-LPS group.

model, and therefore lying a foundation for the therapeutic opportunity of SLDS in treating depression.

Unpredictable chronic stresses have been reported as a promising method to cause a series of depressive behaviors in rodents (Farooq et al., 2012; Nollet et al., 2013; Willner 2017). In the present study, the depressive mouse model was generated using this method and depressive symptoms were assessed by using FST, MWM and OFT. For studies using all kinds of depressive animal models, FST is still one of the most commonly used assay for screening antidepressants in preclinical studies (Petit-Demouliere et al., 2005). MWM has been well defined to examine spatial memory and cognition, while OFT has been widely used to evaluate locomotivity and anxiety levels (Jin et al., 2019; Zhang N., et al., 2020). Consistent with previous researches, our results confirmed that the exposure to unpredictable chronic stress leads to a significant memory loss and volitional activity decline (Gouirand and Matuszewich 2005; Hu et al., 2015; Trofimiuk and Braszko 2015; Li et al., 2017). In recent years, studies have revealed that during pathological process, microglia plays an important role in the destruction of neural plasticity and has deleterious effects on neuroprotection, leading to neuroinflammation and aggravation of depression (Singhal and Baune 2017). Moreover, many drugs fulfill their antidepressant function through regulating the activation of microglia and anti-neuroinflammation in preclinical studies (Han et al., 2019; Feng et al., 2020; Vega-Rivera et al., 2020). These findings emphasized the importance of modulating microglia activity for interfering nervous system disorders.

Salidroside, a phenolic glycosides compound extracted from *Rhodiola rosea*, has been reported in possession of neuroprotective properties (Liu et al., 2018; Wang C., et al., 2018). Researchers also showed that SLDS could suppress

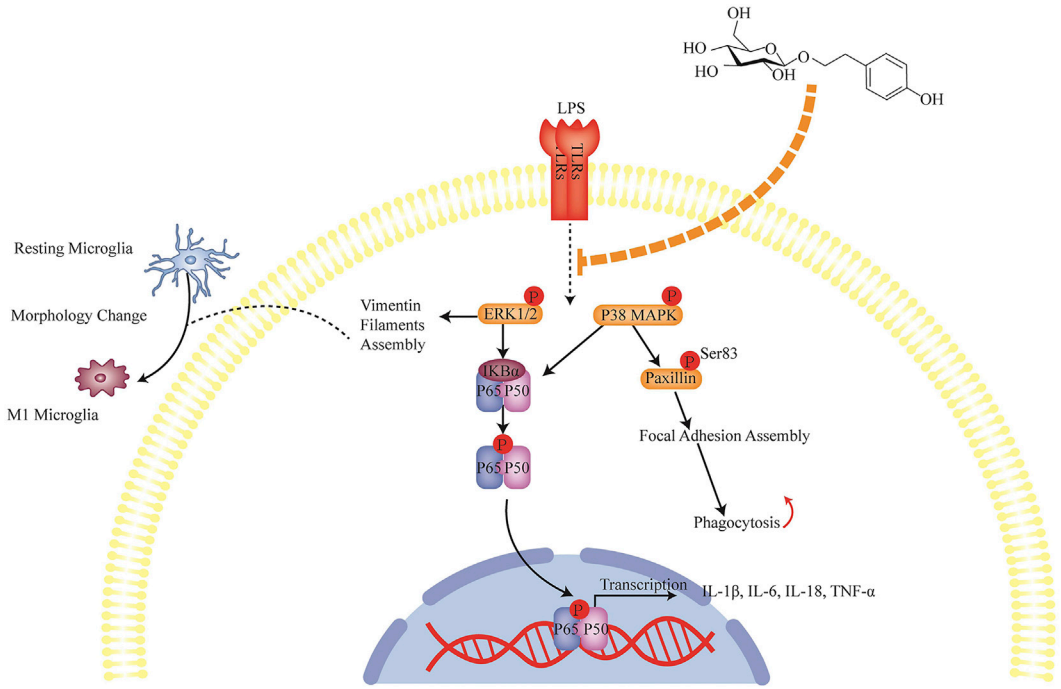

FIGURE 6 | Anti-inflammation mechanism of SLDS in LPS induced primary microglia. LPS signal from infections activates microglia through TLRs and further activates ERK1/2, p38 MAPK, NF-κB signaling. Signals translocate to nucleus and induce the transcription of inflammatory cytokines IL-1β, IL-6, IL-18 and TNF-α. On the other hand, cytoskeleton changes generate the mechanical forces that drive cell motility and phagocytosis which are closely associated with microglial function. LPS signals induce the cytoskeleton protein vimentin filaments assembly which leads to the morphological changes from ramified state to ameboid state. Meanwhile, they regulate focal adhesion assembly which results in the cell attachment state alteration. SLDS can inhibit the LPS signals transduction thus blocking the activation of microglia and prevent cytoskeleton changes.

inflammatory cytokines release and improved depressive symptoms (Vasileva et al., 2018). However, the underlying molecular mechanism remained unclear. In the pathological process, microglia participates in the immune response by migrating to the pathological area and activating itself to fulfill its functions (Domercq et al., 2013). In this study, it was found that SLDS treatment shared a molecular mechanism similar to many other drugs that regulates microglia activation and anti-neuroinflammation. In addition, we also proposed another molecular mechanism in which SLDS might promote anti-depression by altering the morphology and attachment state of microglia and therefore avoid their enrichment in pathological areas.

Microglia, a type of glial cell that is equivalent to macrophages in the brain and spinal cord, is the first and most important immune defense of the CNS. They normally exist in a resting ramified state and become activated in response to different stimuli. Microglia is of great importance in immune defender in the brain by eliminating apoptotic debris and pathogen (Beyer et al., 2000; Gogoleva et al., 2019). Stimulation of microglia by LPS or colony-stimulating factor (CSF) results in an increased expression of CD68, a lysosomal protein, representing a hallmark for M1 phenotype microglia (Lei et al., 2020). Up-regulated CD68 expression in microglia has also been observed in various kinds of neurological diseases, such as Parkinson's disease, Alzheimer's disease, Pelizaeus-Merzbacher disease and brain tumor, which involves in neurodegeneration, neuronal death and neuroinflammation (Aronica et al., 2005; Bachstetter et al., 2013; Bachstetter et al., 2015; Aono et al., 2017). Indeed, the elevated amount of CD68 positive microglia in hippocampus has been observed after chronic stress exposure, indicative of a possible proinflammatory response. We observed that SLDS exhibited strong anti-inflammatory effects by decreasing the CD68 positive microglia cells in hippocampus after chronic stress exposure in mice.

Activated microglia (M1 phenotype) can produce a wide scope of proinflammatory cytokines, such as IL-1β, IL-6, IL-18, TNF-α and other mediators, which eventually induce neuronal damage (Jin et al., 2019; Lajqi et al., 2020). Assessed using ELISA assays and qRT-PCR, the expression levels of cytokines IL-1β, IL-6, IL-18, and TNF-α in hippocampus tissue after chronic stress are increased in a manner similar to that in LPS induced primary microglia, suggesting a robust immune response induced in both model systems. SLDS suppressed the levels of IL-1β, IL-6, IL-18 and TNF-α both *in vitro* and *in vivo*. Interestingly, toxicological tests showed that LPS did not inhibit the proliferation of primary microglia as it does in BV_2 microglia (Lee et al., 2012), suggesting possible physiological differences between BV_2 microglia cells and primary microglia (Fukushima et al., 2015). In addition, the aged microglia cells also showed differences in response to the chemicals, indicating effects of differentiation status of the cells (Perry

et al., 1993). In this study, the results newly uncovered that SLDS might be a potential natural product to inhibit microglial activation and neuroinflammation.

SLDS exhibits its anti-neuroinflammation properties by altering many aspects of microglial activation, such as changes in microglial morphology and the secretion of inflammatory cytokines. In our efforts to illustrate the molecular mechanism of SLDS anti-neuroinflammation effects, it was found that SLDS inhibited the phosphorylation of ERK1/2, p38 MAPK, NF-κB p65 and expression level of iNOS in both chronic stress exposed mice and LPS induced primary microglia. Modulation of NF-κB p65 activity by SLDS has been widely reported (Hu H et al., 2014; Wang et al., 2017). Our findings were consistent with previous results that inactivation of ERK1/2, NF-κB p65 and PI3K/Akt by SLDS, led to the reduction of iNOS and Cyclooxygenase-2 (COX-2) expression (Hu H et al., 2014; Wang et al., 2017; Wang, J et al., 2018). Activation of p38 MAPK has been revealed to regulate microglia morphological changes and phagocytic ability (Fan et al., 2018; Yao and Fu 2020). Therefore, we investigated the effect of SLDS on microglial morphological alterations and phagocytic ability. It was observed that the length of vimentin filaments was significantly shortened in LPS induced primary microglia, consistent with many other studies on activated microglial morphology. In activated microglia, cells become more flattened and loss branches (Kloss et al., 2001; Tynan et al., 2010). Focal adhesions assembling involves in cell attachment and phagocytic ability. With paxillin, a component of focal adhesion as the marker, SLDS was found to disassemble the focal adhesion which is assembled after LPS stimulation, indicating the blockage of microglia spreading. Phagocytic activity has been reported to be regulated by paxillin and cofilin (Gitik et al., 2014). SLDS can significantly attenuated LPS induce phagocytic activity. In this study, chronic stress model for depressive symptoms shares similar properties as LPS induced primary microglia. And a certain number of studies also revealed both chronic stress and LPS challenges induced distinct molecular and behavioral changes in mice (Espinosa-Oliva et al., 2011; Couch et al., 2016). For instance, Toll-like receptors (TLRs) play an important role in this depressive behavioral changes (Habib et al., 2015; Zhang.W., et al., 2020). Further studies are needed to address whether antidepressant effects of SLDS also affects TLRs pathway. In conclusion, our data demonstrated that SLDS could prevent the deleterious M1 microglial activation, and improve the depressive symptoms caused by unpredictable chronic stress. This study suggested a potential application of SLDS in therapeutic treatment of depression.

DATA AVAILABILITY STATEMENT

The raw data supporting the conclusions of this article will be made available by the authors, without undue reservation.

ETHICS STATEMENT

The animal study was reviewed and approved by the Institutional Animal Care and Use committee of Institute of Radiation Medicine, Chinese Academy of Medical Sciences.

AUTHOR CONTRIBUTIONS

YF and YB. performed experiments and analyzed the data. YF and HC conceived the experiments, analyzed the data and wrote the paper.

FUNDING

This work was supported by a grant from Double First Plan of Tianjin University (No. 2900903075103)

ACKNOWLEDGMENTS

We thank members of HC's lab for useful discussions and critical reading of the manuscript. We are indebted to Youcai Zhang for helpful discussions and Huiyuan Wu for critical reading of the manuscript.

SUPPLEMENTARY MATERIAL

The Supplementary Material for this article can be found online at: https://www.frontiersin.org/articles/10.3389/fphar.2021.635762/full#supplementary-material

REFERENCES

Ahmed, S., Kwatra, M., Ranjan Panda, S., Murty, U. S. N., and Naidu, V. G. M. (2021). Andrographolide Suppresses NLRP3 Inflammasome Activation in Microglia through Induction of Parkin-Mediated Mitophagy in In-Vitro and In-Vivo Models of Parkinson Disease. *Brain Behav. Immun.* 91, 142–158. doi:10.1016/j.bbi.2020.09.017

Aono, H., Choudhury, M. E., Higaki, H., Miyanishi, K., Kigami, Y., Fujita, K., et al. (2017). Microglia May Compensate for Dopaminergic Neuron Loss in Experimental Parkinsonism through Selective Elimination of Glutamatergic Synapses from the Subthalamic Nucleus. *Glia* 65 (11), 183–1847. doi:10.1002/glia.23199

Aronica, E., Gorter, J. A., Redeker, S., Ramkema, M., Spliet, W. G. M., van Rijen, P. C., et al. (2005). Distribution, Characterization and Clinical Significance of Microglia in Glioneuronal Tumours from Patients with Chronic Intractable Epilepsy. *Neuropathol. Appl. Neurobiol.* 31 (3), 280–291. doi:10.1111/j.1365-2990.2004.00636.x

Bachstetter, A. D., Van Eldik, L. J., Schmitt, F. A., Neltner, J. H., Ighodaro, E. T., Webster, S. J., et al. (2015). Disease-related Microglia Heterogeneity in the hippocampus of Alzheimer's Disease, Dementia with Lewy Bodies, and Hippocampal Sclerosis of Aging. *Acta Neuropathol. Commun.* 3, 32. doi:10.1186/s40478-015-0209-z

Bachstetter, A. D., Webster, S. J., Van Eldik, L. J., and Cambi, F. (2013). Clinically Relevant Intronic Splicing Enhancer Mutation in Myelin Proteolipid Protein Leads to Progressive Microglia and Astrocyte Activation in white and gray

Matter Regions of the Brain. *J. Neuroinflammation* 10, 146. doi:10.1186/1742-2094-10-146

Bassett, B., Subrmaniyam, S., Fan, Y., Varney, S., Pan, H., Carneiro, A. M. D., et al. (2021). Minocycline Alleviates Depression-like Symptoms by Rescuing Decrease in Neurogenesis in Dorsal hippocampus via Blocking Microglia Activation/phagocytosis. *Brain Behav. Immun.* 91, 519–530. doi:10.1016/j.bbi.2020.11.009

Beyer, M., Gimsa, U., Eyüpoglu, I. Y., Hailer, N. P., and Nitsch, R. (2000). Phagocytosis of Neuronal or Glial Debris by Microglial Cells: Upregulation of MHC Class II Expression and Multinuclear Giant Cell Formation In Vitro. *Glia* 31 (3), 262–266. doi:10.1002/1098-1136(200009)31:3<262:aid-glia70>3.0.co;2-2

Colombo, M., Broadbent, N. J., Taylor, C. S. R., and Frost, N. (2001). The Role of the Avian hippocampus in Orientation in Space and Time. *Brain Res.* 919 (2), 292–301. doi:10.1016/s0006-8993(01)03050-5

Couch, Y., Trofimov, A., Markova, N., Nikolenko, V., Steinbusch, H. W., Chekhonin, V., et al. (2016). Low-dose Lipopolysaccharide (LPS) Inhibits Aggressive and Augments Depressive Behaviours in a Chronic Mild Stress Model in Mice. *J. Neuroinflammation* 13 (1), 108. doi:10.1186/s12974-016-0572-0

Cryan, J. F., Markou, A., and Lucki, I. (2002). Assessing Antidepressant Activity in Rodents: Recent Developments and Future Needs. *Trends Pharmacol. Sci.* 23 (5), 238–245.

da Estrela, C., McGrath, J., Booij, L., and Gouin, J. P. (2020). Heart Rate Variability, Sleep Quality, and Depression in the Context of Chronic Stress. *Ann. Behav. Med.*, 1–10. doi:10.1093/abm/kaaa039

Deng, S.-l., Chen, J.-g., and Wang, F. (2020). Microglia: A Central Player in Depression. *Curr. Med. Sci.* 40 (3), 391–400. doi:10.1007/s11596-020-2193-1

Domercq, M., Vazquez-Villoldo, N., and Matute, C. (2013). Neurotransmitter Signaling in the Pathophysiology of Microglia. *Front Cel Neurosci.* 7, 49. doi:10.3389/fncel.2013.00107

Dong, N., Chang, L., Wang, B., and Chu, L. (2014). Retinal Neuronal MCP-1 Induced by AGEs Stimulates TNF-α Expression in Rat Microglia via P38, ERK, and NF-Kb Pathways. *Mol. Vis.* 20, 616–628.

Ellis, P., and Royal, A. D. (2004). New Zealand College of Psychiatrists Clinical Practice Guidelines Team forAustralian and New Zealand Clinical Practice Guidelines for the Treatment of Depression. *Aust. N. Z. J. Psychiatry* 38 (6), 389–407.

Espinosa-Oliva, A. M., de Pablos, R. M., Villarán, R. F., Argüelles, S., Venero, J. L., Machado, A., et al. (2011). Stress Is Critical for LPS-Induced Activation of Microglia and Damage in the Rat hippocampus. *Neurobiol. Aging* 32 (1), 85–102. doi:10.1016/j.neurobiolaging.2009.01.012

Fan, Y., Xie, L., and Chung, C. Y. (2017). Signaling Pathways Controlling Microglia Chemotaxis. *Mol. Cell* 40 (3), 163–168. doi:10.14348/molcells.2017.0011

Fan, Y., Chen, Z., Pathak, J. L., Carneiro, A. M. D., and Chung, C. Y. (2018). Differential Regulation of Adhesion and Phagocytosis of Resting and Activated Microglia by Dopamine. *Front. Cel Neurosci.* 12, 309. doi:10.3389/fncel.2018.00309

Farooq, R. K., Isingrini, E., Tanti, A., Le Guisquet, A.-M., Arlicot, N., Minier, F., et al. (2012). Is Unpredictable Chronic Mild Stress (UCMS) a Reliable Model to Study Depression-Induced Neuroinflammation?. *Behav. Brain Res.* 231 (1), 130–137. doi:10.1016/j.bbr.2012.03.020

Feng, X., Fan, Y., and Chung, C. Y. (2020). Mefenamic Acid Can Attenuate Depressive Symptoms by Suppressing Microglia Activation Induced upon Chronic Stress. *Brain Res.* 1740, 146846. doi:10.1016/j.brainres.2020.146846

Fukushima, S., Furube, E., Itoh, M., Nakashima, T., and Miyata, S. (2015). Robust Increase of Microglia Proliferation in the Fornix of Hippocampal Axonal Pathway after a Single LPS Stimulation. *J. Neuroimmunology* 285, 31–40. doi:10.1016/j.jneuroim.2015.05.014

Gao, J., Zhou, R., You, X., Luo, F., He, H., Chang, X., et al. (2016). Salidroside Suppresses Inflammation in a D-Galactose-Induced Rat Model of Alzheimer's Disease via SIRT1/NF-Kb Pathway. *Metab. Brain Dis.* 31 (4), 771–778. doi:10.1007/s11011-016-9813-2

Gitik, M., Kleinhaus, R., Hadas, S., Reichert, F., and Rotshenker, S. (2014). Phagocytic Receptors Activate and Immune Inhibitory Receptor SIRPalpha Inhibits Phagocytosis through Paxillin and Cofilin. *Front. Cel Neurosci.* 8, 104. doi:10.3389/fncel.2014.00104

Gogoleva, V. S., Drutskaya, M. S., and Atretkhany, K. S. (2019). [The Role of Microglia in the Homeostasis of the Central Nervous System and Neuroinflammation]. *Mol. Biol. (Mosk)* 53 (5), 790–798. doi:10.1134/s0026893319050054

Goshen, I., Kreisel, T., Ben-Menachem-Zidon, O., Licht, T., Weidenfeld, J., Ben-Hur, T., et al. (2008). Brain Interleukin-1 Mediates Chronic Stress-Induced Depression in Mice via Adrenocortical Activation and Hippocampal Neurogenesis Suppression. *Mol. Psychiatry* 13 (7), 717–728. doi:10.1038/sj.mp.4002055

Gouirand, A. M., and Matuszewich, L. (2005). The Effects of Chronic Unpredictable Stress on Male Rats in the Water Maze. *Physiol. Behav.* 86 (1-2), 21–31. doi:10.1016/j.physbeh.2005.06.027

Habib, M., Shaker, S., El-Gayar, N., and Aboul-Fotouh, S. (2015). The Effects of Antidepressants "fluoxetine and Imipramine" on Vascular Abnormalities and Toll like Receptor-4 Expression in Diabetic and Non-diabetic Rats Exposed to Chronic Stress. *PLoS One* 10 (3), e0120559. doi:10.1371/journal.pone.0120559

Han, Y., Zhang, L., Wang, Q., Zhang, D., Zhao, Q., Zhang, J., et al. (2019). Minocycline Inhibits Microglial Activation and Alleviates Depressive-like Behaviors in Male Adolescent Mice Subjected to Maternal Separation. *Psychoneuroendocrinology* 107, 37–45. doi:10.1016/j.psyneuen.2019.04.021

He, M.-c., Shi, Z., Sha, N.-n., Chen, N., Peng, S.-y., Liao, D.-f., et al. (2019). Paricalcitol Alleviates Lipopolysaccharide-Induced Depressive-like Behavior by Suppressing Hypothalamic Microglia Activation and Neuroinflammation. *Biochem. Pharmacol.* 163, 1–8. doi:10.1016/j.bcp.2019.01.021

Hu, B., Zou, Y., Liu, S., Wang, J., Zhu, J., Li, J., et al. (2014). Salidroside Attenuates Concanavalin A-Induced Hepatitis via Modulating Cytokines Secretion and Lymphocyte Migration in Mice. *Mediators Inflamm.* 2014, 314081. doi:10.1155/2014/314081

Hu, H., Zhang, Y., Xu, Y., Liu, C., and Wang, L. (2015). [Open-field Behavioral Study in Rat Hyperlipidemia Combined with Chronic Unpredictable Mild Stress Model]. *Zhonghua Yi Xue Za Zhi* 95 (23), 1854–1858.

Hu, H., Li, Z., Zhu, X., Lin, R., and Chen, L. (2014). Salidroside Reduces Cell Mobility via NF- Kappa B and MAPK Signaling in LPS-Induced BV2 Microglial Cells. *Evid. Based Complement. Alternat Med.* 2014, 383821. doi:10.1155/2014/383821

Huang, C., Borchers, C. H., Schaller, M. D., and Jacobson, K. (2004). Phosphorylation of Paxillin by p38MAPK Is Involved in the Neurite Extension of PC-12 Cells. *J. Cel Biol.* 164 (4), 593–602. doi:10.1083/jcb.200307081

Huang, Z., Fang, Q., Ma, W., Zhang, Q., Qiu, J., Gu, X., et al. (2019). Skeletal Muscle Atrophy Was Alleviated by Salidroside through Suppressing Oxidative Stress and Inflammation during Denervation. *Front. Pharmacol.* 10, 997. doi:10.3389/fphar.2019.00997

Ilic, D., Furuta, Y., Kanazawa, S., Takeda, N., Sobue, K., Nakatsuji, N., et al. (1995). Reduced Cell Motility and Enhanced Focal Adhesion Contact Formation in Cells from FAK-Deficient Mice. *Nature* 377 (6549), 539–544.

Jiang, Q., Chen, J., Long, X., Yao, X., Zou, X., Yang, Y., et al. (2020). Phillyrin Protects Mice from Traumatic Brain Injury by Inhibiting the Inflammation of Microglia via PPARγ Signaling Pathway. *Int. Immunopharmacology* 79, 106083. doi:10.1016/j.intimp.2019.106083

Jiang, X., Ni, Y., Liu, T., Zhang, M., Ren, H., and Xu, G. (2013). Inhibition of LPS-Induced Retinal Microglia Activation by Naloxone Does Not Prevent Photoreceptor Death. *Inflammation* 36 (1), 42–52. doi:10.1007/s10753-012-9518-6

Jin, X., Liu, M. Y., Zhang, D. F., Zhong, X., Du, K., Qian, P., et al. (2019). Baicalin Mitigates Cognitive Impairment and Protects Neurons from Microglia-mediated Neuroinflammation via Suppressing NLRP 3 Inflammasomes and TLR 4/ NF -κB Signaling Pathway. *CNS Neurosci. Ther.* 25 (5), 575–590. doi:10.1111/cns.13086

Kato, T., and Kanba, S. (2015). Conquering Depression. *Psychiatry Clin. Neurosci.* 69 (1), 1–2. doi:10.1111/pcn.12257

Kloss, C. U. A., Bohatschek, M., Kreutzberg, G. W., and Raivich, G. (2001). Effect of Lipopolysaccharide on the Morphology and Integrin Immunoreactivity of Ramified Microglia in the Mouse Brain and in Cell Culture. *Exp. Neurol.* 168 (1), 32–46. doi:10.1006/exnr.2000.7575

Laffer, B., Bauer, D., Wasmuth, S., Busch, M., Jalilvand, T. V., Thanos, S., et al. (2019). Loss of IL-10 Promotes Differentiation of Microglia to a M1 Phenotype. *Front. Cel Neurosci.* 13, 430. doi:10.3389/fncel.2019.00430

Lajqi, T., Stojiljkovic, M., Williams, D. L., Hudalla, H., Bauer, M., Witte, O. W., et al. (2020). Memory-Like Responses of Brain Microglia Are Controlled by Developmental State and Pathogen Dose. *Front. Immunol.* 11, 546415. doi:10.3389/fimmu.2020.546415

Leaw, B., Zhu, D., Tan, J., Muljadi, R., Saad, M. I., Mockler, J. C., et al. (2017). Human Amnion Epithelial Cells rescue Cell Death via Immunomodulation of Microglia in a Mouse Model of Perinatal Brain Injury. *Stem Cel Res Ther*. 8 (1), 46. doi:10.1186/s13287-017-0496-3

Lee, A. L., Ogle, W. O., and Sapolsky, R. M. (2002). Stress and Depression: Possible Links to Neuron Death in the hippocampus. *Bipolar Disord.* 4 (2), 117–128. doi:10.1034/j.1399-5618.2002.01144.x

Lee, K. W., Jung, S. Y., Choi, S. M., and Yang, E. J. (2012). Effects of Ginsenoside Re on LPS-Induced Inflammatory Mediators in BV2 Microglial Cells. *BMC Complement. Altern. Med.* 12, 196. doi:10.1186/1472-6882-12-196

Lei, F., Cui, N., Zhou, C., Chodosh, J., Vavvas, D. G., and Paschalis, E. I. (2020). CSF1R Inhibition by a Small-Molecule Inhibitor Is Not Microglia Specific; Affecting Hematopoiesis and the Function of Macrophages. *Proc. Natl. Acad. Sci. USA*. 117 (38), 23336–23338. doi:10.1073/pnas.1922788117

Li, Y., Cheng, K. C., Liu, K. F., Peng, W. H., Cheng, J. T., and Niu, H. S. (2017). Telmisartan Activates PPARdelta to Improve Symptoms of Unpredictable Chronic Mild Stress-Induced Depression in Mice. *Sci. Rep.* 7 (1), 14021. doi:10.1038/s41598-017-14265-4

Liu, J., Cai, J., Fan, P., Zhang, N., and Cao, Y. (2019). The Abilities of Salidroside on Ameliorating Inflammation, Skewing the Imbalanced Nucleotide Oligomerization Domain-like Receptor Family Pyrin Domain Containing 3/Autophagy, and Maintaining Intestinal Barrier Are Profitable in Colitis. *Front. Pharmacol.* 10, 1385. doi:10.3389/fphar.2019.01385

Liu, X., Wen, S., Yan, F., Liu, K., Liu, L., Wang, L., et al. (2018). Salidroside Provides Neuroprotection by Modulating Microglial Polarization after Cerebral Ischemia. *J. Neuroinflammation* 15 (1), 39. doi:10.1186/s12974-018-1081-0

Mitchell, P. B., and Malhi, G. S. (2004). Bipolar Depression: Phenomenological Overview and Clinical Characteristics. *Bipolar Disord.* 6 (6), 530–539. doi:10.1111/j.1399-5618.2004.00137.x

Nakagawa, Y., and Chiba, K. (2014). Role of Microglial M1/m2 Polarization in Relapse and Remission of Psychiatric Disorders and Diseases. *Pharmaceuticals* 7 (12), 1028–1048. doi:10.3390/ph7121028

Nicolas, L. B., Kolb, Y., and Prinssen, E. P. (2006). A Combined marble Burying-Locomotor Activity Test in Mice: a Practical Screening Test with Sensitivity to Different Classes of Anxiolytics and Antidepressants. *Eur. J. Pharmacol.* 547 (1-3), 106–115. doi:10.1016/j.ejphar.2006.07.015

Nollet, M., Le Guisquet, A. M., and Belzung, C. (2013). Models of Depression: Unpredictable Chronic Mild Stress in Mice. *Curr. Protoc. Pharmacol.* Chapter 5, 5–65. doi:10.1002/0471141755.ph0565s61

Patriquin, M. A., and Mathew, S. J. (2017). The Neurobiological Mechanisms of Generalized Anxiety Disorder and Chronic Stress. *Chronic Stress (Thousand Oaks)* 1, 2470547017703993. doi:10.1177/2470547017703993

Perry, V. H., Matyszak, M. K., and Fearn, S. (1993). Altered Antigen Expression of Microglia in the Aged Rodent CNS. *Glia* 7 (1), 60–67. doi:10.1002/glia.440070111

Petit-Demouliere, B., Chenu, F., and Bourin, M. (2005). Forced Swimming Test in Mice: a Review of Antidepressant Activity. *Psychopharmacology* 177 (3), 245–255. doi:10.1007/s00213-004-2048-7

Ruggiero, C., Grossi, M., Fragassi, G., Di Campli, A., Di Ilio, C., Luini, A., et al. (2018). The KDEL Receptor Signalling cascade Targets Focal Adhesion Kinase on Focal Adhesions and Invadopodia. *Oncotarget* 9 (12), 10228–10246. doi:10.18632/oncotarget.23421

Sevastre-Berghian, A. C., Ielciu, I., Mitre, A. O., Filip, G. A., Oniga, I., Vlase, L., et al. (2020). Targeting Oxidative Stress Reduction and Inhibition of HDAC1, MECP2, and NF-kB Pathways in Rats with Experimentally Induced Hyperglycemia by Administration of Thymus Marshallianus Willd. Extracts. *Front. Pharmacol.* 11, 581470. doi:10.3389/fphar.2020.581470

Shi, H., Zhang, X., Weng, Y.-L., Lu, Z., Liu, Y., Lu, Z., et al. (2018). m6A Facilitates Hippocampus-dependent Learning and Memory through YTHDF1. *Nature* 563 (7730), 249–253. doi:10.1038/s41586-018-0666-1

Singhal, G., and Baune, B. T. (2017). Microglia: An Interface between the Loss of Neuroplasticity and Depression. *Front. Cell Neurosci.* 11, 270. doi:10.3389/fncel.2017.00270

Smith, K. (2014). Mental Health: a World of Depression. *Nature* 515 (7526), 181. doi:10.1038/515180a

Sterlemann, V., Ganea, K., Liebl, C., Harbich, D., Alam, S., Holsboer, F., et al. (2008). Long-term Behavioral and Neuroendocrine Alterations Following Chronic Social Stress in Mice: Implications for Stress-Related Disorders. *Horm. Behav.* 53 (2), 386–394. doi:10.1016/j.yhbeh.2007.11.001

Szatmari, P., Courtney, D. B., Narrandes, R., and Bennett, K. J. (2018). Locating, Appraising, and Implementing Clinical Practice Guidelines for the Treatment of Adolescent Depression. *J. Am. Acad. Child Adolesc. Psychiatry* 57 (10), S340. doi:10.1016/j.jaac.2018.07.865

Szczepanik, A., Funes, S., Petko, W., and Ringheim, G. E. (2001). IL-4, IL-10 and IL-13 Modulate Aβ(1-42)-Induced Cytokine and Chemokine Production in Primary Murine Microglia and a Human Monocyte Cell Line. *J. Neuroimmunol* 113 (1), 49–62. doi:10.1016/s0165-5728(00)00404-5

Taliaz, D., Stall, N., Dar, D. E., and Zangen, A. (2010). Knockdown of Brain-Derived Neurotrophic Factor in Specific Brain Sites Precipitates Behaviors Associated With Depression and Reduces Neurogenesis. *Mol. Psychiatry* 15 (1), 80–92.

Trofimiuk, E., and Braszko, J. J. (2015). Ciproxifan Differentially Modifies Cognitive Impairment Evoked by Chronic Stress and Chronic Corticosterone Administration in Rats. *Behav. Brain Res.* 283, 145–153. doi:10.1016/j.bbr.2015.01.038

Tynan, R. J., Naicker, S., Hinwood, M., Nalivaiko, E., Buller, K. M., Pow, D. V., et al. (2010). Chronic Stress Alters the Density and Morphology of Microglia in a Subset of Stress-Responsive Brain Regions. *Brain Behav. Immun.* 24 (7), 1058–1068. doi:10.1016/j.bbi.2010.02.001

Üstün, T. B., Ayuso-Mateos, J. L., Chatterji, S., Mathers, C., and Murray, C. J. L. (2004). Global burden of Depressive Disorders in the Year 2000. *Br. J. Psychiatry* 184, 386–392. doi:10.1192/bjp.184.5.386

Vasileva, L. V., Saracheva, K. E., Ivanovska, M. V., Petrova, A. P., Marchev, A. S., Georgiev, M. I., et al. (2018). Antidepressant-like Effect of Salidroside and Curcumin on the Immunoreactivity of Rats Subjected to a Chronic Mild Stress Model. *Food Chem. Toxicol.* 121, 604–611. doi:10.1016/j.fct.2018.09.065

Vega-Rivera, N. M., Ortiz-López, L., Granados-Juárez, A., Estrada-Camarena, E. M., and Ramírez-Rodríguez, G. B. (2020). Melatonin Reverses the Depression-Associated Behaviour and Regulates Microglia, Fractalkine Expression and Neurogenesis in Adult Mice Exposed to Chronic Mild Stress. *Neuroscience* 440, 316–336. doi:10.1016/j.neuroscience.2020.05.014

Wang, C., Wang, Q., Lou, Y., Xu, J., Feng, Z., Chen, Y., et al. (2018). Salidroside Attenuates Neuroinflammation and Improves Functional Recovery after Spinal Cord Injury through Microglia Polarization Regulation. *J. Cel Mol Med.* 22 (2), 1148–1166. doi:10.1111/jcmm.13368

Wang, C., Lou, Y., Xu, J., Feng, Z., Chen, Y., Tang, Q., et al. (2017). Endoplasmic Reticulum Stress and NF-Kb Pathway in Salidroside Mediated Neuroprotection: Potential of Salidroside in Neurodegenerative Diseases. *Am. J. Chin. Med.* 45 (7), 1459–1475. doi:10.1142/s0192415x17500793

Wang, H., Li, Q., Sun, S., and Chen, S. (2020). Neuroprotective Effects of Salidroside in a Mouse Model of Alzheimer's Disease. *Cell Mol Neurobiol.* 40 (7), 1133–1142. doi:10.1007/s10571-020-00801-w

Wang, J., Zhang, Y. L., and Zhuang, N. (2018). [Salidroside Inhibits Inflammatory Factor Release in BV-2 Cells through P38 and JNK Pathways]. *Sheng Li Xue Bao* 70 (3), 245–252.

Wang, N., Song, J., Zhou, G., Li, W., and Ma, H. (2020). Mechanism of Salidroside Relieving the Acute Hypoxia-Induced Myocardial Injury through the PI3K/Akt Pathway. *Saudi J. Biol. Sci.* 27 (6), 1533–1537. doi:10.1016/j.sjbs.2020.04.035

Wang, T., Xu, L., Gao, L., Zhao, L., Liu, X.-h., Chang, Y.-y., et al. (2020). Paeoniflorin Attenuates Early Brain Injury through Reducing Oxidative Stress and Neuronal Apoptosis after Subarachnoid Hemorrhage in Rats. *Metab. Brain Dis.* 35 (6), 959–970. doi:10.1007/s11011-020-00571-w

Wei, R., and Jonakait, G. M. (1999). Neurotrophins and the Anti-inflammatory Agents Interleukin-4 (IL-4), IL-10, IL-11 and Transforming Growth Factor-Beta1 (TGF-Beta1) Down-Regulate T Cell Costimulatory Molecules B7 and CD40 on Cultured Rat Microglia. *J. Neuroimmunol* 95 (1-2), 8–18. doi:10.1016/s0165-5728(98)00248-3

Willner, P. (2017). Reliability of the Chronic Mild Stress Model of Depression: A User Survey. *Neurobiol. Stress* 6, 68–77. doi:10.1016/j.ynstr.2016.08.001

Xiao, Y. Q., Malcolm, K., Worthen, G. S., Gardai, S., Schiemann, W. P., Fadok, V. A., et al. (2002). Cross-talk between ERK and P38 MAPK Mediates Selective Suppression of Pro-inflammatory Cytokines by Transforming Growth Factor-β. *J. Biol. Chem.* 277 (17), 14884–14893. doi:10.1074/jbc.m111718200

Yao, Y., and Fu, K. Y. (2020). Serum-deprivation Leads to Activation-like Changes in Primary Microglia and BV-2 Cells but Not Astrocytes. *Biomed. Rep.* 13 (5), 51. doi:10.3892/br.2020.1358

Yi, S., Jiang, X., Tang, X., Li, Y., Xiao, C., Zhang, J., et al. (2020). IL-4 and IL-10 Promotes Phagocytic Activity of Microglia by Up-Regulation of TREM2. *Cytotechnology* 72 (4), 589–602. doi:10.1007/s10616-020-00409-4

Yoshida, T., Das, N. A., Carpenter, A. J., Izadpanah, R., Kumar, S. A., Gautam, S., et al. (2020). Minocycline Reverses IL-17A/TRAF3IP2-mediated P38 MAPK/NF-κB/iNOS/NO-dependent Cardiomyocyte Contractile Depression and Death. *Cell Signal.* 73, 109690. doi:10.1016/j.cellsig.2020.109690

Zhang, B., Wang, Y., Li, H., Xiong, R., Zhao, Z., Chu, X., et al. (2016). Neuroprotective Effects of Salidroside through PI3K/Akt Pathway Activation in Alzheimer's Disease Models. *Drug Des. Devel Ther.* 10, 1335–1343. doi:10.2147/DDDT.S99958

Zhang, K., Lin, W., Zhang, J., Zhao, Y., Wang, X., and Zhao, M. (2020). Effect of Toll-like Receptor 4 on Depressive-like Behaviors Induced by Chronic Social Defeat Stress. *Brain Behav.* 10 (3), e01525. doi:10.1002/brb3.1525

Zhang, N., Luo, M., He, L., and Yao, L. (2020). Chemical Composition of Essential Oil from Flower of 'Shanzhizi' (Gardenia Jasminoides Ellis) and Involvement of Serotonergic System in its Anxiolytic Effect. *Molecules* 25 (20), 4702. doi:10.3390/molecules25204702

Zong, K., Liu, X., Sun, Z., Piao, L., Xuan, Y., Jin, Y., et al. (2020). Macelignan Inhibits the Inflammatory Response of Microglia and Regulates Neuronal Survival. *J. Neuroimmunology* 339, 577123. doi:10.1016/j.jneuroim.2019.577123

Zuo, W., Yan, F., Zhang, B., Hu, X., and Mei, D. (2018). Salidroside Improves Brain Ischemic Injury by Activating PI3K/Akt Pathway and Reduces Complications Induced by Delayed tPA Treatment. *Eur. J. Pharmacol.* 830, 128–138. doi:10.1016/j.ejphar.2018.04.001

Conflict of Interest: The authors declare that the research was conducted in the absence of any commercial or financial relationships that could be construed as a potential conflict of interest.

frontiers in Pharmacology

MINI REVIEW
published: 29 June 2021
doi: 10.3389/fphar.2021.687935

Mitoprotective Effects of *Centella asiatica* (L.) Urb.: Anti-Inflammatory and Neuroprotective Opportunities in Neurodegenerative Disease

Jia Hui Wong[1], *Anna M. Barron*[1] *and Jafri Malin Abdullah*[2,3]*

[1]*Neurobiology of Aging and Disease Laboratory, Lee Kong Chian School of Medicine, Nanyang Technological University Singapore, Singapore,* [2]*Department of Neurosciences, School of Medical Sciences, Universiti Sains Malaysia, Kota Bharu, Malaysia,* [3]*Brain & Behaviour Cluster and Department of Neurosciences, School of Medical Sciences, Universiti Sains Malaysia, Kota Bharu, Malaysia*

Natural products remain a crucial source of drug discovery for accessible and affordable solutions for healthy aging. *Centella asiatica* (L.) Urb. (CA) is an important medicinal plant with a wide range of ethnomedicinal uses. Past *in vivo* and *in vitro* studies have shown that the plant extract and its key components, such as asiatic acid, asiaticoside, madecassic acid and madecassoside, exhibit a range of anti-inflammatory, neuroprotective, and cognitive benefits mechanistically linked to mitoprotective and antioxidant properties of the plant. Mitochondrial dysfunction and oxidative stress are key drivers of aging and neurodegenerative disease, including Alzheimer's disease and Parkinson's disease. Here we appraise the growing body of evidence that the mitoprotective and antioxidative effects of CA may potentially be harnessed for the treatment of brain aging and neurodegenerative disease.

Keywords: medicinal plants, neuroprotection, mitochondria, neurodegeneration, *centella asiatica* (L.) Urb, antioxidative, mitoprotective

OPEN ACCESS

Edited by:
Tahir Ali,
University of Calgary, Canada

Reviewed by:
Atif Ali Khan Khalil,
National University of Medical Sciences (NUMS), Pakistan
Kevin Spelman,
Consultant, Ashland, OR, United States

***Correspondence:**
Jafri Malin Abdullah
brainsciences@gmail.com

Specialty section:
This article was submitted to Ethnopharmacology, a section of the journal Frontiers in Pharmacology

Received: *30 March 2021*
Accepted: *17 June 2021*
Published: *29 June 2021*

Citation:
Wong JH, Barron AM and Abdullah JM (2021) Mitoprotective Effects of Centella asiatica *(L.) Urb.: Anti-Inflammatory and Neuroprotective Opportunities in Neurodegenerative Disease. Front. Pharmacol. 12:687935. doi: 10.3389/fphar.2021.687935*

INTRODUCTION

Centella asiatica (L.) Urb. (CA) is a medicinal plant commonly consumed in salads or juices in several countries, including Malaysia, India, Sri Lanka, Indonesia and China (Hashim, 2011; Maulidiani et al., 2012; Bachok et al., 2014; Singh et al., 2014). CA has a wide range of ethnomedical applications, including treatment of gastrointestinal disorders, skin diseases, fever, and cognitive and memory problems (Gohil et al., 2010; Jahan et al., 2012; Sabaragamuwa et al., 2018). Studies of the plant extract and its bioactive compounds have revealed a broad range of pharmacological and therapeutic effects, including anti-ulcer (Zheng et al., 2016), anti-microbial (Idris and Nadzir, 2017), cytoprotective (Choi et al., 2016; Tewari et al., 2016), anti-inflammatory (Choi et al., 2016; Park et al., 2017; Ho et al., 2018), anti-oxidant (Zhao et al., 2014; Dewi and Maryani, 2015; Intararuchikul et al., 2019) and mitoprotective (Gray et al., 2017; Zhang et al., 2017; Gray et al., 2018c) properties. The bioactive components of CA readily cross the blood brain barrier and exert beneficial neuroactive effects in a range of models of aging (Zweig et al., 2021) and neurodegenerative disease including Alzheimer's disease (AD) (Gray et al., 2018c; Matthews et al., 2019) and Parkinson's disease (PD) (Gopi and Arambakkam Janardhanam, 2017; Teerapattarakan et al., 2018). Recent studies have associated these neuroprotective and anti-inflammatory effects with increased expression of proteins essential for mitochondrial bioenergetics and antioxidant genes (Gray et al., 2018c; Lu et al., 2021; Zweig et al., 2021). Mitochondria play a pivotal role in aging and

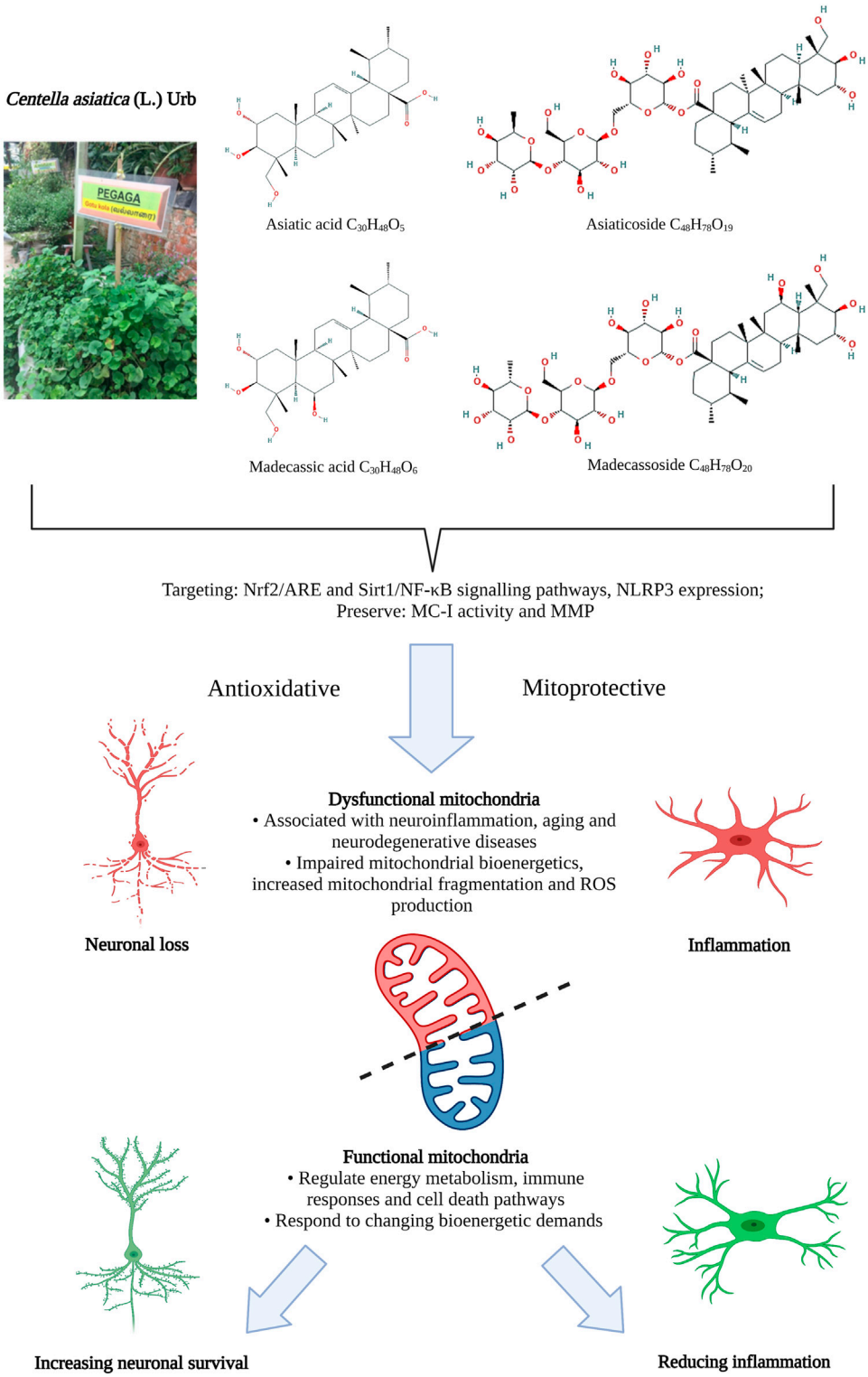

FIGURE 1 | Antioxidative and mitoprotective activities of *Centella asiatica* and its main components. Mitochondrial dysfunction in regulating energy metabolism in response to changing bioenergy demands is closely associated with neuroinflammation in aging and neurodegenerative diseases. The antioxidative and mitoprotective activities of CA targeting mitochondrial and oxidative functions may confer neuroprotective benefits that could potentially be harnessed to treat aging and neurodegenerative diseases and improve functional behavioral outcomes. ARE, antioxidant response element genes; MC-I, mitochondrial complex I; MMP, mitochondrial membrane potential; NF-κB, nuclear factor kappa-light-chain-enhancer of activated B cells; NLRP3, NLR family pyrin domain containing three; Nrf2, NF-E2-p45-related factor 2; Sirt1, Sirtuin 1. Figure created with BioRender.com.

neurodegeneration, regulating energy metabolism, immune responses and cell death pathways (Moreira et al., 2010; Rizzuto et al., 2012; Mills and O'Neill, 2016; Sun et al., 2016; Shah et al., 2019). Hence, this review focuses on the potential therapeutic application of CA for the treatment of brain-aging and neurodegenerative disease through restoration of mitochondrial function and inhibition of oxidative damage.

CENTELLA ASIATICA (L.) URB. (CA): THE MEDICINAL PLANT

Botany and Geographical Distribution of *Centella asiatica* (L.) Urb.

CA is commonly known by several names, including *gotu kola* in Sinhala, *pegaga* in Malay, 'léi gōng gēn' in Chinese and Asian or Indian Pennywort in English (Jahan et al., 2012; Orhan, 2012; Singh et al., 2014; Gajbhiye et al., 2016). CA belongs to the Apiaceae family, which is native to Asian countries and parts of China as well as several other parts of the world, such as northern Australia and the Western Pacific. The plant grows horizontally, with long, slender and tender prostrate stolons that can extend up to 2 m and are characterized by long internodes and nodes. Each node of the stem bears one to three leaves that are about 2–6 cm in length and 1.5–5 cm in width with a slightly cupped circular-reniform shape and palmately netted veins. CA is odorless and flowers from April to June with fascicled umbels that consist of three to four sessile flowers. These flowers bear 4-mm-long fruits that range in shape from oval to globular. Found up to 1800 m above sea level, CA grows in a wide range of habitats, such as open sunny areas, swamps, paddy fields as well as along the banks of lakes and ponds and on stone walls and rocks (Roy et al., 2013; Singh et al., 2014; Sirichoat et al., 2015; Gajbhiye et al., 2016).

Centella asiatica (L.) Urb. and its Major Phytochemical Constituents

CA contains amino acids, alkaloids, carbohydrates, vitamins, minerals, terpenes of various categories (such as monoterpenes, sesquiterpenes, diterpenes, triterpenes and tetraterpene) and phenolic compounds (such as the flavonoids, tannins and other constituents). The phytochemistry of CA has previously been comprehensively reviewed by Brinkhaus et al. (2000), Gray et al. (2018a) and Torbati et al. (2021) therefore will only be summarized briefly here. Terpenes are the dominant group of chemical constituents of CA, with triterpenes being the major and most important component of CA, serving as a marker constituent for quality control analyses (Rafi et al., 2018). The triterpenes (**Figure 1**) found in CA are mostly pentacyclic triterpenic acids (sapogenins), such as the asiatic acid (PubChem CID: 119034, National Center for Biotechnology Information, 2021a) and madecassic acid (PubChem CID: 73412, National Center for Biotechnology Information, 2021b), and their respective triterpenoid glycosides (saponins, with a trisaccharide moiety linked to the aglycones), such as asiaticoside (PubChem CID: 52912190, National Center for Biotechnology Information, 2021c) and madecassoside (PubChem CID: 131801373, National Center for Biotechnology Information, 2021d) (Azerad, 2016; Rafi et al., 2018).

CA extract has been widely studied in the form of ethanolic (Sari et al., 2014; Sari and Rochmah, 2015; Binti Mohd Yusuf Yeo et al., 2018; Suri et al., 2018; Wong et al., 2019; Wong et al., 2020), methanolic (Veerendra Kumar and Gupta, 2003; Arora et al., 2018) and aqueous (Mitha et al., 2016; Gray et al., 2018c; Chintapanti et al., 2018) extract as well as leaf juice (Rao et al., 2007; Thirawarapan et al., 2019). Of these different preparations of CA, it was found that the ethanolic extract retained the highest amount of the triterpenes asiatic acid and asiaticoside compared to other solvents (Puttarak and Panichayupakaranant, 2013; Gajbhiye et al., 2016).

Wide chemotypic variations in triterpenoids were found in CA planted in different growing regions, altitudes and localities (Long et al., 2012; Singh et al., 2014; Srivastava et al., 2014). Genotypic and phenotypic variability have been associated with differences in phytochemicals content of CA including macronutrients, micronutrients, phenolics, flavonoids, tannin, anthocyanin, carotenoids and ascorbic acid (Thomas et al., 2010; Singh et al., 2014; Lal et al., 2017; Chandrasekara et al., 2020). Other than geographical and genotypical influences, the phytochemical compositions of CA also vary due to seasonal variations associated with the cultivation and harvesting procedures, light conditions, as well as the drying conditions post-harvesting (Maulidiani et al., 2012; Rahajanirina et al., 2012; Alqahtani et al., 2015; Plengmuankhae and Tantitadapitak, 2015). This underlines the potential challenges involved in the study of CA plant extract, as differences in specific phytochemical composition may influence the efficacy of the extract.

Neuroactive Effects of *Centella asiatica* (L.) Urb.: Crossing the Blood Brain Barrier

Several pharmacokinetic studies have confirmed that bioactive components of CA can cross the blood brain barrier (BBB) when administered peripherally, although the transport mechanisms of these phytochemicals remain largely unknown. For example, asiatic acid, asiaticoside and madecassoside were found to accumulate in the brains of animals administered with CA extract or the respective single components (Yin et al., 2012; Anukunwithaya et al., 2017a; Anukunwithaya et al., 2017b). A recent study using primary porcine brain endothelial cells as *in vitro* BBB model also reported that asiatic acid, asiaticoside and madecassoside exhibit high permeability across the BBB (Hanapi et al., 2021). The bioavailability of these phytochemicals in brain tissue after peripheral administration (Yin et al., 2012; Anukunwithaya et al., 2017a; Anukunwithaya et al., 2017b) indicates they cross the BBB at adequate concentrations to exert neuroactive effects supporting the potential use of these compounds as neurotherapeutics.

Neuroactive Effects of *Centella asiatica* (L.) Urb.: Cognition

Cognitive-enhancing effects of CA extract have been described in numerous studies, in both normal animals and models of aging

and neurodegenerative disease (Doknark et al., 2014; Sari et al., 2014; Sirichoat et al., 2015; Yolanda et al., 2015; Wong et al., 2019; Sbrini et al., 2020). In early studies, CA extract was found to improve memory and ameliorate biochemical and mitochondrial dysfunction in a mouse model of aging (Kumar et al., 2011). In other studies CA was found to confer protection against hippocampal dysfunction, a region of the brain that plays a critical role in learning and memory and is severely affected in AD (Veerendra Kumar and Gupta, 2003; Giribabu et al., 2014). Further, key bioactive components of CA have also been shown to affect learning and memory in models of aging and neurodegenerative disease. For example, asiaticoside has been found to enhance cognitive performance in aged animals (Lin et al., 2013) and a rat model of AD (Zhang et al., 2017). The cognitive effects of CA extract have been linked to changes in synaptic plasticity (Lin et al., 2013) and excitatory neurotransmission (Wanasuntronwong et al., 2018; Wong et al., 2020) as well as improved neuronal health and survival in models of aging and disease (Gray et al., 2018b; Gray et al., 2018c). Here we will examine the evidence that CA and its phytochemicals provide cognitive benefits in aging and neurodegenerative disease *via* mitoprotective and antioxidant mechanisms (Soumyanath et al., 2012; Chen et al., 2016; Gray et al., 2016; Gray et al., 2017; Matthews et al., 2019).

TARGETING MITOCHONDRIA IN AGING AND NEURODEGENERATIVE DISEASE: ROLE FOR *CENTELLA ASIATICA* (L.) URB.

Mitochondrial dysfunction is closely associated with aging (López-Otín et al., 2013; Sun et al., 2016), AD (Moreira et al., 2010; Yoo et al., 2020) and PD (Yang et al., 2020). Mitochondria regulate energy metabolism, immune responses and cell-death pathways through their highly flexible and dynamic network. The mitochondrial network responds to changing bioenergetic demands by adjusting the rate of mitochondrial fission and fusion—a function that was found to be affected in most age-associated neurodegenerative conditions (Shah et al., 2019). Studies have shown that age-related toxic protein aggregates, such as Alzheimer's beta amyloid (Aβ), induce mitochondrial dysregulation by binding to mitochondrial proteins. For example, Aβ has been found to bind to the mitochondrial fission protein (Drp1), and the mitochondrial voltage-dependent anion channel (VDAC) (Manczak et al., 2011; Manczak et al., 2018). These abnormal protein interactions affect mitochondrial biogenesis, increase mitochondrial fragmentation and induce free radical production (John and Reddy, 2020).

Mitochondria are the primary source of free radicals, otherwise known as reactive oxygen species (ROS), and ROS overproduction leads to oxidative damage. Oxidative damage further affects the mitochondrial respiratory chain function in generating energy in the form of adenosine triphosphate (ATP) through oxidative phosphorylation (OXPHOS) (Elfawy and Das, 2019). Perturbations in the electron transport chain function and/or reduction in the mitochondrial membrane potential lead to a vicious cycle of mitochondrial stress, which results in decreased ATP production and increased ROS production (Szalardy et al., 2015; Zorova et al., 2018). The brain is highly susceptible to both bioenergetic dysfunction and oxidative damage due to the high energy demands associated with neurotransmission and a high lipid content, respectively. The use of antioxidant strategies has been reported to provide a protective benefit against aging and neurodegenerative diseases. Further, enhancing mitochondrial biogenesis and quality control may be an efficient strategy for preventing mitochondrial disorders (Smith et al., 2012; Suliman and Piantadosi, 2016; Murphy and Hartley, 2018) and providing neuroprotection in AD and PD mouse models (Johri and Beal, 2012). Several therapeutic approaches that aim to protect against neurodegeneration and inflammation by improving brain bioenergetics, rescuing mitochondrial dysfunction and reducing oxidative damage are being developed (Cunnane et al., 2020; Fairley et al., 2021). In this section, we will focus on the mitoprotective and antioxidative effects of CA and its key phytochemicals as potential therapeutic agents that can 1) promote neuronal health and survival, and 2) reduce neuroinflammation.

Neuroprotective Effects of *Centella asiatica* (L.) Urb. and its Major Constituents: Antioxidative and Mitoprotective Effects

Neuroprotective effects of CA have been described in several models of neurodegenerative disease and injury, linked to effects on mitochondrial energy production, oxidative stress and mitochondrial-induced apoptosis. For example, the CA extract, asiatic acid has been shown to prevent mitochondrial morphology abnormalities in a rat model of kainic acid-induced seizure, which protected synaptic function and alleviated cognitive deficits (Lu et al., 2021). In a separate study, the CA phytochemical asiaticoside was found to inhibit Aβ-induced neuronal apoptosis by restoring and maintaining mitochondrial membrane potential (Song et al., 2018). Several potential molecular mechanisms mediating the mitoprotective effects of CA have been proposed, including increased conductance and stabilization of VDAC (Tewari et al., 2016). VDAC plays a critical role in cell survival, transport of substrates for energy production and maintenance of mitochondrial membrane potential (Camara et al., 2017), making it a target of interest in regulating mitochondrial function.

Meanwhile, other studies have implicated CA and its bioactive components in the regulation of important antioxidant response signaling pathways. In mouse models of AD, CA extract has been found to promote antioxidative responses, countering Aβ pathology-driven oxidative stress, mitigating neuronal loss around the plaques and improving memory function (Gray et al., 2017; Gray et al., 2018c). CA extract has also been found to protect rotenone-induced parkinsonism rats against lipid peroxidation, dopaminergic neuronal death and locomotor deficit. These protective effects were associated with increased antioxidant enzyme expression and preservation of mitochondrial complex I activity, which is responsible for the rate-limiting step in OXPHOS (Teerapattarakan et al., 2018). Madecassoside was also found to be effective at ameliorating the

deficits observed in PD rat models *via* its antioxidative activities, maintaining the redox balance (Xu et al., 2013). Similarly, asiaticoside has been found to reduce oxidative stress induced by rotenone (Gopi and Arambakkam Janardhanam, 2017; Subaraja and Vanisree, 2019). Likewise, asiatic acid provided antioxidative benefits in a drosophila PD model, protecting mitochondria against rotenone-induced oxidative stress and apoptosis. The antioxidative properties of asiatic acid are also thought to mediate neuroprotection and improve spatial memory function in animals treated with valproic acid (Xu et al., 2012; Umka Welbat et al., 2016). Outside of the brain, antioxidative effects of CA are also observed in other organs and systems. For example, CA extract was found to inhibit lipid peroxidation in rotenone-treated rats (Intararuchikul et al., 2019) and regulate lipid metabolism *via* antioxidant effect (Zhao et al., 2014). These findings support the notion that the neuroprotective effects of CA and its bioactive components are at least in part mediated through enhanced antioxidative responses.

CA-induced antioxidative responses have been linked to the higher expression of antioxidant response element genes (AREs) activated *via* Nrf2 (NF-E2-p45-related factor two, encoded by the NFE2L2 gene) (Matthews et al., 2019). The Nrf2/ARE signaling cascade regulates a plethora of cellular activities, including metabolic reprogramming, mitochondrial physiology and biogenesis, antioxidant stress response, drug detoxification, inflammation, autophagy and unfolded protein response and proteostasis (Dinkova-Kostova and Abramov, 2015; He et al., 2020). Altered expression of Nrf2-targeted genes is associated with AD, and previous studies have demonstrated that the activation of Nrf2 ameliorates Aβ pathology and cognitive deficits in AD mouse models (Bahn et al., 2019). Consequently, activation of Nrf2 pathway represents a promising therapeutic direction for enhancing mitochondrial quality control and biogenesis in aging and neurodegenerative diseases (Kerr et al., 2017; Gureev et al., 2019; Gureev and Popov, 2019; Brandes and Gray, 2020; Bento-Pereira and Dinkova-Kostova, 2021). Subsequent studies found that Nrf2 is a crucial component of the mitoprotective effects of CA, whereby long-term CA treatment improved the cognitive performance of wild type but not Nrf2 deficient mice (Nrf2 knockout) (Zweig et al., 2021). Further, these studies associated hippocampal mitochondrial dysfunction with cognitive performance.

In addition to the general ability to induce antioxidant responses, disease-specific mitoprotective effects of CA have also been identified in models of PD. For example, CA components have been shown to block the translocation of α-synuclein to the mitochondria, therefore maintaining mitochondrial membrane integrity and ATP production (Ding et al., 2018). Further, pre-treatment with asiatic acid significantly decreased mitochondrial ROS production in a 1-methyl-4-phenyl-pyridine (MPP+)-induced neuroblastoma model of PD and protected the cells form the loss of mitochondrial membrane potential (Chen et al., 2019). Additionally, CA and its triterpenoids may also reduce ROS production (Gray et al., 2017; Nataraj et al., 2017), thus potentially restoring mitochondrial function in the central nervous system (Onyango et al., 2017). For example, madecassic acid inhibited ROS production in human retinal microvascular endothelial cells (hMRECs) following hypoxia-induced oxidative stress (Yang et al., 2016). The molecular targets mediating these effects are yet to be elucidated and whether they are generalized to other disease models remains to be determined.

Anti-Inflammatory Effects of *Centella asiatica* (L.) Urb. and its Major Constituents

The mitochondrial and metabolic fitness of the brain's innate immune system plays an important role in the neuroinflammatory responses involved in neurodegenerative diseases (Paolicelli and Angiari, 2019)—a concept known as "immunometabolism" (O'Neill et al., 2016). Mitochondrial-dependent OXPHOS and fatty acid oxidation (FAO) are associated with anti-inflammatory responses (Mills and O'Neill, 2016) while, on the other hand, inflammatory responses are associated with a shift toward non-mitochondrial erobic glycolysis (Rodríguez-Prados et al., 2010; Galván-Peña and O'Neill, 2014). This switch toward erobic glycolysis causes several functional changes: 1) rapid supply of ATP, 2) proinflammatory cytokine production, 3) rearrangement of the tricarboxylic acid (TCA) cycle and accumulation of intermediate metabolites, such as succinate and citrate, and 4) repurposing of the electron transport chain (ETC) to produce ROS (Lampropoulou et al., 2016; Millet et al., 2016; Mills et al., 2016). Furthermore, microglial activation releases neurotoxic factors, such as mitochondrial-generated ROS, that exacerbate the neuroinflammation, thus resulting in neuronal death and neurodegeneration (González et al., 2014; Simpson and Oliver, 2020). Microglia are metabolically plastic and, hence, are potential therapeutic targets for the treatment of AD using metabolic reprogramming strategies (Fairley et al., 2021).

CA and its derivatives have also been shown to affect inflammatory responses through the regulation of mitochondrial and oxidative functions. Asiatic acid, asiaticoside and madecassoside have been found to demonstrate anti-inflammatory effects through a reduction of cytokine levels and the activation of microglia in stroke models (Krishnamurthy et al., 2009; Chen et al., 2014; Luo et al., 2014). Sirtuin 1 (Sirt 1) protein is an important epigenetic regulator for many physiological processes, modulating downstream pathways by targeting proteins such as nuclear factor kappa-light-chain-enhancer of activated B cells (NF-κB) and plays a role in alleviating oxidative stress (Elibol and Kilic, 2018). In an immortalized microglial cell line, asiatic acid was found to prevent LPS-induced neuroinflammation by enhancing Sirt1 expression while suppressing NF-κB activation, attenuated the production of nitric oxide and the expression of inducible nitric oxide synthase (iNOS) and reduced the expression and release of inflammatory cytokines in response to LPS-induced inflammation (Qian et al., 2018). Asiatic acid was shown to protect BV2 cells from LPS-induced damage by suppressing NLRP3 (NLR family pyrin domain containing three) expression and decreasing mitochondrial ROS, effectively ameliorating mitochondrial dysfunction (Chen et al., 2019).

Anti-inflammatory effects have also been reported in models of AD. In a study that used the intracerebroventricular infusion of toxic forms of Alzheimer's Aβ, the neuroprotective effects of asiaticoside in Aβ-infused rats were suggested as being associated with the anti-inflammatory properties of asiaticoside, hence mitigating mitochondrial injuries and regulating the expression of apoptosis markers (Zhang et al., 2017). The mitoprotective effects of asiatic acid have been demonstrated in earlier studies that targeted the regulation of the mitochondrial membrane potential and ROS production (Xiong et al., 2009; Xu et al., 2012). Taken together, these findings demonstrate that CA and its major phytochemicals inhibit ROS production and ameliorate mitochondrial dysfunction, reducing detrimental inflammatory responses.

CONCLUSION

Plants produce chemically, structurally and molecularly diverse phytochemicals that determine their evolutionary success. These compounds represent biological functions and continue to provide crucial novel pharmacological leads for the treatment of human diseases. CA and its phytochemicals have wide ethnopharmacological applications in various cultures, and its biological effects have been substantiated in numerous studies. These findings suggest that CA confers pleiotropic neuroprotective and anti-inflammatory benefits through its mitoprotective and antioxidative effects, which could potentially be harnessed for the treatment of aging and neurodegenerative diseases. Further research is still needed to determine the synergistic effects, safety, efficacy, bioavailability and metabolism of these components.

AUTHOR CONTRIBUTIONS

JW, AB, and JA wrote and reviewed the manuscript. All authors contributed to the article and approved the submitted version.

FUNDING

AB acknowledges funding support from the Nanyang Assistant Professorship from Nanyang Technological University Singapore. JW and JA acknowledge funding support from the NKEA Research Grant Scheme (NRGS Grant, NH1014D049) for the research presented in this article.

REFERENCES

Alqahtani, A., Tongkao-on, W., Li, K. M., Razmovski-Naumovski, V., Chan, K., and Li, G. Q. (2015). Seasonal Variation of Triterpenes and Phenolic Compounds in australian Centella asiatica (L.) Urb. *Phytochem. Anal.* 26 (6), 436–443. doi:10.1002/pca.2578

Anukunwithaya, T., Tantisira, M., Shimada, T., Sai, Y., and Khemawoot, P. (2017a). Multiple Oral Dosing Pharmacokinetics of Standardized Extract of *Centella asiatica* ECa 233 and its Inductive Effect on Efflux Transporters in Rats. *PMIO* 4 (02), e66–e73. doi:10.1055/S-0043-114669

Anukunwithaya, T., Tantisira, M., Tantisira, B., and Khemawoot, P. (2017b). Pharmacokinetics of a Standardized Extract of *Centella asiatica* ECa 233 in Rats. *Planta Med.* 83 (08), 710–717. doi:10.1055/s-0042-122344

Arora, R., Kumar, R., Agarwal, A., Reeta, K. H., and Gupta, Y. K. (2018). Comparison of Three Different Extracts of *Centella asiatica* for Anti-amnesic, Antioxidant and Anticholinergic Activities: *In Vitro* and *In Vivo* Study. *Biomed. Pharmacother.* 105, 1344–1352. doi:10.1016/j.biopha.2018.05.156

Azerad, R. (2016). Chemical Structures, Production and Enzymatic Transformations of Sapogenins and Saponins from *Centella asiatica* (L.) Urban. *Fitoterapia* 114, 168–187. doi:10.1016/j.fitote.2016.07.011

Bachok, M. F., Mohd Yusof, B.-N., Ismail, A., and Hamid, A. A. (2014). Effectiveness of Traditional Malaysian Vegetables ('ulam') in Modulating Blood Glucose Levels. Asia Pac. *J. Clin. Nutr.* 23 (3), 369–376. doi:10.6133/apjcn.2014.23.3.01

Bahn, G., Park, J.-S., Yun, U. J., Lee, Y. J., Choi, Y., Park, J. S., et al. (2019). NRF2/ARE Pathway Negatively Regulates BACE1 Expression and Ameliorates Cognitive Deficits in Mouse Alzheimer's Models. *Proc. Natl. Acad. Sci. USA* 116 (25), 12516–12523. doi:10.1073/pnas.1819541116

Bento-Pereira, C., and Dinkova-Kostova, A. T. (2021). Activation of Transcription Factor Nrf2 to Counteract Mitochondrial Dysfunction in Parkinson's Disease. *Med. Res. Rev.* 41 (2), 785–802. doi:10.1002/med.21714

Binti Mohd Yusuf Yeo, N. A., Muthuraju, S., Wong, J. H., Mohammed, F. R., Senik, M. H., Zhang, J., et al. (2018). Hippocampal Amino-3-hydroxy-5-methyl-4-isoxazolepropionic Acid GluA1 (AMPA GluA1) Receptor Subunit Involves in Learning and Memory Improvement Following Treatment with *Centella asiatica* Extract in Adolescent Rats. *Brain Behav.* 8 (9), e01093. doi:10.1002/brb3.1093

Brandes, M. S., and Gray, N. E. (2020). NRF2 as a Therapeutic Target in Neurodegenerative Diseases. *ASN Neuro* 12, 175909141989978. doi:10.1177/1759091419899782

Brinkhaus, B., Lindner, M., Schuppan, D., and Hahn, E. G. (2000). Chemical, Pharmacological and Clinical Profile of the East Asian Medical Plant Centella Aslatica. *Phytomedicine* 7 (5), 427–448. doi:10.1016/s0944-7113(00)80065-3

Camara, A. K. S., Zhou, Y., Wen, P.-C., Tajkhorshid, E., and Kwok, W.-M. (2017). Mitochondrial VDAC1: A Key Gatekeeper as Potential Therapeutic Target. *Front. Physiol.* 8, 460. doi:10.3389/fphys.2017.00460

Chandrasekara, C. H. W. M. R. B., Sumanarathne, R. A. P. I., and Bandaranayake, P. C. G. (2020). Centellaasiatica Morphotypes Differ Genetically as Well as Macronutrients Content, Total Phenolic Content and Chemical Fingerprints of Leaves. *J. Agric. Sci.* 15, 75. doi:10.4038/jas.v15i1.8673

Chen, S., Yin, Z.-J., Jiang, C., Ma, Z.-Q., Fu, Q., Qu, R., et al. (2014). Asiaticoside Attenuates Memory Impairment Induced by Transient Cerebral Ischemia-Reperfusion in Mice through Anti-inflammatory Mechanism. *Pharmacol. Biochem. Behav.* 122, 7–15. doi:10.1016/j.pbb.2014.03.004

Chen, C.-L., Tsai, W.-H., Chen, C.-J., and Pan, T.-M. (2016). *Centella asiatica* Extract Protects against Amyloid β1-40-induced Neurotoxicity in Neuronal Cells by Activating the Antioxidative Defence System. *J. Traditional Complement. Med.* 6 (4), 362–369. doi:10.1016/j.jtcme.2015.07.002

Chen, D., Zhang, X.-Y., Sun, J., Cong, Q.-J., Chen, W.-X., Ahsan, H. M., et al. (2019). Asiatic Acid Protects Dopaminergic Neurons from Neuroinflammation by Suppressing Mitochondrial ROS Production. *Biomolecules Ther.* 27 (5), 442–449. doi:10.4062/biomolther.2018.188

Chintapanti, S., Pratap Reddy, K., and Sreenivasula Reddy, P. (2018). Behavioral and Neurochemical Consequences of Perinatal Exposure to lead in Adult Male Wistar Rats: Protective Effect by *Centella asiatica*. *Environ. Sci. Pollut. Res.* 25 (13), 13173–13185. doi:10.1007/s11356-018-1500-x

Choi, M.-J., Zheng, H.-M., Kim, J. M., Lee, K. W., Park, Y. H., and Lee, D. H. (2016). Protective Effects of *Centella asiatica* Leaf Extract on Dimethylnitrosamine-Induced Liver Injury in Rats. *Mol. Med. Rep.* 14 (5), 4521–4528. doi:10.3892/mmr.2016.5809

Cunnane, S. C., Trushina, E., Morland, C., Prigione, A., Casadesus, G., Andrews, Z. B., et al. (2020). Brain Energy rescue: an Emerging Therapeutic Concept for Neurodegenerative Disorders of Ageing. *Nat. Rev. Drug Discov.* 19 (9), 609–633. doi:10.1038/s41573-020-0072-x

Dewi, R. T., and Maryani, F. (2015). Antioxidant and α-Glucosidase Inhibitory Compounds of Centella Asiatica. *Proced. Chem.* 17, 147–152. doi:10.1016/j.proche.2015.12.130

Ding, H., Xiong, Y., Sun, J., Chen, C., Gao, J., and Xu, H. (2018). Asiatic Acid Prevents Oxidative Stress and Apoptosis by Inhibiting the Translocation of α-Synuclein into Mitochondria. *Front. Neurosci.* 12, 431. doi:10.3389/fnins.2018.00431

Dinkova-Kostova, A. T., and Abramov, A. Y. (2015). The Emerging Role of Nrf2 in Mitochondrial Function. *Free Radic. Biol. Med.* 88 (Pt B), 179–188. doi:10.1016/j.freeradbiomed.2015.04.036

Doknark, S., Mingmalairak, S., Vattanajun, A., Tantisira, B., and Tantisira, M. H. (2014). Study of Ameliorating Effects of Ethanolic Extract of *Centella asiatica* on Learning and Memory Deficit in Animal Models. *J. Med. Assoc. Thai.* 97 Suppl 2 (Suppl. 2), S68–S76.

Elfawy, H. A., and Das, B. (2019). Crosstalk between Mitochondrial Dysfunction, Oxidative Stress, and Age Related Neurodegenerative Disease: Etiologies and Therapeutic Strategies. *Life Sci.* 218, 165–184. doi:10.1016/j.lfs.2018.12.029

Elibol, B., and Kilic, U. (2018). High Levels of SIRT1 Expression as a Protective Mechanism against Disease-Related Conditions. *Front. Endocrinol.* 9, 614. doi:10.3389/fendo.2018.00614

Fairley, L. H., Wong, J. H., and Barron, A. M. (2021). Mitochondrial Regulation of Microglial Immunometabolism in Alzheimer's Disease. *Front. Immunol.* 12, 257. doi:10.3389/fimmu.2021.624538

Gajbhiye, N. A., Makasana, J., Saha, A., Patel, I., and Jat, R. S. (2016). LC-ESI-MS/MS Method for Simultaneous Determination of Triterpenoid Glycosides and Aglycones in *Centella asiatica* L. *Chromatographia* 79 (11), 727–739. doi:10.1007/s10337-016-3089-x

Galván-Peña, S., and O'Neill, L. A. (2014). Metabolic Reprograming in Macrophage Polarization. *Front. Immunol.* 5, 420. doi:10.3389/fimmu.2014.00420

Giribabu, N., Srinivasarao, N., Swapna Rekha, S., Muniandy, S., and Salleh, N. (2014). Centella asiatica Attenuates Diabetes Induced Hippocampal Changes in Experimental Diabetic Rats. *Evidence-Based Complement. Altern. Med.* 2014, 1–10. doi:10.1155/2014/592062

Gohil, K., Patel, J., and Gajjar, A. (2010). Pharmacological Review on *Centella asiatica*: A Potential Herbal Cure-All. *Indian J. Pharm. Sci.* 72 (5), 546–556. doi:10.4103/0250-474X.78519

González, H., Elgueta, D., Montoya, A., and Pacheco, R. (2014). Neuroimmune Regulation of Microglial Activity Involved in Neuroinflammation and Neurodegenerative Diseases. *J. Neuroimmunol.* 274 (1-2), 1–13. doi:10.1016/j.jneuroim.2014.07.012

Gopi, M., and Arambakkam Janardhanam, V. (2017). Asiaticoside: Attenuation of Rotenone Induced Oxidative burden in a Rat Model of Hemiparkinsonism by Maintaining the Phosphoinositide-Mediated Synaptic Integrity. *Pharmacol. Biochem. Behav.* 155, 1–15. doi:10.1016/j.pbb.2017.02.005

Gray, N. E., Harris, C. J., Quinn, J. F., and Soumyanath, A. (2016). *Centella asiatica* Modulates Antioxidant and Mitochondrial Pathways and Improves Cognitive Function in Mice. *J. Ethnopharmacology* 180, 78–86. doi:10.1016/j.jep.2016.01.013

Gray, N. E., Zweig, J. A., Matthews, D. G., Caruso, M., Quinn, J. F., and Soumyanath, A. (2017). *Centella asiatica* Attenuates Mitochondrial Dysfunction and Oxidative Stress in Aβ-Exposed Hippocampal Neurons. *Oxidative Med. Cell Longevity* 2017, 1–8. doi:10.1155/2017/70230912017

Gray, N. E., Alcazar Magana, A., Lak, P., Wright, K. M., Quinn, J., Stevens, J. F., et al. (2018a). *Centella asiatica*: Phytochemistry and Mechanisms of Neuroprotection and Cognitive Enhancement. *Phytochem. Rev.* 17 (1), 161–194. doi:10.1007/s11101-017-9528-y

Gray, N. E., Zweig, J. A., Caruso, M., Martin, M. D., Zhu, J. Y., Quinn, J. F., et al. (2018b). *Centella asiatica* Increases Hippocampal Synaptic Density and Improves Memory and Executive Function in Aged Mice. *Brain Behav.* 8, e01024. doi:10.1002/brb3.1024

Gray, N. E., Zweig, J. A., Caruso, M., Zhu, J. Y., Wright, K. M., Quinn, J. F., et al. (2018c). *Centella asiatica* Attenuates Hippocampal Mitochondrial Dysfunction and Improves Memory and Executive Function in β-amyloid Overexpressing Mice. *Mol. Cell Neurosci.* 93, 1–9. doi:10.1016/j.mcn.2018.09.002

Gureev, A. P., and Popov, V. N. (2019). Nrf2/ARE Pathway as a Therapeutic Target for the Treatment of Parkinson Diseases. *Neurochem. Res.* 44 (10), 2273–2279. doi:10.1007/s11064-018-02711-2

Gureev, A. P., Shaforostova, E. A., and Popov, V. N. (2019). Regulation of Mitochondrial Biogenesis as a Way for Active Longevity: Interaction between the Nrf2 and PGC-1α Signaling Pathways. *Front. Genet.* 10, 435. doi:10.3389/fgene.2019.00435

Hanapi, N. A., Mohamad Arshad, A. S., Abdullah, J. M., Tengku Muhammad, T. S., and Yusof, S. R. (2021). Blood-brain Barrier Permeability of Asiaticoside, Madecassoside and Asiatic Acid in Porcine Brain Endothelial Cell Model. *J. Pharm. Sci.* 110 (2), 698–706. doi:10.1016/j.xphs.2020.09.015

Hashim, P. (2011). *Centella asiatica* in Food and Beverage Applications and its Potential Antioxidant and Neuroprotective Effect. *Int. Food Res. J.* 18 (4), 1215.

He, F., Ru, X., and Wen, T. (2020). NRF2, a Transcription Factor for Stress Response and beyond. *Ijms* 21 (13), 4777. doi:10.3390/ijms21134777

Ho, P. J., Sung, J. J., Cheon, K. K., and Tae, H. J. (2018). Anti-inflammatory Effect of *Centella asiatica* Phytosome in a Mouse Model of Phthalic Anhydride-Induced Atopic Dermatitis. *Phytomedicine* 43, 110–119. doi:10.1016/j.phymed.2018.04.013

Idris, F. N., and Nadzir, M. M. (2017). Antimicrobial Activity of *Centella asiatica* on Aspergillus niger and Bacillus Subtilis. *Chem. Eng. Trans.* 56, 1381–1386. doi:10.3303/CET1756231

Intararuchikul, T., Teerapattarakan, N., Rodsiri, R., Tantisira, M., Wohlgemuth, G., Fiehn, O., et al. (2019). Effects of Centella Asiatica extract on Antioxidant Status and Liver Metabolome of Rotenone-Treated Rats Using GC-MS. *Biomed. Chromatogr.* 33 (2), e4395. doi:10.1002/bmc.4395

Jahan, R., Hossain, S., Seraj, S., Nasrin, D., Khatun, Z., Das, P. R., et al. (2012). *Centella asiatica* (L.) Urb.: Ethnomedicinal Uses and Their Scientific Validations. *Am. -Eurasian J. Sustain. Agric.* 6 (4), 261–270.

John, A., and Reddy, P. H. (2021). Synaptic Basis of Alzheimer's Disease: Focus on Synaptic Amyloid Beta, P-Tau and Mitochondria. *Ageing Res. Rev.* 65, 101208. doi:10.1016/j.arr.2020.101208

Johri, A., and Beal, M. F. (2012). Mitochondrial Dysfunction in Neurodegenerative Diseases. *J. Pharmacol. Exp. Ther.* 342 (3), 619–630. doi:10.1124/jpet.112.192138

Kerr, F., Sofola-Adesakin, O., Ivanov, D. K., Gatliff, J., Gomez Perez-Nievas, B., Bertrand, H. C., et al. (2017). Direct Keap1-Nrf2 Disruption as a Potential Therapeutic Target for Alzheimer's Disease. *Plos Genet.* 13 (3), e1006593. doi:10.1371/journal.pgen.1006593

Krishnamurthy, R. G., Senut, M.-C., Zemke, D., Min, J., Frenkel, M. B., Greenberg, E. J., et al. (2009). Asiatic Acid, a Pentacyclic Triterpene from Centella Asiatica, Is Neuroprotective in a Mouse Model of Focal Cerebral Ischemia. *J. Neurosci. Res.* 87 (11), 2541–2550. doi:10.1002/jnr.22071

Kumar, A., Prakash, A., and Dogra, S. (2011). Centella asiatica Attenuates D-Galactose-Induced Cognitive Impairment, Oxidative and Mitochondrial Dysfunction in Mice. *Int. J. Alzheimer's Dis.* 2011, 347569. doi:10.4061/2011/347569

Lal, R. K., Gupta, P., and Dubey, B. K. (2017). Genetic Variability and Associations in the Accessions of Manduk Parni {Centella asiatica (L)}. *Ind. Crops Prod.* 96, 173–177. doi:10.1016/j.indcrop.2016.11.056

Lampropoulou, V., Sergushichev, A., Bambouskova, M., Nair, S., Vincent, E. E., Loginicheva, E., et al. (2016). Itaconate Links Inhibition of Succinate Dehydrogenase with Macrophage Metabolic Remodeling and Regulation of Inflammation. *Cel Metab.* 24 (1), 158–166. doi:10.1016/j.cmet.2016.06.004

Lin, X., Huang, R., Zhang, S., Wei, L., Zhuo, L., Wu, X., et al. (2013). Beneficial Effects of Asiaticoside on Cognitive Deficits in Senescence-Accelerated Mice. *Fitoterapia* 87, 69–77. doi:10.1016/j.fitote.2013.03.023

López-Otín, C., Blasco, M. A., Partridge, L., Serrano, M., and Kroemer, G. (2013). The Hallmarks of Aging. *Cell* 153 (6), 1194–1217. doi:10.1016/j.cell.2013.05.039

Long, H. S., Stander, M. A., and Van Wyk, B.-E. (2012). Notes on the Occurrence and Significance of Triterpenoids (Asiaticoside and Related Compounds) and Caffeoylquinic Acids in Centella Species. *South Afr. J. Bot.* 82, 53–59. doi:10.1016/j.sajb.2012.07.017

Lu, C.-W., Lin, T.-Y., Pan, T.-L., Wang, P.-W., Chiu, K.-M., Lee, M.-Y., et al. (2021). Asiatic Acid Prevents Cognitive Deficits by Inhibiting Calpain Activation and Preserving Synaptic and Mitochondrial Function in Rats with Kainic Acid-Induced Seizure. *Biomedicines* 9, 284. doi:10.3390/biomedicines9030284

Luo, Y., Yang, Y.-P., Liu, J., Li, W.-H., Yang, J., Sui, X., et al. (2014). Neuroprotective Effects of Madecassoside against Focal Cerebral Ischemia Reperfusion Injury in Rats. *Brain Res.* 1565, 37–47. doi:10.1016/j.brainres.2014.04.008

Manczak, M., Calkins, M. J., and Reddy, P. H. (2011). Impaired Mitochondrial Dynamics and Abnormal Interaction of Amyloid Beta with Mitochondrial Protein Drp1 in Neurons from Patients with Alzheimer's Disease: Implications

for Neuronal Damage. *Hum. Mol. Genet.* 20 (13), 2495–2509. doi:10.1093/hmg/ddr139

Manczak, M., Kandimalla, R., Yin, X., and Reddy, P. H. (2018). Hippocampal Mutant APP and Amyloid Beta-Induced Cognitive Decline, Dendritic Spine Loss, Defective Autophagy, Mitophagy and Mitochondrial Abnormalities in a Mouse Model of Alzheimer's Disease. *Hum. Mol. Genet.* 27 (8), 1332–1342. doi:10.1093/hmg/ddy042

Matthews, D. G., Caruso, M., Murchison, C. F., Zhu, J. Y., Wright, K. M., Harris, C. J., et al. (2019). *Centella asiatica* Improves Memory and Promotes Antioxidative Signaling in 5XFAD Mice. *Antioxidants* 8 (12), 630. doi:10.3390/antiox812063012

Maulidiani, H., Khatib, A., Shaari, K., Abas, F., Shitan, M., Kneer, R., et al. (2012). Discrimination of Three Pegaga (Centella) Varieties and Determination of Growth-Lighting Effects on Metabolites Content Based on the Chemometry of 1H Nuclear Magnetic Resonance Spectroscopy. *J. Agric. Food Chem.* 60 (1), 410–417. doi:10.1021/jf200270y

Millet, P., Vachharajani, V., McPhail, L., Yoza, B., and McCall, C. E. (2016). GAPDH Binding to TNF-α mRNA Contributes to Posttranscriptional Repression in Monocytes: A Novel Mechanism of Communication between Inflammation and Metabolism. *J.I.* 196 (6), 2541–2551. doi:10.4049/jimmunol.1501345

Mills, E. L., and O'Neill, L. A. (2016). Reprogramming Mitochondrial Metabolism in Macrophages as an Anti-inflammatory Signal. *Eur. J. Immunol.* 46 (1), 13–21. doi:10.1002/eji.201445427

Mills, E. L., Kelly, B., Logan, A., Costa, A. S. H., Varma, M., Bryant, C. E., et al. (2016). Succinate Dehydrogenase Supports Metabolic Repurposing of Mitochondria to Drive Inflammatory Macrophages. *Cell* 167 (2), 457–470.e13. doi:10.1016/j.cell.2016.08.064

Mitha, K. V., Yadav, S., and Ganaraja, B. (2016). Improvement in Cognitive Parameters Among Offsprings Born to Alcohol Fed Female Wistar Rats Following Long Term Treatment with Centella Asiatica. *Indian J. Physiol. Pharmacol.* 60 (2), 167–173.

Moreira, P. I., Carvalho, C., Zhu, X., Smith, M. A., and Perry, G. (2010). Mitochondrial Dysfunction Is a Trigger of Alzheimer's Disease Pathophysiology. *Biochim. Biophys. Acta (Bba) - Mol. Basis Dis.* 1802, 2–10. doi:10.1016/j.bbadis.2009.10.006

Murphy, M. P., and Hartley, R. C. (2018). Mitochondria as a Therapeutic Target for Common Pathologies. *Nat. Rev. Drug Discov.* 17 (12), 865–886. doi:10.1038/nrd.2018.174

Nataraj, J., Manivasagam, T., Justin Thenmozhi, A., and Essa, M. M. (2017). Neuroprotective Effect of Asiatic Acid on Rotenone-Induced Mitochondrial Dysfunction and Oxidative Stress-Mediated Apoptosis in Differentiated SH-SY5Y Cells. *Nutr. Neurosci.* 20 (6), 351–359. doi:10.1080/1028415X.2015.1135559

National Center for Biotechnology Information (2021a). PubChem Compound Summary for CID 119034, Asiatic acid. Retrieved at https://pubchem.ncbi.nlm.nih.gov/compound/Asiatic-acid (Retrieved June 8, 2021)

National Center for Biotechnology Information (2021b). PubChem Compound Summary for CID 73412, Madecassic acid. Retrieved at https://pubchem.ncbi.nlm.nih.gov/compound/Madecassic-acid (Retrieved June 8, 2021)

National Center for Biotechnology Information (2021c). PubChem Compound Summary for CID 52912190. Retrieved at https://pubchem.ncbi.nlm.nih.gov/compound/52912190 (Retrieved June 8, 2021)

National Center for Biotechnology Information (2021d). PubChem Compound Summary for CID 131801373. Retrieved at https://pubchem.ncbi.nlm.nih.gov/compound/131801373 (Retrieved June 8, 2021)

O'Neill, L. A. J., Kishton, R. J., and Rathmell, J. (2016). A Guide to Immunometabolism for Immunologists. *Nat. Rev. Immunol.* 16 (9), 553–565. doi:10.1038/nri.2016.70

Onyango, I. G., Khan, S. M., and Bennett, J. P., Jr (2017). Mitochondria in the Pathophysiology of Alzheimer S and Parkinson S Diseases. *Front. Biosci.* 22, 854–872. doi:10.2741/4521

Orhan, I. E. (2012). *Centella asiatica* (L.) Urban: From Traditional Medicine to Modern Medicine with Neuroprotective Potential. *Evidence-Based Complement. Altern. Med.* 2012, 1–8. doi:10.1155/2012/946259

Paolicelli, R. C., and Angiari, S. (2019). Microglia Immunometabolism: From Metabolic Disorders to Single Cell Metabolism. *Semin. Cel Dev. Biol.* 94, 129–137. doi:10.1016/j.semcdb.2019.03.012

Park, J., Choi, J., Son, D., Park, E., Song, M., Hellström, M., et al. (2017). Anti-inflammatory Effect of Titrated Extract of *Centella asiatica* in Phthalic Anhydride-Induced Allergic Dermatitis Animal Model. *Ijms* 18, 738. doi:10.3390/ijms180407384

Plengmuankhae, W., and Tantitadapitak, C. (2015). Low Temperature and Water Dehydration Increase the Levels of Asiaticoside and Madecassoside in *Centella asiatica* (L.) Urban. *South Afr. J. Bot.* 97, 196–203. doi:10.1016/j.sajb.2015.01.013

Puttarak, P., and Panichayupakaranant, P. (2013). A New Method for Preparing Pentacyclic Triterpene Rich *Centella asiatica* Extracts. *Nat. Product. Res.* 27 (7), 684–686. doi:10.1080/14786419.2012.686912

Qian, Y., Xin, Z., Lv, Y., Wang, Z., Zuo, L., Huang, X., et al. (2018). Asiatic Acid Suppresses Neuroinflammation in BV2 Microgliaviamodulation of the Sirt1/NF-κB Signaling Pathway. *Food Funct.* 9 (2), 1048–1057. doi:10.1039/c7fo01442b

Rafi, M., Handayani, F., Darusman, L. K., Rohaeti, E., Wahyu, Y., Sulistiyani, S., et al. (2018). A Combination of Simultaneous Quantification of Four Triterpenes and Fingerprint Analysis Using HPLC for Rapid Identification of *Centella asiatica* from its Related Plants and Classification Based on Cultivation Ages. *Ind. Crops Prod.* 122, 93–97. doi:10.1016/j.indcrop.2018.05.062

Rahajanirina, V., Rakotondralambo Raoseta, S. n. O., Roger, E., Razafindrazaka, H., Pirotais, S., Boucher, M., et al. (2012). The Influence of Certain Taxonomic and Environmental Parameters on Biomass Production and Triterpenoid Content in the Leaves of *Centella asiatica* (L.) Urb. From Madagascar. *Chem. Biodiversity* 9 (2), 298–308. doi:10.1002/cbdv.201100073

Rao, M. K., Rao, M. S., and Rao, G. S. (2007). Treatment with Centalla Asiatica (Linn) Fresh Leaf Extract Enhances Learning Ability and Memory Retention Power in Rats. *Neurosciences (Riyadh)* 12 (3), 236–241.

Rizzuto, R., De Stefani, D., Raffaello, A., and Mammucari, C. (2012). Mitochondria as Sensors and Regulators of Calcium Signalling. *Nat. Rev. Mol. Cel Biol.* 13 (9), 566–578. doi:10.1038/nrm3412

Rodríguez-Prados, J.-C., Través, P. G., Cuenca, J., Rico, D., Aragonés, J., Martín-Sanz, P., et al. (2010). Substrate Fate in Activated Macrophages: a Comparison between Innate, Classic, and Alternative Activation. *J.I.* 185 (1), 605–614. doi:10.4049/jimmunol.0901698

Roy, D. C., Barman, S. K., and Shaik, M. M. (2013). Current Updates on *Centella asiatica*: Phytochemistry, Pharmacology and Traditional Uses. *Med. Plant Res.* 3. doi:10.5376/mpr.2013.03.0004

Sabaragamuwa, R., Perera, C. O., and Fedrizzi, B. (2018). *Centella asiatica* (Gotu Kola) as a Neuroprotectant and its Potential Role in Healthy Ageing. *Trends Food Sci. Technol.* 79, 88–97. doi:10.1016/j.tifs.2018.07.024

Sari, D. C. R., and Rochmah, M. A. (2015). The Effects of Ethanol Extracts of *Centella asiatica* Leaf on Serial Serum Brain Derived Neurotrophin Factor (BDNF) Concentration of Rats (Sprague Dawley) Following Chronic Stress. *Kls* 2, 159–167. doi:10.18502/kls.v2i1.136

Sari, D. C. R., Aswin, S., Susilowati, R., Ar-Rochmah, M., Prakosa, D., Romi, M., et al. (2014). Ethanol Extracts of *Centella asiatica* Leaf Improves Memory Performance in Rats after Chronic Stress via Reducing Nitric Oxide and Increasing Brain-Derived Neurotrophic Factor (BDNF) Concentration. *GSTF J. Psych* 1, 9. doi:10.7603/s40790-014-0009-01

Sbrini, G., Brivio, P., Fumagalli, M., Giavarini, F., Caruso, D., Racagni, G., et al. (2020). *Centella asiatica* L. Phytosome Improves Cognitive Performance by Promoting BDNF Expression in Rat Prefrontal Cortex. *Nutrients* 12 (2), 355. doi:10.3390/nu12020355

Shah, S. I., Paine, J. G., Perez, C., and Ullah, G. (2019). Mitochondrial Fragmentation and Network Architecture in Degenerative Diseases. *PLoS One* 14 (9), e0223014. doi:10.1371/journal.pone.0223014

Simpson, D. S. A., and Oliver, P. L. (2020). ROS Generation in Microglia: Understanding Oxidative Stress and Inflammation in Neurodegenerative Disease. *Antioxidants* 9 (8), 743. doi:10.3390/antiox9080743

Singh, S., Singh, D. R., Banu, V. S., and N, A. (2014). Functional Constituents (Micronutrients and Phytochemicals) and Antioxidant Activity of *Centella asiatica* (L.) Urban Leaves. *Ind. Crops Prod.* 61, 115–119. doi:10.1016/j.indcrop.2014.06.045

Sirichoat, A., Chaijaroonkhanarak, W., Prachaney, P., Pannangrong, W., Leksomboon, R., Chaichun, A., et al. (2015). Effects of Asiatic Acid on Spatial Working Memory and Cell Proliferation in the Adult Rat hippocampus. *Nutrients* 7 (10), 8413–8423. doi:10.3390/nu7105401

Smith, R. A. J., Hartley, R. C., Cochemé, H. M., and Murphy, M. P. (2012). Mitochondrial Pharmacology. *Trends Pharmacol. Sci.* 33 (6), 341–352. doi:10.1016/j.tips.2012.03.010

Song, D., Jiang, X., Liu, Y., Sun, Y., Cao, S., and Zhang, Z. (2018). Asiaticoside Attenuates Cell Growth Inhibition and Apoptosis Induced by Aβ1-42 via Inhibiting the TLR4/NF-κB Signaling Pathway in Human Brain Microvascular Endothelial Cells. *Front. Pharmacol.* 9, 28. doi:10.3389/fphar.2018.00028

Soumyanath, A., Zhong, Y.-P., Henson, E., Wadsworth, T., Bishop, J., Gold, B. G., et al. (2012). Centella asiatica Extract Improves Behavioral Deficits in a Mouse Model of Alzheimer's Disease: Investigation of a Possible Mechanism of Action. *Int. J. Alzheimer's Dis.* 2012, 1–9. doi:10.1155/2012/381974

Srivastava, S., Verma, S., Gupta, A., Rajan, S., and Rawat, A. (2014). Studies on Chemotypic Variation in Centella asiatica (L.) Urban from Nilgiri Range of India. *J. Planar Chromatogr. - Mod. TLC* 27 (6), 454–459. doi:10.1556/jpc.27.2014.6.9

Subaraja, M., and Vanisree, A. J. (2019). The Novel Phytocomponent Asiaticoside-D Isolated from *Centella asiatica* Exhibits Monoamine Oxidase-B Inhibiting Potential in the Rotenone Degenerated Cerebral Ganglions of Lumbricus Terrestris. *Phytomedicine* 58, 152833. doi:10.1016/j.phymed.2019.152833

Suliman, H. B., and Piantadosi, C. A. (2016). Mitochondrial Quality Control as a Therapeutic Target. *Pharmacol. Rev.* 68 (1), 20–48. doi:10.1124/pr.115.011502

Sun, N., Youle, R. J., and Finkel, T. (2016). The Mitochondrial Basis of Aging. *Mol. Cel* 61 (5), 654–666. doi:10.1016/j.molcel.2016.01.028

Suri, A. A., Handayani, A., Ferhad, A., Farida, S., and Redjeki, S. (2018). Effect of *Centella asiatica* Ethanol Extract in Spatial Working Memory on Adult Male Rats. *Adv. Sci. Lett.* 24 (8), 6109–6111. doi:10.1166/asl.2018.12641

Szalárdy, L., Zádori, D., Klivényi, P., Toldi, J., and Vécsei, L. (2015). Electron Transport Disturbances and Neurodegeneration: From Albert Szent-Györgyi's Concept (Szeged) till Novel Approaches to Boost Mitochondrial Bioenergetics. *Oxidative Med. Cell Longevity* 2015, 1–19. doi:10.1155/2015/498401

Teerapattarakan, N., Benya-Aphikul, H., Tansawat, R., Wanakhachornkrai, O., Tantisira, M. H., and Rodsiri, R. (2018). Neuroprotective Effect of a Standardized Extract of *Centella asiatica* ECa233 in Rotenone-Induced Parkinsonism Rats. *Phytomedicine* 44, 65–73. doi:10.1016/j.phymed.2018.04.028

Tewari, D., Mukhopadhyay, M., Nekkanti, M. S., Vallabhaneni, S., Sahu, G., Jetti, S. K., et al. (2016). Cytoprotective Effect of *Centella asiatica* Is Mediated through the Modulation of Mitochondrial Voltage-dependent Anion Channel (VDAC) and Scavenging of Free Radicals. *J. Funct. Foods* 21, 301–311. doi:10.1016/j.jff.2015.11.047

Thirawarapan, S. S., Jariyapongsakul, A., Suvitayavat, W., Muangnongwa, S., and Sribusarakum, A. (2019). Anti-hypertensive and Cerebral Blood Flow Improving Actions of *Centella asiatica* (L.) Urban Leaves Juice in Deoxycorticosterone Acetate-Salt Hypertensive Rats. *Pharm. Sci. Asia* 46 (3), 184–192. doi:10.29090/psa.2019.03.018.0002

Thomas, M. T., Kurup, R., Johnson, A. J., Chandrika, S. P., Mathew, P. J., Dan, M., et al. (2010). Elite Genotypes/chemotypes, with High Contents of Madecassoside and Asiaticoside, from Sixty Accessions of *Centella asiatica* of South India and the Andaman Islands: For Cultivation and Utility in Cosmetic and Herbal Drug Applications. *Ind. Crops Prod.* 32 (3), 545–550. doi:10.1016/j.indcrop.2010.07.003

Torbati, F. A., Ramezani, M., Dehghan, R., Amiri, M. S., Moghadam, A. T., Shakour, N., et al. (2021). Ethnobotany, Phytochemistry and Pharmacological Features of *Centella asiatica*: A Comprehensive Review. *Adv. Exp. Med. Biol.* 1308, 451–499. doi:10.1007/978-3-030-64872-5_25

Umka Welbat, J., Sirichoat, A., Chaijaroonkhanarak, W., Prachaney, P., Pannangrong, W., Pakdeechote, P., et al. (2016). Asiatic Acid Prevents the Deleterious Effects of Valproic Acid on Cognition and Hippocampal Cell Proliferation and Survival. *Nutrients* 8 (5), 303. doi:10.3390/nu8050303

Veerendra Kumar, M., and Gupta, Y. (2003). Effect of *Centella asiatica* on Cognition and Oxidative Stress in an Intracerebroventricular Streptozotocin Model of Alzheimer's Disease in Rats. *Clin. Exp. Pharmacol. Physiol.* 30 (5-6), 336–342. doi:10.1046/j.1440-1681.2003.03842.x

Wanasuntronwong, A., Wanakhachornkrai, O., Phongphanphanee, P., Isa, T., Tantisira, B., and Tantisira, M. H. (2018). Modulation of Neuronal Activity on Intercalated Neurons of Amygdala Might Underlie Anxiolytic Activity of a Standardized Extract of *Centella asiatica* ECa233. *Evidence-Based Complement. Altern. Med.* 2018, 1–8. doi:10.1155/2018/3853147

Wong, J. H., Muthuraju, S., Reza, F., Senik, M. H., Zhang, J., Mohd Yusuf Yeo, N. A. B., et al. (2019). Differential Expression of Entorhinal Cortex and Hippocampal Subfields α-amino-3-hydroxy-5-methyl-4-isoxazolepropionic Acid (AMPA) and N-Methyl-D-Aspartate (NMDA) Receptors Enhanced Learning and Memory of Rats Following Administration of *Centella asiatica*. *Biomed. Pharmacother.* 110, 168–180. doi:10.1016/j.biopha.2018.11.044

Wong, J. H., Reza, F., Muthuraju, S., Chuang, H. G., Zhang, J., Senik, M. H., et al. (2020). Acute Application of *Centella asiatica* Extract Enhanced AMPAR-Mediated Postsynaptic Currents in Rat Entorhinal Cortex. *J. Integr. Neurosci.* 19 (2), 217–227. doi:10.31083/j.jin.2020.02.50

Xiong, Y., Ding, H., Xu, M., and Gao, J. (2009). Protective Effects of Asiatic Acid on Rotenone- or H2O2-Induced Injury in SH-SY5Y Cells. *Neurochem. Res.* 34 (4), 746–754. doi:10.1007/s11064-008-9844-0

Xu, M.-f., Xiong, Y.-y., Liu, J.-k., Qian, J.-j., Zhu, L., and Gao, J. (2012). Asiatic Acid, a Pentacyclic Triterpene in *Centella asiatica*, Attenuates Glutamate-Induced Cognitive Deficits in Mice and Apoptosis in SH-SY5Y Cells. *Acta Pharmacol. Sin.* 33 (5), 578–587. doi:10.1038/aps.2012.3

Xu, C.-L., Qu, R., Zhang, J., Li, L.-F., and Ma, S.-P. (2013). Neuroprotective Effects of Madecassoside in Early Stage of Parkinson's Disease Induced by MPTP in Rats. *Fitoterapia* 90, 112–118. doi:10.1016/j.fitote.2013.07.009

Yang, B., Xu, Y., Hu, Y., Luo, Y., Lu, X., Tsui, C. K., et al. (2016). Madecassic Acid Protects against Hypoxia-Induced Oxidative Stress in Retinal Microvascular Endothelial Cells via ROS-Mediated Endoplasmic Reticulum Stress. *Biomed. Pharmacother.* 84, 845–852. doi:10.1016/j.biopha.2016.10.015

Yang, L., Mao, K., Yu, H., and Chen, J. (2020). Neuroinflammatory Responses and Parkinson' Disease: Pathogenic Mechanisms and Therapeutic Targets. *J. Neuroimmune Pharmacol.* 15 (4), 830–837. doi:10.1007/s11481-020-09926-7

Yin, M.-C., Lin, M.-C., Mong, M.-C., and Lin, C.-Y. (2012). Bioavailability, Distribution, and Antioxidative Effects of Selected Triterpenes in Mice. *J. Agric. Food Chem.* 60 (31), 7697–7701. doi:10.1021/jf302529x

Yolanda, D. A., Sari, D. C. R., Rochmah, M. A., and Suharmi, S. (2015). The Dose Variations Effect of *Centella asiatica* Ethanol Extract o Escape Latency's Distance Morris Water Maze After Chronic Electrical Stress. *Kls* 2, 146–153. doi:10.18502/kls.v2i1.134

Yoo, S.-M., Park, J., Kim, S.-H., and Jung, Y.-K. (2020). Emerging Perspectives on Mitochondrial Dysfunction and Inflammation in Alzheimer's Disease. *BMB Rep.* 53 (1), 35–46. doi:10.5483/BMBRep.2020.53.1.274

Zhang, Z., Li, X., Li, D., Luo, M., Li, Y., Song, L., et al. (2017). Asiaticoside Ameliorates β-amyloid-induced Learning and Memory Deficits in Rats by Inhibiting Mitochondrial Apoptosis and Reducing Inflammatory Factors. *Exp. Ther. Med.* 13 (2), 413–420. doi:10.3892/etm.2016.4004

Zhao, Y., Shu, P., Zhang, Y., Lin, L., Zhou, H., Xu, Z., et al. (2014). Effect of Centella Asiaticaon Oxidative Stress and Lipid Metabolism in Hyperlipidemic Animal Models. *Oxidative Med. Cell Longevity* 2014, 1–7. doi:10.1155/2014/154295

Zheng, H.-M., Choi, M.-J., Kim, J. M., Cha, K. H., Lee, K. W., Park, Y. H., et al. (2016). Centella asiatica Leaf Extract Protects against Indomethacin-Induced Gastric Mucosal Injury in Rats. *J. Med. Food* 19 (1), 38–46. doi:10.1089/jmf.2015.3464

Zorova, L. D., Popkov, V. A., Plotnikov, E. Y., Silachev, D. N., Pevzner, I. B., Jankauskas, S. S., et al. (2018). Mitochondrial Membrane Potential. *Anal. Biochem.* 552, 50–59. doi:10.1016/j.ab.2017.07.009

Zweig, J. A., Brandes, M. S., Brumbach, B. H., Caruso, M., Wright, K. M., Quinn, J. F., et al. (2021). Loss of NRF2 Accelerates Cognitive Decline, Exacerbates Mitochondrial Dysfunction, and Is Required for the Cognitive Enhancing Effects of *Centella asiatica* during Aging. *Neurobiol. Aging* 100, 48–58. doi:10.1016/j.neurobiolaging.2020.11.019

Conflict of Interest: The authors declare that the research was conducted in the absence of any commercial or financial relationships that could be construed as a potential conflict of interest.

frontiers in Pharmacology

ORIGINAL RESEARCH
published: 09 August 2021
doi: 10.3389/fphar.2021.703894

Carnosic Acid Alleviates Levodopa-Induced Dyskinesia and Cell Death in 6-Hydroxydopamine-lesioned Rats and in SH-SY5Y Cells

*Chun-Yi Lai[1†], Chia-Yuan Lin[1†], Chi-Rei Wu[2], Chon-Haw Tsai[3,4,5] and Chia-Wen Tsai[1]**

[1]Department of Nutrition, China Medical University, Taichung, Taiwan, [2]Department of Chinese Pharmaceutical Sciences and Chinese Medicine Resources, China Medical University, Taichung, Taiwan, [3]Department of Neurology, China Medical University Hospital, Taichung, Taiwan, [4]College of Medicine, China Medical University, Taichung, Taiwan, [5]Graduate Institute of Acupuncture Science, College of Chinese Medicine, China Medical University, Taichung, Taiwan

OPEN ACCESS

Edited by:
Tahir Ali,
University of Calgary, Canada

Reviewed by:
Jue He,
Wenzhou Medical University, China
Muhammad Ikram,
Gyeongsang National University, South Korea

***Correspondence:**
Chia-Wen Tsai
cwtsai@mail.cmu.edu.tw

†These authors have contributed equally to this work

Specialty section:
This article was submitted to Neuropharmacology, a section of the journal Frontiers in Pharmacology

Received: *30 April 2021*
Accepted: *26 July 2021*
Published: *09 August 2021*

Citation:
Lai C-Y, Lin C-Y, Wu C-R, Tsai C-H and Tsai C-W (2021) Carnosic Acid Alleviates Levodopa-Induced Dyskinesia and Cell Death in 6-Hydroxydopamine-lesioned Rats and in SH-SY5Y Cells. Front. Pharmacol. 12:703894. doi: 10.3389/fphar.2021.703894

The present study investigated the impact of carnosic acid (CA) from rosemary on the levodopa ($_L$-dopa)-induced dyskinesia (LID) in rats treated with 6-hydroxydopamine (6-OHDA). To establish the model of LID, 6-OHDA-lesioned rats were injected intraperitoneally with 30 mg/kg $_L$-dopa once a day for 36 days. Rats were daily administrated with 3 or 15 mg/kg CA by oral intubation prior to $_L$-dopa injection for 4 days. Rats pretreated with CA had reduced $_L$-dopa-induced abnormal involuntary movements (AIMs) and ALO scores (a sum of axial, limb, and orofacial scores). Moreover, the increases of dopamine D1-receptor, p-DARPP-32, ΔFosB, p-ERK1/2, and p-c-Jun ser63, along with the decrease in p-c-Jun ser73, induced by $_L$-dopa in 6-OHDA-treated rats were significantly reversed by pretreatment with CA. In addition, we used the model of SH-SY5Y cells to further examine the neuroprotective mechanisms of CA on $_L$-dopa-induced cytotoxicity. SH-SY5Y cells were treated with CA for 18 h, and then co-treated with 400 μM $_L$-dopa for the indicated time points. The results showed that pretreatment of CA attenuated the cell death and nuclear condensation induced by $_L$-dopa. By the immunoblots, the reduction of Bcl-2, p-c-Jun ser73, and parkin and the induction of cleaved caspase 3, cleaved Poly (ADP-ribose) polymerase, p-ERK1/2, p-c-Jun ser63, and ubiquitinated protein by $_L$-dopa were improved in cells pretreated with CA. In conclusion, CA ameliorates the development of LID *via* regulating the D1R signaling and prevents $_L$-dopa-induced apoptotic cell death through modulating the ERK1/2-c-Jun and inducing the parkin. This study suggested that CA can be used to alleviate the adverse effects of LID for PD patients.

Keywords: carnosic acid, 6-hydroxydopamine, levodopa-induced dyskinesia, DARPP-32/ΔFosB, ERK1/2-c-jun

INTRODUCTION

Parkinson's disease (PD) is a progressive neurodegenerative disease. Levodopa ($_L$-dopa), the precursor of dopamine, is the primary drug used to treat PD (Cenci, 2014). However, long-term exposure to $_L$-dopa causes motor complications, called levodopa-induced dyskinesia (LID) (Chaudhuri et al., 2019). LID develops in about 40–50% of patients in the 5 years after treatment and in up to 100% of patients after 10 years of treatment (Manson et al., 2012). The symptoms of LID include chorea, ballism, dystonia, and myoclonus (Calabresi et al., 2010). New adjunct therapies to delay or reduce these adverse effects are needed.

The mechanisms by which LID develops are complex. LID is associated with the hypersensitization of striatum dopamine D1-receptor (D1R) induced by impaired receptor trafficking (Feyder et al., 2011; Spigolon and Fisone, 2018), which results in the abnormal change of proteins of PKA, ΔFosB, and extracellular signal-regulated kinases1/2 (ERK1/2) (Fieblinger et al., 2014). An evidence has shown that pulsatile administration of $_L$-dopa activates the proteins of DARPP-32, ERK, and ΔFosB in 6-OHDA-lesioned rats (Lebel et al., 2010). $_L$-Dopa stimulates D1R coupled with G-protein α/olf to activate PKA, and then phosphorylates DARPP-32 protein at Thr34, leading to increase the ERK1/2 activity. The activation of ERK1/2 results in increased the activation of ΔFosB by cAMP response element-binding protein (CREB) (Fanni et al., 2018; Spigolon and Fisone, 2018). Striatal ΔFosB protein is correlated with the severity of LID in $_L$-dopa-treated monkeys (Berton et al., 2009). ΔFosB is also found in the striatum of PD patients treated with $_L$-dopa (Lindgren et al., 2011). Silencing of striatal ΔFosB-expression neurons improves the motor complication of LID in PD rat model (Engeln et al., 2016). Conversely, overexpression of ΔFosB in 6-hydroxydopamine (6-OHDA)-treated rats exacerbates the effects of LID (Cao et al., 2010).

Accumulating evidence indicates that cells cultured with $_L$-dopa induced neurotoxicity *via* generating oxidative damage (Colamartino et al., 2015). It has been shown that the process of dopamine synthesis from $_L$-dopa enhances the formation of reactive oxygen species (ROS) *via* regulating monoamine oxidase (Stansley and Yamamoto, 2013). This induction is enhanced for PD patients treated with $_L$-dopa and leads to the apoptotic neuronal cell death (Hald and Lotharius, 2005; Dorszewska et al., 2014). Consistent with the results, the increment of cleaved-caspase 3 and -poly (ADP-ribose) polymerase (PARP) proteins is observed in PD patients treated with $_L$-dopa (Hald and Lotharius, 2005). In addition to oxidative stress, study indicates that $_L$-dopa-induced cell death is mediated by ERK1/2-c-Jun pathway (Park et al., 2016). The transcription factor c-Jun regulates cell survival and cell death through regulating its phosphorylation sites by ERK1/2 pathway. An observation by Park et al. suggested that the neurotoxicity caused by long-term $_L$-dopa administration may involve the induction of c-Jun phosphorylation at ser63 and reduction of c-Jun phosphorylation at ser73, which acts as a pro- or anti-apoptotic factor, respectively (Park et al., 2016). An understanding of the possible of neurotoxicity by $_L$-dopa in PD will help to improve the motor complication of LID.

Carnosic acid (CA), a diterpene phenolic compound from rosemary, has multiple physiological benefits, including anti-oxidant and neuroprotective (Guo et al., 2016; Lin et al., 2020). In our previous study, we reveals that the neuroprotective mechanisms of CA are related to the upregulation of anti-oxidant enzymes in PD models (Chen et al., 2012; Wu et al., 2015). CA stimulates glutathione synthesis to inhibit 6-hydroxydopamine (6-OHDA)-induced apoptosis of SH-SY5Y cells through down-regulating of c-Jun NH_2-terminal kinase (JNK) and p38 (Chen et al., 2012). Furthermore, administration of CA with 6-OHDA-lesioned rats improves the antioxidant capacity, neurotoxicity, and motor impairment (Wu et al., 2015). Although CA is currently being investigated for therapeutic benefits in PD, the actions of CA on the development of LID have not yet been described. Therefore, in this study, we explored the roles of CA on LID in 6-OHDA-lesioned rats and further examined the cytotoxicity of $_L$-dopa in SH-SY5Y cells.

MATERIALS AND METHODS

Experimental Animals and Treatments

Eight-week-old male Wistar rats (BioLASCO Experimental Animal Center, Taipei, Taiwan) were used in this study. The protocols for animal-related experiments were approved by the Institutional Animal Care and Use Committee of China Medical University (protocol no. 2017–189). The temperature of the animal husbandry rooms was set at 23 ± 1°C with a 12-h day and night cycle. Animals had ad libitum access to a chow diet and water. After 11 days of adaptation, 6-OHDA (Sigma, St. Louis, MO, United States) injury surgery was performed as described below to induce PD. On day 17 after lesion formation, an apomorphine (0.25 mg/kg)-induced rotation experiment (exhibited >7 full turns/min) were performed to select for next experiment (Zhang et al., 2018). The experimental groups were as follows: 1) vehicle group (6-OHDA lesion, n = 5); 2) $_L$-dopa group: 30 mg/kg $_L$-dopa + 15 mg/kg benserazide (n = 5); 3) $_L$-dopa + CA3 group: 30 mg/kg $_L$-dopa + 15 mg/kg benserazide +3 mg/kg CA (n = 5); 4) $_L$-dopa + CA15 group: 30 mg/kg $_L$-dopa + 15 mg/kg benserazide +15 mg/kg CA (n = 5). $_L$-Dopa (Sigma, St. Louis, MO, United States) and benserazide (Sigma, St. Louis, MO, United States) were injected intraperitoneally with potassium phosphate buffer once per day for 36 consecutive days. In the CA-treated group, CA (Cayman, Ann Arbor, MI, Cat No.89820) was dissolved in 0.5% sodium carboxymethyl cellulose and was administered 4 days before the $_L$-dopa injection by oral intubation once per day until the rats were sacrificed.

6-OHDA Injury Surgery

According to a previous study in our laboratory (Wu et al., 2015), rats were anesthetized with tiletamine/zolazepam (Zoletil50®; Virbac Lab., Carros, France) by intramuscular injection. The rats were fixed on a stereotaxic apparatus and 2.5 μl of 6-OHDA (5 μg/μl) was injected into the right striatum (anteroposterior: +1.5 mm; lateral: −4 mm; dorsoventral: −7.2 mm) with a flow rate of 1 μl/min. The drug delivery tube

was left in place for 1 min before being removed to avoid seepage of 6-OHDA. The sham operation group was injected with 0.5% ascorbic acid-saline.

Abnormal Involuntary Movement Scores

Behavioral analysis subtypes and scoring criteria were based the study by Winkler et al. (Winkler et al., 2002). AIM scores were assessed on days 12, 26, and 33 after L-dopa administration. The rats were placed in a transparent cage for a 2-h photographic record and were scored for 1 min every 20 min. Each rat was assessed for four AIM subtypes: axial, limb, orofacial, and locomotor movements. A severity score ranging from 0 to 4 was assigned for each AIM subtype. The AIM scores from four subtypes were summed for each time point. The ALO score (sum of the axial, limb, and orofacial scores) is more responsive to human dyskinesia than are locomotive scores (Castello et al., 2020). Therefore, the ALO score was also analyzed in this study.

Preparation of Animal Tissues

After the animals were sacrificed, the striatum on the right side was separated and homogenized (10% w/v) in RIPA buffer (Biokit, Taiwan) containing 1% protease inhibitor (Sigma, St. Louis, MO, United States) and 1% phosphatase inhibitor (Sigma, St. Louis, MO, United States). The supernatant was obtained after centrifugation at 15,000 rpm for 30 min at 4°C.

Cell Culture and Sample Preparation

The SH-SY5Y cells were purchased from American Type Culture Collection (ATCC, Manassas, VA, United States). The method of cell culture was based on our previous study (Lin et al., 2016). The cells were plated on 3.5 cm cell culture dishes and incubated with Dulbecco's modified Eagle medium (DMEM) including 10% FBS, 1% L-glutamine, 1% non-essential amino acid, 1 mM sodium pyruvate, 1.5 g/ml sodium bicarbonate, 1% penicillin-streptomycin; pH = 7.4. Cells were pretreated with 0.1% dimethylsulfoxide (DMSO) or 0.5, 1, or 3 μM CA for 18 h followed by treatment with PBS or 20, 200, or 400 μM L-dopa for an additional 24 or 72 h. After treatment, the RIPA buffer containing 1% protease inhibitor and 1% phosphatase inhibitor was added to each plate and the cells were collected for protein analysis. Lysates were centrifuged at 14,000 rpm for 20 min at 4°C to obtain the supernatant. The protein assay dye reagent concentrate (BIO-RAD, Hercules, CA, United States) was used to measure protein concentration.

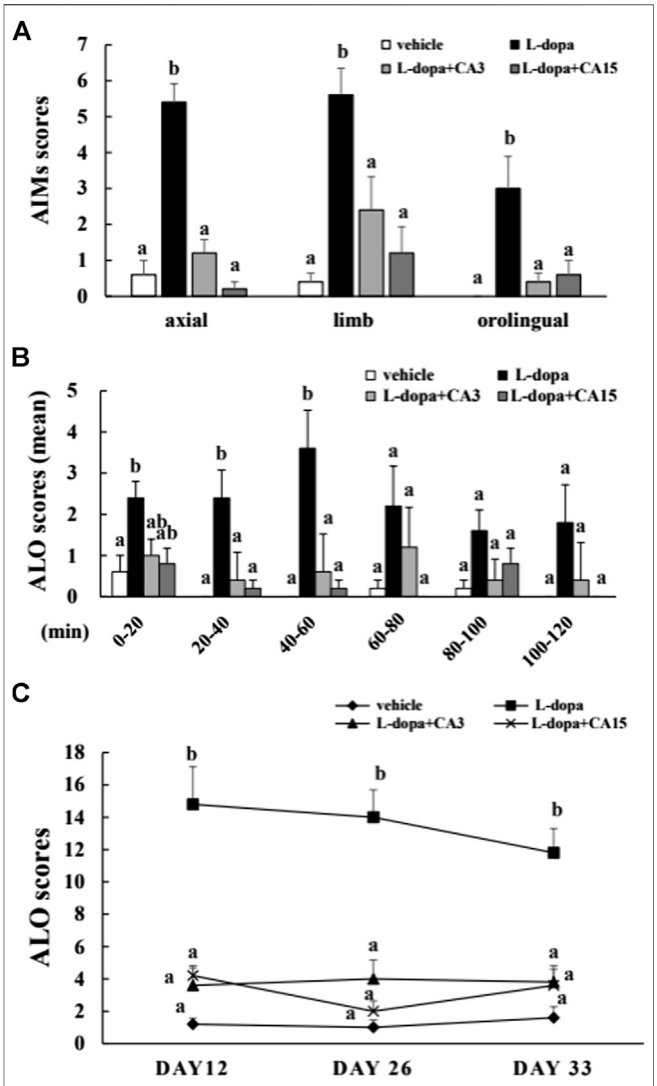

FIGURE 1 | Effect of CA on L-dopa-induced abnormal involuntary movements (AIMs) in 6-OHDA lesioned rats. The axial, limb, and orofacial AIMs were calculated on days 12, 26, and 33 for 1 min every 20 min over 120 min. **(A)** The integrated AIM scores of axial, limb, and orofacial subtype on day 26 over 120 min. **(B)** The ALO score (the sum of axial, limb, and orofacial) on day 26 for 1 min every 20 min over 120 min. **(C)** The ALO score on days 12, 26, and 33. The results are expressed as mean ± SEM (n = 5). Means without a common letter differ, $p < 0.05$.

Western Blot Analysis

Samples containing the same protein concentrations were subjected to sodium dodecyl sulfate-polyacrylamide gel electrophoresis and then transferred to polyvinylidene fluoride membranes (Millipore, Bedford, MA, united States). The membranes were placed in 50 g/L skim milk at 4°C to block the nonspecific binding sites. The membranes were incubated with primary antibodies, including D1R (Santa Cruz Biotechnology (SCBT); sc-33660), p-DARPP-32 (GeneTex; GTX82714), ΔFosB (Cell Signaling Technology (CST); #14695), p-ERK1/2 (SCBT; sc-7383), ERK1/2 (SCBT; sc-93), p-c-Jun ser63 (SCBT; sc-822), p-c-Jun ser73 (CST; #3270), Bcl-2 (CST; #2876), caspase 3 (CST; #9662), cleaved caspase 3 (CST; #9661), PARP (CST; #9542), cleaved PARP (CST; #9541), parkin (SCBT; sc-32282), ubiquitin (Sigma-Aldrich; 05–944), β-tubulin (SCBT; sc-9104) and GAPDH (SCBT; sc-365062) at 4°C overnight and were then subsequently incubated with horseradish peroxidase-conjugated goat anti-rabbit (SCBT; sc-2004), goat anti-mouse IgG (SCBT; sc-2005), or mouse IgG kappa binding protein (m-IgGκ BP)-HRP (SCBT; sc-516102) secondary antibodies. The protein expression on the membrane was detected with an enhanced chemiluminescence reagent (Millipore, Burlington, MA, United States) and analyzed by a luminescent image analyzer (LAS-4000, FUJIFILM).

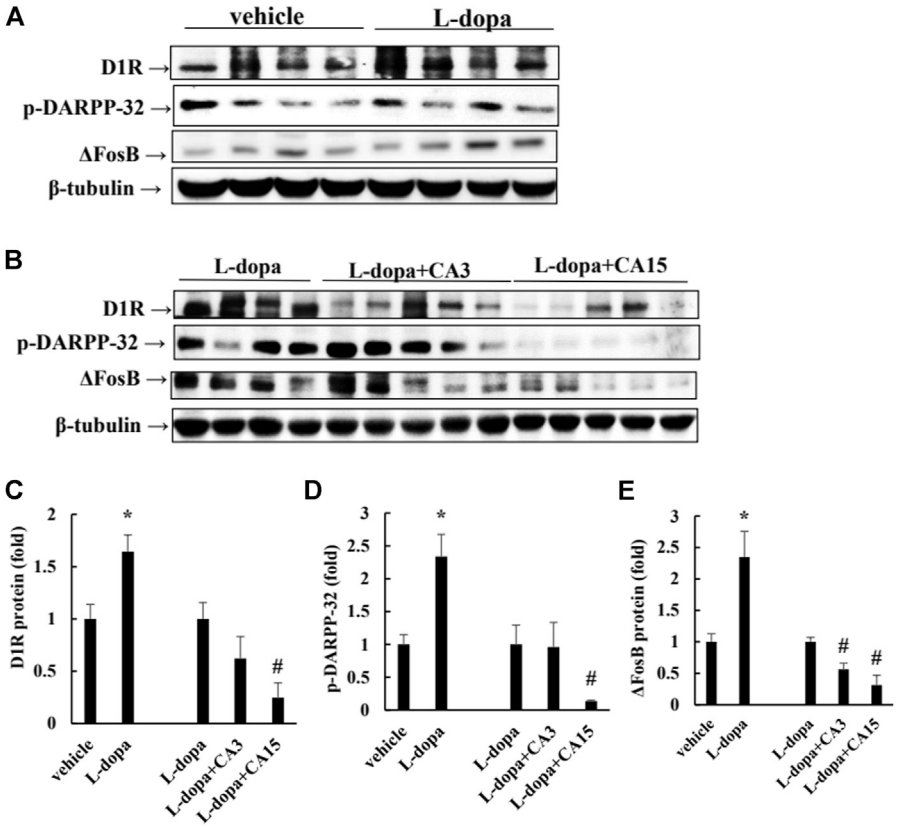

FIGURE 2 | Effect of CA on $_{L}$-dopa-induced D1R, p-DARPP-32, and ΔFosB protein in 6-OHDA-lesioned rats. **(A,B)** D1R, p-DARPP-32, and ΔFosB protein were determined by Western blotting. β-Tubulin was used as the internal control. **(C–E)** The level of the $_{L}$-dopa group was set at 1.0. Values are mean ± SEM ($n = 3$). #$p < 0.05$ compared with $_{L}$-dopa-treated group.

Cell Viability Assay

Cells were washed with phosphate-buffered saline and incubated with DMEM containing 0.5 mg/ml 3-(4,5-dimethylthiazol-2-yl)-2,5-diphenyltetrazolim bromide (MTT) for 2 h at 37°C. After the medium was removed, the formazan crystal was dissolved with 1 ml of isopropanol and then centrifuged at 15,000 rpm for 5 min to get the supernatant. The supernatant was added to a 96-well plate, and absorbance was measured at 570 nm by ELISA (Bio-Rad, Japan). The value in the control cells was set as 100% viability.

Nuclear Staining With Hoechst 33258

Cells were washed with phosphate-buffered saline and fixed with 3.7% paraformaldehyde (pH 7.4) solution for 50 min. Then, the cells were stained with Hoechst 33258 for 1 h at 25°C in the dark and morphological changes were observed by using a fluorescence microscope. Fluorescence intensity was obtained by use of Image-Pro Plus 6.0 (Media Cybernetics, Inc., Bethesda, MD, United States).

Statistical Analysis

All *in vivo* data are presented as the mean ± SEM. The *in vitro* data are expressed as mean ± SD. Statistical analysis was performed with t-tests between two sample comparisons. The multiple comparisons were conducted with a one-way analysis of variance (ANOVA) with SAS software followed by Tukey's post hoc test. Statistically significant differences were considered when the *p*-value was less than 0.05.

RESULTS

CA Improves AIMs Induced by $_{L}$-Dopa in Lesioned Rats

The axial, limb, and orofacial scores on day 26 in the $_{L}$-dopa group were significantly higher than in the vehicle group ($p < 0.05$), whereas those in the groups pretreated with 3 or 15 mg/kg CA were significantly lower than in the $_{L}$-dopa group ($p < 0.05$) (**Figure 1A**). We then divided the total recording time into 20-min intervals, and used a total of 6 intervals for score statistics. In this analysis, CA improved the ALO score (the sum of the axial, limb, and orofacial scores) during the 20–40 min and 40–60 min intervals (**Figure 1B**). In addition, the ALO scores in the $_{L}$-dopa group were significantly higher than in the vehicle group on days 12, 26, and 33. However, the ALO scores in the group pretreated with 3 and 15 mg/kg CA were lower compared with those in the $_{L}$-dopa group ($p < 0.05$) (**Figure 1C**). These results suggest that CA can improve AIMs caused by $_{L}$-dopa.

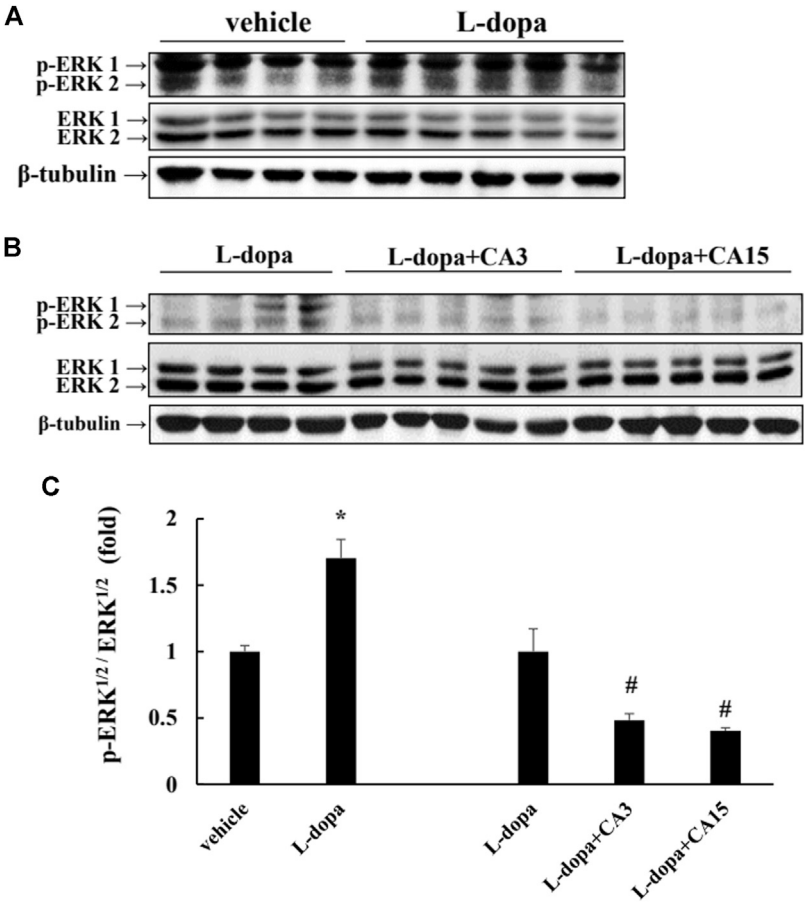

FIGURE 3 | Effect of CA on $_{L}$-dopa-induced activation of ERK1/2 and c-Jun in 6-OHDA lesioned rats. The phosphorylation of ERK1/2 **(A,B)** in striatum tissues were determined by Western blotting. β-Tubulin was used as the internal control. **(C)** The level of the $_{L}$-dopa group was set at 1.0. Values are mean ± SEM (n = 3). #p < 0.05 compared with $_{L}$-dopa-treated group.

CA Reduces LID Marker Proteins in Lesioned Rats

Over-activation of D1R phosphorylates DARPP-32, which ultimately leads to an increase in FosB family proteins, which causes LID (Ahn et al., 2017). Rats treated with $_{L}$-dopa significantly increased D1R and p-DARPP-32, as well as ΔFosB protein ($p < 0.05$). Pretreatment of rats with CA at 15 mg/kg prior to 4 days of $_{L}$-dopa treatment, significantly reduced D1R and p-DARPP-32 compared with that in the $_{L}$-dopa group ($p < 0.05$). However, pretreatment with 3 mg/kg CA had no significant effect. ΔFosB proteins were reduced in the group pretreated with 3 and 15 mg/kg CA by 44 and 69%, respectively, compared with the $_{L}$-dopa group (**Figure 2**). This result suggests that CA reduced the activation of D1R and DARPP-32, leading to improved accumulation of ΔFosB protein induced by $_{L}$-dopa.

Effect of CA on the Phosphorylation of ERK1/2 and c-Jun in Lesioned Rats

It has been reported that $_{L}$-dopa induces continuous activation of ERK1/2 to promote c-Jun phosphorylation at Ser63 (as a pro-apoptotic factor) and reduces c-Jun phosphorylation at Ser73 (as an anti-apoptotic factor) (Park et al., 2016). We found that rats treated with $_{L}$-dopa significantly increased the activation of ERK1/2 and c-Jun Ser63 ($p < 0.05$). (**Figures 3A**, **4A**). However, phosphorylation of ERK1/2 and c-Jun Ser63 was reduced in cells pretreated with 3 and 15 mg/kg CA (**Figures 3B**, **4B**). CA at 15 mg/kg reduced the activation of ERK1/2 and c-Jun Ser63 by 60 and 88%, respectively, compared with that in the $_{L}$-dopa group ($p < 0.05$). However, only the group pretreated with 15 mg/kg CA showed an increase in the phosphorylation of c-Jun Ser73 of about 97% compared with the $_{L}$-dopa group ($p < 0.05$) (**Figure 4B**).

CA Prevents Apoptosis Induced by $_{L}$-Dopa in SH-SY5Y Cells

We further used SH-SY5Y cells to explore the effect of CA on cytotoxicity induced by $_{L}$-dopa. The results indicated that $_{L}$-dopa dose-dependently reduced cell viability. Cell viability in cells treated with 400 μM $_{L}$-dopa was reduced by about 36% compared with the control group (**Figure 5A**) Pretreatment with 1 and 3 μM CA, however, was able to increase cell viability by 21 and 34%, respectively, in $_{L}$-dopa-treated cells compared with that in cells

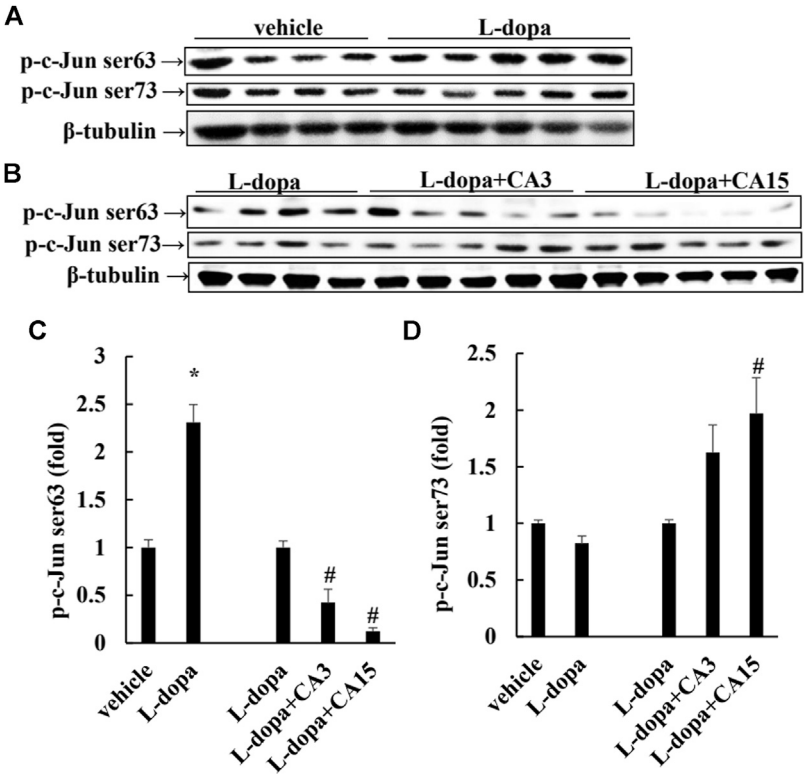

FIGURE 4 | Effect of CA on $_{L}$-dopa-induced activation of ERK1/2 and c-Jun in 6-OHDA lesioned rats. The phosphorylation of c-Jun Ser63 and c-Jun Ser73 in striatum tissues were determined by Western blotting **(A,B)**. β-Tubulin was used as the internal control. **(C,D)** The level of the $_{L}$-dopa group was set at 1.0. Values are mean ± SEM (n = 3). #p < 0.05 compared with $_{L}$-dopa-treated group.

treated with $_{L}$-dopa alone (p < 0.05) (**Figure 5B**). The results of Hoechst 33258 staining were similar, as shown in **Figure 5C**. Exposure to $_{L}$-dopa induced the intensity of Hoechst 33258 fluorescence, suggesting that $_{L}$-dopa treatment increased nuclear condensation and then induced apoptosis. However, the effect of $_{L}$-dopa on nuclear condensation was reduced in cells pretreated with CA. We then used immunoblotting to examine the effect on proteins related to apoptosis. $_{L}$-Dopa dose-dependently reduced the expression of Bcl-2 protein and increased the ratio of cleaved caspase 3/caspase 3 and cleaved PARP/PARP (**Figures 6A,B**). CA pretreatment reversed these findings.

CA Regulates ERK1/2/c-Jun Signaling Induced by $_{L}$-Dopa in SH-SY5Y Cells

The phosphorylation of ERK1/2 and c-Jun Ser63 was increased in cells treated with $_{L}$-dopa, and the activation of c-Jun Ser73 was reduced (**Figure 7**). However, pretreatment with CA improved the effects of $_{L}$-dopa on these proteins (p < 0.05).

CA Improves the Expression of Parkin and Ubiquitinated Protein Induced by $_{L}$-Dopa in SH-SY5Y Cells

Parkin is a ubiquitin protein ligase E3 and plays a critical role in the ubiquitin-proteasome system (UPS) (Higashi et al., 2004). The activation of D1R by $_{L}$-dopa is associated with the dysregulation of the (Berthet et al., 2012). Therefore, in this study, we also examined ubiquitinated-related proteins. We found that parkin protein was reduced and ubiquitinated protein was increased in cells treated with $_{L}$-dopa (**Figure 8**). CA pretreatment improved both proteins in cells treated with $_{L}$-dopa (p < 0.05).

DISCUSSION

LID is the adverse events after long-term use of $_{L}$-dopa in PD patients (Chaudhuri et al., 2019). Several strategies for overcoming LID have been developed, but some of these have limitations (Ryu et al., 2018). In the current study, we revealed that CA could improve the development of LID in a 6-OHDA-lesioned rat model. CA inhibited D1R-induced signaling, including p-DARPP-32, p-ERK1/2, and ΔFosB. Moreover, we revealed that CA attenuated the levels of cleaved-caspase 3 and -PARP by $_{L}$-dopa is associated with the regulation of the ERK1/2-c-Jun pathway. In addition, we found that CA increased parkin protein to reduce the ubiquitinated protein by $_{L}$-dopa. It is the first study to show the favorable effect of CA against the side effects inducing by $_{L}$-dopa treatment for PD.

LID is a serious motor complication that develops after long-term $_{L}$-dopa therapy for PD (Sun et al., 2020). Study indicated

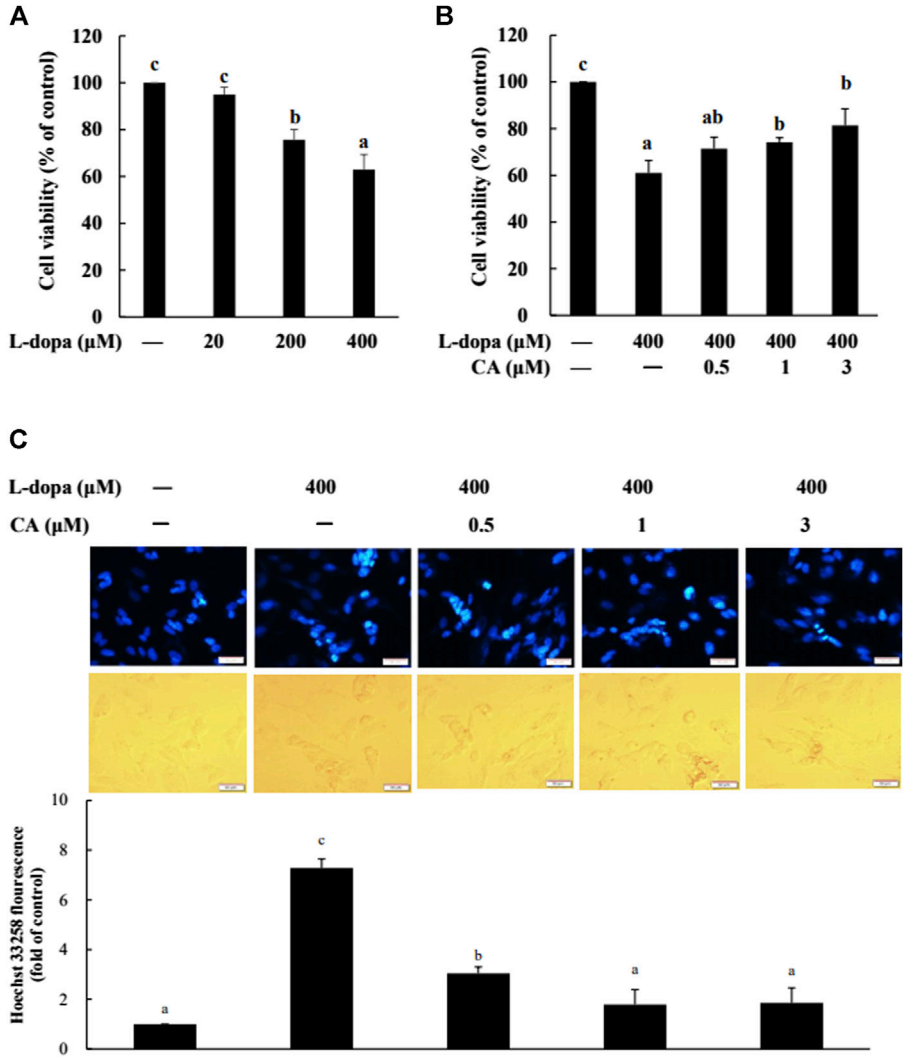

FIGURE 5 | Effect of CA on L-dopa-induced toxicity in SH-SY5Y cells. Cell viability was measured by MTT assay. **(A)** Cells were pretreated with 20, 200, and 400 μM L-dopa for 72 h. Control (–) was treated with PBS. **(B)** Cells were pretreated with 0.1% DMSO alone (–) or 0.5, 1, and 3 μM CA for 18 h and were then treated with 400 μM L-dopa for an additional 72 h. **(C)** Nuclei were visualized with Hoechst 33258 staining. Cells were pretreated with DMSO alone (–) or 0.5, 1, or 3 μM CA for 18 h and were then treated with 400 μM L-dopa for an additional 24 h. One representative image out of three independent experiments is shown. Values are mean ± SD (n = 3). Means not sharing a common letter are significantly different, $p < 0.05$.

that the time-course of L-dopa during 0–60 min exhibits higher total AIM and ALO scores (Ryu et al., 2018). Consistent with these results, our results revealed that the ALO scores are higher after L-dopa administration during 0–60 min. CA group decreased the ALO scores during 20–60 min. Moreover, CA treatment exhibited lower the ALO scores up to 33 days. These results suggested that CA is beneficial for long-term treatment of LID for PD. Recent studies have reported that the behavioral expression of LID is associated with D1R signaling. However, the signaling was unchanged by continuous administration of L-dopa through a subcutaneous mini-pump, suggesting prevention the fluctuation of L-dopa concentrations relieved the LID (Lebel et al., 2010). In the present study, CA attenuated the activation of D1R/DARPP32/ERK1/2 cascade and subsequently led to counteract the effect of LID in 6-OHDA-lesioned rats. Because D1R signaling is triggered by the activation of PKA, study reported that treatment with PKA inhibitor Rp-cAMPS alleviated the LID in 6-OHDA-lesioned rats (Lebel et al., 2010). Similarly, researchers showed that blocking ERK1/2 phosphorylation by SL327 reduces LID in 6-OHDA-lesioned mice treated with L-dopa (Santini et al., 2007). Study also indicated that ΔFosB is accumulated after abusing some drugs and increased the sensitivity to the behavioral effects (Nestler et al., 2001). The present study found that striatal ΔFosB protein induction is related with the AIM and ALO scores by L-dopa. In parallel with behavior reversal, CA treatment reduced D1R/DARPP32/ERK1/2 cascade and decreased ΔFosB protein caused by L-dopa treatment.

Research shows that ERK1/2 activation is involved in the neuronal cell viability induced by L-dopa treatment (Park et al., 2016). Treatment

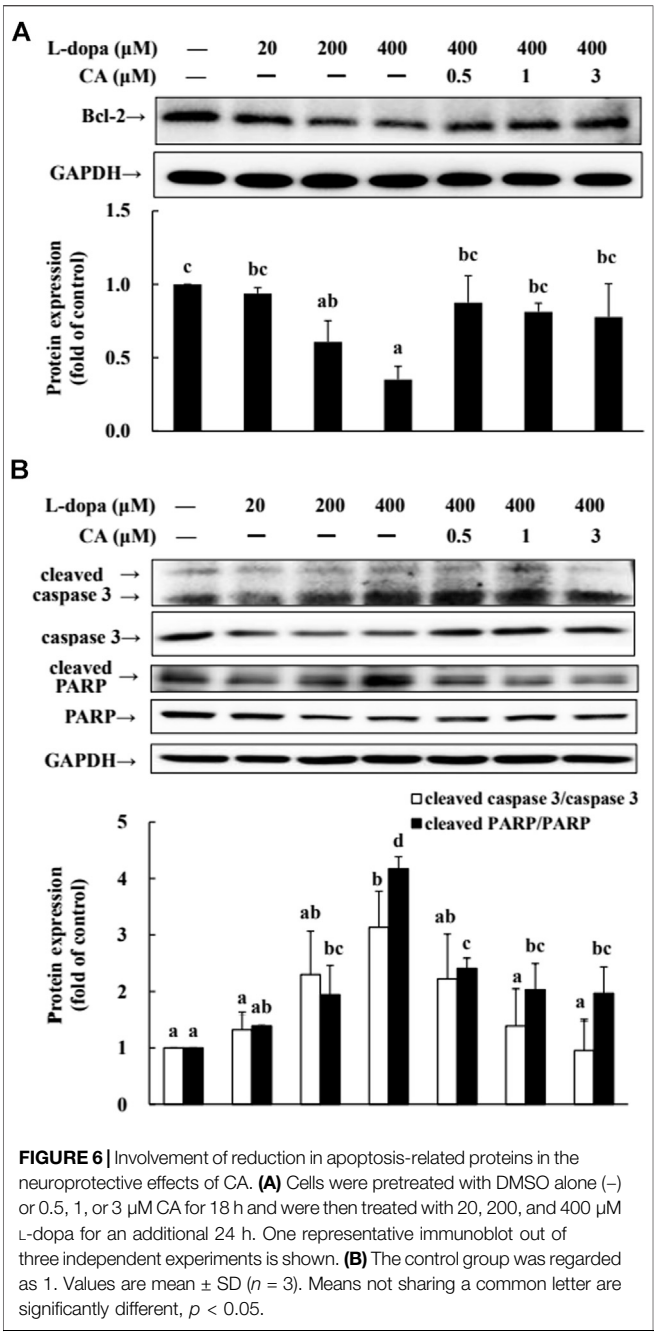

FIGURE 6 | Involvement of reduction in apoptosis-related proteins in the neuroprotective effects of CA. **(A)** Cells were pretreated with DMSO alone (–) or 0.5, 1, or 3 μM CA for 18 h and were then treated with 20, 200, and 400 μM L-dopa for an additional 24 h. One representative immunoblot out of three independent experiments is shown. **(B)** The control group was regarded as 1. Values are mean ± SD (n = 3). Means not sharing a common letter are significantly different, $p < 0.05$.

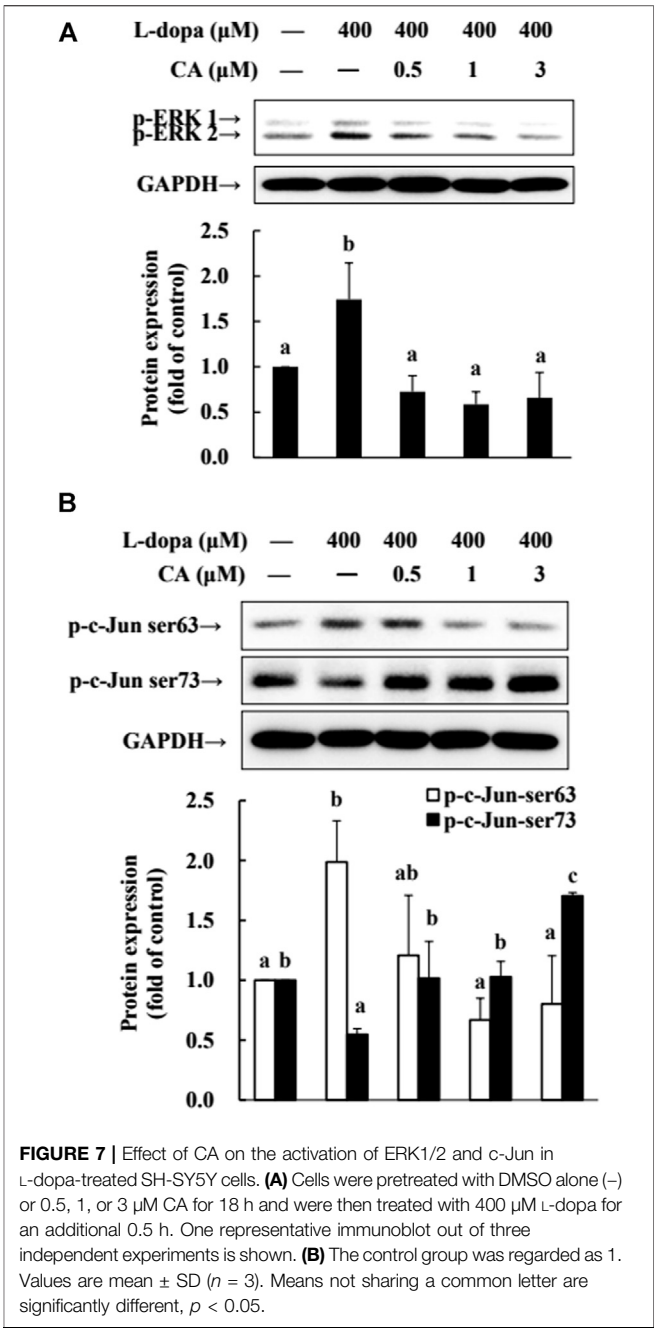

FIGURE 7 | Effect of CA on the activation of ERK1/2 and c-Jun in L-dopa-treated SH-SY5Y cells. **(A)** Cells were pretreated with DMSO alone (–) or 0.5, 1, or 3 μM CA for 18 h and were then treated with 400 μM L-dopa for an additional 0.5 h. One representative immunoblot out of three independent experiments is shown. **(B)** The control group was regarded as 1. Values are mean ± SD (n = 3). Means not sharing a common letter are significantly different, $p < 0.05$.

of PC12 cells with L-dopa induces the activation of ERK1/2 and caspase 3 (Jin et al., 2010; Park et al., 2014). Similarly, in 6-OHDA-lesioned rats, administration of L-dopa upregulated the ERK1/2 activation, leading to increase c-Jun phosphorylation at ser63, but decrease c-Jun phosphorylation at ser73 (Park et al., 2016). It is because L-dopa at high concentrations was cytotoxic and stimulated the activities of ERK1/2 and caspase 3. These results could explain that PD patients after long-term exposure to L-dopa increased neurotoxic events (Blandini et al., 2004) and stimulated abnormal involuntary movements (Chaudhuri et al., 2019). Our results in the present study supported the report that L-dopa increased ERK1/2/c-Jun activation and enhanced caspase 3 activation (**Figures 3**, **4**, **6**, **7**). CA treatment could increase the cell survival through reducing the ERK1/2 activation and alleviating the alternation of c-Jun pathway to prevent apoptotic neuronal cell death.

Recently, evidence reported that dysregulation membrane localization of dopamine D1R impairs the striatal ubiquitin-proteasome system and increases the accumulation of ubiquitinated protein to exaggerate the D1R transmission (Barroso-Chinea et al., 2015). Parkin, an ubiquitin E3 ligase, facilitates multiple misfolded proteins degradation by 26S

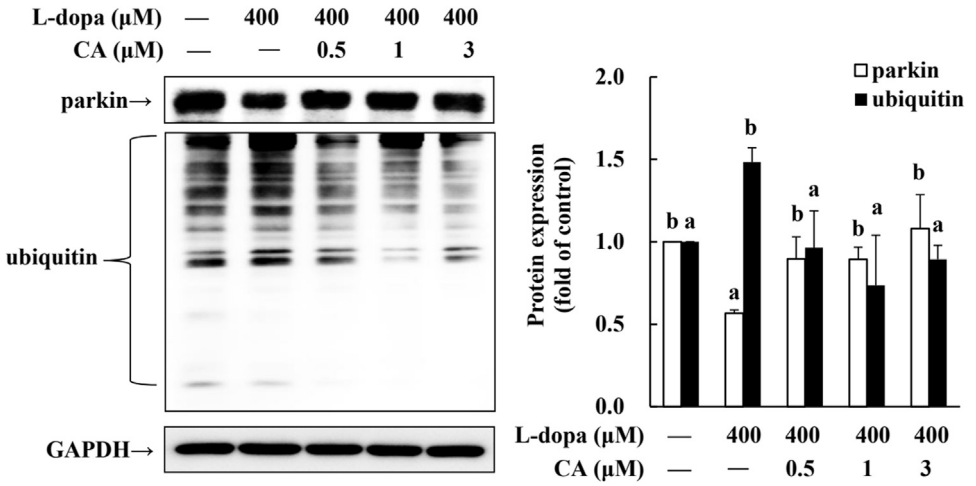

FIGURE 8 | Effect of CA on the expression of parkin and ubiquitinated protein in $_{L}$-dopa-treated SH-SY5Y cells. Cells were pretreated with DMSO alone (–) or 0.5, 1, or 3 μM CA for 18 h and were then treated with 400 μM L-dopa for an additional 24 h. One representative immunoblot out of three independent experiments is shown. The control group was regarded as 1. Values are mean ± SD (n = 3). Means not sharing a common letter are significantly different, $p < 0.05$.

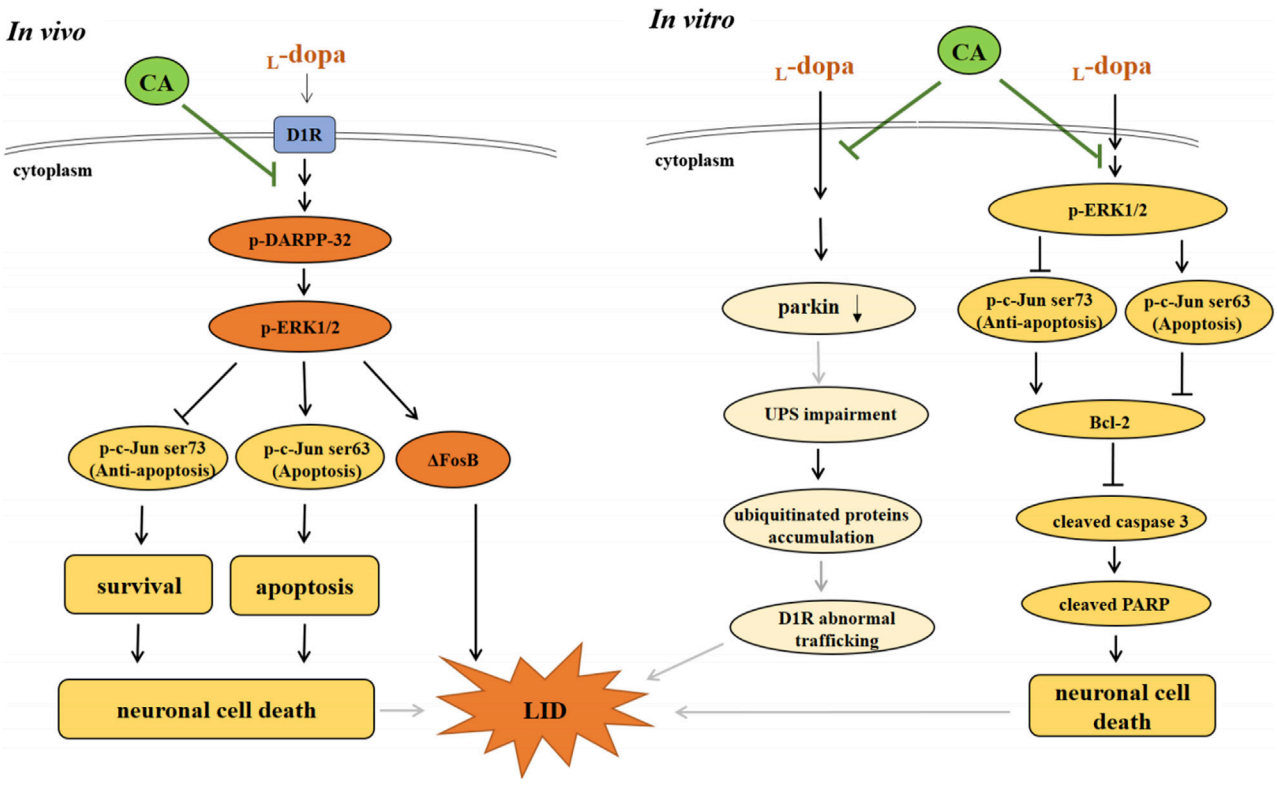

FIGURE 9 | The actions of neuroprotective mechanism of CA on LID in *in vivo* and *in vitro* studies. **(A)** In *in vivo* study, $_{L}$-dopa stimulates DIR protein, and then activates the phosphorylation of DARPP-32 and ERK1/2, which elevates ΔFosB protein, leading to develop the LID in 6-OHDA-lesioned rats. Moreover, $_{L}$-dopa administration induced neuronal cell death through regulating ERK1/2-c-Jun pathway. However, CA alleviates these effects induced by $_{L}$-dopa. **(B)** In *in vitro* study, pretreatment of CA with SH-SY5Y cells attenuates $_{L}$-dopa-triggered apoptotic cell death mediated *via* increasing c-Jun ser73 activation and decreasing c-Jun ser63 activation by ERK1/2. Additionally, CA could be improved the development of LID is related to the induction of parkin protein, leading to prevent the ubiquitinated protein accumulation and D1R abnormal trafficking (gray line).

proteasome, and plays an important role in neuroprotection (Wilhelmus et al., 2012). Study reported that knockdown of parkin displays the higher AIMs scores than in wild-type mice. Moreover, compare to control mice, parkin mutant mice shows an earlier onset of AIMs (Berthet et al., 2012). Our previous study indicated that CA acts to attenuate 6-OHDA-induced neurotoxicity associated with the induction of parkin through enhancing UPS and preventing apoptosis (Lin et al., 2016). In this study, we have shown that SH-SY5Y cells treated with $_{L}$-dopa decreased the parkin and increased the ubiquitinated protein; however, CA pretreatment reversed parkin and ubiquitinated proteins by $_{L}$-dopa. Therefore, we speculated that CA up-regulated the parkin protein and reduced the D1R abnormal trafficking, leading to alleviation of D1R signaling and LID.

In conclusion, the results of the current indicate that CA can alleviate LID-induced behavior changes in 6-OHDA-treated rats by regulating the D1R-mediated activation of DARPP-32 and ΔFosB. The protective mechanisms of CA are involved with the inactivation of ERK1/2/c-Jun pathway and the induction of parkin protein, leading to reduction of apoptotic neuronal cell death and LID (**Figure 9**). CA could be recommended as a beneficial therapy for delaying the development of LID in PD patients.

DATA AVAILABILITY STATEMENT

The raw data supporting the conclusion of this article will be made available by the authors, without undue reservation.

ETHICS STATEMENT

All animal manipulations were carried out according to the Institutional Animal Care and Use Committee of China Medical University (protocol no. 2017–189).

AUTHOR CONTRIBUTIONS

C-WT designed research; C-YLa and C-YLi performed research; C-RW and C-HT contributed analytic tools and ideas; C-YLa and C-WT wrote the paper. C-YLi and C-WT revised the paper.

FUNDING

This study was supported by the Ministry of Science and Technology (MOST 106-2320-B-039-055-MY3) and CMU109-MF-79.

REFERENCES

Ahn, S., Song, T. J., Park, S. U., Jeon, S., Kim, J., Joo-Young, O., et al. (2017). Effects of a Combination Treatment of KD5040 and L-Dopa in a Mouse Model of Parkinson's Disease. *BMC Compl. Altern. Med.* 17, 220. doi:10.1186/s12906-017-1731-2

Barroso-Chinea, P., Thiolat, M.-L., Bido, S., Martinez, A., Doudnikoff, E., Baufreton, J., et al. (2015). D1 Dopamine Receptor Stimulation Impairs Striatal Proteasome Activity in Parkinsonism through 26S Proteasome Disassembly. *Neurobiol. Dis.* 78, 77–87. doi:10.1016/j.nbd.2015.02.024

Berthet, A., Bezard, E., Porras, G., Fasano, S., Barroso-Chinea, P., Dehay, B., et al. (2012). L-DOPA Impairs Proteasome Activity in Parkinsonism through D1 Dopamine Receptor. *J. Neurosci.* 32, 681–691. doi:10.1523/jneurosci.1541-11.2012

Berton, O., Guigoni, C., Li, Q., Bioulac, B. H., Aubert, I., Gross, C. E., et al. (2009). Striatal Overexpression of ΔJunD Resets L-DOPA-Induced Dyskinesia in a Primate Model of Parkinson Disease. *Biol. Psychiatry* 66, 554–561. doi:10.1016/j.biopsych.2009.04.005

Blandini, F., Cosentino, M., Mangiagalli, A., Marino, F., Samuele, A., Rasini, A., et al. (2004). Modifications of Apoptosis-Related Protein Levels in Lymphocytes of Patients with Parkinson's Disease. The Effect of Dopaminergic Treatment. *J. Neural Transm.* 111, 1017–1030. doi:10.1007/s00702-004-0123-1

Calabresi, P., Filippo, M. D., Ghiglieri, V., Tambasco, N., and Picconi, B. (2010). Levodopa-induced Dyskinesias in Patients with Parkinson's Disease: Filling the Bench-To-Bedside gap. *Lancet Neurol.* 9, 1106–1117. doi:10.1016/s1474-4422(10)70218-0

Cao, X., Yasuda, T., Uthayathas, S., Watts, R. L., Mouradian, M. M., Mochizuki, H., et al. (2010). Striatal Overexpression of FosB Reproduces Chronic Levodopa-Induced Involuntary Movements. *J. Neurosci.* 30, 7335–7343. doi:10.1523/jneurosci.0252-10.2010

Castello, J., Cortés, M., Malave, L., Kottmann, A., Sibley, D. R., Friedman, E., et al. (2020). The Dopamine D5 Receptor Contributes to Activation of Cholinergic Interneurons during L-DOPA Induced Dyskinesia. *Sci. Rep.* 10, 2542. doi:10.1038/s41598-020-59011-5

Cenci, M. A. (2014). Presynaptic Mechanisms of L-DOPA-Induced Dyskinesia: The Findings, the Debate, and the Therapeutic Implications. *Front. Neurol.* 5, 242. doi:10.3389/fneur.2014.00242

Chaudhuri, K. R., Jenner, P., and Antonini, A. (2019). Should There Be Less Emphasis on Levodopa-Induced Dyskinesia in Parkinson's Disease? *Move. Disord.* 34, 816. doi:10.1002/mds.27691

Chen, J.-H., Ou, H.-P., Lin, C.-Y., Lin, F.-J., Wu, C.-R., Chang, S.-W., et al. (2012). Carnosic Acid Prevents 6-Hydroxydopamine-Induced Cell Death in SH-Sy5y Cells via Mediation of Glutathione Synthesis. *Chem. Res. Toxicol.* 25, 1893–1901. doi:10.1021/tx300171u

Colamartino, M., Santoro, M., Duranti, G., Sabatini, S., Ceci, R., Testa, A., et al. (2015). Evaluation of Levodopa and Carbidopa Antioxidant Activity in normal Human Lymphocytes *In Vitro*: Implication for Oxidative Stress in Parkinson's Disease. *Neurotox. Res.* 27, 106–117. doi:10.1007/s12640-014-9495-7

Dorszewska, J., Prendecki, M., Lianeri, M., and Kozubski, W. (2014). Molecular Effects of L-Dopa Therapy in Parkinson's Disease. *Curr. Genomics* 15, 11–17. doi:10.2174/1389202914666131210213042

Engeln, M., Bastide, M. F., Toulmé, E., Dehay, B., Bourdenx, M., Doudnikoff, E., et al. (2016). Selective Inactivation of Striatal FosB/ΔFosB-Expressing Neurons Alleviates L-DOPA-Induced Dyskinesia. *Biol. Psychiatry* 79, 354–361. doi:10.1016/j.biopsych.2014.07.007

Fanni, S., Scheggi, S., Rossi, F., Tronci, E., Traccis, F., Stancampiano, R., et al. (2018). 5alpha-reductase Inhibitors Dampen L-DOPA-Induced Dyskinesia via Normalization of Dopamine D1-Receptor Signaling Pathway and D1-D3 Receptor Interaction. *Neurobiol. Dis.* 121, 120–130. doi:10.1016/j.nbd.2018.09.018

Feyder, M., Bonito-Oliva, A., and Fisone, G. (2011). L-DOPA-Induced Dyskinesia and Abnormal Signaling in Striatal Medium Spiny Neurons: Focus on Dopamine D1 Receptor-Mediated Transmission. *Front. Behav. Neurosci.* 5, 71. doi:10.3389/fnbeh.2011.00071

Fieblinger, T., Graves, S. M., Sebel, L. E., Alcacer, C., Plotkin, J. L., et al. (2014). Cell Type-specific Plasticity of Striatal Projection Neurons in Parkinsonism and L-DOPA-Induced Dyskinesia. *Nat. Commun.* 5, 5316. doi:10.1038/ncomms6316

Guo, Q., Shen, Z., Yu, H., Lu, G., Yu, Y., Liu, X., et al. (2016). Carnosic Acid Protects against Acetaminophen-Induced Hepatotoxicity by Potentiating Nrf2-Mediated Antioxidant Capacity in Mice. *Korean J. Physiol. Pharmacol.* 20, 15–23. doi:10.4196/kjpp.2016.20.1.15

Hald, A., and Lotharius, J. (2005). Oxidative Stress and Inflammation in Parkinson's Disease: Is There a Causal Link? *Exp. Neurol.* 193, 279–290. doi:10.1016/j.expneurol.2005.01.013

Higashi, Y., Asanuma, M., Miyazaki, I., Hattori, N., Mizuno, Y., and Ogawa, N. (2004). Parkin Attenuates Manganese-induced Dopaminergic Cell Death. *J. Neurochem.* 89, 1490–1497. doi:10.1111/j.1471-4159.2004.02445.x

Jin, C. M., Yang, Y. J., Huang, H. S., Kai, M., and Lee, M. K. (2010). Mechanisms of L-DOPA-Induced Cytotoxicity in Rat Adrenal Pheochromocytoma Cells: Implication of Oxidative Stress-Related Kinases and Cyclic AMP. *Neuroscience* 170, 390–398. doi:10.1016/j.neuroscience.2010.07.039

Lebel, M., Chagniel, L., Bureau, G., and Cyr, M. (2010). Striatal Inhibition of PKA Prevents Levodopa-Induced Behavioural and Molecular Changes in the Hemiparkinsonian Rat. *Neurobiol. Dis.* 38, 59–67. doi:10.1016/j.nbd.2009.12.027

Lin, C.-Y., Chen, W.-J., Fu, R.-H., and Tsai, C.-W. (2020). Upregulation of OPA1 by Carnosic Acid Is Mediated through Induction of IKKγ Ubiquitination by Parkin and Protects against Neurotoxicity. *Food Chem. Toxicol.* 136, 110942. doi:10.1016/j.fct.2019.110942

Lin, C.-Y., Tsai, C.-W., and Tsai, C.-W. (2016). Carnosic Acid Protects SH-Sy5y Cells against 6-Hydroxydopamine-Induced Cell Death through Upregulation of Parkin Pathway. *Neuropharmacology* 110, 109–117. doi:10.1016/j.neuropharm.2016.04.017

Lindgren, H. S., Rylander, D., Iderberg, H., Andersson, M., O'Sullivan, S. S., Williams, D. R., et al. (2011). Putaminal Upregulation of FosB/ΔFosB-like Immunoreactivity in Parkinson's Disease Patients with Dyskinesia. *J. Parkinsons Dis.* 1, 347–357. doi:10.3233/jpd-2011-11068

Manson, A., Stirpe, P., and Schrag, A. (2012). Levodopa-induced-dyskinesias Clinical Features, Incidence, Risk Factors, Management and Impact on Quality of Life. *J. Parkinsons Dis.* 2, 189–198. doi:10.3233/jpd-2012-120103

Nestler, E. J., Barrot, M., and Self, D. W. (2001). FosB: A Sustained Molecular Switch for Addiction. *Proc. Natl. Acad. Sci.* 98, 11042–11046. doi:10.1073/pnas.191352698

Park, K. H., Park, H. J., Shin, K. S., and Lee, M. K. (2014). Multiple Treatments with L-3,4-Dihydroxyphenylalanine Modulate Dopamine Biosynthesis and Neurotoxicity through the Protein Kinase A-Transient Extracellular Signal-Regulated Kinase and Exchange Protein Activation by Cyclic AMP-Sustained Extracellular Signa. *J. Neurosci. Res.* 92, 1746–1756. doi:10.1002/jnr.23450

Park, K. H., Shin, K. S., Zhao, T. T., Park, H. J., Lee, K. E., and Lee, M. K. (2016). L-DOPA Modulates Cell Viability through the ERK-C-Jun System in PC12 and Dopaminergic Neuronal Cells. *Neuropharmacology* 101, 87–97. doi:10.1016/j.neuropharm.2015.09.006

Ryu, Y.-K., Park, H.-Y., Go, J., Choi, D.-H., Kim, Y.-H., Hwang, J. H., et al. (2018). Metformin Inhibits the Development of L-DOPA-Induced Dyskinesia in a Murine Model of Parkinson's Disease. *Mol. Neurobiol.* 55, 5715–5726. doi:10.1007/s12035-017-0752-7

Santini, E., Valjent, E., Usiello, A., Carta, M., Borgkvist, A., Girault, J.-A., et al. (2007). Critical Involvement of cAMP/DARPP-32 and Extracellular Signal-Regulated Protein Kinase Signaling in L-DOPA-Induced Dyskinesia. *J. Neurosci.* 27, 6995–7005. doi:10.1523/jneurosci.0852-07.2007

Spigolon, G., and Fisone, G. (2018). Signal Transduction in L-DOPA-Induced Dyskinesia: from Receptor Sensitization to Abnormal Gene Expression. *J. Neural Transm.* 125, 1171–1186. doi:10.1007/s00702-018-1847-7

Stansley, B. J., and Yamamoto, B. K. (2013). L-dopa-induced Dopamine Synthesis and Oxidative Stress in Serotonergic Cells. *Neuropharmacology* 67, 243–251. doi:10.1016/j.neuropharm.2012.11.010

Sun, B., Wang, T., Li, N., and Qiao, J. (2020). Analysis of Motor Complication and Relative Factors in a Cohort of Chinese Patients with Parkinson's Disease. *Parkinsons Dis.* 2020, 8692509. doi:10.1155/2020/8692509

Wilhelmus, M. M. M., Nijland, P. G., Drukarch, B., de Vries, H. E., and van Horssen, J. (2012). Involvement and Interplay of Parkin, PINK1, and DJ1 in Neurodegenerative and Neuroinflammatory Disorders. *Free Radic. Biol. Med.* 53, 983–992. doi:10.1016/j.freeradbiomed.2012.05.040

Winkler, C., Kirik, D., Björklund, A., and Cenci, M. A. (2002). L-DOPA-induced Dyskinesia in the Intrastriatal 6-hydroxydopamine Model of Parkinson's Disease: Relation to Motor and Cellular Parameters of Nigrostriatal Function. *Neurobiol. Dis.* 10, 165–186. doi:10.1006/nbdi.2002.0499

Wu, C.-R., Tsai, C.-W., Chang, S.-W., Lin, C.-Y., Huang, L.-C., and Tsai, C.-W. (2015). Carnosic Acid Protects against 6-Hydroxydopamine-Induced Neurotoxicity in *In Vivo* and *In Vitro* Model of Parkinson's Disease: Involvement of Antioxidative Enzymes Induction. *Chemico-Biological Interactions* 225, 40–46. doi:10.1016/j.cbi.2014.11.011

Zhang, S. F., Xie, C. L., Lin, J. Y., Wang, M. H., Wang, X. J., and Liu, Z. G. (2018). Lipoic Acid Alleviates LDOPA induced Dyskinesia in 6OHDA Parkinsonian Rats via Anti-oxidative S-tress. *Mol. Med. Rep.* 17, 1118–1124. doi:10.3892/mmr.2017.7974

Conflict of Interest: The authors declare that the research was conducted in the absence of any commercial or financial relationships that could be construed as a potential conflict of interest.

Publisher's Note: All claims expressed in this article are solely those of the authors and do not necessarily represent those of their affiliated organizations, or those of the publisher, the editors and the reviewers. Any product that may be evaluated in this article, or claim that may be made by its manufacturer, is not guaranteed or endorsed by the publisher.

frontiers in Pharmacology

ORIGINAL RESEARCH
published: 31 August 2021
doi: 10.3389/fphar.2021.688227

Identification of Novel Gene Signatures using Next-Generation Sequencing Data from COVID-19 Infection Models: Focus on Neuro-COVID and Potential Therapeutics

Peter Natesan Pushparaj[1,2]*, *Angham Abdulrahman Abdulkareem*[1,3] and *Muhammad Imran Naseer*[1,2]*

[1]Center of Excellence in Genomic Medicine Research, Faculty of Applied Medical Sciences, King Abdulaziz University, Jeddah, Saudi Arabia, [2]Department of Medical Laboratory Technology, Faculty of Applied Medical Sciences, King Abdulaziz University, Jeddah, Saudi Arabia, [3]Department of Biochemistry, Faculty of Science, King Abdulaziz University, Jeddah, Saudi Arabia

OPEN ACCESS

Edited by:
Ashok Kumar,
University of Florida, United States

Reviewed by:
Mehtab Khan,
Université de Moncton, Canada
Garrett Smith,
University of Florida, United States

***Correspondence:**
Peter Natesan Pushparaj
peter.n.pushparaj@gmail.com
Muhammad Imran Naseer
mimrannaseer@yahoo.com

Specialty section:
This article was submitted to Neuropharmacology, a section of the journal Frontiers in Pharmacology

Received: *30 March 2021*
Accepted: *16 July 2021*
Published: *31 August 2021*

Citation:
Pushparaj PN, Abdulkareem AA and Naseer MI (2021) Identification of Novel Gene Signatures using Next-Generation Sequencing Data from COVID-19 Infection Models: Focus on Neuro-COVID and Potential Therapeutics. Front. Pharmacol. 12:688227. doi: 10.3389/fphar.2021.688227

SARS-CoV-2 is the causative agent for coronavirus disease-19 (COVID-19) and belongs to the family Coronaviridae that causes sickness varying from the common cold to more severe illnesses such as severe acute respiratory syndrome, sudden stroke, neurological complications (Neuro-COVID), multiple organ failure, and mortality in some patients. The gene expression profiles of COVID-19 infection models can be used to decipher potential therapeutics for COVID-19 and related pathologies, such as Neuro-COVID. Here, we used the raw RNA-seq reads (Single-End) in quadruplicates derived using Illumina Next Seq 500 from SARS-CoV-infected primary human bronchial epithelium (NHBE) and mock-treated NHBE cells obtained from the Gene Expression Omnibus (GEO) (GSE147507), and the quality control (QC) was evaluated using the CLC Genomics Workbench 20.0 (Qiagen, United States) before the RNA-seq analysis using BioJupies web tool and iPathwayGuide for gene ontologies (GO), pathways, upstream regulator genes, small molecules, and natural products. Additionally, single-cell transcriptomics data (GSE163005) of meta clusters of immune cells from the cerebrospinal fluid (CSF), such as T-cells/natural killer cells (NK) (TcMeta), dendritic cells (DCMeta), and monocytes/granulocyte (monoMeta) cell types for comparison, namely, Neuro-COVID versus idiopathic intracranial hypertension (IIH), were analyzed using iPathwayGuide. L1000 fireworks display (L1000FWD) and L1000 characteristic direction signature search engine (L1000 CDS^2) web tools were used to uncover the small molecules that could potentially reverse the COVID-19 and Neuro-COVID-associated gene signatures. We uncovered small molecules such as camptothecin, importazole, and withaferin A, which can potentially reverse COVID-19 associated gene signatures. In addition, withaferin A, trichostatin A, narciclasine, camptothecin, and JQ1 have the potential to reverse Neuro-COVID gene signatures. Furthermore, the gene set enrichment analysis (GSEA) preranked method and Metascape web tool were used to decipher and annotate the gene signatures that were

potentially reversed by these small molecules. In conclusion, our study unravels a rapid approach for applying next-generation knowledge discovery (NGKD) platforms to discover small molecules with therapeutic potential against COVID-19 and its related disease pathologies.

Keywords: SARS-CoV-2, COVID-19, Neuro-COVID, bronchial epithelium, cerebrospinal fluid, RNA sequencing, next-generation knowledge discovery platforms, therapeutics

INTRODUCTION

Coronaviruses (CoVs) belong to the order Nidovirales, family Coronaviridae, and subfamily Coronavirinae, which can further be divided into four genera: alpha, beta, gamma, and delta CoVs. SARS CoV2 is the causative agent of coronavirus disease-19 (COVID-19), belongs to the genus beta-CoV, and can cause sickness varying from the common cold to more severe illnesses such as severe acute respiratory syndrome, gastrointestinal complications, sudden stroke, multiple organ failure, and mortality in some cases (Cui et al., 2019). SARS-CoV-2 infected more than 186 million people, resulting in the death of about 4 million people globally (Johns Hopkins COVID-19 Data Center on 10th July 2021) (Dong et al., 2020). SARS-CoV-2 has a positive-sense RNA genome encapsulated by a nucleocapsid. SARS-CoV-2 infects host cells through surface receptors, angiotensin-converting enzyme 2 (hACE2), and transmembrane protease serine-type 2 (TMPRSS2) (Hoffmann et al., 2020). An increase in the expression of ACE2, a tissue-protective mediator during lung damage, was found to be associated with interferon signaling in airway epithelial cells, and SARS-CoV-2 could exploit interferon-mediated stimulation of ACE2 to augment infection (Ziegler et al., 2020). The differential expression of genes that are necessary for SARS-CoV-2 interaction and subsequent host response determine susceptibility to COVID-19, disease progression, and recovery (Kasela et al., 2021).

RNA sequencing is a recently developed NGS methodology for whole transcriptome or single-cell transcriptomic approaches (Liu and Di, 2020). Single-cell RNA sequencing of COVID-19 infected bronchial epithelial cells and bronchioalveolar immune cells revealed important cellular and molecular processes implicated in COVID-19 infection at the single-cell level and provided information about the mechanisms of disease severity (Liu T. et al., 2020; Liao et al., 2020; Zhou et al., 2020). Notably, IL-17-associated signaling was significantly increased but not Th2-related inflammation following COVID-19 infection (Kasela et al., 2021). A recent study showed that SARS-CoV-2 infection caused a twofold higher induction of interferon stimulation compared to SARS-CoV in Calu-3 human epithelial cells and subsequent induction of cytokines such as IL6 or IL-10 (Wyler et al., 2021). The interferon-induced genes IFIT2 and OAS2 were widely stimulated compared to interferon lambda (IFNL) and interferon-beta (IFNB). Besides, scRNA-seq data suggested that interferon regulatory factor (IRF) activity occurs before the induction of nuclear factor-κB (NF-κB) in SARS-CoV-2-infected cells (Wyler et al., 2021).

COVID-19 patients, especially those with greater disease severity, can develop neurological complications such as neuroinflammation, headache, and cerebrovascular disease called Neuro-COVID (Heming et al., 2021). Developing novel drug candidates and identifying suitable existing therapeutics for drug repurposing for COVID-19 and Neuro-COVID are critical for controlling this ongoing pandemic and reducing the enormous economic burden on health care systems and socioeconomic devastation of individuals, families, small to large businesses, and countries. Understanding COVID-19-associated gene signatures is essential for developing robust therapeutics for treating infected patients effectively and reducing infection rates and mortality. To address this important issue, the gene expression profiles of COVID-19 infection models can be used to identify potential therapeutic targets that could be targeted by known drugs. Here, we used RNA-seq datasets from the COVID-19 infection model of human bronchial epithelial cells (NHBE) and the scRNA-seq datasets of immune cells isolated from the cerebrospinal fluid (CSF) of Neuro-COVID patients, obtained from public repositories and analyzed using next-generation knowledge discovery (NGKD) platforms to understand disease-specific gene signatures and uncover drugs from synthetic and natural sources that can reverse these gene signatures for potential therapeutics.

MATERIALS AND METHODS

Ethical Statement

This study was exempted from Institutional Review Board (IRB) approval since it did not involve any animal models or human subjects and was conducted using RNA-seq datasets retrieved from the Gene Expression Omnibus (GEO) (Barrett et al., 2013).

Data Source

In the present study, the raw RNA-seq reads (Single-End) (*FASTQ format*) in quadruplicates derived using Illumina Next Seq 500 from SARS-CoV-infected and mock-treated NHBE cells were obtained from the GEO (*Accession No: GSE147507*) (Blanco-Melo, et al., 2020). Additionally, the single-cell transcriptomics data (*Accession No: GSE163005*) of immune cells isolated from the CSF of Neuro-COVID patients (Heming et al., 2021) were used for additional analysis using high-throughput knowledge discovery platforms. Heming et al. (2021) provided the entire dataset for the open-source interactive platform *cerebroApp* at http://covid.mheming.de/ (Hillje et al., 2020).

COVID-19 RNA-seq Data: Quality Control (QC)

Raw RNA-seq reads (Single-End) (*FASTQ format*) in quadruplicates were evaluated for quality using the CLC Genomics Workbench 20.0 (Qiagen, United States) as described previously (Ewing and Green, 1998; Liu and Di, 2020).

BioJupies Analysis of the RNA-seq Data

BioJupies is a freely available web-based application (http://biojupies.cloud) that has 14 RNA-seq analysis library plug-ins and provides the user with the automatic generation, storage, and deployment of Jupyter Notebooks containing RNA-seq data analyses (Torre et al., 2018). In BioJupies, the RNA-seq datasets were user-submitted, compressed in an HDF5 data package, and uploaded to Google Cloud. Raw counts were normalized to log10-Counts per million (log CPM) and the differentially expressed genes (DEGs) were derived between the control group and the experimental group using the limma R package (Ritchie et al., 2015). The Jupyter Notebooks created for each RNA-seq raw data analysis were permanently available through a URL and stored in the cloud. The notebooks consist of executable code of the whole pipeline, description of the methods, enrichment analysis, interactive data visualizations, differential expression, and so on (Torre et al., 2018).

Principal component analysis (PCA) was performed using the PCA function from the sklearn Python module by transforming the log CPM using the Z-score method. An interactive heatmap was generated using a clustergram (Fernandez et al., 2017). In the volcano plots, the log2 fold changes of the DEGs are shown on the *x*-axis and *p*-values were corrected using the Benjamini-Hochberg method, transformed (–log10), and presented on the *y*-axis (Benjamini and Hochberg, 1995; Benjamini and Yekutieli, 2001). In contrast, for the MA plot, average gene expression is shown on the x-axis; *p*-values were corrected using the Benjamini-Hochberg method (Benjamini and Hochberg, 1995; Benjamini and Yekutieli, 2001), transformed (–log10), and presented on the y-axis.

In Silico Analysis of the RNA-seq Expression Data Using iPathwayGuide

The impact analysis method (IAM) (Draghici et al., 2007; Khatri et al., 2007; Tarca et al., 2009) was used to determine the significantly impacted gene signatures and pathways from the DEGs (log2FC cut-off 0.6, adjusted false discovery rate (FDR) *p*-value ≤ 0.05) obtained from the COVID-19 using BioJupies and the DEGs with log2FC (cut-off 0.3) and adjusted *p*-value ≤ 0.001 based on Bonferroni method in meta clusters of T-cells/natural killer cells (NK) (TcMeta), dendritic cells (DCMeta), and monocytes/granulocyte (monoMeta) cell types of the comparison, namely, Neuro-COVID versus idiopathic intracranial hypertension (IIH) for the Neuro-COVID infection models in the iPathwayGuide (Advaita Bioinformatics, United States). Here, the *p*-value calculated based on Fisher's method was used to compute the pathway score method (Fisher, 1925). The *p*-value was further corrected based on multiple testing corrections for FDR and Bonferroni corrections (Bonferroni, 1935; Bonferroni, 1936). The gene interactions and pathways based on the DEGs were generated using the Kyoto Encyclopedia of Genes and Genomes (KEGG) database (Kanehisa and Goto, 2000; Kanehisa et al., 2002; Kanehisa et al., 2010; Kanehisa et al., 2012; Kanehisa et al., 2014). For each gene ontology (GO) term (Ashburner et al., 2000; Gene Ontology Consortium, 2001; Ashburner and Lewis, 2002; Gene Ontology Consortium, 2004), the number of DEGs annotated to the term was compared to that expected by chance. iPathwayGuide uses an overrepresentation approach to compute the statistical significance of observing at least a given number of DEGs (Draghici et al., 2003a; Draghici et al., 2003b; Draghici 2011). The hypergeometric distribution was used to compute the *p*-values in the iPathwayGuide analysis and corrected using FDR and Bonferroni for multiple comparisons (Draghici et al., 2003a; Draghici et al., 2003b; Draghici 2011). The prediction of upstream chemicals, drugs, and toxins (CDTs), either as present (or overly abundant) or absent (or insufficient), is based on two types of information: *1*) the enrichment of DEGs from the experiment and *2*) a network of interactions from the Advaita Knowledge Base (AKB v2012) (Draghici et al., 2003a; Draghici 2011). The analysis uses Fisher's standard method to combine *p*-values into one test statistic (Fisher, 1925).

L1000CDS2 and L1000FWD Queries

The L1000 characteristic direction signature search engine (L1000CDS2) analysis was performed by submitting the top 2000 DEGs to the L1000CDS2 signature search application programming interface (API) (Duan et al., 2016). Similarly, the L1000FWD analysis was performed by submitting the top 2000 DEGs to the L1000 Fire Works Display (L1000FWD) signature search API (Wang et al., 2018). Similarly, the DEGs obtained from TcMeta, DCMeta, and monoMeta cell types were compared; namely, Neuro-COVID versus IIH were subjected to both L1000CDS2 and L1000FWD analyses to identify drugs that reverse the gene signatures differentially regulated by COVID-19. An FDR (q-value) of 0.05 was considered statistically significant.

Gene Set Enrichment Analysis (GSEA) Preranked

GSEA against a ranked list of genes was performed using the GSEA preranked method (Subramanian et al., 2005). The RNK-formatted files were created to the comparison of SARS-CoV-2-NHBE vs. Mock-NHBE, Neuro-COVID vs. IIH-TcMeta, Neuro-COVID vs. IIH-DCMeta, and Neuro-COVID vs. IIH-monoMeta, based on the ranking metric log2FC of the DEGs. Gene matrix files (GMTs) were created using the gene signatures (combined, up, and down) of withaferin A, importazole, camptothecin, trichostatin A, narciclasine, and JQ1 from the L1000FWD web tool (Wang et al., 2018). GSEA preranked was run by weighting each gene's contribution to the enrichment score by the value of its ranking metric against GMT files using Java-based

desktop application GSEA 4.1.0 (Broad Institute, United States) under default settings as described previously (Subramanian et al., 2005).

Metascape Analysis of Gene Signatures Reversed by Small Molecules

The Metascape web tool (http://metascape.org) offers an easy and effective way to explore and understand gene lists derived from experimental data. The gene signatures reversed by small molecules identified in our study in COVID-19 and Neuro-COVID models were first automatically converted into Human Entrez Gene ID in Metascape. Then, all statistically enriched terms, accumulative hypergeometric *p*-values, and enrichment factors were calculated and used for filtering to obtain enrichment ontology clusters based on GO/KEGG terms, canonical pathways, and hallmark gene sets (Zhou et al., 2019).

RESULTS

Raw RNA-seq reads (Single-End) (*FASTQ format*) derived using Illumina Next Seq 500 from SARS-CoV-infected NHBE and mock-treated NHBE cells were obtained from the GEO and the QC was evaluated using the CLC Genomics Workbench 20.0, before the RNA-seq analysis using BioJupies web tool. iPathwayGuide analysis was performed to decipher the disease-specific signatures, pathways, and small molecules, either synthetic or derived from natural sources, to reverse disease-specific gene signatures. In addition, single-cell transcriptomic data of immune cells isolated from the CSF of Neuro-COVID-19 patients were further analyzed using iPathwayGuide, L1000CDS2, and L1000FWD analyses.

Hierarchically clustered heatmaps were generated using the Clustergrammer web tool to visualize and analyze high-dimensional RNA-seq data of SARS-CoV-infected NHBE cells and mock-treated NHBE cells (**Supplementary Figure S1A**). PCA was used to uncover global patterns in RNA-seq datasets analyzed and helped to understand the difference between COVID-19-infected and mock-treated NHBE cells (**Supplementary Figure S1B**). The volcano plot was generated using transformed gene fold changes using log2 and is shown on the *x*-axis (**Supplementary Figure S1C**). The MA plot was based on the average gene expression, which was calculated using the mean of the normalized gene expression values and shown on the *x*-axis (**Supplementary Figure S1D**).

iPathwayGuide Analysis of DEGs From COVID-19 and Neuro-COVID Infection Models

In this experiment, 1,072 DEGs were identified from a total of 10,663 DEGs obtained from BioJupies analysis of the RNA-seq reads of the SARS-CoV-infected NHBE cells and mock-treated NHBE cells based on a *p*-value cut-off of 0.05 and a log2 fold change cut-off of 0.6. In contrast, DEGs with a logFC cut-off of 0.3 and adjusted *p*-value based on the Bonferroni method from clusters in TcMeta, DCMeta, and monoMeta of the comparison, namely, Neuro-COVID versus IIH, were also subjected to iPathwayGuide analysis separately, followed by comparative analyses. Subsequently, the DEGs were analyzed in the context of pathways obtained from the KEGG database (Kanehisa and Goto, 2000; Kanehisa et al., 2002), GO from the Gene Ontology Consortium database, a network of regulatory relationships from BioGRID: Biological General Repository for Interaction Datasets v4.0.189 (Szklarczyk et al., 2017), chemicals/drugs/toxicants from the Comparative Toxicogenomics Database (Davis et al., 2021), and diseases from the KEGG database. In summary, 22 pathways were found to be significantly impacted in SARS-CoV-2-infected NHBE cells compared to mock-treated NHBE cells. In addition, 503 GO terms, 18 miRNAs, 190 gene upstream regulators, 213 chemical upstream regulators, and 14 diseases were found to be significantly enriched before correction for multiple comparisons.

COVID-19 infection of NHBE cells triggers key immune-related pathways, such as cytokine-cytokine receptor interactions and viral protein interactions with cytokine receptors (**Table 1**). The top five upstream regulators, IL-17, TNF-alpha, STAT2, IRF9, and TLR4, were predicted to be activated (**Table 2**). The top identified biological processes, molecular functions, and cellular components for each pruning type are provided in **Tables 3–5**.

The bar chart (**Figure 1A**) shows the top small molecules identified by the L1000CDS2 query using the DEGs identified from SARS-CoV-2-NHBE. The left panel shows small molecules such as geldanamycin, radicicol, AZD8330, trametinib, NVP-AYU922, GSK2126458, and JW-7-24-1, which mimic the observed gene expression signature; the right panel displays small molecules such as camptothecin (**Figure 1B**), importazole (**Figure 1C**), and withaferin A (**Figure 1D**). The upstream regulator drugs and natural products that reverse the molecular signatures based on iPathwayGuide analysis are shown as a dendrogram (**Figure 1E**). The top five upstream drugs, natural products,

TABLE 1 | Top identified pathways and their associated *p*-values are given in the table.

Pathway name	Pathway ID	*p*-value	*p*-value (FDR)	*p*-value (Bonferroni)
Cytokine-cytokine receptor interaction	04060	6.711e–8	2.0202e–5	2.020e–5
Staphylococcus aureus infection	05150	4.009e–7	6.034e–5	1.207e–4
Viral protein interaction with cytokine and cytokine receptor	04061	1.050e–7	1.053e–4	3.160e–4
Systemic lupus erythematosus	05322	3.414e–4	0.026	0.103
Herpes simplex virus 1 infection	05168	6.444e–4	0.039	0.194

The p*-value corresponding to the pathway was calculated based on overrepresentation analysis.*

TABLE 2 | Top identified upstream regulators activated based on Bonferroni correction were listed in the table.

Upstream regulator (u)	DTA (u)	DT (u)	*p*-value	*p*-value (FDR)	*p*-value (Bonferroni)
IL17A	13	17	1.139e–6	0.001	0.001
TNF	23	28	1.857e–6	0.001	0.002
STAT2	9	9	5.589e–6	0.002	0.007
IRF9	8	8	2.248e–5	0.007	0.028
TLR4	8	8	8.493e–5	0.021	0.106

Table 2 indicates the number of differentially expressed (DE) targets supporting the hypothesis that each upstream regulator (u) is activated (DTA(u)), the total number of DE genes downstream of u (DT(u)), the combined raw p-value, and the corrected p-value for multiple comparisons.

TABLE 3 | Top identified biological processes for each pruning type.

Pruning type: none				Pruning type: high specificity		Pruning type: smallest common denominator	
Go term	***p*-value**	***p*-value (FDR)**	***p*-value (Bonferroni)**	**Go term**	***p*-value**	**Go term**	***p*-value**
Keratinization	6.600e–9	4.710e–5	4.710e–5	Cornification	1.713e–4	Keratinization	4.710e–5
Cornification	2.400e–8	8.563e–5	1.713e–4	Acute-phase response	0.033	Acute-phase response	0.100
Humoral immune response	2.900e–7	6.898e–4	0.002	Peptide cross-linking	0.209	Humoral immune response	0.167
DNA replication initiation	9.000e–6	0.002	0.064	Double-strand break repair *via* break-induced replication	0.371	Peptide cross-linking	0.371
Acute-phase response	9.300e–6	0.012	0.066	Antimicrobial humoral immune response mediated by antimicrobial peptide	0.371	Double-strand break repair *via* break-induced replication	0.371

TABLE 4 | Top identified molecular functions for each pruning type.

Pruning type: none				Pruning type: high specificity		Pruning type: smallest common denominator	
Go term	***p*-value**	***p*-value (FDR)**	***p*-value (Bonferroni)**	**Go term**	***p*-value**	**Go term**	***p*-value**
Cytokine activity	1.200e–7	1.691e–4	1.691e–4	Cytokine activity	0.061	Cytokine activity	1.691e–4
Receptor regulator activity	6.500e–7	4.579e–4	9.158e–4	Chemokine activity	0.061	Serine hydrolase activity	0.341
Signaling receptor activator activity	4.500e–6	0.002	0.006	DNA replication origin binding	0.341	DNA replication origin binding	0.341
Receptor-ligand activity	7.900e–6	0.003	0.011	2'-5'-Oligodenylate synthetase activity	0.341	2'-5'-Oligodenylate synthetase activity	0.341
Chemokine activity	6.000e–5	0.017	0.085	Structural constituent of skin epidermis	0.341	Structural constituent of skin epidermis	0.341

TABLE 5 | Top identified cellular components for each pruning type.

Pruning type: none				Pruning type: high specificity		Pruning type: smallest common denominator	
Go term	***p*-value**	***p*-value (FDR)**	***p*-value (Bonferroni)**	**Go term**	***p*-value**	**Go term**	***p*-value**
Cornified envelope	3.600e–5	0.024	0.033	Cornified envelope	0.033	Cornified envelope	0.024
Intermediate filament	5.200e–5	0.024	0.048	Intermediate filament	0.279	Intermediate filament	0.024
DNA packaging complex	2.700e–4	0.082	0.247	Blood microparticle	0.485	DNA packaging complex	0.082
Intermediate filament cytoskeleton	0.001	0.209	0.924	MCM complex	0.492	Blood microparticle	0.364
Extracellular matrix	0.001	0.209	1.000	Nucleosome	0.492	MCM complex	0.470

and chemicals predicted as absent (or insufficient) based on iPathwayGuide analysis were coumestrol, methylprednisolone, JinFuKang (JFK), selenium, and gold sodium thiomalate (**Figure 1F**). However, withaferin A was found to reverse the COVID-19-induced molecular signatures in both L1000CDS2 and L1000FWD analyses, along with other small-molecule drugs (**Table 6**) in the SARS-CoV-2-infected NHBE cells.

We identified 14 genes that were commonly expressed between Neuro-COVID and IIH (TcMeta, DCMeta, and monoMeta), as depicted in the Venn diagram (**Figure 2A**). The upregulated genes (**Figure 2B**), downregulated genes (**Figure 2C**), and the common genes between the meta clusters of immune cells in Neuro-COVID were presented as rank diagrams based on log2FC values. The genes GABARAP, GNAI2, COTL1, ATP5F1D, CD81, GNAS,

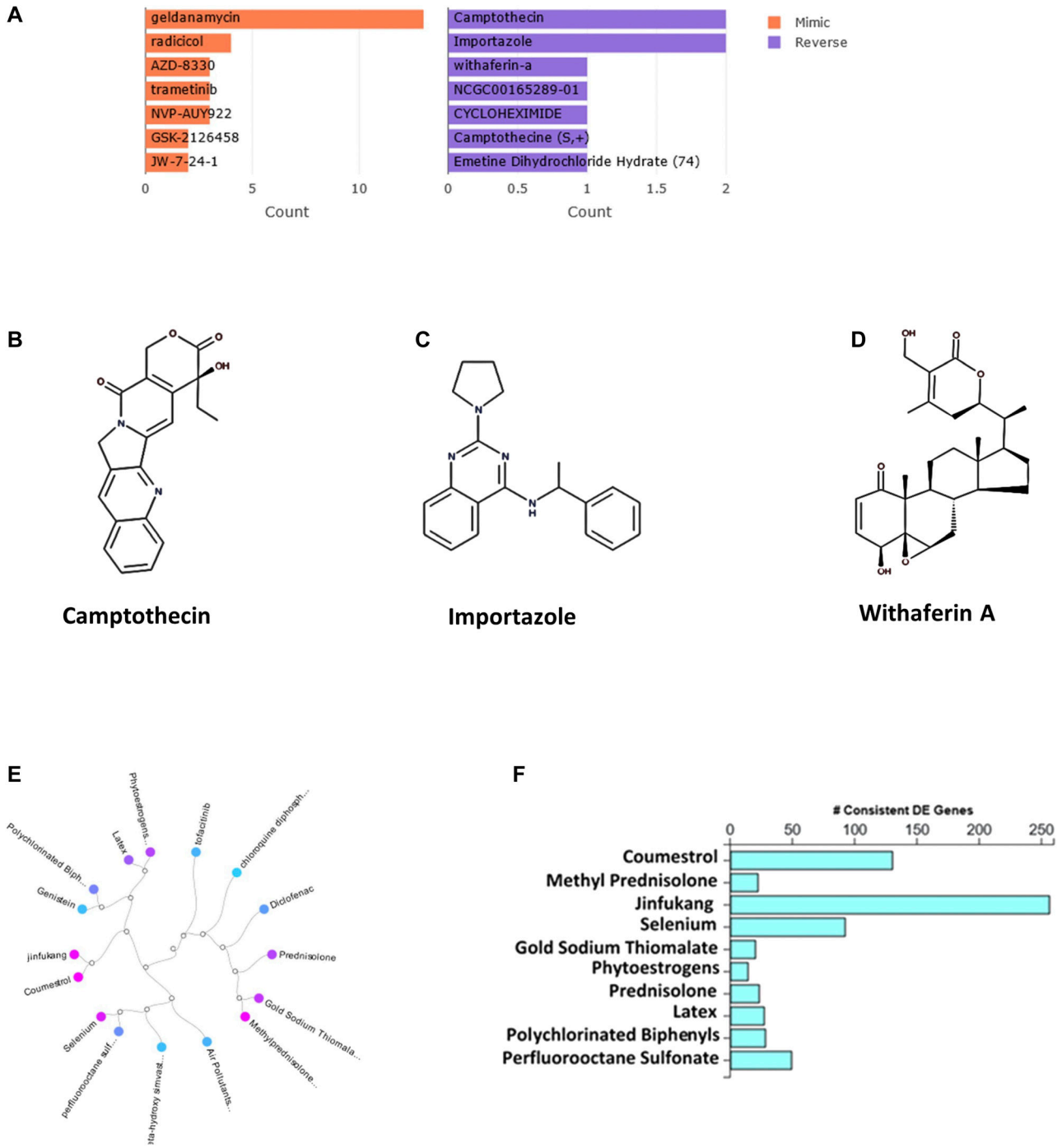

FIGURE 1 | (A) The bar chart displaying the top five small molecules identified by the L1000CDS2 query. The left panel displays the small molecules which mimic the observed gene expression signature, while the right panel displays the small molecules which reverse it. **(B–D)** The two-dimensional structures of camptothecin, importazole, and withaferin A. **(E)** Dendrogram show the drugs and natural products that reverse the COVID-19 associated molecular signatures and **(F)** bar graph shows the drugs and natural products that potentially reverse COVID-19 associated molecular signatures based on iPathwayGuide analysis.

TABLE 6 | Natural products and drugs with opposite molecular signatures based on L1000FWD web-based tool for querying gene expression signatures (SARS-CoV-2-NHBE vs. Mock-NHBE) against signatures created from human cell lines treated with over 20,000 small molecules and drugs for the LINCS project.

Signature ID	Drug or natural product	Similarity SCORE	*p*-value	q-value	Z-score	Combined score
CPC006_PC3_6H:BRD-A36630025-001-02-6:0.35	SN-38	−0.0598	1.04e−11	2.02e−08	1.79	−19.61
CPC011_A549_24H:BRD-K97514127-045-02-0:10	Vinorelbine	−0.0598	2.32e−11	3.82e−08	1.72	−18.26
CPC015_MCF7_24H:BRD-K52075715-001-03-4:10	Oxibendazole	−0.0573	2.91e−10	3.37e−07	1.67	−15.88
CPC019_HT29_6H:BRD-K67870070-001-01-4:10	SA-247615	−0.0560	7.96e−11	1.22e−07	1.69	−17.05
ERG005_VCAP_6H:BRD-K88378636-001-02-8:20	Withaferin A	−0.0547	1.28e−09	1.19e−06	1.65	−14.71
CPC012_MCF7_24H:BRD-K69496360-001-01-5:10	BRD-K69496360	−0.0522	1.03e−08	5.72e−06	1.73	−13.81
CPC015_MCF7_24H:BRD-K47869605-001-18-9:10	Podophyllotoxin	−0.0509	1.78e−08	8.35e−06	1.67	−12.97
CPC001_HCC515_24H:BRD-K82823804-001-01-7:10	SA-792987	−0.0509	3.61e−08	1.44e−05	1.81	−13.45
MUC.CP003_MCF7_24H:BRD-K02407574-001-04-8:3.3333	Parbendazole	−0.0496	8.46e−08	2.85e−05	1.62	−11.45
CPC002_PC3_6H:BRD-K06926592-001-01-7:10	Tretinoin	−0.0496	7.24e−08	2.54e−05	1.79	−12.80

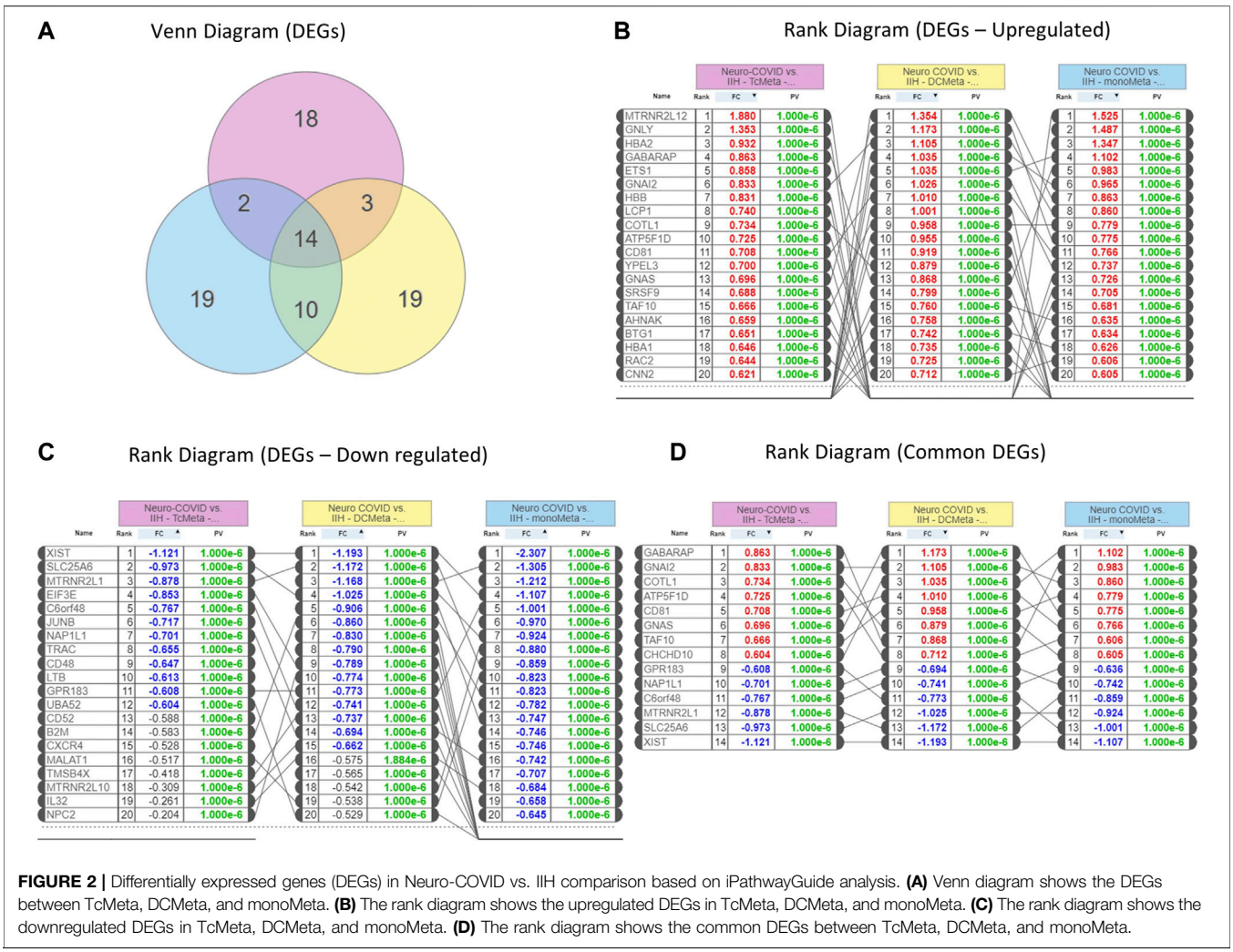

FIGURE 2 | Differentially expressed genes (DEGs) in Neuro-COVID vs. IIH comparison based on iPathwayGuide analysis. **(A)** Venn diagram shows the DEGs between TcMeta, DCMeta, and monoMeta. **(B)** The rank diagram shows the upregulated DEGs in TcMeta, DCMeta, and monoMeta. **(C)** The rank diagram shows the downregulated DEGs in TcMeta, DCMeta, and monoMeta. **(D)** The rank diagram shows the common DEGs between TcMeta, DCMeta, and monoMeta.

TAF10, and CHCHD10 were significantly upregulated, and genes such as XIST, SLC25A6, MTRNR2L1, C6orf48, NAP1L1, and GPR183 were significantly downregulated in the meta clusters of immune cells in Neuro-COVID (**Figure 2D**).

GO analysis showed that 61 biological processes (**Figure 3A**), 13 molecular functions (**Figure 3C**), and 12 cellular components (**Figure 3E**) were commonly enriched in the meta clusters of immune cells in Neuro-COVID. The top five biological processes enriched were bicarbonate transport,

B

Rank Diagram (BP))

Name	Neuro-COVID vs. IIH - TcMeta -... Rank	PV	Neuro COVID vs. IIH - DCMeta -... Rank	PV	Neuro COVID vs. IIH - monoMeta -... Rank	PV
bicarbonate transp...	1	0.007	1	0.098	1	0.048
gas transport	2	0.007	2	0.098	2	0.048
oxygen transport	3	0.007	3	0.107	3	0.048
hydrogen peroxide ...	4	0.014	4	0.254	4	0.048
drug transport	5	0.017	5	0.254	5	0.048
osteoclast differe...	6	0.017	6	0.266	6	0.048
antibiotic catabol...	7	0.018	7	0.289	7	0.048
antibiotic metabol...	8	0.018	8	0.295	8	0.048
hydrogen peroxide ...	9	0.018	9	0.334	9	0.048
reactive oxygen sp...	10	0.020	10	0.349	10	0.048
cofactor catabolic...	11	0.048	11	0.385	11	0.048
response to stimul...	12	0.104	12	0.493	12	0.048
defense response t...	13	0.153	13	0.517	13	0.048
leukocyte chemotax...	14	0.242	14	0.638	14	0.048
response to extern...	15	0.242	15	0.705	15	0.048
G protein-coupled ...	16	0.263			16	0.048
G protein-coupled ...	17	0.263			17	0.048
adenylate cyclase-...	18	0.263			18	0.050
cell chemotaxis	19	0.263			19	0.053
neutrophil chemota...	20	0.263			20	0.065

D

Rank Diagram (MF))

Name	Neuro-COVID vs. IIH - TcMeta -... Rank	PV	Neuro COVID vs. IIH - DCMeta -... Rank	PV	Neuro COVID vs. IIH - monoMeta -... Rank	PV
haptoglobin bindin...	1	2.565e-4	1	0.006	1	0.003
oxygen binding	2	2.565e-4	2	0.006	2	0.003
oxygen carrier act...	3	6.839e-4	3	0.011	3	0.004
heme binding	4	0.010	4	0.014	4	0.004
tetrapyrrole bindi...	5	0.016	5	0.030	5	0.005
peroxidase activit...	6	0.023	6	0.095	6	0.005
G-protein beta/gam...	7	0.028	7	0.095	7	0.005
organic acid bindi...	8	0.028	8	0.393	8	0.006
oxidoreductase act...	9	0.028	9	0.404	9	0.019
signaling receptor...	10	0.030	10	0.592	10	0.019
receptor antagonis...	11	0.036	11	0.605	11	0.019
antioxidant activi...	12	0.045			12	0.022
receptor inhibitor...	13	0.045			13	0.026
sterol binding	14	0.122			14	0.026
receptor regulator...	15	0.125			15	0.026
steroid binding	16	0.125			16	0.026
G protein-coupled ...	17	0.263			17	0.026
MHC class II prote...	18	0.298			18	0.026
cytokine activity	19	0.438			19	0.026
receptor ligand ac...	20	0.551			20	0.026

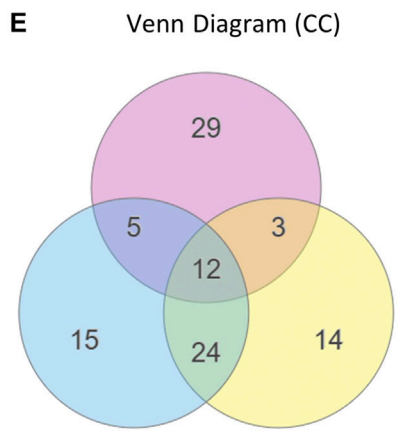

F

Rank Diagram (CC)

Name	Neuro-COVID vs. IIH - TcMeta -... Rank	PV	Neuro COVID vs. IIH - DCMeta -... Rank	PV	Neuro COVID vs. IIH - monoMeta -... Rank	PV
endocytic vesicle ...	1	2.450e-4	1	0.087	1	0.016
haptoglobin-hemogl...	2	2.940e-4	2	0.211	2	0.016
hemoglobin complex	3	7.840e-4	3	0.224	3	0.016
cytosolic small ri...	4	0.003	4	0.224	4	0.088
cytosolic ribosome	5	0.005	5	0.224	5	0.121
extracellular regi...	6	0.005	6	0.380	6	0.154
endocytic vesicle	7	0.015	7	0.563	7	0.189
small ribosomal su...	8	0.015	8	0.621	8	0.189
extracellular spac...	9	0.021			9	0.189
blood microparticl...	10	0.036			10	0.294
actin cytoskeleton	11	0.040			11	0.297
extracellular exos...	12	0.040			12	0.330
extracellular orga...	13	0.040			13	0.409
extracellular vesi...	14	0.040			14	0.437
side of membrane	15	0.415			15	0.811

FIGURE 3 | Enrichment of gene ontologies (GO) such as biological process (BP), molecular function (MF), and cellular component (CC) in Neuro-COVID vs. IIH comparison based on iPathwayGuide analysis. **(A)** Venn and **(B)** rank diagrams show the BP enriched between TcMeta, DCMeta, and monoMeta. **(C)** Venn and **(D)** rank diagrams show the MF enriched between TcMeta, DCMeta, and monoMeta. **(E)** Venn and **(F)** rank diagrams show the CC enriched between TcMeta, DCMeta, and monoMeta.

gas transport, oxygen transport, hydrogen peroxide, and drug transport (**Figure 3B**), the top five molecular functions enriched were haptoglobin binding, oxygen binding, oxygen carrier activity, heme binding, and tetrapyrrole binding (**Figure 3D**), and the top five cellular components enriched were endocytic vesicle, haptoglobin-hemoglobin complex,

TABLE 7 | Top small molecules with opposite molecular signatures based on L1000FWD web-based tool for querying gene expression signatures (Neuro-COVID vs. IIH-Tc Meta) against signatures created from human cell lines treated with over 20,000 small molecules and drugs for the LINCS project.

Signature ID	Drug or natural product	Similarity score	*p*-value	q-value	Z-score	Combined score
ERG005_VCAP_6H:BRD-K88378636-001-02-8:20	Withaferin A	–0.0492	3.55e–16	1.52e–11	1.65	–25.55
CPC012_VCAP_24H:BRD-A59985574-003-01-9:10	Topotecan	–0.0303	6.34e–05	4.35e–01	1.75	–7.36
CPC012_VCAP_24H:BRD-K62459624-001-08-7:10	BRD-K62459624	–0.0293	1.66e–04	8.86e–01	1.77	–6.69
CPC006_HCC515_6H:BRD-K16406336-311-01-2:10	Methylene-blue	–0.0303	8.54e–04	1.00e+00	1.77	–5.43
CPC011_PC3_6H:BRD-K04548931-003-11-6:10	Pidorubicine	–0.0278	1.04e–03	1.00e+00	1.77	–5.27
NMH002_NPC_24H:BRD-K32610195-001-14-9:10	Androstenedione	–0.0269	1.58e–03	1.00e+00	1.63	–4.57
CPC012_VCAP_24H:BRD-K56196992-001-01-2:10	BRD-K56196992	–0.0269	9.60e–03	1.00e+00	1.72	–3.47
CPC015_NPC_24H:BRD-K14920963-304-01-9:10	Erythrosine	–0.0269	1.51e–03	1.00e+00	1.75	–4.93
CPC013_SKB_24H:BRD-K16798053-001-01-0:10	ST-4029573	–0.0269	4.94e–04	1.00e+00	1.76	–5.82
CPC004_PC3_6H:BRD-A41519720-001-03-0:10	Ezetimibe	–0.0264	1.21e–02	1.00e+00	1.78	–3.42

TABLE 8 | Top small molecules with opposite molecular signatures based on L1000FWD web-based tool for querying gene expression signatures (Neuro-COVID vs. IIH-DC Meta) against signatures created from human cell lines treated with over 20,000 small molecules and drugs for the LINCS project.

Signature ID	Drug or natural product	Similarity score	*p*-value	q-value	Z-score	Combined score
ERG005_VCAP_6H:BRD-K88378636-001-02-8:20	Withaferin A	–0.0587	2.84e–19	1.21e–14	1.65	–30.67
CPC015_NPC_24H:BRD-K14920963-304-01-9:10	Erythrosine	–0.0304	2.85e–04	7.64e–01	1.75	–6.19
CPC006_HCC515_6H:BRD-K16406336-311-01-2:10	Methylene-blue	–0.0330	3.94e–04	8.88e–01	1.77	–6.02
CPC012_HCC515_6H:BRD-K56653679-001-01-2:10	MD-041	–0.0317	4.22e–04	9.03e–01	1.72	–5.81
CVD001_HUH7_6H:BRD-K81142122-001-14-1:10	STK-249718	–0.0323	3.91e–04	8.88e-01	1.62	–5.52
CPC004_HT29_6H:BRD-K77830450-001-02-4:10	Forskolin	–0.0264	1.31e–03	1.00e+00	1.90	–5.47
CPC013_SKB_24H:BRD-K16798053-001-01-0:10	ST-4029573	–0.0277	9.86e–04	1.00e+00	1.76	–5.29
CPC014_HA1E_6H:BRD-U66370498-000-01-0:10	Androstanol	–0.0264	1.43e–03	1.00e+00	1.77	–5.03
CPC005_A375_24H:BRD-A78360835-001-01-1:10	Cercosporin	–0.0290	2.06e–03	1.00e+00	1.82	–4.90
CPC014_HCC515_6H:BRD-A80960055-001-01-7:10	Celastrol	–0.0290	2.78e–03	1.00e+00	1.72	–4.40

TABLE 9 | Top small molecules with opposite molecular signatures based on L1000FWD web-based tool for querying gene expression signatures (Neuro-COVID vs. IIH-monoMeta) against signatures created from human cell lines treated with over 20,000 small molecules and drugs for the LINCS project.

Signature ID	Drug or natural product	Similarity score	*p*-value	q-value	Z-score	combined score
ERG005_VCAP_6H:BRD-K88378636-001-02-8:20	Withaferin A	–0.0533	2.68e–13	1.06e–08	1.65	–20.79
CPC006_SNUC5_6H:BRD-A19633847-050-20-6:10	Perhexiline	–0.0414	4.51e–08	3.85e–04	1.80	–13.23
CPC013_SKB_24H:BRD-K16798053-001-01-0:10	ST-4029573	–0.0382	2.01e–07	8.62e–04	1.76	–11.79
CPC017_SKB_24H:BRD-A20968261-001-01-3:10	WAY-213613	–0.0414	2.81e–07	1.00e–03	1.68	–11.01
CPC006_CORL23_6H:BRD-A04706586-236-01-7:10	Bucladesine	–0.0358	2.08e–06	4.95e–03	1.84	–10.48
CPC007_A375_24H:BRD-K03067624-003-19-3:10	Emetine	–0.0398	1.42e–06	3.80e–03	1.78	–10.42
CPC007_A375_6H:BRD-K03067624-003-19-3:10	emetine	–0.0374	3.86e–06	8.48e–03	1.81	–9.79
CPC012_MCF7_6H:BRD-K41652870-001-01-9:10	BRD-K41652870	–0.0366	7.70e–06	1.32e–02	1.75	–8.97
CPC005_A375_24H:BRD-A78360835-001-01-1:10	Cercosporin	–0.0358	2.49e–05	2.74e–02	1.83	–8.40
CPC006_PL21_6H:BRD-K78659596-001-01-3:10	MLN-2238	–0.0334	3.27e–05	3.33e–02	1.85	–8.28

hemoglobin complex, cytosolic small ribosomes, and cytosolic ribosomes (**Figure 3F**). The top five differentially expressed pathways identified based on iPathwayGuide analysis of immune cell meta clusters from Neuro-COVID patients were malaria, African trypanosomiasis, cocaine addiction, Parkinson's disease, and leukocyte transendothelial migration. The differentially regulated pathways in the meta clusters of immune cells from patients with Neuro-COVID are provided in **Supplementary Table S1**. The upstream genes activated in TcMeta, DCMeta, and monoMeta clusters are listed in **Supplementary Table S2**.

L1000FWD and L1000CDS2 Analyses

The L1000FWD analysis of DEGs of meta clusters of Tc, DC, and Mono of Neuro-COVID compared to IIH revealed that withaferin A was the top molecule capable of reversing the COVID-19 induced gene signatures (**Tables 7–9**). Furthermore, the rank diagram (**Figure 4A**) showed that JQ1 was the top drug based on the *in silico* prediction of insufficient signaling of drugs, natural products, and chemicals in the meta clusters of Tc, DC, and Mono of Neuro-COVID compared to IIH using iPathwayGuide (**Figure 4B**). The L100CDS2 analysis of DEGs of meta

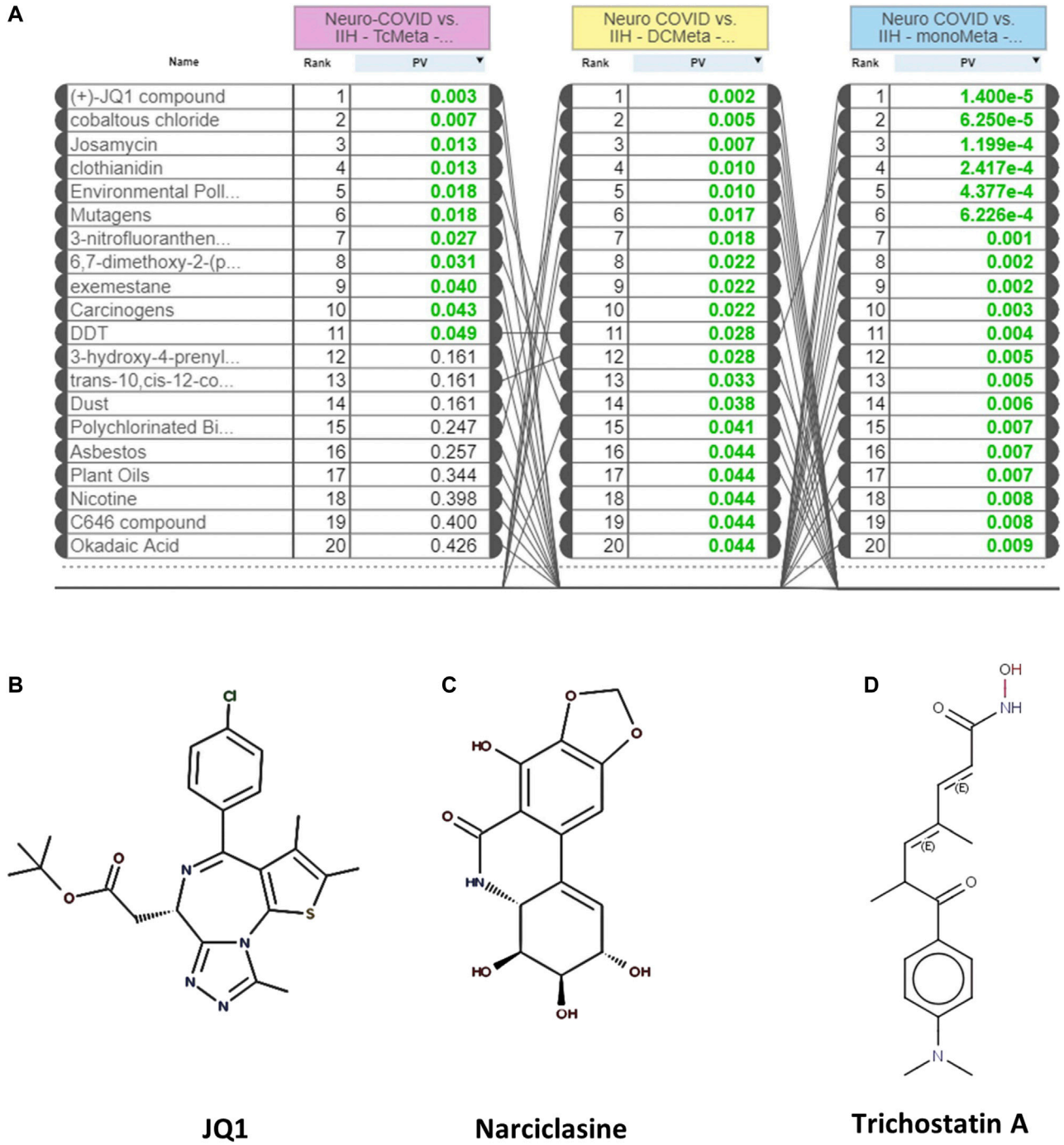

FIGURE 4 | (A) The rank diagram based on the *in silico* prediction of insufficient signaling of drugs and natural products in TcMeta, DCMeta, and monoMeta using iPathwayGuide analysis. **(B–D)** The two-dimensional structures of JQ1, narciclasine, and trichostatin A.

clusters of Tc, DC, and Mono of Neuro-COVID compared to IIH revealed that narciclasine (**Figure 4C**) and trichostatin A (**Figure 4D**) were some of the top molecules potentially reversing the Neuro-COVID gene signatures (**Tables 10–12**).

GSEA Preranked and Metascape Analyses

To obtain the specific gene signatures potentially reversed by camptothecin, importazole, and withaferin A, GSEA preranked analysis was performed using ranked DEGs from SARS-CoV-2-NHBE vs. Mock-NHBE comparison against

TABLE 10 | Top small molecules identified by the L1000CDS2 query that reverse the Neuro-COVID vs. IIH-TcMeta gene signature.

Rank	Overlap	Perturbation	Cell line	Dose	Time (h)
1	0.0358	T5212475	VCAP	10.0 μm	24.0
2	0.0353	BRD-K56411643	VCAP	10.0 μm	24.0
3	0.0278	F3055	A375	10.0 μm	6.0
4	0.0254	Narciclasine	HA1E	10.0 μm	24.0
5	0.0249	Ro 31-8220 mesylate	HCC515	10.0 μm	24.0
6	0.0244	Erythrosine sodium	HA1E	10.0 μm	24.0
7	0.0244	Parthenolide	A375	20.0 μm	24.0
8	0.0239	Teniposide	A375	1.25 μm	24.0
9	0.0239	Daunorubicin	A549	10.0 μm	6.0
10	0.0239	EI-293	PC3	10.0 μm	6.0

TABLE 12 | Top small molecules identified by the L1000CDS2 query that reverse the Neuro-COVID vs. IIH-monoMeta gene signature.

Rank	Overlap	Perturbation	Cell line	Dose	Time (h)
1	0.0398	Trichostatin A	A375	10.0 μm	24.0
2	0.0390	Narciclasine	A375	10.0 μm	24.0
3	0.0366	Parthenolide	A375	20.0 μm	24.0
4	0.0350	HY-10518	VCAP	10.0 μm	24.0
5	0.0334	Vorinostat	A375	11.1 μm	24.0
6	0.0326	Teniposide	A375	1.25 μm	24.0
7	0.0326	BRD-K56411643	VCAP	10.0 μm	24.0
8	0.0326	BL-081	VCAP	10.0 μm	24.0
9	0.0326	Camptothecin (S,+)	PC3	10.0 μm	24.0
10	0.0310	Erythrosine sodium	HA1E	10.0 μm	24.0

gene signatures differentially regulated by these small molecules derived from the L1000FWD web tool. The gene signature (Signature ID: CPC002_PC3_24H: BRD-A30437061:10.0) downregulated by camptothecin was positively enriched (normalized enrichment score (NES) = 1.32**,** and q-value = 0.065) and the upregulated genes were negatively enriched (NES = −1.12 and q-value = 0.27) in the SARS CoV2-NHBE cells (**Supplementary Figure S2A**). The gene signature (Signature ID: CPC006_A375_24H: BRD-A02481876:60.0) downregulated by importazole was positively enriched (NES = 1.31 and q-value = 0.036) (**Supplementary Figure S2B**) and the gene signature (Signature ID: CPC014_VCAP_6H: BRD-A52193669:10.0) downregulated by withaferin A was significantly enriched (NES = 1.21 and q-value = 0)**,** and the upregulated genes were negatively enriched (NES = −1.21 and q-value = 0.14) in the SARS CoV2-NHBE cells (**Supplementary Figure S2C**).

Camptothecin potentially reversed 28 genes that were positively enriched in SARS-CoV-2 in NHBE cells, and the top 10 genes were COL6A2, CSE1L, TMEM135, PPA2, MNAT1, BNIP3L, DLGAP5, TMEM47, ARHGAP29, and OLA1. In contrast, 11 genes upregulated by CPT were negatively enriched in SARS-CoV-2- NHBE cells, including RSAD2, CD74, HSPA2, SDC3, ZDHHC11, NEU1, S100A8, ISG15, MAFB, TSPAN7, and PEG3. Importazole potentially reversed 66 genes that were positively enriched in SARS-CoV-2-NHBE cells, and the top 10 genes were CDH19, CD58, TFF3, SNX10, SMC4, TMEM135, MNAT1, PBK, and TFPI. Withaferin A potentially reversed 134 genes that were positively enriched in SARS-CoV-2-NHBE cells, and the top 10 genes were NUDT4, CCNG1, ASPM, NLGN4X, USP1, SERP1, DIAPH2, PLEKHF2, XPO1, SUB1, SMC4, and HSPA6. In contrast, 23 genes upregulated by withaferin A were negatively enriched in SARS-CoV-2- NHBE cells and the top 10 genes were MT1F, CBR3, RAB20, SLC22A18, SLC37A4, EIF4EBP1, IRX5, S100A8, COL1A1, and ABHD14A. In addition, the gene signatures enriched in SARS-CoV-2-NHBE cells that were potentially reversed by withaferin A, camptothecin, and importazole were analyzed using Metascape to identify the enrichment ontology clusters based on GO/KEGG terms, canonical pathways, and hallmark gene sets (**Figure 5**). The genes enriched in GSEA preranked analysis of SARS CoV2-NHBE vs. Mock-NHBE against the gene signatures of camptothecin, importazole, and withaferin A are provided in **Supplementary Datasheet S1**.

TABLE 11 | Top small molecules identified by the L1000CDS2 query that reverse the Neuro-COVID vs. IIH-DCMeta gene signature.

Rank	Overlap	Perturbation	Cell line	Dose	Time (h)
1	0.0337	Trichostatin A	A375	10.0 μm	24.0
2	0.0304	Narciclasine	HA1E	10.0 μm	24.0
3	0.0297	Camptothecin (S,+)	PC3	10.0 μm	24.0
4	0.0277	Erythrosine sodium	HA1E	10.0 μm	24.0
5	0.0277	Vorinostat	A375	11.1 μm	24.0
6	0.0271	F3055	A375	10.0 μm	6.0
7	0.0264	Parthenolide	A375	20.0 μm	24.0
8	0.0257	Curcumin	MCF7	48.0 μm	24.0
9	0.0257	BRD-K56411643	VCAP	10.0 μm	24.0
10	0.0257	Celastrol	HME1	10 μm	3

Similarly, the GSEA preranked analysis was performed using ranked DEGs from Neuro-COVID vs. IIH-TcMeta, Neuro-COVID vs. IIH-DCMeta, and Neuro-COVID vs. IIH_monoMeta comparisons against gene signatures differentially regulated by withaferin A, camptothecin, trichostatin A, narciclasine, and JQ1 small molecules. The gene signature (Signature ID: CPC014_VCAP_6H: BRD-A52193669:10.0) upregulated by withaferin A was positively enriched (NES = 1.62, q = 0.028) in TcMeta, DCMeta (NES = 1.23, q-value <= 0.24)**,** and monoMeta (NES = 1.50, q-value = 0.06). However, the downregulated genes of withaferin A were moderately enriched in TcMeta and DCMeta (**Supplementary Figure S3**). The gene signature (Signature ID: CPC002_PC3_24H: BRD-A30437061:10.0) downregulated by camptothecin was significantly enriched (NES = 1.52, q = 0.051) in TcMeta and moderately enriched in DCMeta and monoMeta (**Supplementary Figure S4**).

The gene signature (Signature ID: CPC012_A375_6H: BRD-K68202742:10.0) downregulated by trichostatin A was moderately enriched (NES = 1.34 and q = 0.11) in TcMeta, DCMeta (NES = 0.92 and q-value = 0.59), and monoMeta (NES = 1.2 and q = 0.20). The upregulated genes of trichostatin A were negatively enriched in DCMeta (NES = −1.39 and q-value = 0.085) and monoMeta (NES = −1.47 and q-value = 0.10) (**Supplementary Figure S5**). The gene signature (Signature ID: CPC006_HA1E_24H: BRD-K06792661:10.0) upregulated by

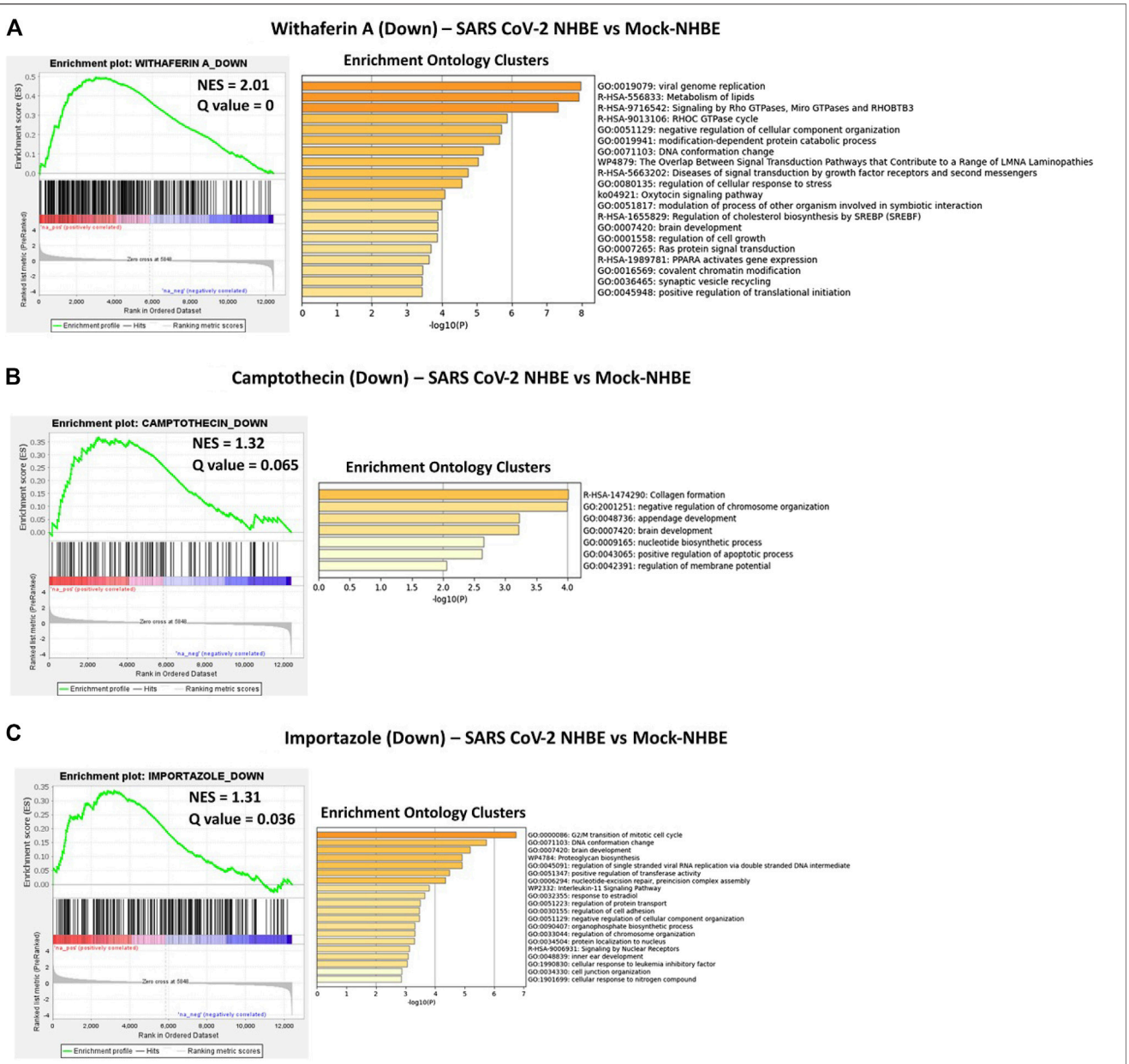

FIGURE 5 | GSEA preranked analysis was performed to decipher the potential gene signatures downregulated by camptothecin, importazole, and withaferin A using the RNK file generated from DEGs of SARS CoV2-NHBE vs. Mock-NHBE comparison. The Metascape analyses to decipher the gene ontology clusters based on the **(A)** enrichment of gene signature (Signature ID: CPC014_VCAP_6H: BRD-A52193669:10.0) downregulated by withaferin A **(B)** enrichment of gene signature (Signature ID: CPC002_PC3_24H: BRD-A30437061:10.0) downregulated by camptothecin, and **(C)** enrichment of gene signature (Signature ID: CPC006_A375_24H: BRD-A02481876:60.0) downregulated by importazole in SARS CoV2-NHBE cells.

narciclasine was negatively enriched in TcMeta (NES = −1.97 and q-value = 0), DCMeta (NES = −1.65 and q-value = 0), and monoMeta (NES = −2.77 and q-value = 0). The differentially regulated genes of narciclasine were negatively enriched in monoMeta (NES = −2.01 and q-value = 0). However, the downregulated genes of narciclasine were moderately enriched in TcMeta (NES = 1.22 and q-value = 0.19) and DCMeta (NES = 1.32 and q = 0.15) (**Supplementary Figure S6**). The gene signature (Signature ID: LJP008_A549_24H: BRD-K54606188: 10) downregulated by JQ1 was negatively enriched in the DCMeta (NES = −0.68 and q-value = 0.98) and Neuro-COVID vs. IIH-monoMeta (NES = −1.40 and q = 0.14) groups. The upregulated genes of JQ1 were moderately enriched in all three meta clusters of immune cells in Neuro-COVID (**Supplementary Figure S7**).

The gene signatures upregulated by withaferin A (GNLY CST7 PPIB TSPO BCL2 S100A10 GSTP1), (S100A10, TSPO, PPIB, HLA-DQB1, BCL2, GSTP1, EDF1, and FLOT1), and (S100A9,

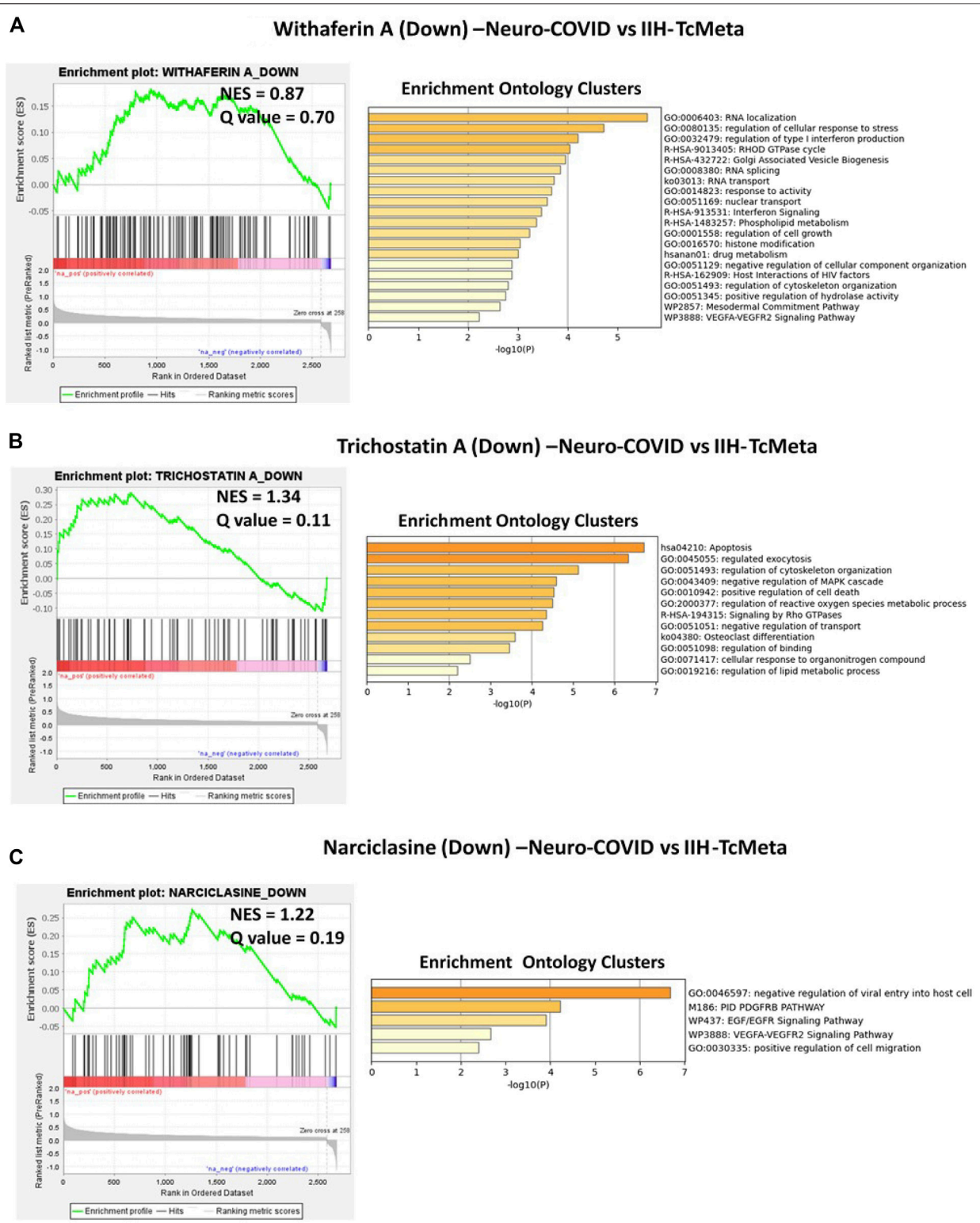

FIGURE 6 | GSEA preranked analysis was performed to decipher the potential gene signatures downregulated by withaferin A, trichostatin A, and narciclasine using the RNK file generated from DEGs of Neuro-COVID vs. IIH (TcMeta) comparison. The Metascape analyses to decipher the GO clusters based on the **(A)** enrichment of gene signature (Signature ID: CPC014_VCAP_6H: BRD-A52193669:10.0) downregulated by withaferin A, **(B)** enrichment of gene signature (Signature ID: CPC012_A375_6H: BRD-K68202742:10.0) downregulated by trichostatin A, and **(C)** enrichment of gene signature (Signature ID: CPC006_HA1E_24H: BRD-K06792661:10.0) downregulated by narciclasine in Neuro-COVID vs. IIH-TcMeta.

S100A8, TSPO, and HOMER3) were positively enriched in TcMeta, DCMeta, and monoMeta clusters in Neuro-COVID. Camptothecin potentially reversed seven genes that were positively enriched in TcMeta, including AHNAK, MBNL1, LGALS1, HNRNPA2B1, S100A10, TGFBR2, and CAPN2. Trichostatin A potentially reverses five genes that were positively enriched in DCMeta, such as RGS2. IL32, ZFP36, SRGN, and STAB1, as well as nine genes that were positively enriched in monoMeta, such as SRGN, RGS2, IL32, ZFP36, JUNB, SAT1, PADI2, ALOX5AP, and IL2RG. The upregulated gene signatures of narciclasine (H3F3B, ZFP36, RGS2, and XIST) and (XIST, CREM, ZFP36, JUNB, NR4A2, FOS, EGR1, EVI2A, SAT1, EGR2, IER2, NR4A1, and KDM5A) were negatively enriched in DCMeta and monoMeta, respectively. JQ1 potentially increased six genes that were negatively enriched in DCMeta, such as H3F3B, AP2A2, PIGF, SOS1, TRIO, FHL3, H3F3B, MBNL2, TRIO, AP2A2, PSIP1, and ARHGEF6 in monoMeta. In addition, the gene signatures enriched in Neuro-COVID vs. IIH (TcMeta, DCMeta, and monoMeta) that are potentially reversed by withaferin A, camptothecin, trichostatin A, narciclasine, and JQ1 were analyzed using Metascape to find the enrichment ontology clusters based on GO/KEGG terms, canonical pathways, and hallmark gene sets. The enrichment ontology clusters derived for the gene signatures reversed by withaferin A, trichostatin A, and narciclasine in Neuro-COVID vs. IIH-TcMeta are shown in **Figure 6**. The genes enriched in GSEA preranked analysis of Neuro-COVID vs. IIH comparison against the gene signatures of withaferin A, camptothecin, trichostatin A, narciclasine, and JQ1 are provided in **Supplementary Datasheet S2**.

DISCUSSION

COVID-19 caused by SARS-CoV-2 infection remains an ongoing pandemic (Huang C. et al., 2020; Liu J. et al., 2020; Novel Coronavirus Pneumonia Emergency Response Epidemiology Team, 2020) and patients with severe COVID-19 may also develop neurological complications called Neuro-COVID (Heming et al., 2021). RNA sequencing is a very recently developed NGS methodology for the whole transcriptome or single-cell transcriptomics approaches (Liu and Di, 2020) and is broadly used to explore biological, cellular, and molecular processes implicated in COVID-19 infection (Liu T. et al., 2020; Liao et al., 2020; Zhou et al., 2020). Hence, either developing novel drug candidates or identifying suitable existing therapeutics for drug repurposing for COVID-19 and Neuro-COVID is essential to decrease the infection rate and control the COVID-19 pandemic and reduce the enormous economic burden on healthcare systems. Because the gene expression profiles of COVID-19 infection models can be used to decipher potential therapeutic targets that could be targeted by known drugs (Daamen et al., 2021), we used RNA-seq datasets from the COVID-19 infection models of NHBE cells, and the scRNA-seq datasets of immune cells isolated from the CSF of Neuro-COVID patients and analyzed using NGKD platforms to understand the disease-specific gene signatures and pathways and further uncover small molecules from both synthetic and natural sources that potentially reverse these diseases.

Here, we found that COVID-19 infection of NHBE cells activated upstream genes such as IL-17, TNF-alpha, STAT2, IRF9, and TLR-4. Biological processes such as humoral immune response, acute-phase response, and molecular functions such as cytokine activity, receptor regulator activity, signaling receptor activity, receptor-ligand activity, and chemokine activity were enriched in the COVID-infected cells. Importantly, the cytokine and cytokine receptor interaction and viral protein interaction with the cytokine and cytokine receptors were activated in COVID-infected NHBE cells. Cytokines are important for both innate and adaptive inflammatory host responses, cell differentiation, cell death, growth, repair and development, and cellular homeostasis (Pushparaj, 2019; Bahlas et al., 2020; Harakeh et al., 2020; Jafri et al., 2020; Pushparaj, 2020). Studies have shown that several circulating cytokines and chemokines such as TNFα, CXCL-10, IL-6, and IL-8 are differentially expressed during SARS-CoV-2 infection, and this cytokine/chemokine storm likely contributes to the poor prognosis of COVID-19 (Liu J. et al., 2020; Vaninov, 2020). RNA sequencing analysis of cell and animal models of SARS-CoV-2 infection, blood, lung, and airway biopsies from COVID-19 patients showed inflammatory responses characterized by low levels of type I and III IFNs, increased interleukin-6 (IL-6), and a variety of chemokines (Blanco-Melo et al., 2020; Daamen et al., 2021). The spike protein (S protein) of SARS-CoV-2 is essential for the attachment between the coronavirus and hACE2 surface receptor through its receptor-binding domain (RBD) (Lan et al., 2020) and is proteolytically activated by human proteases, thus helping the coronavirus to enter the host cells (Shang et al., 2020). A recent study showed that hACE2 was stimulated by IFN in human airway epithelial cells (Ziegler et al., 2020) and thus helps in the entry of SARS-CoV-2 into host cells.

SARS-CoV-2 and other coronaviruses have developed different mechanisms to avoid detection and subsequent destruction by copying and repurposing cytokine and cytokine receptor genes in the host (Heimfarth et al., 2020; Choudhary et al., 2021). COVID-19 induced cytokines and cytokine receptors, chemokines, and other specific cytokine receptors and binding proteins may subvert and alter the host cytokine networks (Choudhary et al., 2021). Here, the COVID-19-induced cytokines, cytokine receptors, receptor-binding proteins, and chemokines may stimulate or prevent cytokine signaling and may significantly alter various facets of host immunity. In addition, Daamen et al. (2021) found that COVID-19 pathogenesis was driven by highly inflammatory myeloid-lineage cells with distinct transcriptional signatures and the absence of cytotoxic cells in the lungs, leading to reduced viral clearance.

Heming et al. (2021) stated that lumbar puncture to obtain immune cells from COVID-19 patients without neurological manifestations as controls was not ethically permitted for scientific purposes. Since IIH is a benign disorder associated with high pressure in the brain, the immune cells derived from the CSF of patients with IIH were used as controls to compare Neuro-COVID. The cluster of differentiation molecule 81 (CD81) is one

of the commonly regulated genes in the meta clusters of immune cells from the CSF of patients with Neuro-COVID and belongs to the tetraspanin superfamily, which has been shown to regulate viral entry, viral replication, infectivity, and virion exit of different types of viruses (Benayas et al., 2020). Therefore, it is essential to investigate the importance of CD81 in patients with COVID-19 and Neuro-COVID. One of the upstream genes activated in TcMeta cluster, Cell cycle division 37 (CDC37), a heat shock protein 90 (HSP90) cochaperone that could play an important role in the pathogenesis of Neuro-COVID. COVID-19 progression to a systemic disease could be associated with HSP-related molecular mimicry autoimmune phenomena (Cappello et al. 2020; Kasperkiewicz, 2021). It was postulated that Hsp90 inhibition could also be a potential treatment option for cytokine storm-mediated acute respiratory distress syndrome in COVID-19 patients (Kasperkiewicz, 2021). Recently, Wyler et al. (2021) identified HSP90 as a target for COVID therapy based on transcriptomic profiling of SARS-CoV-2 infected human cell lines.

Interestingly, the top five differentially expressed pathways identified based on iPathwayGuide analysis of immune cell meta clusters from Neuro-COVID patients were malaria, African trypanosomiasis, cocaine addiction, Parkinson's disease, and leukocyte transendothelial migration. Studies have shown a potential link between the presentation of malaria and COVID-19. The opposite relationship between COVID 19 and malaria has been suggested to be linked with the wide use of antimalarial drugs, including hydroxychloroquine (HCQ) and chloroquine (CQ), in countries that are endemic to malaria (Hussein et al., 2020).

There are many types of COVID-19 vaccines currently available for prophylaxis, and many are under development (Mandolesi et al., 2021). Several therapeutics are available based on WHO guidelines to treat the complications of COVID-19 and related complications (Lamontagne et al., 2021); however, these therapeutics are not specifically designed for the treatment of COVID-19 and its related complications such as Neuro-COVID, and their efficacies substantially differ across the globe and are not very effective in ameliorating disease severity (Surnar et al., 2020). In this study, we utilized NGKD platforms such as iPathwayGuide, L1000FWD, and L1000CDS2 tools to identify promising druggable molecules based on their *in silico* potential to reverse gene signatures induced by COVID-19 and Neuro-COVID. We found that camptothecin, importazole, and withaferin A had insufficient signaling or gene signatures (or absent) in COVID-19 infected NHBE cells. Based on L1000CDS2 analysis, trichostatin A, a histone deacetylase inhibitor, mildly inhibited the ACE receptors (Takahashi et al., 2021), and narciclasine and camptothecin are some of the top small molecules that reverse the gene signatures in Neuro-COVID vs. IIH immune datasets. In addition, a comparative analysis of the Neuro-COVID vs. IIH immune cell meta cluster datasets showed that JQ1 had insufficient signaling (or absence).

The GSEA preranked analysis calculates if *a priori* defined sets of genes display statistically significant enrichment at either end of the ranking (Subramanian et al., 2005). The gene signature potentially reversed by withaferin A in SARS-CoV-2 NHBE vs. Mock-NHBE based on preranked GSEA involved in various biological, molecular, and cellular processes, including viral genome replication (GO: 0019079), modulation of the process of other organisms involved in symbiotic interactions (GO:0051817), and positive regulation of translational initiation (GO:0045948). The gene signature potentially reversed by importazole in SARS-CoV-2 NHBE vs. Mock-NHBE based on preranked GSEA involved in various biological, molecular, and cellular processes, including regulation of single-stranded viral RNA replication via a double-stranded DNA intermediate (GO: 0045091). The gene signature potentially reversed by withaferin A in Neuro-COVID vs. IIH-TcMeta based on preranked GSEA involved in various biological, molecular, and cellular processes, including regulation of type 1 interferon production (GO:0032479) and interferon signaling (R-HSA-913531). The gene signature potentially reversed by withaferin A in Neuro-COVID vs. IIH-TcMeta based on preranked GSEA involved in various biological, molecular, and cellular processes, including regulation of type 1 interferon production (GO:0032479) and interferon signaling (R-HSA-913531). The gene signature potentially reversed by narciclasine in Neuro-COVID vs. IIH-TcMeta based on preranked GSEA involved in negative regulation of viral entry into host cells (GO: 0046597), PDGFR beta signaling pathway (PID-M186), EGF/EGFR signaling pathway (WP437), VEGFA/VEGFR2 signaling pathway (WP3888), and positive regulation of cell migration (GO: 0030335). The gene signatures upregulated by withaferin A (GNLY CST7 PPIB TSPO BCL2 S100A10 GSTP1), (S100A10, TSPO, PPIB, HLA-DQB1, BCL2, GSTP1, EDF1, and FLOT1), and S100A9, S100A8, TSPO, and HOMER3) were positively enriched in Neuro-COVID. Granulysin (GNLY) is a member of the saposin-like protein (SAPLIP) family, is located in the cytotoxic granules of T-cells and NK cells, is released on antigen stimuli, and has antimicrobial activity. The S100 genes include 13 members and have antibacterial and antifungal properties (Crinier et al., 2018).

Our L1000FWD analyses showed that withaferin A was the top natural product that reverses the signature of Neuro-COVID in all the meta clusters of immune cells from the CSF of Neuro-COVID patients. Withaferin A is a component of Withania somnifera (*ashwagandha or Indian ginseng*) (Srivastava et al., 2020). W. somnifera has been used in traditional medicine as an antioxidant, antianxiety, anti-inflammatory, antibacterial, aphrodisiac, and herbal tonic for general health (Sood et al., 2018). The active ingredients include withanolides, saponins, alkaloids, and steroidal lactones. *In vitro* studies have shown that ashwagandha has neuroprotective, cardioprotective, immunomodulating, and anticancer properties (Singh et al., 2021).

Adjunctive treatment with ashwagandha improved symptoms and stress in patients with schizophrenia, offering beneficial effects on cognitive function in patients with bipolar disorder and improves balance in patients with progressive degenerative cerebral ataxias (Sood et al., 2018; Singh et al., 2021). It was recently shown that withanolides present in ashwagandha possess anti-COVID-19 properties**,** and these compounds exhibit good absorption and transport kinetics with no related mutagenic or adverse effects (Srivastava et al., 2020). Withaferin A was predicted to bind and stably interact with the binding site of TMPRSS2, similar to its known inhibitor, camostat mesylate (Kumar et al., 2020). Camostat was found to reduce SARS-CoV-2 infection in TMPRSS2 expressing Vero cells (Hoffmann et al., 2020). David et al., 2021 in their

MedRixv preprint showed that a common variant of TMPRSS2 protects against COVID-19. *In silico* screening of several phytochemicals identified that Withanone, one of the constituents of ashwagandha, showed a potential inhibition of ACE2 (Balkrishna et al., 2021). Additionally, Ghosh et al. (2021) used molecular dynamic simulations and pharmacophore modeling approaches to predict the highly potent small-molecule derivative of withaferin A that potentially inhibits SARS-CoV-2 protease (Mpro), a favorable future therapeutic against COVID-19.

Recent studies have demonstrated the antiviral properties of narciclasine, an alkaloid found in various Amaryllidaceae species, and camptothecin, a topoisomerase inhibitor first isolated from the stem of *Camptotheca acuminata* (used in Chinese traditional medicine) against SARS-CoV-2 (Huang C.-T. et al., 2020; Mamkulathil Devasia et al., 2021). However, importazole, an inhibitor of importin-β transport receptors, and other small molecules identified to reverse COVID-19-induced gene signatures need to be further explored because developing effective therapeutics is essential to control the COVID-19 pandemic (Surnar et al., 2020).

In conclusion, the present study unravels a rapid approach to using high-throughput RNA sequencing technologies coupled with NGKD platforms to decipher specific drugs and small molecules derived either synthetically or from natural sources for the amelioration of COVID-19 related disease pathologies such as Neuro-COVID. Further studies are warranted to validate the small molecules identified in our study using *in vitro* and *in vivo* model systems of COVID-19 and Neuro-COVID to determine their mechanism(s) of action followed by suitable clinical trials to confirm the efficacy and safety for possible therapeutic intervention for COVID-19-related disease pathologies.

DATA AVAILABILITY STATEMENT

Publicly available datasets were analyzed in this study. This data can be found here: Gene Expression Omnibus GSE147507 and GSE163005.

AUTHOR CONTRIBUTIONS

PP, MN, and AA designed the experiments. PP and MN conducted the experiments. PP, AA, and MN analyzed the data. PP wrote the manuscript. PP and MN finally revised the manuscript. All authors contributed to the editing of the manuscript and the scientific discussions.

FUNDING

The research work was funded by Institutional Fund Project under grant no. (IFPHI-110-117-2020). Therefore, the authors gratefully acknowledge technical and financial support from the Ministry of Education and King Abdulaziz University, DSR, Jeddah. Saudi Arabia.

SUPPLEMENTARY MATERIAL

The Supplementary Material for this article can be found online at: https://www.frontiersin.org/articles/10.3389/fphar.2021.688227/full#supplementary-material

Supplementary Table S1 | The differentially regulated pathways in the meta clusters of immune cells from patients with Neuro-COVID are provided in Supplementary Table S1.

Supplementary Table S2 | The upstream genes activated in TcMeta, DCMeta, and monoMeta clusters are listed in Supplementary Table S2.

Supplementary Datasheet S1 | The genes enriched in GSEA preranked analysis of SARS CoV2-NHBE vs. Mock-NHBE against the gene signatures of camptothecin, importazole, and withaferin A are provided in Supplementary Datasheet S1.

Supplementary Datasheet S2 | The genes enriched in GSEA preranked analysis of Neuro-COVID vs. IIH comparison against the gene signatures of withaferin A, camptothecin, trichostatin A, narciclasine, and JQ1 are provided in Supplementary Datasheet S2.

Supplementary Figure S1 | **(A)** Hierarchically clustered interactive heatmaps were generated using the Clustergrammer web tool for visualizing and analyzing high-dimensional RNASeq data (NHBE-SARS CoV2 vs NHBE-Mock). **(B)** Principal Component Analysis (PCA) was applied to identify global patterns in high-dimensional RNASeq datasets **(C)** Volcano plot was generated using transformed gene fold changes using log2 and displayed on the x-axis **(D)** MA plot was based on average gene expression which was calculated using the mean of the normalized gene expression values and displayed on the x-axis.

Supplementary Figure S2 | GSEA Preranked analysis was performed to decipher the potential gene signatures differentially regulated (Combined, Downregulated, and Upregulated) by camptothecin, importazole, and withaferin A using the RNK file generated from DEGs of SARS CoV-NHBE vs Mock-NHBE comparison. **(A)** The enrichment of gene signature (Signature_ID: CPC002_PC3_24H: BRD-A30437061:10.0) differentially regulated by camptothecin, **(B)** the enrichment of gene signature (Signature ID: CPC006_A375_24H: BRD-A02481876:60.0) differentially regulated by importazole and **(C)** the enrichment of gene signature (Signature ID: CPC014_VCAP_6H: BRD-A52193669:10.0) differentially regulated by withaferin A in SARS CoV2-NHBE cells.

Supplementary Figure S3 | GSEA Preranked analysis was performed to decipher the potential gene signatures differentially regulated (Combined, Downregulated, and Upregulated) by withaferin A using the RNK file generated from DEGs of Neuro-COVID vs IIH (TcMeta, DCMeta, and monoMeta) comparisons. The enrichment of gene signature (Signature ID: CPC014_VCAP_6H: BRD-A52193669:10.0) differentially regulated by withaferin A in **(A)** Neuro-COVID vs IIH-TcMeta **(B)** Neuro-COVID vs IIH-DCMeta, and **(C)** Neuro-COVID vs IIH-monoMeta.

Supplementary Figure S4 | GSEA Preranked analysis was performed to decipher the potential gene signatures differentially regulated (Combined, Downregulated, and Upregulated) by camptothecin using the RNK file generated from DEGs of Neuro-COVID vs IIH (TcMeta, DCMeta, and monoMeta) comparisons. The enrichment of gene signature (Signature ID: CPC002_PC3_24H: BRD-A30437061:10.0) differentially regulated by camptothecin in **(A)** Neuro-COVID vs IIH-TcMeta **(B)** Neuro-COVID vs IIH-DCMeta, and **(C)** Neuro-COVID vs IIH-monoMeta.

Supplementary Figure S5 | GSEA Preranked analysis was performed to decipher the potential gene signatures differentially regulated (Combined, Downregulated, and Upregulated) by trichostatin A using the RNK file generated from DEGs of Neuro-COVID vs IIH (TcMeta, DCMeta, and monoMeta) comparisons. The enrichment of gene signature (Signature ID: CPC012_A375_6H: BRD-K68202742:10.0) differentially regulated by trichostatin A in **(A)** Neuro-COVID vs IIH-TcMeta **(B)** Neuro-COVID vs IIH-DCMeta, and **(C)** Neuro-COVID vs IIH-monoMeta.

Supplementary Figure S6 | GSEA Preranked analysis was performed to decipher the potential gene signatures differentially regulated (Combined, Downregulated, and Upregulated) by narciclasine using the RNK file generated from DEGs of Neuro-COVID vs IIH (TcMeta, DCMeta, and monoMeta) comparisons. The enrichment of gene signature (Signature ID:

CPC006_HA1E_24H: BRD-K06792661:10.0) differentially regulated by narciclasine in **(A)** Neuro-COVID vs IIH-TcMeta **(B)** Neuro-COVID vs IIH-DCMeta, and **(C)** Neuro-COVID vs IIH-monoMeta.

Supplementary Figure S7 | GSEA Preranked analysis was performed to decipher the potential gene signatures differentially regulated (Combined, Downregulated, and Upregulated) by JQ1 using the RNK file generated from DEGs of Neuro-COVID vs IIH (TcMeta, DCMeta, and monoMeta) comparisons. The enrichment of gene signature (Signature ID: LJP008_A549_24H: BRD-K54606188:10) differentially regulated by JQ1 in **(A)** Neuro-COVID vs IIH-TcMeta **(B)** Neuro-COVID vs IIH-DCMeta, and **(C)** Neuro-COVID vs IIH-monoMeta.

REFERENCES

Ashburner, M., and Lewis, S. (2002). On Ontologies for Biologists: The Gene Ontology-Uuntangling the Web. *Novartis Found. Symp.* 247, 66–52. doi:10.1002/0470857897.ch6

Ashburner, M., Ball, C. A., Blake, J. A., Botstein, D., Butler, H., Cherry, J. M., et al. (2000). Gene Ontology: Tool for the Unification of Biology. *Nat. Genet.* 25 (1), 25–29. doi:10.1038/75556

Bahlas, S., Damiati, L. A., Al-Hazmi, A. S., and Pushparaj, P. N. (2020). Decoding the Role of Sphingosine-1-Phosphate in Asthma and Other Respiratory System Diseases Using Next Generation Knowledge Discovery Platforms Coupled with Luminex Multiple Analyte Profiling Technology. *Front. Cel Dev. Biol.* 8, 444. doi:10.3389/fcell.2020.00444

Balkrishna, A., Pokhrel, S., Singh, H., Joshi, M., Mulay, V. P., Haldar, S., et al. (2021). Withanone from *Withania Somnifera* Attenuates SARS-CoV-2 RBD and Host ACE2 Interactions to Rescue Spike Protein Induced Pathologies in Humanized Zebrafish Model. *Dddt* 15, 1111–1133. doi:10.2147/DDDT.S292805

Barrett, T., Wilhite, S. E., Ledoux, P., Evangelista, C., Kim, I. F., Tomashevsky, M., et al. (2013). NCBI GEO: Archive for Functional Genomics Data Sets-Update. *Nucleic Acids Res.* 41 (Database issue), D991–D995. doi:10.1093/nar/gks1193

Benayas, B., Sastre, I., López-Martín, S., Oo, A., Kim, B., Bullido, M. J., et al. (2020). Tetraspanin CD81 Regulates HSV-1 Infection. *Med. Microbiol. Immunol.* 209 (4), 489–498. doi:10.1007/s00430-020-00684-0

Benjamini, Y., and Hochberg, Y. (1995). Controlling the False Discovery Rate: A Practical and Powerful Approach to Multiple Testing. *J. R. Stat. Soc. Ser. B (Methodological)* 57 (1), 289–300. doi:10.1111/j.2517-6161.1995.tb02031.x

Benjamini, Y., and Yekutieli, D. (2001). The Control of the False Discovery Rate in Multiple Testing Under Dependency. *Ann. Stat.* 29 (4), 1165–1188. doi:10.1214/aos/1013699998

Blanco-Melo, D., Nilsson-Payant, B. E., Liu, W.-C., Uhl, S., Hoagland, D., Møller, R., et al. (2020). Imbalanced Host Response to SARS-CoV-2 Drives Development of COVID-19. *Cell* 181 (5), 1036–1045.e9. doi:10.1016/j.cell.2020.04.026

Bonferroni, C. E. (1935). "Il calcolo delle assicurazioni su gruppi di teste," in *Studi in Onore del Professore Salvatore Ortu Carboni* (Rome: Tipografia del Senato), 13–60.

Bonferroni, C. E. (1936). "Teoria statistica delle classi e calcolo delle probabilita," in *Pubblicazioni del Istituto Superiore di Scienze Economiche e Commerciali di Firenze* (Firenze: Seeber), 8, 3–62.

Cappello, F., Marino Gammazza, A., Dieli, F., Conway de Macario, E., and Macario, A. J. (2020). Does SARS-CoV-2 Trigger Stress-Induced Autoimmunity by Molecular Mimicry? A Hypothesis. *Jcm* 9 (7), 2038. doi:10.3390/jcm9072038

Choudhary, S., Sharma, K., and Silakari, O. (2021). The Interplay Between Inflammatory Pathways and COVID-19: A Critical Review on Pathogenesis and Therapeutic Options. *Microb. pathogenesis* 150, 104673. doi:10.1016/j.micpath.2020.104673

Crinier, A., Milpied, P., Escalière, B., Piperoglou, C., Galluso, J., Balsamo, A., et al. (2018). High-Dimensional Single-Cell Analysis Identifies Organ-specific Signatures and Conserved NK Cell Subsets in Humans and Mice. *Immunity* 49 (5), 971–986.e5. doi:10.1016/j.immuni.2018.09.009

Cui, J., Li, F., and Shi, Z.-L. (2019). Origin and Evolution of Pathogenic Coronaviruses. *Nat. Rev. Microbiol.* 17, 181–192. doi:10.1038/s41579-018-0118-9

Daamen, A. R., Bachali, P., Owen, K. A., Kingsmore, K. M., Hubbard, E. L., Labonte, A. C., et al. (2021). Comprehensive Transcriptomic Analysis of COVID-19 Blood, Lung, and Airway. *Sci. Rep.* 11 (1), 7052. doi:10.1038/s41598-021-86002-x

David, A., Parkinson, N., Peacock, T. P., Pairo-Castineira, E., Khanna, T., Cobat, A., et al. (2021). A Common TMPRSS2 Variant Protects Against Severe COVID-19. MedRxiv [Preprint]. Available at: https://www.medrxiv.org/content/10.1101/2021.03.04.21252931v1.full.pdf. doi:10.1101/2021.03.04.21252931

Davis, A. P., Grondin, C. J., Johnson, R. J., Sciaky, D., Wiegers, J., Wiegers, T. C., et al. (2021). Comparative Toxicogenomics Database (CTD): Update 2021. *Nucleic Acids Res.* 49 (D1), D1138–D1143. doi:10.1093/nar/gkaa891

Dong, E., Du, H., and Gardner, L. (2020). An Interactive Web-Based Dashboard to Track COVID-19 in Real Time. *Lancet Infect. Dis.* 20 (5), 533–534. doi:10.1016/S1473-3099(20)30120-1

Draghici, S., Khatri, P., Martins, R. P., Ostermeier, G. C., and Krawetz, S. A. (2003a). Global Functional Profiling of Gene Expression. *Genomics* 81 (2), 98–104. doi:10.1016/s0888-7543(02)00021-6

Draghici, S. (2011). *Statistics and Data Analysis for Microarrays Using R and Bioconductor*. 2nd Edn. London: Chapman and Hall/CRC.

Draghici, S., Khatri, P., Bhavsar, P., Shah, A., Krawetz, S., and Tainsky, M. A. (2003b). Onto-Tools, the Toolkit of the Modern Biologist: Onto-Express, Onto-Compare, Onto-Design and Onto-Translate. *Nucleic Acids Res.* 31 (13), 3775–3781. doi:10.1093/nar/gkg624

Draghici, S., Khatri, P., Tarca, A. L., Amin, K., Done, A., Voichita, C., et al. (2007). A Systems Biology Approach for Pathway Level Analysis. *Genome Res.* 17 (10), 1537–1545. doi:10.1101/gr.6202607

Duan, Q., Reid, S. P., Clark, N. R., Wang, Z., Fernandez, N. F., Rouillard, A. D., et al. (2016). L1000CDS2: LINCS L1000 Characteristic Direction Signatures Search Engine. *Npj Syst. Biol. Appl.* 2, 16015. doi:10.1038/npjsba.2016.15

Ewing, B., and Green, P. (1998). Base-Calling of Automated Sequencer Traces UsingPhred.II. Error Probabilities. *Genome Res.* 8 (3), 186–194. doi:10.1101/gr.8.3.186

Fernandez, N. F., Gundersen, G. W., Rahman, A., Grimes, M. L., Rikova, K., Hornbeck, P., et al. (2017). Clustergrammer, A Web-Based Heatmap Visualization and Analysis Tool for High-Dimensional Biological Data. *Sci. Data* 4, 170151. doi:10.1038/sdata.2017.151

Fisher, R. A. (1925). *Statistical Methods for Research Workers*. 11th Edn. Edinburgh, UK: Oliver & Boyd.

Gene Ontology Consortium (2001). Creating the Gene Ontology Resource: Design and Implementation. *Genome Res.* 11, 1425–1433. doi:10.1101/gr.180801

Gene Ontology Consortium (2004). The Gene Ontology (GO) Database and Informatics Resource. *Nucleic Acids Res.* 32 (Suppl. 1), D258–D261.

Ghosh, A., Chakraborty, M., Chandra, A., and Alam, M. P. (2021). Structure-activity Relationship (SAR) and Molecular Dynamics Study of Withaferin-A Fragment Derivatives as Potential Therapeutic Lead Against Main Protease (Mpro) of SARS-CoV-2. *J. Mol. Model.* 27 (3), 97. doi:10.1007/s00894-021-04703-6

Harakeh, S., Kalamegam, G., Pushparaj, P. N., Al-Hejin, A., Alfadul, S. M., Al Amri, T., et al. (2020). Chemokines and Their Association with Body Mass Index Among Healthy Saudis. *Saudi J. Biol. Sci.* 27 (1), 6–11. doi:10.1016/j.sjbs.2019.03.006

Heimfarth, L., Serafini, M. R., Martins-Filho, P. R., Quintans, J. d. S. S., and Quintans-Júnior, L. J. (2020). Drug Repurposing and Cytokine Management in Response to COVID-19: A Review. *Int. immunopharmacology* 88, 106947. doi:10.1016/j.intimp.2020.106947

Heming, M., Li, X., Räuber, S., Mausberg, A. K., Börsch, A.-L., Hartlehnert, M., et al. (2021). Neurological Manifestations of COVID-19 Feature T Cell Exhaustion and Dedifferentiated Monocytes in Cerebrospinal Fluid. *Immunity* 54 (1), 164–175.e6. doi:10.1016/j.immuni.2020.12.011

Hillje, R., Pelicci, P. G., and Luzi, L. (2020). Cerebro: Interactive Visualization of scRNA-Seq Data. *Bioinformatics (Oxford, England)* 36 (7), 2311–2313. doi:10.1093/bioinformatics/btz877

Hoffmann, M., Kleine-Weber, H., Schroeder, S., Krüger, N., Herrler, T., Erichsen, S., et al. (2020). SARS-CoV-2 Cell Entry Depends on ACE2 and TMPRSS2 and Is Blocked by a Clinically Proven Protease Inhibitor. *Cell* 181, 271–280.e8. doi:10.1016/j.cell.2020.02.052

Huang, C.-T., Chao, T.-L., Kao, H.-C., Pang, Y.-H., Lee, W.-H., Hsieh, C.-H., et al. (2020b). Enhancement of the IFN-β-Induced Host Signature Informs Repurposed Drugs for COVID-19. *Heliyon* 6 (12), e05646. doi:10.1016/j.heliyon.2020.e05646

Huang, C., Wang, Y., Li, X., Ren, L., Zhao, J., Hu, Y., et al. (2020a). Clinical Features of Patients Infected with 2019 Novel Coronavirus in Wuhan, China. *Lancet* 395 (10223), 497–506. doi:10.1016/s0140-6736(20)30183-5

Hussein, M. I. H., Albashir, A. A. D., Elawad, O. A. M. A., and Homeida, A. (2020). Malaria and COVID-19: Unmasking Their Ties. *Malar. J.* 19 (1), 457. doi:10.1186/s12936-020-03541-w

Jafri, M. A., Kalamegam, G., Abbas, M., Al-Kaff, M., Ahmed, F., Bakhashab, S., et al. (2020). Deciphering the Association of Cytokines, Chemokines, and Growth Factors in Chondrogenic Differentiation of Human Bone Marrow Mesenchymal Stem Cells Using an Ex Vivo Osteochondral Culture System. *Front. Cel Dev. Biol.* 7, 380. doi:10.3389/fcell.2019.00380

Kanehisa, M., Goto, S., Furumichi, M., Tanabe, M., and Hirakawa, M. (2010). KEGG for Representation and Analysis of Molecular Networks Involving Diseases and Drugs. *Nucleic Acids Res.* 38, D355–D360. doi:10.1093/nar/gkp896

Kanehisa, M., Goto, S., Kawashima, S., and Nakaya, A. (2002). The KEGG Databases at GenomeNet. *Nucleic Acids Res.* 30, 42–46. doi:10.1093/nar/30.1.42

Kanehisa, M., and Goto, S. (2000). KEGG: Kyoto Encyclopedia of Genes and Genomes. *Nucleic Acids Res.* 28, 27–30. doi:10.1093/nar/28.1.27

Kanehisa, M., Goto, S., Sato, Y., Furumichi, M., and Tanabe, M. (2012). KEGG for Integration and Interpretation of Large-Scale Molecular Data Sets. *Nucleic Acids Res.* 40, D109–D114. doi:10.1093/nar/gkr988

Kanehisa, M., Goto, S., Sato, Y., Kawashima, M., Furumichi, M., and Tanabe, M. (2014). Data, Information, Knowledge and Principle: Back to Metabolism in KEGG. *Nucl. Acids Res.* 42, D199–D205. doi:10.1093/nar/gkt1076

Kasela, S., Ortega, V. E., Ortega, V. E., Martorella, M., Garudadri, S., Nguyen, J., et al. (2021). Genetic and Non-genetic Factors Affecting the Expression of COVID-19-Relevant Genes in the Large Airway Epithelium. *Genome Med.* 13 (1), 66. doi:10.1186/s13073-021-00866-2

Kasperkiewicz, M. (2021). Covid-19, Heat Shock Proteins, and Autoimmune Bullous Diseases: A Potential Link Deserving Further Attention. *Cell Stress and Chaperones* 26 (1), 1–2. doi:10.1007/s12192-020-01180-3

Khatri, P., Draghici, S., Tarca, A. D., Hassan, S. S., and Romero, R. (2007). A System Biology Approach for the Steady-State Analysis of Gene Signaling Networks. *Lecture Notes Comput. Sci. (Lncs)* 4756, 32–41. doi:10.1007/978-3-540-76725-1_4

Kumar, V., Dhanjal, J. K., Bhargava, P., Kaul, A., Wang, J., Zhang, H., et al. (2020). Withanone and Withaferin-A Are Predicted to Interact with Transmembrane Protease Serine 2 (TMPRSS2) and Block Entry of SARS-CoV-2 into Cells. *J. Biomol. Struct. Dyn.* 1–13, 1–13. doi:10.1080/07391102.2020.1775704

Lamontagne, F., Agoritsas, T., Siemieniuk, R., Rochwerg, B., Bartoszko, J., Askie, L., et al. (2021). A Living WHO Guideline on Drugs to Prevent Covid-19. *Bmj* 372, n526. doi:10.1136/bmj.n526

Lan, J., Ge, J., Yu, J., Shan, S., Zhou, H., Fan, S., et al. (2020). Structure of the SARS-CoV-2 Spike Receptor-Binding Domain Bound to the ACE2 Receptor. *Nature* 581 (7807), 215–220. doi:10.1038/s41586-020-2180-5

Liao, M., Liu, Y., Yuan, J., Wen, Y., Xu, G., Zhao, J., et al. (2020). Single-cell Landscape of Bronchoalveolar Immune Cells in Patients with COVID-19. *Nat. Med.* 26, 842–844. doi:10.1038/s41591-020-0901-9

Liu, C.-H., and Di, Y. P. (2020). Analysis of RNA Sequencing Data Using CLC Genomics Workbench. *Methods Mol. Biol. (Clifton, N.J.)* 2102, 61–113. doi:10.1007/978-1-0716-0223-2_4

Liu, J., Zheng, X., Tong, Q., Li, W., Wang, B., Sutter, K., et al. (2020b). Overlapping and Discrete Aspects of the Pathology and Pathogenesis of the Emerging Human Pathogenic Coronaviruses SARS-CoV, MERS-CoV, and 2019-nCoV. *J. Med. Virol.* 92, 491–494. doi:10.1002/jmv.25709

Liu, T., Jia, P., Fang, B., and Zhao, Z. (2020a). Differential Expression of Viral Transcripts from Single-Cell RNA Sequencing of Moderate and Severe COVID-19 Patients and its Implications for Case Severity. *Front. Microbiol.* 11, 603509. doi:10.3389/fmicb.2020.603509

Mamkulathil Devasia, R., Altaf, M., Fahad Alrefaei, A., and Manoharadas, S. (2021). Enhanced Production of Camptothecin by Immobilized Callus of *Ophiorrhiza mungos* and a Bioinformatic Insight into its Potential Antiviral Effect against SARS-CoV-2. *J. King Saud Univ. - Sci.* 33 (2), 101344. doi:10.1016/j.jksus.2021.101344

Mandolesi, M., Sheward, D. J., Hanke, L., Ma, J., Pushparaj, P., Perez Vidakovics, L., et al. (2021). SARS-CoV-2 Protein Subunit Vaccination of Mice and Rhesus Macaques Elicits Potent and Durable Neutralizing Antibody Responses. *Cel Rep. Med.* 2 (4), 100252. doi:10.1016/j.xcrm.2021.100252

Novel Coronavirus Pneumonia Emergency Response Epidemiology Team (2020). [The Epidemiological Characteristics of an Outbreak of 2019 Novel Coronavirus Diseases (COVID-19) in China]. *Zhonghua Liu Xing Bing Xue Za Zhi* 41, 145–151. doi:10.3760/cma.j.issn.0254-6450.2020.02.003

Pushparaj, P. N. (2019). Multiple Analyte Profiling (xMAP) Technology Coupled with Functional Bioinformatics Strategies: Potential Applications in Protein Biomarker Profiling in Autoimmune Inflammatory Diseases. *Essentials of Bioinformatics* Vol. II, 151–165. doi:10.1007/978-3-030-18375-2_9

Pushparaj, P. N. (2020). Translational Interest of Immune Profiling. *Precision Med. Investigators, Pract. Providers* 1, 105–122. doi:10.1016/b978-0-12-819178-1.00011-3

Ritchie, M. E., Phipson, B., Wu, D., Hu, Y., Law, C. W., Shi, W., et al. (2015). Limma powers Differential Expression Analyses for RNA-Sequencing and Microarray Studies. *Nucleic Acids Res.* 43, e47. doi:10.1093/nar/gkv007

Shang, J., Wan, Y., Luo, C., Ye, G., Geng, Q., Auerbach, A., et al. (2020). Cell Entry Mechanisms of SARS-CoV-2. *Proc. Natl. Acad. Sci. USA* 117 (21), 11727–11734. doi:10.1073/pnas.2003138117

Singh, N., Yadav, S. S., Rao, A. S., Nandal, A., Kumar, S., Ganaie, S. A., et al. (2021). Review on Anticancerous Therapeutic Potential of Withania Somnifera (L.) Dunal. *J. ethnopharmacology* 270, 113704. doi:10.1016/j.jep.2020.113704

Sood, A., Mehrotra, A., Dhawan, D. K., and Sandhir, R. (2018). Indian Ginseng (Withania Somnifera) Supplementation Ameliorates Oxidative Stress and Mitochondrial Dysfunctions in Experimental Model of Stroke. *Metab. Brain Dis.* 33 (4), 1261–1274. doi:10.1007/s11011-018-0234-2

Srivastava, A., Siddiqui, S., Ahmad, R., Mehrotra, S., Ahmad, B., and Srivastava, A. N. (2020). Exploring Nature's Bounty: Identification of Withania Somnifera as a Promising Source of Therapeutic Agents against COVID-19 by Virtual Screening and In Silico Evaluation. *J. Biomol. Struct. Dyn.*, 1–51. [Advance online publication]. doi:10.1080/07391102.2020.1835725

Subramanian, A., Tamayo, P., Mootha, V. K., Mukherjee, S., Ebert, B. L., Gillette, M. A., et al. (2005). Gene Set Enrichment Analysis: A Knowledge-Based Approach for Interpreting Genome-wide Expression Profiles. *Proc. Natl. Acad. Sci.* 102 (43), 15545–15550. doi:10.1073/pnas.0506580102

Surnar, B., Kamran, M. Z., Shah, A. S., and Dhar, S. (2020). Clinically Approved Antiviral Drug in an Orally Administrable Nanoparticle for COVID-19. *ACS Pharmacol. Transl. Sci.* 3 (6), 1371–1380. doi:10.1021/acsptsci.0c00179

Szklarczyk, D., Morris, J. H., Cook, H., Kuhn, M., Wyder, S., Simonovic, M., et al. (2017). The STRING Database in 2017: Quality-Controlled Protein-Protein Association Networks, Made Broadly Accessible. *Nucleic Acids Res.* 45 (D1), D362–D368. doi:10.1093/nar/gkw937

Takahashi, Y., Hayakawa, A., Sano, R., Fukuda, H., Harada, M., Kubo, R., et al. (2021). Histone Deacetylase Inhibitors Suppress ACE2 and ABO Simultaneously, Suggesting a Preventive Potential against COVID-19. *Sci. Rep.* 11 (1), 3379. doi:10.1038/s41598-021-82970-2

Tarca, A. L., Draghici, S., Khatri, P., Hassan, S. S., Mittal, P., Kim, J.-s., et al. (2009). A Novel Signaling Pathway Impact Analysis. *Bioinformatics* 25 (1), 75–82. doi:10.1093/bioinformatics/btn577

Torre, D., Lachmann, A., and Ma'ayan, A. (2018). BioJupies: Automated Generation of Interactive Notebooks for RNA-Seq Data Analysis in the Cloud. *Cel Syst.* 7 (5), 556–561.e3. doi:10.1016/j.cels.2018.10.007

Vaninov, N. (2020). In the Eye of the COVID-19 Cytokine Storm. *Nat. Rev. Immunol.* 20, 277. doi:10.1038/s41577-020-0305-6

Wang, Z., Lachmann, A., Keenan, A. B., and Ma'ayan, A. (2018). L1000FWD: Fireworks Visualization of Drug-Induced Transcriptomic Signatures. *Bioinformatics*, 34, 2150, 2152. doi:10.1093/bioinformatics/bty060

Wyler, E., Mösbauer, K., Franke, V., Diag, A., Gottula, L. T., Arsiè, R., et al. (2021). Transcriptomic Profiling of SARS-CoV-2 Infected Human Cell Lines Identifies HSP90 as Target for COVID-19 Therapy. *iScience* 24 (3), 102151. doi:10.1016/j.isci.2021.102151

Zhou, P., Yang, X.-L., Wang, X.-G., Hu, B., Zhang, L., Zhang, W., et al. (2020). A Pneumonia Outbreak Associated with a New Coronavirus of Probable Bat Origin. *Nature* 579, 270–273. doi:10.1038/s41586-020-2012-7

Zhou, Y., Zhou, B., Pache, L., Chang, M., Khodabakhshi, A. H., Tanaseichuk, O., et al. (2019). Metascape Provides a Biologist-Oriented Resource for the Analysis of Systems-Level Datasets. *Nat. Commun.* 10 (1), 1523. doi:10.1038/s41467-019-09234-6

Ziegler, C. G. K., Allon, S. J., Nyquist, S. K., Mbano, I. M., Miao, V. N., Tzouanas, C. N., et al. (2020). SARS-CoV-2 Receptor ACE2 Is an Interferon-Stimulated Gene in Human Airway Epithelial Cells and Is Detected in Specific Cell Subsets across Tissues. *Cell* 181, 1016–1035.e19. doi:10.1016/j.cell.2020.04.035

Conflict of Interest: The authors declare that the research was conducted in the absence of any commercial or financial relationships that could be construed as a potential conflict of interest.

frontiers in Pharmacology

ORIGINAL RESEARCH
published: 02 November 2021
doi: 10.3389/fphar.2021.770329

Neuroprotective and Anti-Inflammatory Effect of Pterostilbene Against Cerebral Ischemia/Reperfusion Injury *via* Suppression of COX-2

Wenjun Yan, Dongqing Ren, Xiaoxue Feng, Jinwen Huang, Dabin Wang, Ting Li and Dong Zhang*

Department of Anesthesiology, Gansu Provincial Hospital, Lanzhou, China

OPEN ACCESS

Edited by:
Muhammad Ayaz, University of Malakand, Pakistan

Reviewed by:
Muhammad Ikram, Gyeongsang National University, South Korea
Muhammad Shahid, Sarhad University of Science and Information Technology (SUIT), Pakistan
Irshad Ahmad, King Fahd University of Petroleum and Minerals, Saudi Arabia

***Correspondence:**
Wenjun Yan
yanwenjun0700@126.com

Specialty section:
This article was submitted to Neuropharmacology, a section of the journal Frontiers in Pharmacology

Received: *03 September 2021*
Accepted: *13 October 2021*
Published: *02 November 2021*

Citation:
Yan W, Ren D, Feng X, Huang J, Wang D, Li T and Zhang D (2021) Neuroprotective and Anti-Inflammatory Effect of Pterostilbene Against Cerebral Ischemia/Reperfusion Injury via Suppression of COX-2. Front. Pharmacol. 12:770329. doi: 10.3389/fphar.2021.770329

Background: The incidence of cerebral ischemia disease leading cause of death in human population worldwide. Treatment of cerebral ischemia remains a clinical challenge for researchers and mechanisms of cerebral ischemia remain unknown. During the cerebral ischemia, inflammatory reaction and oxidative stress plays an important role. The current investigation scrutinized the neuroprotective and anti-inflammatory role of pterostilbene against cerebral ischemia in middle cerebral artery occlusion (MCAO) rodent model and explore the underlying mechanism.

Methods: The rats were divided into following groups viz., normal, sham, MCAO and MCAO + pterostilbene (25 mg/kg) group, respectively. The groups received the oral administration of pterostilbene for 30 days followed by MCAO induction. The neurological score, brain water content, infarct volume and Evan blue leakage were estimated. Hepatic, renal, heart, inflammatory cytokines and inflammatory mediators were estimated.

Results: Pterostilbene treatment significantly ($p < 0.001$) improved the body weight and suppressed the glucose level and brain weight. Pterostilbene significantly ($p < 0.001$) reduced the hepatic, renal and heart parameters. Pterostilbene significantly ($p < 0.001$) decreased the level of glutathione (GSH), glutathione peroxidase (GPx), superoxide dismutase (SOD) and decreased the level of malonaldehyde (MDA), 8-Hydroxy-2′-deoxyguanosine (8-OHdG). Pterostilbene significantly ($p < 0.001$) inflammatory cytokines and inflammatory parameters such as cyclooxygenase-2 (COX-2), inducible

Abbreviations: MCAO, Middle cerebral artery occlusion; GSH, Glutathione; GPx, Glutathione peroxidase; SOD, Superoxide dismutase; MDA, Malonaldehyde; 8-OHdG, 8-Hydroxy-2′-deoxyguanosine; COX-2, Cyclooxygenase-2; iNOS Inducible nitric oxidase synthase; PGE2, Prostaglandin; MMP, Metalloproteinases; NVU, Neurovascular unit; BBB, Blood brain barrier; ECM, Extracellular Matrix; WHO, World Health Organization; ROS, Reactive oxygen species; NO, Nitric oxide; H2O2, Hydrogen peroxide; O2, Superoxide anion; NF-Kb, Nuclear factor kappa B; Tcm, Traditional Chinese medicine; CRP, C-reactive protein; LDH, Lactate dehydrogenase; HDL-c, High-density lipoprotein cholesterol; TG, Triglyceride; TC, Total cholesterol; LDL-c, Low-density lipoprotein cholesterol; VLDL-c, Very low-density lipoprotein cholesterol; BUN, Blood urea nitrogen; ALP, Alkaline phosphatase; ALT, Alanine aminotransferase; AST, Aspartate aminotransferase; IL-1β, Interleukin-1β; IL-4, Interleukin-4; TNF-α, Tumor necrosis factor-α; IL-6, Interleukin-6; IL-10, Interleukin-1; IL-1, Interleukin-1; ELISA, Enzyme-Linked Immunosorbent Assay Kits; SEM, Standard error mean; PUFA, Polyunsaturated fatty acid; LPO, Lipid peroxidation.

nitric oxidase synthase (iNOS) and prostaglandin (PGE_2). Pterostilbene significantly ($p < 0.001$) down-regulated the level of metalloproteinases (MMP) such as MMP-2 and MMP-9. Pterostilbene suppressed the cellular swelling, cellular disintegration, macrophage infiltration, monocyte infiltration and polymorphonuclear leucocyte degranulation in the brain.

Conclusion: In conclusion, Pterostilbene exhibited the neuroprotective effect against cerebral ischemia in rats *via* anti-inflammatory mechanism.

Keywords: cerebral ischemia reperfusion, pterostilbene, inflammation, oxidative stress, COX-2

INTRODUCTION

Stroke is a complicated disease that causes the number of death and disability whole over the world, and it is accompanied by cognitive dysfunctions (Vakili et al., 2014; Wang K. et al., 2020). According to the World Health Organization (WHO), over 15 million people are affected by stroke (Alva-Díaz et al., 2020). Ischemia stroke is the most frequent type of stroke, accounting for 87 percent of all instances. It is caused by thromboembolic blockage of cerebral arteries, which causes an ischemic cascade and tissue injury (Özön and Cüce, 2020; Tuo et al., 2021). Cerebral ischemia disease is the major neurological disease worldwide and incidence of cerebral ischemia rapidly increases last few decades (Yuan et al., 2020). The treatment of cerebral ischemia still challenge to the researcher (Wang et al., 2018; Leung et al., 2020). But few research suggest that neurovascular units involve in the disease (Pan et al., 2018) and the researcher targeting the neurovascular unit (NVU) for the treatment of overall disease, which exhibited the protective against the neuronal damage, neurons and blood brain barrier (BBB) such as extracellular matrix, vascular endothelial cells, microglia and astrocytes (Crofts et al., 2020; Lake et al., 2017).

During the ischemic cascade, oxygen and energy deprivation start the production of reactive oxygen species (ROS), followed through inflammatory reaction, deposition of intracellular calcium and glutamate excitotoxicity (Michalski et al., 2017; Tuo et al., 2021). Ischemic tissue reperfusion enhances the neuroinflammatory reaction and production of ROS. Various studies have shown that oxidative stress is linked to neuronal cell death in ischemic lesions (Patel et al., 2020; Yan et al., 2020). ROS such as nitric oxide (NO), hydrogen peroxide (H_2O_2), superoxide anion (O_2) and hydroxyl free radicals destroys the cellular structures includes nucleic acid, proteins, lipids, redox sensitive enzymes, membrane receptors and channels, which eventually induces the neuronal injury in the ischemic lesions (Jin et al., 2016; Liang et al., 2019; Leung et al., 2020). Furthermore, the increased proportion of ROS leakage from the mitochondrial cytochrome C, which further recruits caspases, worsening neuronal death after ischemia and reperfusion injury (Tang et al., 2016; Han et al., 2018; Zhang et al., 2020). Due to increase the level of ROS leading the cell death, inflammatory reaction and neural dysfunction after the reperfusion (Zhang et al., 2018; Leung et al., 2020). Following cerebral ischemia, an inflammatory response plays a key role in the development of secondary brain injury. Inflammatory mediators include COX-2, nuclear factor kappa B (NF-κB) and MMPs play a significant role in the expansion of cerebral ischemic (Li et al., 2017; Zhang et al., 2018). During the cerebral ischemia injury, the level of above discuss enzymes boosted to considerable level in the brain area. In the treatment of cerebral ischemia, antioxidants and anti-inflammatory agents are helpful (Liang et al., 2020).

Extracellular Matrix (ECM) degrading enzymes such as MMP-2 and MMP-9, are most directly linked to BBB degradation (Traystman, 2003; Ma et al., 2020). The inhibition of ECM degrading enzymes considerably suppresses the cerebral infarct volume and cerebral edema induced *via* ischemia and suppress the BBB injury (Turner and Sharp, 2016). Previous study showed that the reperfusion is the protective in suppressing the ischemic brain injury and also showed the beneficial effect for recovering the various reversible injury (Gresoiu and Christou, 2020; Yu et al., 2020). Though, few research suggest that the blood reperfusion for ischemic tissue could causes the dysfunction and injury in some cases (Gresoiu and Christou, 2020). Furthermore, consideration is always taken of how to inhibit reperfusion injury during the treatment of ischemic stroke (Vakili et al., 2014). During the ischemic reperfusion stop or abrupt the blood supply in the brain area which resultant shortage the oxygen and glucose level in the brain that leading to the anaerobic pathway of glycolytic cycle. The glycolytic cycle generate the high H+ ion, lactic acid and reversal to the mitochondrial matrix (Liang et al., 2019; Wang et al., 2020a; Zhao et al., 2020). All the cascade suppressed the cytoplasmic pH and increase the formation of free radicals. Due to continuous production of free radicals, its finally induces the oxidative stress and start the inflammatory reaction (Li et al., 2017; Zhang et al., 2018).

More than hundred traditional Chinese medicine (TCM) patents have been filed in China in the last few years for the treatment of ischemic stroke, including therapies for ischemia reperfusion injury (Gupta et al., 2010; Peng et al., 2019; Singh et al., 2020). Dietary phytochemicals getting more popularity due to its wide range of benefits includes regulation of immune system, anti-oxidation and suppression of inflammation. Resveratrol (polyphenol flavonoids) isolated from the skin of red grape and suggested the protective effect against various inflammatory reaction. Pterostilbene (*trans*-3,5-dimethoxy-4′-hydroxystilbene) is a stilbene, that is naturally occurring methoxylated analog of Revesterol, commonly found in blueberry (Acharya and Ghaskadbi, 2013; Shi et al., 2019). Pterostilbene shows the higher bioactivity and bioavailability than resveratrol due to presence of two extra methyl group in the structure (**Supplementary Figure S1**). The structure of pterostilbene showed

the removal of two hydroxy group with two methoxy group, which increase the bioactivity and oral bioavailability and demonstrate the prolong metabolism (Wu et al., 2017; Yang et al., 2017; Shi et al., 2019). Pterostilbene having the bioavailability (85%) as compared to the bioavailability of revesterol (20%) in animal model. Additionally, clinical studies showed that the pterostilbene may be a potent anti-inflammatory drug against various diseases (Acharya and Ghaskadbi, 2013; Shi et al., 2019; Zhang et al., 2021). In this experimental study, we try to explore the neuroprotective and anti-inflammatory effect of pterostilbene against the MCAO rat model.

MATERIAL AND METHODS

Experimental Rodent

Swiss Wistar rats (weight 200 ± 20 g, sex-both, aged 8–10 weeks) were used in this study. The whole experimental study was carried out using the institutional animal ethical committee guidelines. All the rats were kept in the standard laboratory condition 20 ± 5°C temperature, 12 h dark and 12 h light cycle and 65% relative humidity. All the rats were received the standard pellet (rat chow) and water *ab libitum*. The rats were kept 7 days for acclimatization for adopting the laboratory condition.

MCAO/R Method

Briefly, the rats were anesthetized using the 50 mg/kg intraperitoneal injection of ketamine hydrochloride and 5 mg/kg xylazine and monitored accordingly. The common carotid artery was isolated and the branches of external carotid artery (right) were carefully removed (Pan et al., 2018). To obstruct the source of MCAO, a nylon monofilament suture (4–0) with a silicon coated tip was pushed to the internal carotid artery (Yuan et al., 2020). The same operation was performed on the normal group (sham group), but no suture was put. After cerebral ischemia (2 h), the suture was removed for reperfusion (24 h). The rats were divided into different groups such as Group I: control; Group II: Sham; Group III: MCAO and Group IV: MCAO + pterostilbene (35 mg/kg), respectively.

Neurological Deficits

Neurological dysfunction were assessed after 2 h of MCAO and then every day for the next 5 days (Shamim and Khan, 2019). The behavioural impairments and post chemical motor were examined using a 4-point neuro score (Yuan et al., 2020). The grade for neurological impairments was as follows:

Symptoms are absent in grade 0.

Grade 1: bending of the forelimbs
Grade 2: reduced lateral push (and forelimb flexion) resistance without circling
Grade 3: circle and the same conduct as grade 2.

Blood and Tissue Sampling

The rats were euthanized at the end of the protocol so that blood (plasma/serum) and organs (liver and brain) could be collected and kept at 80°C. All the blood and tissue samples kept for the histopathological evaluation and biochemical estimation.

BBB Permeability

For the determination of BBB permeability, the all-group rats were received the Evans blue (2%) in the tail vein before the sacrifice (2 h). after that removed the brain tissue and weighted and placed into the 1 ml dimethylformamide and incubated for next 24 h at 60°C. Afterthat centrifuge at 1 g rpm for 10 min to separate the supernatant (Pan et al., 2018). The supernatant collected and take absorbance at 620 nm wavelength using the spectrophotometer.

Cerebral Edema

For the determination of cerebral edema, the brain water content was estimated using the dry weight method of previous reported method with minor modification (Yang et al., 2020). Briefly, the brain tissue was successfully removed after the reperfusion (24 h) and weight immediately and baked in the oven for 24 h at 120°C and again weight.

The brain water content was estimated using the following formula

$$Brain\ water\ content = \frac{(a-b)}{a}\ X\ 100.$$

Biochemical Assays

Turbid Metric Immunoassay model was used for the estimation of serum C-reactive protein (CRP) using the kit (Conformidad Europea, Spain).

Enzymatic colorimetric GOD-POD kit was used for the estimation of blood glucose (Global, United Kingdom). Lactate dehydrogenase (LDH) assay kit was used for the determination of LDH activity (Institute of Biological Engineering of Nanjing Jiancheng, Nanjing, China) following the manufacture protocol.

For the estimation of lipid parameters such as high-density lipoprotein cholesterol (HDL-c), triglyceride (TG) and cholesterol (TC) was estimated using the enzymatic kit kit (Institute of Biological Engineering of Nanjing Jiancheng, Nanjing, China). The low-density lipoprotein cholesterol (LDL-c) and very low-density lipoprotein cholesterol (VLDL-c) were determined using the Friedewald's formula (Mendes de Cordova et al., 2018).

Berthelot colorimetric model was used for the estimation of urea concentration in the serum. Jaffe's method was used for the determination of creatinine using the enzymatic kit (Biogene Diagnostics, United States). Blood urea nitrogen (BUN) and uric acid was estimated using the previous reported method with minor modification (Pandey et al., 2018; Kumar et al., 2021).

The hepatic parameters include alkaline phosphatase (ALP), alanine aminotransferase (ALT) and aspartate aminotransferase (AST) using the enzymatic kit (Institute of Biological Engineering of Nanjing Jiancheng, Nanjing, China).

Antioxidant Parameters

The antioxidant parameters include SOD, GSH, GPx, MDA and CAT were estimated using the previous reported method with minor modification (Bhatt et al., 2017, 2018).

MMP Levels

MMP-2 and MMP-9 were estimated using the gelatinase assay kit (Chemicon International, Inc. Temecula, CA, United States) following the manufacture protocol.

Inflammatory Cytokines

Pro-inflammatory cytokines such as interleukin-1β (IL-1β), interleukin-4 (IL-4), tumor necrosis factor-α (TNF-α), interleukin-6 (IL-6), interleukin-1 (IL-10) and interleukin-1 (IL-1) were estimated using the Enzyme-Linked Immunosorbent Assay Kits (ELISA) (Institute of Biological Engineering of Nanjing Jiancheng, Nanjing, China) following the manufacture protocol.

Inflammatory Mediators

Inflammatory mediators such as NF-κB, i-NOS, NO, COX-2 and PGE2 using the Enzyme-Linked Immunosorbent Assay Kits (ELISA) (Institute of Biological Engineering of Nanjing Jiancheng, Nanjing, China) following the manufacture protocol.

Statistical Analysis

The current study's findings were given as a mean standard error mean (S.E.M.). The statistical analysis was performed using Graphpad Prism 7. The difference between the intergroups was determined using a post hoc *t* test. The significance level was set at $p < 0.05$.

RESULTS

Effect of Pterostilbene on Neurological Parameter

During cerebral ischemia, it increases the neurological score. A neurological score of 0 was observed in the normal and sham group rats. The MCAO group rats showed an enhanced neurological score, which started from day 0 and reached its maximum on day 1 and remained at the higher end of the protocol (day 5). Pterostilbene treated rats significantly ($p < 0.001$) suppressed the neurological score. Pterostilbene treated rats exhibited a reduced neurological score at different time intervals (day 0, 1, and 5) as compared to the MCAO group (**Figure 1A**).

Infarct volume (**Figure 1B**), brain edema (**Figure 1C**), Evans blue leakage (**Figure 1D**) and brain water content (**Figure 1E**) were higher observed in the MCAO group rats. Pterostilbene treated rats exhibited the suppressed level of infarct volume, brain edema, Evans blue leakage and brain water content.

Effect of Pterostilbene on Body Weight, Glucose Level and Organ Weight

The body weight was slightly reduced in the sham control and MCAO group rats. MCAO group rats receiving pterostilbene significantly ($p < 0.001$) improved their body weight (**Figure 2A**).

The blood glucose remained constant in the normal and sham control group rats. The blood glucose level slightly decreased in the MCAO group. Pterostilbene treated group rats improved the blood glucose level (**Figure 2B**).

The brain weight slightly enhanced in the sham group rats as compared to the normal rats. MCAO group rats exhibited the increased brain weight as compared to all experimental group. MCAO group rats treated with the pterostilbene treated group rats demonstrated the reduced brain weight (**Figure 3**).

Effect of Pterostilbene on LDH and CRP

The level of LDH (**Figure 4A**) and CRP (**Figure 4B**) were estimated in the different groups. The level of LDH (691 ± 12.45 U/L) and CRP (10.89 ± 1.32 mg/dl) slightly enhanced in the MCAO group and pterostilbene treated rats significantly ($p < 0.05$) reduced the level of LDH (687 ± 11.34 U/L) and CRP (9.91 ± 1.93 mg/dl).

Effect of Pterostilbene on Hepatic Parameter

MCAO group rats displayed the boosted level of ALT (25.45 ± 2.38 U/L), AST (40.73 ± 4.93 U/L) and ALP (51.61 ± 2.83 U/L) as compared to normal and sham group rats. After the pterostilbene treatment reduced the level of hepatic parameters ALT (23.04 ± 2.93 U/L), AST (31.59 ± 3.82 U/L) and ALP (42.82 ± 3.89 U/L) (**Figure 5**).

Effect of Pterostilbene on Renal Parameters

The levels of Uric acid (4.67 ± 0.83 mg/dl) (**Figure 6A**), creatinine (0.56 ± 0.03 mg/dl) (**Figure 6B**), BUN (22.51 ± 1.34 mg/dl) (**Figure 6C**) and urea (49.46 ± 3.94 mg/dl) (**Figure 6D**) were observed in different experimental group. MCAO group rats demonstrated the increased level of uric acid (2.62 ± 0.67 mg/dl), creatinine (0.35 ± 0.04 mg/dl), BUN (16.54 ± 2.32 mg/dl) and urea (33.05 ± 2.93 mg/dl), which was significantly ($p < 0.001$) diminished after the pterostilbene treatment.

Effect of Pterostilbene on NO Level

The NO level was considerably boosted in the MCAO group rats as compared to normal and sham control. MCAO group rats received the NO significantly ($p < 0.001$) repressed the level (**Figure 7**).

Effect of Pterostilbene on Lipid Parameters

Figure 8 exhibited the lipid parameters in experimental groups. The level of lipid parameters such as TG, LDL, TC, VLDL boosted and HDL level reduced in the MCAO group. Pterostilbene treated rats exhibited the reduced level of TG, LDL, TC, VLDL and enhanced level of HDL.

Effect of Pterostilbene on Antioxidant Parameters

Figure 9 exhibited the antioxidant parameters of different group rats. MCAO group rats exhibited the decreased level of SOD (55.03 ± 5.32 U/mg protein) (**Figure 9A**), CAT (5.57 ± 0.83 U/mg protein) (**Figure 9B**), GPx (7.11 ± 0.93 U/mg protein) (**Figure 9C**), GSH (0.47 ± 0.04 U/mg protein) (**Figure 9D**) and enhanced level of MDA (263.4 ± 10.34 U/mg protein) (**Figure 9E**), 8OdhG OdhG (0.97 ± 0.09 μg/mg protein) (**Figure 9F**) as compared to normal and sham group rats. MCAO group rats treated with pterostilbene significantly ($p < 0.001$) improved the level of SOD (102.34 ± 7.54 U/mg protein),

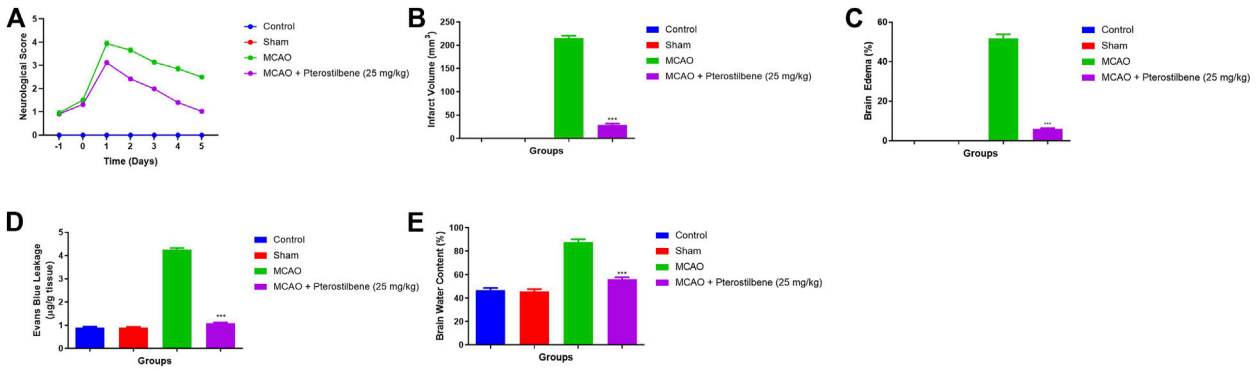

FIGURE 1 | showed the neurological parameter and score of among experimental groups. **(A)** neurological score, **(B)** infarct volume, **(C)** brain edema, **(D)** evans blue leakage and **(E)** brain water content. Values are expressed as mean ± SEM. The *t*-test was used for the significant difference between groups: $^{*}p < 0.05$, $^{**}p < 0.01$, $^{***}p < 0.005$. NS, non-significant.

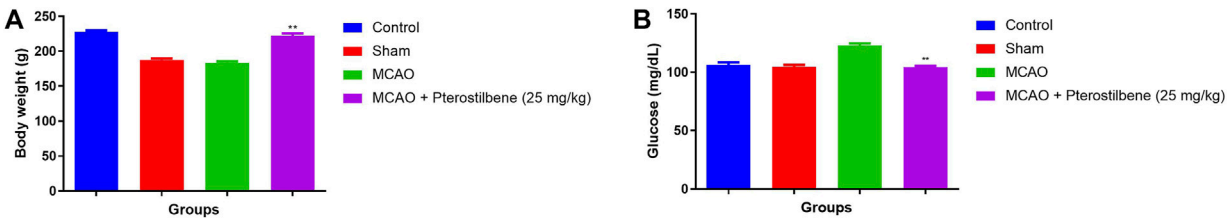

FIGURE 2 | showed the body weight and glucose level of among experimental groups. **(A)** body weight and **(B)** blood glucose level. Values are expressed as mean ± SEM. The *t*-test was used for the significant difference between groups: $^{*}p < 0.05$, $^{**}p < 0.01$, $^{***}p < 0.005$. NS, non-significant.

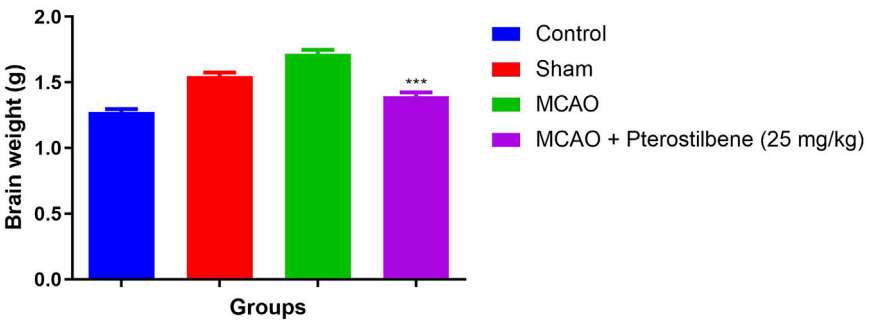

FIGURE 3 | showed the brain weight of among experimental groups. Values are expressed as mean ± SEM. The *t*-test was used for the significant difference between groups: $^{*}p < 0.05$, $^{**}p < 0.01$, $^{***}p < 0.005$. NS, non-significant.

CAT (28.85 ± 1.33 U/mg protein), GPx (33.73 ± 4.34 U/mg protein), GSH (1.34 ± 0.45 U/mg protein) and suppressed the level of MDA (89.45 ± 3.45 U/mg protein), 8-OdhG (0.28 ± 0.05 µg/mg protein).

Effect of Pterostilbene on Inflammatory Cytokines

The level of inflammatory cytokines boosted during the cerebral ischemia due to expansion of inflammatory disease. MCAO group rats exhibited the increased level of TNF-α (41.34 ± 1.57 pg/mg) (**Figure 10A**), IL-1β (14.37 ± 1.23 pg/mg) (**Figure 10B**), IL-6 (41.45 ± 2.34 pg/mg) (**Figure 10C**) and reduced level of (9.89 ± 1.34 pg/mg) IL-10 (**Figure 10D**). MCAO group rats received the pterostilbene treatment significantly diminished the level of TNF-α (10.34 ± 0.89 pg/mg) (**Figure 10A**), IL-1β (5.23 ± 0.83 pg/mg) (**Figure 10B**), IL-6 (17.04 ± 2.93 pg/mg) (**Figure 10C**) and improved the level of IL-10 (28.34 ± 1.83 pg/mg) (**Figure 10D**).

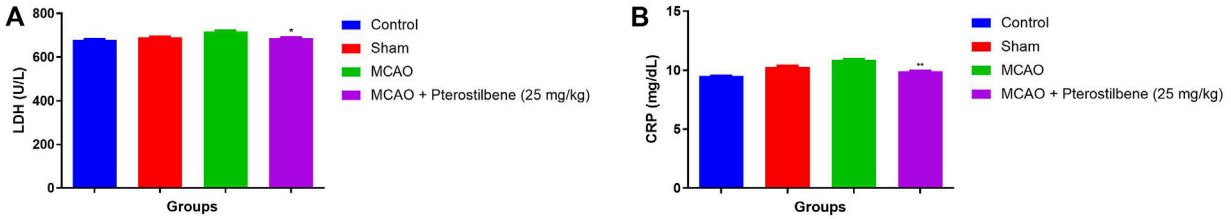

FIGURE 4 | showed the LDH and CRP level of among experimental groups. **(A)** LDH and **(B)** CRP. Values are expressed as mean ± SEM. The *t*-test was used for the significant difference between groups: $^{*}p < 0.05$, $^{**}p < 0.01$, $^{***}p < 0.005$. NS, non-significant.

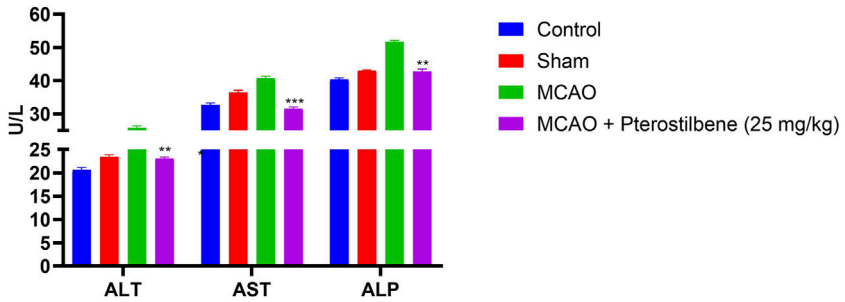

FIGURE 5 | showed the hepatic parameters of among experimental groups. Values are expressed as mean ± SEM. The *t*-test was used for the significant difference between groups: $^{*}p < 0.05$, $^{**}p < 0.01$, $^{***}p < 0.005$. NS, non-significant.

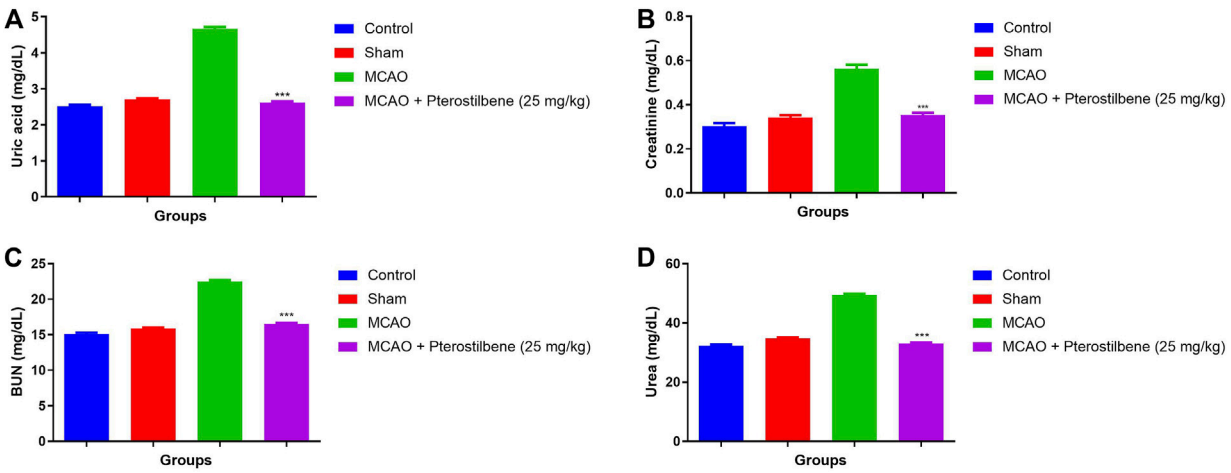

FIGURE 6 | showed the renal parameters of among experimental groups. **(A)** uric acid, **(B)** creatinine, **(C)** BUN and **(D)** urea. Values are expressed as mean ± SEM. The *t*-test was used for the significant difference between groups: $^{*}p < 0.05$, $^{**}p < 0.01$, $^{***}p < 0.005$. NS, non-significant.

Effect of Pterostilbene on Inflammatory Mediators

Figures 11A–C showed the level of inflammatory parameters in different experimental group. MCAO group rats showed the improved level of COX-2 (37.34 ± 2.34 pg/mg) (**Figure 11A**), PGE_2 (41.93 ± 3.23 pg/mg) (**Figure 11B**) and iNOS (36.54 ± 2.93 pg/mg) (**Figure 11C**) and pterostilbene treatment reduced the inflammatory parameters such as COX-2 (12.34 ± 0.45 pg/mg), PGE2 (10.02 ± 0.93 pg/mg) and iNOS (10.34 ± 1.83 pg/mg).

Effect of Pterostilbene on MMP

MCAO group showed the increased level of MMP-2 (1.13 ± 0.37 pg/mg) (**Figure 12A**) and MMP-9 (1.08 ± 0.89 pg/mg) (**Figure 12B**) as compared to different group. MCAO group treated with the pterostilbene significantly ($p < 0.001$) suppressed

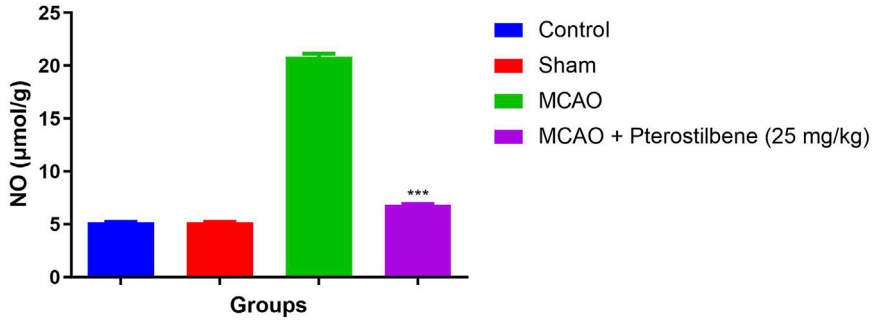

FIGURE 7 | showed the level of nitric oxide of among experimental groups. Values are expressed as mean ± SEM. The *t*-test was used for the significant difference between groups: *$p < 0.05$, **$p < 0.01$, ***$p < 0.005$. NS, non-significant.

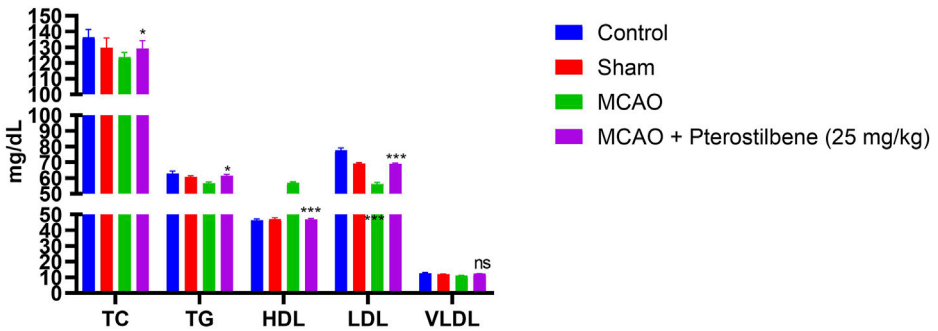

FIGURE 8 | showed the lipid parameters of among experimental groups. Values are expressed as mean ± SEM. The *t*-test was used for the significant difference between groups: *$p < 0.05$, **$p < 0.01$, ***$p < 0.005$. NS, non-significant.

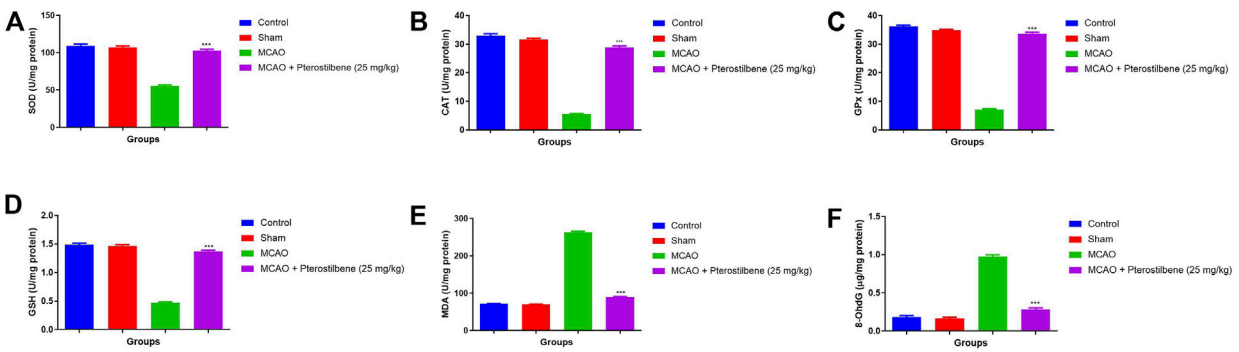

FIGURE 9 | showed the antioxidant parameters of among experimental groups. **(A)** SOD, **(B)** CAT, **(C)** GPx, **(D)** GSH, **(E)** MDA and **(F)** 8-OhdG. Values are expressed as mean ± SEM. The *t*-test was used for the significant difference between groups: *$p < 0.05$, **$p < 0.01$, ***$p < 0.005$. NS, non-significant.

the level of MMP-2 (0.28 ± 0.08 pg/mg) and MMP-9 (0.56 ± 0.04 pg/mg).

Effect of Pterostilbene on Histopathology

Table 1 demonstrated the effect of pterostilbene on the brain tissue histopathology. MCAO group rats demonstrated the development of cellular swelling, cellular disintegration, macrophage infiltration, monocyte infiltration and polymorphonuclear leucocyte degranulation. Pterostilbene treatment suppressed the cellular swelling, cellular disintegration, macrophage infiltration, monocyte infiltration and polymorphonuclear leucocyte degranulation.

DISCUSSION

Stroke and its related disorder cause the disability and death whole over the world. The loss of cerebral blood flow during an ischemic stroke causes metabolic, biochemical and hemodynamic

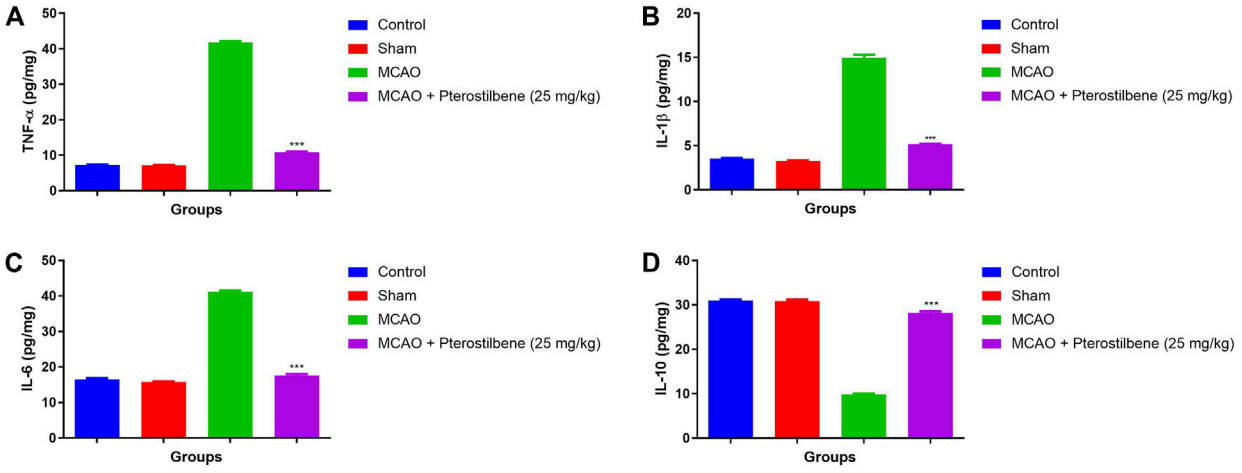

FIGURE 10 | showed the inflammatory cytokines of among experimental groups. **(A)** TNF-α, **(B)** IL-1β, **(C)** IL-6 and **(D)** IL-10. Values are expressed as mean ± SEM. The *t*-test was used for the significant difference between groups: $^{*}p < 0.05$, $^{**}p < 0.01$, $^{***}p < 0.005$. NS, non-significant.

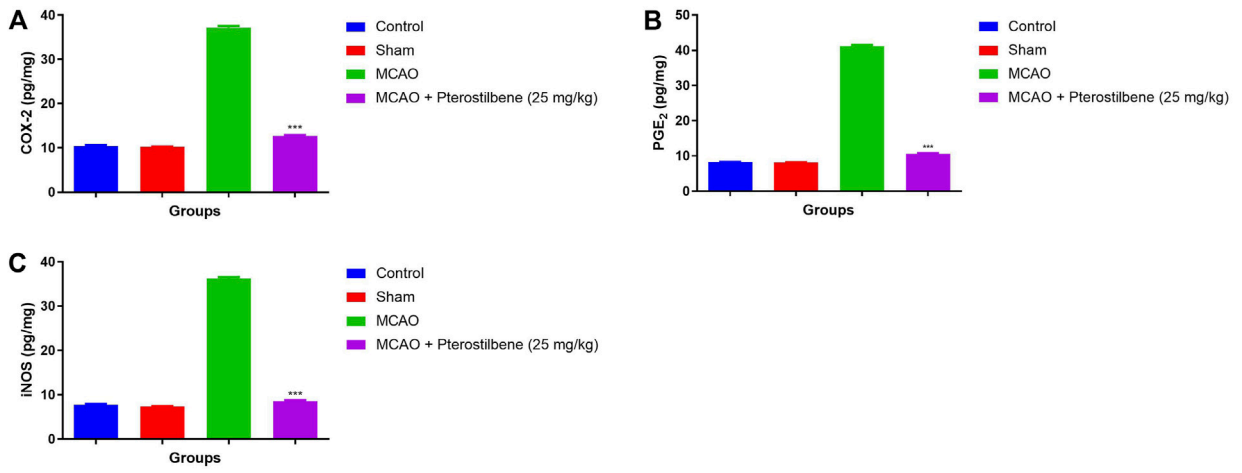

FIGURE 11 | showed the inflammatory mediators of among experimental groups. **(A)** COX-2, **(B)** PGE_2 and **(C)** iNOS. Values are expressed as mean ± SEM. The *t*-test was used for the significant difference between groups: $^{*}p < 0.05$, $^{**}p < 0.01$, $^{***}p < 0.005$. NS, non-significant.

alteration in the damaged brain area to shut down, resulting in brain injury and reduced or lost brain function (Wang et al., 2020b; Yuan et al., 2021b). The neuronal necrosis is aggravated by reperfusion after an ischemic insult. Although the cause of cerebral ischemic stroke is complicated, some pathogenic mechanisms have shown that increasing oxidative stress and reducing endogenous antioxidant enzymes, can restore the most harmful effects of the disease (Bu et al., 2019; Shi et al., 2021). Some studies showed that oxidate stress and inflammatory reactions play a significant role to induces the serve toxicity in the biological macromolecules, which further leading the injury in the cell and tissue (Wang et al., 2020b; Shi et al., 2021). MCAO is a well-established animal model for ischemic stroke-related brain injury in order to study about the stroke phenomena and to assess the efficacy of possible neuroprotection therapies. Furthermore, neutralizing the oxidative stress, inflammatory reaction, enhanced antioxidant intake would be a beneficial therapy for the treatment of ischemic disease (Pan et al., 2018). Herb and its phytoconstituent having long history to treat the oxidative stress and inflammatory disease. Previous studies showed that the plant and its phytoconstituent having the potent anti-inflammatory, antitumor, antidiabetic and antioxidant activity (Wang et al., 2020b; Tian et al., 2020; Shi et al., 2021). The neuroprotective effect of pterostilbene against MCAO-induced cerebral ischemia reperfusion was studied in this experimental study.

During the cerebral ischemia, start the production of oxygen free radicals (OFR) *via* enzymatic and non-enzymatic systems and later on they can attack on the polyunsaturated fatty acid

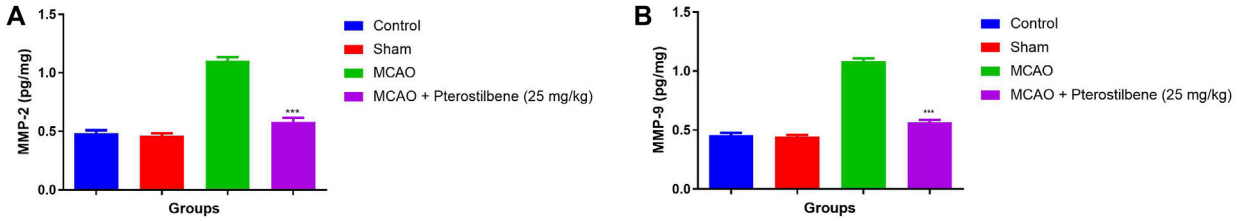

FIGURE 12 | showed the MMP level of among experimental groups. **(A)** MMP-2 and **(B)** MMP-9. Values are expressed as mean ± SEM. The *t*-test was used for the significant difference between groups: $*p < 0.05$, $**p < 0.01$, $***p < 0.005$. NS, non-significant.

TABLE 1 | showed the histopathological index of brain.

S. NO	Pathology type	Groups			
		Normal	Sham	MCAO	MCAO + pterostilbene
1	Cellular swelling	-	+1	+3	+1
2	Cellular disintegration	-	-	+3	+2
3	Macrophage infiltration	-	+1	+3	+1
4	Monocyte infiltration	-	+1	+3	+1
5	Polymorphonuclear leucocyte degranulation	-	+1	+3	+1

(PUFA), which are commonly found in the brain cells and vascular endothelial cells (Bu et al., 2019; Yuan et al., 2021b; Shi et al., 2021). Free radical starts the lipid peroxidation reaction which further start the production of various products such as hydroxy, aldehyde (MDA), keto, inner peroxy or carbonyl radicals. Some reported suggest that oxidant and free radicals play a crucial role in the expansion of edema and disruption of BBB after the cerebral ischemia (Chen et al., 2013; Bu et al., 2019). Drugs that exhibited the neuroprotective effect *via* targeting the production of free radicals to treat the disease. MDA (an indicator of lipid peroxidation, LPO) used to estimation of LPO degree and indirectly shows the cell injury in the brain (Stegner et al., 2019; Wang et al., 2020b). According to the results, pterostilbene showed the neuroprotective effect *via* decreasing the brain lesions and edema may be related to its effect in restriction the free radical production and improved the antioxidant effect. GSH neutralize the hydroperoxides and other toxic free radicals in the brain tissue (Wang et al., 2020b; Yuan et al., 2021b). GSH is endogenous antioxidant enzymes against the oxidative stress. SOD averts formation of hydroxyl radical through catalyzing the super radicals into the H2O2. CAT detoxifies the H2O2 into the water and molecular oxygen. In the brain tissue, CAT is the 2nd line antioxidant that protect brain from oxidative injury. During the cerebral ischemia and oxidation of free radical, the activity of SOD reduced in the brain tissue and serum (Si et al., 2009; Zhang et al., 2019). Large amount of SOD in consumed for neutralize or scavenge the free radicals. Due to continues uses of the SOD to neutralize or scavenge the free radicals, the activity of SOD reduces. However, the activity of SOD indirectly reflects the level of scavenged free radicals (Si et al., 2009; Li et al., 2020). Our result clearly showed that pterostilbene may contribute to suppressing the excessive production of free radical and enhance the SOD activity in the serum and brain. Pterostilbene treated group exhibited the reduction in the MDA content and enhancement of SOD content, but the result not significant (He et al., 2019; Chen et al., 2020). On the basis of result, we can say that Pterostilbene altered the cerebral ischemia *via* scavenging pathway of LPO, not antioxidant effects.

Stroke is a primary cause of acquired impairment in adults and one of the top causes of death worldwide, with a complicated pathological process (He et al., 2019; Chen et al., 2020). Recently, the researcher targeting the neurovascular unit for the treatment of stroke. Neurovascular unit is made up to several neurons, glial cells (microglia and astrocyte), extracellular matrix (ECM), endothelial cells (vascular cells) and BBB (Pan et al., 2018). The BBB is the most important component of the neurovascular unit, and MMPs have long been thought to play a role in the breakdown of the BBB following a stroke. During the early stage of stroke, MMPs induce the various neruo vascular dysfunction includes leakage of BBB and neuronal death. Previous report showed that MMP-9 is unusually expressed in brains suffering from cerebral ischemia injury and its enhance the brain injury and breakdown of BBB (Li et al., 2017). The patients suffer from the ischemic stroke exhibit the enhance level of MMP (MMP-2 and MMP-9) in the circulation (Gu et al., 2013; Li et al., 2017). The increase level of MMP-9 in the circulation related with the poorer prognosis. The reduction of MMP-9 in the circulation and gene considerably decreased the bleeding complications and infarct size (Li et al., 2017). Our result showed that pterostilbene may protect the BBB permeability *via* suppressing of MMP-9. Studies that used MMP inhibitors before a stroke, showed similar benefits, which matched our findings.

The recruitment of systemic macrophages and endogenous microglia indicates an early inflammatory response in cerebral ischemia injury. Inflammatory cells interact with the cerebral stimulus through production of pleiotropic mediators such as prostanoids, cytokines and chemokines (Chen et al., 2020; Li et al., 2020). The inflammatory or immune response following a stroke includes changes in numerous pro and anti-inflammatory cytokines and chemokines in the brain tissue. Previous reports suggest that targeting the inflammatory cytokines is beneficial for the treatment of cerebral ischemia (Li et al., 2020). Inflammatory reaction initiates the tissue lesions such as accumulation of free radicals as well targeting the toxic enzyme of brain tissue. Report suggest that various inflammatory mediators interact with each other and enhance the brain injury. Increases the level of inflammatory cytokines in the brain and begins the breakdown of BBB during cerebral ischemia (Gong et al., 2014; Li et al., 2020).

Report suggests that the TNF-α is activated during the brain ischemia. TNF-α generated through monocytes and macrophages and its over generated due to activation of inflammation related cells during the cerebral ischemia, that boost the local inflammation reaction in the brain tissue (Chen et al., 2020; Li et al., 2020). The level of cytokines increased as a result of leukocyte leakage into the circulation, causing an influx of neutrophils, macrophages, and microglia to enter the ischemic area, causing neuronal cell death and injury. TNF-α induces the cerebral endothelial cells injury and also enhance the BBB permeability, thus contributing to the formation of brain edema (Gong et al., 2014; Li et al., 2020). Moreover, the antiedematous effect of pterostilbene due to reduction the synthesis of TNF-α and also provide the protection of the BBB against disruption. Other inflammatory cytokines such as IL-6 and IL-1β and NF-κB activation play an important role in the pathogenesis of brain edema (He et al., 2017; Hou et al., 2018; Li et al., 2020). Recently report suggest that pterostilbene considerably suppressed the inflammatory cytokines and activated the NF-κB in the endothelial cells and lipopolysaccharide induced lung injury (Liu et al., 2016). All these results suggest that the preventive effect of pterostilbene, at least in part, from suppression the cytokines production and subsequently their signaling pathways. More molecular research needs to elucidate these possibilities.

During cerebral ischemic injury, enhance the level of iNOS due to development of injury cause by inflammatory cytokines and mediators (Li et al., 2017; Zhang et al., 2020). During the normal process, NO generated from the oxidation of L-arginine and further catalysed through synthesis of nitric oxide. The iNOS level boosted in the cerebral ischemic group, confirm the expansion of inflammation and pterostilbene considerably suppressed the iNOS level and confirm the reduction in the inflammatory reaction. Inflammatory mediators and cytokines increased the level of immunocyte such as neutrophils and macrophages (Gong et al., 2014; Li et al., 2017; Zhang et al., 2020). The boosted level of iNOS, PGE2 and COX-2, observed after the cerebral ischemia, which further expand the brain injury *via* inducing the damage in the neuronal cells (Gong et al., 2014; Li et al., 2021).

Prostaglandin is formed when arachidonic acid (AA) is metabolised, and it has been shown to have both a pro and anti-inflammatory effect in mammalian systems, as well as other physiological activities (Liang et al., 2020; Yuan and Zhang, 2021). COX is thought to have a role in brain homeostasis, such as blood flow regulation. Due to COX's important involvement in vasodilation, rodents lacking the enzyme were more prone to stroke. COX is divided into two isomers (COX-1 and COX-2), which have similar catalytic actions but differing physiological functions (Liang et al., 2020). COX-2 is an inducible COX that catalyses the first committed step in prostaglandin production from arachidonic acid (Liang et al., 2020; Yuan et al., 2021a). COX-2 levels and PG production increase in endothelial cells, neurons, and glial cells in the brain tissue in response to diverse stimuli such as inflammatory mediators, excitatory synaptic activity, hypoxia, and growth factors. Previous report suggest that the COX-2 enzymatic activity involved in the stroke animal model that leads to the enhanced stroke damage and neuronal death (Wei et al., 2016; Liang et al., 2020). The use of pharmacological or genetic techniques to suppress COX-2-dependent PG production reduces infarct volume. As a result, a major effort is ongoing to investigate how to minimise the PG receptor pathways that cause COX-2-mediated cerebral damage after stroke. COX-2 levels are higher in infarcted human brains, according to clinical and prior studies, and it is found in both glial and neuronal cells. Previous research suggests that the enhanced level of COX-2 infiltrating the vascular cells, neutrophils and neurons in the peri-infarct zone (Abd El-Aal et al., 2013; Yu et al., 2015; Wei et al., 2016). It is well documented that COX-2 play an important role to providing the protection of brain tissue against cerebral ischemic injury during the brain injury in the rodents. The higher level of COX-2 rodent having higher infarcts volume after experimental stroke. In animal models, selective pharmacologic suppression of COX-2 activity has shown to be a *via*ble therapeutic target for stroke. Prostanoids (prostaglandin E2 and prostaglandin D2) formed through the COX pathway. (Liang et al., 2020; Yuan et al., 2021a). The level of PGE2 have been boosted in the brain after the cerebral ischemia (Liang et al., 2020). Following doubts regarding the safety of COX-2 inhibitors in 2004, most research on the role of the cyclooxygenase system in stroke focused on the PGE2 and PGD2 receptors (Ahmad and Graham, 2010). The actions of PGE2 receptors are triggered by four G-protein coupled receptors, which are the mediators of stroke injury (Liang et al., 2020; Yuan and Zhang, 2021). The level of PGE2 rose during cerebral ischemia due to the production of brain damage. Our control group rats showed a similar finding, with pterostilbene administration significantly suppressing COX-2 and PGE2, indicating an anti-inflammatory effect (Duan et al., 2016; Sotomayor-Sobrino et al., 2019). NF-κB is another significant transcription factors which activates after the reperfusion of cerebral ischemia (Simão et al., 2012; Yuan et al., 2021a). It is well known that oxidative stress/ROS activates the NF-κB signaling pathway that are involved in the various inflammatory reaction initiate after the cerebral ischemia. NF-κB play a crucial role in implementation of various inflammatory reactions that induces the brain injury during the cerebral ischemia (Abd El-Aal et al., 2013; Wei et al.,

2016). NF-κB triggered the various parameters such as inflammatory cytokines and inflammatory mediators that are involved in the brain injury during the cerebral ischemia injury (Liang et al., 2020). Targeting the NF-κB is the novel approach to treat the cerebral ischemia. In this study, pterostilbene considerably suppressed the level of COX-2, PGE2 and NF-κB, suggesting the anti-inflammatory potential against cerebral ischemia.

CONCLUSION

In conclusion, the current investigation showed that pterostilbene has beneficial and protective effect against cerebral ischemia reperfusion injury. Pterostilbene significantly reduced the brain edema, infarct volume and neurological score. Pterostilbene maintain the liver enzymes, renal and lipid parameters at a baseline level. Pterostilbene considerably altered the level of antioxidant enzymes in the brain tissue and reduces the oxidative stress. Pterostilbene significantly suppressed the level of inflammatory cytokines, inflammatory mediators and increased the level of anti-inflammatory cytokines. These findings show that pterostilbene may be an effective treatment for cerebral ischemic stroke. It also emphasises pterostilbene's clinical applications in the treatment of cerebral ischemia reperfusion.

DATA AVAILABILITY STATEMENT

The raw data supporting the conclusions of this article will be made available by the authors, without undue reservation.

ETHICS STATEMENT

The animal study was reviewed and approved by All the experimental study was approved from the Gansu Provincial Hospital and performed as per the guidelines of the Institute.

AUTHOR CONTRIBUTIONS

WY design and performed the experimental study. DR, XF, JH, DW, TL, and DZ. interpret the biochemical data. All the authors equally contributed in proof reading.

SUPPLEMENTARY MATERIAL

The Supplementary Material for this article can be found online at: https://www.frontiersin.org/articles/10.3389/fphar.2021.770329/full#supplementary-material

REFERENCES

Abd El-Aal, S. A., El-Sawalhi, M. M., Seif-El-Nasr, M., and Kenawy, S. A. (2013). Effect of Celecoxib and L-NAME on Global Ischemia-Reperfusion Injury in the Rat Hippocampus. *Drug Chem. Toxicol.* 36, 385–395. doi:10.3109/01480545.2012.749270

Acharya, J. D., and Ghaskadbi, S. S. (2013). Protective Effect of Pterostilbene against Free Radical Mediated Oxidative Damage. *BMC Complement. Altern. Med.* 13(1), 238. doi:10.1186/1472-6882-13-238

Ahmad, M., and Graham, S. H. (2010). Inflammation after Stroke: Mechanisms and Therapeutic Approaches. *Transl. Stroke Res.* 1, 74–84. doi:10.1007/s12975-010-0023-7

Alva-Díaz, C., Huerta-Rosario, A., Pacheco-Barrios, K., Molina, R. A., Navarro-Flores, A., Aguirre-Quispe, W., et al. (2020). Neurological Diseases in Peru: a Systematic Analysis of the Global burden Disease Study. *Arq. Neuropsiquiatr.* 78, 282–289. doi:10.1590/0004-282x20200018

Bhatt, P. C., Verma, A., Al-Abbasi, F. A., Anwar, F., Kumar, V., and Panda, B. P. (2017). Development of Surface-Engineered PLGA Nanoparticulate-Delivery System of Tet1-Conjugated Nattokinase Enzyme for Inhibition of Aβ40 Plaques in Alzheimer's Disease. *Int. J. Nanomed.* 12, 8749–8768. doi:10.2147/IJN.S144545

Bhatt, P. C., Pathak, S., Kumar, V., and Panda, B. P. (2018). Attenuation of Neurobehavioral and Neurochemical Abnormalities in Animal Model of Cognitive Deficits of Alzheimer's Disease by Fermented Soybean Nanonutraceutical. *Inflammopharmacol* 26, 105–118. doi:10.1007/s10787-017-0381-9

Bu, J., Shi, S., Wang, H.-Q., Niu, X.-S., Zhao, Z.-F., et al. (2019). Acacetin Protects against Cerebral Ischemia-Reperfusion Injury via the NLRP3 Signaling Pathway. *Neural Regen. Res.* 14, 605. doi:10.4103/1673-5374.247465

Chen, X.-m., Chen, H.-s., Xu, M.-j., and Shen, J.-g. (2013). Targeting Reactive Nitrogen Species: A Promising Therapeutic Strategy for Cerebral Ischemia-Reperfusion Injury. *Acta Pharmacol. Sin.* 34, 67–77. doi:10.1038/aps.2012.82

Chen, X., Yao, Z., Peng, X., Wu, L., Wu, H., Ou, Y., et al. (2020). Eupafolin Alleviates Cerebral Ischemia/reperfusion Injury in Rats via Blocking the TLR4/NF-κB Signaling Pathway. *Mol. Med. Rep.* 22, 5135–5144. doi:10.3892/mmr.2020.11637

Crofts, A., Kelly, M. E., and Gibson, K. L. (2020). Imaging Functional Recovery Following Ischemic Stroke: Clinical and Preclinical fMRI Studies. *J. Neuroimaging* 30 (1), 5–14. doi:10.1111/jon.12668

Duan, X., Wen, Z., Shen, H., Shen, M., and Chen, G. (2016). Intracerebral Hemorrhage, Oxidative Stress, and Antioxidant Therapy. *Oxid. Med. Cell Longev.* 2016, 1–17. doi:10.1155/2016/1203285

Gong, G., Xiang, L., Yuan, L., Hu, L., Wu, W., Cai, L., et al. (2014). Protective Effect of Glycyrrhizin, a Direct HMGB1 Inhibitor, on Focal Cerebral Ischemia/reperfusion-Induced Inflammation, Oxidative Stress, and Apoptosis in Rats. *PLoS One* 9, e89450. doi:10.1371/journal.pone.0089450

Gresoiu, M., and Christou, S. (2020). Hypoxic Ischaemic Brain Injury. *Anaesth. Intensive Care Med.* 21, 298–304. doi:10.1016/j.mpaic.2020.03.009

Gu, J.-H., Ge, J.-B., Li, M., Xu, H.-D., Wu, F., and Qin, Z.-H. (2013). Poloxamer 188 Protects Neurons against Ischemia/Reperfusion Injury through Preserving Integrity of Cell Membranes and Blood Brain Barrier. *PLoS One* 8, e61641. doi:10.1371/journal.pone.0061641

Gupta, Y. K., Briyal, S., and Gulati, A. (2010). Therapeutic Potential of Herbal Drugs in Cerebral Ischemia. *Indian J. Physiol. Pharmacol.* 54 (2), 99–122. doi:10.25259/IJPP_90_2010

Han, X. R., Wen, X., Wang, Y. J., Wang, S., Shen, M., Zhang, Z. F., et al. (2018). Retracted : Protective Effects of microRNA-431 against Cerebral Ischemia-reperfusion Injury in Rats by Targeting the Rho/Rho-kinase Signaling Pathway. *J. Cel. Physiol.* 233, 5895–5907. doi:10.1002/jcp.26394

He, Q., Li, Z., Wang, Y., Hou, Y., Li, L., and Zhao, J. (2017). Resveratrol Alleviates Cerebral Ischemia/reperfusion Injury in Rats by Inhibiting NLRP3 Inflammasome Activation through Sirt1-dependent Autophagy Induction. *Int. Immunopharmacol.* 50, 208–215. doi:10.1016/j.intimp.2017.06.029

He, J., Li, H., Li, G., and Yang, L. (2019). Hyperoside Protects against Cerebral Ischemia-Reperfusion Injury by Alleviating Oxidative Stress, Inflammation and Apoptosis in Rats. *Biotechnol. Biotechnol. Equip.* 33, 798–806. doi:10.1080/13102818.2019.1620633

Hou, Y., Wang, Y., He, Q., Li, L., Xie, H., Zhao, Y., et al. (2018). Nrf2 Inhibits NLRP3 Inflammasome Activation through Regulating Trx1/TXNIP Complex in Cerebral Ischemia Reperfusion Injury. *Behav. Brain Res.* 336, 32–39. doi:10.1016/j.bbr.2017.06.027

Jin, F. M., Zhang, Z. X., Wang, Y., Zhao, H. R., Yang, Y. Y., Huang, X., et al. (2016). Protective Effect of Ento-I Plastic against Cerebral Ischemia-Reperfusion Injury in Rats 12, 947. *J. Int. Pharm. Res.* doi:10.13220/j.cnki.jipr.2016.03.019

Kumar, V., Sachan, R., Rahman, M., Rub, R. A., Patel, D. K., Sharma, K., et al. (2021). Chemopreventive Effects of *Melastoma malabathricum* L. Extract in Mammary Tumor Model via Inhibition of Oxidative Stress and Inflammatory Cytokines. *Biomed. Pharmacother.* 137, 111298. doi:10.1016/j.biopha.2021.111298

Lake, E. M. R., Bazzigaluppi, P., Mester, J., Thomason, L. A. M., Janik, R., Brown, M., et al. (2017). Neurovascular Unit Remodelling in the Subacute Stage of Stroke Recovery. *Neuroimage* 146, 869–882. doi:10.1016/j.neuroimage.2016.09.016

Leung, S. W., Lai, J. H., Wu, J. C.-C., Tsai, Y.-R., Chen, Y.-H., Kang, S.-J., et al. (2020). Neuroprotective Effects of Emodin against Ischemia/Reperfusion Injury through Activating Erk-1/2 Signaling Pathway. *Ijms* 21, 2899. doi:10.3390/ijms21082899

Li, W., Suwanwela, N. C., and Patumraj, S. (2017). Curcumin Prevents Reperfusion Injury Following Ischemic Stroke in Rats via Inhibition of NF-κB, ICAM-1, MMP-9 and Caspase-3 Expression. *Mol. Med. Rep.* 16, 4710–4720. doi:10.3892/mmr.2017.7205

Li, L., Sun, L., Qiu, Y., Zhu, W., Hu, K., and Mao, J. (2020). Protective Effect of Stachydrine against Cerebral Ischemia-Reperfusion Injury by Reducing Inflammation and Apoptosis through P65 and JAK2/STAT3 Signaling Pathway. *Front. Pharmacol.* 11, 64. doi:10.3389/fphar.2020.00064

Li, F., Xu, Y., Li, X., Wang, X., Yang, Z., Li, W., et al. (2021). Triblock Copolymer Nanomicelles Loaded with Curcumin Attenuates Inflammation via Inhibiting the NF-Kb Pathway in the Rat Model of Cerebral Ischemia. *Ijn* 16, 3173–3183. doi:10.2147/IJN.S300379

Liang, W., Lin, C., Yuan, L., Chen, L., Guo, P., Li, P., et al. (2019). Preactivation of Notch1 in Remote Ischemic Preconditioning Reduces Cerebral Ischemia-Reperfusion Injury through Crosstalk with the NF-Kb Pathway. *J. Neuroinflamm.* 16. doi:10.1186/s12974-019-1570-9

Liang, S., Chen, Z., Li, H., Cang, Z., Yin, K., Wu, M., et al. (2020). Neuroprotective Effect of Umbelliferone against Cerebral ischemia/Reperfusion Induced Neurological Deficits: *In-Vivo* and In-Silico Studies. *J. Biomol. Struct. Dyn.* 0, 1–11. doi:10.1080/07391102.2020.1780153

Liu, J., Fan, C., Yu, L., Yang, Y., Jiang, S., Ma, Z., et al. (2016). Pterostilbene Exerts an Anti-inflammatory Effect via Regulating Endoplasmic Reticulum Stress in Endothelial Cells. *Cytokine* 77, 88–97. doi:10.1016/j.cyto.2015.11.006

Ma, R., Xie, Q., Li, Y., Chen, Z., Ren, M., Chen, H., et al. (2020). Animal Models of Cerebral Ischemia: A Review. *Biomed. Pharmacother.* 131, 110686. doi:10.1016/j.biopha.2020.110686

Mendes de Cordova, C. M., de Santa Helena, E. T., Galgowski, C., Figueira, V. H., Setter, G. B., Markus, M. R. P., et al. (2018). Evaluation of a New Equation for LDL-C Estimation and Prediction of Death by Cardiovascular Related Events in a German Population-Based Study Cohort. *Scand. J. Clin. Lab. Invest.* 78, 187–196. doi:10.1080/00365513.2018.1432070

Michalski, D., Hofmann, S., Pitsch, R., Grosche, J., and Härtig, W. (2017). Neurovascular Specifications in the Alzheimer-like Brain of Mice Affected by Focal Cerebral Ischemia: Implications for Future Therapies. *Jad* 59, 655–674. doi:10.3233/JAD-170185

Özön, A. Ö., and Cüce, F. (2020). Clinical and Radiological Evaluation of Epilepsy after Ischemic Cerebrovascular Disease. *Gulhane Med. J.*, 62(2):126–130. doi:10.4274/gulhane.galenos.2019.998

Pan, Z., Cui, M., Dai, G., Yuan, T., Li, Y., Ji, T., et al. (2018). Protective Effect of Anthocyanin on Neurovascular Unit in Cerebral Ischemia/Reperfusion Injury in Rats. *Front. Neurosci.* 12. doi:10.3389/fnins.2018.00947

Pandey, P., Bhatt, P. C., Rahman, M., Patel, D. K., Anwar, F., Al-Abbasi, F., et al. (2018). Preclinical Renal Chemo-Protective Potential of Prunus Amygdalus Batsch Seed Coat via Alteration of Multiple Molecular Pathways. *Arch. Physiol. Biochem.* 124, 88–96. doi:10.1080/13813455.2017.1364773

Patel, P., Barve, K., and Bhatt, L. K. (2020). Naringin-rich Fraction from Grape Fruit Peel Protects against Transient Cerebral Ischemia Reperfusion Injury in Rats. *Nutr. Neurosci.* 2020, 1–10. doi:10.1080/1028415X.2020.1821518

Peng, T., Jiang, Y., Farhan, M., Lazarovici, P., Chen, L., and Zheng, W. (2019). Anti-Inflammatory Effects of Traditional Chinese Medicines on Preclinical *In Vivo* Models of Brain Ischemia-Reperfusion-Injury: Prospects for Neuroprotective Drug Discovery and Therapy. *Front. Pharmacol.* 10, 204. doi:10.3389/fphar.2019.00204

Shamim, M., and Khan, N. I. (2019). Neuroprotective Effect ofPanax Ginsengextract against Cerebral Ischemia-Reperfusion-Injury-Induced Oxidative Stress in Middle Cerebral Artery Occlusion Models. *Facets* 4, 52–68. doi:10.1139/facets-2018-0025

Shi, L., Liu, Q., Tang, J.-h., Wen, J.-j., and Li, C. (2019). Protective Effects of Pterostilbene on Ulcerative Colitis in Rats via Suppressing NF-Kb Pathway and Activating PPAR-γ. *Eur. J. Inflamm.* 17, 205873921984015. doi:10.1177/2058739219840152

Shi, C. X., Ding, Y. B., Yu, F., Jin, J., Li, T., Ma, J. H., et al. (2021). Effects of Sevoflurane post-conditioning in Cerebral Ischemia-Reperfusion Injury via TLR4/NF-Kb Pathway in Rats. *Eur. Rev. Med. Pharmacol. Sci.* 22(6):1770–1775. doi:10.26355/eurrev_201803_14595

Si, Y. l., Zhang, J. y., and Yan, G. T. (2009). Protective Effect of Leptin against Cerebral Ischemia/reperfusion Injury in Mice. *Nan Fang Yi Ke Da Xue Xue Bao* 29 (4), 598–601. doi:10.27382/IJPP_1-_2009

Simão, F., Matté, A., Pagnussat, A. S., Netto, C. A., and Salbego, C. G. (2012). Resveratrol Preconditioning Modulates Inflammatory Response in the Rat hippocampus Following Global Cerebral Ischemia. *Neurochem. Int.* 61, 659–665. doi:10.1016/j.neuint.2012.06.009

Singh, S., Shafi, S., Shrivastav, A., Khan, S., Ahmad, T., and Khan, N. A. (2020). A Review on Herbal Plants Used in Brain Ischemic and Reperfusion Injury. *J. Drug Deliv. Ther.* 10, 376–379. doi:10.22270/jddt.v10i5.4415

Sotomayor-Sobrino, M. A., Ochoa-Aguilar, A., Méndez-Cuesta, L. A., and Gómez-Acevedo, C. (2019). Interacciones Neuroinmunológicas en el ictus. *Neurología* 34, 326–335. doi:10.1016/j.nrl.2016.08.003

Stegner, D., Klaus, V., and Nieswandt, B. (2019). Platelets as Modulators of Cerebral Ischemia/Reperfusion Injury. *Front. Immunol.* 10, 2505. doi:10.3389/fimmu.2019.02505

Tang, X.-J., Yang, M.-H., Cao, G., Lu, J.-T., Luo, J., Dai, L.-J., et al. (2016). Protective Effect of microRNA-138 against Cerebral Ischemia/reperfusion Injury in Rats. *Exp. Ther. Med.* 11, 1045–1050. doi:10.3892/etm.2016.3021

Tian, F., Liu, R., Fan, C., Sun, Y., Huang, X., Nie, Z., et al. (2020). Effects of Thymoquinone on Small-Molecule Metabolites in a Rat Model of Cerebral Ischemia Reperfusion Injury Assessed Using Maldi-Msi. *Metabolites* 10, 27. doi:10.3390/metabo10010027

Traystman, R. J. (2003). Animal Models of Focal and Global Cerebral Ischemia. *ILAR J.* 44, 85–95. doi:10.1093/ilar.44.2.85

Tuo, Q. z., Zhang, S. T., and Lei, P. (2021). Mechanisms of Neuronal Cell Death in Ischemic Stroke and Their Therapeutic Implications. *Med. Res. Rev.* doi:10.1002/med.21817

Turner, R. J., and Sharp, F. R. (2016). Implications of MMP9 for Blood Brain Barrier Disruption and Hemorrhagic Transformation Following Ischemic Stroke. *Front. Cel. Neurosci.* 10, 56. doi:10.3389/fncel.2016.00056

Vakili, A., Einali, M. R., and Bandegi, A. R. (2014). Protective Effect of Crocin against Cerebral Ischemia in a Dose-dependent Manner in a Rat Model of Ischemic Stroke. *J. Stroke Cerebrovasc. Dis.* 23, 106–113. doi:10.1016/j.jstrokecerebrovasdis.2012.10.008

Wang, Y., Ren, Q., Zhang, X., Lu, H., and Chen, J. (2018). Neuroprotective Mechanisms of Calycosin against Focal Cerebral Ischemia and Reperfusion Injury in Rats. *Cell. Physiol. Biochem.* 45, 537–546. doi:10.1159/000487031

Wang, K., Ru, J., Zhang, H., Chen, J., Lin, X., Lin, Z., et al. (2020a). Melatonin Enhances the Therapeutic Effect of Plasma Exosomes against Cerebral Ischemia-Induced Pyroptosis through the TLR4/NF-Kb Pathway. *Front. Neurosci.* 14, 848. doi:10.3389/fnins.2020.00848

Wang, Y., Xiao, G., He, S., Liu, X., Zhu, L., Yang, X., et al. (2020b). Protection against Acute Cerebral Ischemia/reperfusion Injury by QiShenYiQi via Neuroinflammatory Network Mobilization. *Biomed. Pharmacother.* 125, 109945. doi:10.1016/j.biopha.2020.109945

Wei, J., Sun, C. L., Liu, C., and Zhang, Q. M. (2016). Cerebrovascular Protective Effect of Combination of Tetradrine and Atorvastatin against Cerebral Ischemia-Reperfusion Injury in Rats via Inhibition of Inflammatory Mediators. *Int. J. Clin. Exp. Med.* 9 (11), 22807–22813.

Wu, M., Lu, S., Zhong, J., Huang, K., and Zhang, S. (2017). Protective Effects of Pterostilbene against Myocardial Ischemia/Reperfusion Injury in Rats. *Inflammation* 40, 578–588. doi:10.1007/s10753-016-0504-2

Yan, M., Li, M., Gu, S., Sun, Z., Ma, T., and Ma, X. (2020). Ginkgo Biloba Extract Protects Diabetic Rats against Cerebral Ischemia-Reperfusion Injury by Suppressing Oxidative Stress and Upregulating the Expression of Glutamate Transporter 1. *Mol. Med. Rep.* 21, 1809–1818. doi:10.3892/mmr.2020.10990

Yang, Y., Fan, C., Wang, B., Ma, Z., Wang, D., Gong, B., et al. (2017). Pterostilbene Attenuates High Glucose-Induced Oxidative Injury in Hippocampal Neuronal Cells by Activating Nuclear Factor Erythroid 2-related Factor 2. *Biochim. Biophys. Acta (Bba) - Mol. Basis Dis.* 1863, 827–837. doi:10.1016/j.bbadis.2017.01.005

Yang, T., Feng, C., Wang, D., Qu, Y., Yang, Y., Wang, Y., et al. (2020). Neuroprotective and Anti-inflammatory Effect of Tangeretin against Cerebral Ischemia-Reperfusion Injury in Rats. *Inflammation* 43, 2332–2343. doi:10.1007/s10753-020-01303-z

Yu, H., Wu, M., Zhao, P., Huang, Y., Wang, W., and Yin, W. (2015). Neuroprotective Effects of Viral Overexpression of microRNA-22 in Rat and Cell Models of Cerebral Ischemia-Reperfusion Injury. *J. Cel. Biochem.* 116, 233–241. doi:10.1002/jcb.24960

Yu, L., Su, X., Li, S., Zhao, F., Mu, D., and Qu, Y. (2020). Microglia and Their Promising Role in Ischemic Brain Injuries: An Update. *Front. Cel. Neurosci.* 14, 211. doi:10.3389/fncel.2020.00211

Yuan, S., and Zhang, T. (2021). Boeravinone B Protects Brain against Cerebral Ichemia Reperfusion Injury in Rats: Possible Role of Anti-inflammatory and Antioxidant. *J. Oleo Sci.* 70, 927–936. doi:10.5650/jos.ess21037

Yuan, Y., Men, W., Shan, X., Zhai, H., Qiao, X., Geng, L., et al. (2020). Baicalein Exerts Neuroprotective Effect against Ischaemic/Reperfusion Injury via Alteration of NF-kB and LOX and AMPK/Nrf2 Pathway. *Inflammopharmacology* 28, 1327–1341. doi:10.1007/s10787-020-00714-6

Yuan, H., Yang, Q., Yang, B., Xu, H., Nasif, O., Muruganantham, S., et al. (2021a). Phyllanthin Averts Oxidative Stress and Neuroinflammation in Cerebral Ischemic-Reperfusion Injury through Modulation of the NF-Kb and AMPK/Nrf2 Pathways. *J. Environ. Pathol. Toxicol. Oncol.* 40, 85–97. doi:10.1615/JEnvironPatholToxicolOncol.2020036307

Yuan, Q., Yuan, Y., Zheng, Y., Sheng, R., Liu, L., Xie, F., et al. (2021b). Anti-cerebral Ischemia Reperfusion Injury of Polysaccharides: A Review of the Mechanisms. *Biomed. Pharmacother.* 137, 111303. doi:10.1016/j.biopha.2021.111303

Zhang, W., Song, J. K., Zhang, X., Zhou, Q. M., He, G. R., Xu, X. N., et al. (2018). Salvianolic Acid A Attenuates Ischemia Reperfusion Induced Rat Brain Damage by Protecting the Blood Brain Barrier through MMP-9 Inhibition and Anti-inflammation. *Chin. J. Nat. Med.* 16(3):184–193. doi:10.1016/S1875-5364(18)30046-3

Zhang, W. F., Jin, Y. C., Li, X. M., Yang, Z., Wang, D., and Cui, J. J. (2019). Protective Effects of Leptin against Cerebral Ischemia/reperfusion Injury. *Exp. Ther. Med.* 17, 3282–3290. (Review). doi:10.3892/etm.2019.7377

Zhang, C., Chen, S., Zhang, Z., Xu, H., Zhang, W., Xu, D., et al. (2020). Asiaticoside Alleviates Cerebral Ischemia-Reperfusion Injury via NOD_2/Mitogen-Activated Protein Kinase (MAPK)/Nuclear Factor Kappa B (NF-κB) Signaling Pathway. *Med. Sci. Monit.* 26, e920325. doi:10.12659/MSM.920325

Zhang, Y., Han, Z., Jiang, A., Wu, D., Li, S., Liu, Z., et al. (2021). Protective Effects of Pterostilbene on Lipopolysaccharide-Induced Acute Lung Injury in Mice by Inhibiting NF-Kb and Activating Nrf2/HO-1 Signaling Pathways. *Front. Pharmacol.* 11, 591836. doi:10.3389/fphar.2020.591836

Zhao, M., Hou, S., Feng, L., Shen, P., Nan, D., Zhang, Y., et al. (2020). Vinpocetine Protects against Cerebral Ischemia-Reperfusion Injury by Targeting Astrocytic Connexin43 via the PI3K/AKT Signaling Pathway. *Front. Neurosci.* 14, 223. doi:10.3389/fnins.2020.00223

Conflict of Interest: The authors declare that the research was conducted in the absence of any commercial or financial relationships that could be construed as a potential conflict of interest.

Publisher's Note: All claims expressed in this article are solely those of the authors and do not necessarily represent those of their affiliated organizations, or those of the publisher, the editors and the reviewers. Any product that may be evaluated in this article, or claim that may be made by its manufacturer, is not guaranteed or endorsed by the publisher.

frontiers in Neuroscience

ORIGINAL RESEARCH
published: 11 November 2021
doi: 10.3389/fnins.2021.743705

Anti-inflammatory Effects of a Novel Herbal Extract in the Muscle and Spinal Cord of an Amyotrophic Lateral Sclerosis Animal Model

*Sun Hwa Lee[1], Mudan Cai[2] and Eun Jin Yang[2]**

[1] Department of Clinical Research, Korea Institute of Oriental Medicine, Daejeon, South Korea, [2] Department of Korea Medicine (KM) Science Research, Korea Institute of Oriental Medicine, Daejeon, South Korea

OPEN ACCESS

Edited by:
Muhammad Imran Naseer, King Abdulaziz University, Saudi Arabia

Reviewed by:
Yoichiro Abe, Keio University, Japan
Paola Fabbrizio, Mario Negri Pharmacological Research Institute, Scientific Institute for Research, Hospitalization and Healthcare (IRCCS), Italy

***Correspondence:**
Eun Jin Yang
yej4823@gmail.com

Specialty section:
This article was submitted to Neuropharmacology, a section of the journal Frontiers in Neuroscience

Received: *19 July 2021*
Accepted: *30 September 2021*
Published: *11 November 2021*

Citation:
Lee SH, Cai M and Yang EJ (2021) Anti-inflammatory Effects of a Novel Herbal Extract in the Muscle and Spinal Cord of an Amyotrophic Lateral Sclerosis Animal Model. Front. Neurosci. 15:743705. doi: 10.3389/fnins.2021.743705

Amyotrophic lateral sclerosis (ALS) is a complex disease characterized by motor neuron loss and muscle atrophy. There is no prominent treatment for ALS as the pathogenic process in the skeletal muscle and spinal cord is complex and multifactorial. Therefore, we investigated the effects of a herbal formula on the multi-target effects in the skeletal muscle and spinal cord in hSOD1^{G93A} transgenic mice. We prepared a herbal extract (HE) from *Glycyrrhiza uralensis*, *Atractylodes macrocephala Koidzumi*, *Panax ginseng*, and *Astragalus membranaceus*. Control and HE-treated mice underwent rotarod and footprint tests. We also performed immunohistochemical and Western blotting analyses to assess expression of inflammation-related and oxidative stress-related proteins in the muscle and spinal cord tissues. We found that the HE increased motor activity and reduced motor neuron loss in hSOD1^{G93A} mice. In addition, the HE significantly reduced the levels of inflammatory proteins and oxidative stress-related proteins in the skeletal muscles and spinal cord of hSOD1^{G93A} mice. Furthermore, we demonstrated that the HE regulated autophagy function and augmented neuromuscular junction in the muscle of hSOD1^{G93A} mice. Based on these results, we propose that the HE formula may be a potential therapeutic strategy for multi-target treatment in complex and multifactorial pathological diseases.

Keywords: amyotrophic lateral sclerosis, herbal medicine, oxidative stress, inflammation, skeletal muscle

INTRODUCTION

Amyotrophic lateral sclerosis (ALS) is a neurodegenerative disease that leads to progressive degeneration and death of the motor neurons and muscle paralysis. Ten percent of patients with ALS are known to have familial ALS that is caused by genetic mutations in genes, such as *SOD1* and *C9ORF72*. However, 90% of the cases are sporadic. Despite several attempts to find effective therapy, only two drugs are permitted for the treatment of ALS—riluzole reduces excessive glutamate excitotoxicity and edaravone reduces oxidative stress. However, even these show only a mild effect in delaying disease progression and extending life (Miller et al., 2012; Watanabe et al., 2018).

Amyotrophic lateral sclerosis is caused by the loss of motor neurons and muscle atrophy. However, it remains controversial whether muscle atrophy is caused by the loss of the motor neurons or pathogenic mechanisms in the muscle that lead to death of motor neurons. Wong and Martin (2010) demonstrated that expression of mutant human SOD1 (hSOD1) in the skeletal muscles causes motor neuron degeneration in an ALS animal model and suggested that the muscles could be the primary site for pathogenesis in ALS. Boillee et al. (2006) showed that microglia and astrocytes contribute to the degeneration of motor neurons, leading to disease pathogenesis. Therefore, therapeutic strategies should target both the motor neurons and skeletal muscles to alleviate the disease suffering and to improve the quality of life of patients with ALS and their families.

Herbal medicines, which are common, complementary, alternative medicines, are used worldwide for the treatment of various diseases, such as cancer (Molassiotis et al., 2005), immune dysfunction diseases (Liu et al., 2018), and neurodegenerative diseases (Zhang et al., 2015; Jarrell et al., 2018) and muscle regeneration and energy metabolism in muscle (Tan et al., 2014; Go et al., 2020).

Based on herbal function, herbal combinations, with each herb having differing mechanisms of action, help increase the therapeutic efficacy. According to a previous study by our group, Bojungikgi-tang (BJIGT) has neuroprotective effects and delays the progression of disease in an ALS animal model (Cai et al., 2019). Therefore, we designed the present study to find a herbal formula in BJIGT that increases the anti-inflammatory and anti-oxidative effects in the ALS model and to examine combined herbal extracts (HEs), including *Glycyrrhiza uralensis*, *Atractylodes macrocephala Koidzumi*, *Panax ginseng*, and *Astragalus membranaceus*, in the skeletal muscles and spinal cord in the ALS animal model. *G. uralensis* is primarily used for its anti-inflammatory effects on gastric ulcers (Katakai et al., 2002), as well as its anti-allergic and neuroprotective effects (Kobayashi et al., 1995; Yu et al., 2008; Hasanein, 2011). *Atractylodes macrocephala Koidzumi* is also used in traditional medicine for its anti-inflammatory (Li et al., 2007) and antitumor effects (Kimura, 2006). *P. ginseng* has been widely used to improve the motor functions in spinal cord injury models (Kim et al., 2015), and its active compound, ginsenoside Re, has increased anti-inflammatory effects in hSOD1^{G93A} mice and LPS-induced BV2 microglial cells (Lee et al., 2012; Cai and Yang, 2016). *A. membranaceus* is reported to have bioactive compounds with immunomodulatory, anti-inflammatory, and antioxidant effects in diabetic nephropathy and heart disease (Fu et al., 2014). Additionally, *A. macrocephala* regulates the mitochondrial function and energy metabolism in C_2C_{12} myotubes (Song et al., 2015).

In the present study, we performed behavioral tests, including rotarod test and foot printing, immunohistochemistry, and Western blotting, in hSOD1^{G93A} mice. We found that the herbal combination extracts improved motor activity and increased anti-neuroinflammation and anti-oxidation activity in the skeletal muscle (tibialis anterior and gastrocnemius) and spinal cord of hSOD1^{G93A} mice.

MATERIALS AND METHODS

Animals

Hemizygous male hSOD1^{G93A} mice were used as the ALS model. They were purchased from the Jackson Laboratory (Bar Harbor, ME, United States). hSOD1^{G93A} B6SJL mice carry a mutation of a glycine-to-alanine at the 93rd codon of the cytosolic Cu/Zn superoxide dismutase gene and were maintained as described previously (Yang et al., 2010). They were handled in accordance with the United States National Institutes of Health guidelines (Bethesda, MD, United States). Animal experiments were approved by the Institutional Animal Care and Use Committee of the Korea Institute of Oriental Medicine (protocol number: 17-061). All mice were housed in Specific Pathogen Free (SPF) animal facility and acclimatized at a constant temperature ($21 \pm 3°C$) and humidity ($50 \pm 10\%$) under a 12 h light/dark cycle with free access to water and stand chow *ad libitum*.

Preparation of Herbal Extracts and Treatment

Medicinal herbs, such as *G. uralensis*, *A. macrocephala Koidzumi*, *P. ginseng*, and *A. membranaceu*, were purchased from Kwangmyungdang Medicinal Herbs Co. (Ulsan, South Korea). For water extraction of medicinal herbs, these four medicinal herbs were mixed in a 1:1:1:1 ratio. Mixed herbs were extracted with distilled water for 24 h at room temperature, filtered through Whatman filter paper, and concentrated under reduced pressure. The extracts were then freeze-dried to obtain a powdered extract. The extracts were stored at $-20°C$ for further use. For the treatment of HEs, the powdered extract was dissolved in distilled water before use.

Twenty-four male mice were randomly divided into the following groups: non-transgenic mice (nTg) = 8, hSOD1^{G93A} transgenic mice (Tg) = 8, and HE-treated hSOD1^{G93A} transgenic mice (Tg-HE) = 8. HEs were administered once daily for 6 weeks as an oral dose of 1 mg/g, starting in 8-week-old hSOD1^{G93A} transgenic mice. The nTg and hSOD1^{G93A} transgenic mice were the controls and were treated with distilled water.

Rotarod Test

The mice were trained for 2 weeks before the test. To measure motor coordination, each mouse was placed on the rotating rod (10 rpm), as described previously (Yang et al., 2010). Each mouse was tested three times, and the average time spent on the rod was determined for each group.

Footprint Test

Footprint tests were performed the day before the mice were euthanized to determine the extent of muscle loosening (Filali et al., 2011; Mancuso et al., 2011). The hind paws of mice were painted with a non-toxic, water-soluble ink to pass through an alley that was 70 cm in width, 16 cm in length, and 6 cm in height. At least three attempts were made to obtain a clearly visible footprint.

Tissue Preparation

The tibialis anterior (TA) and gastrocnemius (GC) muscles and the spinal cords of mice were collected from hSOD1^{G93A} mice. Mice tissue were homogenized in radioimmunoprecipitation assay (RIPA) lysis buffer [50 mM Tris–Cl pH 7.4, 1% NP-40, 0.1% sodium dodecyl sulfate (SDS), and 150 mM NaCl], containing a protease and phosphatase inhibitor cocktail (Thermo Fisher Scientific, Waltham, MA, United States). Homogenate was quantified using bicinchoninic acid assay kit (Pierce, IL, United States).

Western Blotting Analysis

Total proteins (20 μg) were separated by SDS-polyacrylamide gel electrophoresis and transferred to polyvinylidene difluoride membrane for Western blotting. The membranes were blocked with 5% skim milk (Sigma) in Tris–buffered saline for 1 h at room temperature and then incubated with various primary antibodies overnight at 4°C: tumor necrosis factor (TNF)-α, cluster of differentiation 11b (CD11b), heme oxygenase (HO)-1, ferritin, and tubulin (all 1:1,000; Abcam, Cambridge, MA, United States); NAD(P)H quinone dehydrogenase 1 (NQO1), B-cell lymphoma-2 (Bcl-2)-associated X protein (BAX), transferrin, and actin (all 1:1,000; Santa Cruz Biotechnology, Santa Cruz, CA, United States); p62 and microtubule-associated protein 1A/1B light chain (LC) 3B (all 1:1,000; Cell Signaling Technology, Danvers, MA, United States); and glial fibrillary acidic protein (GFAP) (1:5,000; Agilent Technologies, Santa Clara, CA, United States). Further, the blots were probed with horseradish peroxidase-conjugated anti-mouse or anti-rabbit secondary antibodies (Santa Cruz Biotechnology) and visualized using SuperSignal West Femto Substrate Maximum Sensitivity Substrate (Thermo Fisher Scientific). A ChemiDoc image analyzer was used to detect immunoblotted bands (Bio-Rad, Hercules, CA, United States).

Immunohistochemistry

For neuromuscular junction, the experiment was performed, as described previously (Cai et al., 2019). Briefly, the GC tissue was fixed with 4% paraformaldehyde and incubated in 20% sucrose for 24 h. The GC tissue was then embedded in optimal temperature cutting compound, and the sections were cryo-sectioned. For staining, the sections were incubated with α-bungarotoxin (1:500 dilution) for 2 h.

Nissl Staining

The spinal cord tissues were fixed with 4% paraformaldehyde and paraffinized. Further, the tissue slices were gradually dehydrated in alcohol (70, 80, 90, and 100%) for 5 min with two changes and placed in xylene for 5 min with three changes. Then, the slices were stained with 0.1% cresyl violet (Sigma, St. Louis, MO, United States) for 5 min, washed three times in distilled water, and dehydrated two times in gradient alcohol (70, 80, 90, and 100%) for 5 min each. Finally, the slices were transferred and rinsed again in xylene for three times, 5 min each time, and covered with a coverslip using Histomount media and dried at room temperature. The following criteria were used to quantify motor neuron loss: neurons must be located in the ventral horn of spinal cord L4∼5, the diameter of soma should be more than 20 μm, and neurons should have a distinct nucleolus (Lance-Jones, 1982).

Statistical Analyses

Data are presented as the mean ± standard error of the mean (SEM), where indicated. The experiments were performed at least three independently and analyzed using GraphPad Prism 9.0 (GraphPad Software, San Diego, CA, United States). Comparisons between each group were analyzed by one-way analysis of variance (ANOVA) followed by Bonferroni's multiple comparison tests or Newman-Keuls test.

RESULTS

Herbal Extract Improves Motor Function in hSOD1^{G93A} Mice

The body weight and muscle weight of the mice were significantly reduced by 1.1- and 1.7-fold ($p < 0.05$, $p < 0.001$), respectively, in the Tg group compared with the nTg group (**Figure 1A**). There was no change in the body weight of mice in the Tg-HE group, although the muscle weights of TA and GC of mice in the Tg-HE group were significantly increased by 1.3- and 1.2-fold, respectively, compared with those of mice in the Tg group (**Figure 1A**).

The rotarod and footprint tests were performed as behavioral tests to determine the effect of HE administration on the motor function of the hSOD1^{G93A} mice after administration of the HE (1 g/kg) for 6 weeks. As shown in **Figure 1B**, compared with the motor function in the nTg group, motor function in the Tg group was reduced by 4.1-fold ($p < 0.05$) in the rotarod test. However, the Tg-HE group showed a 3.8-fold ($p < 0.05$) increase in motor function compared with the Tg group. Additionally, the Tg group showed stride length of 4.7 ± 0.3 cm, which was reduced by 1.3-fold ($p < 0.01$) compared with the nTg group; and the Tg-HE group showed stride length of 5.5 ± 0.2 cm, which was 1.2-fold ($p < 0.05$) that of the Tg group (**Figure 1B**).

Herbal Extract Reduces Inflammation in the Muscles of hSOD1^{G93A} Mice

To examine the effect of HE on inflammation in the muscles of hSOD1^{G93A} mice, we investigated the expression of inflammation-related proteins—GFAP, TNF-α, and CD11b—by Western blotting. Quantitative analysis showed that the expressions of GFAP and TNF-α were increased by 3.3- and 4.6-fold ($p < 0.01$), respectively, in the TA of the Tg group compared with that in the nTg group (**Figures 2A,B**). However, treatment with HE significantly decreased their expressions by 1.7- and 2.0-fold ($p < 0.05$), respectively, in the Tg-HE group compared with the Tg group.

Moreover, the expressions of TNF-α, GFAP, and CD11b were increased by 2. 8−, 2. 0−, and 6.3-fold ($p < 0.01$, $p < 0.05$, and $p < 0.01$), respectively, in the GC of the Tg group compared with that in the nTg group; whereas treatment with HE significantly

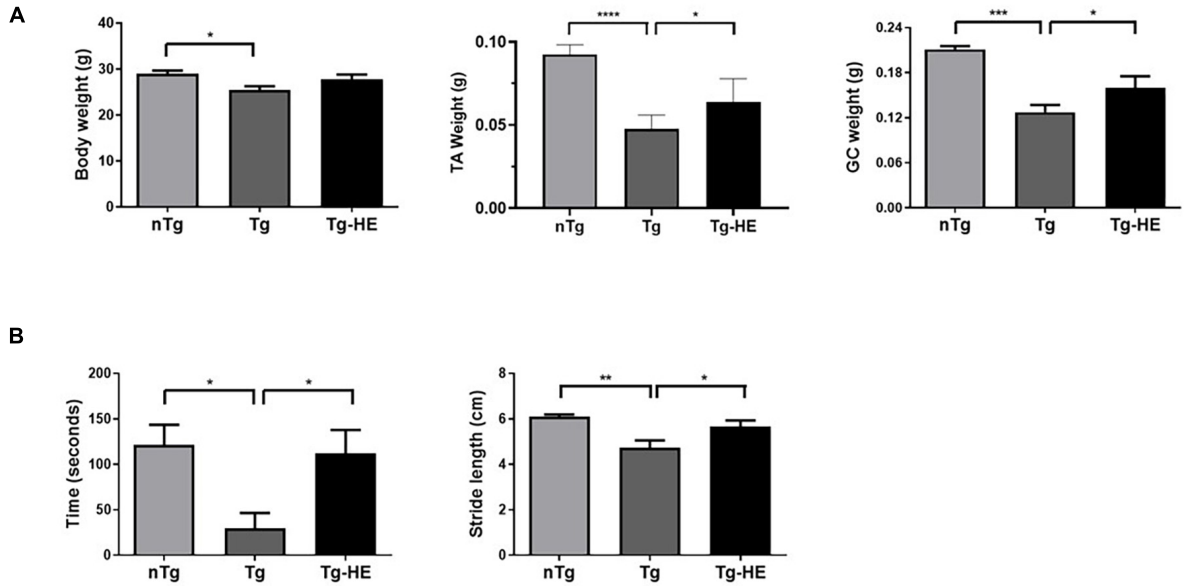

FIGURE 1 | Effect of herbal extract (HE) on the motor functions in hSOD1^{G93A} mice. **(A)** The body weight and tibialis anterior (TA) or gastrocnemius (GC) muscle weight of non-transgenic mice, hSOD1^{G93A} mice, and HE-treated hSOD1^{G93A} mice. **(B)** Comparison of outcome of rotarod and footprint tests between groups. Data are expressed as the mean ± SEM ($N = 8$, $^{*}p < 0.05$, $^{**}p < 0.01$, $^{***}p < 0.001$, and $^{****}p < 0.0001$). The statistical analyses were conducted using one-way ANOVA followed by Bonferroni's multiple comparison tests. nTg, non-transgenic mice; Tg, hSOD1^{G93A} mice; Tg-HE, HE-treated hSOD1^{G93A} mice.

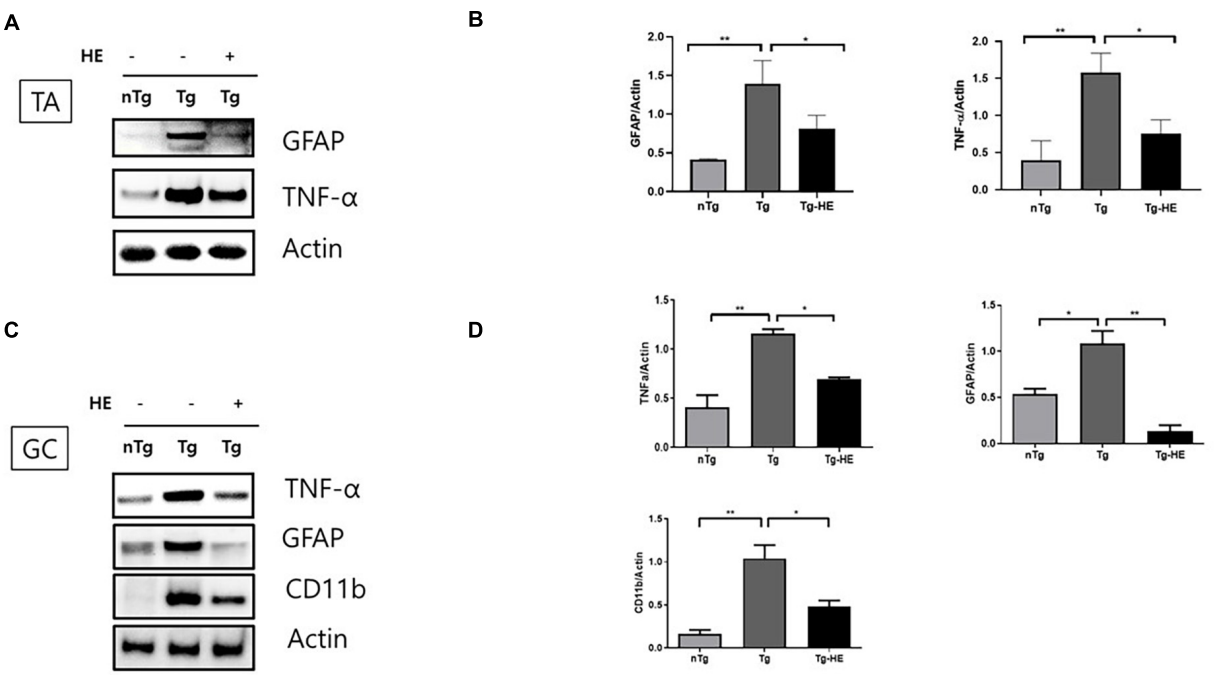

FIGURE 2 | Herbal extract (HE) relieves inflammation in the tibialis anterior (TA) and gastrocnemius (GC) of hSOD1^{G93A} mice. **(A–D)** Western blotting of non-transgenic mice (nTg, $N = 3$), hSOD1^{G93A} mice (Tg, $N = 3$), and HE-treated hSOD1^{G93A} mice (Tg-HE, $N = 3$). **(A)** Data for Western blotting analysis of glial fibrillary acidic protein (GFAP) and tumor necrosis factor (TNF)-α in the TA. **(B)** Quantification of levels of GFAP and TNF-α with respect to levels of actin that is used as a loading control. **(C)** GC is immunoblotted with TNF-α, GFAP, and cluster of differentiation 11b (CD11b) using nTg, Tg, and Tg-HE ($N = 3$). **(D)** Quantification of levels of TNF-α, GFAP, and CD11b with respect to that of or actin that is used as a loading control. Data are shown as mean ± SEM. The statistical analyses were conducted with one-way ANOVA followed by Bonferroni's multiple comparison tests ($^{*}p < 0.05$ and $^{**}p < 0.01$).

decreased expression of the same proteins by 1. 6−, 8. 0−, and 2.1-fold ($p < 0.05$, $p < 0.01$, and $p < 0.05$), respectively, in the Tg-HE group compared with the Tg group (**Figures 2C,D**).

Herbal Extract Attenuates Oxidative Stress in the Muscles of hSOD1^{G93A} Mice

We analyzed the effects of HE on the expression of oxidative stress-related proteins in the muscles of hSOD1^{G93A} mice. The expressions of HO1, NQO1, BAX, and ferritin in the TA of the Tg group increased by 7. 5−, 2. 6−, 7. 9−, and 2.8-fold ($p < 0.05$, $p < 0.001$, $p < 0.001$, and $p < 0.05$), respectively, compared with that in the nTg group. In contrast, in the GC, they were increased by 2. 1−, 2. 8−, 2. 1−, and 5.3-fold ($p < 0.01$, $p < 0.01$, $p < 0.01$, and $p < 0.01$), respectively, in the Tg group compared with the nTg group (**Figures 3A–D**). However, after administration of HE, expressions of HO1, NQO1, BAX, and ferritin in the TA significantly decreased by 2. 9−, 2. 2−, 2. 9−, and 2.3-fold ($p < 0.05$, $p < 0.01$, $p < 0.05$, and $p < 0.01$), respectively, in the Tg-HE group compared with the Tg group. On the other hand, they decreased in the GC by 4. 0−, 1. 7−, 1. 4−, and 2.2-fold ($p < 0.05$), respectively, in the Tg-HE group compared with that in the Tg group (**Figures 3A–D**).

Herbal Extract Reduces the Expression of Autophagy-Associated Proteins in the Gastrocnemius of hSOD1^{G93A} Mice

We investigated the expression of autophagy-related proteins, p62 and LC3B, to examine the effect of HE on autophagy dysfunction in the GC of hSOD1^{G93A} mice. The expression of p62 and LC3B increased by 1.5− and 28.0-fold ($p < 0.05$ and $p < 0.001$), respectively, in the GC in the Tg group compared with that in the nTg group (**Figures 4A,B**). However, treatment with HE significantly decreased their expression by 3.8− and 10.0-fold, respectively, in the Tg-HE group compared with that in the Tg group.

In a previous study, we observed a relatively small muscle fiber diameter and abnormal muscle fiber nuclei in the skeletal muscles of hSOD1^{G93A} transgenic mice (Cai et al., 2015). To analyze the alterations in the structure of the GC muscle fiber following administration of HE, we performed hematoxylin/eosin staining of the cross sections of the muscle tissues. HE administration reduced the abnormal nuclei in GC by 4.7-fold and enlarged the fiber diameter compared to those of the Tg (**Figure 5A**). In addition, we found that enlarged the fiber diameter in GC of HE-treated group compared to those of the Tg but it was not significant (**Figure 5A**).

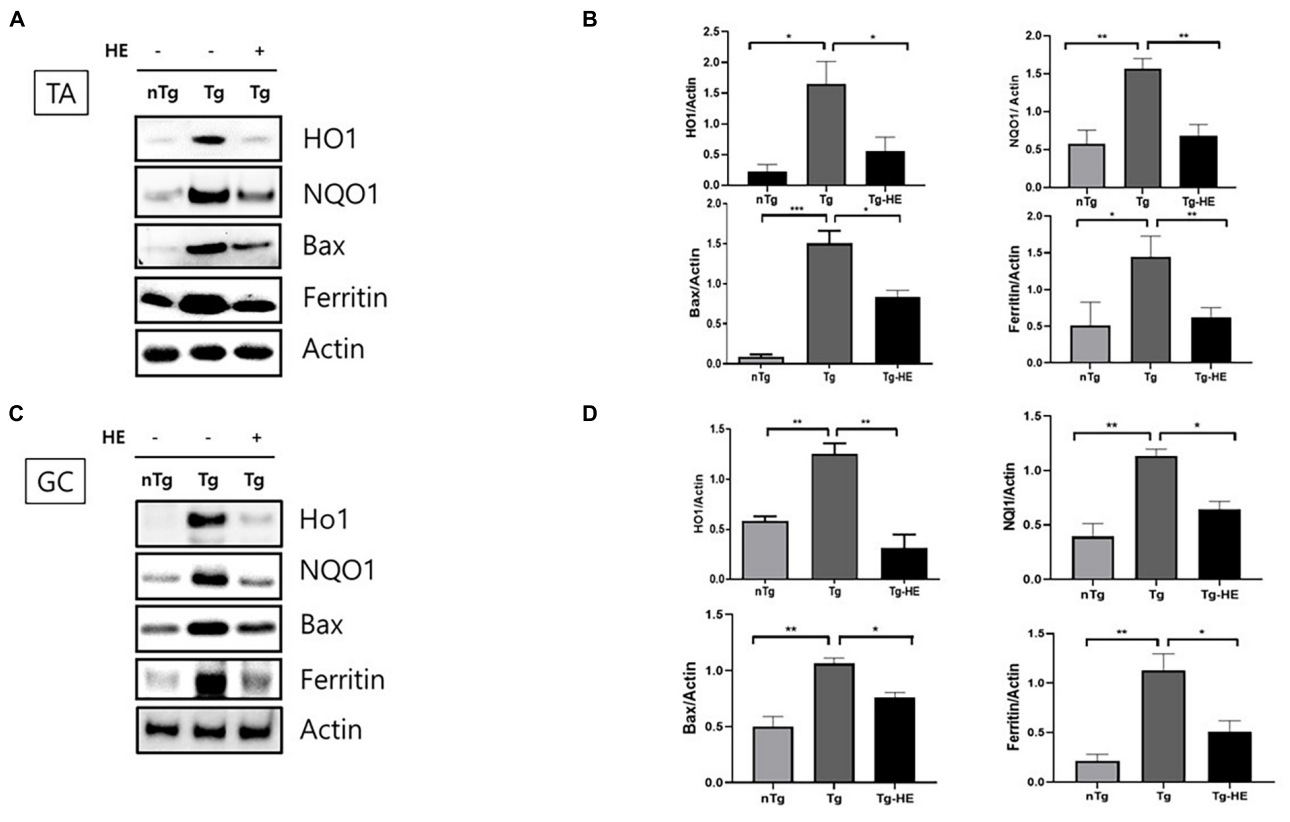

FIGURE 3 | Herbal extract (HE) reduces oxidative stress in the muscles of hSOD1^{G93A} mice. Representative data for Western blotting analysis of HO1, NQO1, BAX, and ferritin in the **(A)** tibialis anterior (TA) and **(C)** gastrocnemius (GC) using nTg, Tg, and Tg-HE ($N = 3$); and quantitative analysis of the expression level of each protein in **(B)** TA and **(D)** GC. Data are shown as the mean ± SEM. The statistical analyses were conducted with a one-way ANOVA followed by Bonferroni's multiple comparison tests (*$p < 0.05$, **$p < 0.01$, and ***$p < 0.001$).

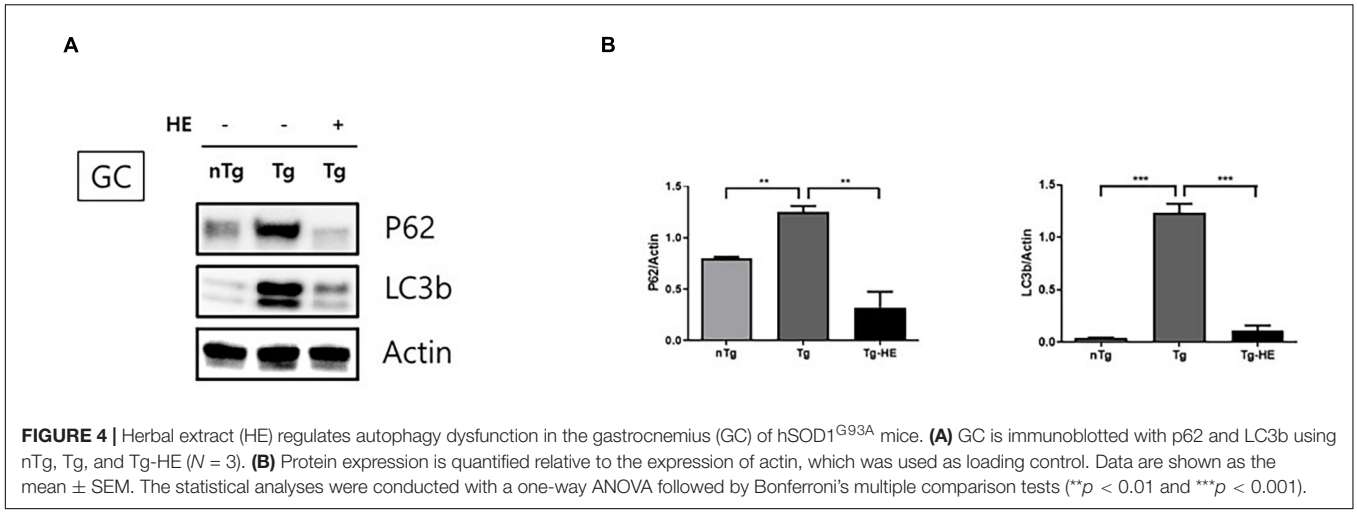

FIGURE 4 | Herbal extract (HE) regulates autophagy dysfunction in the gastrocnemius (GC) of hSOD1^{G93A} mice. **(A)** GC is immunoblotted with p62 and LC3b using nTg, Tg, and Tg-HE ($N = 3$). **(B)** Protein expression is quantified relative to the expression of actin, which was used as loading control. Data are shown as the mean ± SEM. The statistical analyses were conducted with a one-way ANOVA followed by Bonferroni's multiple comparison tests (**$p < 0.01$ and ***$p < 0.001$).

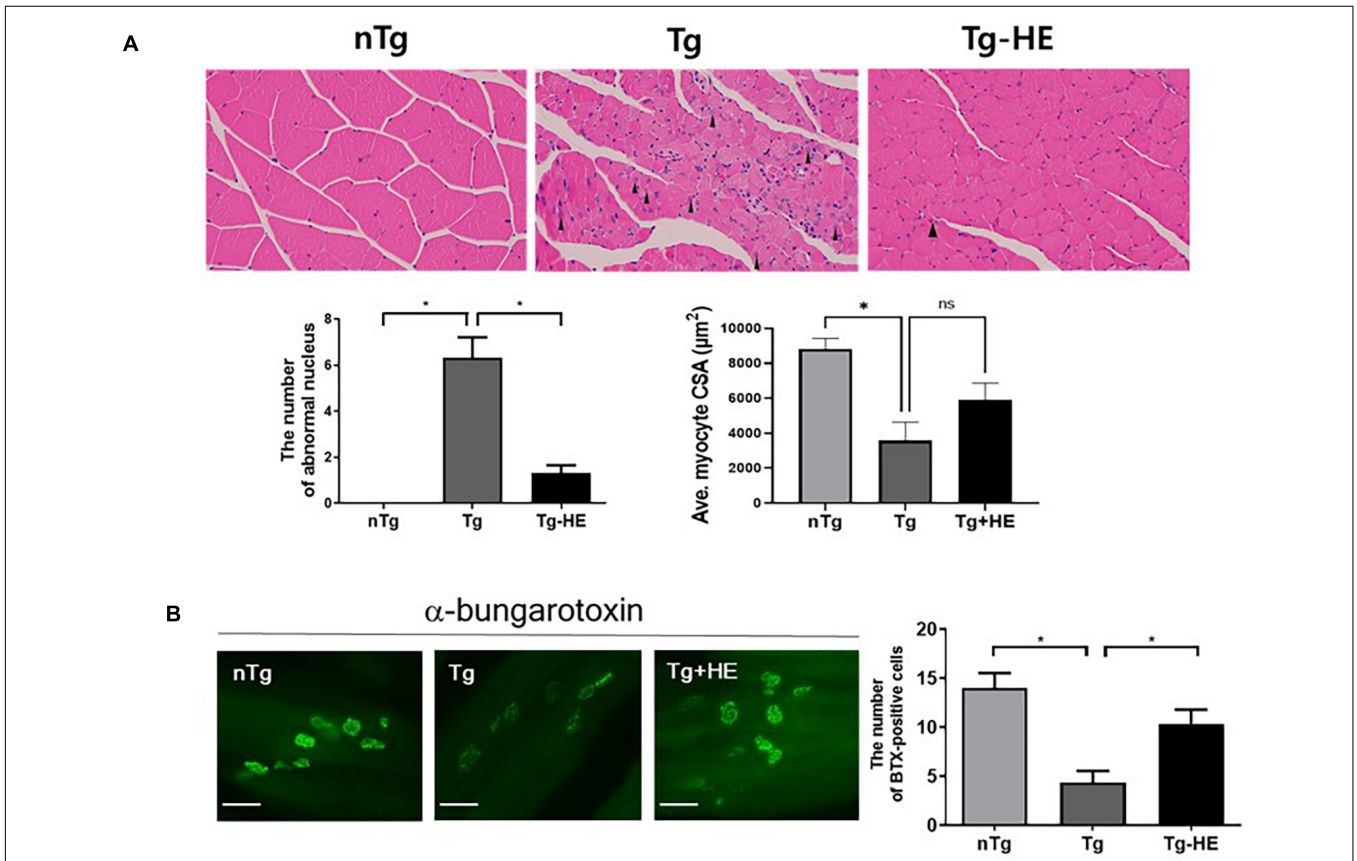

FIGURE 5 | Herbal extract (HE) prevents muscle degeneration in the gastrocnemius (GC) of hSOD1^{G93A} mice. **(A)** Representative images of H&E staining of the GC of the nTg, Tg, and Tg-HE groups and quantification of the number of abnormal of nucleus and myocyte cross-sectional area (CSA). The arrowhead indicates an abnormal nucleus. **(B)** α-bungarotoxin staining of the GC and quantification of the number of BTX-positive cells ($N = 3$); scale bar = 500 μm. Data are shown as the mean ± SEM. The statistical analyses were conducted with a one-way ANOVA followed by Bonferroni's multiple comparison tests (*$p < 0.05$).

Next, we determined the effect of HE on the pathological morphology of the GC. We found that treatment with HE retarded the typical features of muscle atrophy, such as increases in the number of small muscle fibers and abnormal nuclei (**Figure 5A**). Additionally, α-bungarotoxin staining demonstrated that treatment with HE increased the number of neuromuscular junctions (NMJs) in the GC by 2.4-fold ($p < 0.05$)

in the Tg-HE group compared with that in the Tg group (**Figure 5B**).

Herbal Extract Reduces Expression of Neuroinflammation or Oxidative Stress-Related Proteins in the Spinal Cord of hSOD1^{G93A} Amyotrophic Lateral Sclerosis Mice

Neuroinflammation is a key cellular process in the pathogenesis of ALS (Liu and Wang, 2017). Nissl staining showed that the loss of motor neurons in the saline-treated Tg mice was dramatically reduced by 4.5-fold in the anterior horn of the lumbar spinal cord compared with that in the nTg mice ($p < 0.05$; **Figure 6A**). However, treatment with HE reduced the loss of motor neurons by 4.1-fold in the spinal cord of the hSOD1^{G93A} mice. This was consistent with the choline acetyltransferase immunohistochemistry data ($p < 0.05$; **Figure 6A**). To study the molecular mechanism of the motor neuron protection by HE, we investigated the levels of neuroinflammation-related proteins, such as GFAP, CD11b, and TNF-α, in the spinal cord of the hSOD1^{G93A} mice using Western blotting (**Figures 6B,C**). The analysis indicated that the expressions of GFAP, CD11b, and TNF-α were dramatically increased by 1. 8−, 15. 1−, and 1.8-fold ($p < 0.05$, $p < 0.01$, and $p < 0.05$), respectively, in the Tg group compared with in the nTg group; while treatment with the HE in the Tg-HE group significantly reduced the levels of GFAP, CD11b, and TNF-α by 2−, 2. 3−, and 1.8-fold ($p < 0.05$), respectively, compared with those in the Tg group (**Figures 6B,C**). In addition, we confirmed that HE treatment reduced by 2.4− and 2.5-fold ($p < 0.01$), respectively, the immunoreactivity of GFAP and Iba1 in anterior horn of the spinal cord compared to those of the Tg group (**Figure 6D**).

Oxidative stress is a mechanism contributing to ALS that leads to motor neuron cell death (Barber et al., 2006). To determine whether treatment with HE regulates oxidative stress, we evaluated the levels of oxidative stress-related proteins, transferrin and BAX, using Western blotting in the spinal cord of ALS mice (**Figures 6E,F**). The expression levels of transferrin and BAX were significantly increased by 1.9− and 2.7-fold ($p < 0.05$ and $p < 0.001$), respectively, in the Tg group compared with the nTg group, while treatment with HE in the Tg-HE group dramatically reduced their expression levels each by 1.8-fold ($p < 0.05$ and $p < 0.01$) compared with those in the Tg group.

DISCUSSION

Amyotrophic lateral sclerosis is a complex and incurable disease that leads to motor neuronal cell death and muscle paralysis. Studies have attempted to find treatment against ALS, but there is still no effective drug to treat ALS patients. Riluzole and edaravone have been used for the treatment of patients with ALS, but they do not offer complete cure. Therefore, it is necessary to develop drugs against multiple targets because ALS is a complex disease of the muscles and spinal cord.

Herbal medicine comprises multiple components and is primarily used to improve the immune system. Therefore, we investigated whether a herbal formula extract could be helpful in achieving immunity and anti-oxidation in the muscle and spinal cord of the hSOD1^{G93A} transgenic mice. The hSOD1^{G93A} transgenic mice have decreased muscle function in their skeletal muscles, such as strength, mitochondrial structure, and contractile apparatus, as well as loss of motor neurons in the spinal cord (Dobrowolny et al., 2008; Martin and Wong, 2020). Many studies have focused on the pathological mechanisms of motor neuron death (Renton et al., 2014; Alsultan et al., 2016; Taylor et al., 2016); however, only some studies have demonstrated that the skeletal muscles are a critical target for developing effective treatment for patients with ALS (Wong and Martin, 2010).

Oxidative stress is a critical factor leading to motor neuron death and muscle atrophy in ALS because oxidative stress impairs mitochondrial function and dysregulates protein homeostasis (Le Gall et al., 2020). Reactive oxygen species cause oxidative stress and increase production of cytokines and chemokines involved in abnormal glial oxidative responses in neurodegeneration (Nijssen et al., 2017). In the ALS model, immune cell infiltration is observed in the extensor digitorum longus muscle (Trias et al., 2018). Additionally, oxidative stress accelerates presynaptic decline in the NMJs and causes abnormal secretion of acetylcholinesterase. Therefore, the subsequent reduction in acetylcholine levels in the synaptic cleft can lead to the loss of muscle strength in patients with ALS (Pollari et al., 2014). Edaravone, an antioxidant, is a free radical scavenger and is used for the treatment of patients with ALS (Yoshino and Kimura, 2006), although it does not extend patients' survival. Other antioxidants, including vitamin E, acetylcysteine, and creatine, were effective in ALS animal models, but they are not valuable for disease symptoms in patients with ALS (Louwerse et al., 1995). Therefore, studies on the discovery of multitarget treatment should be considered in ALS pathology as neuroinflammation and oxidative stress are linked and together causes loss of motor neurons and muscle degeneration. We focused on the anti-inflammatory and anti-oxidative effects of the herbal formula (*G. uralensis*, *A. macrocephala Koidzumi*, *P. ginseng*, and *A. membranaceus*) in the spinal cord and skeletal muscles of 14-week-old (presymptomatic stage) hSOD1^{G93A} mice to determine its preventive effect. We found that treatment with HE increased muscle weight and motor activity in the rotarod and foot printing tests. Additionally, we demonstrated that the expression levels of inflammation-related proteins (GFAP, TNF-α, and CD11b) and oxidative stress-related proteins (HO1, NQO1, Bax, and ferritin) were significantly reduced by HE in the TA and GC of hSOD1^{G93A} mice compared with those of the control mice.

Glial fibrillary acidic protein expression was increased in the hindlimb of GFAP-luc/SOD1^{G93A} mice at disease onset in damaged sciatic nerves ALS, suggesting that GFAP upregulation could be a valid marker at peripheral axons/neuromuscular junction and in the spinal cord/brain area according to the ALS pathogenesis stage (Keller et al., 2009).

Furthermore, we found that treatment with HE increased NMJ in the muscles to raise the motor function in hSOD1^{G93A} mice.

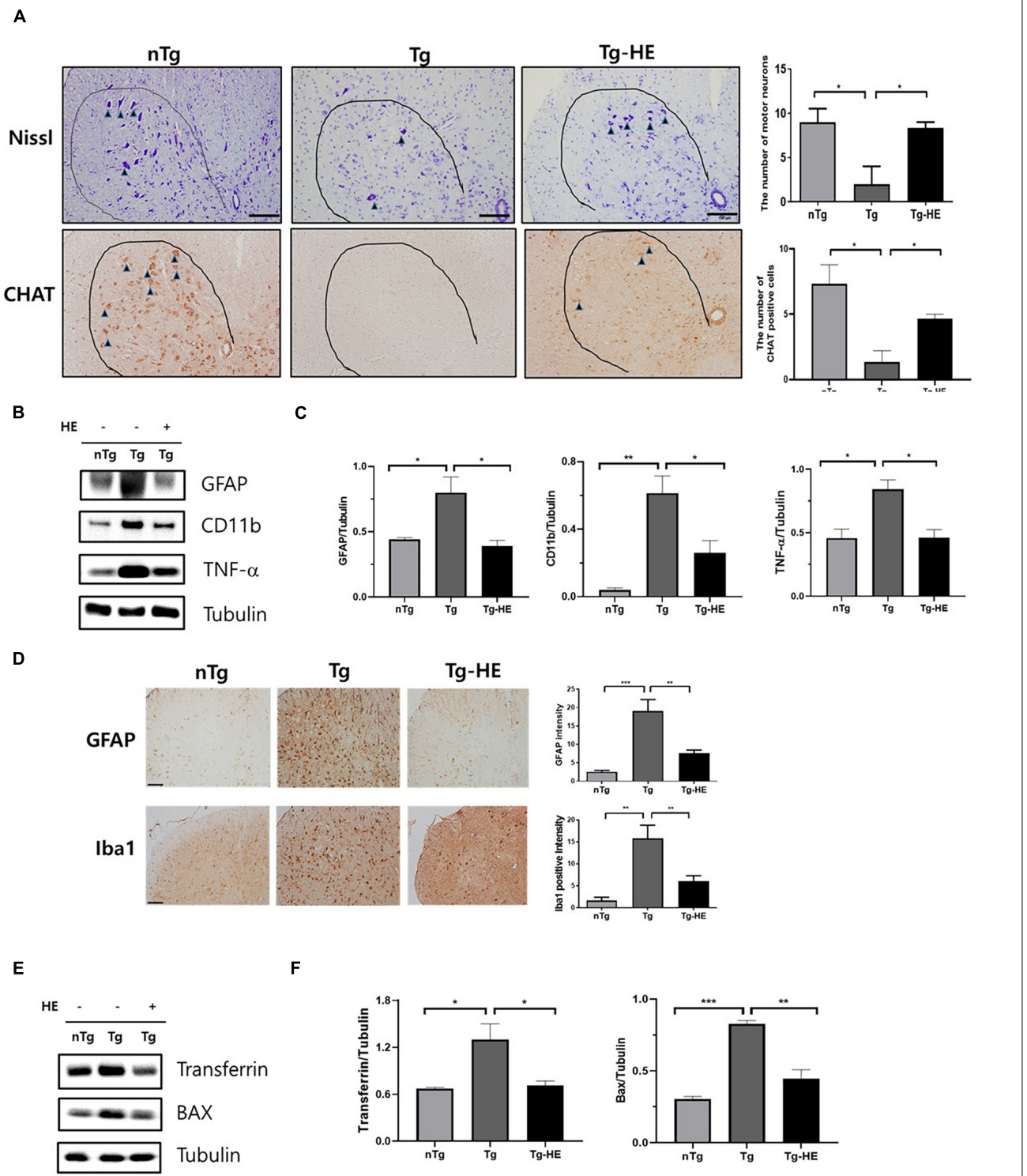

FIGURE 6 | Herbal extract (HE) inhibits motor neuron death and increases anti-neuroinflammatory and anti-oxidative effects. **(A)** Nissl staining of the motor neurons (arrowheads) in the anterior horn of L4-5 lumbar spinal cords ($N = 3$); scale bar = 100 μm. **(B)** Representative Western blotting images showing the expression of inflammation-related proteins [glial fibrillary acidic protein (GFAP), cluster of differentiation 11b (CD11b), and tumor necrosis factor (TNF)-α] in the spinal cord of each group of mice ($N = 3$). **(C)** Quantification of immunoblots normalized to the expression of tubulin. **(D)** Immunohistochemistry with anti-GFAP and anti-Iba1 in spinal cord. scale bar = 2 mm. **(E)** Representative Western blotting images showing the expression of transferrin and BAX in the spinal cord of each group of mice ($N = 3$). **(F)** Quantification of immunoblots normalized to the expression of tubulin. Data are shown as the mean ± SEM. The statistical analyses were conducted with a one-way ANOVA followed by Newman-Keuls multiple or Bonferroni's multiple comparison tests (*$p < 0.05$, **$p < 0.01$, and ***$p < 0.001$).

These findings suggest that treatment with HE can delay disease progression through anti-inflammatory and anti-oxidative effects in the skeletal muscles of mice with ALS. However, whether HE can extend the survival of hSOD1^{G93A} mice remains to be investigated.

Mitochondrial dysfunction is detected in the muscles and spinal cord of hSOD1^{G93A} mice (Mattiazzi et al., 2002; Scaricamazza et al., 2020), plays a critical role in the degeneration of motor neurons in ALS, and is considered a therapeutic target due to its involvement in disease onset. Oxidative stress modulates the autophagy signaling pathway in the muscles and motor neurons (Rodney et al., 2016; Le Gall et al., 2020). Olivan et al. (2015) demonstrated a significant activation of the autophagy marker, LC3-II/LC3-I, in the muscles derived from hSOD1^{G93A} mice (Olivan et al., 2015). Furthermore, Zhou et al. (2019) showed that oxidative stress, mitochondrial dysfunction, and reduction in autophagy function promoted recurrent mitochondrial damage. Therefore, we suggest that an increase in motor activity and NMJ following treatment with HE results from loss of mitochondrial damage by anti-oxidation and autophagy regulation in hSOD1^{G93A} mice. As fiber transition from glycolysis to β-oxidation in the ALS muscle correlates with disease onset and defects in motor functions (Dobrowolny et al., 2018; Scaricamazza et al., 2020), the relationship between metabolic changes and motor function after treatment with HE should be investigated.

CONCLUSION

This study demonstrated that treatment with HE improved motor activity and prevented the loss of motor neurons in hSOD1^{G93A} mice. Additionally, we identified anti-inflammatory and anti-oxidative mechanisms of HE in the skeletal muscles and spinal cord of ALS mice. Treatment with HE reduced the expression levels of inflammation-related proteins (GFAP, CD11b, and TNF-α) and oxidative stress-related proteins (HO1, NQO1, Bax, and ferritin) in the muscles (GC and TA) and spinal cord of hSOD1^{G93A} mice. The limitation is that we did not investigate the bio-active components of the anti-inflammatory and anti-oxidative effects of HE in the ALS model. Taken together, HE can be helpful for the treatment of multi-target complex diseases, such as ALS.

DATA AVAILABILITY STATEMENT

The raw data supporting the conclusions of this article will be made available by the authors, without undue reservation.

ETHICS STATEMENT

The animal study was reviewed and approved by the Institutional Animal Care and Use Committee of the Korea Institute of Oriental Medicine (protocol number: 17-061).

AUTHOR CONTRIBUTIONS

SL performed the rotarod test, western blotting, and immunohistochemistry with the muscles, and partially wrote the manuscript. MC contributed to the foot printing test, western blotting, and immunohistochemistry with the spinal cord. EY designed the study, analyzed the data, and prepared the final version of the manuscript. All authors contributed to the article and approved the submitted version.

FUNDING

This work was supported by the Basic Science Research Program through the National Research Foundation of Korea funded by the Ministry of Science, ICT and Future Planning, South Korea, under Grant NRF-2020R1A2C2006703 and the Korea Institute of Oriental Medicine, C18040.

REFERENCES

Alsultan, A. A., Waller, R., Heath, P. R., and Kirby, J. (2016). The genetics of amyotrophic lateral sclerosis: current insights. *Degener. Neurol. Neuromuscul. Dis.* 6, 49–64. doi: 10.2147/dnnd.s84956

Barber, S. C., Mead, R. J., and Shaw, P. J. (2006). Oxidative stress in ALS: a mechanism of neurodegeneration and a therapeutic target. *Biochim. Biophys. Acta* 1762, 1051–1067. doi: 10.1016/j.bbadis.2006.03.008

Boillee, S., Vande Velde, C., and Cleveland, D. W. (2006). ALS: a disease of motor neurons and their nonneuronal neighbors. *Neuron* 52, 39–59. doi: 10.1016/j.neuron.2006.09.018

Cai, M., Choi, S. M., and Yang, E. J. (2015). The effects of bee venom acupuncture on the central nervous system and muscle in an animal hSOD1G93A mutant. *Toxins* 7, 846–858. doi: 10.3390/toxins7030846

Cai, M., Lee, S. H., and Yang, E. J. (2019). Bojungikgi-tang improves muscle and spinal cord function in an amyotrophic lateral sclerosis model. *Mol. Neurobiol.* 56, 2394–2407. doi: 10.1007/s12035-018-1236-0

Cai, M., and Yang, E. J. (2016). Ginsenoside re attenuates neuroinflammation in a symptomatic ALS animal model. *Am. J. Chin. Med.* 44, 401–413. doi: 10.1142/s0192415x16500233

Dobrowolny, G., Aucello, M., Rizzuto, E., Beccafico, S., Mammucari, C., Boncompagni, S., et al. (2008). Skeletal muscle is a primary target of SOD1G93A-mediated toxicity. *Cell Metab.* 8, 425–436. doi: 10.1016/j.cmet.2008.09.002

Dobrowolny, G., Lepore, E., Martini, M., Barberi, L., Nunn, A., Scicchitano, B. M., et al. (2018). Metabolic changes associated with muscle expression of SOD1(G93A). *Front. Physiol.* 9:831. doi: 10.3389/fphys.2018.00831

Filali, M., Lalonde, R., and Rivest, S. (2011). Sensorimotor and cognitive functions in a SOD1(G37R) transgenic mouse model of amyotrophic lateral sclerosis. *Behav. Brain Res.* 225, 215–221. doi: 10.1016/j.bbr.2011.07.034

Fu, J., Wang, Z., Huang, L., Zheng, S., Wang, D., Chen, S., et al. (2014). Review of the botanical characteristics, phytochemistry, and pharmacology of *Astragalus membranaceus* (Huangqi). *Phytother. Res.* 28, 1275–1283. doi: 10.1002/ptr.5188

Go, G. Y., Jo, A., Seo, D. W., Kim, W. Y., Kim, Y. K., So, E. Y., et al. (2020). Ginsenoside Rb1 and Rb2 upregulate Akt/mTOR signaling-mediated muscular hypertrophy and myoblast differentiation. *J. Ginseng. Res.* 44, 435–441. doi: 10.1016/j.jgr.2019.01.007

Hasanein, P. (2011). Glabridin as a major active isoflavan from *Glycyrrhiza glabra* (licorice) reverses learning and memory deficits in diabetic rats. *Acta Physiol. Hung.* 98, 221–230. doi: 10.1556/aphysiol.98.2011.2.14

Jarrell, J. T., Gao, L., Cohen, D. S., and Huang, X. (2018). Network medicine for Alzheimer's disease and traditional chinese medicine. *Molecules* 23:1143.

Katakai, M., Akamaru, T., and Tani, T. (2002). An analysis of the frequency of formulations and crude drugs described in Shan-Han-Lun. *Yakushigaku Zasshi* 37, 28–35.

Keller, A. F., Gravel, M., and Kriz, J. (2009). Live imaging of amyotrophic lateral sclerosis pathogenesis: disease onset is characterized by marked induction of GFAP in Schwann cells. *Glia* 57, 1130–1142. doi: 10.1002/glia.20836

Kim, Y. O., Kim, Y., Lee, K., Na, S. W., Hong, S. P., Valan Arasu, M., et al. (2015). Panax ginseng improves functional recovery after contusive spinal cord injury by regulating the inflammatory response in rats: an in vivo study. *Evid. Based Complement. Alternat. Med.* 2015:817096.

Kimura, I. (2006). Medical benefits of using natural compounds and their derivatives having multiple pharmacological actions. *Yakugaku Zasshi* 126, 133–143. doi: 10.1248/yakushi.126.133

Kobayashi, S., Miyamoto, T., Kimura, I., and Kimura, M. (1995). Inhibitory effect of isoliquiritin, a compound in licorice root, on angiogenesis in vivo and tube formation in vitro. *Biol. Pharm. Bull.* 18, 1382–1386. doi: 10.1248/bpb.18.1382

Lance-Jones, C. (1982). Motoneuron cell death in the developing lumbar spinal cord of the mouse. *Brain Res.* 256, 473–479. doi: 10.1016/0165-3806(82)90192-4

Le Gall, L., Anakor, E., Connolly, O., Vijayakumar, U. G., Duddy, W. J., and Duguez, S. (2020). Molecular and cellular mechanisms affected in ALS. *J. Pers. Med.* 10:101. doi: 10.3390/jpm10030101

Lee, K. W., Jung, S. Y., Choi, S. M., and Yang, E. J. (2012). Effects of ginsenoside Re on LPS-induced inflammatory mediators in BV2 microglial cells. *BMC Complement. Altern. Med.* 12:196. doi: 10.1186/1472-6882-12-196

Li, C. Q., He, L. C., Dong, H. Y., and Jin, J. Q. (2007). Screening for the anti-inflammatory activity of fractions and compounds from *Atractylodes macrocephala* koidz. *J. Ethnopharmacol.* 114, 212–217. doi: 10.1016/j.jep.2007.08.002

Liu, J., and Wang, F. (2017). Role of neuroinflammation in amyotrophic lateral sclerosis: cellular mechanisms and therapeutic implications. *Front. Immunol.* 8:1005. doi: 10.3389/fimmu.2017.01005

Liu, L., Wang, L. P., He, S., and Ma, Y. (2018). Immune homeostasis: effects of chinese herbal formulae and herb-derived compounds on allergic asthma in different experimental models. *Chin. J. Integr. Med.* 24, 390–398. doi: 10.1007/s11655-018-2836-2

Louwerse, E. S., Weverling, G. J., Bossuyt, P. M., Meyjes, F. E., and De Jong, J. M. (1995). Randomized, double-blind, controlled trial of acetylcysteine in amyotrophic lateral sclerosis. *Arch. Neurol.* 52, 559–564. doi: 10.1001/archneur.1995.00540300031009

Mancuso, R., Olivan, S., Osta, R., and Navarro, X. (2011). Evolution of gait abnormalities in SOD1(G93A) transgenic mice. *Brain Res.* 1406, 65–73. doi: 10.1016/j.brainres.2011.06.033

Martin, L. J., and Wong, M. (2020). Skeletal muscle-restricted expression of human SOD1 in transgenic mice causes a fatal ALS-like syndrome. *Front. Neurol.* 11:592851. doi: 10.3389/fneur.2020.592851

Mattiazzi, M., D'aurelio, M., Gajewski, C. D., Martushova, K., Kiaei, M., Beal, M. F., et al. (2002). Mutated human SOD1 causes dysfunction of oxidative phosphorylation in mitochondria of transgenic mice. *J. Biol. Chem.* 277, 29626–29633. doi: 10.1074/jbc.m203065200

Miller, R. G., Mitchell, J. D., and Moore, D. H. (2012). Riluzole for amyotrophic lateral sclerosis (ALS)/motor neuron disease (MND). *Cochrane Database Syst. Rev.* 2012:CD001447.

Molassiotis, A., Fernandez-Ortega, P., Pud, D., Ozden, G., Scott, J. A., Panteli, V., et al. (2005). Use of complementary and alternative medicine in cancer patients: a European survey. *Ann. Oncol.* 16, 655–663.

Nijssen, J., Comley, L. H., and Hedlund, E. (2017). Motor neuron vulnerability and resistance in amyotrophic lateral sclerosis. *Acta Neuropathol.* 133, 863–885.

Olivan, S., Calvo, A. C., Gasco, S., Munoz, M. J., Zaragoza, P., and Osta, R. (2015). Time-point dependent activation of autophagy and the UPS in SOD1G93A mice skeletal muscle. *PLoS One* 10:e0134830. doi: 10.1371/journal.pone.0134830

Pollari, E., Goldsteins, G., Bart, G., Koistinaho, J., and Giniatullin, R. (2014). The role of oxidative stress in degeneration of the neuromuscular junction in amyotrophic lateral sclerosis. *Front. Cell Neurosci.* 8:131. doi: 10.3389/fncel.2014.00131

Renton, A. E., Chio, A., and Traynor, B. J. (2014). State of play in amyotrophic lateral sclerosis genetics. *Nat. Neurosci.* 17, 17–23.

Rodney, G. G., Pal, R., and Abo-Zahrah, R. (2016). Redox regulation of autophagy in skeletal muscle. *Free Radic. Biol. Med.* 98, 103–112. doi: 10.1016/j.freeradbiomed.2016.05.010

Scaricamazza, S., Salvatori, I., Giacovazzo, G., Loeffler, J. P., Rene, F., Rosina, M., et al. (2020). Skeletal-muscle metabolic reprogramming in ALS-SOD1(G93A) mice predates disease onset and is a promising therapeutic target. *iScience* 23:101087.

Song, M. Y., Kang, S. Y., Oh, T. W., Kumar, R. V., Jung, H. W., and Park, Y. K. (2015). The Roots of *Atractylodes macrocephala* koidzumi enhanced glucose and lipid metabolism in C2C12 Myotubes via mitochondrial regulation. *Evid. Based Complement. Alternat. Med.* 2015:643654.

Tan, S. J., Li, N., Zhou, F., Dong, Q. T., Zhang, X. D., Chen, B. C., et al. (2014). Ginsenoside Rb1 improves energy metabolism in the skeletal muscle of an animal model of postoperative fatigue syndrome. *J. Surg. Res.* 191, 344–349. doi: 10.1016/j.jss.2014.04.042

Taylor, J. P., Brown, R. H. Jr., and Cleveland, D. W. (2016). Decoding ALS: from genes to mechanism. *Nature* 539, 197–206. doi: 10.1038/nature20413

Trias, E., King, P. H., Si, Y., Kwon, Y., Varela, V., Ibarburu, S., et al. (2018). Mast cells and neutrophils mediate peripheral motor pathway degeneration in ALS. *JCI Insight.* 3:e123249.

Watanabe, K., Tanaka, M., Yuki, S., Hirai, M., and Yamamoto, Y. (2018). How is edaravone effective against acute ischemic stroke and amyotrophic lateral sclerosis? *J. Clin. Biochem. Nutr.* 62, 20–38. doi: 10.3164/jcbn.17-62

Wong, M., and Martin, L. J. (2010). Skeletal muscle-restricted expression of human SOD1 causes motor neuron degeneration in transgenic mice. *Hum. Mol. Genet.* 19, 2284–2302. doi: 10.1093/hmg/ddq106

Yang, E. J., Jiang, J. H., Lee, S. M., Yang, S. C., Hwang, H. S., Lee, M. S., et al. (2010). Bee venom attenuates neuroinflammatory events and extends survival in amyotrophic lateral sclerosis models. *J. Neuroinflamm.* 7:69. doi: 10.1186/1742-2094-7-69

Yoshino, H., and Kimura, A. (2006). Investigation of the therapeutic effects of edaravone, a free radical scavenger, on amyotrophic lateral sclerosis (Phase II study). *Amyotroph. Lateral Scler.* 7, 241–245.

Yu, X. Q., Xue, C. C., Zhou, Z. W., Li, C. G., Du, Y. M., Liang, J., et al. (2008). In vitro and in vivo neuroprotective effect and mechanisms of glabridin, a major active isoflavan from *Glycyrrhiza glabra* (licorice). *Life Sci.* 82, 68–78. doi: 10.1016/j.lfs.2007.10.019

Zhang, G., Xiong, N., Zhang, Z., Liu, L., Huang, J., Yang, J., et al. (2015). Effectiveness of traditional Chinese medicine as an adjunct therapy for Parkinson's disease: a systematic review and meta-analysis. *PLoS One* 10:e0118498. doi: 10.1371/journal.pone.0118498

Zhou, J., Li, A., Li, X., and Yi, J. (2019). Dysregulated mitochondrial Ca(2+) and ROS signaling in skeletal muscle of ALS mouse model. *Arch. Biochem. Biophys.* 663, 249–258. doi: 10.1016/j.abb.2019.01.024

Conflict of Interest: The authors declare that the research was conducted in the absence of any commercial or financial relationships that could be construed as a potential conflict of interest.

Publisher's Note: All claims expressed in this article are solely those of the authors and do not necessarily represent those of their affiliated organizations, or those of the publisher, the editors and the reviewers. Any product that may be evaluated in this article, or claim that may be made by its manufacturer, is not guaranteed or endorsed by the publisher.

frontiers in Pharmacology

ORIGINAL RESEARCH
published: 10 December 2021
doi: 10.3389/fphar.2021.794933

The Mechanisms of Cucurbitacin E as a Neuroprotective and Memory-Enhancing Agent in a Cerebral Hypoperfusion Rat Model: Attenuation of Oxidative Stress, Inflammation, and Excitotoxicity

Zhiyong Liu[1], *Manish Kumar*[2]*†, *Sushma Devi*[3] *and Atul Kabra*[4]

[1]Henan University of Traditional Chinese Medicine, Zhengzhou, China, [2]Chitkara College of Pharmacy, Chitkara University, Punjab, India, [3]Department of Pharmacy, Guru Nanak Institute of Technology, Ambala, India, [4]University Institute of Pharma Sciences, Chandigarh University, Mohali, India

OPEN ACCESS

Edited by:
Muhammad Ayaz,
University of Malakand, Pakistan

Reviewed by:
Jelena Zivkovic,
Institute for Medicinal Plants Reserach "Dr. Josif Pančić," Serbia
Ajay Singh Kushwah,
Amar Shaheed Baba Ajit Singh Jujhar Singh Memorial College, India
Zia Uddin,
COMSATS University Islamabad, Abbottabad Campus, Pakistan

***Correspondence:**
Manish Kumar
mkpharmacology@gmail.com
manish.kumar@chitkara.edu.in

†ORCID:
Manish Kumar
https://orcid.org/0000-0001-6697-544X

Specialty section:
This article was submitted to Ethnopharmacology, a section of the journal Frontiers in Pharmacology

Received: 14 October 2021
Accepted: 09 November 2021
Published: 10 December 2021

Citation:
Liu Z, Kumar M, Devi S and Kabra A (2021) The Mechanisms of Cucurbitacin E as a Neuroprotective and Memory-Enhancing Agent in a Cerebral Hypoperfusion Rat Model: Attenuation of Oxidative Stress, Inflammation, and Excitotoxicity. Front. Pharmacol. 12:794933. doi: 10.3389/fphar.2021.794933

Impaired cerebral hemodynamic autoregulation, vasoconstriction, and cardiovascular and metabolic dysfunctions cause cerebral hypoperfusion (CH) that triggers pro-oxidative and inflammatory events. The sequences linked to ion-channelopathies and calcium and glutamatergic excitotoxicity mechanisms resulting in widespread brain damage and neurobehavioral deficits, including memory, neurological, and sensorimotor functions. The vasodilatory, anti-inflammatory, and antioxidant activities of cucurbitacin E (CuE) can alleviate CH-induced neurobehavioral impairments. In the present study, the neuroprotective effects of CuE were explored in a rat model of CH. Wistar rats were subjected to permanent bilateral common carotid artery occlusion to induce CH on day 1 and administered CuE (0.25, 0.5 mg/kg) and/or Bay-K8644 (calcium agonist, 0.5 mg/kg) for 28 days. CH caused impairment of neurological, sensorimotor, and memory functions that were ameliorated by CuE. CuE attenuated CH-triggered lipid peroxidation, 8-hydroxy-2′-deoxyguanosine, protein carbonyls, tumor necrosis factor-α, nuclear factor-kappaB, myeloperoxidase activity, inducible nitric oxide synthase, and matrix metalloproteinase-9 levels in brain resulting in a decrease in cell death biomarkers (lactate dehydrogenase and caspase-3). CuE decreased acetylcholinesterase activity, glutamate, and increased γ-aminobutyric acid levels in the brain. An increase in brain antioxidants was observed in CuE-treated rats subjected to CH. CuE has the potential to alleviate pathogenesis of CH and protect neurological, sensorimotor, and memory functions against CH.

Keywords: cerebral hypoperfusion, cucurbitacin E, memory, GABA, bay-K8644, caspase-3, inflammation, working memory

INTRODUCTION

Cerebral hypoperfusion (CH) originates from cardiovascular abnormalities that result in severe neurobehavioral deficits similar to Alzheimer's-type dementia and vascular cognitive impairment and dementia (Dong et al., 2018). A decease in cerebral blood flow (CBF) is typically observed in old age along with other comorbidities that share some major risk factors, such as cardiac disorders (e.g., cardiac arrest), hypertension, atherosclerosis, dyslipidemia, and metabolic diseases (e.g., hyperglycemia, obesity) (Duncombe et al., 2017). The brain is vulnerable to hemodynamic alterations owing to the need of an uninterrupted supply of glucose and oxygen to meet the energy requirements for fulfillment of metabolic demands. However, vascular impairments and deregulation of hemodynamic autoregulatory mechanisms cause hypoperfused states in the brain that give rise to a sequence of events detrimental to brain architecture and functions (Liu and Zhang, 2012; Saxena et al., 2015). At present, the pharmacotherapeutic approaches in patients of CH are limited to symptomatic treatment only, and there is a dearth of some novel therapeutic agents that can modify or even reverse the pathogenesis of CH (Farkas et al., 2002).

Hemodynamic aberrations hamper aerobic respiration and energy supply that results in failure of ion-channel activity and biogenesis of reactive oxygen species in the mitochondria. A pathogenic increase in free radicals not only depletes endogenous antioxidants, but also instigates catastrophic events of oxidative stress and inflammation in the hypoperfused brain (Chen et al., 2011). Ion channelopathy, such as hyperactivation of postsynaptic *N*-methyl D-aspartate receptors (NMDAR), leads to a calcium (Ca^{2+}) influx that initiates proteolytic mechanisms (e.g., calpains) and Ca^{2+}-dependent cell death pathways (e.g., caspase-3). Ca^{2+} plays a vital role in long-term brain damage by increasing free radicals and expression of pro-inflammatory cytokines during brain hypoperfusion (Warner et al., 2004; Daulatzai, 2017). An excessive rise in cytoplasmic Ca^{2+} levels activates the nitric oxide synthase–nitric oxide pathway that fortifies the glutamatergic activation of NMDARs, thereby establishing a vicious cycle of neurodegenerative pathways. Together, free radicals, inflammatory molecules, proteolytic enzymes (e.g., matrix metalloproteinases, myeloperoxidase), and adhesion molecules damage the vascular architecture in the brain, including the blood–brain barrier (BBB) (Wang et al., 2020). These events lead to infiltration of neutrophils and monocytes and activation of macrophages and microglia that further amplify brain damage (Liu and Zhang, 2012). Inhibition of glutamatergic excitatory drive and reestablishment of CBF can alleviate the oxidative and inflammatory insult and protect neurobehavioral functions (Farkas et al., 2002).

Cucurbitacins are steroidal tetracyclic terpenes abundantly found in Cucurbitaceae (e.g., cucumbers, pumpkins, gourds) and several other plant families, such as Scrophulariaceae, Begoniaceae, Primulaceae, Liliaceae, Tropaeolaceae, and Rosaceae (Kaushik et al., 2015). *Cucumis melo* L. and cucurbitacin are Chinese traditional medicines used as antimalarial, emetics, narcotics, and against jaundice (Dhiman et al., 2012; Zhong et al., 2020). Cucurbitacin B and E are the most common and widely studied (Chung et al., 2015). In earlier studies, cucurbitacin showed cytotoxic, antitumor, hepatoprotective, anti-inflammatory, antimicrobial, anthelmintic, cardiovascular, and antidiabetic effects (Dhiman et al., 2012; Chung et al., 2015; Kaushik et al., 2015; Garg et al., 2018; Zhong et al., 2020). Many of the pharmacological activities (e.g., antiproliferative, antiobesity, immunomodulatory, and neuroprotective) of Cucurbitacin E (CuE) are attributed to antioxidant and anti-inflammatory properties (Murtaza et al., 2017; Song et al., 2018; Xie et al., 2020). CuE can modulate several molecular mechanisms (e.g., Janus kinase, signal transducer and activator of transcription, cyclo-oxygenase-2, autophagy, cofilin) that may be exploited for potential benefits in various cerebral disorders (Murtaza et al., 2017; Song et al., 2018). Yuan et al. (2019) showed that pretreatment with cucurbitacin-rich extract of *Cucumis melo* L. inhibited phenylephrine-mediated vasoconstriction, enhanced acetylcholine-mediated vasodilation, and suppressed the angiotensin II-induced increase in systolic blood pressure in mice. Furthermore, anti-inflammatory and antioxidant effects of CuE were observed in carrageenan-induced paw edema and liver damage animal models (Peters et al., 1997; Hussein et al., 2017). Cell culture studies revealed the neuroprotective effects of CuE against 1-methyl-4-phenylpyridinium (MPP^+) induced Parkinson's disease by modulating lysosomal-autophagic mechanisms (Arel-Dubeau et al., 2014). These findings indicate that CuE may have therapeutic value against CH states and improve the behavioral outcomes by improving the blood flow and attenuating oxidative and inflammatory cascades in the brain. The present study investigated the neuroprotective and memory-enhancing effects of CuE in permanent 2-vessel occlusion (2-VO)-induced CH in rats.

MATERIALS AND METHODS

Experimental Subjects

The research protocol was accepted by the Animal Ethics Committee of Henan Hospital of Traditional Chinese Medicine (The Second Affiliated Hospital of Henan University of Chinese Medicine) (Henan, China) *vide* approval reference no. ky20210429001 on April 29, 2021. Wistar rats (7–8 month adults) of male sex (body weight range 220 ± 10 g) were housed under a standard laboratory environment. Each rat was housed individually in polyacrylic cages and nurtured using a regular diet and water with unlimited access. Rats were fasted for 12 h before surgery, but water was provided *ad libitum*. The caregivers were blinded to the treatment groups. The experiments on animals were conducted after 2 weeks of an acclimatization phase. Experiments were performed between 0900 and 1600 h.

Drugs and Chemicals

CuE (mol. weight 556.69, purity >95%) was acquired from Merck (China). Monosodium phosphate (NaH_2PO_4), dipotassium phosphate (K_2HPO_4), sodium cyanide (NaCN),

p-Nitrobluetetrazolium chloride (NBT), ethylenediaminetetraacetic acid (EDTA), riboflavin, hydrogen peroxide (H_2O_2), Folin–Ciocalteu's reagent, formaldehyde, bovine serum albumin (BSA), trichloroacetic acid, *n*-butanol, thiobarbituric acid (TBA), acetic acid, 5,5′-Dithiobis-(2-nitrobenzoic acid) (DTNB), sulfosalicylic acid, dimethyl sulfoxide (DMSO), pyridine, and sodium dodecyl sulphate (SDS) (TCI, Shanghai, China); acetylthiocholine (AcTh) iodide, methanol, acetonitrile (HPLC grade), copper sulfate ($CuSO_4$), 2,4 dinitrophenylhydrazine (DNPH), sodium-potassium tartrate, sodium nitrite ($NaNO_2$), sodium carbonate (Na_2CO_3), sulphanilamide, *N*-1-Napthyl ethylenediamine dihydrochloride, 0.5% hexadecyltrimethylammonium bromide (HETAB), 3,3′,5,5′-tetramethylbenzidine (TMB), N, N′-dimethylformamide, heptanes (Fischer-Scientific); catalase (Cayman Chemicals, Ann Arbor, MI, United States) were used. The standards including amino acids *viz.* glutamate and GABA used were procured from Sigma Chemical Co., St. Louis, MO, United States.

Surgery-CH

The procedure and techniques used in bilateral common carotid arteries occlusion (BCCAo)-induced CH are adopted from previous protocols (Yanpallewar et al., 2005; Bhuvanendran et al., 2019). Atropine sulfate (0.5 mg/kg, *i.p.*) was injected as a preanesthetic treatment. An anesthesia cocktail of ketamine (90 mg/kg) and xylazine (10 mg/kg) was administered through the intraperitoneal (*i.p.*) route in rats. Eye reflex, toe or tail pinch responses were checked to determine the level of general anesthesia. The surgical zone was disinfected using 70% ethanol. A skin incision in the ventral side of the neck (midline) was performed between the sternocleidomastoid and sternohyoid muscles in line with the windpipe (area in the middle of the neck and sternum to reveal the windpipe). Common carotid arteries (both right and left) next to the sternocleidomastoid muscle were isolated vigilantly from the vagosympathetic nerve and adventitial sheath. Bilateral common carotid arteries were permanently double-ligated (*p*-BCCAo) using a sterilized 3–0 silk suture in the CH model. The skin incision was applied with penicillin and 0.5% bupivacaine and then sutured. The first carotid to be ligated, either right or left, was interchanged throughout the experiment (Soria et al., 2013). The temperature of the animals was monitored at regular intervals by a rectal thermometer probe. Body temperature at 37°C ± 0.5°C was maintained during the entire phase using a feedback-adjusted heat-cushion. After sutures, a warm atmosphere (37°C ± 0.5°C) was preserved to avoid hypothermia in animals. Each rat was kept independently in a distinct cage and allowed unhindered access to a semisolid standard diet, and purified water was given. Rats showing reluctance to drinking water postsurgery were given buprenorphine (0.05%, *i.p*) once. Sham rats were exposed to matching surgery without carotid artery ligation.

Experimental Design

CuE was homogenously suspended in a vehicle (0.5% carboxymethylcellulose; CMC) and given in doses 0.25 and 0.5 mg/kg in rats through the oral route (Lu et al., 2017; Murtaza et al., 2017). The rats were dispersed in six groups in a single blind manner by a random distribution technique (n = 12): 1) Sham (S), 2) S + CuE(0.5), 3) CH, 4) CH + CuE(0.25), 5) CH + CuE(0.5), 6) CH + Bay-K8644 + CuE(0.5). Rats were subjected to sham or CH surgery on day 1. CuE was administered for 28 consecutive days after CH or sham procedure on day 1. Bay-K8644 (0.5 mg/kg, *i.p.*, 28 days) (Jackson and Damaj, 2009) was given to rats that were subjected to CuE (0.5 mg/kg) treatment for 28 days and CH on day 1. Animals in sham or CH groups were given the vehicle (0.5% CMC dose volume 5 ml/kg) from days 1–28. The neurological functions and sensorimotor performance were assessed on days 1, 7, 14, 21, and 28. Working memory of rats was evaluated on day 25 using the novel object recognition test (NORT). On days 26 and 27, the animals were exposed to a passive avoidance test. Afterward, whole brain samples were collected for histopathological examination and assessment of biochemical parameters of oxidative stress, such as 8-hydroxy-2′-deoxyguanosine (8-OHdG), thiobarbituric acid reactive substances (TBARS), superoxide dismutase (SOD), catalase, and glutathione (GSH), protein carbonyls, cellular demise *viz.* lactate dehydrogenase (LDH) and caspase-3, acetylcholinesterase (AChE), γ-aminobutyric acid (GABA), glutamate, inducible nitric oxide synthase (iNOS), inflammation such as tumor necrosis factor-α (TNF-α), nuclear factor-kappaB (NF-κB), myeloperoxidase (MPO), and vascular injury such as matrix metalloproteinase 9 (MMP-9).

Evaluation of Neurological Deficits

Abnormal gait, reflexes, and hemiplegia functions were determined by adopting the standard technique of assessing neurological deficits using a modified 12-point neurological scale (mNSS) (**Table 1**).

Sensorimotor Test

The rotarod test was used for determining the balance and coordination aspects of sensorimotor performance in rodents. The rats were trained until they were able to run for more than 60 s on a rod rotating at nine rotations per min (rpm). After the training, each rat was placed on the rod and the rotation speed was enhanced incrementally every 10 s from 6 rpm (initial speed) to 30 rpm (final speed) over the course of 50 s. The fall-off latency (s) over the rotating rod before induction of and after CH was noted.

Evaluation of Working Memory

The assessment of recognition type working memory used discrimination between a familiar and a new article *via* innate probing behavior of rodents in novel object recognition task (NORT) (Ennaceur and Delacour, 1988). An open arena with plywood walls (80 × 40 × 60 cm^3) and solid-wood objects (three similar copies) of three varied shapes (compact cube, cylinder, and pyramid) having a height of 10 cm were used. Experiments were performed in a noise-attenuated place with uniform lighting conditions. Rats were familiarized prior to testing for 3 successive days by permitting search of the vacant arena for 5 min duration.

TABLE 1 | Scoring scale (12-point) for modified neurological severity score test (mNSS) in rats. Each animal was exposed to four different tests (twisting of thorax, forelimb flexion, beam-walk test, and hanging-wire test) and scores added to obtain neurological deficit score (NDS) of an individual animal.

S. No.	Test	Score	Interpretation
1	*Twisting of thorax*	0	No twisting (animal tries to grasp floor)
		1	Wobble to contralateral side (damaged striatum or cortex)
	Each rat was dangled freely by tail (5 s), 25 cm above the floor. Bending of thorax (upward movement of rat toward its tail) was noted	2	Bending upwardly, not touch tail
		3	Bending upwardly, touch tail
2	*Forelimb flexion*	0	Extension of both forepaws towards the ground
		1	Contralateral side flexion of contralateral forepaw with slight flexion
	Rat was suspended by tail and forelimb observed as it reaches floor	2	45° flexion
		3	Distinct 90° flexion
3	*Walk-beam test*	0	Grip normal and no slipping
		1	Grip not firm with irregular slipping
	This method evaluates fore- and hind-limbs motor coordination (limb paralysis). Each rat was placed on the narrow beam (70 cm length × 1.5 cm width) situated at 50 cm height and observed for 15 s	2	Grip completely lost, feet resting on beam
		3	Grip completely lost, feet sagging over beam, immovable
4	*Prehensile traction test*	0	>4 s
		1	≤4 s
	Forelimbs of rat were placed on a nylon rope (70 cm height) with 5 cm thick underneath foam sheet (cutoff period 5 s) and duration of adherence to rope noted	2	≤3 s
		3	≤1 s

In the training trial, two alike objects were situated at indiscriminately designated divergent angles of the arena with a 10 cm gap from the plywood walls. Each animal was positioned in the center of the arena facing at a 90° angle away from the alike objects. Afterward, time expended by the animal to scrutinize the individual objects (z1 and z2) was observed (cutoff period 5 min). In probing behavior, sniffing, touching, or investigating the object within a 2 cm zone was acceptable. After 5 min of intertrial pause, the retention trial was initiated. A new article replaced one of the former articles, and time expended in investigation of each article (z3 and y) by the animal was observed. To decline plausible partiality caused by fondness for specific places or articles, complete amalgamations and settings within the arena were compensated. After every single trial, olfactive signs were circumvented by wiping the apparatus using 20% ethanol. The discrimination index (DI) mirrors the variation in time expended examining the familiar article and the new article (y—z3) that represents the memory. DI was quantified using formula (y—z3)/entire investigation time during the retention trial.

Passive Avoidance (PA) Test

Restriction over the impulsive investigative habit of rodents is used in this inhibitory avoidance test in which the animal adapts to circumvent the aversive stimulus given in the form of a foot shock (1.0 mA for 5 s). The step-through PA instrument is made of twin alike dimensions light–dark compartments (23 × 22 × 23 cm^3) separated by a guillotine gate. The dark box consists of plywood walls, and the light box consists of plexiglass walls having a light source (bulb 60 W). A grid floor arrangement *viz.* 3.1 mm stainless-steel rods placed at a distance 8 mm away from each other made the floor of the dark compartment to issue a scrambled electric shock to rodents. A noise-attenuated place was used to perform the trials. During the training trial (day 26), an individual rat was positioned in the light compartment with the snout contrary to the guillotine gate, which was opened after 10 s, and the rat was permitted to pass into the dark compartment. The time taken to pass into the dark compartment from the light compartment was determined using a digital stopwatch. Afterward, the guillotine gate was shut, and an inevitable foot shock ensued. The animal escaped from the dark compartment after 15 s of termination of shock and placed in its home cage. A retrieval test was performed 24 h post training trial (i.e., on day 27) with an identical practice excepting the foot shock. The step-through latency time (STL) to pass into the dark compartment was noted during acquisition and retrieval trials for the individual rat, giving a 300 s cutoff period (Gimenez De Bejar et al., 2017).

Estimation of Biochemical Parameters

The rats were euthanized by the cervical dislocation method (Sodium pentobarbitone 150 mg/kg). Instantly, the complete brain was harvested and bathed with freezing sterile isotonic normal saline. The brain was homogenized using tissue homogenizer in ice-cold 50 mM sodium-phosphate phosphate buffer (pH 7.40) to prepare 10% w/v brain homogenate. Subsequently, a clear supernatant was obtained by centrifuging the whole brain homogenate for 15 min at 4°C at 12,000 × *g* force. The clear supernatant was separated for evaluation of biochemical parameters.

Lipid Peroxidation

For assessment of thiobarbituric acid reactive substances (TBARS) (Ohkawa et al., 1979) the assay blend (final volume 4 ml) containing 0.10 ml homogenized brain, 1.50 ml TBA (0.8%), 1.50 ml glacial acetic acid (20%, pH 3.50), 0.20 ml SDS (8.10%), and 0.70 ml purified water was boiled at 95°C for 1 h, *n*-butanol/pyridine (5 ml in 15:1 ratio) was added into test tubes, assay blend centrifuged at 4000 × *g* (10 min), and supernatant was

separated. Optical density (O.D.) of the malondialdehyde-thiobarbituric acid (MDA-TBA_2) chromophore was determined at the wavelength (λ_{max} = 532 nm) using a two-beam UV1700 spectrophotometer (Shimadzu, Japan). The molar extinction coefficient (ε) = 1.56×10^5 /M/cm at λ_{max} = 532 nm was used to estimate TBARS expressed as nmol per mg protein.

Glutathione Levels

Glutathione was assessed adopting the technique of Ellman (1959). Briefly, the test blend comprising homogenate supernatant (1.0 ml) and 4% sulfosalicylic acid (1 ml) was centrifuged for 10 min (4°C) at 2000 × *g* force. Subsequently, 2.7 ml sodium-potassium phosphate buffer (50.0 mM, pH 7.80) and 0.20 ml DTNB (0.10 mM, pH 8.0) was mixed with 0.10 ml separated supernatant. Glutathione (μmol GSH per mg protein) was enumerated spectrophotometrically (λ_{max} = 412 nm) by using $\varepsilon = 1.36 \times 10^4$ /M/cm at λ_{max} = 532 nm.

Superoxide Dismutase Activity

The activity of superoxide dismutase (SOD) was appraised by following the technique of Winterbourn et al. (1975). Briefly, the test tubes (final volume 3 ml) containing 0.05 ml supernatant of homogenized whole brain, 0.05 ml riboflavin (0.12 mM), 0.10 ml NBT (1.50 mM), 0.20 ml of 0.10 M EDTA (0.30 mM NaCN), and Na^+/K^+ PO_4^{3-} buffer (67.0 mM, pH 7.81) *q.s.* were illuminated for 13 ± 3 min below a 100 W fluorescent-tube (Bajaj®) and O.D. variability (λ_{max} = 560 nm) noted. The SOD in the sample impedes the reduction of NBT by O_2− and formazan synthesis. SOD activity (μmol NBT reduced per min per mg protein) is quantified using ε (formazan) = 15,000 /M/cm.

Catalase Activity

For estimation of catalase activity, the disparity in O.D. of the analyte (3.0 ml) containing 0.05 ml homogenized brain supernatant, 1.10 ml H_2O_2 (0.02 M) in Na^+/K^+ PO_4^{3-} buffer (pH 7.80, 0.05 M), and 1.85 ml of 0.05 M Na^+/K^+ phosphate buffer (pH 7.0) was noted at λ_{max} = 240 nm (Claiborne, 1985). Catalase activity (μmol H_2O_2 decomposed per min per mg protein of brain) was enumerated by means of ε = 43.6 /M/cm.

Acetylcholinesterase Activity

Acetylcholinesterase (AChE) activity was determined by following the technique of Ellman et al. (1961). Briefly, the test tube volume was made of 0.10 ml acetylthiocholine (AcTh) iodide (1.585 M), 0.10 ml DTNB (0.01 M), 3 ml Na^+/K^+ PO_4^{3-} buffer (0.10 M, pH 8.0), and 0.05 ml supernatant. Variation in O.D. was observed at λ_{max} = 412 nm by employing twin-beam UV-spectrophotometer. The activity of AChE (μmol acetylthiocholine iodide hydrolyzed per min per mg protein) was determined utilizing $\varepsilon = 1.36 \times 10^4$ /M/cm at λ_{max} = 412 nm.

Lactate Dehydrogenase Activity

The lactate dehydrogenase activity (μmol NADH oxidized/min/mg protein) was examined using a technique given by Horecker and Kornberg (1948) using $\varepsilon = 6220\ M^{-1}cm^{-1}$ at λ_{max} = 340 nm. The total reaction mixture (3 ml) contained 1 ml of 0.2 M Tris-HCl buffer (pH 7.4), 0.15 ml of 0.1 M KCl, 0.15 ml of 50 mM sodium pyruvate, 0.20 ml of 2.4 mM NADH and supernatant. A decrease in extinction for 2 min at 25°C was measured, and the result was expressed in micromole NADH oxidized/min/mg protein.

Total Protein

The total protein content (mg per mL of homogenate) was quantified using a typical curve of BSA with a concentration range 0.2–2.4 mg/ml. The test blend was arranged using 0.25 ml homogenate supernatant, Lowry's reagent (5.0 ml), Na^+/K^+ PO_4^{3-} buffer (1.0 ml), and Folin–Ciocalteu reagent (0.50 ml of 1.0 N). O.D. was determined at λ_{max} = 650 nm (Lowry et al., 1951).

Estimation of Myeloperoxidase Activity

A pellet was used for determination of myeloperoxidase (MPO) activity (units per mg protein) used as a biomarker of inflammatory neutrophil extravasation (Grisham et al., 1990). The pellet is homogenized in 10 volumes of 50 mM potassium phosphate buffer (ice cold, pH 6.2) added with 0.5% hexadecyltrimethylammonium bromide (HETAB) and 10 mM EDTA. MPO catalyzes the oxidation of 3,3′,5,5′-tetramethylbenzidine (TMB) by hydrogen peroxide to produce a blue chromophore that has λ_{max} = 655 nm. The above homogenate is mixed with 0.5 ml reaction mixture having 80 mM potassium phosphate buffer (pH 5.4), HETAB (0.5% w/v), and TMB (1.6 mM) added as a stock solution (10 mM) prepared in N, N′-dimethylformamide. The reaction is then heated to 37°C and started with hydrogen peroxide (0.3 mM). Each test tube is incubated for 3 min (37°C). The reaction is ended by sequential addition of catalase (20 μg/ml) and 0.2 M sodium acetate (2 ml, pH 3.0) at 4-min intervals and ice cooled. Centrifugation can be used to eliminate extraneous membranous material that can affect spectrophotometric analysis. The O.D. of each reaction test tube is noted at λ_{max} = 655 nm and subsequently corrected by subtracting the blank value. One unit of activity is the quantity of enzyme existing that produces an alteration in O.D. per minute of 1.0 at 37°C in concluding reaction volume comprising sodium acetate. MPO activity was calculated: MPO activity (U/mg protein) = N/tissue weight with N = 10 × (change in O.D./min)/volume of supernatant taken in final reaction.

Estimation of Protein Carbonyl Content

Brain homogenates were diluted to 750–800 µg/ml of protein in individual samples, and 1 ml of diluted sample was added with 10.1 mM DNPH (0.2 ml) or the same volume of 2 M HCl. The sample was incubated at 25°C for 1 h in a dark environment. Subsequently, 0.6 ml of denaturing buffer (150 mM sodium phosphate buffer, pH 6.8 with 3% SDS), 1.8 ml of heptanes (99.5%), and 1.8 ml of ethanol (99.8%) were added. The sample was vortexed for 40 s and centrifuged at 4000 × *g* force for 15 min. Protein was secluded from the interface and washed twice with 1 ml of ethyl acetate/ethanol 1:1 (v/v). Separated protein was suspended in 1 ml of denaturing buffer and absorbance noted at λ_{max} = 370 nm spectrophotometrically. Protein carbonylation was quantified using ε = 22,000 /M/cm (Reznick and Packer, 1994; Yan et al., 1995).

HPLC-FLD Analysis of Neurotransmitters

The brain was swiftly harvested on frozen ice, weighed, and homogenized using 15 volumes of methanol/water (85:15 v/v). The homogenate was centrifuged (7800 × *g* for 15 min at 4°C) and supernatants detached, filtered by means of a cellulose membrane of pore size 0.22 μm, and then kept at −20°C until derivatization for GABA/glutamate analysis. The filtered supernatant (10 μL) was diluted with deionized water (990 μL). The OPA derivatization technique was used for assessment of GABA and glutamate. Standard (glutamate or GABA) or supernatant (100 μL) was subjected to precolumn derivatization in microcentrifuge tubes (Eppendorf) using OPA solution (22 μL) at room temperature in the dark for 10 min. The OPA solution consisted of methanolic OPA (5 mg/ml), 75 μL borate buffer (pH 9.9), and 5 μL 3-mercaptopropionic acid. The derivatization product (20 μL) was inoculated into the column (C18 column; 5 μm, 4.6 × 250 mm) of HPLC system (Waters) with fluorescence detection (Agilent 1260 Infinity FLD G1321C) coupled with an LC-10 AD pump. The mobile phase used comprised 0.05 M sodium acetate, tetrahydrofuran, and methanol (HPLC grade) (49:1:50 v/v/v) (pH 4.1) and filtered through 0.22 μm and vacuum degassed before disseminated in HPLC at flow rate 0.05–0.1 ml/min. The column temperature was upheld at 23°C–27°C. Compounds were eluted isocratically over a 15-min runtime at a flow rate of 1 ml/min. The fluorescent detector was set at an excitation wavelength of λ_{max} = 337 nm and an emission wavelength of λ_{max} = 454 nm. The concentrations of neurotransmitters were measured by means of external standards and the zone under the peak procedure. The peak zones were determined by injecting serial dilutions of standards. Peak zones (upright axis) versus matching concentrations (flat axis) of individual discrete amino acid were plotted to obtain a linear standard arc and used to quantify the concentrations in samples. Concentration of glutamate and GABA reported as μg/mg of the brain tissue.

Enzyme-Linked Immunosorbent Assay

A double antibody sandwich ELISA method was employed to measure the TNF-α (#KB3145, Krishgen Biosystems), NF-κB (#K11-0,288, KinesisDX, United States), MMP-9 (E-EL-R3021, Elabscience), caspase-3 (#E4592, Biovision), 8-hydroxy-2′-deoxyguanosine (#ADI-EKS-350, Enzo LifeSciences), and iNOS (#E4649, Biovision) levels in the rat brain samples. The assay procedure specified in the instruction brochure provided in the kits was appropriately followed. Briefly, whole brain tissue was homogenized and then centrifuged at 2500 × *g* for 20 min. Supernatant was taken and filled in wells (12 × 8 wells) that were precoated with rat monoclonal antibodies. The plates were incubated at 37°C for 1 h. Biotin-labeled detection antibody followed by streptavidin-horseradish peroxidase were added and plates were covered and again incubated. A bluish coloration was obtained by the addition of chromogenic solution A/B or TMB substrate. The reaction was stopped by adding stop solution, and instantly (within 15 min) O.D. was observed at a wavelength λ_{max} = 450 nm by using an ELISA reader (iMARK, BIORAD). A standard curve of different biomarkers (concentrations standard rat TNF-α 450, 225, 56.25, 28.13, 14.06, 7.03, and 3.51 pg/ml; NF-κB 12, 6, 3, 1.5, and 0.75 ng/ml; MMP-9 7.81, 15.63, 31.25, 62.5, 125, 250, and 500 ng/ml; caspase-3 and iNOS 0.313, 0.625, 1.25, 2.5, 5, 10, and 20 ng/ml, 8-OHdG 0.94, 1.875, 3.75, 7.5, 15, 30, and 60 ng/ml) was plotted to estimate TNF-α (pg/ml), NF-κB (ng/ml), MMP-9 (ng/ml), caspase-3 (ng/ml), iNOS (ng/ml), and 8-OHdG (ng/ml) in the samples.

Brain Histopathology

Animals were deeply anesthetized and intracardially (*via* left ventricle) perfused with 10% neutral buffered formalin solution (10% NBF) by using a gravity fed perfusion setup. The cortex were fixed for 6 days (4°C) in 10% neutral buffered formalin with 0.05% sodium azide (pH 7.0) in a fixative-to-tissue ratio of 10:1. A 70% ethanol was used as storage medium (4°C) for the previously fixed brain tissues. A rotary microtome was used to section out thin slices (5.0 μm) that were stained using hematoxylin and eosin (H&E) dye. Permanent slides were prepared using DPX-resin mounting medium and subsequently coverslipped. These slides were scrutinized using light microscopy at ×40 magnifications. In histomorphometric analysis, cortical neuron densities (per μm^2) were determined by counting viable neurons using ImageJ software (NIH Image 1.61; National Institute of Health; Bethesda, MD).

Statistical Analysis

Data were analyzed by a skilled experimenter blinded to miscellaneous treatments received by diverse clusters of rats. Data from the PA test, NORT, biochemical and histomorphometry parameters were analyzed using one-way ANOVA and Tukey's honestly significant difference (HSD) *post hoc* test. Grubb's test was applied to eradicate likely outliers even though no outliers were detected. To determine the typical distribution of variables, the Kolmogorov–Smirnov test was used. Levene's test was applied to test the homogeneity of variance (HOV). One-way ANOVA was applied to compare the means of normally distributed variables. If the variance was homogeneous ($p > .05$, Levene's test) and the outcomes of one-way ANOVA were substantial ($p < .05$, F-statistic), Tukey's HSD *post hoc* test was used for multiple comparisons. If the variance was unequal ($p < .05$, Levene's test), Welch's ANOVA was used (F′-statistic), and if the matching p was <.05, the Games–Howell technique was used for the *post hoc* analyses. The *post hoc* tests were only applied when ANOVA results were significant ($p < .05$). Box and whisker plots (Tukey) demonstrate mean (+), median (bold horizontal line), quartiles (box), and total range (whisker). Data from mNSS and rotarod were analyzed using two-way ANOVA. When two-way ANOVA generated a significant interaction, then Bonferroni's *post hoc* test was applied. Results of mNSS and rotarod expressed as mean ± standard deviation (S.D.). Statistical significance was considered at $p < .05$.

RESULTS

CuE Attenuated CH-Induced Neurological and Sensorimotor Deficits

Rats exposed to CH on day 1 showed substantial neurological and sensorimotor deficits (days 1, 7, 14, 21, and 28, $p < .001$) relative

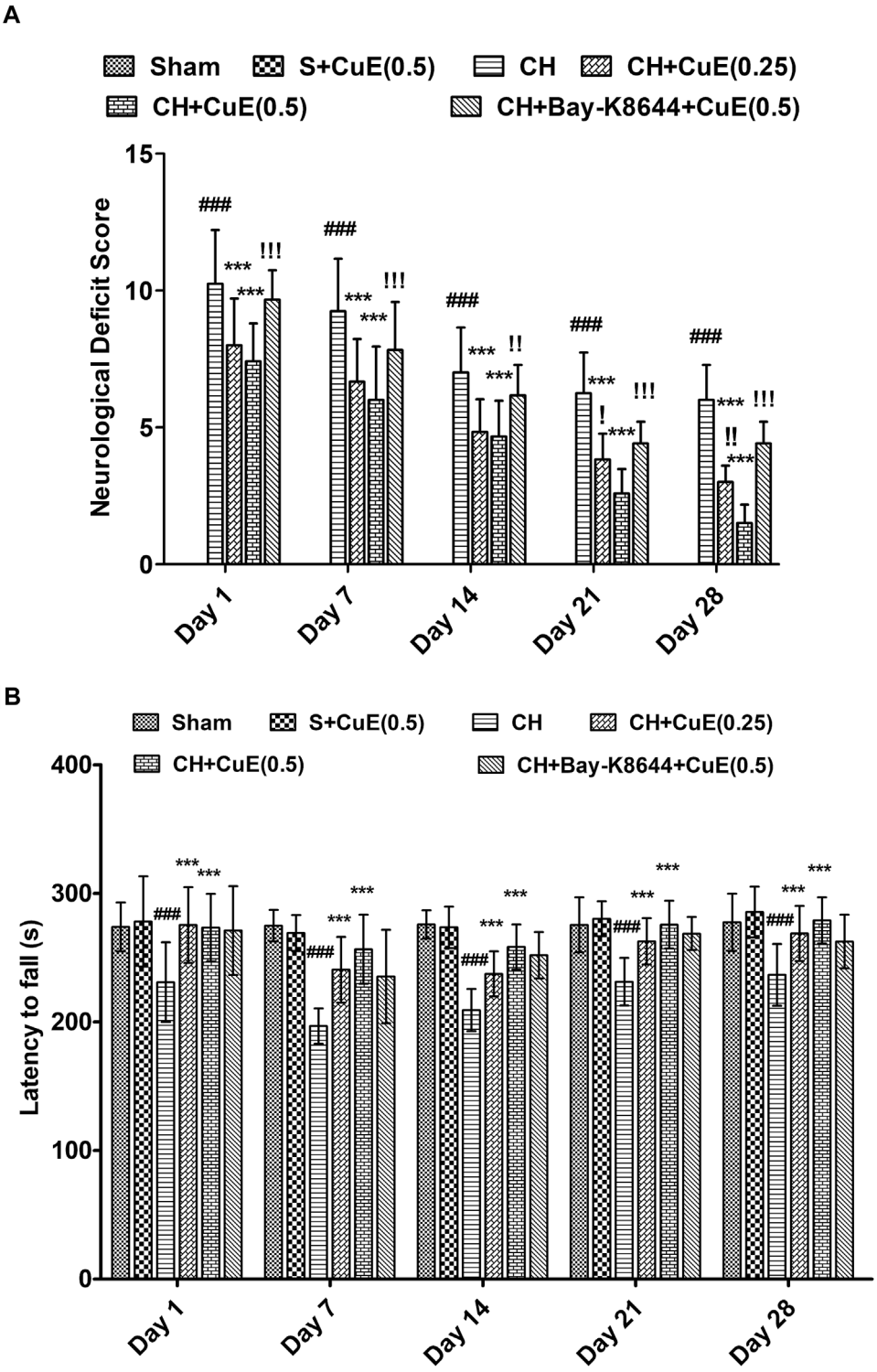

FIGURE 1 | CuE, 0.25 and 0.5 mg/kg, *p.o.*, post-treatment for 28 days attenuated neurological and sensorimotor deficits in rats subjected to CH on day 1. Neurological deficit scores (12-point scale) **(A)** and latency to fall (s) in rotarod test **(B)** evaluated on different days. Bay-K8644 significantly attenuated CuE-induced decrease in mNSS. Data expressed as mean ± S.D. (n = 12). $^{###}$ ($p < .001$) *vs.* Sham (S) group; *** ($p < .001$) *vs.* CH group; ($p < .05$), ($p < .01$), ($p < .001$) *vs.* CH + CuE(0.5) group

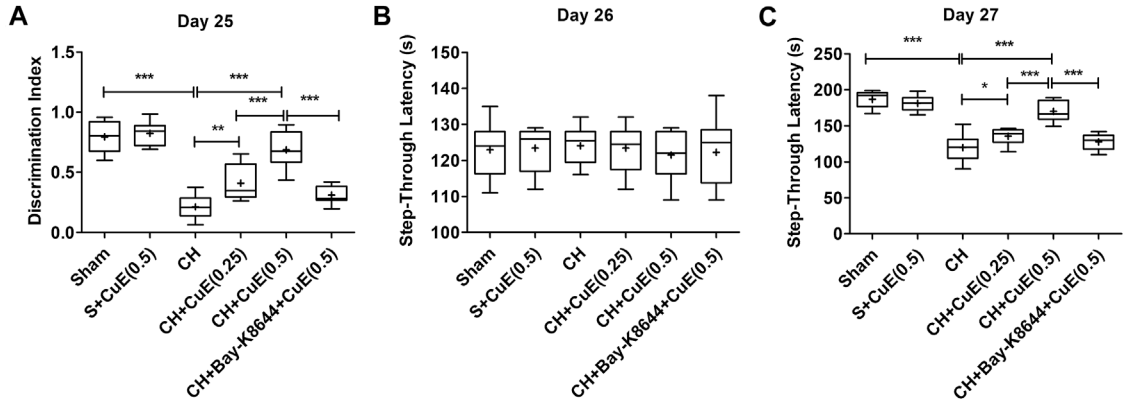

FIGURE 2 | Post-treatment with CuE, 0.25 and 0.5 mg/kg, *p.o.*, decreased CH-induced loss of memory in rats. In a novel object recognition task, animals treated with CuE exhibited increase in discrimination index **(A)**. STL (s) during acquisition trials in PA tests showed no significant difference **(B)**, CuE significantly decreased retention trial STL **(C)**. Bay-K8644 significantly attenuated increase in DI and STL by CuE. Box and whisker plots (Tukey) show mean (+), median (bold horizontal line), quartiles (box), and total range (whisker) (n = 12). *(p < .05), ** (p < .01), *** (p < .001)

to sham rats. CuE (0.25 and 0.5 mg/kg) post-treatment in rats for 28 days attenuated CH-induced neurological deficits (p < .001) [$F_{(20,330)}$ = 12.63, p < .001] (**Figure 1A**) and also improved sensorimotor performance (p < .001) [$F_{(20,330)}$ = 1.41, p < .001] (**Figure 1B**) compared with rats that were given CH and vehicle treatments alone. Interestingly, administration of Bay-K8644 (Ca^{2+} agonist) significantly attenuated CuE (0.5 mg/kg) induced decline in mNSS (day 1 p < .001, day 7 p < .001, day 14 p < .01, day 21 p < .001, and day 28 p < .001) in rats exposed to CH relative to rats that were subjected to CuE (0.5 mg/kg) and CH surgery. Furthermore, CuE (0.5 mg/kg) showed a dose-dependent decrease in mNSS (day 21 p < .05; day 28 p < .01) in comparison with CuE (0.25 mg/kg) in rats subjected to CH.

CuE Attenuated CH-Induced Memory Deficits

Estimation of DI in NORT on day 25 revealed that permanent 2-VO on day 1 debilitated recognition type of working memory in rats. Rats subjected to CH showed a considerable decrease (p < .001) in DI relative to sham [$F_{(5,71)}$ = 60.52, p < .001]. CuE (0.25 and 0.5 mg/kg) post-treatment in rats subjected to CH attenuated the memory deficits (p < .01, p < .001) relative to rats that were exposed to CH and vehicle administrations (**Figure 2A**). In the PA test, STL was evaluated to determine the effects of CuE on memory of rats subjected to CH. In acquisition trials, no significant intergroup variation in day 26 STL of rats was noted in the PA test [$F_{(5,71)}$ = 0.2264, p > .05] (**Figure 2B**). In the retrieval trials (day 27), a significant increase (p < .001) in the STL (**Figure 2C**) was noted in rats subjected to CH in reference to vehicle-treated sham. CuE (0.25 and 0.5 mg/kg) treatment attenuated the CH-triggered decline in the STL (p < .05, p < .001) with respect to the rats that were subjected to CH and vehicle treatments only [$F_{(5,71)}$ = 62.67, p < .001]. CuE (0.5 mg/kg) significantly enhanced the DI (p < .001) and STL (p < .001) in comparison with CuE (0.25 mg/kg) in p-BCCAo operated rats. Bay-K8644 (Ca^{2+} agonist) significantly attenuated (p < .001) CuE (0.5 mg/kg) induced improvement in DI and STL relative to CuE (0.5 mg/kg) in p-BCCAo operated rats.

CuE Decreased Brain Oxido-Nitrosative Stress Against CH

Rats subjected to vehicle treatments and CH displayed a substantial (p < .001) upsurge in the brain lipid peroxidation (TBARS content), 8-OHdG, and protein carbonyls, and decrease of endogenous antioxidants (GSH, SOD, and catalase activities) relative to vehicle-treated sham rats (**Figure 3**). CuE (0.25 and 0.5 mg/kg) post-treatment for 28 days daily in rats exposed to CH attenuated the lipid peroxidation (p < .05, p < .001) [$F_{(5,41)}$ = 45.64, p < .001], 8-OHdG (p < .05, p < .001) [$F_{(5,41)}$ = 59.65, p < .001], and protein carbonyls (p < .01, p < .001) [$F_{(5,41)}$ = 26.94, p < .001], and significantly enhanced the GSH (p < .05, p < .001) [$F_{(5,41)}$ = 79.92, p < .001], SOD (p < .001, p < .001) [$F_{(5,41)}$ = 41.61, p < .001], and catalase (p < .01, p < .001) [$F_{(5,41)}$ = 58.36, p < .001] activities in relation to rats that had undergone CH and vehicle treatments. CuE (0.5 mg/kg) post-treatment for 28 days caused a dose-dependent decline in TBARS (p < .001), 8-OHdG (p < .001), protein carbonyls (p < .05), and increase in GSH (p < .001), SOD (p < .01), and catalase (p < .001) in the brain with respect to CuE (0.25 mg/kg) post-treatment for the same duration in rats operated to p-BCCAo on day 1. Bay-K8644 (Ca^{2+} agonist) significantly attenuated (p < .001) CuE (0.5 mg/kg) induced decline in TBARS, 8-OHdG, protein carbonyls, and increase in antioxidants (GSH, SOD, catalase) relative to CuE (0.5 mg/kg) in p-BCCAo operated rats.

CuE Attenuated CH-Triggered Inflammation in the Brain

Data from ELISA showed a significant rise (p < .001) in inflammatory cytokines (TNF-α, NF-κB, MPO, MMP-9, and iNOS) in the brain of rats in response to CH when juxtaposed with sham rats. In the present study, CuE (0.25 and 0.5 mg/kg)

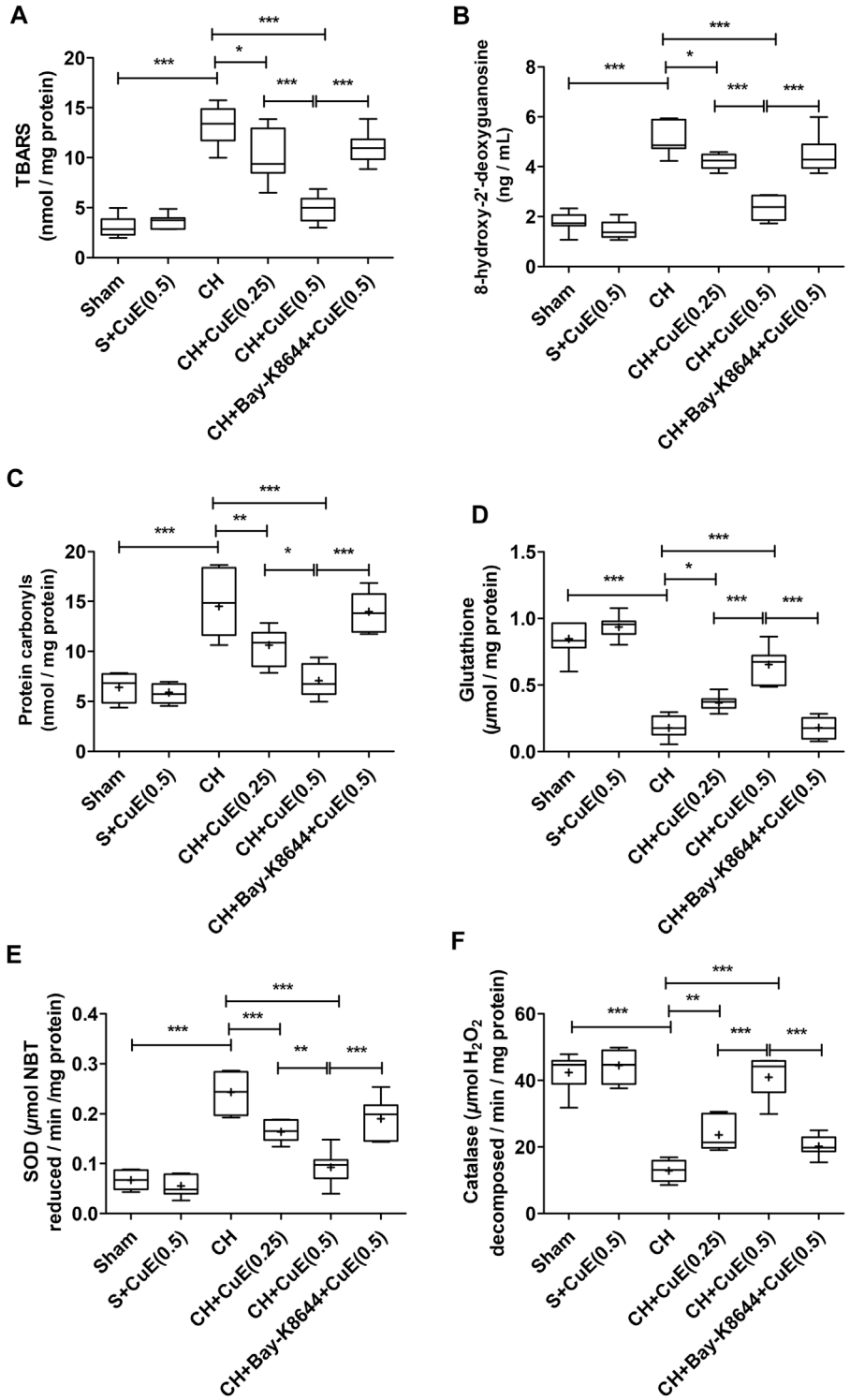

FIGURE 3 | CuE post-treatment (0.25 and 0.5 mg/kg, *p.o.*) for 28 days decreased oxido-nitrosative stress against CH. CuE significantly decreased the brain **(A)** lipid peroxidation (TBARS) level, **(B)** 8-hydroxy-2' -deoxyguanosine (8-OHdG) content, and **(C)** protein carbonyls levels. A significant increase in **(D)** GSH content, **(E)** SOD activity, and **(F)** catalase activity was observed in CuE-treated rats subjected to CH on day 1. Bay-K8644 attenuated antioxidant activity of CuE. Box and whisker plots (Tukey) show mean (+), median (bold horizontal line), quartiles (box), and total range (whisker) ($n = 7$). * ($p < .05$), ** ($p < .01$), *** ($p < .001$)

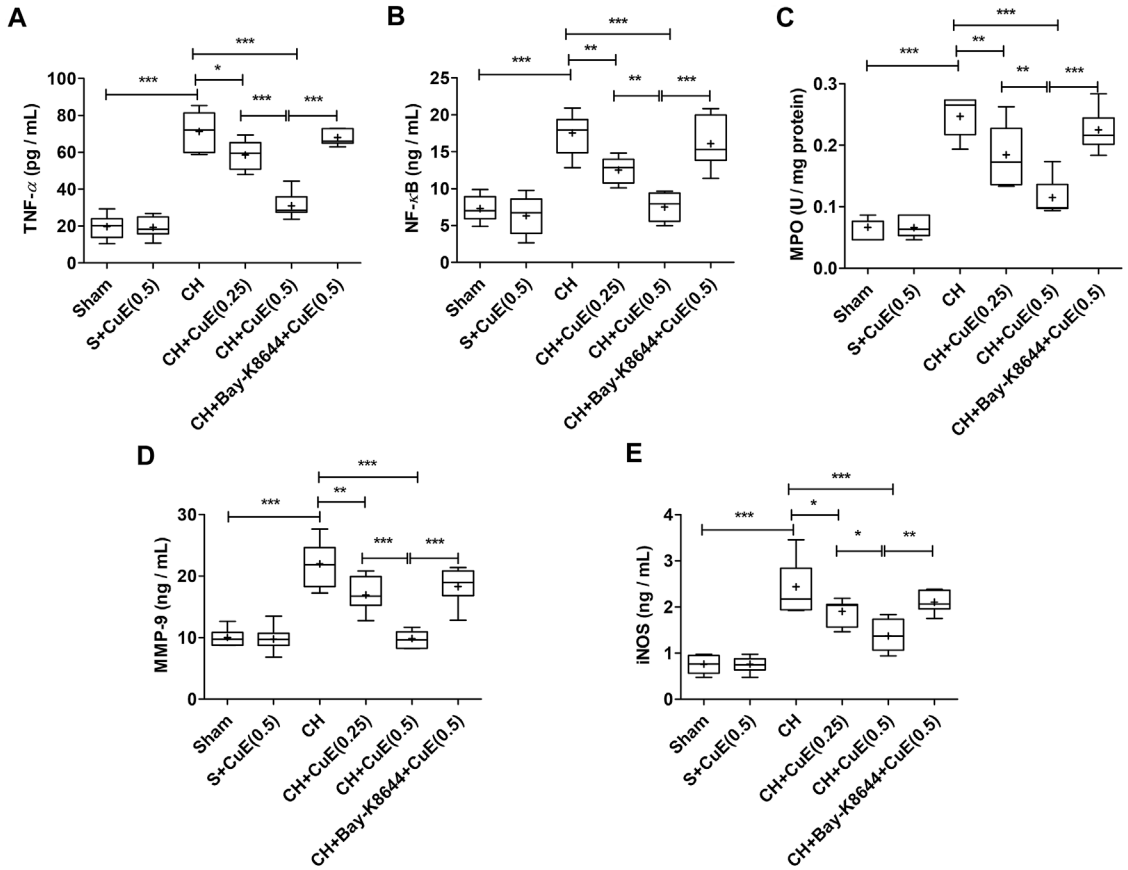

FIGURE 4 | CuE post-treatment (0.25 and 0.5 mg/kg, *p.o.*) for 28 days decreased inflammatory cascade against CH. CuE significantly lowered **(A)** TNF-α, **(B)** NF-κB level, **(C)** MPO activity, **(D)** MMP-9, and **(E)** iNOS in the brain of rats exposed to CH on day 1. Bay-K8644 attenuated anti-inflammatory activity of CuE. Box and whisker plots (Tukey) show mean (+), median (bold horizontal line), quartiles (box), and total range (whisker) (n = 7). * (p < .05), ** (p < .01), *** (p < .001)

post-treatment for 28 successive days attenuated the CH-induced increase in TNF-α (p < .05, p < .001) [$F_{(5,41)}$ = 81.95, p < .001], NF-κB (p < .01, p < .001) [$F_{(5,41)}$ = 27.97, p < .001], MPO (p < .01, p < .001) [$F_{(5,41)}$ = 43.84, p < .001], MMP-9 (p < .01, p < .001) [$F_{(5,41)}$ = 31.52, p < .001], and iNOS (p < .05, p < .001) [$F_{(5,41)}$ = 33.60, p < .001] in the brain of rats with respect to rats that were exposed to CH and vehicle treatments (**Figure 4**). Bay-K8644 (Ca^{2+} agonist) significantly attenuated CuE (0.5 mg/kg) induced decline in TNF-α (p < .001), NF-κB (p < .001), MPO (p < .001), MMP-9 (p < .001), and iNOS (p < .01) relative to CuE (0.5 mg/kg) in p-BCCAo operated rats. CuE (0.5 mg/kg) post-treatment caused substantial reduction in TNF-α (p < .001), NF-κB (p < .01), MPO (p < .01), MMP-9 (p < .001), and iNOS (p < .05) relative to CuE (0.25 mg/kg) in p-BCCAo operated rats.

CuE Attenuated CH-Triggered Cell Death in the Brain

LDH activity and caspase-3 were quantified to assess the extent of cell death in the brain of rats. In the present study, LDH activity and caspase-3 contents were substantially enhanced (p < .001) in the brain of rats that were subjected to CH when juxtaposed with sham rats. CuE (0.25 and 0.5 mg/kg) post-treatment for 28 successive days considerably attenuated (p < .001, p < .001) the LDH activity [$F_{(5,41)}$ = 39.55, p < .001] (**Figure 5A**) and caspase-3 content [$F_{(5,41)}$ = 46.58, p < .001] (**Figure 5B**) in rats subjected to CH with respect to rats that were exposed to CH and vehicle treatments. CuE (0.5 mg/kg) post-treatment caused substantial reduction (p < .01) in caspase-3 levels relative to CuE (0.25 mg/kg) in rats exposed to CH. Bay-K8644 (Ca^{2+} agonist) significantly attenuated (p < .001) CuE (0.5 mg/kg) induced decline in LDH activity and caspase-3 relative to CuE (0.5 mg/kg) in p-BCCAo operated rats.

CuE Attenuated Acetylcholinesterase Activity and Ameliorated Neurotransmitter Levels in the Brain of Rats Subjected to CH

Biochemical analysis revealed a substantial (p < .001) upsurge in brain acetylcholinesterase (AChE) activity in rats exposed to CH and vehicle treatments observed with respect to vehicle-treated sham rats. In HPLC-FLD chromatograms (**Figure 6**), we detected a significant increase in glutamate levels and decline in GABA levels in rats exposed to CH and vehicle treatments observed with

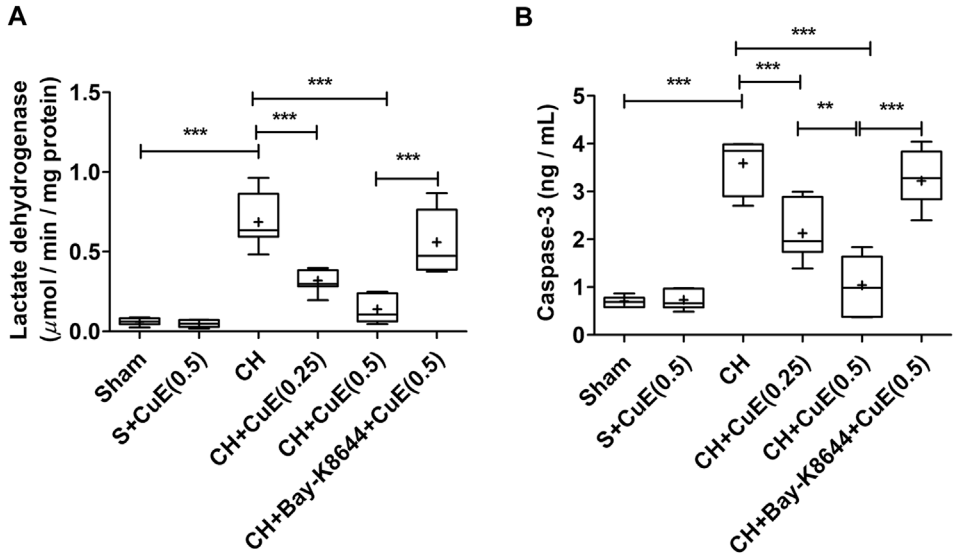

FIGURE 5 | CuE post-treatment (0.25 and 0.5 mg/kg, *p.o.*) for 28 days attenuated cell death against CH. CuE significantly lowered **(A)** LDH activity and **(B)** caspase-3 levels in the brain of rats exposed to CH on day 1. Bay-K8644 attenuated pro-survival effects of CuE. Box and whisker plots (Tukey) show mean (+), median (bold horizontal line), quartiles (box), and total range (whisker) (n = 7). * (p < .05), ** (p < .01), *** (p < .001)

respect to vehicle-treated sham rats. Post-treatment with CuE (0.25 and 0.5 mg/kg) for 28 successive days diminished the AChE activity (p < .001, p < .001) [$F_{(5,41)}$ = 44.51, p < .001] (**Figure 7A**), glutamate levels (p < .05, p < .001) [$F_{(5,41)}$ = 90.03, p < .001] (**Figure 7B**), and enhanced the GABA levels (p < .05, p < .01) [$F_{(5,41)}$ = 32.52, p < .001] (**Figure 7C**) in the brain of rats subjected to CH in comparison to rats that were exposed to CH and vehicle treatments only. CuE (0.5 mg/kg) post-treatment caused substantial reduction in AChE activity (p < .01), glutamate level (p < .001), and enhanced GABA content (p < .05) relative to CuE (0.25 mg/kg) in rats exposed to CH. Bay-K8644 (Ca^{2+} agonist) significantly attenuated CuE (0.5 mg/kg) induced decline in AChE activity (p < .001), glutamate level (p < .001), and increase in GABA (p < .01) relative to CuE (0.5 mg/kg) in p-BCCAo operated rats.

CuE Attenuated CH-Triggered Neurodegenerative Changes

In histopathological examination using H&E stain, rats subjected to permanent BCCAo exhibited neurodegenerative deviations highlighted by blebbing of the plasma membrane (b), swelling (s), and pyknosis (p) in the cortex areas of the brain. Sham rats displayed no signs of neurodegeneration. Administration of rats with CuE (0.25 and 0.5 mg/kg) attenuated CH-induced neuropathological changes in plasma membrane and genetic material (**Figure 8**). Bay-K8644 was found to enhance the neurodegenerative signs in the brain of rats subjected to CuE (0.5 mg/kg) treatment and CH. CH significantly reduced (p < .001) the cortical neuron density relative to sham. Viable neuron density was significantly increased by CuE (0.25 and 0.5 mg/kg) in the cortex (p < .05; p < .001) [$F_{(5,29)}$ = 23.21, p < .001] that were subjected to CH. CuE (0.5 mg/kg) caused substantial increase in cortical neuron density (p < .05) relative to CuE (0.25 mg/kg) in p-BCCAo operated rats. Bay-K8644 (Ca^{2+} agonist) significantly attenuated CuE (0.5 mg/kg) induced protection of cortical neurons (p < .001) relative to CuE (0.5 mg/kg) in rats subjected to CH.

DISCUSSION

Several risk factors (e.g., age, cardiovascular disorders, metabolic disorders) and mechanisms related to vascular and hemodynamic alterations underlie the pathogenesis of CH and related disorders, such as dementia (Dong et al., 2018). Uninterrupted CBF is indispensable in the brain owing to glucose dependence, high metabolic rate, and energy recoupment *via* mitochondrial aerobic respiration (Duncombe et al., 2017). An inequality in the demand/supply relation of nutrients and oxygen to the brain owing to hemodynamic turbulences unfavorably affects the mitochondrial electron transport chain, oxidative phosphorylation, and cellular energy-homeostasis that accentuates free radicals, glutamate activity, ionic imbalance, recruitment of inflammatory biomolecules, amyloid-β burden, and tauopathy in the brain. Subsequently, electrical inactivity, edema, microangiopathy, and vascular resistance unite to cause irrevocable damage to the brain leading to extensive neurobehavioral discrepancies (Dong et al., 2018). Findings from prior studies suggest that cucurbitacins, particularly CuE, modulate diverse molecular targets and pathways that may protect against hypoperfusion states (Murtaza et al., 2017; Song et al., 2018; Xie et al., 2020). Although a few studies indicate promising effects of CuE in neurodegenerative disorders (Arel-Dubeau et al., 2014), nevertheless, the potential of CuE against perfusion defects has received very little emphasis so far.

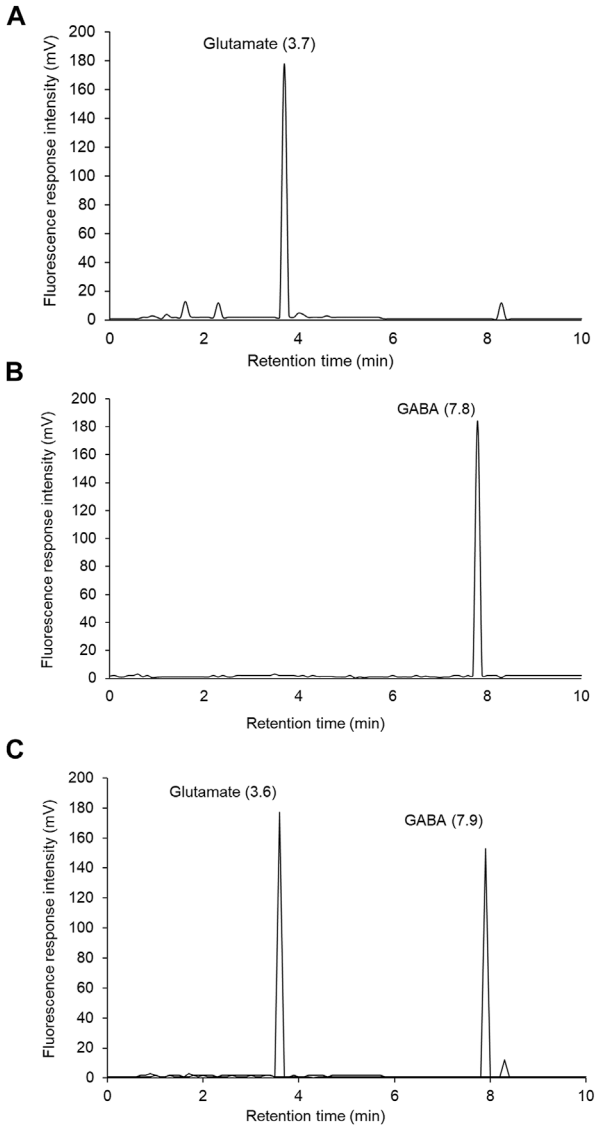

FIGURE 6 | Representative HPLC-FLD chromatograms of glutamate and GABA OPA derivatives: **(A)** glutamate standard solution (0.75 μg), **(B)** GABA standard solution (0.1 μg), **(C)** brain sample showing glutamate and GABA peaks.

Free radicals instigate endothelial damage and infiltration of leucocytes (neutrophils) *via* cellular lipid and protein modifications (Saxena et al., 2015). Free radicals readily react with polyunsaturated fatty acids that generate extremely reactive aldehydes (e.g., malondialdehyde, 4-hydroxy 2-nonenal, acrolein), which further modify proteins (Schiff base or Michael addition) and lipoproteins (e.g., low-density lipoproteins) (Chen et al., 2011). Malondialdehydes defunctionalize the autophagic process, form toxic adducts such as advanced lipid peroxidation end products (ALEs) (e.g., malondialdehyde-methylglyoxal), and react with genetic material (Liu et al., 2017). Under the hypoperfusion state, activation of iNOS culminates in nitrosative stress that leads to protein carbonylation and nitrosylation by peroxynitrites. Excess nitric oxide can cause irreversible cell injury, necrosis, and microvascular abnormalities by attenuating complex I and II activity in the mitochondrial electron transport chain, damage to DNA, and instigation of poly(ADP-ribose) polymerase (Daulatzai, 2017). In this study, CH caused increases in brain lipid peroxidation and DNA damage marked by increase in TBARS and 8-OHdG, which were substantially reduced by CuE post-treatment in rats. Hyperactivation of iNOS resulted in a disproportionate rise in protein carbonyls in rat brains exposed to CH. The present findings indicate that CuE treatment for 28 days daily alleviated the accumulation of protein carbonyls in the brain by decreasing the iNOS hyperactivity in rats against CH. Although antioxidants present in the brain scavenge the free radicals and detoxify dysfunctional proteins, however, under extreme oxidative stress, depletion of antioxidants severely hampers the defense mechanisms against CH. Experiments on transgenic animal models indicate that endogenous antioxidants, such as SOD and catalase, protect the brain against CH (Warner et al., 2004). Oral administration of CuE for 28 days increased the endogenous antioxidants (GSH, SOD, and catalase) in the brain of rats that were previously exposed to CH on day 1.

Hemodynamic aberrations damage the brain capillary network (e.g., BBB) by instigating unsolicited proteins (e.g., MPO and matrix metalloproteinases), cytokines (e.g., TNF-α), inflammatory transcription factor (e.g., NF-κB), and reactive oxygen species (Wang et al., 2020), which, in turn, paves the way for invasion of neurotoxins, monocytes, neutrophils, and chemotactic factors in the brain parenchyma. TNF-α triggers caspase-associated apoptotic cell death and excitotoxic-nitric oxide pathway-mediated necrotic cell death. It augments transcription activity of NF-κB that enhances expression of interleukins, matrix metalloproteinases, MPO, C-reactive protein, cell adhesion molecules, cyclo-oxygenase-2, and iNOS (Liu et al., 2017; Duncan et al., 2020). MPO in neutrophils, macrophages, and neurons promote oxidative stress and inflammation by catalyzing the production of hypochlorous acid (Chen et al., 2020). Activation of MMP-9 degrades the capillary vasculature (basal lamina) including BBB integrity (Vafadari et al., 2016). In the current study, CH increased TNF-α level, NF-κB, MPO activity, and vascular injury biomarker MMP-9 in the brain of rats over a 28-day period. CuE post-treatment for 28 days significantly attenuated the TNF-α level, NF-κB, MPO activity, and MMP-9 in the brain of rats subjected to CH. In this study, the biomarkers of necrotic cell death (LDH) and apoptotic cell death (caspase-3) were measured in the brain of rats. A significant increase in brain LDH activity and caspase-3 expression in rats subjected to CH indicated coparticipation of necrotic and apoptotic cell death mechanisms. The histopathological analysis well supported the biochemical findings. CH caused significant neurodegenerative changes marked by pyknosis, swelling, and blebbing of membranes in the cortical regions. However, CuE post-treatment for 28 days attenuated cell death and neurodegenerative changes in the CH rat model. Forebrain regions (e.g., cerebrum particularly temporal and parietal

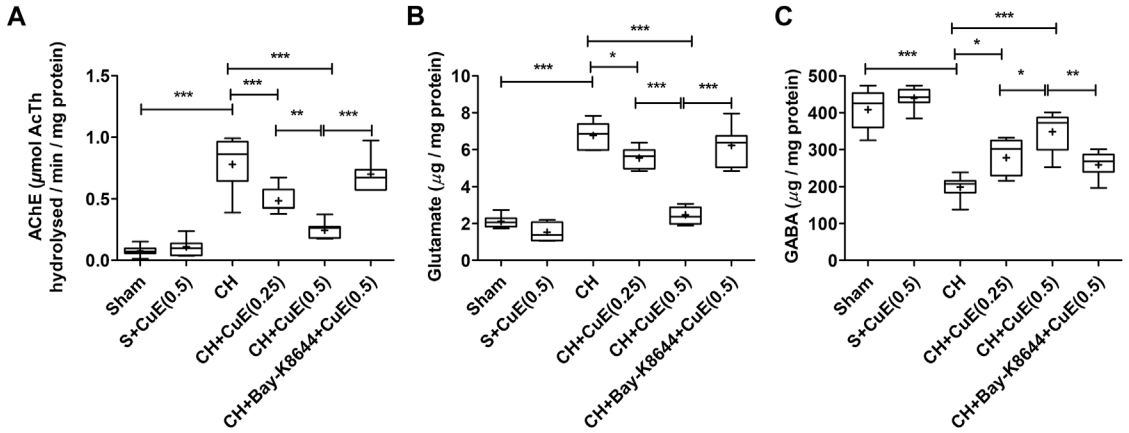

FIGURE 7 | CuE post-treatment (0.25 and 0.5 mg/kg, *p.o.*) for 28 days decreased AChE activity and ameliorated neurotransmitter levels against CH. CuE significantly lowered **(A)** AChE activity, **(B)** glutamate levels, and enhanced **(C)** γ-aminobutyric acid (GABA) level in the brain of rats exposed to CH on day 1. Bay-K8644 attenuated amelioration of neurotransmitters by CuE. Box and whisker plots (Tukey) show mean (+), median (bold horizontal line), quartiles (box), and total range (whisker) (n = 7). * (p < .05), ** (p < .01), *** (p < .001)

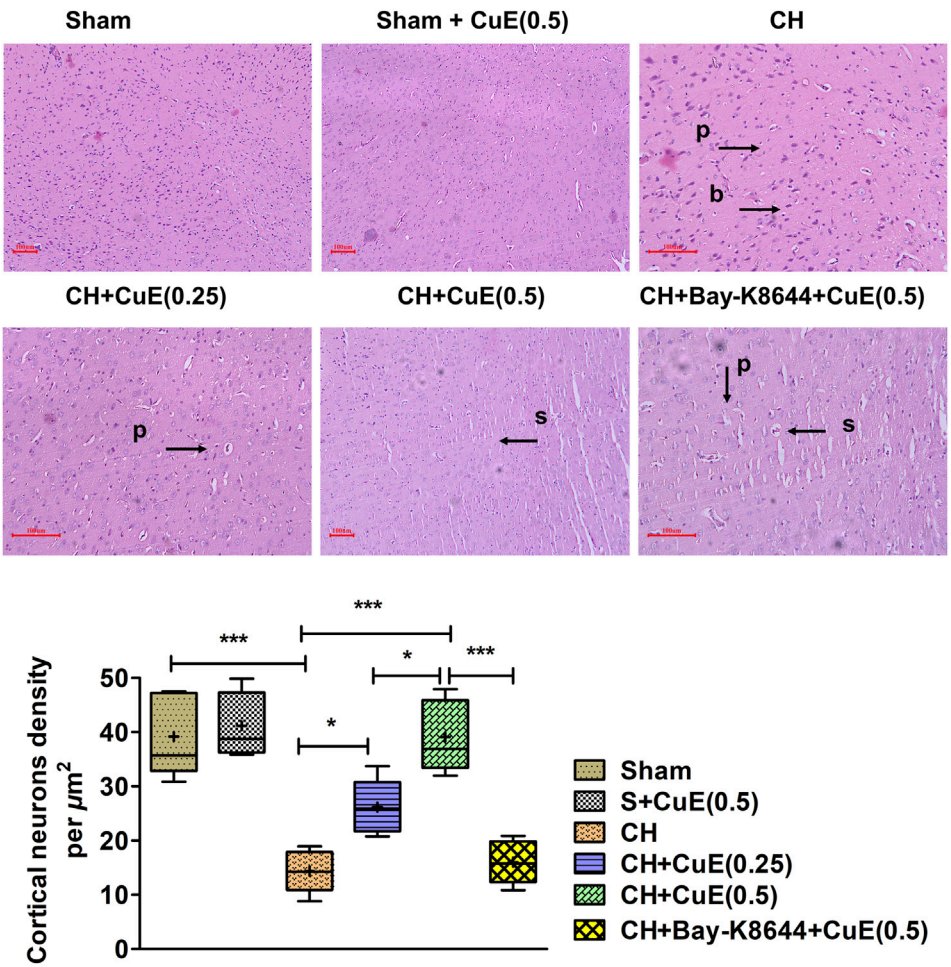

FIGURE 8 | CuE, 0.25 and 0.5 mg/kg, *p.o.*, attenuated CH triggered neurodegenerative changes in the cortical regions (n = 5) (H & E stain, × 40, scale 100 μm). Pyknosis (p), bulging of plasma membrane (b), and swelling (s) were observed. Histomorphometric determinations indicate cortical neuron density per μm^2. Box and whisker plots (Tukey) show mean (+), median (bold horizontal line), quartiles (box), and total range (whisker) (n = 5). *p < .05, **p < .01, ***p < .001

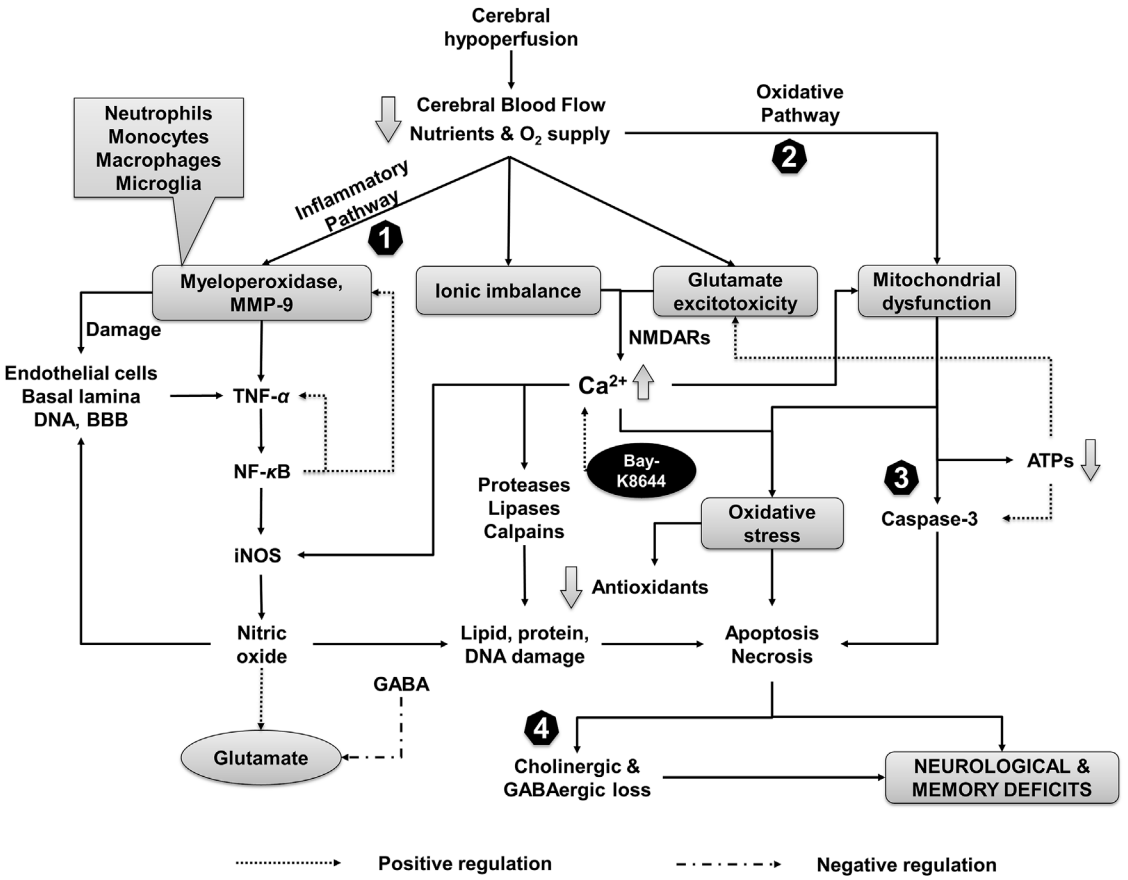

FIGURE 9 | Events associated with CH injury and putative neuroprotective mechanism of CuE. Inflammation, oxidative stress, and ion influx are the primary events associated with reduced CBF followed by derangement of neurotransmitters. CH recruit MMP-9 and myeloperoxidase leading to sequential activation of TNF-α, NF-κB, and iNOS. CH-induced formation of reactive oxygen species and mitochondrial dysfunction leads to decline of endogenous antioxidants and damage to biomolecules (e.g., lipids, proteins, genetic material). A decrease in adenosine triphosphates (ATPs) further potentiates the glutamate toxicity and activates apoptotic and necrotic pathways of cell death through caspases in the brain. Ionic imbalance and glutamate excess increase the intracellular calcium (Ca^{2+}) levels that aggravates oxidative stress and activate proteases, lipases (e.g., phospholipase A_2), and Ca^{2+} dependent calpains. Reduction in GABAergic transmission in response to CH paves the way for undeterred glutamate excitotoxicity. CuE attenuates inflammatory cascade (1) and free radicals (2) that protect brain against proteolytic damage (3). Improvement in GABA levels by CuE antagonizes the CH triggered glutamate toxicity (4) and enhances the cholinergic function in the brain against CH leading to neuroprotective effects and improvement in cognitive functions. Bay-K8644 (Ca^{2+} agonist) can enhance the Ca^{2+}-induced catastrophe and antagonize the brain protective effects of CuE in CH rat model.

cortices) form the major seat of cognitive functions and processing of inputs and evidence indicate that these regions are most adversely affected during CH (Farkas et al., 2007). Histomorphometry analysis showed that CuE protected the neurons against CH in the cortical portion of the brain of rats marked by a substantial higher number of viable neurons. Bay-K8644 attenuated the prosurvival function of CuE in CH rat model.

Acetylcholine regulates cognitive functions by modulating synaptic plasticity, long-term potentiation, acquisition, encoding, consolidation, reconsolidation, extinction, and retrieval of memory (Resende and Adhikari, 2009). Acetylcholine plays an important part in regulating biological rhythms (e.g., wakefulness, sleep), stress response, inflammatory response, and vascular tone (Jin et al., 2015). In line with earlier findings (Sun et al., 2020), in this study, CH increased the AChE activity that might adversely affect the acetylcholine levels in the brain. Following the energy depletion and ionic imbalance, accumulation of glutamate in synapse depolarizes the postsynaptic membrane, triggers Ca^{2+} influx and nitric oxide release that establishes a vicious cycle of Ca^{2+}-dependent catabolic (proteolytic) mechanisms (Belov Kirdajova et al., 2020). These excitotoxic pathways perpetuate inflammatory and oxidative mechanisms during CH. Recently, GABA is proposed to counter the glutamatergic excitatory drive in the brain. GABA can impart neuroprotective, antioxidant, antiapoptotic, and anti-inflammatory effects through improvement in CBF, glucose utilization, and energy production (Chen et al., 2019; Ngo and Vo, 2019). Because hyperpolarization of neurons decreases the metabolic rate, free radicals, and inflammatory cascade, analogous to hypothermia (Neumann et al., 2013; Lee et al., 2018), GABA refereed hyperpolarization of neurons is a documented neuroprotective tactic used in brain

ailments involving excitotoxic pathogenesis. In this study, CuE post-treatment in rats attenuated the brain AChE activity and glutamate level and enhanced the GABA levels in the CH model.

In the current study, neurological scores, sensorimotor performance, and memory functions were evaluated in all the animals. Results displayed that CH severely hampered the neurological and motor functions over a 4-week period. CuE post-treatment improved the neurological and sensorimotor functions evident by a decline in mNSS and increase in latency to fall from the rotating rod, respectively, in the CH rat model. Earlier findings also substantiate CH-triggered decrease in neurological and motor performance and damage to memory skills in animals (Yanpallewar et al., 2005; Bhuvanendran et al., 2019). In the present study, oral administration of CuE significantly increased DI and STL, which highlighted enhancement in the memory performance of rats exposed to CH on day 1. Furthermore, we detected a dose-dependent betterment of biochemical parameters and neurobehavioral activity in rats by CuE. Administration of CuE (0.5 mg/kg) exhibited a substantial improvement in the parameters of oxidative stress, inflammation, cell death, and neurotransmitters in comparison to CuE (0.25 mg/kg) in rats against CH. Commensurate with biochemical findings, CuE (0.5 mg/kg) enhanced the cognitive functions relative to CuE (0.25 mg/kg) in rats against CH.

Interestingly the current findings highlight that Bay-K8644 (Ca^{2+} agonist) attenuates the antioxidative and anti-inflammatory effects of CuE (0.5 mg/kg) in a rat model of CH that promoted brain damage evident by an increase in caspase-3. Glutamate induced *N*-methyl D-aspartate receptor hyperactivation is known to enhance the cytoplasmic Ca^{2+} levels that trigger catastrophic cell death pathways. Furthermore, Ca^{2+}-induced excessive nitric oxide biogenesis perpetuates this vicious cycle, resulting in profound brain damage. In the present study, administration of Bay-K8644 revealed a pathogenic increase in iNOS, protein carbonyls, and glutamate levels in the rat CH model that substantiated involvement of Ca^{2+} pathways in cerebroprotective effects of CuE in the current prototype. Bay-K8644 significantly attenuated the CuE induced decrease in AChE activity and rise in GABA content in rats subjected to CH. Behavioral data also reflected a decrease in neurological, sensorimotor, and cognitive performance of rats treated with Bay-K8644. Taken together, it might be possible that CuE exerted the antioxidative, anti-inflammatory, neuroprotective, and memory-enhancing effects *via* suppression of Ca^{2+}-linked pathways in the CH state (**Figure 9**).

CONCLUSION

The findings of the present study suggest that CuE possess therapeutic worth against CH. CuE mitigated neurobehavioral discrepancies against CH by antioxidant, anti-inflammatory, and neuroprotective effects. CuE can ameliorate brain cholinergic neurotransmission by declining AChE activity and has the potential to alleviate glutamate excitatory drive *via* GABAergic activity that may resurrect neurobehavioral functions in hypoperfusion states. The current research findings specify that CuE has potential against CH-associated cerebral disorders.

DATA AVAILABILITY STATEMENT

The raw data supporting the conclusion of this article will be made available by the authors, without undue reservation.

ETHICS STATEMENT

The animal study was reviewed and approved by Animal Ethics Committee of Henan Hospital of Traditional Chinese Medicine (The Second Affiliated Hospital of Henan University of Chinese Medicine) (Henan, China) vide approval reference no. ky20210429001 on April 29, 2021.

AUTHOR CONTRIBUTIONS

Conceptualization and design of research: MK and ZL; Methodology: MK and ZL; Validation: AK and SD; Formal Analysis: SD; Investigation: ZL; Resources: ZL and MK; Data Curation: AK and ZL; Writing Original Draft Preparation: MK and ZL; Writing, review, & editing: MK and ZL; Supervision: MK; Project Administration: ZL. All authors approved the final article for publication.

FUNDING

This research was funded by Special Research Project of Traditional Chinese Medicine in Henan Province (Grant No. 20-21ZY1024).

REFERENCES

Arel-Dubeau, A. M., Longpré, F., Bournival, J., Tremblay, C., Demers-Lamarche, J., Haskova, P., et al. (2014). Cucurbitacin E Has Neuroprotective Properties and Autophagic Modulating Activities on Dopaminergic Neurons. *Oxid. Med. Cel. Longev.* 2014, 425496. doi:10.1155/2014/425496

Belov Kirdajova, D., Kriska, J., Tureckova, J., and Anderova, M. (2020). Ischemia-triggered Glutamate Excitotoxicity from the Perspective of Glial Cells. *Front. Cel. Neurosci.* 14, 51. doi:10.3389/fncel.2020.00051

Bhuvanendran, S., Bakar, S. N. S., Kumari, Y., Othman, I., Shaikh, M. F., and Hassan, Z. (2019). Embelin Improves the Spatial Memory and Hippocampal Long-Term Potentiation in a Rat Model of Chronic Cerebral Hypoperfusion. *Sci. Rep.* 9, 14507–14511. doi:10.1038/s41598-019-50954-y

Chen, C., Zhou, X., He, J., Xie, Z., Xia, S., and Lu, G. (2019). The Roles of GABA in Ischemia-Reperfusion Injury in the central Nervous System and Peripheral Organs. *Oxid. Med. Cel. Longev.* 2019, 4028394. doi:10.1155/2019/4028394

Chen, H., Yoshioka, H., Kim, G. S., Jung, J. E., Okami, N., Sakata, H., et al. (2011). Oxidative Stress in Ischemic Brain Damage: Mechanisms of Cell Death and Potential Molecular Targets for Neuroprotection. *Antioxid. Redox Signal.* 14, 1505–1517. doi:10.1089/ars.2010.3576

Chen, S., Chen, H., Du, Q., and Shen, J. (2020). Targeting Myeloperoxidase (MPO) Mediated Oxidative Stress and Inflammation for Reducing Brain Ischemia Injury: Potential Application of Natural Compounds. *Front. Physiol.* 11, 433. doi:10.3389/fphys.2020.00433

Chung, S. O., Kim, Y. J., and Park, S. U. (2015). An Updated Review of Cucurbitacins and Their Biological and Pharmacological Activities. *EXCLI J.* 14, 562–566. doi:10.17179/excli2015-283

Claiborne, A. (1985). "Catalase Activity," in *CRC Handbook of Methods for Oxygen Radical Research*. Editor R.A. Greenwald (Boca Raton, FL: CRC Press), 283–284.

Daulatzai, M. A. (2017). Cerebral Hypoperfusion and Glucose Hypometabolism: Key Pathophysiological Modulators Promote Neurodegeneration, Cognitive Impairment, and Alzheimer's Disease. *J. Neurosci. Res.* 95, 943–972. doi:10.1002/jnr.23777

Dhiman, K., Gupta, A., Sharma, D. K., Gill, N. S., and Goyal, A. (2011). A Review on the Medicinally Important Plants of the Family Cucurbitaceae. *Asian J. Clin. Nutr.* 4, 16–26. doi:10.3923/ajcn.2012.16.26

Dong, S., Maniar, S., Manole, M. D., and Sun, D. (2018). Cerebral Hypoperfusion and Other Shared Brain Pathologies in Ischemic Stroke and Alzheimer's Disease. *Transl. Stroke Res.* 9, 238–250. doi:10.1007/s12975-017-0570-2

Duncan, J. W., Younes, S. T., Hildebrandt, E., Ryan, M. J., Granger, J. P., and Drummond, H. A. (2020). Tumor Necrosis Factor-α Impairs Cerebral Blood Flow in Pregnant Rats: Role of Vascular β-epithelial Na+ Channel. *Am. J. Physiol. Heart Circ. Physiol.* 318, H1018–H1027. doi:10.1152/ajpheart.00744.2019

Duncombe, J., Kitamura, A., Hase, Y., Ihara, M., Kalaria, R. N., and Horsburgh, K. (2017). Chronic Cerebral Hypoperfusion: A Key Mechanism Leading to Vascular Cognitive Impairment and Dementia. Closing the Translational gap between Rodent Models and Human Vascular Cognitive Impairment and Dementia. *Clin. Sci. (Lond)* 131 (19), 2451–2468. doi:10.1042/CS20160727

Ellman, G. L., Courtney, K. D., Andres, V., Jr., and Feather-Stone, R. M. (1961). A New and Rapid Colorimetric Determination of Acetylcholinesterase Activity. *Biochem. Pharmacol.* 7, 88–95. doi:10.1016/0006-2952(61)90145-9

Ellman, G. L. (1959). Tissue Sulfhydryl Groups. *Arch. Biochem. Biophys.* 82, 70–77. doi:10.1016/0003-9861(59)90090-6

Ennaceur, A., and Delacour, J. (1988). A New One-Trial Test for Neurobiological Studies of Memory in Rats. 1: Behavioral Data. *Behav. Brain Res.* 31 (1), 47–59. doi:10.1016/0166-4328(88)90157-x

Farkas, E., de Wilde, M. C., Kiliaan, A. J., and Luiten, P. G. (2002). Chronic Cerebral Hypoperfusion-Related Neuropathologic Changes and Compromised Cognitive Status: Window of Treatment. *Drugs Today (Barc)* 38 (5), 365–376. doi:10.1358/dot.2002.38.5.677137

Farkas, E., Luiten, P. G., and Bari, F. (2007). Permanent, Bilateral Common Carotid Artery Occlusion in the Rat: a Model for Chronic Cerebral Hypoperfusion-Related Neurodegenerative Diseases. *Brain Res. Rev.* 54 (1), 162–180. doi:10.1016/j.brainresrev.2007.01.003

Garg, S., Kaul, S. C., and Wadhwa, R. (2018). Cucurbitacin B and Cancer Intervention: Chemistry, Biology and Mechanisms (Review). *Int. J. Oncol.* 52 (1), 19–37. doi:10.3892/ijo.2017.4203

Giménez De Béjar, V., Caballero Bleda, M., Popović, N., and Popović, M. (2017). Verapamil Blocks Scopolamine Enhancement Effect on Memory Consolidation in Passive Avoidance Task in Rats. *Front. Pharmacol.* 8, 566. doi:10.3389/fphar.2017.00566

Grisham, M. B., Benoit, J. N., and Granger, D. N. (1990). Assessment of Leukocyte Involvement during Ischemia and Reperfusion of Intestine. *Methods Enzymol.* 186, 729–742. doi:10.1016/0076-6879(90)86172-r

Horecker, B. L., and Kornberg, A. (1948). The Extinction Coefficients of the Reduced Band of Pyridine Nucleotides. *J. Biol. Chem.* 175, 385–390. doi:10.1016/s0021-9258(18)57268-9

Hussein, M. A., El-Gizawy, H. A., Gobba, N. A. E. K., and Mosaad, Y. O. (2017). Synthesis of Cinnamyl and Caffeoyl Derivatives of Cucurbitacin-Eglycoside Isolated from *Citrullus colocynthis* Fruits and Their Structures Antioxidant and Anti-inflammatory Activities Relationship. *Curr. Pharm. Biotechnol.* 18 (8), 677–693. doi:10.2174/1389201018666171004144615

Jackson, K. J., and Damaj, M. I. (2009). L-type Calcium Channels and Calcium/calmodulin-dependent Kinase II Differentially Mediate Behaviors Associated with Nicotine Withdrawal in Mice. *J. Pharmacol. Exp. Ther.* 330 (1), 152–161. doi:10.1124/jpet.109.151530

Jin, X., Wang, R. H., Wang, H., Long, C. L., and Wang, H. (2015). Brain protection against Ischemic Stroke Using Choline as a New Molecular Bypass Treatment. *Acta Pharmacol. Sin.* 36, 1416–1425. doi:10.1038/aps.2015.104

Kaushik, U., Aeri, V., and Mir, S. R. (2015). Cucurbitacins - an Insight into Medicinal Leads from Nature. *Pharmacogn. Rev.* 9 (17), 12–18. doi:10.4103/0973-7847.156314

Lee, R. H. C., Lee, M. H. H., Wu, C. Y. C., Couto E Silva, A., Possoit, H. E., Hsieh, T. H., et al. (2018). Cerebral Ischemia and Neuroregeneration. *Neural Regen. Res.* 13, 373–385. doi:10.4103/1673-5374.228711

Liu, H., and Zhang, J. (2012). Cerebral Hypoperfusion and Cognitive Impairment: The Pathogenic Role of Vascular Oxidative Stress. *Int. J. Neurosci.* 122, 494–499. doi:10.3109/00207454.2012.686543

Liu, T., Zhang, L., Joo, D., and Sun, S. C. (2017). NF-κB Signaling in Inflammation. *Signal. Transduct. Target. Ther.* 2, 17023. doi:10.1038/sigtrans.2017.23

Lowry, O. H., Rosebrough, N. J., Farr, A. L., and Randall, R. J. (1951). Protein Measurement with the Folin Phenol Reagent. *J. Biol. Chem.* 193, 265–275. doi:10.1016/s0021-9258(19)52451-6

Lu, J., Ding, T., Qin, X., Liu, M., and Wang, X. (2017). *In Vitro* and *In Vivo* Evaluation of Cucurbitacin E on Rat Hepatic CYP2C11 Expression and Activity Using LC-MS/MS. *Sci. China Life Sci.* 60 (2), 215–224. doi:10.1007/s11427-015-4911-7

Murtaza, M., Khan, G., Aftab, M. F., Afridi, S. K., Ghaffar, S., Ahmed, A., et al. (2017). Cucurbitacin E Reduces Obesity and Related Metabolic Dysfunction in Mice by Targeting JAK-STAT5 Signaling Pathway. *Plos One* 12 (6), e0178910. doi:10.1371/journal.pone.0178910

Neumann, J. T., Cohan, C. H., Dave, K. R., Wright, C. B., and Perez-Pinzon, M. A. (2013). Global Cerebral Ischemia: Synaptic and Cognitive Dysfunction. *Curr. Drug Targets* 14, 20–35. doi:10.2174/138945013804806514

Ngo, D. H., and Vo, T. S. (2019). An Updated Review on Pharmaceutical Properties of Gamma-Aminobutyric Acid. *Molecules* 24, 2678. doi:10.3390/molecules24152678

Ohkawa, H., Ohishi, N., and Yagi, K. (1979). Assay for Lipid Peroxides in Animal Tissues by Thiobarbituric Acid Reaction. *Anal. Biochem.* 95, 351–358. doi:10.1016/0003-2697(79)90738-3

Peters, R. R., Farias, M. R., and Ribeiro-do-Valle, R. M. (1997). Anti-inflammatory and Analgesic Effects of Cucurbitacins from *Wilbrandia Ebracteata*. *Planta Med.* 63 (6), 525–528. doi:10.1055/s-2006-957755

Resende, R. R., and Adhikari, A. (2009). Cholinergic Receptor Pathways Involved in Apoptosis, Cell Proliferation and Neuronal Differentiation. *Cell Commun. Signal.* 7, 20. doi:10.1186/1478-811X-7-20

Reznick, A. Z., and Packer, L. (1994). Oxidative Damage to Proteins: Spectrophotometric Method for Carbonyl Assay. *Methods Enzymol.* 233, 357–363. doi:10.1016/s0076-6879(94)33041-7

Saxena, A. K., Abdul-Majeed, S. S., Gurtu, S., and Mohamed, W. M. (2015). Investigation of Redox Status in Chronic Cerebral Hypoperfusion-Induced Neurodegeneration in Rats. *Appl. Transl Genom* 5, 30–32. doi:10.1016/j.atg.2015.05.004

Song, H., Wang, Y., Li, L., Sui, H., Wang, P., and Wang, F. (2018). Cucurbitacin E Inhibits Proliferation and Migration of Intestinal Epithelial Cells via Activating Cofilin. *Front. Physiol.* 9, 1090. doi:10.3389/fphys.2018.01090

Soria, G., Tudela, R., Márquez-Martín, A., Camón, L., Batalle, D., Muñoz-Moreno, E., et al. (2013). The Ins and Outs of the BCCAo Model for Chronic Hypoperfusion: a Multimodal and Longitudinal MRI Approach. *Plos One* 8, e74631. doi:10.1371/journal.pone.0074631

Sun, Y., Zhao, Z., Li, Q., Wang, C., Ge, X., Wang, X., et al. (2020). Dl-3-n-butylphthalide Regulates Cholinergic Dysfunction in Chronic Cerebral Hypoperfusion Rats. *J. Int. Med. Res.* 48, 300060520936177. doi:10.1177/0300060520936177

Vafadari, B., Salamian, A., and Kaczmarek, L. (2016). MMP-9 in Translation: from Molecule to Brain Physiology, Pathology, and Therapy. *J. Neurochem.* 139 (Suppl. 2), 91–114. doi:10.1111/jnc.13415

Wang, X. X., Zhang, B., Xia, R., and Jia, Q. Y. (2020). Inflammation, Apoptosis and Autophagy as Critical Players in Vascular Dementia. *Eur. Rev. Med. Pharmacol. Sci.* 24, 9601–9614. doi:10.26355/eurrev_202009_23048

Warner, D. S., Sheng, H., and Batinić-Haberle, I. (2004). Oxidants, Antioxidants and the Ischemic Brain. *J. Exp. Biol.* 207, 3221–3231. doi:10.1242/jeb.01022

Winterbourn, C. C., Hawkins, R. E., Brian, M., and Carrell, R. W. (1975). The Estimation of Red Cell Superoxide Dismutase Activity. *J. Lab. Clin. Med.* 85, 337–341.

Xie, H., Tuo, X., Zhang, F., Bowen, L., Zhao, W., and Xu, Y. (2020). Dietary Cucurbitacin E Reduces High-Strength Altitude Training Induced Oxidative Stress, Inflammation and Immunosuppression. *Acad. Bras. Cienc.* 92 (4), e20200012. doi:10.1590/0001-3765202020200012

Yan, L. J., Traber, M. G., and Packer, L. (1995). Spectrophotometric Method for Determination of Carbonyls in Oxidatively Modified Apolipoprotein B of Human Low-Density Lipoproteins. *Anal. Biochem.* 228, 349–351. doi:10.1006/abio.1995.1362

Yanpallewar, S., Rai, S., Kumar, M., Chauhan, S., and Acharya, S. B. (2005). Neuroprotective Effect of *Azadirachta indica* on Cerebral post-ischemic Reperfusion and Hypoperfusion in Rats. *Life Sci.* 76, 1325–1338. doi:10.1016/j.lfs.2004.06.029

Yuan, R. Q., Qian, L., Yun, W. J., Cui, X. H., Lv, G. X., Tang, W. Q., et al. (2019). Cucurbitacins Extracted from *Cucumis Melo* L. (CuEC) Exert a Hypotensive Effect via Regulating Vascular Tone. *Hypertens. Res.* 42 (8), 1152–1161. doi:10.1038/s41440-019-0258-y

Zhong, H., Huang, Y., Deng, X., Liu, M., and Luo, W. (2020). Cucurbitacin B Supplementation Reduces Inflammatory Responses and Alveolar Bone Loss via Regulating MPO, COX-2 and RANK/RANKL/OPG Signals in a Rodent Model of Ligature-Induced Periodontitis. *J. King Saud Univ. - Sci.* 32 (3), 1889–1895. doi:10.1016/j.jksus.2020.01.028

Conflict of Interest: The authors declare that the research was conducted in the absence of any commercial or financial relationships that could be construed as a potential conflict of interest.

Publisher's Note: All claims expressed in this article are solely those of the authors and do not necessarily represent those of their affiliated organizations, or those of the publisher, the editors, and the reviewers. Any product that may be evaluated in this article, or claim that may be made by its manufacturer, is not guaranteed or endorsed by the publisher.

frontiers in Pharmacology

ORIGINAL RESEARCH
published: 28 February 2022
doi: 10.3389/fphar.2021.720170

Decoding the Role of Astrocytes in the Entorhinal Cortex in Alzheimer's Disease Using High-Dimensional Single-Nucleus RNA Sequencing Data and Next-Generation Knowledge Discovery Methodologies: Focus on Drugs and Natural Product Remedies for Dementia

Peter Natesan Pushparaj[1,2]*, *Gauthaman Kalamegam*[2], *Khalid Hussain Wali Sait*[3] and *Mahmood Rasool*[1]*

[1]Center of Excellence in Genomic Medicine Research, Department of Medical Laboratory Technology, Faculty of Applied Medical Sciences, King Abdulaziz University, Jeddah, Saudi Arabia, [2]Center for Transdisciplinary Research, Department of Pharmacology, Saveetha Dental College and Hospitals, Saveetha Institute of Medical and Technical Sciences, Chennai, India, [3]Department of Obstetrics and Gynaecology, King Abdulaziz University Hospital, King Abdulaziz University, Jeddah, Saudi Arabia

OPEN ACCESS

Edited by:
Tahir Ali,
University of Calgary, Canada

Reviewed by:
Luc Ver Donck,
Janssen Research and Development, Belgium
Satoshi Saito,
National Cerebral and Cardiovascular Center, Japan

***Correspondence:**
Peter Natesan Pushparaj
peter.n.pushparaj@gmail.com
Mahmood Rasool
mahmoodrasool@yahoo.com

Specialty section:
This article was submitted to Neuropharmacology, a section of the journal Frontiers in Pharmacology

Received: 03 June 2021
Accepted: 10 December 2021
Published: 28 February 2022

Citation:
Pushparaj PN, Kalamegam G, Wali Sait KH and Rasool M (2022) Decoding the Role of Astrocytes in the Entorhinal Cortex in Alzheimer's Disease Using High-Dimensional Single-Nucleus RNA Sequencing Data and Next-Generation Knowledge Discovery Methodologies: Focus on Drugs and Natural Product Remedies for Dementia. Front. Pharmacol. 12:720170. doi: 10.3389/fphar.2021.720170

Introduction: Alzheimer's disease (AD) is a major cause of the development of cognitive decline and dementia. AD and associated dementias (ADRD) are the major contributors to the enormous burden of morbidity and mortality worldwide. To date, there are no robust therapies to alleviate or cure this debilitating disease. Most drug treatments focus on restoring the normal function of neurons and the cells that cause inflammation, such as microglia in the brain. However, the role of astrocytes, the brain's housekeeping cells, in the development of AD and the initiation of dementia is still not well understood.

Objective: To decipher the role of astrocytes in the entorhinal cortex of AD patients using single nuclear RNA sequencing (snRNASeq) datasets from the Single Cell RNA-seq Database for Alzheimer's Disease (scREAD). The datasets were originally derived from astrocytes, isolated from the entorhinal cortex of AD brain and healthy brain to decipher disease-specific signaling pathways as well as drugs and natural products that reverse AD-specific signatures in astrocytes.

Methods: We used snRNASeq datasets from the scREAD database originally derived from astrocytes isolated from the entorhinal cortex of AD and healthy brains from the Gene Expression Omnibus (GEO) (GSE138852 and GSE147528) and analyzed them using next-generation knowledge discovery (NGKD) platforms. scREAD is a user-friendly open-source interface available at https://bmbls.bmi.osumc.edu/scread/that enables more discovery-oriented strategies. snRNASeq data and metadata can also be visualized and downloaded via an interactive web application at adsn.ddnetbio.com. Differentially expressed genes (DEGs) for each snRNASeq dataset were analyzed using iPathwayGuide

to compare and derive disease-specific pathways, gene ontologies, and in silico predictions of drugs and natural products that regulate AD -specific signatures in astrocytes. In addition, DEGs were analyzed using the L1000FWD and L1000CDS2 signature search programming interfaces (APIs) to identify additional drugs and natural products that mimic or reverse AD-specific gene signatures in astrocytes.

Results: We found that PI3K/AKT signaling, Wnt signaling, neuroactive ligand-receptor interaction pathways, neurodegeneration pathways, etc. were significantly impaired in astrocytes from the entorhinal cortex of AD patients. Biological processes such as glutamate receptor signaling pathway, regulation of synapse organization, cell-cell adhesion via plasma membrane adhesion molecules, and chylomicrons were negatively enriched in the astrocytes from the entorhinal cortex of AD patients. Gene sets involved in cellular components such as postsynaptic membrane, synaptic membrane, postsynapse, and synapse part were negatively enriched ($p < 0.01$). Moreover, molecular functions such as glutamate receptor activity, neurotransmitter receptor activity, and extracellular ligand-gated ion channels were negatively regulated in the astrocytes of the entorhinal cortex of AD patients ($p < 0.01$). Moreover, the application of NGKD platforms revealed that antirheumatic drugs, vitamin-E, emetine, narciclasine, cephaeline, trichostatin A, withaferin A, dasatinib, etc. can potentially reverse gene signatures associated with AD.

Conclusions: The present study highlights an innovative approach to use NGKD platforms to find unique disease-associated signaling pathways and specific synthetic drugs and natural products that can potentially reverse AD and ADRD-associated gene signatures.

Keywords: astrocytes, alzheimer's disease and dementia, scREAD, single-nucleus RNA sequencing, in silico tools, anti-rheumatic agents, dasatinib, natural products

1 INTRODUCTION

Alzheimer's disease (AD) is a major cause of the development of cognitive decline and dementia in the elderly (Winblad et al., 2016; Matthews et al., 2019). AD-related dementias (ADRD) contribute to 50-70 percent of dementias worldwide (Winblad et al., 2016). AD and associated dementias (ADRD) are the largest contributors to the burden of morbidity and mortality and higher costs in health care systems worldwide (Hurd et al., 2013). Important risk factors for ADRD include ethnicity, age, and gender. Approximately 6.2 million Americans aged 65 years or older were affected by AD and this number is expected to double to 13.8 million by 2060 in the United States of America (United States) (Claxton et al., 2015; Matthews et al., 2019; Alzheimer's Disease Facts and Figures, 2021). Therefore, ADRD has been declared a health priority worldwide (World Health Organization, 2012). In the United States of America (United States), AD is the sixth leading cause of death in the general population and the fifth leading cause of death in Americans aged 65 years and older. In contrast, reported deaths from other debilitating diseases such as stroke, heart disease, and HIV have declined, while deaths from AD have increased by more than 145% in the U.S. between 2000 and 2019 (Alzheimer's Disease Facts and Figures, 2021).

AD is a neurodegenerative disease of the brain (**Figure 1**), and symptoms such as cognitive decline and language difficulties have slowly developed in AD patients in recent years. It is mostly diagnosed in the older population with an average age of 65 years or more and is referred to as late-onset AD (LOAD) (Gauthaman et al., 2014; Rasool et al., 2018; Rasool et al., 2021). The progressive damage to neurons from the aggregation of amyloid-beta (Ab) protein and tau protein, as well as neuroinflammation in certain parts of the brain, significantly impairs learning, speech, memory, and other cognitive abilities (Gauthaman et al., 2014; Rasool et al., 2018; Rasool et al., 2021). Importantly, the risk of ADRD is significantly increased in AD patients with diabetes mellitus (Gauthaman et al., 2014; Rasool et al., 2018; Rasool et al., 2021). Moreover, the cellular and molecular mechanisms of AD pathology and the role of specific cells in the brain in the development of ADRD are poorly understood (Rasool et al., 2021).

AD and ADRD pathology differ by brain region, cell type, age, and gender (Sala Frigerio et al., 2019; Rasool et al., 2021). Genome-wide association studies (GWAS) using genetic mapping concepts have revealed genes enriched in AD susceptibility loci, and transcriptomics of whole brain tissue using next-generation sequencing (NGS) platforms or microarray applications have shown an increase in microglial

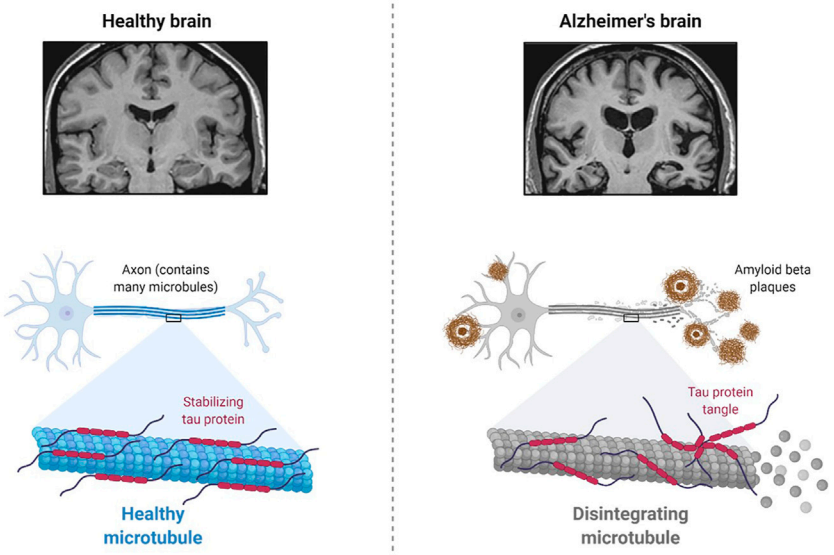

FIGURE 1 | Pathology of Alzheimer's Disease (Created using Biorender.com).

TABLE 1 | Information on the snRNASeq datasets obtained from scREAD database for NGKD analysis (Human)*.

scREAD Data ID	File name	Condition	Brain region	Sex	Braak Stage	GEO ID	Number of cells
AD00201	H-H-Entorhinal Cortex-Male	Control	Entorhinal cortex	Male	NA	GSE138852 (*n* = 6); GSE147528 (*n* = 3)	29,993
AD00202	H-H-Entorhinal Cortex-Female	Control	Entorhinal cortex	Female	NA	GSE138852 (*n* = 2)	1,122
AD00203	H-AD-Entorhinal Cortex-Male_001	Disease	Entorhinal cortex	Male	4–5	GSE138852 (*n* = 6)	3,770
AD00204	H-AD-Entorhinal Cortex-Female_001	Disease	Entorhinal cortex	Female	4	GSE138852 (*n* = 2)	2,303
AD00205	H-AD.Braak 2-Entorhinal cortex -Male_001	Disease	Entorhinal cortex	Male	2	GSE147528 (*n* = 3)	25,492
AD00206	H-AD.Braak 6-Entorhinal cortex -Male_001	Disease	Entorhinal cortex	Male	6	GSE147528 (*n* = 3)	25,537

NA, not applicable; the mean age range of samples from the GSE138852 dataset was 77.6 (range 67.3–91 years) and the mean age range of samples from the GSE147528 dataset was 74.4 (range, 50–91 years).

gene connectivity and impairment of neuronal connectivity in AD (Hitzemann et al., 2014). Although transcriptional network dynamics of mass analysis can provide more information about AD pathogenesis, it does not reveal all the dynamic changes at the cellular and molecular levels that contribute to AD pathology. A detailed understanding of the underlying role of individual cell types in AD patients is therefore essential for the development of new therapeutics to treat dementia.

Recent advances in NGS applications such as single-cell RNA sequencing (scRNA-Seq) have enabled researchers to study and understand the dynamic transcriptomic profile of individual cells in brain tissue or other biological samples. RNA-sequencing of posterior cingulate astrocytes (PC) in AD patients revealed differential expression of mitochondria-related genes, including TRMT61B, FASTKD2, and NDUFA4L2. In addition, immune response genes such as CLU, C3, and CD74 were identified to play a central role in the generation or clearance of amyloid-beta (Sekar et al., 2015). scRNASeq provides a higher resolution of cellular dynamics and a better understanding of individual cells in the tissue microenvironment (Grubman et al., 2019; Jiang et al., 2020; Wu and Zhang, 2020). Similarly, the single nucleus RNA sequencing (snRNA-Seq) technique is used to study frozen samples where dissociation of single cells becomes a problem and affects gene expression patterns. Although AD is one of the

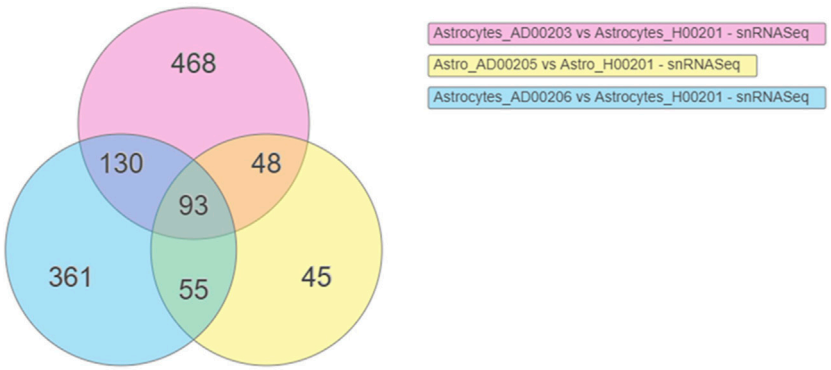

FIGURE 2 | Venn diagram showing the DEGs obtained using the scREAD analysis of snRNASeq data from astrocytes of AD groups (AD00203, AD00205, and AD00206) compared to astrocytes of the healthy control group (AD00201) were 739, 241, and 639 respectively after filtering with a *p*-value cut off of 0.05 and log2 fold change (Log2Fc) of ±0.3. Further analysis of DEGs using iPathwayGuide software showed that 93 DEGs were commonly regulated in all the disease groups.

TABLE 2 | Top 15 pathways ranked based on their associated differentially expressed genes derived from astrocytes based on the comparison AD00203 (disease) vs. AD00201 (control).

pName	countDE	countAll	pv	pAcc	pComb	pORA
Metabolic pathways	66	74	0.646507	—	—	0.57601
Pathways of neurodegeneration- multiple diseases	32	33	0.065081	0.114443	0.065081	0.10487
Pathways in cancer	26	29	0.402445	0.22089	0.402445	0.604649
Protein processing in endoplasmic reticulum	25	25	0.041699	0.133433	0.041699	0.05241
Amyotrophic lateral sclerosis	25	26	0.274844	0.384808	0.274844	0.200526
Salmonella infection	23	24	0.024458	0.015492	0.024458	0.239293
MAPK signaling pathway	22	25	0.023567	0.004998	0.023567	0.710082
Prion disease	22	22	0.248451	0.894553	0.248451	0.075041
Huntington disease	22	22	0.268695	0.996502	0.268695	0.075041
Alzheimer disease	22	23	0.493084	0.69965	0.493084	0.260971
Parkinson disease	21	21	0.194912	0.572214	0.194912	0.084551
PI3K-Akt signaling pathway	20	23	0.022861	0.004498	0.022861	0.761224
Shigellosis	18	18	0.346957	0.888556	0.346957	0.120833
Human papillomavirus infection	18	19	0.66544	0.832584	0.66544	0.364583
Non-alcoholic fatty liver disease	16	16	0.239509	0.416792	0.239509	0.153188

TABLE 3 | Top 15 pathways ranked based on their associated differentially expressed genes derived from astrocytes based on the comparison AD00205 (disease) vs. AD00201 (control).

pName	countDE	countAll	pv	pAcc	pComb	pORA
Metabolic pathways	26	39	0.681028	—	—	0.633724
MAPK signaling pathway	10	12	0.050732	0.044978	0.050732	0.196978
Pathways in cancer	10	14	0.694137	0.646677	0.694137	0.507905
PI3K-Akt signaling pathway	9	11	0.308503	0.358821	0.308503	0.252895
Cell adhesion molecules	8	8	0.103009	—	—	0.042457
Pathways of neurodegeneration—multiple diseases	8	15	0.881576	0.596702	0.881576	0.929541
Alzheimer disease	8	15	0.913995	0.661669	0.913995	0.929541
Morphine addiction	7	7	0.188261	0.729635	0.188261	0.063322
Calcium signaling pathway	7	8	0.307444	0.431284	0.307444	0.209381
Mineral absorption	7	8	0.340951	—	—	0.209381
Axon guidance	7	10	0.878371	0.934533	0.878371	0.587743
Prion disease	7	13	0.923744	0.695152	0.923744	0.914648
Hippo signaling pathway	6	6	0.110827	0.246877	0.110827	0.09431
Purine metabolism	6	6	0.191181	—	—	0.09431
Phospholipase D signaling pathway	6	7	0.398858	0.470265	0.398858	0.280235

TABLE 4 | Top 15 pathways ranked based on their associated differentially expressed genes derived from astrocytes based on the comparison AD00206 (disease) vs. AD00201 (control).

pName	countDE	countAll	pv	pAcc	pComb	pORA
Metabolic pathways	56	65	0.305591	—	—	0.179067
Pathways in cancer	27	33	0.873799	0.96052	0.873799	0.563988
MAPK signaling pathway	22	27	0.588314	0.409295	0.588314	0.596373
PI3K-Akt signaling pathway	20	21	0.188374	0.663668	0.188374	0.069671
Axon guidance	20	23	0.69189	0.96052	0.69189	0.339855
Pathogenic *Escherichia coli* infection	18	21	0.361799	0.273863	0.361799	0.416672
cAMP signaling pathway	18	23	0.547391	0.290855	0.547391	0.743484
Alzheimer disease	18	24	0.631722	0.324838	0.631722	0.850642
Pathways of neurodegeneration - multiple diseases	17	23	0.927345	0.735632	0.927345	0.875279
Ribosome	16	16	0.085705	—	—	0.033724
Human T-cell leukemia virus 1 infection	15	20	0.164459	0.045977	0.164459	0.841122
Salmonella infection	15	22	0.722322	0.369315	0.722322	0.960377
Regulation of actin cytoskeleton	15	19	0.882177	0.773113	0.882177	0.718756
Osteoclast differentiation	15	19	0.886352	0.783108	0.886352	0.718756
Rap1 signaling pathway	14	17	0.283435	0.135432	0.283435	0.594732

major reasons for the development of cognitive decline and dementia (Gauthaman et al., 2014; Rasool et al., 2018; Rasool et al., 2021), there are still no robust therapies to alleviate or cure this debilitating disease (Gao et al., 2016; Rasool et al., 2018) and most drug treatments focus on restoring normal function of cells that cause inflammation, such as microglia and neurons in the brain (Oksanen et al., 2017). However, the genetic basis of astrocytes in the development of AD, and the triggering of dementia is still not clearly understood (Oksanen et al., 2017; Kery et al., 2020). Therefore, a precise understanding of the underlying role of astrocytes in AD patients may provide clues for the development of effective therapies to treat dementia. Here, we used an innovative approach to leverage next-generation knowledge discovery (NGKD) platforms to decipher the AD -specific gene signatures in astrocytes isolated from the entorhinal cortex of AD patients and specific synthetic drugs and natural products to improve AD and associated disease pathologies such as dementia.

2 MATERIALS AND METHODS

2.1 Ethical Statement

This study was exempt from Institutional Review Board (IRB) approval because it did not involve animal models or human subjects. It was performed using DEGs derived from the Single Cell RNA-seq Database for Alzheimer's Disease (scREAD) based on publicly available and previously published single nucleus RNA sequencing datasets from the Gene Expression Omnibus (GEO).

2.2 Data Source

In the present study, we snRNASeq data from the scREAD, originally obtained from astrocytes isolated from the entorhinal cortex of AD brains and healthy brains from the Gene Expression Omnibus (GEO) (GSE138852 and GSE147528). scREAD is a user-friendly open-source interface available at https://bmbls.bmi.osumc.edu/scread/to enable more discovery-oriented strategies (Wu and Zhang, 2020; Jiang et al., 2020; Jiang et al., 2021) (**Supplementary Figure S1**). Datasets were filtered in scREAD by selecting the options for species (human), condition (all), region in the brain (entorhinal cortex), and gender (all), and are listed in **Table 1** with the corresponding Braak levels (Braak and Braak, 1991). scREAD webtool was also used to visualize all cell types and sub-clusters of astrocytes in the entorhinal cortex region of the brain using Uniform Manifold Approximation and Projection (UMAP) (Becht et al., 2018). All snRNASeq data are freely available in the Gene Expression Omnibus (GEO) under accession numbers GSE138852 and GSE147528.

Importantly, the snRNAseq datasets (GSE138852) are available via an interactive web application at adsn.ddnetbio.com (Grubman et al., 2019). The characteristics of all AD and healthy snRNASeq scREAD datasets used in this study are provided in **Table 1**. As of May 2021, the snRNASeq datasets used for this study had been already published and are publicly available (Barrett et al., 2013).

2.3 The snRNASeq Data Analysis Using iPathwayGuide

DEGs were obtained using scREAD analysis of snRNASeq data from astrocytes of AD groups (AD00203, AD00205, and AD00206) compared with the healthy control group (AD00201). DEGs of AD groups (AD00203, AD00205, and AD00206) were further filtered using a p-value cut-off of 0.05, and log2 fold change (Log2Fc) of ±0.3 in iPathwayGuide Software (Advaita Bioinformatics, United States) to obtain 739, 241, and 639 DEGs. Further analysis of these DEGs using iPathwayGuide software showed that 93 DEGs were commonly regulated in all disease groups (**Figure 2**). The Kyoto Encyclopedia of Genes and Genomes (KEGG) database was used to decipher differentially regulated pathways (Kanehisa and Goto, 2000; Kanehisa et al., 2002; Kanehisa et al., 2010; Kanehisa et al., 2012; Kanehisa et al., 2014), and the Gene Ontology Consortium database (Ashburner

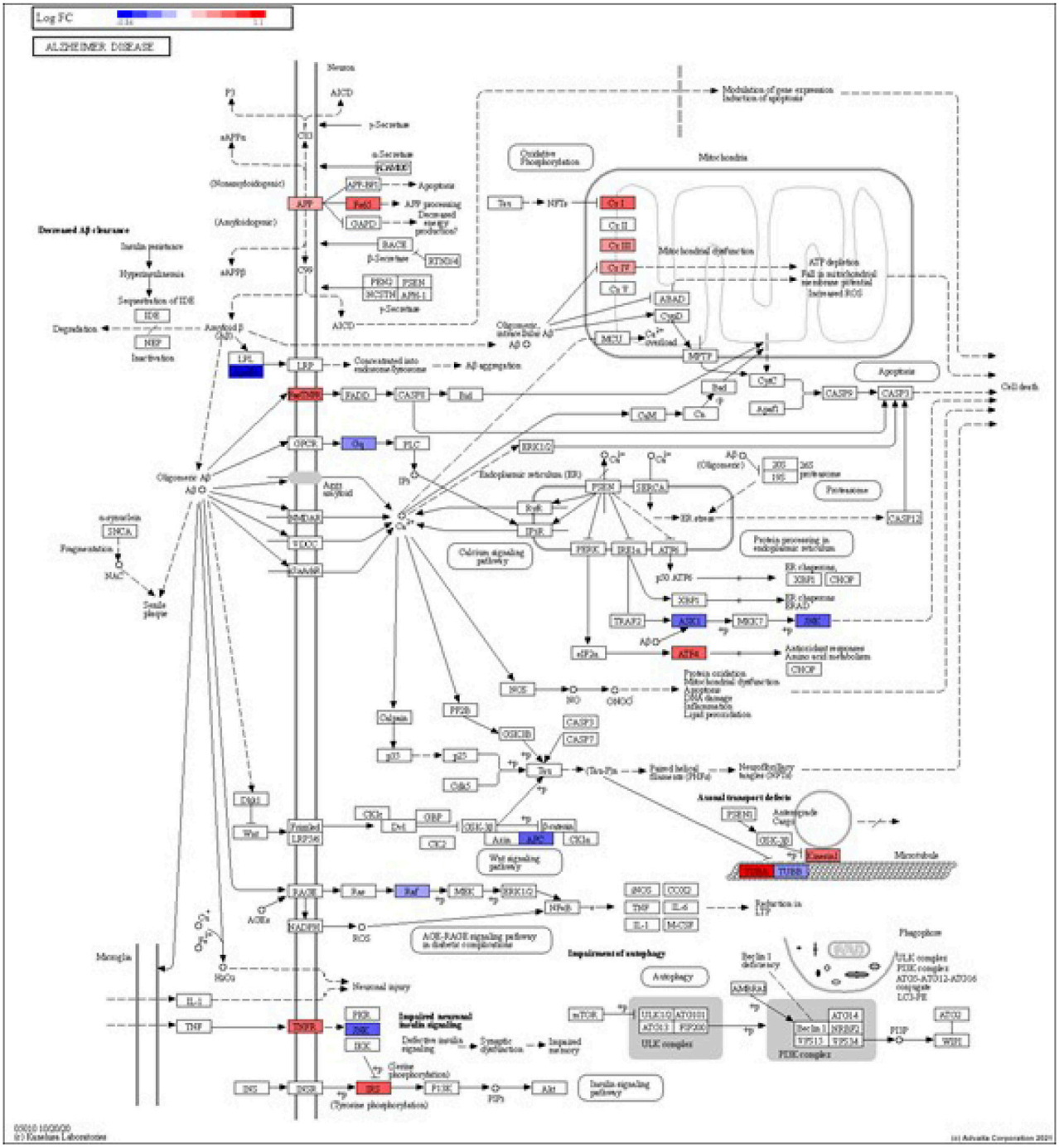

FIGURE 3 | iPathwayGuide analysis shows the differentially regulated genes in the KEGG Alzheimer's disease pathway in astrocytes from the AD group (AD00203) compared to astrocytes from the healthy control group (AD00201).

et al., 2000; Gene Ontology Consortium 2001) was used to identify the differentially regulated GO functions, and the Comparative Toxicogenomics Database was used to find the chemicals/drugs/toxicants (CDT and the KEGG database for diseases (Kanehisa and Goto, 2000; Kanehisa et al., 2002). The iPathwayGuide software used the Impact Analysis Method (IAM) (Draghici et al., 2003; Draghici et al., 2007; Draghici, 2011) to obtain significantly impacted DEGs and pathways compared with the corresponding control group; the *p*-value computed using Fisher's method was used to determine the pathway score, and the *p*-value was adjusted based on the false discovery rate (FDR) (Benjamini and Hochberg, 1995; Benjamini and Yekutieli, 2001).

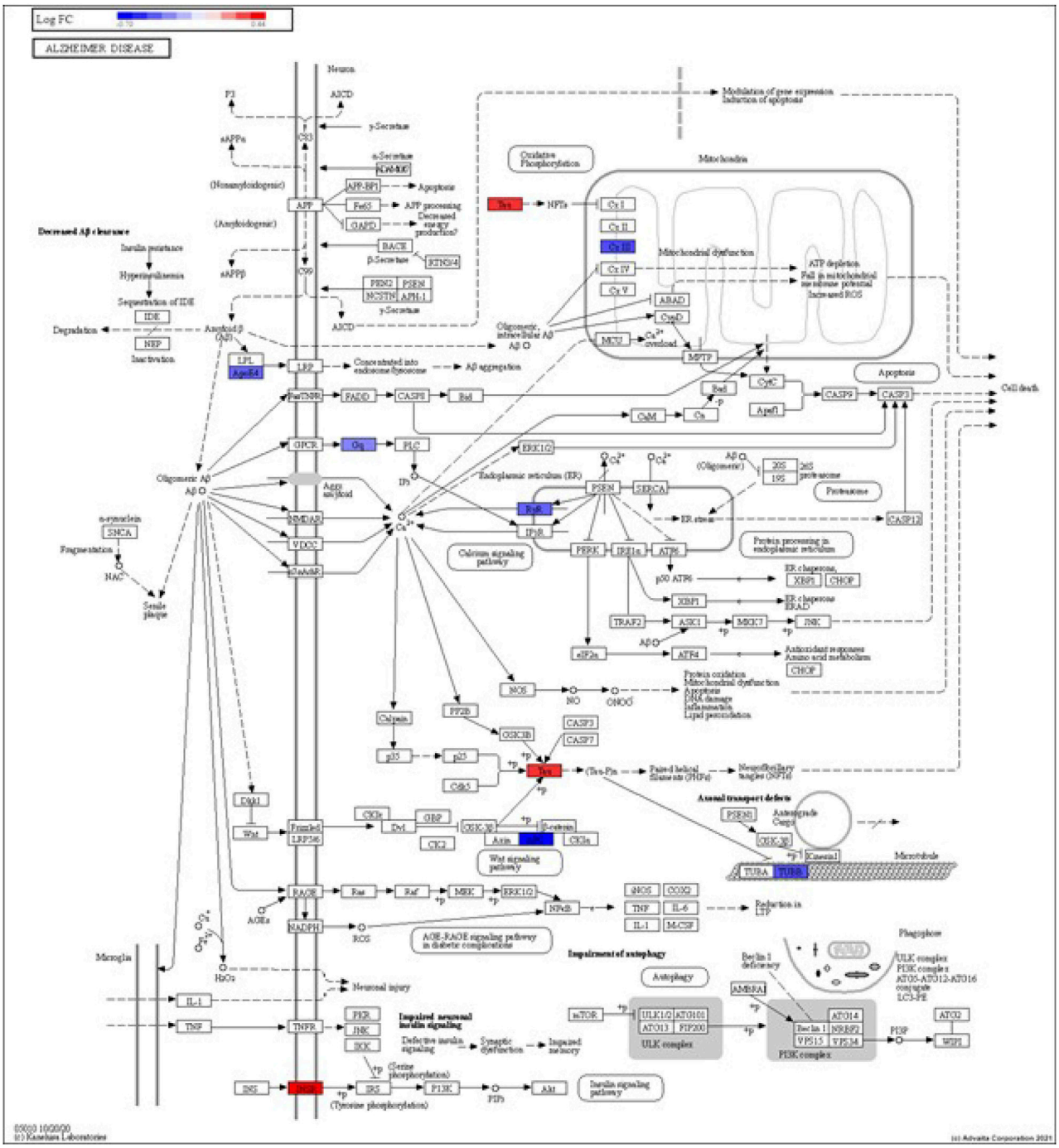

FIGURE 4 | iPathwayGuide analysis shows the differentially regulated genes in the KEGG Alzheimer's disease pathway in astrocytes from the AD group (AD00205) compared to astrocytes from the healthy control group (AD00201).

and Bonferroni multiple testing corrections (Bonferroni, 1935). The *p*-values were computed based on the hypergeometric distribution in iPathwayGuide analysis and the FDR and Bonferroni methods for multiple testing corrections (Draghici et al., 2003; Draghici, 2011).

2.4 Determination of Upstream Drugs and Natural Products Using iPathwayGuide

The determination of upstream drugs or natural products was predicted based on the enrichment of DEGs and 2) a network of connections or interactions from the Advaita Knowledge

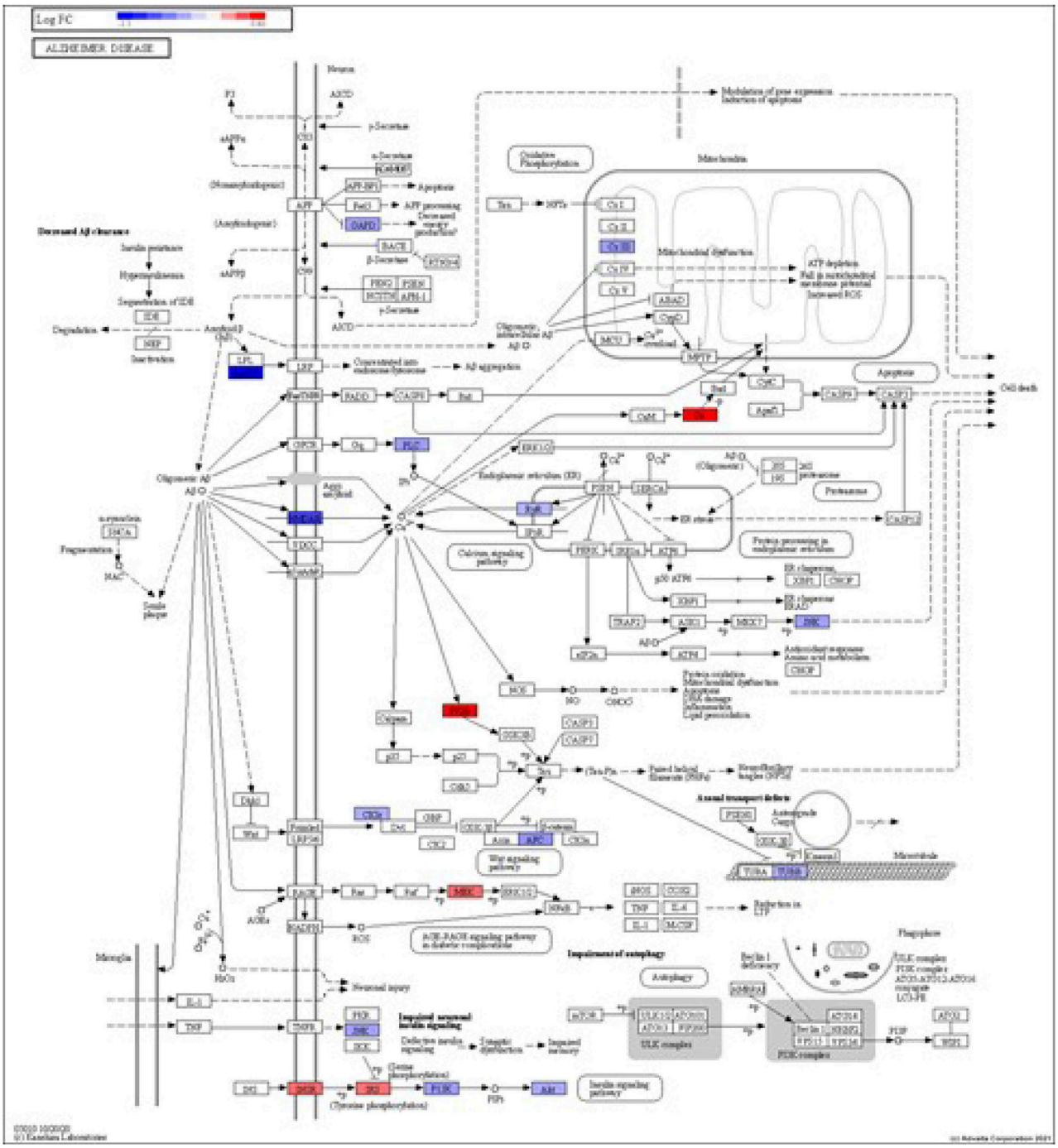

FIGURE 5 | iPathwayGuide analysis shows the differentially regulated genes in the KEGG Alzheimer's disease pathway in astrocytes from the AD group (AD00206) compared to astrocytes from the healthy control group (AD00201).

Base (Draghici et al., 2003; Draghici, 2011). The iPathwayGuide analysis was based on two hypotheses (HP and HA). The overly abundant or present upstream chemical, drug, or toxicant (CDT) was predicted under the conditions analyzed under the first hypothesis called HP and the upstream CDT. is insufficient (or absent) was predicted under the conditions analyzed under the second hypothesis. HA. iPathwayGuide calculates a Z-score for each CDT z(u) by iterating over the genes in DT(u) and their incoming edges in (g) in testing both HP and HA. Subsequently, the *p*-value was computed corresponding to the z-score Pz (One-Tailed) under the probability density

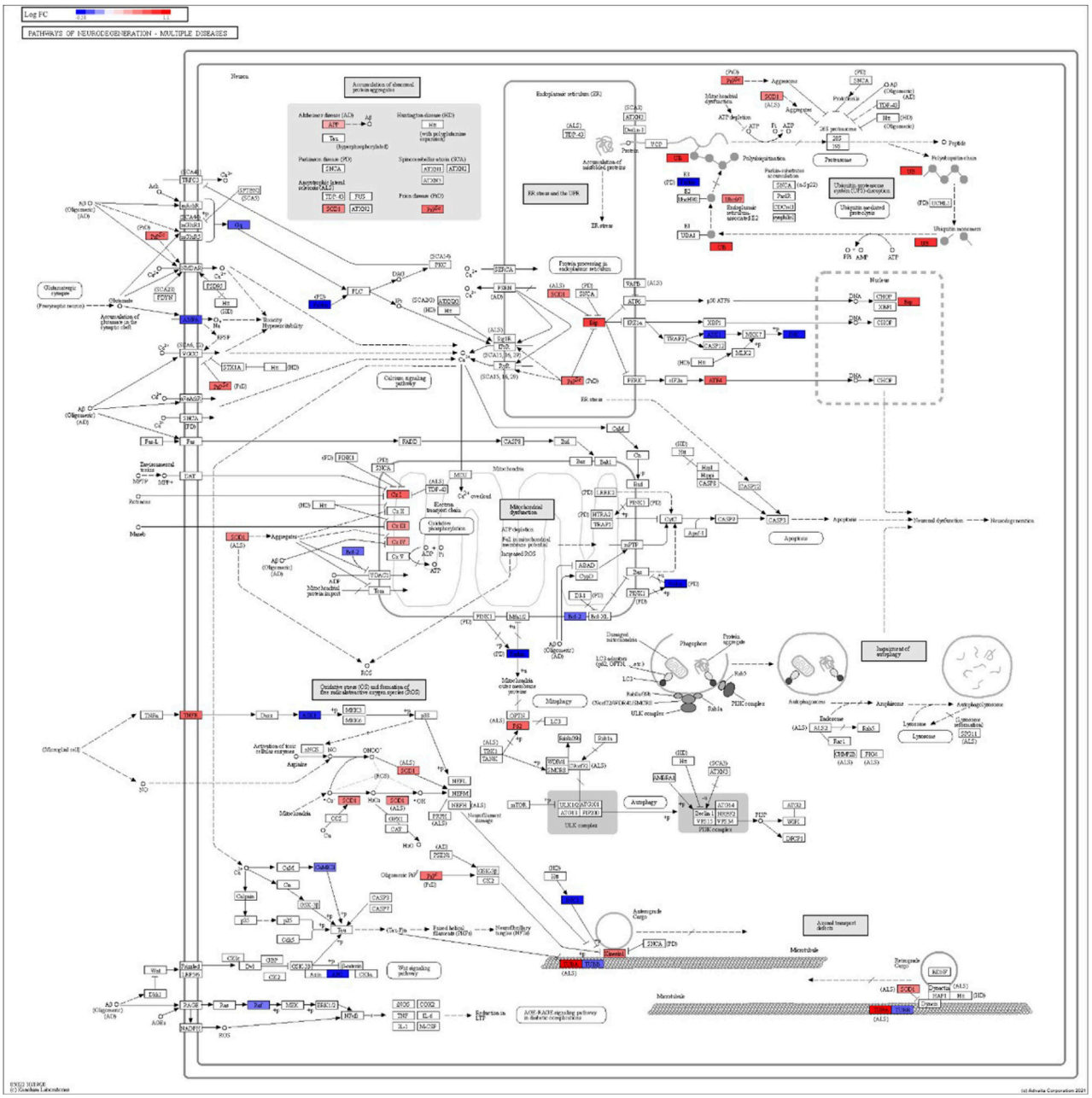

FIGURE 6 | iPathwayGuide analysis shows the differentially regulated genes in the KEGG neurodegeneration pathway (multiple diseases) in the astrocytes of the AD group (AD00203) compared to the astrocytes of the healthy control group (AD00201).

function for a normal distribution, N (0,1) (Draghici et al., 2003; Draghici, 2011).

2.4.1 Determination of Upstream Drugs and Natural Products Present or Overly Abundant Using iPathwayGuide

To determine the presence or abundance of CDTs based on the differentially expressed (DE) genes, CDT u, DE genes downstream of u, DTA (u) were compared to measured target genes predicted by chance to be both DE and consistent. An over-representation method was applied to calculate the statistical significance (p-value) based on the number of consistent DE genes in the iPathwayGuide analysis. The Ppres (p-value) was calculated based on the hypergeometric distribution (Draghici et al., 2003; Draghici, 2011). Then, the global probability value (PG) was computed by combining Pz and Ppres: and was used to rank the upstream regulators and test the HP research hypothesis. The p-values were combined into one test statistic using the standard Fisher's method.

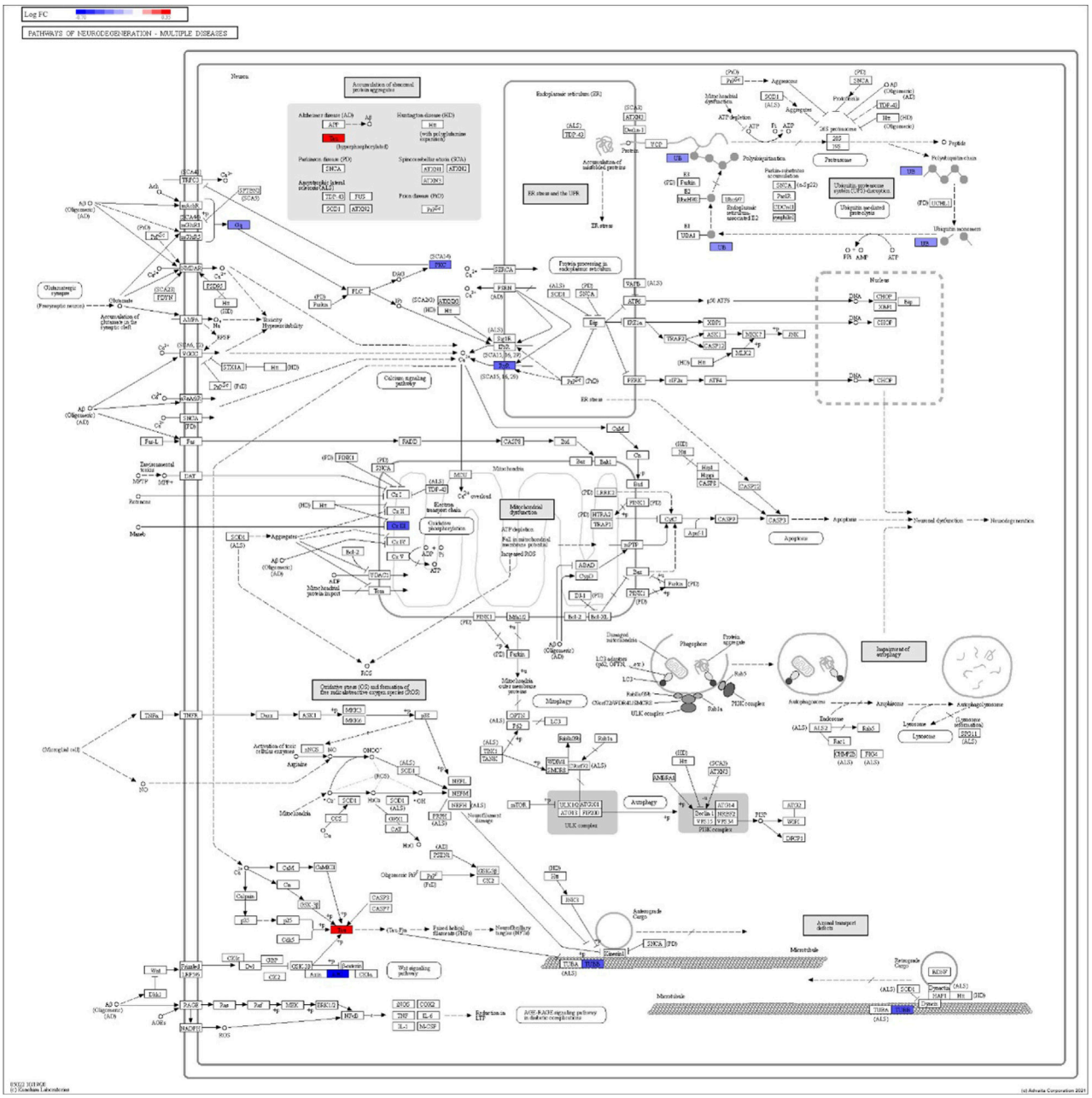

FIGURE 7 | iPathwayGuide analysis shows the differentially regulated genes in the KEGG neurodegeneration pathway (multiple diseases) in the astrocytes of the AD group (AD00205) compared to the astrocytes of the healthy control group (AD00201).

2.4.2 Determination of Upstream Drugs and Natural Products Absent or Insufficient Using iPathwayGuide

To determine the absence or insufficiency of CDTs based on the DE genes, Pabs was calculated using the iPathwayGuide analysis. The upstream CDTs that were absent or insufficient under the conditions investigated based on the number of consistent DE genes downstream of u, and DTI (u) was compared to the measured target genes predicted by chance to be both DE and consistent. The Pabs (*p*-value) was calculated based on the hypergeometric distribution (Draghici et al., 2003; Draghici, 2011). Then the PG was computed by combining Pz and Pabs and was used to rank the upstream regulators that were absent or insufficient and to test the research hypothesis HA. The analysis combines Pabs and Pz, using Fisher's method as described previously, where Pz was measured only for significant negative z-scores ($z \leq -2$) (Draghici et al., 2003; Draghici, 2011).

2.5 L1000FWD and L1000CDS^2 Analyses

DEGs were subjected to L1000 Fire Works Display (L1000FWD) analysis using the L1000FWD signature

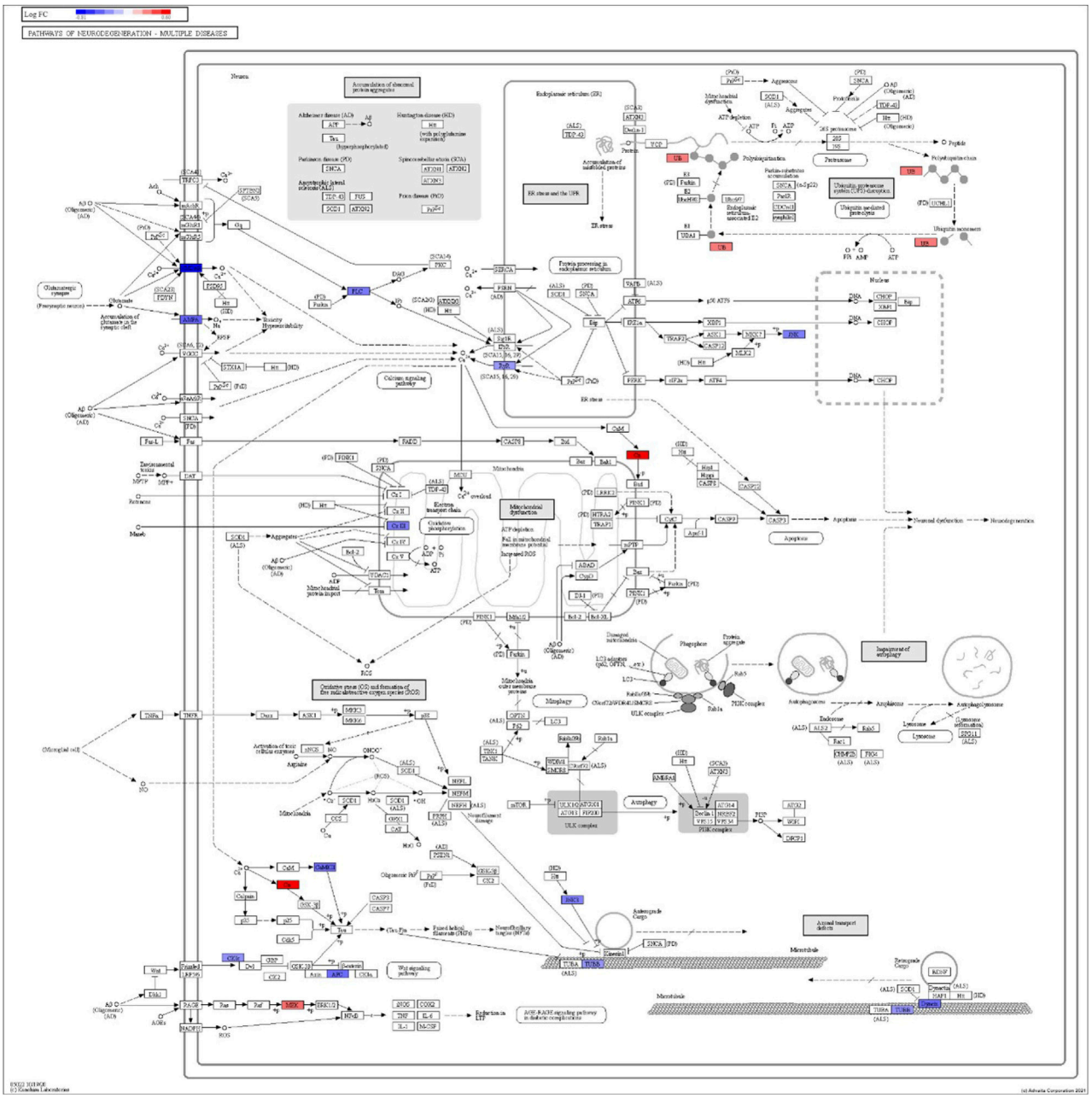

FIGURE 8 | iPathwayGuide analysis shows the differentially regulated genes in the KEGG neurodegeneration pathway (multiple diseases) in the astrocytes of the AD group (AD00206) compared to the astrocytes of the healthy control group (AD00201).

search application programming interface (API) (Wang et al., 2018) to identify the top 50 drugs and natural products that have the potential to reverse AD-associated signaling. Similarly, the same set of DEGs was subjected to L1000 Characteristic Direction Signature Search Engine (L1000CDS2) analysis using the L1000CDS2 Signature Search API to identify the top 50 drugs and natural products with the potential to reverse AD-associated signaling (Duan et al., 2016).

3 RESULTS

In the present study, snRNASeq datasets of astrocytes isolated from the entorhinal cortex region of AD patients and healthy brains were obtained from the scREAD database for NGKD platform analysis (**Table 1**). The scREAD web tool was used to visualize all cell types and sub-clusters of astrocytes in the entorhinal cortex region of the brain in AD and healthy snRNASeq datasets using UMAP (**Supplementary Figure S1**).

TABLE 5 | Top 25 Impacted Pathways obtained using Gene Set Enrichment Analysis (GSEA) based on Normalized Enrichment Score (NES) and False Discovery Rate (FDR) using the web tool available at http://adsn.ddnetbio.com/

BP/CC/MF/KEGG	Impacted pathway	NES	FDR
CC	Postsynaptic membrane	−2.02	0.001283
CC	Synaptic membrane	−1.858	0.001283
CC	Postsynapse	−1.653	0.001283
CC	Synapse	−1.484	0.001283
CC	Synapse part	−1.47	0.001997
KEGG	Neuroactive ligand receptor interaction	−1.98	0.004235
MF	Glutamate receptor activity	−2.169	0.005663
MF	Extracellular ligand gated ion channel activity	−2.11	0.005663
CC	Transporter complex	−1.685	0.006176
MF	Neurotransmitter receptor activity	−2.081	0.009856
BP	Glutamate receptor signaling pathway	−2.206	0.011
BP	Regulation of synapse organization	−1.985	0.011
BP	Single organism behavior	−1.744	0.011
BP	Behavior	−1.675	0.011
BP	Heterophilic cell-cell adhesion via plasma membrane cell adhesion molecules	−2.09	0.01224
BP	Regulation of synaptic transmission glutamatergic	−2.03	0.01224
BP	Synaptic signaling	−1.682	0.01224
CC	Chylomicron	−1.639	0.01265
BP	Cell-cell adhesion *via* plasma membrane adhesion molecules	−1.895	0.01373
BP	Synapse organization	−1.876	0.01619
BP	Learning	−1.831	0.01867
MF	Extracellular glutamate gated ion channel activity	−2.007	0.01954
MF	Ligand-gated channel activity	−1.83	0.02148
CC	Plasma membrane region	−1.353	0.02471
BP	Startle response	−2.044	0.02524

A UMAP example for the healthy control and AD scREAD datasets is shown in **Supplementary Figure S2**.

DEGs in astrocytes from the entorhinal cortex compared to healthy controls were determined using paired comparisons with the healthy control (AD00201) and AD (AD00203, AD00205, and AD00206) datasets (**Supplementary Tables S1–S3**) The 93 DEGs common to all AD datasets can be found in **Supplementary Table S4**. The 15 pathways most affected by DEGs in the AD groups compared to healthy controls are listed in **Tables 2–4**. Based on the number of DEGs, the top signaling pathways differentially regulated in the astrocytes of AD patients in the context of neurodegeneration include Alzheimer's disease, prion disease, Parkinson's disease, Huntington's disease, neurodegeneration signaling pathways (multiple diseases), amyotrophic lateral sclerosis, and the phosphatidylinositol 3-kinases/protein kinase B (PI3K/AKT) pathway. The differentially regulated KEGG pathways of Alzheimer's disease in the groups of AD are shown in **Figures 3–5**, and the differentially regulated KEGG pathways of neurodegenerative degeneration (multiple diseases) are shown in **Figures 6–8**. Analysis of WNT pathway perturbation and PI3K/AKT pathways followed by iPathwayGuide coherent cascade activation revealed the dysregulation of these pathways in the astrocytes of AD patients from the entorhinal cortex (**Supplementary Figure S3A** and **Supplementary Figure S4B**). The differentially regulated genes in the WNT pathways and the PI3K/AKT pathways are also shown in **Supplementary Figure S3B** and **Supplementary Figure S4B**, respectively. In addition to the neurodegenerative diseases, we also observed the signaling pathways associated with *Salmonella* infection, human papillomavirus (HPV) infection, and human T-cell leukemia virus infection in the astrocytes of the severe AD groups (**Table 2** and **Table 4**) compared with the healthy controls. Gene set enrichment analysis (GSEA) showed that gene sets involved in cellular components, such as postsynaptic

TABLE 6 | Top 25 differentially expressed GWAS genes in astrocytes from entorhinal cortex in AD brain based on analysis using the web tool available at http://adsn.ddnetbio.com/.

Gene Name	LogFc	FDR	Category
NKAIN3	−1.965	8.226e-103	Biomarkers
LRRC4C	−1.54	1.055e-51	Biomarkers
CADM2	−0.9309	3.203e-43	Alzheimer's
DLC1	−1.269	2.297e-38	Alzheimer's | LOAD
APOE	−1.136	5.424e-35	Alzheimer's | Biomarkers | LOAD
TNIK	−0.8955	3.230e-34	Biomarkers
GADD45G	1.232	1.193e-33	Biomarkers
FRMD4A	−1.263	1.728e-28	Alzheimer's
CTNNA2	−0.7049	5.649e-28	Alzheimer's | Biomarkers
NPAS3	−0.5062	6.715e-28	Biomarkers
NCKAP5	−1.027	9.935e-26	Alzheimer's
RORA	−0.6096	4.061e-25	Alzheimer's | Biomarkers
FBXL7	−0.8531	7.555e-24	Alzheimer's
AHNAK	1.015	1.846e-23	Alzheimer's | Biomarkers | LOAD
FAT3	−1.066	4.009e-22	Alzheimer's | Biomarkers | LOAD
SLCO3A1	0.9594	5.436e-19	Biomarkers | Neuropathologic
SH3RF1	−1.016	5.596e-17	Alzheimer's
CACNA2D3	0.8438	2.955e-16	Alzheimer's
DLG2	−0.6662	1.094e-15	Biomarkers
PDE7B	−0.7986	8.458e-14	Alzheimer's
SPON1	−0.7795	1.476e-13	Alzheimer's
PTPRG	−0.764	2.860e-13	Alzheimer's
CDH23	0.785	3.357e-12	Biomarkers
AUTS2	−0.5907	2.649e-11	Biomarkers
LUZP2	−0.8184	7.842e-11	Alzheimer's | Biomarkers

TABLE 7 | The upstream Chemicals, Drugs, or Toxicants (CDTs) were predicted as absent (or insufficient) in the astrocytes of AD based on the number of DEGs significantly impacted in each category.

Name	cDE_n (Astrocytes_AD00203 vs. Astrocytes_AD00201)	cDE (Astrocytes_AD00203 vs. Astrocytes_AD00201)	pv_comb_n (Astrocytes_AD00203 vs. Astrocytes_AD00201)	cDE_n (Astro_AD00205 vs. Astro_AD00201)	cDE (Astro_AD00205 vs. Astro_H00201)	pv_comb_n (Astro_AD00205 vs. Astro_AD00201)	cDE_n (Astrocytes_AD00206 vs. Astrocytes_AD00201)	cDE (Astrocytes_AD00206 vs. Astrocytes_AD00201)	pv_comb_n (Astrocytes_AD00206 vs. Astrocytes_AD00201)
Antirheumatic Agents	116	193	0.017467	36	67	1	131	189	9.71E-07
perfluorooctanoic acid	43	64	0.029342	13	17	0.906879	23	40	0.99999999
Vitamin E	40	110	1	10	31	1	50	76	0.0281796
Vanadates	35	65	1	15	19	0.035627	51	76	0.01079637
Piroxicam	28	34	0.001769	6	11	0.988182	13	21	0.99599971
Propionaldehyde	28	61	1	17	29	0.999354	46	68	0.01320547
MT19c compound	19	25	0.029523	3	7	0.943716	4	18	1
Uranium Compounds	16	19	0.010291	1	4	0.999381	9	10	0.02177297
methylselenic acid	15	30	1	9	12	0.900238	20	25	0.03745406
nickel chloride	15	32	1	9	11	0.048969	8	30	1
3-(4'-hydroxy-3'-adamantylbiphenyl-4-yl)acrylic acid	15	16	0.000817	3	6	0.988999	11	12	0.00697841
CD 437	14	15	0.002889	2	6	0.999675	11	15	0.89309347
Salinomycin	11	13	0.034563		4	1	10	18	0.99353861
cylindrospermopsin	10	17	0.999219	8	9	0.034748	5	15	0.99999998
Clorgyline	10	11	0.021724	5	5	0.039888	8	9	0.0461479
Aldehydes	10	23	1	11	14	0.045315	22	28	0.00958826
Environmental Pollutants	8	8	0.020578	1	1	0.646199	2	2	0.61565284
chloroacetaldehyde	7	15	0.999971	2	3	0.871198	11	13	0.03735946
Dinitrochlorobenzene	7	14	0.999971	9	10	0.003928	6	16	0.99998432
cadmium sulfate	5	20	1	7	8	0.018781	3	10	0.99,987,959
Sulforafan	3	11	1	6	6	0.020331	6	12	0.9998163
Bezafibrate	2	3	0.94972	1	1	0.875495	4	4	0.04,955,141

membrane, synaptic membrane, postsynapse, synapse, and synapse, were negatively enriched ($p < 0.01$). Neuroactive ligand-receptor interaction based on KEGG pathways was significantly downregulated ($p < 0.01$), and cellular function of the transporter complex was also negatively enriched ($p < 0.01$). Similarly, genes associated with glutamate receptor activity, neurotransmitter receptor activity, glutamate receptor signaling, heterophilic cell-cell adhesion via plasma membrane cell adhesion molecules, cell-cell adhesion via plasma membrane adhesion molecules, and behavior were also negatively enriched ($p < 0.01$) in astrocytes from AD patients (**Table 5**). Importantly, differential expression of GWAS genes in astrocytes from the entorhinal cortex in the brain of AD is listed in **Table 6**. The most downregulated GWAS genes in astrocytes from the entorhinal cortex associated with the pathogenesis of AD were NKAIN3, LRRC4C, CADM2, DLC1, APOE, TNIK, GADD45G, FRMD4A, CTNNA2, NPAS3, NCKAP5, and RORA.

Comparative analysis of the AD datasets from the scREAD based on the DEGs with iPathwayGuide showed that the antirheumatic drugs, vitamin E, salinomycin, and clorgyline have insufficient ($p < 0.05$) signaling effect in the astrocytes of AD patients (**Table 7**). In addition, **Tables 8–10** list the drugs or natural products that could potentially reverse the gene signatures of astrocytes in the AD groups (AD00203, AD00205, and AD00206) based on the L1000FWD web tool analysis. L1000FWD analysis revealed that natural products such as emetine, cephaeline, homoharringtonine, narciclasine, withaferin A and several synthetic drugs such as dasatinib can significantly reverse gene signatures associated with AD pathology.

The drugs or natural products that could potentially reverse the gene signatures of astrocytes in AD groups (AD00203, AD00205, and AD00206) based on the L1000CDS^2 web tool are provided in **Supplementary Tables S1–S3**, respectively. The L1000CDS^2 analysis uncovered the natural products emetine, narciclasine, trichostatin A, homoharringtonine, ouabain, bufalin, and withaferin A, as well as synthetic drugs, such as dasatinib, that have the potential to reverse AD-associated gene signatures in astrocytes from AD patients.

4 DISCUSSION

AD is a neurodegenerative disease of the brain and a major cause of the development of cognitive decline and dementia in the elderly (Winblad et al., 2016; Matthews et al., 2019). ADRD contributes to the majority of dementia cases worldwide (Winblad et al., 2016). Recent advances in genome sequencing technologies such as scRNA-Seq and snRNASeq are critical for deciphering the roles of heterogeneous cell populations in the brain at the single-cell level, and subsequent dissecting of these datasets using high throughput knowledge discovery platforms may provide clues as to why a particular group of cells is susceptible to AD and ADRD (Jiang et al., 2020; Wu and Zhang, 2020; Wang et al., 2021). Here, snRNASeq datasets of astrocytes isolated from the entorhinal cortex region of AD patients and healthy brains were obtained and analyzed using scREAD web-tool. scREAD includes 73 datasets from 16 studies, 10 brain regions, and 713,640 cells, and provides cell type and sub-cluster predictions, decipherment of DEGs, and

TABLE 8 | The top 50 drugs or natural products that reverse DEGs of astrocytes from entorhinal cortex in AD (AD00203 (disease) vs AD00201 (control) based on L1000FWD analysis.

Signature ID	Drug	Similarity score	*p*-value	q-value	Z-score	Combined score
CPC006_HEPG2_6H:BRD-K01976263-003-04-5:0.63	Emetine	−0.0673	1.16E-10	7.11E-07	1.79	−17.83
CPC017_MCF7_24H:BRD-A62184259-001-02-8:10	Cycloheximide	−0.0617	6.64E-10	3.28E-06	1.72	−15.78
HOG003_A549_24H:BRD-K01976263-003-04-5:3.3333	Emetine	−0.0598	7.55E-09	2.31E-05	1.62	−13.18
CVD001_HEPG2_24H:BRD-K03067624-001-01-5:10	Emetine	−0.0579	1.59E-08	4.25E-05	1.69	−13.16
CPC006_HT29_6H:BRD-K01976263-003-04-5:0.63	Emetine	−0.0561	3.40E-07	3.41E-04	1.77	−11.45
CPC014_SKB_24H:BRD-M16762496-001-01-9:10	PIK-75	−0.0542	8.37E-07	5.60E-04	1.69	−10.25
CPC004_HCC515_24H:BRD-A25687296-300-03-5:10	Emetine	−0.0523	1.60E-06	8.80E-04	1.83	−10.6
CPC018_MCF7_24H:BRD-K36055864-001-09-3:10	Cycloheximide	−0.0523	6.02E-07	4.47E-04	1.71	−10.61
CPC002_HCC515_24H:BRD-K80348542-001-01-4:10	Cephaeline	−0.0505	7.75E-06	2.67E-03	1.8	−9.2
CPC008_A375_24H:BRD-K66032149-001-01-9:10	VU-0365117-1	−0.0486	2.18E-05	5.87E-03	1.74	−8.12
CPC017_HEPG2_6H:BRD-A25687296-300-03-5:10	Emetine	−0.0486	3.66E-06	1.61E-03	1.7	−9.22
CPC004_HT29_6H:BRD-A25687296-300-03-5:10	Emetine	−0.0467	2.11E-05	5.82E-03	1.82	−8.51
CPC009_PC3_6H:BRD-K21773564-001-01-8:10	BRD-K21773564	−0.0467	2.26E-05	6.04E-03	1.73	−8.05
CPC004_HEPG2_6H:BRD-A62184259-001-02-8:10	Cycloheximide	−0.0467	1.10E-05	3.52E-03	1.85	−9.2
CPC006_HEPG2_6H:BRD-A45889380-300-04-8:10	Mepacrine	−0.0467	1.28E-05	3.96E-03	1.84	−8.99
CPC016_HEPG2_6H:BRD-K80348542-001-01-4:10	Cephaeline	−0.0449	2.86E-05	7.24E-03	1.74	−7.92
CPC017_A549_24H:BRD-K11927976-050-01-1:10	ER-27319	−0.0449	4.63E-05	9.86E-03	1.72	−7.44
CPC013_SKB_24H:BRD-K87909389-001-01-2:10	Alvocidib	−0.0449	3.78E-05	8.51E-03	1.72	−7.62
CPC018_A549_6H:BRD-K63606607-001-01-8:10	Bufalin	−0.0449	3.07E-05	7.68E-03	1.72	−7.74
CPC004_VCAP_24H:BRD-A01593789-001-02-3:10	Chlormadinone	−0.0449	1.07E-04	1.71E-02	1.81	−7.19
CPC004_HA1E_6H:BRD-K14920963-304-01-9:10	Erythrosine	−0.0449	8.86E-05	1.49E-02	1.83	-7.42
CVD001_HUH7_6H:BRD-K03067624-001-01-5:10	Emetine	−0.0449	1.03E-04	1.68E-02	1.65	−6.59
CPC017_MCF7_6H:BRD-A25687296-300-03-5:10	Emetine	−0.043	6.30E-05	1.22E-02	1.73	−7.25
CPC008_A375_6H:BRD-U88878891-000-01-9:10	BRD-U88878891	−0.043	3.61E-04	3.91E-02	1.74	−5.98
CPC014_HT29_6H:BRD-A26002865-001-01-5:10	Verrucarin-a	−0.043	2.88E-04	3.38E-02	1.71	−6.06
CPC017_MCF7_6H:BRD-K60511616-236-01-4:10	Pravastatin	−0.043	2.80E-04	3.35E-02	1.65	−5.84
CPC007_HT29_24H:BRD-K03067624-003-19-3:10	Emetine	−0.043	5.00E-04	4.75E-02	1.76	−5.82
CPC010_A375_6H:BRD-A24643465-001-05-3:10	Homoharringtonine	−0.043	2.03E-04	2.79E-02	1.76	−6.48
CPC015_MCF7_6H:BRD-K63550407-001-08-5:10	Erythromycin	−0.043	8.50E-05	1.47E-02	1.71	−6.96
CPC004_MCF7_6H:BRD-A25687296-300-03-5:10	Emetine	−0.043	8.78E-05	1.49E-02	1.87	−7.6
CPC008_MCF7_24H:BRD-K64409586-001-04-5:10	KU-C104488	−0.043	3.13E-05	7.79E-03	1.82	−8.19
CPC006_PC3_24H:BRD-A75517195-001-01-3:40	Thiazolopyrimidine	−0.043	2.03E-04	2.79E-02	1.79	−6.61
CPC006_LOVO_6H:BRD-K01976263-003-04-5:0.63	Emetine	−0.043	1.55E-04	2.30E-02	1.79	−6.81
CPC014_SKB_24H:BRD-K80622725-001-10-2:10	STK-397047	−0.043	2.50E-04	3.13E-02	1.7	−6.12
CPC012_MCF7_24H:BRD-K48935217-001-01-3:10	Epothilone	−0.0411	3.41E-04	3.77E-02	1.73	−5.99
CPC006_MCF7_24H:BRD-K01976263-003-04-5:0.63	Emetine	−0.0411	4.29E-04	4.34E-02	1.77	−5.96
CPC014_PC3_6H:BRD-K70549064-001-03-3:10	Staurosporine	−0.0411	4.54E-04	4.46E-02	1.69	−5.64
CPC008_A375_24H:BRD-K14749055-001-01-3:10	BRD-K14749055	−0.0411	6.13E-04	5.37E-02	1.76	−5.65
CPC017_A375_6H:BRD-A25687296-300-03-5:10	Emetine	−0.0411	2.18E-04	2.91E-02	1.72	−6.3
CPC002_HCC515_6H:BRD-K80348542-001-01-4:10	Cephaeline	−0.0411	8.58E-05	1.47E-02	1.9	−7.72
CPC019_HT29_6H:BRD-A70311631-001-05-9:10	BRD-A70311631	−0.0411	1.06E-03	7.60E-02	1.64	−4.87
LJP001_SKBR3_6H:BRD-K99252563-001-01-1:2	QL-XII-47	−0.0411	3.13E-04	3.56E-02	1.63	−5.7
LJP001_SKBR3_6H:BRD-K04923131-001-10-5:10	GSK-3-inhibitor-IX	−0.0411	3.94E-04	4.12E-02	1.61	−5.48
CPC014_HEPG2_6H:BRD-K83794624-001-01-7:10	Pirarubicin	−0.0411	7.99E-04	6.43E-02	1.67	−5.18
CPC006_SW948_6H:BRD-K05649647-001-03-7:20	BRD-K05649647	−0.0411	1.70E-04	2.45E-02	1.81	−6.83
CPC010_HEPG2_6H:BRD-A24643465-001-05-3:10	Homoharringtonine	−0.0411	5.07E-04	4.77E-02	1.72	−5.68
CPC013_SKB_24H:BRD-A14178283-001-01-1:10	BRD-A14178283	−0.0411	6.74E-05	1.26E-02	1.77	−7.39
MUC.CP004_MCF7_24H:BRD-K09638361-001-01-4:3.3333	SA-63133	−0.0411	3.13E-04	3.56E-02	1.61	−5.64
CPC013_VCAP_6H:BRD-A81530502-001-01-6:10	BRD-A81530502	−0.0393	9.82E-04	7.25E-02	1.71	−5.13
CPC006_HCC515_6H:BRD-K14696368-001-01-8:10	9-methyl-5H-6-thia-4,5-diaza-chrysene-6,6-dioxide	−0.0393	2.90E-04	3.38E-02	1.85	−6.54

discovery of cell type-specific regulons (Jiang et al., 2020; Wu and Zhang, 2020; Wang et al., 2021).

We observed that Wnt signaling and PI3K/AKT signaling pathways were dysregulated or impaired in astrocytes from the entorhinal cortex of AD patients. Wnt signaling is very important at the synapse and necessary for synaptic plasticity and maintenance in the brain (Palomer et al., 2019). The PI3K/AKT pathway regulates apoptosis, cell proliferation, and metabolism and is essential for protection against amyloid protein (Aβ)-induced neurotoxicity (Long et al., 2021). Neuroactive ligand-receptor interaction, axon guidance, Alzheimer's disease, GABAergic synapse, glutamatergic synapse, etc. were negatively enriched or dysregulated in astrocytes from AD patients. GABAergic transmission is essential for all central nervous system functions (Luscher et al., 2011) and the GABAergic synapse pathway is impaired

TABLE 9 | The top 50 drugs or natural products that reverse DEGs of astrocytes from entorhinal cortex in AD (AD00205 (disease) vs AD00201 (control) based on L1000FWD analysis.

Signature ID	Drug	Similarity score	*p*-value	q-value	Z-score	Combined score
CPC003_PC3_6H:BRD-K76534306-001-11-0:10	Enrofloxacin	−0.1071	7.61E-10	1.09E-05	1.87	−17.05
CPC006_U937_6H:BRD-K78126613-001-16-0:10	Menadione	−0.0893	5.38E-07	1.62E-03	1.78	−11.15
CPC019_HA1E_6H:BRD-K98824517-001-06-4:10	BRD-K98824517	−0.0893	3.48E-07	1.43E-03	1.67	−10.8
CPC018_MCF7_24H:BRD-K36055864-001-09-3:10	Cycloheximide	−0.0893	3.68E-07	1.43E-03	1.71	−10.97
CPC014_MCF7_24H:BRD-K16485616-001-03-0:10	Mocetinostat	−0.0893	6.83E-07	1.62E-03	1.73	−10.64
CPC016_A375_6H:BRD-K63516691-003-01-2:10	T-0156	−0.0833	2.78E-06	4.25E-03	1.7	−9.44
CPD001_MCF7_24H:BRD-K21680192-300-11-0:10	Mitoxantrone	−0.0833	1.51E-06	2.93E-03	1.67	−9.71
CPC016_MCF7_24H:BRD-K80348542-001-01-4:10	Cephaeline	−0.0833	2.64E-06	4.19E-03	1.68	−9.39
CPC017_HEPG2_6H:BRD-K04546108-066-01-5:10	JAK3-inhibitor-VI	−0.0833	1.18E-06	2.67E-03	1.72	−10.21
CPC013_A375_6H:BRD-K35638681-001-01-5:10	BRD-K35638681	−0.0833	2.27E-06	3.90E-03	1.74	−9.82
CPC014_PC3_24H:BRD-K95901403-001-01-1:10	XL-147	−0.0774	2.79E-05	1.44E-02	1.68	−7.66
CPC013_HCC515_6H:BRD-K94493764-001-01-3:10	BRD-K94493764	−0.0774	1.12E-05	9.40E-03	1.72	−8.53
CPC006_MCF7_6H:BRD-A67788537-001-01-7:120	Salermide	−0.0774	8.02E-06	8.18E-03	1.82	−9.25
CPD002_MCF7_6H:BRD-K42635745-001-19-8:10	Suloctidil	−0.0774	6.60E-06	7.63E-03	1.7	−8.79
CPC006_A375_6H:BRD-K05402890-001-02-7:0.35	BRD-K05402890	−0.0774	1.07E-05	9.40E-03	1.81	−9.01
CPC018_A549_6H:BRD-A71459254-001-02-8:10	Cymarin	−0.0774	1.09E-05	9.40E-03	1.69	−8.4
CPC010_A549_6H:BRD-K28916077-001-04-0:10	BRD-K28916077	−0.0714	4.69E-05	1.82E-02	1.76	−7.64
CPC014_PC3_24H:BRD-A18497,530-001-05-3:10	5-iodotubercidin	−0.0714	4.03E-05	1.79E-02	1.73	−7.62
LJP002_BT20_6H:BRD-A24396574-001-02-3:10	Celastrol	−0.0714	4.21E-05	1.79E-02	1.66	−7.25
CPC006_HT29_24H:BRD-K19894101-001-01-6:11.1	MST-312	−0.0714	4.79E-05	1.83E-02	1.8	−7.77
CPC018_HT29_6H:BRD-A80383043-001-01-7:10	BRD-A80383043	−0.0714	4.99E-05	1.87E-02	1.66	−7.13
CPC010_HEPG2_6H:BRD-K28916077-001-04-0:10	BRD-K28916077	−0.0714	2.41E-05	1.37E-02	1.8	−8.32
CPC004_PC3_6H:BRD-A09472452-015-11-9:10	Flecainide	−0.0714	3.16E-05	1.56E-02	1.84	−8.28
CPC019_A375_6H:BRD-K98824517-001-06-4:10	BRD-K98824517	−0.0714	2.64E-05	1.44E-02	1.7	−7.8
BRAF001_A375_24H:BRD-K16478699-001-05-0:0.625	PLX-4720	−0.0714	4.30E-05	1.79E-02	1.84	−8.05
CPC001_HA1E_6H:BRD-K02590140-001-01-2:10	O-2050	−0.0714	4.39E-05	1.79E-02	1.85	–
LJP001_MCF7_6H:BRD-K99252563-001-01-1:10	QL-XII-47	−-0.0714	5.90E-05	1.90E-02	1.62	−6.87
CPC012_MCF7_24H:BRD-K08307026-001-01-4:10	BRD-K08307026	−0.0714	4.49E-05	1.81E-02	1.76	−7.67
NMH001_NPC_24H:BRD-K14282469-001-09-8:10	LY-165163	−0.0714	5.10E-05	1.88E-02	1.61	−6.92
CPC010_HCC515_6H:BRD-K78385490-019-02-2:10	BRD-K78385490	−0.0714	1.01E-04	2.54E-02	1.73	−6.91
CPC006_MCF7_24H:BRD-K28360340-001-01-8:10	TW-37	−0.0714	5.54E-05	1.88E-02	1.81	−7.69
CPC008_A549_6H:BRD-K32944375-019-01-3:10	BRD-K32944375	−0.0714	8.47E-05	2.29E-02	1.75	−7.13
CPC012_PC3_6H:BRD-K28610502-001-01-0:10	RAN-05	−0.0714	1.36E-04	3.22E-02	1.7	−6.56
CPC009_A549_6H:BRD-K95138506-019-01-8:10	BRD-K95138506	−-0.0714	4.30E-05	1.79E-02	1.78	−7.77
CVD001_HUH7_6H:BRD-K76674262-001-01-7:2.5	Homoharringtonine	−0.0714	6.94E-05	2.07E-02	1.65	-6.85
CPC013_MCF7_6H:BRD-K35638681-001-01-5:10	BRD-K35638681	−0.0714	1.03E-04	2.57E-02	1.69	−6.73
CPC010_PC3_6H:BRD-K69676861-001-02-4:10	BRD-K69676861	−0.0714	4.39E-05	1.79E-02	1.76	−7.67
CPC015_A375_6H:BRD-K15409150-001-01-7:10	Penfluridol	−0.0655	3.01E-04	4.42E-02	1.69	−5.94
CPC014_PC3_6H:BRD-U86922168-000-01-3:10	QL-XII-47	−0.0655	1.65E-04	3.56E-02	1.73	−6.53
CPC002_HA1E_6H:BRD-K91370081-001-10-3:10	Anisomycin	−0.0655	1.62E-04	3.53E-02	1.85	−7.02
CPC006_TYKNU_6H:BRD-K92317137-001-04-0:10	BRD-K92317137	−0.0655	2.60E-04	4.26E-02	1.77	−6.36
CPC008_VCAP_24H:BRD-K44432556-001-03-0:10	VU-0418946-1	−0.0655	2.55E-04	4.26E-02	1.77	−6.36
CPC006_MCF7_6H:BRD-A62025033-001-01-8:10	Temsirolimus	−0.0655	3.59E-04	4.85E-02	1.77	−6.1
CPC006_HCC515_24H:BRD-K04430056-001-09-4:80	7-nitroindazole	−0.0655	1.43E-04	3.28E-02	1.84	−7.07
CPC014_A375_6H:BRD-U33728988-000-01-6:10	QL-X-138	−0.0655	2.85E-04	4.34E-02	1.69	−6.01
HOG001_MCF7_24H:BRD-K06854232-001-03-3:0.0045	AM-580	−0.0655	3.53E-04	4.80E-02	1.62	−5.58
CPC014_HT29_6H:BRD-K50720187-050-04-1:10	Flupirtine	−0.0655	1.55E-04	3.44E-02	1.71	−6.53
CPC019_VCAP_24H:BRD-K20000640-001-01-5:10	SA-247384	−0.0655	3.17E-04	4.59E-02	1.66	−5.82
CPC019_HT29_6H:BRD-K86027709-001-01-7:10	BRD-K86027709	−0.0655	2.95E-04	4.42E-02	1.65	−5.82
CPC006_SW620_6H:BRD-K06792661-001-01-9:10	Narciclasine	−0.0655	2.24E-04	4.00E-02	1.78	−6.49

in the astrocytes of AD. This was also confirmed by GSEA analysis, which showed that the sets of genes involved in cellular components such as postsynaptic membrane, synaptic membrane, postsynapse, transporter complex, and interaction between neuroactive ligands and receptors were negatively enriched in the astrocytes of AD patients. Similarly, genes associated with glutamate receptor activity, neurotransmitter receptor activity, glutamate receptor signaling, heterophilic cell-cell adhesion via plasma membrane cell adhesion molecules, cell-cell adhesion via plasma membrane adhesion molecules, and behavior were also negatively enriched in the astrocytes of AD patients. Importantly, the downregulated GWAS genes in astrocytes derived from the entorhinal cortex, such as NKAIN3, LRRC4C, CADM2, DLC1, APOE, TNIK, GADD45G, FRMD4A, CTNNA2, NPAS3, NCKAP5, RORA, etc., associated with AD pathogenesis, can be used either as biomarkers for neuropathology, AD or LOAD (Riaz et al., 2021). Interestingly, we found signaling pathways associated with *Salmonella* infection, HPV infection, and human T-cell leukemia virus infection in the astrocytes of severe AD groups.

TABLE 10 | The top 50 drugs or natural products that reverse DEGs of astrocytes from entorhinal cortex in AD (AD00206 (disease) vs AD00201 (control) based on L1000FWD analysis.

Signature ID	Drug	Similarity score	*p*-value	q-value	Z-score	Combined score
CPC006_A375_24H:BRD-A75817871-001-04-2:40	Blebbistatin	−0.0593	1.31E-07	1.12E-03	1.79	−12.29
CPC004_MCF7_6H:BRD-K37991163-003-06-8:10	Paroxetine	−0.0571	1.12E-06	3.67E-03	1.79	−10.68
CPC014_HT29_6H:BRD-K53561341-001-02-6:10	KIN001-220	−0.0549	2.43E-06	4.92E-03	1.69	−9.5
CPC014_VCAP_24H:BRD-A52886023-001-01-7:10	Antimycin-a	−0.0527	4.90E-06	7.23E-03	1.69	−8.97
CPC009_VCAP_24H:BRD-K94390040-019-01-9:10	BRD-K94390040	−0.0527	7.95E-06	8.74E-03	1.75	−8.93
LJP001_SKBR3_24H:BRD-K19540840-001-04-5:10	Saracatinib	−0.0505	5.57E-06	7.94E-03	1.67	−8.77
CPC015_HEPG2_6H:BRD-K92093830-003-05-0:10	Doxorubicin	−0.0505	1.21E-05	1.19E-02	1.71	−8.42
CPC006_JHUEM2_6H:BRD-K12502280-001-01-5:11.1	TG-101348	−-0.0505	5.98E-06	8.08E-03	1.84	−9.63
CPC006_LOVO_6H:BRD-A62182663-001-01-4:10	YK-4279	−0.0484	2.82E-05	2.11E-02	1.8	−8.21
CPC003_HA1E_24H:BRD-K72783841-001-01-0:10	Tyrphostin-AG-555	−0.0484	4.68E-05	2.78E-02	1.82	−7.9
CPC006_A375_6H:BRD-K13049116-001-01-6:10	BMS-754807	−0.0484	3.53E-05	2.47E-02	1.82	−8.1
PCLB003_A375_24H:BRD-K95309561-001-19-7:0.12	Dienestrol	−0.0484	2.64E-05	2.02E-02	1.64	−7.5
CPC013_HEPG2_6H:BRD-K00954209-001-01-0:10	BRD-K00954209	−0.0484	1.04E-04	4.04E-02	1.71	−6.82
CPC013_VCAP_6H:BRD-A81530502-001-01-6:10	BRD-A81530502	−0.0484	4.39E-05	2.77E-02	1.72	−7.47
CPC018_A375_6H:BRD-K18787,491-001-07-8:10	U-0126	−0.0462	4.13E-05	2.77E-02	1.71	−7.5
CPC011_PC3_6H:BRD-K92093830-003-23-3:10	Doxorubicin	−0.0462	6.26E-05	3.18E-02	1.77	−7.46
CPC003_HA1E_24H:BRD-K17415526-001-02-7:10	Tyrphostin-AG-835	−0.0462	2.64E-04	6.89E-02	1.81	−6.46
CPC008_HEPG2_6H:BRD-K54687541-001-01-8:10	BRD-K54687541	−0.0462	6.26E-05	3.18E-02	1.8	−7.57
CPC006_HA1E_24H:BRD-K28360340-001-01-8:10	TW-37	−0.0462	1.66E-04	4.87E-02	1.79	−6.76
CPC014_SKB_24H:BRD-K89014967-001-01-9:10	AS-703026	−0.0462	1.48E-04	4.79E-02	1.7	−6.51
CPC018_A375_6H:BRD-K12244279-001-02-5:10	MEK1-2-inhibitor	−0.0462	6.46E-05	3.18E-02	1.7	−7.11
LJP001_SKBR3_24H:BRD-K49328571-001-06-9:2	Dasatinib	−0.0462	2.86E-04	7.25E-02	1.6	−5.67
CPC006_VCAP_6H:BRD-K12994359-001-07-7:177.6	Valdecoxib	−0.0462	9.89E-05	3.92E-02	1.78	−7.15
CPC014_HCC515_6H:BRD-M16762496-001-01-9:10	PIK-75	−0.0462	1.62E-04	4.87E-02	1.71	−6.47
LJP001_SKBR3_24H:BRD-K49328571-001-06-9:10	Dasatinib	−0.0462	2.50E-04	6.68E-02	1.62	−5.85
HOG002_A549_6H:BRD-K34581968-001-01-2:11.1	BMS-536924	−0.0462	1.32E-04	4.61E-02	1.65	−6.38
CPC013_SKB_24H:BRD-K49328571-001-04-4:10	Dasatinib	−0.0462	1.86E-04	5.27E-02	1.71	−6.38
CPC014_SKB_24H:BRD-K05804044-001-01-1:10	AZ-628	−0.0462	1.11E-04	4.14E-02	1.72	−-6.8
CPC012_MCF7_24H:BRD-K45842176-001-01-3:10	BRD-K45842176	−0.0462	1.62E-04	4.87E-02	1.73	−6.55
CPC014_MCF7_6H:BRD-K73293050-001-01-5:10	WZ-3146	−0.044	2.58E-04	6.78E-02	1.71	−6.14
CPC012_PC3_6H:BRD-A19248578-001-03-7:10	Latrunculin-b	−0.044	1.22E-04	4.37E-02	1.78	−6.97
CPC018_HEPG2_6H:BRD-K15588452-003-01-9:10	R-96544	−0.044	2.24E-04	6.12E-02	1.69	−6.15
CPC006_HA1E_24H:BRD-K68336408-001-04-2:56.78	Tyrphostin-AG-1478	−0.044	6.76E-04	1.10E-01	1.78	−5.64
CPC019_HT29_6H:BRD-K65366129-001-04-0:10	SD-6-035-A3	−0.044	1.25E-04	4.39E-02	1.69	−6.59
CPC014_HT29_6H:BRD-K16478699-001-02-7:10	PLX-4720	−0.044	2.24E-04	6.12E-02	1.71	−6.24
CPC006_A549_6H:BRD-K20285085-001-01-4:10	Fostamatinib	−0.044	9.80E-05	3.92E-02	1.83	−7.33
LJP002_MCF10A_6H:BRD-K41859756-001-03-5:0.4	NVP-AUY922	−0.044	1.69E-04	4.91E-02	1.65	−6.23
CPC018_HEPG2_6H:BRD-K46419649-001-01-8:10	U0126	−0.044	1.37E-04	4.69E-02	1.7	−6.57
CPC013_MCF7_24H:BRD-K16541732-001-01-3:10	BRD-K16541732	−0.044	9.90E-04	1.32E-01	1.67	−5.03
CPC006_A375_24H:BRD-K10705233-003-02-8:40	GW-405833	−0.044	8.40E-04	1.22E-01	1.76	−5.41
CPC012_SKB_24H:BRD-K08307026-001-01-4:10	BRD-K08307026	−0.044	2.51E-04	6.68E-02	1.72	−6.21
CPC012_MCF7_24H:BRD-K41220170-236-01-4:10	BRD-K41220170	−0.044	4.08E-04	8.32E-02	1.75	−5.94
MUC.CP004_MCF7_6H:BRD-K36627727-001-01-3:1.1111	Tamibarotene	−0.0418	4.72E-04	9.18E-02	1.62	−5.38
CPC006_HA1E_6H:BRD-K64634304-001-01-5:40	Tretinoin	−0.0418	7.53E-04	1.17E-01	1.8	−5.61
CPC003_HA1E_24H:BRD-K37691127-001-02-2:10	Hinokitiol	−0.0418	4.35E-04	8.70E-02	1.89	−6.34
CPC010_VCAP_6H:BRD-A04327189-001-11-0:10	Synephrine	−0.0418	3.12E-04	7.52E-02	1.81	−6.33
CPC018_NPC_24H:BRD-K22385716-001-01-7:10	LY-303511	−0.0418	6.46E-04	1.09E-01	1.66	−5.31
CPC003_PC3_24H:BRD-K17415526-001-02-7:10	Tyrphostin-AG-835	−0.0418	5.39E-04	9.88E-02	1.84	−6.02
CPC006_SW620_6H:BRD-K34581968-001-01-2:11.1	BMS-536924	−0.0418	1.25E-03	1.51E-01	1.77	−5.14
CPC019_PC3_24H:BRD-K92817986-001-01-7:10	BJM-CSC-19	−0.0418	7.34E-04	1.15E-01	1.68	−5.28

Previous studies have shown that infections with *Salmonella* (Himmelhoch et al., 1947), HPV (Lin et al., 2020), and human T-cell leukemia virus (Lycke et al., 1993) are associated with dementia and cognitive decline in humans.

We have previously shown that natural products such as albiziasaponin-A, iso-orientin, and salvadorin can ameliorate the pathologies associated with AD *in vivo* (Rasool et al., 2018) and that the natural products could be useful for the treatment of age-related degenerative diseases (Kalamegam et al., 2020). In addition, we have recently shown that NGKD platforms can be successfully used to find drugs and natural products that may reverse disease-specific gene signatures (Pushparaj et al., 2021). Therefore, NGKD platforms can be used to find drugs and natural products that can potentially reverse AD-associated gene signatures in astrocytes. Here, we used iPathwayGuide, L1000FWD, and L1000CDS2 tools to identify promising drug-responsive molecules for ADRD. Comparative analysis of AD datasets using iPathwayGuide showed that antirheumatic drugs have insufficient signaling in astrocytes from AD patients. Disease-modifying antirheumatic drugs (DMARDs) are used to treat patients with rheumatoid arthritis (Bahlas et al.,

2019) and recent studies have found that patients with rheumatoid arthritis taking antirheumatic drugs have a lower risk of developing dementia (Judge et al., 2017; Huang et al., 2019). Our finding is consistent with these studies that antirheumatic drugs can reverse AD-associated gene signatures in astrocytes. Similarly, vitamin E gene signatures were absent in astrocytes from AD. The role of vitamin E in the treatment of AD remains a controversial topic to date (Browne et al., 2019) and our results provide some evidence for the importance of vitamin E in the treatment of AD and ADRD. A recent study found that emetine may have the potential to clear amyloid-beta plaques in AD (Ahmad et al., 2019). The isoquinoline alkaloids emetine and its desmethyl analog cepaheline have been predicted to be protective against cognitive decline and AD (Fernández-Martínez et al., 2020). Withaferin A is a steroidal lactone and a withanolide found in the medicinal plant Withania somnifera, and a number of studies have shown that it plays a neuroprotective role in AD (Das et al., 2021). Narciclasine is an active constituent of the Lycoris radiata (L'Her.) herb. It is used in traditional Chinese medicine for the treatment of AD (Shen et al., 2019). A recent study found that senolytic therapy with a combination of dasatinib and quercetin reduced Aβ-associated oligodendrocyte progenitor cell senescence and cognitive decline in an AD model (Zhang et al., 2019). The histone deacetylase inhibitor trichostatin A (Hsing et al., 2015) increased albumin expression and Aβ clearance in APP/PS1 mice and improved cognitive deficits (Su et al., 2021). Trichostatin A increased the antioxidant capacity and cell viability of SH -SY5Y cells by enhancing Keap1-mediated inhibition of the Nrf2 pathway, thereby reducing amyloid-β peptide-mediated cell damage (Li et al., 2020). Importantly, we recently predicted the potential of withaferin A, narciclasine, and trichostatin A to reverse gene signatures in neuro- COVID (Pushparaj et al., 2021). However, the effects of natural products such as emetine, cephaeline, narciclasine, withaferin A, trichostatin A and drugs such as DMARDs and dasatinib which may be able to reverse AD gene signatures in astrocytes should be validated with appropriate experimental models from AD before being used for further clinical testing.

5 CONCLUSION

The present study provides a valuable method for analyzing snRNASeq datasets deposited in open-source repositories with NGKD platforms to decipher AD -specific pathways, genes, and drugs from synthetic and natural sources for the amelioration of AD-related disease pathologies such as ADRD. However, further studies are required to confirm these drugs and natural products that reverse the gene signatures of AD using appropriate experimental models to deduce the precise mechanisms of action, followed by appropriate clinical trials to evaluate the safety and efficacy of the likely therapeutic interventions for AD and ADRD in a typical clinical milieu. Our innovative approach of applying NGKD platforms to uncover AD-specific pathways and potential drugs and natural products that reverse the AD-specific signatures could be useful in the future for developing personalized medicine for AD patient care.

DATA AVAILABILITY STATEMENT

The datasets presented in this study can be found in online repositories. The names of the repository/repositories and accession number(s) can be found in the article/ **Supplementary Material**.

AUTHOR CONTRIBUTIONS

PP, KG, and MR were involved in conceptualization, intellectual contribution, statistical evaluation, and manuscript writing. PP was involved in the NGKD work and data analysis. PP, GK, KHWS and MR were involved in the coordination of the work, review, and editing of the manuscript. All authors contributed to the article and approved the submitted version.

ACKNOWLEDGMENTS

We acknowledge this project funded by the King Abdulaziz City for Science and Technology (KACST), Riyadh, Kingdom of Saudi Arabia, under grant number 13-MED2437-03. We acknowledge with thanks the KACST and the Science and Technology Unit, King Abdulaziz University for technical and financial support.

SUPPLEMENTARY MATERIAL

The Supplementary Material for this article can be found online at: https://www.frontiersin.org/articles/10.3389/fphar.2021.720170/full#supplementary-material

Supplementary Figure S1 | scREAD. A Single Cell RNA Sequencing Database for Alzheimer's Disease (*Adapted from Jiang et al., 2020 and shared under CC BY-NC-ND 4.0 license*)

Supplementary Figure S2 | An example UMAP of healthy control and AD scREAD datasets. scREAD web tool was used to visualize all the cell types and sub-clusters of astrocytes in the entorhinal cortex region of the brain in AD and Healthy snRNASeq datasets using UMAP.

Supplementary Figure S3 | (A) The iPathwayGuide analysis showing the differentially regulated genes in the Wnt signaling KEGG pathway in the astrocytes of the AD group (AD00203) compared to astrocytes of the healthy control group (AD00201). **(B)** Bar graph depicting the differentially regulated genes in the Wnt signaling pathway in the astrocytes of AD compared to healthy control.

Supplementary Figure S4 | (A) The iPathwayGuide perturbation analysis based on the differentially regulated genes in the PI3K/AKT KEGG pathway in the astrocytes of the AD group (AD00203) compared to astrocytes of the healthy control group (AD00201). **(B)** Bar graph depicting the differentially regulated genes in the PI3K/AKT signaling pathway in the astrocytes of AD compared to healthy control.

REFERENCES

Ahmad, S. S., Khan, H., Danish Rizvi, S. M., Ansari, S. A., Ullah, R., Rastrelli, L., et al. (2019). Computational Study of Natural Compounds for the Clearance of Amyloid-Beta: A Potential Therapeutic Management Strategy for Alzheimer's Disease. *Molecules* 24 (18), 3233. doi:10.3390/molecules24183233

Alzheimer's Disease Facts and Figures (2021). 2021 Alzheimer's Disease Facts and Figures. *Alzheimers Demen.* 17 (3), 327–406. doi:10.1002/alz.12328

Ashburner, M., Ball, C. A., Blake, J. A., Botstein, D., Butler, H., Cherry, J. M., et al. (2000). Gene Ontology: Tool for the Unification of Biology. The Gene Ontology Consortium. *Nat. Genet.* 25 (1), 25–29. doi:10.1038/75556

Bahlas, S., Damiati, L., Dandachi, N., Sait, H., Alsefri, M., and Pushparaj, P. N. (2019). Rapid Immunoprofiling of Cytokines, Chemokines and Growth Factors in Patients with Active Rheumatoid Arthritis Using Luminex Multiple Analyte Profiling Technology for Precision Medicine. *Clin. Exp. Rheumatol.* 37 (1), 112–119.

Barrett, T., Wilhite, S. E., Ledoux, P., Evangelista, C., Kim, I. F., Tomashevsky, M., et al. (2013). NCBI GEO: Archive for Functional Genomics Data Sets-Uupdate. *Nucleic Acids Res.* 41 (Database issue), D991–D995. doi:10.1093/nar/gks1193

Becht, E., McInnes, L., Healy, J., Dutertre, C.-A., Kwok, I. W. H., Ng, L. G., et al. (2018). Dimensionality Reduction for Visualizing Single-Cell Data Using UMAP. *Nat. Biotechnol.* 37, 38–44. doi:10.1038/nbt.4314

Benjamini, Y., and Hochberg, Y. (1995). Controlling the False Discovery Rate: A Practical and Powerful Approach to Multiple Testing. *J. R. Stat. Soc. Ser. B Methodol.* 57 (1), 289–300. doi:10.1111/j.2517-6161.1995.tb02031.x

Benjamini, Y., and Yekutieli, D. (2001). The Control of the False Discovery Rate in Multiple Testing under Dependency. *Ann. Stat.* 29 (4), 1165–1188. doi:10.1214/aos/1013699998

Bonferroni, C. E. (1935). "Il calcolo delle assicurazioni su gruppi di teste," in *Studi in Onore del Professore Salvatore Ortu Carboni* (Rome: Tipografia del Senato), 13–60.

Braak, H., and Braak, E. (1991). Neuropathological Stageing of Alzheimer-Related Changes. *Acta Neuropathol.* 82 (4), 239–259. doi:10.1007/BF00308809

Browne, D., McGuinness, B., Woodside, J. V., and McKay, G. J. (2019). Vitamin E and Alzheimer's Disease: what Do We Know So Far? *Clin. Interv. Aging* 14, 1303–1317. doi:10.2147/CIA.S186760

Claxton, A., Baker, L. D., Hanson, A., Trittschuh, E. H., Cholerton, B., Morgan, A., et al. (2015). Long Acting Intranasal Insulin Detemir Improves Cognition for Adults with Mild Cognitive Impairment or Early-Stage Alzheimer's Disease Dementia. *J. Alzheimers Dis.* 45 (4), 1269–1270. doi:10.3233/JAD-159002

Das, R., Rauf, A., Akhter, S., Islam, M. N., Emran, T. B., Mitra, S., et al. (2021). Role of Withaferin A and its Derivatives in the Management of Alzheimer's Disease: Recent Trends and Future Perspectives. *Molecules* 26 (12), 3696. doi:10.3390/molecules26123696

Draghici, S., Khatri, P., Martins, R. P., Ostermeier, G. C., and Krawetz, S. A. (2003). Global Functional Profiling of Gene Expression. *Genomics* 81 (2), 98–104. doi:10.1016/s0888-7543(02)00021-6

Draghici, S., Khatri, P., Tarca, A. L., Amin, K., Done, A., Voichita, C., et al. (2007). A Systems Biology Approach for Pathway Level Analysis. *Genome Res.* 17 (10), 1537–1545. doi:10.1101/gr.6202607

Draghici, S. (2011). *Statistics and Data Analysis for Microarrays Using R and Bioconductor*. 2nd edition. London: Chapman and Hall/CRC.

Duan, Q., Reid, S. P., Clark, N. R., Wang, Z., Fernandez, N. F., Rouillard, A. D., et al. (2016). L1000CDS2: LINCS L1000 Characteristic Direction Signatures Search Engine. *NPJ Syst. Biol. Appl.* 2, 16015. doi:10.1038/npjsba.2016.15

Fernández-Martínez, J. L., Álvarez-Machancoses, Ó., deAndrés-Galiana, E. J., Bea, G., and Kloczkowski, A. (2020). Robust Sampling of Defective Pathways in Alzheimer's Disease. Implications in Drug Repositioning. *Int. J. Mol. Sci.* 21 (10), 3594. doi:10.3390/ijms21103594

Gao, L. B., Yu, X. F., Chen, Q., and Zhou, D. (2016). Alzheimer's Disease Therapeutics: Current and Future Therapies. *Minerva Med.* 107 (2), 108–113.

Gauthaman, K., Pushparaj, P. N., Rajeshkumar, M., Narasimhan, K., Al-Qahtani, M., Cheung, N. S., et al. (2014). Common Cellular and Molecular Mechanisms Underlying Alzheimer's Disease and Type 2 Diabetes: a Knowledge-Driven Approach. *CNS Neurol. Disord. Drug Targets* 13 (2), 247–258. doi:10.2174/18715273113126660138

Gene Ontology Consortium (2001). Creating the Gene Ontology Resource: Design and Implementation. *Genome Res.* 11 (8), 1425–1433. doi:10.1101/gr.180801

Grubman, A., Chew, G., Ouyang, J. F., Sun, G., Choo, X. Y., McLean, C., et al. (2019). A Single-Cell Atlas of Entorhinal Cortex from Individuals with Alzheimer's Disease Reveals Cell-type-specific Gene Expression Regulation. *Nat. Neurosci.* 22 (12), 2087–2097. doi:10.1038/s41593-019-0539-4

Himmelhoch, E., Latham, O., and Mcdonald, C. G. (1947). Alzheimer's Disease Complicated by a Terminal salmonella Infection. *Med. J. Aust.* 1 (23), 701–703. doi:10.5694/j.1326-5377.1947.tb94344.x

Hitzemann, R., Darakjian, P., Walter, N., Iancu, O. D., Searles, R., and McWeeney, S. (2014). Introduction to Sequencing the Brain Transcriptome. *Int. Rev. Neurobiol.* 116, 1–19. doi:10.1016/B978-0-12-801105-8.00001-1

Hsing, C. H., Hung, S. K., Chen, Y. C., Wei, T. S., Sun, D. P., Wang, J. J., et al. (2015). Histone Deacetylase Inhibitor Trichostatin A Ameliorated Endotoxin-Induced Neuroinflammation and Cognitive Dysfunction. *Mediators Inflamm.* 2015, 163140. doi:10.1155/2015/163140

Huang, L. C., Chang, Y. H., and Yang, Y. H. (2019). Can Disease-Modifying Anti-Rheumatic Drugs Reduce the Risk of Developing Dementia in Patients with Rheumatoid Arthritis? *Neurotherapeutics.* 16 (3), 703–709. doi:10.1007/s13311-019-00715-6

Hurd, M. D., Martorell, P., Delavande, A., Mullen, K. J., and Langa, K. M. (2013). Monetary Costs of Dementia in the United States. *New Engl. J. Med.* 368 (14), 1326–1334. doi:10.1056/NEJMsa1204629

Jiang, J., Wang, C., Qi, R., Fu, H., and Ma, Q. (2020). scREAD: A Single-Cell RNA-Seq Database for Alzheimer's Disease. *iScience* 23 (11), 101769. doi:10.1016/j.isci.2020.101769

Judge, A., Garriga, C., Arden, N. K., Lovestone, S., Prieto-Alhambra, D., Cooper, C., et al. (2017). Protective Effect of Antirheumatic Drugs on Dementia in Rheumatoid Arthritis Patients. *Alzheimers Demen.* 3 (4), 612–621. doi:10.1016/j.trci.2017.10.002

Kalamegam, G., Alfakeeh, S. M., Bahmaid, A. O., AlHuwait, E. A., Gari, M. A., Abbas, M. M., et al. (2020). *In Vitro* Evaluation of the Anti-inflammatory Effects of Thymoquinone in Osteoarthritis and In Silico Analysis of Inter-Related Pathways in Age-Related Degenerative Diseases. *Front. Cel Develop. Biol.* 8, 646. doi:10.3389/fcell.2020.00646

Kanehisa, M., and Goto, S. (2000). KEGG: Kyoto Encyclopedia of Genes and Genomes. *Nucleic Acids Res.* 28 (1), 27–30. doi:10.1093/nar/28.1.27

Kanehisa, M., Goto, S., Kawashima, S., and Nakaya, A. (2002). The KEGG Databases at GenomeNet. *Nucleic Acids Res.* 30 (1), 42–46. doi:10.1093/nar/30.1.42

Kanehisa, M., Goto, S., Furumichi, M., Tanabe, M., and Hirakawa, M. (2010). KEGG for Representation and Analysis of Molecular Networks Involving Diseases and Drugs. *Nucleic Acids Res.* 38 (Database issue), D355–D360. doi:10.1093/nar/gkp896

Kanehisa, M., Goto, S., Sato, Y., Furumichi, M., and Tanabe, M. (2012). KEGG for Integration and Interpretation of Large-Scale Molecular Data Sets. *Nucleic Acids Res.* 40 (Database issue), D109–D114. doi:10.1093/nar/gkr988

Kanehisa, M., Goto, S., Sato, Y., Kawashima, M., Furumichi, M., and Tanabe, M. (2014). Data, Information, Knowledge and Principle: Back to Metabolism in KEGG. *Nucleic Acids Res.* 42 (Database issue), D199–D205. doi:10.1093/nar/gkt1076

Kery, R., Chen, A., and Kirschen, G. W. (2020). Genetic Targeting of Astrocytes to Combat Neurodegenerative Disease. *Neural Regen. Res.* 15 (2), 199–211. doi:10.4103/1673-5374.265541

Li, L. H., Peng, W. N., Deng, Y., Li, J. J., and Tian, X. R. (2020). Action of Trichostatin A on Alzheimer's Disease-like Pathological Changes in SH-SY5Y Neuroblastoma Cells. *Neural Regen. Res.* 15 (2), 293–301. doi:10.4103/1673-5374.265564

Lin, C. H., Chien, W. C., Chung, C. H., Chiang, C. P., Wang, W. M., Chang, H. A., et al. (2020). Increased Risk of Dementia in Patients with Genital Warts: A Nationwide Cohort Study in Taiwan. *J. Dermatol.* 47 (5), 503–511. doi:10.1111/1346-8138.15277

Long, H. Z., Cheng, Y., Zhou, Z. W., Luo, H. Y., Wen, D. D., and Gao, L. C. (2021). PI3K/AKT Signal Pathway: A Target of Natural Products in the Prevention and

Treatment of Alzheimer's Disease and Parkinson's Disease. *Front. Pharmacol.* 12, 648636. doi:10.3389/fphar.2021.648636

Luscher, B., Fuchs, T., and Kilpatrick, C. L. (2011). GABAA Receptor Trafficking-Mediated Plasticity of Inhibitory Synapses. *Neuron* 70 (3), 385–409. doi:10.1016/j.neuron.2011.03.024

Lycke, J., Svennerholm, B., Svenningsson, A., Horal, P., Nordqvist-Brandt, E., and Andersen, O. (1993). Possible Association of HTLV-I Infection and Dementia. *Acta Neurol. Scand.* 88 (3), 199–203. doi:10.1111/j.1600-0404.1993.tb04216.x

Matthews, K. A., Xu, W., Gaglioti, A. H., Holt, J. B., Croft, J. B., Mack, D., et al. (2019). Racial and Ethnic Estimates of Alzheimer's Disease and Related Dementias in the United States (2015-2060) in Adults Aged ≥65 Years. *Alzheimers Demen.* 15 (1), 17–24. doi:10.1016/j.jalz.2018.06.3063

Oksanen, M., Petersen, A. J., Naumenko, N., Puttonen, K., Lehtonen, Š., Gubert Olivé, M., et al. (2017). PSEN1 Mutant iPSC-Derived Model Reveals Severe Astrocyte Pathology in Alzheimer's Disease. *Stem Cel Rep.* 9 (6), 1885–1897. doi:10.1016/j.stemcr.2017.10.016

Palomer, E., Buechler, J., and Salinas, P. C. (2019). Wnt Signaling Deregulation in the Aging and Alzheimer's Brain. *Front. Cell Neurosci.* 13, 227. doi:10.3389/fncel.2019.00227

Pushparaj, P. N., Abdulkareem, A. A., and Naseer, M. I. (2021). Identification of Novel Gene Signatures Using Next-Generation Sequencing Data from COVID-19 Infection Models: Focus on Neuro-COVID and Potential Therapeutics. *Front. Pharmacol.* 12, 688227. doi:10.3389/fphar.2021.688227

Rasool, M., Malik, A., Waquar, S., Tul-Ain, Q., Jafar, T. H., Rasool, R., et al. (2018). In-Silico Characterization and *In-Vivo* Validation of Albiziasaponin-A, Iso-Orientin, and Salvadorin Using a Rat Model of Alzheimer's Disease. *Front. Pharmacol.* 9, 730. doi:10.3389/fphar.2018.00730

Rasool, M., Malik, A., Waquar, S., Zaheer, A., Asif, M., Iqbal, Z., et al. (2021). Cellular and Molecular Mechanisms of Dementia: Decoding the Causal Link of Diabetes Mellitus in Alzheimer's Disease. *CNS Neurol. Disord. Drug Targets* 20, 602. doi:10.2174/1871527320666210212114116

Riaz, M., Huq, A., Ryan, J., Orchard, S. G., Tiller, J., Lockery, J., et al. (2021). Effect of APOE and a Polygenic Risk Score on Incident Dementia and Cognitive Decline in a Healthy Older Population. *Aging Cell* 20, e13384. doi:10.1111/acel.13384

Sala Frigerio, C., Wolfs, L., Fattorelli, N., Thrupp, N., Voytyuk, I., Schmidt, I., et al. (2019). The Major Risk Factors for Alzheimer's Disease: Age, Sex, and Genes Modulate the Microglia Response to Aβ Plaques. *Cel Rep.* 27 (4), 1293–1306. doi:10.1016/j.celrep.2019.03.099

Sekar, S., McDonald, J., Cuyugan, L., Aldrich, J., Kurdoglu, A., Adkins, J., et al. (2015). Alzheimer's Disease Is Associated with Altered Expression of Genes Involved in Immune Response and Mitochondrial Processes in Astrocytes. *Neurobiol. Aging* 36 (2), 583–591. doi:10.1016/j.neurobiolaging.2014.09.027

Shen, C. Y., Xu, X. L., Yang, L. J., and Jiang, J. G. (2019). Identification of Narciclasine from Lycoris Radiata (L'Her.) Herb. And its Inhibitory Effect on LPS-Induced Inflammatory Responses in Macrophages. *Food Chem. Toxicol.* 125, 605–613. doi:10.1016/j.fct.2019.02.003

Su, Q., Li, T., He, P. F., Lu, X. C., Yu, Q., Gao, Q. C., et al. (2021). Trichostatin A Ameliorates Alzheimer's Disease-Related Pathology and Cognitive Deficits by Increasing Albumin Expression and Aβ Clearance in APP/PS1 Mice. *Alzheimers Res. Ther.* 13 (1), 7. doi:10.1186/s13195-020-00746-8

Wang, Z., Lachmann, A., Keenan, A. B., and Ma'ayan, A. (2018). L1000FWD: Fireworks Visualization of Drug-Induced Transcriptomic Signatures. *Bioinformatics* 34 (12), 2150–2152. doi:10.1093/bioinformatics/bty060

Wang, C., Xiang, Y., Fu, H., and Ma, Q. (2021). Use of scREAD to Explore and Analyze Single-Cell and Single-Nucleus RNA-Seq Data for Alzheimer's Disease. *STAR Protoc.* 2 (2), 100513. doi:10.1016/j.xpro.2021.100513

Winblad, B., Amouyel, P., Andrieu, S., Ballard, C., Brayne, C., Brodaty, H., et al. (2016). Defeating Alzheimer's Disease and Other Dementias: a Priority for European Science and societyThe Lancet. *Neurology* 15 (5), 455–532. doi:10.1016/S1474-4422(16)00062-4

World Health Organization (2012). Dementia: a public health priority. World Health Organization. Available at: https://apps.who.int/iris/handle/10665/75263 (Accessed June 1, 2021).

Wu, Y., and Zhang, K. (2020). Tools for the Analysis of High-Dimensional Single-Cell RNA Sequencing Data. *Nat. Rev. Nephrol.* 16 (7), 408–421. doi:10.1038/s41581-020-0262-0

Zhang, P., Kishimoto, Y., Grammatikakis, I., Gottimukkala, K., Cutler, R. G., Zhang, S., et al. (2019). Senolytic Therapy Alleviates Aβ-Associated Oligodendrocyte Progenitor Cell Senescence and Cognitive Deficits in an Alzheimer's Disease Model. *Nat. Neurosci.* 22 (5), 719–728. doi:10.1038/s41593-019-0372-9

Conflict of Interest: The authors declare that the research was conducted in the absence of any commercial or financial relationships that could be construed as a potential conflict of interest.

Publisher's Note: All claims expressed in this article are solely those of the authors and do not necessarily represent those of their affiliated organizations, or those of the publisher, the editors and the reviewers. Any product that may be evaluated in this article, or claim that may be made by its manufacturer, is not guaranteed or endorsed by the publisher.

Advantages of publishing in Frontiers

OPEN ACCESS
Articles are free to read for greatest visibility and readership

FAST PUBLICATION
Around 90 days from submission to decision

HIGH QUALITY PEER-REVIEW
Rigorous, collaborative, and constructive peer-review

TRANSPARENT PEER-REVIEW
Editors and reviewers acknowledged by name on published articles

Frontiers
Avenue du Tribunal-Fédéral 34
1005 Lausanne | Switzerland

Visit us: www.frontiersin.org
Contact us: frontiersin.org/about/contact

REPRODUCIBILITY OF RESEARCH
Support open data and methods to enhance research reproducibility

DIGITAL PUBLISHING
Articles designed for optimal readership across devices

FOLLOW US
@frontiersin

IMPACT METRICS
Advanced article metrics track visibility across digital media

EXTENSIVE PROMOTION
Marketing and promotion of impactful research

LOOP RESEARCH NETWORK
Our network increases your article's readership